NATIONAL TECHNICAL UNIVERSITY OF ATHENS

SCHOOL OF CIVIL ENGINEERING

KINETIC MODELING OF REDUCTIVE BIODEGRADATION OF CHLOROETHENES IN GROUNDWATER

DOCTORAL THESIS

KYRIAKOS K. KANDRIS
Civil Engineer, M.Sc., NTUA

SUPERVISOR:
MARINA PANTAZIDOU
Associate Professor, NTUA

CO-SUPERVISOR:
DANIEL MAMAIS
Professor, NTUA

ATHENS, March 2017

NATIONAL TECHNICAL UNIVERSITY OF ATHENS

SCHOOL OF CIVIL ENGINEERING

KINETIC MODELING OF REDUCTIVE BIODEGRADATION OF CHLOROETHENES IN GROUNDWATER

DOCTORAL THESIS

KYRIAKOS K. KANDRIS

Civil Engineer, M.Sc., NTUA

ADVISORY COMMITTEE

1. Marina Pantazidou, Assoc. Prof., NTUA (Supervisor)
2. Daniel Mamais, Prof., NTUA (Co-supervisor)
3. Andreas Andreadakis, Prof., NTUA

EXAMINATION COMMITTEE

1. Marina Pantazidou, Assoc. Prof., NTUA (Supervisor)
2. Daniel Mamais, Prof., NTUA (Co-supervisor)
3. Andreas Andreadakis, Prof., NTUA
4. Nicolas Kalogerakis, Prof., Technical University of Crete (TUC)
5. Georgios Karatzas, Prof., TUC
6. Nymfodora Papassiopi, Prof., NTUA
7. Konstantinos Noutsopoulos, Assist. Prof., NTUA

ATHENS, March 2017

ΕΘΝΙΚΟ ΜΕΤΣΟΒΙΟ ΠΟΛΥΤΕΧΝΕΙΟ

ΣΧΟΛΗ ΠΟΛΙΤΙΚΩΝ ΜΗΧΑΝΙΚΩΝ

ΜΑΘΗΜΑΤΙΚΗ ΠΡΟΣΟΜΟΙΩΣΗ ΤΩΝ ΚΙΝΗΤΙΚΩΝ ΤΗΣ ΑΝΑΓΩΓΙΚΗΣ ΒΙΟΛΟΓΙΚΗΣ ΑΠΟΔΟΜΗΣΗΣ ΤΩΝ ΧΛΩΡΙΩΜΕΝΩΝ ΑΙΘΥΛΕΝΙΩΝ ΣΤΟ ΥΠΟΓΕΙΟ ΝΕΡΟ

ΔΙΔΑΚΤΟΡΙΚΗ ΔΙΑΤΡΙΒΗ

ΚΥΡΙΑΚΟΥ Κ. ΚΑΝΔΡΗ

Διπλωματούχου Πολιτικού Μηχανικού, Μ.Δ.Ε., ΕΜΠ

ΣΥΜΒΟΥΛΕΥΤΙΚΗ ΕΠΙΤΡΟΠΗ

1. Μαρίνα Πανταζίδου, Αναπ.Καθ. ΕΜΠ (Επιβλέπουσα)
2. Δανιήλ Μαμάης, Καθ., ΕΜΠ (Συνεπιβλέπων)
3. Ανδρέας Ανδρεαδάκης, Καθ., ΕΜΠ

ΕΞΕΤΑΣΤΙΚΗ ΕΠΙΤΡΟΠΗ

1. Μαρίνα Πανταζίδου, Assoc. Prof., NTUA (Επιβλέπουσα)
2. Δανιήλ Μαμάης, Καθ., ΕΜΠ (Συνεπιβλέπων)
3. Ανδρέας Ανδρεαδάκης, Καθ., ΕΜΠ
4. Νικόλας Καλογεράκης, Καθ., Πολυτεχνείο Κρήτης
5. Γεώργιος Καρατζάς, Καθ., Πολυτεχνείο Κρήτης
6. Νυμφοδώρα Παπασιώπη Καθ., ΕΜΠ
7. Κωνσταντίνος Νουτσόπουλος, Επίκ. Καθ., ΕΜΠ

ΑΘΗΝΑ, Μάρτιος 2017

This research was conducted at the Geotechnical Department of the School of Civil Engineering of the National Technical University of Athens and it was supported by the "IKY Fellowships of Excellence for Postgraduate Studies in Greece - Siemens Program".

The approval of the doctoral thesis on behalf of the School of Civil Engineering of the National Technical University of Athens does not imply the acceptance of the author's opinions (Law 5343/1932, Article 202).

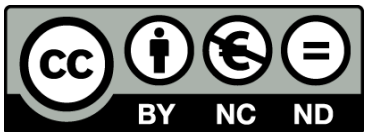

Acknowledgements

This thesis would never have come to fruition without the support of many individuals. Hereby, I would like to acknowledge their names and sincerely thank them. However, while grateful to them, I bear the sole responsibilities for all the mistakes made in the thesis.

First and foremost, I would like to express my gratitude to my supervisors, Assoc. Prof. Marina Pantazidou and Prof. Daniel Mamais. I am profoundly indebted to Marina Pantazidou for her mentoring and guidance througouhout these years. Our collaboration was an honour and a priviledge. I also owe my gratitude to Daniel Mamais for accepting to be my supervisor and offering me the opportunity to work with him. He was very generous with his time and knowledge and assisted me in each step of my research.

Besides my supervisors, I would like to thank the members of my thesis examination committee: Prof. A. Andreadakis, Prof. N. Papassiopi, Prof. N. Kalogerakis, Prof. G. Karatzas, and Assist. Prof. K. Noutsopoulos. Their insightful comments and hard questions incented me to widen my research from various perspectives.

Special thanks are directed to Dr. Iraklis Panagiotakis and Ms. Cornelia Antoniou for providing access to both published and unpublished experimental results of the work they performed in the Sanitary Engineering Laboratory of the National Technical University of Athens. I praise the amount of help provided by both throughout these years.

Finally, I feel that there are no proper words to convey my deep gratitude to my parents, Kostas and Anthoula, to my brother, Giannis, and my companion-in-life, Christina. If it was not for their sacrifices and unremitting support this thesis would not have materialized.

Kyriakos Kandris,
Athens, March 2017

Abstract

Chloroethenes, and particularly the most chlorinated perchloroethene (PCE) and trichloroethene (TCE), are common groundwater contaminants, because of wide industrial use and improper management and disposal. In contaminated subsurface environments, PCE and TCE are often accompanied by dichloroethenes (DCEs) and the monochlorinated vinyl chloride (VC), which are produced by the microbially-mediated degradation of PCE and TCE.

Anaerobic reductive dechlorination (referred to simply as dechlorination in the context of the thesis) has emerged as the most efficient biodegradation pathway of chloroethenes. Dechlorination is a stepwise microbial respiratory process, during which chloroethenes serve as electron acceptors and H_2 serves as the electron donor. Ultimately, the environmentally benign ethene (ETH) is produced.

Dechlorination depends upon, besides H_2 availability, the presence of specific microbes (namely dechlorinators), often naturally-occurring, that mediate each step of the reaction and gain energy to support their maintenance and growth. In field settings, when H_2 is insufficient for the complete or timely detoxification of chloroethenes, H_2 precursors are supplied, an approach referred to as biostimulation (or enhanced, as opposed to intrinsic, biodegradation). Typically, H_2 is not readily available to dechlorinators, hence, the presence of bacteria that can mediate the production of H_2 is also a prerequisite for successful biostimulation. But, H_2 will not stimulate only dechlorinators; H_2 under strictly anaerobic conditions is an electron donor for competitor H_2 scavengers, such as sulfate-reducers and methanogens. Consequently, dechlorination is part of a complex food web involving populations that help (syntrophs) or hinder (competitors) dechlorinators.

The composition of mixed dechlorinating communities varies considerably both in field and laboratory conditions. Differences in the make-up of chloroethene-degrading communities (i.e. different dechlorinating and non-dechlorinating microorganisms) have resulted in mixed cultures with diverse dechlorinating abilities. Consequently, dechlorination rates reported in the literature vary significantly, almost by two orders of magnitude. Considering the metabolic properties of dechlorinators, when the goal is their preferential stimulation, a reasonable remedial approach appears to be the addition of slowly fermentable substrates that provide H_2 (and acetate) steadily at low concentrations. Yet, several biostimulation efforts in the literature deviated from this reasoning (mainly in the laboratory) and managed to successfully effect complete dechlorination to ethene.

The study of dechlorination in mixed communities becomes especially challenging when multiple underlying microbial processes are involved in the explanation of the observed outcomes. In the laboratory, it is hard to separate dechlorination from its side reactions and systematically observe the interspecies flow of H_2. Kinetic models, however, can aid experimental approaches and provide insight into the relevance of dechlorinating and non-dechlorinating processes.

In this research, a comprehensive kinetic model was developed and calibrated, and suitable applications were devised, with the aim to shed light on the non-dechlorinating part of dechlorinating communities. A model that integrates the key microbial processes that are typically anticipated under strictly anaerobic conditions can offer plausible explanations for the distinctive behaviors of dechlorinating cultures in laboratory settings and natural environments. The model

can be used to perform numerical experiments and evaluate the outcome of targeted what-if scenarios that corroborate laboratory investigations, in search of supporting evidence for selecting strategies to optimize chloroethene detoxification.

To this end, the kinetic model presented herein accounted for dechlorination in conjunction with cooperative (i.e. fermentation of H_2 precursors) and competing processes (methane formation and sulfate reduction). A heuristic multistart global optimization approach was developed in order to calibrate the model with experimental observations from research previously performed at NTUA. The multistart optimization technique was also tested with two models and mixed chloroethene-degrading cultures reported in the literature: in one of them, it was found to offer greater insight into the type of dechlorinators. Confidence in model structure and the multistart strategy was gained by testing them under distinctive conditions, ranging from non-limiting conditions (e.g. ample donor supply in the absence of sulfate reducers) to competitive conditions for dechlorinators (e.g. when sulfate reduction and methane formation compete with dechlorination for limited quantities of H_2). Finally, a series of numerical tests was performed to simulate the performance of alternate mixed communities under distinct scenarios of enhanced dechlorination, with emphasis given on the activity and the make-up of non-dechlorinators.

The findings of this thesis offer a framework through which to interpret the observations of dechlorination under methanogenic conditions reported in the literature. The results delineated a group of mixed dechlorinating cultures, containing mostly acetate-consuming methanogens, for which the addition of H_2 in significant quantities will not put dechlorinators in disadvantage, thereby explaining why this is so on the basis of the composition of the non-dechlorinating portion of the microbial community. This is important, because most of the well-studied dechlorinating cultures, including several commercially available ones, exhibit the opposite trend: as a result, perceptions of good practice for efficient dechlorination have often stemmed from over-generalizations that did not apply to the universe of the mixed cultures capable of fully dechlorinating PCE and TCE.

This work investigated systematically the activities of non-dechlorinators for the first time, thus highlighting the need to examine the performance of chloroethene-degrading cultures by considering the interplay of the main microbial groups. Specifically, it showed that moderate differences in the metabolic properties of non-dechlorinators (methanogens and H_2-producing fermenters), even if they are minority populations, influenced significantly the performance of dechlorinators following biostimulation.

Overall, the type of inquiry presented herein frames the use of slowly fermentable substrates to communities where efficient H_2-utilizing methanogens thrive and compete with dechlorinators. In addition, this is the first time that the competition for fermentation daughter-products besides H_2 (i.e. acetate) is assessed. Model results indicated that acetate can dictate the extent of dechlorination, especially under limiting H_2 conditions, i.e. conditions typically encountered during the natural attenuation of chloroethenes.

Simulations performed under sulfate-reducing conditions revealed the role of sulfate-reducing pathways that involve electron donors other than H_2; competition for H_2 precursors (fermentable substrates and acetate) can jeopardize the success of dechlorination, apart from direct competition for H_2. Specifically, the results quantified differences in dechlorination extent depending on the

type of the pathway followed for sulfate reduction. Finally, model results provide evidence supporting the hypothesis that the long-term exposure of dechlorinators to sulfides (the end-product of sulfate reduction) preferentially inhibit the most efficient dechlorinating species, giving room to slow-growing dechlorinators to dominate. The preferential inhibition of dechlorinators by sulfides provides a suitable explanatory framework for the inconsistent findings regarding dechlorination under-sulfate reducing conditions.

Perhaps more importantly, this work showed that kinetic modeling of the fate of priority groundwater pollutants can become more than a fitting exercise and be trusted not only in a predictive mode but also to evaluate alternate hypotheses of the composition of mixed microbial communities and their remediation potential.

ΜΑΘΗΜΑΤΙΚΗ ΠΡΟΣΟΜΟΙΩΣΗ ΤΩΝ ΚΙΝΗΤΙΚΩΝ ΤΗΣ ΑΝΑΓΩΓΙΚΗΣ ΒΙΟΛΟΓΙΚΗΣ ΑΠΟΔΟΜΗΣΗΣ ΤΩΝ ΧΛΩΡΙΩΜΕΝΩΝ ΑΙΘΥΛΕΝΙΩΝ ΣΤΟ ΥΠΟΓΕΙΟ ΝΕΡΟ

Εκτεταμένη περίληψη

1. Το υπόβαθρο του προβλήματος

Τα χλωροαιθυλένια αποτελούν μια οικογένεια ρύπων που περιλαμβάνει το τετραχλωροαιθυλένιο (perchloroethylene – PCE, με τέσσερα άτομα χλωρίου στο μόριο του), το τριχλωροαιθυλένιο (trichloroethylene – TCE, με τρία άτομα χλωρίου στο μόριο του), τα διχλωοροαιθυλένια (dichloroethenes – DCEs) και το μονοχλωριωμένο βινυλοχλωρίδιο (VC). Τα χλωροαιθυλένια είναι στο σύνολό τους ιδιαιτέρως τοξικά για τον άνθρωπο. Μεταξύ της οικογένειας των χλωροαιθυλενίων, τα TCE και VC είναι χαρακτηρισμένα ως καρκινογόνες ουσίες για τον άνθρωπο, ενώ το PCE έχει χαρακτηριστεί ως δυνάμει καρκινογόνο. Κατά συνέπεια, τα χλωροαιθυλένια θεωρούνται ρύποι προτεραιότητας για την Υπηρεσία Περιβάλλοντος των ΗΠΑ (US Environmental Protection Agency – EPA), ενώ τα PCE και TCE συμπεριλαμβάνονται στην Οδηγία περί ουσιών προτεραιότητας της Ευρωπαϊκής Ένωσης (ΕΕ) (Οδηγία 2008/105) και στην Οδηγία για την προστασία των υπογείων υδάτων (Οδηγία 2006/118).

Οι πιο χλωριωμένες ουσίες, δηλαδή τα PCE και TCE, είναι από τους πλέον διαδεδομένους ρύπους στον εκβιομηχανισμένο κόσμο. Αν και τα PCE και TCE παράγονται και από φυσικές διεργασίες, η συχνότητα και πρωτίστως η έκταση των περιστατικών ρύπανσης από το PCE το TCE υποδεικνύουν την ανθρωπογενή προέλευση των χλωροαιθυλενίων στο υπόγειο νερό. Οι δύο αυτοί ρύποι έχουν χρησιμοποιηθεί εκτεταμένα σε βιομηχανικές δραστηριότητες – κυρίως σε στεγνοκαθαριστήρια και σε βιομηχανικές εφαρμογές για τον καθαρισμό και την απολίπανση μετάλλων. Ενδεικτικά, οι Löffler et al. (2013) αναφέρουν τιμές ζήτησης για το PCE και το TCE στις ΗΠΑ και την ΕΕ: για το έτος 2007 η ζήτηση για το PCE στις ΗΠΑ ήταν ίση με 168.000 τόνους, ενώ οι πωλήσεις TCE στην ΕΕ ήταν 28.000 τόνοι για το έτος 2005. Παρά την αυστηροποίηση των κανόνων χρήσης των συγκεκριμένων ουσιών, η χρήση τους παραμένει διαδομένη.

Οι λιγότερο χλωριωμένες ουσίες, τα DCEs και το VC, επίσης απαντώνται συχνά σε ρυπασμένους χώρους. Συνήθως, εμφανίζονται ως τα προϊόντα της βιολογικής αποδόμησης (βιοαποδόμησης) των PCE και TCE. Το συχνότερα απαντώμενο DCE στο υπόγειο νερό είναι το cis-DCE (cDCE), που αποτελεί το κύριο παραπροϊόν της βιολογικής αποδόμησης του TCE. Τέλος, η αναγωγή του cDCE παράγει το VC.

Η επί τόπου βιοαποδόμηση των χλωροαιθυλενίων αποτελεί μια αποτελεσματική επιλογή για την εξυγίανση των υπόγειων υδροφορέων. Τα PCE και TCE ως ρύποι χαμηλής διαλυτότητας και μεγαλύτερης πυκνότητας από το νερό είναι δυνατόν να εισέλθουν στο υπέδαφος ως ξεχωριστές μη υδατικές φάσεις (nonaqueous phase liquids – NAPLs) και να διεισδύσουν σε μεγάλα βάθη του υπόγειου υδροφορέα. Κατά συνέπεια, οι φυσικοχημικές τεχνολογίες απορρύπανσης είναι συχνά δαπανηρές και αναποτελεσματικές λύσεις, ιδιαιτέρως για μεγαλύτερης κλίμακας περιστατικά (Löffler et al., 2013).

Η αναερόβια αναγωγική αποχλωρίωση των χλωροαιθυλενίων αποτελεί τον πιο σημαντικό μηχανισμό βιοαποδόμησής τους στο υπόγειο νερό. Αν και τα χλωροαιθυλένια αποδομούνται τόσο αναγωγικά, όσο και οξειδωτικά, η συχνή παρουσία των ρύπων σε μεγάλα βάθη, όπου το οξυγόνο σχεδόν απουσιάζει, καθιστά το αναερόβιο αναγωγικό μονοπάτι της αποδόμησης των χλωροαιθυλενίων σημαντικό.

Η αναερόβια αναγωγική αποχλωρίωση (θα αναφέρεται απλώς ως αποχλωρίωση στο εξής) είναι η αντικατάσταση ενός ατόμου χλωρίου από ένα άτομο υδρογόνου (H_2). Η αποχλωρίωση αποτελεί μια διεργασία μικροβιακής αναπνοής, κατά την οποία τα χλωροαιθυλένια δρουν ως δέκτες ηλεκτρονίων και το H_2 δρα ως δότης. Όταν όλη η μάζα του PCE ή του TCE έχει μετατραπεί σταδιακά μέσω της παραγωγής DCEs και VC στο περιβαλλοντικώς λιγότερο προβληματικό αιθυλένιο (ethylene – ETH), η αποχλωρίωση είναι πλήρης.

Η πλήρης αποχλωρίωση των χλωροαιθυλενίων σε ETH απαιτεί, εκτός από επαρκές H_2 (για 1 mol ενός χλωροαιθυλενίου απαιτείται 1 mol H_2), την παρουσία συγκεκριμένων μικροοργανισμών-αποχλωριωτών (αποχλωριωτές στο εξής). Οι αποχλωριωτές, που είναι συχνά αυτόχθονες στους ρυπασμένους χώρους, διευκολύνουν κάθε στάδιο της αντίδρασης (δηλαδή την απομάκρυνση ενός ατόμου χλωρίου ανά στάδιο) αντλώντας ενέργεια για τη συντήρηση και τον πολλαπλασιασμό τους. Οι αποχλωριωτές χωρίζονται σε δύο κατηγορίες: (α) τα βακτήρια μερικής αποχλωρίωσης, που μπορούν να αποδομήσουν μόνο τα PCE και TCE, και (β) τα βακτήρια πλήρους αποχλωρίωσης που μπορούν να αποδομήσουν και τα λιγότερο χλωριωμένα DCEs ή/και VC. Η πρώτη κατηγορία αποχλωριωτών περιλαμβάνει βακτήρια με ποικίλες μεταβολικές ιδιότητες που ανήκουν σε διαφορετικά φύλα (πχ Firmicutes ή Proteobacteria). Ωστόσο, η δεύτερη κατηγορία περιλαμβάνει συγκεκριμένα βακτήρια που ανήκουν αποκλειστικά στο φύλο Chloroflexi, το γένος *Dehalococcoides* και το είδος *Dehalococcoides mccartyi* (πρώην *Dehalococcoides ethenogenes*) και χρησιμοποιούν μόνο χλωροαιθυλένια και το H_2 κατά την αναπνοή τους.

Η αποχλωρίωση είναι μόλις ένα τμήμα από ένα σύνθετο μεταβολικό σύστημα με μικροβιακές ομάδες οι οποίες είτε υποβοηθούν είτε παρεμποδίζουν τους αποχλωριωτές. Σε ρυπασμένους χώρους, όπου το υπάρχον H_2 δεν επιτρέπει την ολοκλήρωση όλων των σταδίων της αποχλωρίωσης σε εύλογο χρονικό διάστημα, συνήθως προστίθενται οργανικές ενώσεις που διασπώμενες παράγουν H_2 (πρόδρομες ενώσεις του H_2, όπως είναι οι αλκοόλες και τα λιπαρά οξέα). Αυτή η μέθοδος αποκατάστασης ονομάζεται βιοδιέγερση (ή ενισχυμένη, σε αντίθεση με την ενδογενή, βιοαποκατάσταση). Η διάσπαση των πρόδρομων ενώσεων απαιτεί άλλη μια κατηγορία βακτηρίων, τα υδρογονοπαραγωγικά βακτήρια ζύμωσης των πρόδρομων ενώσεων του H_2 (fermenters). Όμως, το παραγόμενο H_2 δεν είναι διαθέσιμο αποκλειστικά στους αποχλωριωτές. Υπό αυστηρώς αναερόβιες συνθήκες υπάρχουν και άλλοι υποψήφιοι ανταγωνιστές για την κατανάλωσή του. Τέτοιοι είναι οι ομοακετογόνοι μικροοργανισμοί (homoacetogens), οι υδρογονοτροφικοί μεθανογόνοι μικροοργανισμοί (υδρογονοτροφικοί μεθανογόνοι) και τα υδρογονοτροφικά βακτήρια αναγωγής θειικών ιόντων (υδρογονοτροφικοί θειικοαναγωγείς). Η διάσπαση των πρόδρομων ενώσεων παράγει και ανιόντα οξικού (οξικό), διεγείροντας μια δεύτερη κατηγορία μικροοργανισμών, τους οξικοτροφικούς. Το οξικό μπορεί να λειτουργήσει είτε ως απευθείας δότης ηλεκτρονίων (πχ κατά την παραγωγή μεθανίου ή την θειικοαναγωγή), είτε ως πηγή H_2 μέσω της οξείδωσής του από μια δεύτερη κατηγορία υδρογονοπαραγωγών βακτηρίων, τα βακτήρια συντροφικής οξείδωσης του οξικού.

2. Η περιγραφή του προβλήματος

Η σύσταση των κοινοτήτων αποχλωρίωσης ποικίλλει σημαντικά τόσο σε συνθήκες πεδίου, όσο και στο εργαστήριο. Στο πεδίο, οι γεωχημικές συνθήκες του ρυπασμένου υδροφορέα καθορίζουν τη σύσταση της μικροβιακής κοινότητας. Στο εργαστήριο, τα χαρακτηριστικά της μικροβιακής κοινότητας εξαρτώνται από (α) την προέλευσή της (πχ αν προέρχεται από κάποιο ρυπασμένο υδροφορέα ή από αναερόβιους αντιδραστήρες), (β) τον τύπο και την ποσότητα του δότη ηλεκτρονίων που παρέχεται, (γ) το είδος και τις ποσότητες των χλωροαιθυλενίων που προστίθενται, και (δ) την παρουσία εναλλακτικών αποδεκτών ηλεκτρονίων. Η ποικιλία των κοινοτήτων αποχλωρίωσης στη βιβλιογραφία έχει οδηγήσει σε αναφορές ρυθμών αποχλωρίωσης που κυμαίνονται σε εύρος σχεδόν δύο τάξεων μεγέθους. Οι διαφορετικές συμπεριφορές που παρατηρούνται δημιουργούν εύλογα ερωτήματα για τις πρακτικές που πρέπει να υιοθετηθούν κατά τις απόπειρες ενίσχυσης της βιοαποκατάστασης των χλωροαιθυλενίων.

Η αποχλωρίωση υπό συνθήκες μεθανογένεσης έχει μελετηθεί συστηματικά στη βιβλιογραφία, χωρίς ωστόσο να εξάγεται με ασφάλεια ένα συμπέρασμα για τον τύπο και την ποσότητα των πρόδρομων ενώσεων του H_2 που στοχευμένα θα ενισχύσουν τους αποχλωριωτές. Πρώτοι οι Fennell et al. (1997) και οι Yang και McCarty (1998) έδειξαν ότι οργανικές ενώσεις που απαιτούν χαμηλές συγκεντρώσεις H_2 για τη ζύμωσή τους, όπως είναι το βουτυρικό ανιόν (βουτυρικό), προσφέρουν ένα συγκριτικό πλεονέκτημα στους αποχλωριωτές έναντι των μεθανογόνων. Οι χαμηλές συγκεντρώσεις H_2 (συγκεντρώσεις H_2 < 100 nM ή 0.01 kPa) είναι επιθυμητές για δύο λόγους. Πρώτον, το κατώφλι H_2 που απαιτείται για να είναι εφικτή η αποχλωρίωση είναι χαμηλότερο από το αντίστοιχο κατώφλι H_2 για τη μεθανογένεση. Για την αποχλωρίωση απαιτούνται συγκεντρώσεις από 0.1 ως 24 nM H_2 (Luijten et al., 2004), ενώ για τη μεθανογένεση τα κάτω όρια H_2 εντοπίζονται μεταξύ 5 και 100 nM (Löffler et al., 1999). Δεύτερον, οι αποχλωριωτές παρουσιάζουν μεγαλύτερη ικανότητα πρόσληψης του H_2, με τιμές του συντελεστή ημικορεσμού (half-velocity coefficients, K_S) να κυμαίνονται από 7 εως 100 nM (Ballapragada et al., 1997, Smatlak et al., 1996 και Cupples et al., 2004), ενώ οι αντίστοιχοι συντελεστές για τους μεθανογόνους κυμαίνονται από 500 έως 22.000 nM (Clapp et al., 2004). Παρά το θεωρητικό μεταβολικό πλεονέκτημα των αποχλωριωτών σε χαμηλές συγκεντρώσεις H_2, πρόδρομες ενώσεις του H_2 που παράγουν γρήγορα και σημαντικές συγκεντρώσεις H_2 (πχ το γαλακτικό ανιόν ή αλκοόλες, όπως η αιθανόλη) έχουν ενισχύσει την αποχλωρίωση σε μεικτές καλλιέργειες με μεθανογόνο δραστηριότητα τόσο στο εργαστήριο (πχ Richardson et al., 2002 ή Aulenta et al., 2005), όσο και στο πεδίο (πχ Macbeth et al., 2004). Συνεπώς, δεν προκύπτει μια ξεκάθαρη εικόνα για το πως επιλέγεται η ποσότητα και το είδος του δότη ηλεκτρονίων για την ενίσχυση της βιοαποδόμησης των χλωροαιθυλενίων.

Η ανεπαρκής κατανόηση της πορείας της αποχλωρίωσης υπό συνθήκες μεθανογένεσης προέρχεται, έστω εν μέρει, από τις λίγες απόπειρες προσδιορισμού της σύστασης των μεθανογόνων σε μεικτές καλλιέργειες αποχλωρίωσης. Σε λίγες περιπτώσεις είναι γνωστά τα μεταβολικά μονοπάτια παραγωγής μεθανίου (Macbeth et al., 2004, Duhamel και Edwards, 2006, Richardson et al., 2002, Rowe et al., 2008). Επομένως, ο σχεδιασμός της βιοενίσχυσης γίνεται υποθέτοντας πως οι αποχλωριωτές έχουν να ανταγωνιστούν αποκλειστικά υδρογονοτροφικούς μεθανογόνους, μια υπόθεση που δεν είναι πάντα ακριβής – για παράδειγμα η παραγωγή μεθανίου στην καλλιέργεια Donna II είναι κυρίως οξικοτροφικής προέλευσης (Rowe et al., 2008 και Heavner et al., 2013).

Η αποχλωρίωση παρουσία θειικών ιόντων έχει μελετηθεί λιγότερο διεξοδικά στη βιβλιογραφία. Συνηθέστερα καταγράφεται ότι η παρουσία θειικών ιόντων έχει μερικώς ή και πλήρως αναχαιτίσει την

αποχλωρίωση (πχ El Mamouni et al., 2002, Hoelen και Reinhard, 2004, Mao et al., 2017). Ωστόσο, υπάρχουν λίγες αναφορές που περιγράφεται μηδενική ή και θετική επίδραση των θειικών στην αποχλωρίωση (Harkness et al., 2012, Aulenta et al., 2007). Πιθανές αιτίες για τις αρνητικές επιπτώσεις της παρουσίας θειικών στην αποχλωρίωση (όταν παρατηρήθηκαν) είναι ο ανταγωνισμός για το H_2 και η παρεμπόδιση της ανάπτυξης των αποχλωριωτών εξαιτίας της τοξικής παρουσίας σουλφιδίων, δηλαδή των προϊόντων αναγωγής των θειικών ιόντων (Hoelen και Reinhard, 2004; Berggren et al., 2013; Mao et al., 2017). Εκτιμήσεις για την έκβαση του ανταγωνισμού μεταξύ αποχλωριωτών και υδρογονοτροφικών θειικοαναγωγέων βασίζονται στις επιδόσεις των τελευταίων σε καλλιέργειες που δεν παρατηρείται αποχλωρίωση και διαφέρουν θεμελιωδώς από τις καλλιέργειες αποχλωρίωσης. Επιπλέον, ο μηχανισμός παρεμπόδισης της αποχλωρίωσης από τα σουλφίδια δεν έχει μελετηθεί συστηματικά. Έτσι, σε αυτό το πλαίσιο περιορισμένης γνώσης, σε συνθήκες πεδίου συνηθίζεται η προσθήκη μεγάλων ποσοτήτων πρόδρομων ενώσεων του H_2 με στόχο τη γρήγορη απομάκρυνση των θειικών και την ανάπτυξη των αποχλωριωτών σε λιγότερο ανταγωνιστικές συνθήκες.

3. Ο στόχος και η μεθοδολογία της διατριβής

Η μελέτη της αποχλωρίωσης σε μεικτές μικροβιακές κοινότητες γίνεται ιδιαίτερα περίπλοκη καθώς η ερμηνεία των εμπειρικών παρατηρήσεων εμπλέκει πολλές παράλληλες μικροβιακές διεργασίες. Στο εργαστήριο είναι δύσκολο να απομονωθεί η αποχλωρίωση από τις συνοδές αντιδράσεις και να παρατηρηθεί συστηματικά η παραγωγή και η κατανάλωση του H_2 από τις διαφορετικές μικροβιακές ομάδες. Εδώ βοηθούν τα κινητικά μοντέλα τα οποία σε συνδυασμό με πειραματικά δεδομένα μπορούν να αποτυπώσουν ποσοτικά την αλληλεπίδραση μεταξύ αποχλωριωτικών και μη διεργασιών.

Στόχος της παρούσας διατριβής είναι, μέσω της ανάπτυξης ενός κινητικού μοντέλου που θα περιγράφει και μη αποχλωριωτικές διεργασίες, (α) να προσφέρει πιθανές εξηγήσεις για τις διαφορετικές συμπεριφορές που παρουσιάζουν οι καλλιέργειες αποχλωρίωσης στο πεδίο και το εργαστήριο, και (β) να αναζητήσει στοιχεία που θα προσφέρουν απαντήσεις στο θεμελιώδες ερώτημα της ενισχυμένης βιοαποκατάστασης των χλωροαιθυλενίων: πώς να οδηγηθεί στοχευμένα το H_2 στους αποχλωριωτές και να βελτιστοποιηθεί η αποδόμηση των ρύπων.

Για τον λόγο αυτό αναπτύχθηκε ένα κινητικό μοντέλο που περιγράφει την αποχλωρίωση παράλληλα με συνεργατικές (η ζύμωση των πρόδρομων ενώσεων του H_2) και ανταγωνιστικές διεργασίες (παραγωγή μεθανίου και αναγωγή θειικών ιόντων). Για να περιγράψει τη συμπεριφορά πραγματικών καλλιεργειών αποχλωρίωσης, το μοντέλο βαθμονομήθηκε χρησιμοποιώντας δεδομένα από μεικτές καλλιέργειες αποχλωρίωσης που αναπτύχθηκαν και συντηρήθηκαν στο Εθνικό Μετσόβιο Πολυτεχνείο (Panagiotakis, 2010 και Antoniou, 2017): (α) μια μεθανογόνο καλλιέργεια αποχλωρίωσης (NTUA-M), και (β) μια μεικτή καλλιέργεια αποχλωρίωσης με δυνατότητες αναγωγής θειικών ιόντων και παραγωγής μεθανίου (NTUA-S).

Για τον προσδιορισμό των παραμέτρων του μοντέλου, αναπτύχθηκε μια ευρετική μέθοδος βελτιστοποίησης με πολλαπλά σημεία εκκίνησης (heuristic multistart global optimization approach). Η μέθοδος βελτιστοποίησης δοκιμάστηκε και σε δύο μοντέλα για δύο αποχλωριωτικές κοινότητες από τη βιβλιογραφία. Η εμπιστοσύνη στη δομή του μοντέλου και στην επαναληπτική μέθοδο βελτιστοποίησης ενισχύθηκε με δοκιμές υπό διακριτές συνθήκες, οι οποίες κάλυπταν το φάσμα από μη περιοριστικές συνθήκες (π.χ. προσθήκη ικανής ποσότητας δότη εν τη απουσία θειικών) έως συνθήκες έντονου ανταγωνισμού (π.χ. όταν η αναγωγή θειικών και η παραγωγή μεθανίου ανταγωνίζεται με την αποχλωρίωση για περιορισμένες ποσότητες H_2). Επιπρόσθετα, μια σειρά από αριθμητικά

πειράματα προσομοίωσαν την επίδοση εναλλακτικών μεικτών αποχλωριωτικών κοινοτήτων για διαφορετικές στρατηγικές βιοενίσχυσης, δίνοντας έμφαση στη δράση και στη σύνθεση των μη αποχλωριωτών μελών της κοινότητας.

4. Η ανάπτυξη του μοντέλου για μεικτές καλλιέργειες αποχλωρίωσης
(Κεφάλαιο 4)

Καταρχήν, ο σχεδιασμός του μοντέλου θα πρέπει να λαμβάνει υπόψιν όλες τις βασικές πληροφορίες που παρέχονται από τις εμπειρικές παρατηρήσεις των καλλιεργειών στο εργαστήριο, ώστε το παραγόμενο μοντέλο να συμβαδίζει με την πραγματικότητα. Έτσι, ο εννοιακός σχεδιασμός του μοντέλου συμπεριέλαβε όλες τις βασικές συμβιωτικές και ανταγωνιστικές διεργασίες που μπορούν να εξηγήσουν τη συμπεριφορά των δύο αποχλωριωτικών καλλιεργειών που αναπτύχθηκαν και συντηρήθηκαν από τους Panagiotakis (2010) και Antoniou (2017). Ο εννοιακός σχεδιασμός του μοντέλου συμπεριλαμβάνει για πρώτη φορά πεδία μικροβιακού ανταγωνισμού πέραν του H_2, δημιουργώντας ένα μοντέλο ευρύτερης εφαρμογής που περιγράφει διεργασίες που εν δυνάμει λαμβάνουν χώρα σε μεικτές κοινότητες αποχλωρίωσης πέραν των NTUA-M και NTUA-S και οι οποίες σπάνια λαμβάνονται υπόψιν.

4.1 Οι καλλιέργειες αποχλωρίωσης NTUA-M και NTUA-S

Οι καλλιέργειες NTUA-M και NTUA-S θεωρούνται συγγενικές καλλιέργειες. Προήλθαν από το συνδυασμό δύο μητρικών αποχλωριωτικών καλλιεργειών και μίας καλλιέργειας αναγωγής θειικών (Panagiotakis, 2010). Επίσης, συντηρήθηκαν σε αντιδραστήρες ημι-διακοπτόμενου έργου, οι οποίοι σε εβδομαδιαία βάση τροφοδοτούνταν με 500 μM (ή 65,7 mg/l) TCE και 300 μM (ή 26,1 mg/l) βουτυρικού, προσομοιώνοντας τις συνθήκες περιορισμένης διαθεσιμότητας H_2 που συνήθως απαντώνται στο πεδίο. Επίσης, τα αποτελέσματα μοριακών αναλύσεων και των δύο καλλιεργειών έδειξαν ότι σε ποσοτικό επίπεδο κυριαρχούν στελέχη των βακτηρίων πλήρους αποχλωρίωσης *Dehalococcoides mccartyi*.

Η καλλιέργεια NTUA-M διήλθε δύο ξεχωριστών περιόδων λειτουργίας με βάση τη μέση εβδομαδιαία αποχλωριωτική επίδοσή της. Οι δύο ξεχωριστές περίοδοι λειτουργίας της καλλιέργειας θα αντιμετωπίζονται ως δύο ξεχωριστές καλλιέργειες στο εξής και θα αναφέρονται ως η καλλιέργεια NTUA-M1 και η καλλιέργεια NTUA-M2. Στην καλλιέργεια NTUA-M1, οι αποχλωριωτές αποχλωρίωναν κατά μέσο όρο το διαθέσιμο TCE σε ποσοστό 65%, παράγοντας σε εβδομαδιαία βάση κυρίως cDCE και VC και μικρές ποσότητες ETH (Panagiotakis, 2010). Στην καλλιέργεια NTUA-M2, οι αποχλωριωτές ήταν ελαφρώς πιο αποδοτικοί και κατά μέσο όρο αποχλωρίωναν το 71% των χλωροαιθυλενίων – παρήγαγαν κυρίως VC και ελαφρώς υψηλότερες συγκεντρώσεις ETH (Antoniou, 2017). Ένα κοινό χαρακτηριστικό των δύο καλλιεργειών ήταν η ασταθής παραγωγή μεθανίου: ανά περιόδους παρατηρούνταν εξάρσεις και υφέσεις της παραγωγής μεθανίου που συνδυάστηκαν με αντιστρόφως μεταβαλλόμενες συγκεντρώσεις οξικού. Κατά τις έντονα μεθανοπαραγωγικές περιόδους το οξικό καταναλωνόταν σε υψηλούς ρυθμούς, ενώ σε περιόδους χαμηλής παραγωγής μεθανίου το οξικό συσσωρευόταν.

Η καλλιέργεια NTUA-S, πέραν της προσθήκης TCE και βουτυρικού, δεχόταν σε εβδομαδιαία βάση σχετικά χαμηλές συγκεντρώσεις θειικών ιόντων: για μια περίοδο περίπου πέντε ετών τροφοδοτούνταν με 300 μM (ή 28 mg/l) θειικών και για περίπου ένα έτος με 729 μM (ή 70 mg/l) θειικών. Οι συγκεντρώσεις θεωρούνται χαμηλές λαμβάνοντας υπόψιν ότι σε χώρους ρυπασμένους από

χλωροαιθυλένια έχουν αναφερθεί συγκεντρώσεις θειικών ιόντων που κυμαίνονται από 200 μM έως 30.000 μM. Παρά την παρουσία εναλλακτικών αποδεκτών ηλεκτρονίων, οι αποχλωριωτές κατά το τελευταίο έτος λειτουργίας της καλλιέργειας αποχλωρίωναν κατά μέσο όρο το TCE σε ποσοστό 67%, παράγοντας συγκρίσιμες ποσότητες ETH με τις καλλιέργειες NTUA-M1 και NTUA-M2. Η παραγωγή μεθανίου στην καλλιέργεια ήταν ιδιαίτερα χαμηλή, αφού αντιστοιχούσε μόλις στο 1% των διαθέσιμων ισοδύναμων ηλεκτρονίων.

4.2 Ο εννοιακός σχεδιασμός του μοντέλου

Το κινητικό μοντέλο που αναπτύχθηκε περιγράφει την αποχλωρίωση σε σύνθετες μικροβιακές κοινότητες που συμπεριλαμβάνουν συντροφικές και ανταγωνιστικές αλληλεπιδράσεις ανάμεσα σε αποχλωριωτές, υδρογονοπαραγωγά βακτήρια που αποδομούν τις πρόδρομες ενώσεις του H_2, μεθανογόνους και θειικοαναγωγείς. Πιο συγκεκριμένα, το μοντέλο περιγράφει (α) την αποχλωρίωση του TCE από δύο πληθυσμούς αποχλωριωτών (αποχλωριωτές μερικής και πλήρους αποχλωρίωσης), (β) τη συντροφική οξείδωση του βουτυρικού και του οξικού (πρόδρομες ενώσεις του H_2), (γ) την υδρογονοτροφική και οξικοτροφική μεθανογένεση, και (δ) την αναγωγή θειικών με δότες ηλεκτρονίων το H_2, το οξικό και το βουτυρικό. Συνολικά, εννέα κύριες ομάδες μικροοργανισμών θεωρείται ότι έχουν εν δυνάμει αναπτυχθεί στις καλλιέργειες. Τέλος, σύνθετες οργανικές ενώσεις, που προέρχονται από την αποδόμηση της βιομάζας και την προσθήκη εκχυλίσματος ζύμης, προσομοιώθηκαν ως πηγές βουτυρικού συνεισφέροντας κατ' αυτόν τον τρόπο επιπλέον ηλεκτρόνια για τις καταβολικές διεργασίες των μικροοργανισμών.

Τρία επίπεδα ανταγωνισμού περιγράφονται από το μοντέλο, ο ανταγωνισμός για το H_2, το οξικό και το βουτυρικό. Ο ανταγωνισμός για το H_2 είναι κρίσιμος, αφού επηρεάζει άμεσα την έκβαση της αποχλωρίωσης. Η προσθήκη βουτυρικού σε καλλιέργειες αποχλωρίωσης με στόχο τη βιοενίσχυση των αποχλωριωτών έχει οδηγήσει σε συγκεντρώσεις H_2 που κυμαίνονται από 0,05 μM (Fennell και Gossett, 1998) σε 1,20 μM (Mao et al., 2015) και, ως εκ τούτου, όλες οι διεργασίες που καταναλώνουν H_2 είναι θερμοδυναμικά εφικτές (Löffler et al., 1999). Μετά την προσθήκη των πρόδρομων ενώσεων του H_2, παράγεται και οξικό, για το οποίο ανταγωνίζονται οξικοτροφικοί μεθανογόνοι και θειικοαναγωγείς και βακτήρια συντροφικής οξείδωσης του οξικού. Το αποτέλεσμα του ανταγωνισμού μεταξύ των τριών οξικοτροφικών πληθυσμών δεν έχει διερευνηθεί διεξοδικά στη βιβλιογραφία και ιδιαίτερα σε κοινότητες αποχλωρίωσης. Ειδικά, η χρήση του οξικού ως πηγή H_2 συνοδεύεται από αντικρουόμενα ευρήματα στη βιβλιογραφία. Ως εκ τούτου, δεν μπορεί να προβλεφθεί εκ των προτέρων η έκβαση του ανταγωνισμού για το οξικό. Το ίδιο ισχύει και για τον ανταγωνισμό για το βουτυρικό. Ακόμα λιγότερες μελέτες έχουν εξετάσει πως ανταγωνίζονται θειικοαναγωγείς και βακτήρια συντροφικής οξείδωσης του βουτυρικού για το διαθέσιμο βουτυρικό (Stams et al., 2005). Ακόμη και αν οι συντροφικοί πληθυσμοί τυπικά αναπτύσσονται με αργούς ρυθμούς, παρουσία περιοριστικών ποσοτήτων θειικών ιόντων θα μπορούσαν να ανταγωνιστούν τα θειικοαναγωγικά βακτήρια (Muyzer και Stams, 2008).

4.3 Η μαθηματική περιγραφή των διεργασιών

Η μαθηματική περιγραφή των διεργασιών που λήφθηκαν υπόψιν στο μοντέλο βασίστηκε σχεδόν εξολοκλήρου σε κινητικές εξισώσεις τύπου Monod κατάλληλα τροποποιημένες για να περιγράφουν τα ιδιαίτερα χαρακτηριστικά κάθε διεργασίας. Στις αντιδράσεις αποχλωρίωσης θεωρήθηκαν δύο περιοριστικοί παράγοντες: τα χλωροαιθυλένια (αποδέκτης ηλεκτρονίων) και το H_2 (δότης ηλεκτρονίων), για το οποίο χρησιμοποιήθηκε ένα κατώφλι συγκέντρωσης κάτω από το οποίο η

αποχλωρίωση δεν είναι εφικτή. Επίσης, θεωρήθηκε πως η παρουσία του cDCE λειτουργεί παρεμποδιστικά για την κατανάλωση του VC, ένας μηχανισμός που προσομοιώνεται για τα βακτήρια πλήρους αποχλωρίωσης περιγράφοντας τις συχνές καθυστερήσεις στο τελικό στάδιο της αποχλωρίωσης. Οι αντιδράσεις μεθανογένεσης (υδρογονοτροφική και οξικοτροφική) περιείχαν έναν περιοριστικό παράγοντα, το H_2 ή το οξικό, ανάλογα με το είδος του μεθανογόνου μικροοργανισμού. Οι κινητικές της θειικοαναγωγής περιεγράφηκαν με δύο περιοριστικούς παράγοντες, όμοια με τις αντιδράσεις αποχλωρίωσης. Ο πρώτος περιοριστικός παράγοντας είναι η παρουσία θειικών ιόντων (ο αποδέκτης ηλεκτρονίων, όπως κατ' αναλογία είναι τα χλωροαιθυλένια), ενώ ο δεύτερος περιοριστικός παράγοντας είναι ο δότης ηλεκτρονίων, δηλαδή το H_2 ή το οξικό ή το βουτυρικό. Τέλος, οι ρυθμοί οξείδωσης των πρόδρομων ενώσεων του H_2 (δηλαδή του βουτυρικού και του οξικού) υπολογίστηκαν από εξισώσεις τύπου Monod, στις οποίες η πρόδρομη ένωση του H_2 αποτελεί τον μόνο περιοριστικό παράγοντα ανάπτυξης των μικροοργανισμών. Για το θερμοδυναμικό έλεγχο των δύο αντιδράσεων, χρησιμοποιήθηκαν απλές εκθετικές συναρτήσεις της συγκέντρωσης του H_2 σύμφωνα με τις οποίες ο εκάστοτε ρυθμός κατανάλωσης μηδενίζεται όταν η συγκέντρωση του H_2 ξεπεράσει ένα άνω όριο – για το βουτυρικό το όριο είναι 1,20 μM H_2 και για το οξικό είναι 0,40 μM H_2.

Η φθορά των μικροοργανισμών και η αποδόμηση των πιο σύνθετων οργανικών μορίων προσομοιώθηκαν με απλές κινητικές πρώτης τάξης. Ειδικά για την αποδόμηση των σύνθετων οργανικών ενώσεων, θεωρήθηκε απλοποιητικά πως η αποδόμησή τους παράγει αποκλειστικά βουτυρικό, συνεισφέροντας κατ' αυτόν τον τρόπο ισοδύναμα ηλεκτρόνια στην αποχλωριωτική κοινότητα.

5. Η εκτίμηση παραμέτρων του μοντέλου – Μεθοδολογικά ζητήματα
(Κεφάλαιο 5)

Σε κινητικά μοντέλα που βασίζονται σε εξισώσεις τύπου Monod το πρόβλημα εκτίμησης παραμέτρων (το αποκαλούμενο ως αντίστροφο πρόβλημα) είναι συχνά κακώς τεθειμένο (ill-posed). Πολλές λύσεις περιγράφουν εξίσου καλά τα πειραματικά δεδομένα. Η μη μοναδικότητα των λύσεων έχει δύο επιπτώσεις. Πρώτον, μοντέλα με διαφορετικές συμπεριφορές μπορούν να θεωρούνται αποδεκτές λύσεις του αντίστροφου προβλήματος. Για παράδειγμα, στο παρόν μοντέλο η παραγωγή μεθανίου με ταυτόχρονη μείωση του οξικού θα μπορούσε να είναι προϊόν (α) της δράσης οξικοτροφικών μεθανογόνων ή (β) της συνεργασίας συντροφικών βακτηρίων οξείδωσης του οξικού και υδρογονοτροφικών μεθανογόνων. Συνεπώς, το ίδιο αποτέλεσμα μπορεί να παράγεται από διαφορετικά μονοπάτια. Έτσι, υπάρχει περιορισμένη εμπιστοσύνη ότι οι λύσεις του αντίστροφου προβλήματος μπορούν να προσομοιώσουν επαρκώς την πραγματική συμπεριφορά της καλλιέργειας. Δεύτερον, η παρουσία πολλών λύσεων δυσκολεύει τον εντοπισμό αποδεκτών λύσεων. Η εύρεση μιας αποδεκτής λύσης προϋποθέτει τη θεώρηση ενός ορθού αρχικού σημείου εκκίνησης της αναζήτησης. Ένα τέτοιο σημείο, ωστόσο, απαιτεί καλή γνώση της συμπεριφοράς της καλλιέργειας, που είναι σπανίως διαθέσιμη. Επίσης, μια λανθασμένη λύση του αντίστροφου προβλήματος που αναπαράγει ανεπαρκώς τις πειραματικές μετρήσεις μπορεί να οδηγήσει στο εσφαλμένο συμπέρασμα ότι η δομή του μοντέλου είναι λάθος, ενώ η αποτυχία μπορεί να οφείλεται στον εγκλωβισμό της αναζήτησης λύσεων σε περιοχές του χώρου των λύσεων που δεν περιγράφουν ικανοποιητικά τα δεδομένα.

Στην παρούσα διατριβή για τον προσδιορισμό των παραμέτρων του μοντέλου, αναπτύχθηκε μια ευρετική μέθοδος βελτιστοποίησης με πολλαπλά σημεία εκκίνησης. Η μέθοδος αυτή έχει δύο πλεονεκτήματα. Πρώτον, είναι μια απλή στη σύλληψη μέθοδος που παρακάμπτει τη δυσκολία προσδιορισμού ενός μοναδικού σημείου εκκίνησης. Δεύτερον, και ίσως το πλέον σημαντικό, η

βελτιστοποίηση με πολλαπλά σημεία εκκίνησης παρέχει την ευκαιρία εντοπισμού ισοδύναμων αλλά διαφορετικών λύσεων του προβλήματος. Έτσι, χαρτογραφείται ο χώρος των λύσεων του αντίστροφου προβλήματος και εντοπίζονται λύσεις που αντιπροσωπεύουν καλλιέργειες με διαφορετικές συμπεριφορές. Η εκτίμηση μίας μοναδικής λύσης (ακόμα κι αν είναι πράγματι η ολικά βέλτιστη λύση) μπορεί να υποκρύπτει διαφορές στις διεργασίες που είναι ασήμαντες κατά τη φάση προσδιορισμού του μοντέλου, αλλά σημαντικές κατά τη φάση πρόβλεψης, όταν προσομοιώνονται διαφορετικές αρχικές συνθήκες.

Η στρατηγική πολλαπλών εκκινήσεων πραγματοποιείται σε τρία βήματα. Πρώτα, επιλέγεται ένα οιονεί τυχαίο (quasi-random) σημείο εκκίνησης από τον παραμετρικό χώρο. Στη συνέχεια, καλείται ένα τοπικός επιλυτής που εντοπίζει μια λύση του αντίστροφου προβλήματος στη γειτονιά του σημείου εκκίνησης. Τέλος, ελέγχεται ένα κριτήριο τερματισμού του αλγορίθμου. Αν οι τοπικές λύσεις που έχουν προσδιοριστεί είναι ίσες με την Μπεϋζιανή εκτίμηση του ολικού αριθμού τοπικών λύσεων του προβλήματος, τότε σταματά ο αλγόριθμος. Σε διαφορετική περίπτωση, ο αλγόριθμος επιστρέφει στο πρώτο βήμα επιλέγοντας ένα νέο σημείο εκκίνησης.

Δύο εναλλακτικοί αλγόριθμοι πολλαπλών εκκινήσεων προγραμματίστηκαν στο MATLAB®. Η μόνη τους διαφορά είναι ο τοπικός επιλυτής που καλείται κατά το δεύτερο βήμα. Συγκεκριμένα, επιλέχθηκαν: (α) μια μέθοδος επαναληπτικού τετραγωνικού προγραμματισμού (sequential quadratic programming method – SQP), η οποία ανήκει στην οικογένεια των μεθόδων κλίσης (gradient-based method), και (β) μια γενικευμένη μέθοδος αναζήτησης προτύπων (generalized pattern search method – GPS), η οποία ανήκει στην οικογένεια των μεθόδων άμεσης αναζήτησης (gradient-free method).

Η ευρετική μέθοδος βελτιστοποίησης με πολλαπλά σημεία εκκίνησης δοκιμάστηκε σε τρία διαφορετικά κινητικά μοντέλα, τα οποία περιγράφουν αποκλειστικά την αποχλωρίωση υπό μη περιοριστικές συνθήκες H_2 και με παραλλαγές των εξισώσεων τύπου Monod. Συγκεκριμένα, η μέθοδος βελτιστοποίησης ελέγχθηκε: (α) στην καλλιέργεια NTUA-M2 με μια απλοποιημένη εκδοχή του μοντέλου που αναπτύχθηκε στην παρούσα διατριβή, (β) στην εμπορικά διαθέσιμη αποχλωριωτική καλλιέργεια SDC-9 με το μοντέλο των Schäfer et al. (2009), το οποίο λαμβάνει υπόψιν την ανταγωνιστική παρεμπόδιση των χλωροαιθυλενίων, και (γ) στην καλλιέργεια PM με το μοντέλο των Yu και Semprini (2004), που περιγράφει την τοξική επίδραση υψηλών συγκεντρώσεων των PCE και TCE στην αποδόμησή τους.

Η εφαρμογή της μεθόδου πολλαπλών σημείων εκκίνησης εντόπισε αποδεκτές προσεγγίσεις της συμπεριφοράς των καλλιεργειών αποχλωρίωσης NTUA-M2, SDC-9 και PM, χωρίς να εγκλωβίζεται σε περιοχές του παραμετρικού χώρου με ανεπαρκείς λύσεις. Επιπλέον, η μέθοδος τοπικής αναζήτησης SQP ήταν αποτελεσματικότερη της GPS παρουσιάζοντας υψηλότερους ρυθμούς σύγκλισης σε τοπικές λύσεις. Τέλος, η χρήση του Μπεϋζιανού κριτηρίου τερματισμού ήταν άκαρπη, καθώς εξαιτίας της γραμμικής συσχέτισης των παραμέτρων του προβλήματος, έπρεπε να εντοπιστεί μεγάλος αριθμός τοπικών λύσεων του προβλήματος που απαιτεί σημαντικό υπολογιστικό φόρτο. Έτσι, στα συνθετότερα μοντέλα της διατριβής, ο αλγόριθμος πολλαπλών σημείων εκκίνησης σταματούσε στα 1000 σημεία εκκίνησης.

Η διερεύνηση μεγάλων περιοχών του παραμετρικού χώρου παρέχει εμπιστοσύνη ότι το μοντέλο που περιγράφεται από τη βέλτιστη λύση της στρατηγικής πολλαπλών σημείων εκκίνησης είναι ορθό. Το σύνολο των αποδεκτών λύσεων για την καλλιέργεια αποχλωρίωσης NTUA-M2 είχε κοινά λειτουργικά χαρακτηριστικά επιβεβαιώνοντας ότι (α) δύο είδη αποχλωριωτών αποτελούν την κοινότητα των

αποχλωριωτών – τα βακτήρια μερικής αποχλωρίωσης που καταναλώνουν το περισσότερο TCE και τα βακτήρια πλήρους αποχλωρίωσης που καταναλώνουν μικρό τμήμα του TCE και, κυρίως, cDCE και VC, και (β) ότι η παρουσία του cDCE έχει ανασταλτική επίδραση στην απομάκρυνση VC. Για την καλλιέργεια αποχλωρίωσης SDC-9, η εφαρμογή της στρατηγικής πολλαπλών σημείων εκκίνησης επίσης επιβεβαίωσε την υπόθεση ότι το cDCE παρεμποδίζει την αποδόμηση του VC. Για την καλλιέργεια PM, η εφαρμογή της μεθόδου πολλαπλών εκκινήσεων εντόπισε αποδεκτές λύσεις του αντίστροφου προβλήματος που αμφισβητούν τη διαπίστωση των Yu και Semprini (2004) σχετικά με την τοξική επίδραση των υψηλών συγκεντρώσεων TCE.

Αυτός ο πρώτος γύρος προσομοιώσεων οδήγησε την παρούσα διατριβή να εκμεταλλευθεί το διαπιστωμένο πρόβλημα της μη μοναδικότητας των λύσεων του αντίστροφου προβλήματος. Η παρουσία πολλών αποδεκτών λύσεων αποτέλεσε ευκαιρία προσδιορισμού εναλλακτικών μεικτών αποχλωριωτικών κοινοτήτων, η μελέτη των οποίων υπό διαφορετικά σενάρια βιοενίσχυσης θα μπορούσε να δώσει πιθανές εξηγήσεις για τις αντικρουόμενες παρατηρήσεις αναφορικά με το τι αποτελεί καλή πρακτική βιοενίσχυσης των αποχλωριωτών.

6. Η χρήση του μοντέλου για την κατανόηση της σύστασης των μη-αποχλωριωτών σε μεικτές κοινότητες αποχλωρίωσης

Το αναπτυχθέν κινητικό μοντέλο χρησιμοποιήθηκε και σε αντίστροφη και σε ευθεία λογική για να (α) εξετάσει τη λειτουργική δομή των αποχλωριωτικών καλλιεργειών NTUA-M και NTUA-S και (β) να διεξαγάγει στοχευμένα αριθμητικά πειράματα που εξετάζουν την επίδραση των μη αποχλωριωτών στην έκβαση της αποχλωρίωσης υπό συνθήκες μεθανογένεσης ή/και αναγωγής θειικών σε διαφορετικά σενάρια βιοενίσχυσης.

6.1 Εκτιμώντας τη σύσταση της κοινότητας των μη-αποχλωριωτών της καλλιέργειας NTUA-M2 (Κεφάλαιο 7)

Αρχικά, διερευνήθηκε η σύσταση και ο λειτουργικός ρόλος των μη αποχλωριωτών της μεικτής αποχλωριωτικής καλλιέργειας NTUA-M2. Όπως προαναφέρθηκε, η καλλιέργεια NTUA-M2 κατά τη συντήρησή της παρουσίασε σταθερή αποχλωριωτική δράση συνοδευόμενη από ασταθή παραγωγή μεθανίου. Οι διακυμάνσεις στην παραγωγή μεθανίου συνέπεσαν με μεταβολές των συγκεντρώσεων οξικού, υποδεικνύοντας πως το κύριο μονοπάτι μεθανογένεσης είναι οξικοτροφικό. Ωστόσο, το ίδιο αποτέλεσμα θα μπορούσε να έχει επιτευχθεί εναλλακτικά, δηλαδή από τη συντροφική σχέση υδρογονοτροφικών μεθανογόνων και βακτηρίων οξείδωσης του οξικού. Με τη χρήση του μοντέλου, αναζητήθηκαν στοιχεία που να επιβεβαιώνουν την υπόθεση ότι η μεθανογένεση στην αποχλωριωτική κοινότητα NTUA-M2 είναι οξικοτροφική και να διαφωτίζουν τη σύσταση της κοινότητας των μη αποχλωριωτών, δηλαδή των μεθανογόνων και των υδρογονοπαραγωγών βακτηρίων.

Για το σκοπό αυτό, εφαρμόστηκε μια στρατηγική αντεπιβεβαίωσης λύσεων (cross-confirmation strategy). Η στρατηγική αυτή εκτελείται σε δύο στάδια. Κατά το πρώτο, εντοπίζονται διαφορετικές, ισοδύναμες προσεγγίσεις της καλλιέργειας NTUA-M2. Στο δεύτερο στάδιο οι εναλλακτικές λύσεις προσομοιώνουν πειράματα που πραγματοποιήθηκαν σε διαφορετικές φάσεις της καλλιέργειας και για διαφορετικά σενάρια παροχής του δότη ηλεκτρονίων. Όποια λύση αναπαράγει τη συμπεριφορά της καλλιέργειας στα πειράματα του δεύτερου σταδίου θεωρείται ως αποδεκτή προσέγγιση της καλλιέργειας NTUA-M2.

Κατά το πρώτο στάδιο της στρατηγικής αντεπιβεβαίωσης των λύσεων, εφαρμόστηκε η μέθοδος βελτιστοποίησης πολλαπλών εκκινήσεων σε ένα πείραμα που πραγματοποιήθηκε υπό συνθήκες περιορισμένης παροχής βουτυρικού και διήρκησε σχεδόν έξι μήνες επιτυγχάνοντας τελικώς την πλήρη αποχλωρίωση 500 μM TCE. Η στρατηγική πολλαπλών εκκινήσεων εφαρμόστηκε σε επιμέρους βήματα κατά τα οποία εντοπίζονταν διακριτές και ολοένα μικρότερες γειτονιές του χώρου των λύσεων. Αυτή η ευρετική προσέγγιση του αντίστροφου προβλήματος παρείχε εμπιστοσύνη ότι δεν αγνοήθηκαν σημαντικές διεργασίες που περιγράφουν τις πειραματικές παρατηρήσεις. Συνολικά εντοπίστηκαν τέσσερις λύσεις, οι οποίες διέφεραν στις κινητικές παραμέτρους και τη σχετική πυκνότητα των δύο μεθανογόνων και των βακτηρίων οξείδωσης του οξικού. Αυτές οι ομάδες βακτηρίων καταλάμβαναν μόλις το 20% της συνολικής βιομάζας, αφού όπως προαναφέρθηκε κυρίαρχη μικροβιακή ομάδα στην καλλιέργεια NTUA-M2 ήταν τα στελέχη των *Dehalococcoides mccartyi*. Εκτός από τη σχετική κατανομή του 20% της βιομάζας στις τρεις ομάδες μη αποχλωριωτών, οι λύσεις διέφεραν κυρίως ως προς τα μεταβολικά χαρακτηριστικά των υδρογονοτροφικών μεθανογόνων: σε τρεις λύσεις οι υδρογονοτροφικοί μεθανογόνοι μπορούσαν να αναπτυχθούν με υψηλούς μέγιστους ρυθμούς ανάπτυξης (μ_{max}) και σε μία λύση με χαμηλές τιμές μ_{max}.

Για κάθε εναλλακτική μεικτή καλλιέργεια προσομοιώθηκαν δύο διαφορετικά πειράματα. Το πρώτο πείραμα πραγματοποιήθηκε με απευθείας προσθήκη H_2 και πραγματοποιήθηκε σε μια περίοδο της καλλιέργειας NTUA-M2 που παρατηρούνταν ύφεση της μεθανογένεσης. Το δεύτερο πείραμα πραγματοποιήθηκε με υψηλή περίσσεια βουτυρικού (σχεδόν επταπλάσια συγκέντρωση βουτυρικού σε σχέση με τις συγκεντρώσεις που προστίθενται κατά τη συντήρηση της καλλιέργειας) και σε μια περίοδο που η μεθανογένεση είχε ανακάμψει από μια περίοδο ύφεσης.

Η χρήση των τεσσάρων προσεγγίσεων της καλλιέργειας NTUA-M2 σε ευθεία προσομοίωση (forward modeling) ανέδειξε μια μοναδική λύση που περιγράφει τη συμπεριφορά της καλλιέργειας NTUA-M2 σε ένα σημαντικό εύρος αρχικών συνθηκών. Η επιτυχής προσομοίωση των πειραματικών παρατηρήσεων προσφέρει σιγουριά ότι το τελικό μοντέλο αναπαράγει τη ροή ηλεκτρονίων στο πλέγμα των καταβολικών αντιδράσεων της NTUA-M2, παρά τις απλοποιητικές παραδοχές για την περιγραφή των θερμοδυναμικών περιορισμών στην κατανάλωση του βουτυρικού και του οξικού και την αποδόμηση της βιομάζας.

Η λύση που βρέθηκε υποδεικνύει ότι η μεθανογένεση στην καλλιέργεια NTUA-M2 είναι κυρίως οξικοτροφική ακόμα και μετά την απευθείας προσθήκη H_2 ή την προσθήκη υψηλών συγκεντρώσεων βουτυρικού. Η παρουσία υδρογονοτροφικών μεθανογόνων δεν μπορεί να αποκλειστεί, αλλά εφόσον έχουν επιβιώσει στην καλλιέργεια, αποτελούν έναν μικρό πληθυσμό που αναπτύσσεται αργά (δηλαδή με χαμηλές τιμές μ_{max}) και δεν μπορεί να συναγωνισθεί τους αποχλωριωτές.

Οι προσομοιώσεις με τις τέσσερις εναλλακτικές καλλιέργειες υπογράμμισαν επίσης τη σημασία του ρόλου των βακτηρίων συντροφικής οξείδωσης του οξικού στην κατανομή των ηλεκτρονίων στις επιμέρους καταβολικές διεργασίες. Η δράση τους στην καλλιέργεια NTUA-M2 δείχνει ότι, πέραν του ανταγωνισμού για το H_2, ο ανταγωνισμός για το οξικό δεν θα πρέπει να αγνοείται, κυρίως σε συνθήκες που επικρατούν χαμηλές συγκεντρώσεις H_2, καθώς το οξικό μπορεί να λειτουργήσει ως πηγή H_2.

Η παρούσα απόπειρα προσομοίωσης είναι από τις ελάχιστες (ειδικά εν συγκρίσει με το σημαντικό αριθμό δημοσιευμένων κοινοτήτων αποχλωρίωσης) που εξετάζει το σύνολο των διεργασιών της κοινότητας αποχλωρίωσης, ενώ είναι η πρώτη που εξετάζει συστηματικά τα λειτουργικά

χαρακτηριστικά των μη αποχλωριωτών. Ο ρόλος των μη αποχλωριωτών έχει αναγνωρισθεί εσχάτως στη βιβλιογραφία με το ενδιαφέρον να επικεντρώνεται στο φυλογενετικό χαρακτηρισμό των μη αποχλωριωτών. Ωστόσο, συνάγοντας τις μεταβολικές δραστηριότητες των πληθυσμών με βάση φυλογενετικές αναλύσεις μπορεί να οδηγήσει σε εσφαλμένα συμπεράσματα. Η σημασία τέτοιων σφαλμάτων εξετάστηκε στο πλαίσιο της διατριβής, όπως περιγράφεται παρακάτω στην Ενότητα 6.3.

6.2 Εξετάζοντας πιθανές μεταβολές στη σύσταση και τη λειτουργία της καλλιέργειας NTUA-M (Κεφάλαιο 8)

Όπως αναφέρθηκε, η μέση επίδοση των αποχλωριωτών βελτιώθηκε στην καλλιέργεια NTUA-M συν τω χρόνω, δημιουργώντας δύο διακριτές περιόδους, την περίοδο της καλλιέργειας NTUA-M1 (Panagiotakis, 2010) και την περίοδο της καλλιέργειας NTUA-M2 (Antoniou, 2017). Οι δύο καλλιέργειες συμπεριφέρθηκαν ελαφρώς διαφορετικά υπό συνθήκες περιορισμένης παροχής βουτυρικού και διαφοροποιήθηκαν σημαντικά σε συνθήκες υψηλών πλεονασμάτων βουτυρικού. Όταν η καλλιέργεια NTUA-M2 τροφοδοτήθηκε με υψηλές συγκεντρώσεις βουτυρικού, αποχλωρίωσε πλήρως το διαθέσιμο TCE πέντε φορές ταχύτερα από την καλλιέργεια NTUA-M1, παράγοντας τέσσερις φορές λιγότερο μεθάνιο. Η αλλαγή στη συμπεριφορά των καλλιεργειών μπορεί να είναι το αποτέλεσμα μιας μεταβολής της σύνθεσης των μη αποχλωριωτών ή το αποτέλεσμα της εξέλιξης των αποχλωριωτών. Για να ελεγχθούν οι υποθέσεις αυτές, προσομοιώθηκε η συμπεριφορά της καλλιέργειας NTUA-M1. Πιο συγκεκριμένα, η λύση που προκρίθηκε ως πιθανή προσέγγιση της καλλιέργειας NTUA-M2 αποτέλεσε το εναρκτήριο σημείο για την εξέταση της δομής της καλλιέργειας NTUA-M1. Συγκεκριμένα, χρησιμοποιώντας τρία πειράματα που πραγματοποιήθηκαν με την καλλιέργεια NTUA-M1 με διαφορετικές ποσότητες βουτυρικού, επιλύθηκε το αντίστροφο πρόβλημα θεωρώντας ως μεταβλητές μόνο δύο παραμέτρους του προβλήματος: τους μέγιστους ρυθμούς ανάπτυξης των μικροοργανισμών, μ_{max}, και τις αρχικές συγκεντρώσεις τους. Εάν υπάρχουν σημαντικές διαφορές στην ποιοτική και ποσοτική σύσταση των καλλιεργειών, θα πρέπει να αντικατοπτρίζονται στις μεταβολικές ιδιότητες και τη σχετική αφθονία της κάθε μικροβιακής ομάδας που υπάρχει στην καλλιέργεια.

Η επίλυση του αντίστροφου προβλήματος για τα τρία πειράματα που πραγματοποιήθηκαν έδειξε ότι οι διαφορές στη συμπεριφορά των δύο καλλιεργειών οφείλονται κυρίως στη μεταβολή των ιδιοτήτων των υδρογονοτροφικών μεθανογόνων και σε μικρότερο βαθμό σε αλλαγές στην επίδοση των βακτηρίων μερικής αποχλωρίωσης του TCE.

Τα αποτελέσματα υποδεικνύουν ότι κατά την πρώτη περίοδο της καλλιέργειας NTUA-M είναι πιθανή η παρουσία υδρογονοτροφικών μεθανογόνων με υψηλές τιμές μ_{max}. Στις χαμηλές συγκεντρώσεις H_2 που επικρατούν κατά τη συντήρηση της καλλιέργειας, οι υδρογονοτροφικοί μεθανογόνοι παρά τις υψηλές τιμές μ_{max} δεν μπορούν να είναι ιδιαίτερα αποδοτικοί καταναλωτές του H_2 και, συνεπώς, η συνολική συμπεριφορά των καλλιεργειών είναι ελαφρώς διαφορετική. Όμως, σε υψηλές περίσσειες βουτυρικού η παρουσία τους ήταν καταστροφική για την αποχλωρίωση, παρά το γεγονός ότι ποσοτικά ήταν λίγοι. Αυτή η αλλαγή στα μεταβολικά χαρακτηριστικά των μεθανογόνων επιβεβαιώνει προηγούμενες βιβλιογραφικές αναφορές (Duhamel και Edwards, 2006 και Hug et al., 2012) που έδειξαν ότι πλούσιες φυλογενετικά ομάδες μη αποχλωριωτών μπορούν να επιβιώνουν παράλληλα με τους αποχλωριωτές. Έτσι, όταν ένα είδος αναχαιτιστεί, ένα άλλο αναπτύσσεται κερδοσκοπικά για να καλύψει το κενό που δημιουργήθηκε στην καλλιέργεια. Μια τέτοια αλλαγή στην ποιοτική δομή των υδρογονοτροφικών μεθανογόνων έλαβε χώρα και κατά τη συντήρηση της καλλιέργειας NTUA-M.

Σύμφωνα με τα αποτελέσματα του αντίστροφου προβλήματος, μεταβλήθηκε και το αποτέλεσμα του ανταγωνισμού για το TCE μεταξύ των αποχλωριωτών στις καλλιέργειες NTUA-M1 και NTUA-M2. Στην καλλιέργεια NTUA-M1, οι αποχλωριωτές μερικής αποχλωρίωσης ήταν πιο αποδοτικοί και κατανάλωναν σχεδόν αποκλειστικά το διαθέσιμο TCE. Με το πέρασμα του χρόνου, όμως, η επίδοση των αποχλωριωτών μερικής αποχλωρίωσης μειώθηκε και τα στελέχη *Dehalococcoides mccartyi* άρχισαν να καταναλώνουν τμήμα του διαθέσιμου TCE. Έτσι, στην καλλιέργεια NTUA-M2 τα δύο κρίσιμα τελικά στάδια της αποχλωρίωσης (δηλαδή η αποχλωρίωση των cDCE και VC) πραγματοποιούνταν από μεγαλύτερους πληθυσμούς *Dehalococcoides mccartyi*. Μια τέτοια αλλαγή στις αποχλωριωτικές κοινότητες είναι επίσης αναμενόμενη. Για παράδειγμα, οι Duhamel και Edwards (2006) έδειξαν ότι η σύσταση της κοινότητας των αποχλωριωτών σε διάφορες εκδοχές της εμπορικά διαθέσιμης καλλιέργειας KB-1 ήταν σημαντικά διαφορετική, ακόμη και για καλλιέργειες που διατηρήθηκαν με το ίδιο είδος και ποσότητα του δότη ηλεκτρονίων. Στην περίπτωση της καλλιέργειας NTUA-M, η αλλαγή αυτή ήταν υπέρ των στελεχών πλήρους αποχλωρίωσης, βελτιώνοντας τη συνολική απόδοση της καλλιέργειας. Λαμβάνοντας υπόψη τα παραπάνω, ο ανταγωνισμός για το TCE και η δυναμική των πληθυσμών των αποχλωριωτών του TCE δεν πρέπει να παραμεληθεί, καθώς θα μπορούσε να επηρεάσει τους πληθυσμούς που εκτελούν τα τελευταία και, συνήθως, πιο κρίσιμα βήματα της αποχλωρίωσης.

Συνολικά, η μελέτη των δύο γενιών της καλλιέργειας NTUA-M προσέφερε πιθανές εξηγήσεις για τα αίτια της διαφορετικής συμπεριφοράς που παρουσιάζεται στη βιβλιογραφία με καλλιέργειες που συντηρούνται με παρόμοιες συνθήκες παροχής του δότη ηλεκτρονίων. Μια μεταβολή στη συμπεριφορά των υδρογονοτροφικών μεθανογόνων οδήγησε δύο φαινομενικά πανομοιότυπες κοινότητες αποχλωρίωσης να συμπεριφερθούν εντελώς διαφορετικά μετά την απόπειρα ενίσχυσης της αποχλωρίωσης.

6.3 Διερευνώντας τις επιπτώσεις των μη αποχλωριωτών σε αποχλωριωτικές καλλιέργειες υπό συνθήκες μεθανογένεσης

(Κεφάλαιο 9)

Οι δύο προηγούμενες ενότητες άνοιξαν τη συζήτηση αναφορικά με την επίδοση της αποχλωρίωσης και τη λειτουργική δομή των μη αποχλωριωτών. Έτσι, το αναπτυχθέν κινητικό μοντέλο χρησιμοποιήθηκε σε μια σειρά αριθμητικών πειραμάτων με στόχο να εκτιμήσει πως η σύσταση και οι μεταβολικές ιδιότητες των μη αποχλωριωτών επιδρούν στην κατανομή των ισοδυνάμων ηλεκτρονίων στις επιμέρους διεργασίες και, κατά συνέπεια, στην επίδοση της αποχλωρίωσης.

Η μεθοδολογία που εφαρμόστηκε οδήγησε στον προσδιορισμό τεσσάρων υποψήφιων προσεγγίσεων της συμπεριφοράς της NTUA-M2, μία από τις οποίες προκρίθηκε ως αποδεκτή προσομοίωση της πραγματικής συμπεριφοράς της καλλιέργειας. Οι τέσσερις υποψήφιες λύσεις προσφέρουν, ωστόσο, τη δυνατότητα να ελεγχθεί πώς οι μη αποχλωριωτές επιδρούν στην επίδοση της αποχλωρίωσης σε διαφορετικά σενάρια ενισχυμένης βιοαποκατάστασης. Δεδομένου ότι όλες οι λύσεις περιέγραφαν ικανοποιητικά τη συμπεριφορά της πραγματικής καλλιέργειας σε συνθήκες χαμηλής περίσσειας του βουτυρικού, όλες θα μπορούσαν να περιγράφουν μια πραγματική καλλιέργεια αποχλωρίωσης στο εργαστήριο ή στο πεδίο. Έτσι, οι τέσσερις λύσεις αντιμετωπίστηκαν ως διαφορετικές καλλιέργειες και χρησιμοποιήθηκαν σε μια σειρά αριθμητικών πειραμάτων που πραγματοποιήθηκαν με διαφορετικές ποσότητες και τρόπο παροχής βουτυρικού, H_2 και οξικού.

Οι αριθμητικές προσομοιώσεις που πραγματοποιήθηκαν με τις τέσσερις καλλιέργειες ανέδειξαν ότι ήπιες διαφορές στη σύσταση και τις μεταβολικές δυνατότητες των μη αποχλωριωτών σε μια καλλιέργεια που επικρατούν στελέχη των αποχλωριωτών *Dehalococcoides mccartyi* μπορούν να οδηγήσουν σε διαφορετικές στρατηγικές ενίσχυσης της αποχλωρίωσης.

Σε καλλιέργειες όπου η μεθανογένεση είναι πρωτίστως οξικοτροφική, η προσθήκη απευθείας H_2 ή πρόδρομων ενώσεων που αποδομούνται γρήγορα (όπως το γαλακτικό ή οι αλκοόλες), μπορούν να είναι οι βέλτιστες λύσεις για την ενίσχυση των αποχλωριωτών. Η παρουσία υδρογονοτροφικών μεθανογόνων δεν είναι απαραιτήτως παράγοντας προβληματισμού, καθώς θα μπορούσαν να είναι αργά αναπτυσσόμενοι και, συνεπώς, να μην μπορούν να αναχαιτίσουν την ανάπτυξη των αποχλωριωτών μετά τις απόπειρες βιοενίσχυσης.

Οι προσομοιώσεις επιβεβαίωσαν πως αν οι υδρογονοτροφικοί μεθανογόνοι μπορούν να αναπτύσσονται γρήγορα στη μεικτή καλλιέργεια αποχλωρίωσης, η προσθήκη υψηλών ποσοτήτων των πρόδρομων ενώσεων H_2 μπορεί να έχει αρνητικό αποτέλεσμα στην επίδοση της αποχλωρίωσης ανεξάρτητα από το αρχικό μέγεθος του πληθυσμού των μεθανογόνων. Τα υψηλά επίπεδα συγκέντρωσης του παραγόμενου H_2 ακυρώνουν το όποιο κινητικό πλεονέκτημα των αποχλωριωτών. Σε αυτές τις περιπτώσεις, η σταδιακή προσθήκη της πρόδρομης ένωσης H_2 εμφανίστηκε ως μια ελπιδοφόρος εναλλακτική προσέγγιση. Συνεπώς, σύνθετες οργανικές ενώσεις (οι οποίες διασπώμενες αποδίδουν αργά πρόδρομες ενώσεις του H_2) θα ήταν η κατάλληλη στρατηγική για την ενίσχυση της αποχλωρίωσης.

Ο ανταγωνισμός για το οξικό μελετήθηκε συστηματικά και αποδείχθηκε σημαντικός για τις καλλιέργειες με σημαντική υδρογονοτροφική δραστηριότητα και συνθήκες έντονου ανταγωνισμού για το H_2. Πιο συγκεκριμένα, όταν τα βακτήρια οξείδωσης του οξικού συνυπήρχαν με μια κοινότητα γρήγορα αναπτυσσόμενων υδρογονοτροφικών μεθανογόνων, οι συγκεντρώσεις του H_2 παρέμεναν αρκούντως χαμηλές για να λειτουργεί το οξικό ως πηγή H_2. Έτσι, παρά τον υψηλό ανταγωνισμό για το H_2 και την απώλεια ηλεκτρονίων προς τη μεθανογένεση, η συντροφική αποδόμηση του οξικού μετρίαζε τη ζημία για τους αποχλωριωτές. Η θερμοδυναμική απαίτηση για χαμηλές συγκεντρώσεις H_2 εξηγεί γιατί η λειτουργία των βακτηρίων συντροφικής οξείδωσης του οξικού παρατηρείται συνήθως σε συνθήκες πεδίου (πχ He et al., 2002) και σπάνια στο εργαστήριο, όπου σημαντικές ποσότητες πρόδρομων ενώσεων του H_2 προσφέρονται και πιθανώς διατηρούν υψηλά επίπεδα H_2 αναχαιτίζοντας θερμοδυναμικά την οξείδωση του οξικού.

Τα ευρήματα προσφέρουν ένα πλαίσιο μέσα από το οποίο ερμηνεύονται οι ποικίλες αποχλωριωτικές συμπεριφορές που αναφέρονται στη βιβλιογραφία: η επίδοση της αποχλωριωτικής δράσης των καλλιεργειών δεν καθορίζεται αποκλειστικά από τη δραστηριότητα των αποχλωριωτών, ακόμα και αν είναι ποσοτικά η σημαντικότερη πληθυσμιακή ομάδα. Συνολικά, τα αποτελέσματα τονίζουν ότι η μελέτη της αποχλωρίωσης σε μεικτές καλλιέργειες προϋποθέτει (α) τον προσδιορισμό των μονοπατιών μεθανογένεσης και των λειτουργικών χαρακτηριστικών των μεθανογόνων πληθυσμών, και (β) την εξέταση συμβιωτικών αλληλεπιδράσεων που αναπτύσσονται μεταξύ των βακτηρίων συντροφικής οξείδωσης του οξικού και υδρογονοτροφικών πληθυσμών.

6.4 Κατανοώντας τη δομή της αποχλωριωτικής καλλιέργειας NTUA-S
(Κεφάλαιο 10)

Όπως προαναφέρθηκε, η αποχλωρίωση υπό συνθήκες αναγωγής θειικών έχει μελετηθεί λιγότερο συστηματικά σε σχέση με την αποχλωρίωση υπό συνθήκες μεθανογένεσης. Οι διαθέσιμες βιβλιογραφικές αναφορές που μελετούν τον ανταγωνισμό αποχλωρίωσης και θειικοαναγωγής στο πεδίο και στο εργαστήριο δεν συνεισφέρουν προς τη δημιουργία μια ενιαίας αντίληψης για το πώς επιδρά η παρουσία θειικών στην έκβαση και το ρυθμό της αποχλωρίωσης. Ωστόσο, η παρουσία θειικών συνήθως εμφανίζεται να έχει αρνητικές επιπτώσεις στους ρυθμούς αποχλωρίωσης των cDCE και VC. Οι μηχανισμοί που εξηγούν την καθυστέρηση στην απομάκρυνση των cDCE και VC υπό συνθήκες θειικοαναγωγής είναι ακόμα ασαφείς.

Από τη σκοπιά των υπαρχόντων μοντέλων, ο ανταγωνισμός μεταξύ αποχλωρίωσης και αναγωγής θειικών είναι ακόμα λιγότερο μελετημένος. Μόλις δύο προσπάθειες προσομοίωσης τέτοιων καλλιεργειών έχουν πραγματοποιηθεί: οι εργασίες των Malaguerra et al. (2011) και Kouznetsova et al. (2010). Στις δύο απόπειρες, ο ανταγωνισμός για το H_2 ήταν στο επίκεντρο των προσομοιώσεων. Συνεπώς, η μόνη αποδεκτή εξήγηση για την καθυστέρηση της αποχλωρίωσης είναι η απώλεια H_2 για τους αποχλωριωτές προς την ανταγωνιστική διεργασία της αναγωγής θειικών. Ωστόσο, η θειικοαναγωγή πραγματοποιείται και από εναλλακτικά μονοπάτια, καθώς σημαντικός αριθμός μικροοργανισμών μπορεί να ανάγει τα θειικά χρησιμοποιώντας πλήθος οργανικών ενώσεων ως δότη ηλεκτρονίων, συμπεριλαμβανομένων του βουτυρικού και του οξικού. Η σημασία των εναλλακτικών, μη υδρογονοτροφικών μονοπατιών αναγωγής θειικών σε καλλιέργειες αποχλωρίωσης παραμένει άγνωστη.

Όπως έχει αναφερθεί, η καλλιέργεια NTUA-S θεωρείται συγγενική καλλιέργεια με τις NTUA-M1 και NTUA-M2. Προέκυψε από τις ίδιες μητρικές καλλιέργειες και διατηρήθηκε με τις ίδιες συγκεντρώσεις βουτυρικού και TCE. Επίσης, στην καλλιέργεια έχει αναπτυχθεί μια ισχυρή καλλιέργεια αποχλωριωτών πλήρους αποχλωρίωσης, οι οποίοι επιτυγχάνουν συγκρίσιμους βαθμούς αποχλωρίωσης με τους αποχλωριωτές στις καλλιέργειες NTUA-M1 και NTUA-M2. Ωστόσο, η καλλιέργεια απέτυχε να απομακρύνει γρήγορα το TCE ακόμα και μετά από την παροχή υψηλών ποσοτήτων βουτυρικού: χρειάστηκε 10πλάσιο χρόνο σε σχέση με την καλλιέργεια NTUA-M2 και σχεδόν διπλάσιο σε σχέση με την καλλιέργεια NTUA-M1.

Με τη χρήση του μοντέλου επιχειρήθηκε να προσδιορισθεί η δομή της αποχλωριωτικής καλλιέργειας NTUA-S με απώτερο στόχο να εξηγηθεί η συμπεριφορά της καλλιέργειας στις συνθήκες που δοκιμάστηκε. Για να ληφθούν υπόψιν τα διαφορετικά μονοπάτια θειικοαναγωγής που ενδεχόμενα εξηγούν τη συμπεριφορά της καλλιέργειας, θεωρήθηκαν δύο διαφορετικές εκδοχές: (α) στην πρώτη εκδοχή, η κοινότητα θειικοαναγωγέων αποτελείται από δύο μέλη που χρησιμοποιούν το H_2 και το οξικό ως δότες ηλεκτρονίων, και (β) στη δεύτερη εκδοχή, η κοινότητα των θειικοαναγωγέων αποτελείται από οξικοτροφικά βακτήρια και από έναν πληθυσμό που χρησιμοποιεί το βουτυρικό ως δότη ηλεκτρονίων. Στις δύο εκδοχές, τα υπόλοιπα μέλη της κοινότητας αποχλωρίωσης είναι όμοια: (α) ένα είδος αποχλωριωτών επικρατεί στην καλλιέργεια, (β) δύο συντροφικοί υδρογονοπαραγωγοί πληθυσμοί επιβιώνουν και αποδομούν το βουτυρικό και το οξικό, και (γ) η χαμηλή παραγωγή μεθανίου που παρατηρείται αποδίδεται σε μια μικρή οξικοτροφική κοινότητα μεθανογόνων.

Η θεώρηση δύο εναλλακτικών μοντέλων συμπεριφοράς της καλλιέργειας NTUA-S θα πρέπει να θεωρηθεί ως μια απλοποιημένη εκδοχή της στρατηγικής που είχε χρησιμοποιηθεί για τον εντοπισμό

εναλλακτικών μοντέλων της καλλιέργειας NTUA-M2. Εδώ, καθώς η κοινότητα αποχλωρίωσης είναι πιο σύνθετη, τα μοντέλα προ-επιλέχθηκαν χρησιμοποιώντας τη γνώση της συμπεριφοράς της καλλιέργειας κατά τη συντήρησή της. Στη συνέχεια, τα δύο υποψήφια μοντέλα προσαρμόσθηκαν με τον αλγόριθμο πολλαπλών εκκινήσεων σε παρατηρήσεις από δύο πειράματα διακοπτόμενου έργου: (α) ένα πείραμα που διήρκησε 149 ημέρες με χαμηλή περίσσεια βουτυρικού (300 μM βουτυρικού), (β) ένα πείραμα που διήρκησε 83 ημέρες με υψηλή περίσσεια βουτυρικού (2200 μM βουτυρικού). Η επίλυση του αντίστροφου προβλήματος με παρατηρήσεις από δύο πειράματα περιόρισε τη συμπεριφορά των μοντέλων και οδήγησε στον εντοπισμό πρακτικά μοναδικών λύσεων για κάθε εναλλακτική εκδοχή.

Οι δύο λύσεις που προέκυψαν εξήγησαν εξίσου καλά τη συμπεριφορά της καλλιέργειας NTUA-S στο πείραμα με περιορισμένη προσθήκη βουτυρικού. Το κύριο μονοπάτι θειικοαναγωγής ήταν οξικοτροφικό και στις δύο περιπτώσεις. Η ουσιαστικότερη διαφορά των λύσεων ήταν το δευτερεύον μονοπάτι θειικοαναγωγής: στην πρώτη εκδοχή βασιζόταν στο H_2 και στη δεύτερη στο βουτυρικό. Τα υπόλοιπα μέλη της κοινότητας (αποχλωριωτές, υδρογονοπαραγωγοί και μεθανογόνοι) είχαν όμοια συμπεριφορά στις δύο λύσεις. Τα δύο μοντέλα συμπεριφοράς της καλλιέργειας απέτυχαν να περιγράψουν ικανοποιητικά την περίπτωση υψηλής περίσσειας του δότη. Σε αυτήν την περίπτωση, μόνο εφόσον θεωρηθεί πως η θειικοαναγωγή βασίστηκε εξολοκλήρου στο βουτυρικό μπορεί να περιγραφεί ορθά η εικόνα του πειράματος. Συνεπώς, η δεύτερη εκδοχή θεωρείται η πιο πιθανή προσέγγιση της συμπεριφοράς της καλλιέργειας NTUA-S.

Η παρούσα προσέγγιση είναι η πρώτη που εξετάζει και τονίζει τη σημασία μονοπατιών θειικοαναγωγής που απαιτούν την κατανάλωση του οξικού και του βουτυρικού ως δότες ηλεκτρονίων. Συνεπώς, ακόμα και αν η παρουσία υδρογονοτροφικών θειικοαναγωγέων είναι μια προφανής ανησυχία κατά το σχεδιασμό της ενισχυμένης βιοαποκατάστασης, όταν χρησιμοποιούνται λιπαρά οξέα ως πρόδρομες ενώσεις του H_2 για την ενίσχυση της αποχλωρίωσης, η άμεση κατανάλωσή τους μπορεί να θέσει σε κίνδυνο τις απόπειρες ενίσχυσης της αποχλωρίωσης. Τέλος, τα αποτελέσματα επιβεβαίωσαν τη μεταβολική ευελιξία των βακτηρίων θειικοαναγωγής. Όπως αναφέρθηκε, η μεταβολή από την κυρίως οξικοτροφική θειικοαναγωγή στη θειικοαναγωγή με χρήση βουτυρικού ήταν απαραίτητη για να εξηγήσει τη συμπεριφορά της καλλιέργειας.

Η ανάλυση που πραγματοποιήθηκε για την καλλιέργεια NTUA-S αποκάλυψε ότι η παρουσία των θειικών έχει επηρεάσει τη δομή της κοινότητας των αποχλωριωτών. Στην καλλιέργεια NTUA-S, οι αποχλωριωτές εκτιμήθηκαν με (α) αυξημένη ικανότητα πρόσληψης του H_2 (αυξημένο K_s για το H_2), και (β) μειωμένες κινητικές ιδιότητες για την κατανάλωση του VC σε σχέση με τους αποχλωριωτές των συγγενικών καλλιεργειών NTUA-M1 και NTUA-M2 (μειωμένη τιμή μ_{max} για το VC). Η αύξηση του K_s για το H_2 εξηγεί γιατί η αποχλωρίωση του TCE και cDCE προχώρησε γρήγορα, ανεξάρτητα από την παρουσία των θειικών, που ενεργεί ως ανταγωνιστική διεργασία. Από την άλλη πλευρά, η μειωμένη τιμή μ_{max} για το VC εξηγεί τους χαμηλούς ρυθμούς κατανάλωσης του VC, ακόμα και στο πείραμα με υψηλό πλεόνασμα του δότη ηλεκτρονίων. Είναι πιθανό ότι η μακροχρόνια έκθεση σε σουλφίδια προκάλεσε τη διαφορά μεταξύ των αποχλωριωτών που επικράτησαν εν τέλει στην καλλιέργεια NTUA-S και τους αποχλωριωτές των καλλιεργειών NTUA-M1 και NTUA-M2. Ένα παρόμοιο εύρημα έχει αναφερθεί από τους Berggren et al. (2013), σύμφωνα με τους οποίους όταν εισήχθησαν θειικά σε μια κοινότητα αποχλωρίωσης, η παραγωγή σουλφιδίων παρεμπόδισε επιλεκτικά τα πιο αποδοτικά αποχλωριωτικά στελέχη, ενώ παράλληλα ευνόησε αποχλωριωτικά στελέχη που αναπτύσσονται με χαμηλότερα μ_{max}, επιβραδύνοντας έτσι το συνολικό ρυθμό της αποχλωρίωσης.

Τέλος, αναδείχτηκε και πάλι ο ρόλος των συντροφικών πληθυσμών οξείδωσης του οξικού. Όπως στις καλλιέργειες NTUA-M1 και NTUA-M2, αυτό το συνήθως παραμελημένο μονοπάτι παραγωγής H_2 ήταν σημαντικό υπό συνθήκες περιορισμένης διαθεσιμότητας H_2, δηλαδή συνθήκες που απαντώνται συνήθως σε ρυπασμένους υδροφορείς. Το οξικό στην καλλιέργεια NTUA-S λειτούργησε ως μια σημαντική πηγή H_2 παρά τη δράση των οξικοτροφικών θειικοαναγωγέων.

6.5 Ελέγχοντας τους παράγοντες που επιδρούν στην επίδοση της αποχλωρίωσης υπό συνθήκες θειικοαναγωγής

(Κεφάλαιο 11)

Η προηγούμενη ενότητα ήταν μια προσπάθεια να εξηγηθεί η δομή της καλλιέργειας NTUA-S εξετάζοντας (α) το ρόλο των αποχλωριωτών και των υδρογονοπαραγωγών συντροφικών πληθυσμών και (β) τη σύσταση της κοινότητας των θειικοαναγωγέων. Τα ευρήματα έδειξαν ότι σε σχέση με τις καλλιέργειες NTUA-M1 και NTUA-M2, η NTUA-S έχει (α) αποχλωριωτές με μειωμένες δυνατότητες αποδόμησης του VC, (β) αποχλωριωτές με αυξημένες δυνατότητες πρόσληψης του H_2, και (γ) συντροφικούς πληθυσμούς οξείδωσης του οξικού που καταναλώνουν αποτελεσματικότερα το οξικό και μετριάζουν για τους αποχλωριωτές την απώλεια ηλεκτρονίων προς την άμεσα ανταγωνιστική διεργασία της θειικοαναγωγής.

Οι εναλλακτικές προσεγγίσεις της καλλιέργειας NTUA-S χρησιμοποιήθηκαν σε ευθείες προσομοιώσεις και εξέτασαν την επίδραση των προαναφερθεισών αλλαγών στην επίδοση της αποχλωρίωσης. Υπό μία έννοια, πραγματοποιήθηκε μια στοχευμένη ανάλυση ευαισθησίας κατά την οποία αναιρέθηκαν οι διαφορές των καλλιεργειών NTUA-S με τις συγγενικές καλλιέργειες NTUA-M. Έτσι, ποσοτικοποιήθηκε η έκβαση της αποχλωρίωσης θεωρώντας πως (α) στην καλλιέργεια NTUA-S βρίσκονται στελέχη των *Dehalococcoides mccartyi* που αποδομούν γρήγορα το VC, (β) οι αποχλωριωτές καταναλώνουν το H_2 λιγότερο αποτελεσματικά, και (γ) τα βακτήρια οξείδωσης του οξικού είναι λιγότερο αποδοτικά αναπτυσσόμενα με μικρότερες τιμές μ_{max}. Τέλος, μια σειρά αριθμητικών πειραμάτων πραγματοποιήθηκε εξετάζοντας πώς οι εναλλακτικές προσεγγίσεις της καλλιέργειας NTUA-S θα λειτουργούσαν υπό αυξημένες συγκεντρώσεις θειικών, μια παράμετρος που υποδείχθηκε από τους Malaguerra et al. (2011) ως κρίσιμη για την έκβαση της αποχλωρίωσης.

Ο τελικός βαθμός και ο ρυθμός της αποχλωρίωσης στην καλλιέργεια NTUA-S καθορίστηκαν από τις παραμέτρους αποδόμησης του VC, ανεξάρτητα από το σενάριο βιοενίσχυσης ή τη σύσταση της κοινότητας των θειικοαναγωγέων. Αυτό το εύρημα επιβεβαιώνει την ανάλυση ευαισθησίας των Kouznetsova et al. (2010), οι οποίοι επίσης είχαν θεωρήσει κρίσιμες τις παραμέτρους κατανάλωσης του VC.

Η ικανότητα πρόσληψης του H_2 ήταν κρίσιμη μόνο σε πειράματα κατά τα οποία η καλλιέργεια είχε τροφοδοτηθεί με χαμηλές ποσότητες βουτυρικού. Σε αυτές τις περιπτώσεις, η τιμή της παραμέτρου K_s για την κατανάλωση H_2 καθορίζει αν οι αποχλωριωτές μπορούν (α) να ανταγωνιστούν τους αποδοτικούς και ταχέως αναπτυσσόμενους υδρογονοτροφικούς θειικοαναγωγείς, και (β) να διατηρήσουν τα επίπεδα H_2 χαμηλά, ώστε η συντροφική οξείδωση του βουτυρικού και του οξικού να είναι εφικτή, αποδίδοντας επιπλέον ποσότητες H_2. Ωστόσο, μετά από σημαντικές προσθήκες βουτυρικού, το K_s για το H_2 έπαψε να είναι σημαντικό, αφού το H_2 δεν ήταν περιοριστικό και η αποχλωρίωση εξαρτιόταν μόνο από τη συγκέντρωση των χλωροαιθυλενίων.

Τα μεταβολικά χαρακτηριστικά των βακτηρίων συντροφικής οξείδωσης του οξικού είναι σημαντικά μόνο για περιπτώσεις περιορισμένων συγκεντρώσεων H_2. Στα σενάρια βιοενίσχυσης, εξαιτίας του χαμηλού ρυθμού αποδόμησης των χλωροαιθυλενίων, οι αποχλωριωτές αναπτύσσονταν αργά και το H_2 παρέμενε σταθερά σε υψηλές συγκεντρώσεις αναχαιτίζοντας τη δράση των υδρογονοπαραγωγών βακτηρίων.

Οι αρχικές συγκεντρώσεις θειικών ιόντων δεν ήταν κρίσιμες για την επίδοση της καλλιέργειας NTUA-S. Εξαίρεση αποτελούν οι περιπτώσεις που μπορούν να παραχθούν υψηλές συγκεντρώσεις σουλφιδίων (>5000 μM ή 160 mg/l). Αυτό το εύρημα έρχεται σε αντίθεση με την ανάλυση ευαισθησίας των Malaguerra et al. (2011), που τόνισαν ότι η συγκέντρωση θειικών ήταν η πιο σημαντική παράμετρος για τη λειτουργία της αποχλωρίωσης.

Οι προσομοιώσεις που πραγματοποιήθηκαν με υψηλές ποσότητες βουτυρικού επιβεβαίωσαν τη συνήθη πρακτική του πεδίου, κατά την οποία σημαντικές ποσότητες πρόδρομων ενώσεων του H_2 προσφέρονται στους μικροοργανισμούς, ώστε να αναχθούν γρήγορα τα υπάρχοντα θειικά και να μπορέσουν οι αποχλωριωτές να αναπτυχθούν χωρίς ανταγωνιστικές διεργασίες. Αν και με την πάροδο του χρόνου σημαντικές ποσότητες μεθανίου εμφανίστηκαν, η μεθανογένεση ήταν οξικοτροφική και το H_2 ήταν αποκλειστικά διαθέσιμο στους αποχλωριωτές. Οι προσομοιώσεις που πραγματοποιήθηκαν έδειξαν ότι στα σενάρια ενισχυμένης βιοαποκατάστασης είναι σημαντικό (α) να αποσαφηνιστεί το μονοπάτι θειικοαναγωγής, και (β) να εξεταστεί η πιθανή παρεμπόδιση των αποχλωριωτών λόγω της αυξημένης παραγωγής σουλφιδίων. Αν οι αποχλωριωτές επηρεάζονται από την τοξικότητα των σουλφιδίων, τότε γίνεται κρίσιμο το μονοπάτι της θειικοαναγωγής. Όταν η θειικοαναγωγή βασίζεται στην απευθείας κατανάλωση βουτυρικού, παράγονται μικρότερες ποσότητες σουλφιδίων, καθώς αυτό το μεταβολικό μονοπάτι είναι απαιτητικότερο σε ισοδύναμα ηλεκτρόνια. Συνεπώς, λιγότερα θειικά ανάγονται και κατ' επέκταση επικρατούν λιγότερο τοξικές συνθήκες λόγω της περιορισμένης παραγωγής σουλφιδίων.

7. Πρωτοτυπία και κύρια συμβολή

Για πρώτη φορά μελετήθηκαν συστηματικά οι δραστηριότητες των μη αποχλωριωτών, καταδεικνύοντας την ανάγκη της αξιολόγησης της αποχλωριωτικής επίδοσης μιας μεικτής καλλιέργειας υπό το πρίσμα της παράλληλης δράσης των κύριων μικροβιακών ομάδων που την συναποτελούν.

Τα ευρήματα της διατριβής προσφέρουν ένα ερμηνευτικό πλαίσιο για τις διαφορετικές αποχλωριωτικές συμπεριφορές που περιγράφονται στη βιβλιογραφία υπό συνθήκες μεθανογένεσης. Τα αποτελέσματα ανέδειξαν μια κατηγορία μεικτών αποχλωριωτικών κοινοτήτων με κυρίως οξικοτροφικούς μεθανογόνους, για τις οποίες η βιοδιέγερση με H_2 σε υψηλές συγκεντρώσεις δεν θα φέρει τους αποχλωριωτές σε μειονεκτική θέση. Έτσι, αυτή η μη αναμενόμενη αποχλωριωτική συμπεριφορά εξηγείται με βάση τον θεωρούμενο λιγότερο συνήθη τύπο των μεθανογόνων (δηλαδή των οξικοτροφικών αντί των υδρογονοτροφικών). Η ανάδειξη του πλαισίου αυτού είναι σημαντική γιατί οι περισσότερες καλομελετημένες αποχλωριωτικές καλλιέργειες, συμπεριλαμβανομένων και αρκετών διαθέσιμων στο εμπόριο, έχουν την αντίθετη συμπεριφορά: ως αποτέλεσμα, οι αντιλήψεις για το τι συνιστά καλή πρακτική συχνά προέκυπταν από γενικεύσεις που δεν αντιπροσώπευαν το σύμπαν των μεικτών καλλιεργειών που είναι ικανές να αποχλωριώσουν πλήρως τους ρύπους PCE και TCE.

Το είδος της διερεύνησης που παρουσιάστηκε μπόρεσε να επιβεβαιώσει την ορθή πρακτική της χρήσης αργά διασπώμενων πρόδρομων ενώσεων σε μεικτές καλλιέργειες οι οποίες περιέχουν υδρογονοτροφικούς μεθανογόνους ικανούς να συναγωνιστούν τους αποχλωριωτές όταν επικρατούν υψηλότερες συγκεντρώσεις H_2. Επιπλέον, για πρώτη φορά αξιολογήθηκε ο ανταγωνισμός για τα προϊόντα της διάσπασης των πρόδρομων ενώσεων πλην του H_2, δηλαδή για το οξικό. Τα αποτελέσματα έδειξαν ότι το οξικό μπορεί να καθορίσει τον βαθμό ολοκλήρωσης της αποχλωρίωσης, ιδιαίτερα υπό περιοριστικές συνθήκες χαμηλών ποσοτήτων H_2, δηλαδή τις συνθήκες που συνήθως επικρατούν κατά τη φυσική εξασθένηση των χλωροαιθυλενίων, η οποία –όταν είναι επιτυχής– στηρίζεται σε μεγάλο βαθμό στην ενδογενή βιοαποκατάσταση.

Οι προσομοιώσεις σε καλλιέργειες με θειικοαναγωγείς αποκάλυψαν τον ρόλο των θειικοαναγωγικών μονοπατιών που εμπλέκουν δότες ηλεκτρονίων πλην του H_2: ο ανταγωνισμός για πρόδρομες ενώσεις (λιπαρά οξέα συμπεριλαμβανομένου του οξικού) αποτελεί ένα ακόμα εμπόδιο για την επιτυχή έκβαση της αποχλωρίωσης, εκτός από τον απευθείας ανταγωνισμό για H_2. Επίσης, τα αποτελέσματα ισχυροποίησαν την υπόθεση ότι η μακροχρόνια έκθεση των αποχλωριωτών στα σουλφίδια (το προϊόν της αναγωγής θειικών) παρεμποδίζει επιλεκτικά τα πιο αποδοτικά αποχλωριωτικά στελέχη, ενώ παράλληλα ευνοεί αποχλωριωτικά στελέχη που αναπτύσσονται με βραδύτερους ρυθμούς, επιβραδύνοντας έτσι τον ρυθμό της αποχλωρίωσης. Η επιλεκτική παρεμπόδιση των αποχλωριωτών από τα σουλφίδια προσφέρει ένα κατάλληλο ερμηνευτικό πλαίσιο για τα αντικρουόμενα ευρήματα που αναφέρονται στη βιβλιογραφία σχετικά με την αποχλωρίωση σε συνθήκες αναγωγής θειικών.

Τέλος, ως πιθανώς πλέον σημαντική συμβολή της διατριβής κρίνεται ότι έδειξε πως τα κινητικά μοντέλα μπορούν, πέρα από την προσομοίωση πειραματικών δεδομένων, να είναι έμπιστα εργαλεία όχι μόνο για προβλέψεις της εξέλιξης του ρυπαντικού φορτίου, αλλά και για την αξιολόγηση εναλλακτικών υποθέσεων για τη σύσταση μεικτών μικροβιακών κοινοτήτων και τις εξυγιαντικές δυνατότητές τους.

Contents

Table of Figures

List of Tables

Chapter 1: Goal setting

The present chapter introduces the problem to be addressed in the thesis. It discusses the goals of this work, its methodology and, finally, presents the thesis outline.

1.1 Background of the problem

Chloroethenes, and especially the most chlorinated perchloroethene (PCE) and trichloroethene (TCE), are widespread subsurface contaminants, due to their extensive use as dry-cleaning solvents and degreasing agents in military and industrial facilities. Dichloroethenes (DCEs) and the monochlorinated vinyl chloride (VC) are also frequently detected in groundwater, as they result from the *in situ* biodegradation of PCE and TCE. Laboratory and field evidence indicate that the predominant biodegradation pathway of chloroethenes is anaerobic reductive dechlorination (for convenience purposes referred to as dechlorination herein), where PCE and TCE are sequentially dechlorinated to DCEs (mainly cis-DCE), VC and, ultimately to the environmentally benign ethene (ETH).

Dechlorination is catalyzed by bacteria capable of chloroethene respiration, referred to as dechlorinators, i.e. bacteria that use chloroethenes as electron acceptors in an energy-yielding process. Various species gain energy from chloroethene respiration, but *Dehalococcoides mccartyi* can remove PCE all the way to ETH. All the strains of *Dehalococcoides mccartyi* isolated to date are obligately H_2-utilizing; molecular H_2 serves as the electron donor and couples chloroethenes in dechlorination. Thus, reductive dechlorination apart from the presence of specific bacterial populations necessitates the presence of sufficient H_2.

In field settings, the production of H_2 comes from the fermentation of organic substrates (electron donor sources), such as hydrocarbon co-contaminants or decaying biomass. Thus, the presence of bacteria that can mediate the use of H_2 is also a prerequisite for the complete detoxification of chloroethenes. Nevertheless, H_2 is an attractive electron donor under strictly anaerobic conditions not only for dechlorinators, but for competitive H_2 scavengers as well. Homoacetogens, sulfate-reducers and methanogens, which are ubiquitous in contaminated subsurface environments, also utilize H_2 to gain energy to support their growth. Consequently, dechlorination is a part of complex, multi-parametric systems, which involve side-reactions catalyzed by cooperative or antagonistic microbial populations.

In laboratory enrichments, dechlorinators thrive in mixed communities too (the reasons explaining why they fail to grow well in isolation are discussed in Chapter 2). Community composition varies remarkably, primarily because of the different (a) origins of the inocula utilized (e.g. contaminated sites or anaerobic reactors), (b) types and quantities of electron donor sources supplied, (c) types and quantities of chloroethenes added, and (d) alternate electron acceptors present or added (such as sulfate). Composition variability has created cultures with diverse dechlorinating abilities and, consequently, dechlorination rates reported in the literature vary vastly, nearly by two orders of magnitude. The variability of the composition of dechlorinating communities inevitably results in the absence of a firm consensus regarding the reasons that explain performance differences.

The study of dechlorination in mixed cultures is thought-provoking, as multiple microbial processes underlie laboratory observations. In the laboratory, it is hard to separate dechlorination from its side reactions, create controlled conditions and systematically assess the mechanisms that potentially affect dechlorination. Kinetic models, however, can corroborate experimental efforts and provide insight into the relevance of the non-dechlorinating processes.

The goal of the thesis is, through the development of a comprehensive kinetic model, to (a) offer plausible explanations for the distinctive behaviors of dechlorinating cultures in enrichment cultures and in the field, and (b) search for evidence that support answers related to the core question of enhanced dechlorination: how to preferentially stimulate dechlorinators and optimize chloroethene detoxification.

1.2 Methodology

A kinetic model that describes dechlorination in conjunction with cooperative (i.e. fermentation of electron donor sources) and competing processes (methane formation and sulfate reduction) was designed. In order to yield meaningful simulations, the model was fitted to experimental observations from two mixed chloroethene-degrading cultures that were created and maintained at the National Technical University of Athens (NTUA) by Panagiotakis (2010) and Antoniou (2017): (a) a methane-producing, chloroethene-degrading culture, and (b) a sulfate-reducing, methane-producing, chloroethene-degrading culture. A heuristic multistart global optimization strategy was developed for the estimation of the parameters of the model. Confidence in the model structure and the multistart strategy was gained by testing them under distinctive conditions, ranging from non-limiting conditions for dechlorinators to conditions where sulfate-reduction and methane formation compete with dechlorination for limited quantities of H_2. This confidence-building stage of the work also considered two kinetic models and respective experimental data from the literature. Finally, a series of numerical tests was performed to simulate the performance of alternate mixed communities undergoing different scenarios of engineered dechlorination.

1.3 Outline of the thesis

The thesis is divided in three parts, which contain twelve chapters. The three parts are divided according to the topics they address.

Part 1 provides the reader with all the information required to follow the discussion taking place in Parts 2 to 3. A discussion of chloroethene biodegradation in groundwater and enrichment cultures takes place in Chapter 2. There, a brief discussion on the make-up of mixed chloroethene communities takes place focusing mostly on the metabolic interactions of dechlorinators with non-dechlorinators. In Chapter 3, a review of the existing kinetic models describing dechlorination in mixed chloroethene-degrading cultures is provided, focusing on the conceptual designs of the models, the mathematical formulations of the processes and the employed parameter estimation approaches.

Part 2 deals with the methodological issues concerning the current thesis. The conceptual set-up of the model and its mathematical formulation are given in Chapter 4. The design of the multistart strategy used for the parameter estimation processes is given in Chapter 5. There, the developed strategy is applied for the calibration of three simple kinetic models describing dechlorination, i.e. a simplified version of the model developed in Chapter 4 and two models reported in the literature.

Finally, Chapter 6 puts forth the concept of model simplification and the selection among candidate conceptual models describing dechlorination kinetics.

In Part 3, the model is employed both in inverse and forward mode, in order to (a) examine the make-up of the two dechlorinating communities developed at NTUA and (b) perform targeted numerical tests assessing the relevance of non-dechlorinators under methanogenic and sulfate-reducing conditions. Chapter 7 sheds light on the make-up of non-dechlorinators in the methane-producing, chloroethene-degrading culture. The model is used inversely to estimate plausible approximations of the mixed culture that differ only in the make-up of the non-dechlorinating part of the culture. The distinctive-yet-plausible approximations of the culture are subsequently tested in a forward fashion simulating actual experiments performed under different phases of the culture and diverse electron donor amendment scenarios. With this cross-confirmation strategy employed, a single approximation of the culture is selected as the most probable to represent reality. Chapter 8 investigates, always with a modeling approach, possible shifts in the qualitative characteristics of the culture over the years of its maintenance. Chapter 9 makes use of the distinctive-yet-plausible realizations of the culture (the three less probable and the most probable selected) in a forward mode in order to examine the impact of the functional structure of non-dechlorinators on dechlorination extent and efficiency under varying electron donor supply scenarios. In Chapter 10 the make-up of the more complex sulfate-reducing, methane-producing, chloroethene-degrading culture is investigated. The different approximations of the behavior of the culture are used in Chapter 11 to elucidate the factors that predominantly affect dechlorination in the sulfate-reducing, methane-producing, chloroethene-degrading culture.

Chapter 12 gathers the main findings of the thesis, discusses its contribution to the understanding of dechlorination in complex communities and highlights which aspects of them are in need of extra experimental data.

PART 1. LITERATURE REVIEW

Chapter 2: Review of chloroethene biodegradation in groundwater

2.1 Introduction

The present chapter provides the reader with the requisite context for the microbial aspects of this work. It does not hold the position of an extensive review on chloroethene occurrence in groundwater, neither aims to discuss extensively all the aspects of natural and enhanced biodegradation of chloroethenes in groundwater. Instead, it demonstrates the main features of anaerobic biodegradation of chloroethenes in enrichment cultures. The reader is referred to: (a) the work of Bradley (2003) for a review discussing the historical and ecological aspects of chloroethene biodegradation, (b) the work of Tas et al. (2010) for a review on the physiology of dechlorinators, and (c) the work of Aulenta et al. (2006) for a review on the parameters influencing enhanced biodegradation.

2.2 Chloroethene occurrence and biodegradation pathways in groundwater

Chloroethenes vary from the most chlorinated compounds, perchloroethene (PCE, with four chlorine atoms in its molecule) and trichloroethene (TCE, with three chlorine atoms in its molecule, to dichloroethenes (DCEs, i.e. cis-DCE, trans-DCE and 1,1-DCE) and the monochlorinated vinyl chloride (VC).

Chloroethenes have been found at numerous contaminated sites worldwide. Natural production of PCE and TCE is recognized nowadays, with reports of PCE and TCE production in marine algae (Abrahamsson et al., 1995) or salt lake sediments (Weissflog et al., 2005). But, the frequency and magnitude of PCE and TCE contamination indicate that PCE and TCE are entering the subsurface from anthropogenic sources (Löffler et al., 2013). Both chlorinated compounds have been used extensively in dry cleaning, metal cleaning and degreasing. In order to have an inkling of the quantities produced and consumed even after the stringent regulations imposed over the last years, Löffler et al. (2013) offer some indicative figures for the demand for PCE and TCE in the United States (US) and the European Union (EU): the magnitude of PCE demand in United States was in the range of 168,000 metric tons for year 2005, while the sales of TCE in the European union in 2005 was 28,000 metric tons. Similar to PCE and TCE, DCEs and VC are also commonly detected in contaminated sites. They typically occur as the daughter products of *in situ* microbial degradation of more chlorinated compounds. The most commonly found DCE in groundwater is cis-DCE (cDCE), because it is the main daughter product of microbially-mediated TCE reduction. Finally, the anaerobic reduction of cDCE yields VC.

Chloroethenes are priority pollutants for the US Environmental Protection Agency (EPA), while PCE and TCE are included in the EU Directive on Environmental Quality Standards (Directive 2008/105/EC), also known as the Priority Substances Directive. Chloroethenes are highly toxic to humans with PCE, TCE, cDCE and VC having an EPA maximum contaminant level (MCL) for drinking water equal to 5 μg/l, 5 μg/l, 70 μg/l and 2 μg/l, respectively. Among chloroethenes, TCE and VC are known human carcinogens, while PCE is likely to be carcinogenic.

The most chlorinated compounds share some common physical-chemical properties that affect their fate, distribution and longevity in contaminated aquifers. First, their solubility in water is orders of magnitude greater than the aforementioned drinking water standards; PCE and TCE solubility in water at 20° C is 200 mg/l and 1100 mg/l, respectively. Second, they are denser than water. The liquid densities of PCE and TCE at 20° C are 1.62 g/cm^3 and 1.46 g/cm^3, respectively. Thus, they typically enter the subsurface as immiscible liquids denser than water and, thus, migrate to significant depths below groundwater table. There, they slowly dissolve into groundwater, posing a continuous source of cDCE and VC, apart from PCE and TCE. Physical and chemical technologies are often costly and inefficient solutions for large-scale contamination incidents (Löffler et al., 2013). Therefore, in situ biodegradation is an attractive alternative for the treatment of chloroethenes.

Chloroethenes can be degraded biologically to the environmentally benign ethene (ETH) via both reductive and oxidative pathways. As Bradley (2003) postulates, the tendency of chloroethenes to undergo reduction is proportional to the number of chlorine atoms in their molecules. Thus, VC does not readily undergo reduction, but it is more easily oxidized. On the contrary, TCE as a highly-oxidized molecule is easily reduced. Nevertheless, as chloroethene contamination typically exists in depths where oxygen is limited or absent, anaerobic reductive pathways are more relevant.

2.3 Anaerobic reductive degradation of chloroethenes

Anaerobic reductive dechlorination is the replacement of a chlorine atom with a hydrogen atom (Fig. 2.1). For convenience purposes, microbially-mediated anaerobic reductive dechlorination of chloroethenes will be simply referred to as dechlorination throughout the thesis. Dechlorination is a stepwise redox reaction constituting a respiratory process, which yields energy to support the maintenance and growth of bacteria that catalyze it. Complete detoxification of chloroethenes is achieved when VC is reduced to ETH. Complete dechlorination of TCE to ETH requires the presence of bacteria that can gain energy from dechlorination and the input of electrons from an electron donor. These requirements are discussed in the following sections.

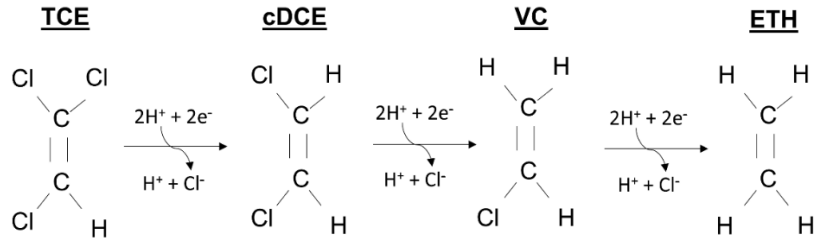

Fig. 2.1. Reductive dechlorination of TCE to cDCE, VC and ETH.

2.3.1 Dechlorinating microorganisms

Currently known microbes respiring chloroethenes (namely dechlorinators) belong to diverse phylogenetic groups, from Chloroflexi and Firmicutes to Proteobacteria. Inevitably, such diverse populations possess diverse physiological and genetic characteristics. Yet, they have one common feature. They all benefit from specific enzymes (namely reductive dehalogenases), which give them the opportunity to utilize chloroethenes as electron acceptors. Based on the type of reductive dehalogenases they have, dechlorinators can be roughly divided in two categories, those that can

respire that respire PCE and TCE only (these were identified first) and those capable of respiring DCEs and/or VC (identified first by Maymó-Gattell et al., 1997). The first (partial dechlorinators) belong to diverse phyla, Firmicutes, delta-, epsilon- and gamma-Proteobacteria, while the second belong to the phylum Chloroflexi, the genus *Dehalococcoides* and the species *Dehalococcoides mccartyi* (previously designated *Dehalococcoides ethenogenes*).

Members of the species *Dehalococcoides mccartyi* are extreme specialists. They obligately respire chloroethenes and require H_2 as an electron donor. According to Hendrickson et al. (2002), these bacteria can be further divided into three subgroups each of which contains strains with different metabolic abilities (Fig. 2.2): (a) the "Cornell" subgroup that contains strain 195, (b) the "Victoria" subgroup that contains strain VC, and (c) the "Pinellas" subgroup that contains strain FL2, GT and BAV 1.

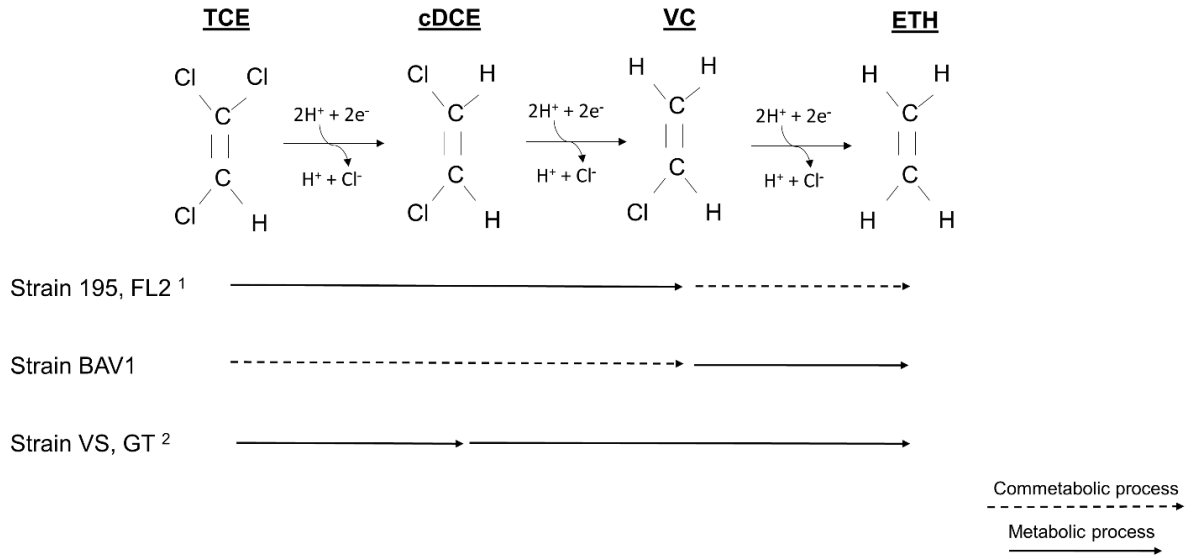

Fig. 2.2. Dechlorinating abilities of the *Dehalococcoides mccartyi* strains isolated to date. 1: Strain 195 dechlorinate also PCE, while strain FL2 dechlorinates PCE commetabolically. 2: Strains VS, GT dechlorinate TCE, but not with the same reductive dehalogenases as strains 195, FL2 do.

Partial dechlorinators demonstrate a wide spectrum of physiological properties, different electron donor requirements and diverse end-points of dechlorination. To date, members belonging to the genera *Dehalobacter*, *Desulfitobacterium*, *Sulfurospirillum*, *Desulfuromonas*, and *Geobacter* have been identified as partial dechlorinators. Examples of bacterial isolates and their metabolic properties are given in Table 2.1. An exhaustive discussion on their phylogenetic characteristics and properties is provided by Maillard and Holliger (2016), Futagami and Furakawa (2016), Goris and Diekert (2016), and Sanford et al. (2016).

In field settings, detection of *Dehalococcoides mccartyi* is a necessary but not a sufficient condition for the complete detoxification of chloroethenes. As a rule of thumb, concentrations of *Dehalococcoides mccartyi* greater than 10^6 cells/l are considered sufficient (Stroo et al., 2013) and enhanced bioremediation can proceed with the stimulation of dechlorinators by adding electron donor and nutrients. Otherwise, the augmentation of the existing *Dehalococcoides mccartyi* populations should be considered as an option. Typically, mixed dechlorinating consortia are used as bioaugmentation

cultures containing at least one *Dehalococcoides mccartyi* strain in concentrations ranging from 10^{10} cells/l to 10^{12} cells/l.

Table 2.1. Examples of partial dechlorinators, their electron donor requirements and end-products of dechlorination.

Partial dechlorinator	Electron donor	Activity
Dehalobacter restrictus	H_2	PCE-to-cDCE
Desulfitobacterium PCE1	Formate, lactate, pyruvate	PCE-to-cDCE
Desulfitobacterium TCE1	Formate, lactate, pyruvate and H_2	PCE-to-cDCE
Sulfurospirillum halorespirans	H_2, lactate and pyruvate	PCE-to-cDCE
Sulfurospirillum multivorans	H_2, lactate and pyruvate	PCE-to-cDCE
Desulfuromonas chloroethenica	Acetate, pyruvate	PCE-to-cDCE
Desulfuromonas michiganensis	Lactate, acetate, pyruvate, succinate, malate and fumarate	PCE-to-cDCE
Geobacter lovleyi	Acetate	PCE-to-cDCE

2.3.2 Electron donor, carbon source and nutrient requirements

All *Dehalococcoides mccartyi* are extreme specialists and require H_2 as an electron donor. Consequently, the supply of H_2 in support of dechlorination has drawn wide attention in the literature. In field and laboratory studies, several strategies for H_2 supply have been tested. Usually, dechlorinators should compete with other bacteria and archaea for the available H_2. So, electron donor delivery aims to minimize competition for H_2 in favor of dechlorinators by maintaining H_2 at low levels (in the range of a few nM); at this range of concentrations, dechlorinators have a competitive advantage due to their higher affinity for H_2 (see Section 2.4 for a detailed discussion on the competitive fitness of dechlorinators).

A careful investigation of the literature regarding the substrates used to sustain dechlorination challenges the uniqueness of the strategy that aims to maintain low H_2. Fennell et al. (1997) and Yang and McCarty (1998) showed that organic substrates that necessitate low H_2 concentrations for their fermentation (low H_2-ceiling donor sources), such as butyrate, propionate or benzoate, gave dechlorinators an advantage over methanogens. Thereafter, the findings of Yang and McCarty (2000) strengthened the belief that low H_2-ceiling substrates are desirable. Yet, in the following years a wide range of substrates that produce H_2 at high levels (i.e. high H_2-ceiling donor sources) has promoted efficient dechlorination in enrichment cultures and in the field. Such electron donor sources are lactate (e.g. Heimann et al., 2007; Malaguerra et al., 2011), formate (e.g. Azizian et al., 2010), methanol (e.g. Aulenta et al., 2005) or sugars (Lee et al., 2004). In addition, three of the most prominent mixed dechlorinating cultures have been maintained for years with high H_2-ceiling substrates. Various subcultures of the commercially available culture KB-1 have been maintained with mixtures of ethanol and methanol or H_2 (Duhamel and Edwards, 2006),

while cultures ANAS (Richardson et al., 2002) and SDC-9 (Schäfer et al., 2009) are both lactate-fed cultures. Even direct addition of H_2 has been reported to be a promising approach (Aulenta et al., 2005 and 2007) in some cultures, even if it promoted methane formation in others (Ma et al., 2003, 2006 and 2007). Finally, conflicting findings have been reported for the supply of acetate, which can function as a low H_2-ceiling donor. Acetate sustained complete dechlorination in the cases of He et al. (2002), Wei and Finneran (2011) and Harkness et al. (2012), but failed to sustain complete detoxification of chloroethenes in the works of Aulenta et al. (2002) and Lee et al. (2007).

Apart from the requirement for sufficient amounts of electron donors (H_2) and acceptors (chloroethenes), *Dehalococcoides mccartyi* strains require acetate as a carbon source, cofactors (e.g. corrinoids) and nutrients (Löffler et al., 2013). The supply of fermentable substrates, which produce acetate, typically covers the need for carbon sources. But, the vast majority of *Dehalococcoides mccartyi* are not able to synthesize essential cofactors *de novo* and they must retrieve them from the environment (Hug et al., 2012). As Hug et al. (2012) report, many methanogens and fermenters are in position to cover cofactor requirements for dechlorinators. This may be partially the reason why *Dehalococcoides mccartyi* grows poorly in pure cultures (they rarely grow above 10^{11} cells/l) and thrives in mixed anaerobic cultures (reported concentrations are in the range of 10^{12} cells/l).

2.3.3 Non-dechlorinating microorganisms

Enrichment cultures with dechlorinating abilities regularly contain a wide range of non-dechlorinators. The make-up of the non-dechlorinating part of the culture is affected from the availability and the quantity of the electron donor fed, incubation conditions (e.g. pH, temperature etc.), and the availability of alternate electron acceptors, such as sulfate. Additionally, the origin of the culture affects the make-up of the community, as even after years of selective enrichment on specific substrates, non-dechlorinators may retain metabolic abilities that seem useless under the conditions prevailing (Richardson, 2016).

Non-dechlorinators vary both phylogenetically and metabolically. Yet, there are populations more frequently observed than others, probably due to their functional characteristics (Hug et al., 2012). Non-dechlorinators have a dual function within the culture: (a) they influence the interspecies flow of reducing power among the various microbial groups, (b) they provide dechlorinators with cofactors and nutrients. This work focuses on the direct catabolic interactions among the microbial populations. Therefore, the functional groups of non-dechlorinators will be discussed on the basis of their role in the production or consumption of reducing power. Non-dechlorinators are segregated as: (a) fermenters and homoacetogens, (b) methanogens, and (c) sulfate reducers (Fig. 2.3).

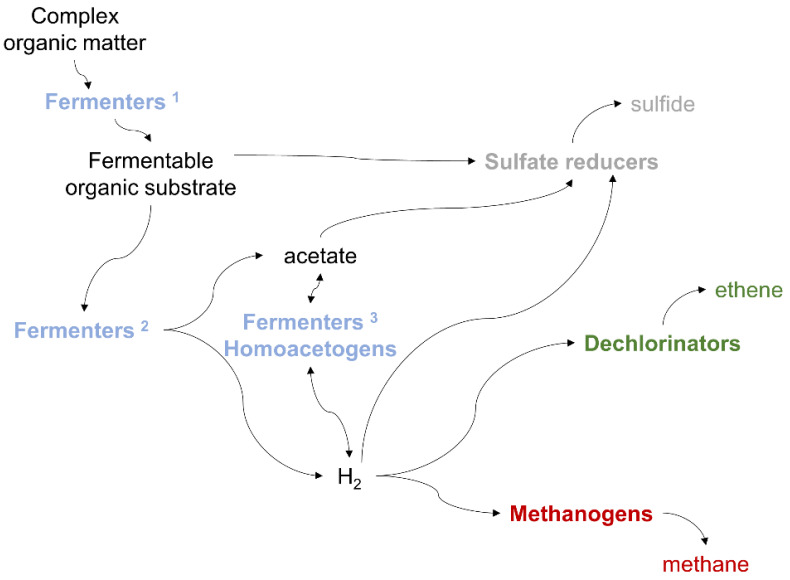

Fig. 2.3. Schematic presentation of the main catabolic interactions observed in mixed dechlorinating consortia. 1: primary fermenters. 2: secondary fermenters (e.g. butyrate oxidizers), 3: acetate oxidizers.

2.3.3.1 Fermenters and homoacetogens

The terms "fermentation", "acetogenesis" and "homoacetogenesis" have been widely used in the literature to describe different reactions mediated by diverse microbial populations (Drake, 2006). Hence, they can be confusing. In the context of this thesis, the term "fermenters" refers collectively to microbial populations that (a) consume complex organic substrates and produce organic intermediates (such as butyrate or propionate) and H_2 (primary fermenters), (b) consume organic intermediates and produce H_2 and acetate (secondary fermenters, such as butyrate oxidizers), and (c) further oxidize acetate and produce H_2 (acetate oxidizers). For the third category, discussion will be held separately, as this is only the second work that models their function in conjunction with dechlorination. Finally, the term "homoacetogens" comprises bacteria that can produce acetate from H_2; homoacetogens also can provide H_2 from substrates such as methanol.

Frequently detected fermenters in dechlorinating consortia belong to delta-Proteobacteria (e.g. *Desulfovibrio*), Clostridiales (e.g. *Clostridium*, *Acetobacterium* etc.), and Bacteroidetes. With regard to dechlorination, their most important function is to produce H_2 (electron donor) and acetate (carbon source) from the fermentation of organic substrates. For various organic substrates, fermentation is thermodynamically infeasible, unless other microbial species consume their end-products and especially H_2. Thus, a syntrophic cooperation of (at least) two populations is required, one to oxidize the organic substrate and (at least) one to consume the end-products of oxidation. Substrates like lactate or methanol can be fermented even at high levels of H_2, but substrates as propionate or butyrate require H_2 concentrations to be maintained low by H_2-utilizing species (such as dechlorinators, methanogens etc.). Mao et al. (2015) reported that butyrate fermentation in a co-culture of *Dehalococcoides mccartyi* strain 195 with a butyrate-oxidizing syntroph stopped at H_2 concentrations around 1.2 μM during VC dechlorination, as dechlorinators failed to maintain low H_2 levels.

In addition, H_2 can be produced from the further oxidation of acetate. This is a syntrophic reaction requiring low H_2 concentrations; Zinder (1994) claims that an H_2 concentration of around 50 nM

is required in natural habitats with low temperatures, while Löffler et al. (1999) indicate that acetate oxidation can be feasible at concentrations below 400 nM. To date, four bacteria have been isolated with the ability to oxidize acetate syntrophically: they all belong to Firmicutes (Hattori, 2008) and are close relatives of some fermenting bacteria. But, syntrophic oxidation of acetate has been reported in various environments by non-fermenters as well (Hattori, 2008). For example, strains of *Geobacter sulfurreducens* can carry out acetate oxidation (Caccavo et al., 1994; Cord-Ruwisch et al., 1998). Finally, H_2 production coupled with acetate consumption has been reported by Heimann et al. (2006) as a side reaction of acetate-dependent methanogenesis in a KB-1 dechlorinating culture.

Homoacetogenesis is the reverse reaction of acetate oxidation. Homoacetogens consume H_2 and produce acetate. The most frequently reported homoacetogens in dechlorinating consortia belong to phylum Firmicutes (e.g. Clostridiales, Selenomonadales). As the reverse reaction of acetate oxidation, homoacetogenesis requires a threshold concentration of H_2 in order to be thermodynamically feasible; Löffler et al. (1999) mention that homoacetogenesis is feasible for concentrations above 400 nM H_2. Homoacetogens have also the ability to produce H_2 from reduced one-carbon compounds, like methanol. Thus, they are typically present in cultures fed with H_2 or methanol (e.g. culture KB-1, Duhamel and Edwards, 2006; culture DehaloR^2, Ziv-El et al., 2011).

2.3.3.2 Methanogens

Methane is a common end-product in mixed dechlorinating cultures. The pathways of methane formation, however, are rarely reported; methanogenesis can depend on H_2, acetate or methanol, substrates that are frequently present in dechlorinating enrichment cultures and in the field. Thus, the metabolic pathways of methane formation can only be inferred based on the populations detected.

Most methanogens are hydrogenotrophs meaning that they can utilize H_2 as electron donor and reduce CO_2 to produce methane. Only two genera use acetate for methane formation: *Methanosarcina* and *Methanosaeta*. Genus *Methanosarcina* is not strictly acetotrophic, as members of *Methanosarcina* prefer methanol and methylamine to acetate, while many species can also utilize H_2 (Liu and Whitman, 2008). On the other hand, *Methanosaeta* is a specialist that uses only acetate. *Methanosaeta* is superior acetate utilizer at concentrations as low as 5–20 μM, while *Methanosarcina* species require a minimum concentration of about 1000 μM (Demirel, 2008). Finally, methanogens belonging to the order Methanosarcinales (apart from *Methanosphaera* species, which belong to the order Methanobacteriales) can use methyl-group containing compounds, including methanol, methylated amines and methylated sulfides, to produce methane (Liu and Whitman, 2008).

As already mentioned, the make-up of methanogenic populations in dechlorinating consortia has been reported in limited cases. In dechlorinating, lactate-fed culture ANAS, the H_2-utilizing methanogens *Methanobacterium* and *Methanospirillum* have been identified (Richardson et al. 2002; Brisson et al. 2012). In KB-1 subcultures (maintained with alcohols and/or H_2 as electron donors), methanogenic populations comprise mainly *Methanomethylovorans* (methanol-utilizing methanogen), Methanomicrobiales (an order containing mostly H_2-utilizing methanogens) and to a smaller degree the acetate-utilizing, *Methanosarcina* and *Methanosaeta*. Culture Donna II, which is maintained with butyrate (electron donor source) and PCE, comprises the H_2-utilizing *Methanospirillum* and the

acetate-utilizing *Methanosaeta* (Rowe et al., 2008), with methane formation being mostly acetate-dependent (Heavner et al., 2013). Dennis et al. (2003) found mostly *Methanosaeta* in a soil column fed with methanol and butyrate while treating PCE non-aqueous phase liquid (NAPL). Macbeth et al. (2004) identified mostly *Methanosaeta* in a chloroethene-degrading culture established with material from a contaminated site undergoing biostimulation with lactate.

2.3.3.3 Sulfate reducers

The presence of alternate electron acceptors, such as sulfate, potentially results in the growth of populations that can compete with dechlorinators and non-dechlorinators for the available H_2, acetate or more complex organic substrates, such as lactate, butyrate etc. Mixed dechlorinating cultures are seldom maintained with sulfate in the laboratory and, therefore, the make-up of such communities is rarely characterized. Notable exceptions are the studies reported by Berggren et al. (2013) and Panagiotakis et al. (2014). Therefore, knowledge on the occurrence of sulfate-reducers in chloroethene-contaminated sites is restricted.

Widening the search to include non-dechlorinating cultures yields a huge range of novel sulfate reducers, which have been described over the past 25 years, that can grow on various substrates. The most prominent genera are *Desulfovibrio*, *Desulfobacter*, *Desulfuromonas*. Sulfate reducers are flexible populations from a metabolic viewpoint. Sulfate reducers can be roughly divided in two groups: (a) sulfate reducers that can degrade organic substrates incompletely and, ultimately, produce acetate (e.g. *Desulfovibrio*, *Desulfotomaculum, Desulfomicrobium* etc.) and (b) sulfate reducers that can degrade organic substrates completely to carbon dioxide (e.g. *Desulfobacter*, *Desulfobacterium*, *Desulfosarcina* etc.). Lactate, H_2 and pyruvate serve as electron donors for most of sulfate reducers, regardless of the group they belong. Madigan et al. (2014) and Rabus et al. (2013) provide a comprehensive discussion on the metabolic abilities of sulfate reducers.

2.4 Metabolic interactions in mixed dechlorinating communities

2.4.1 Competition for H_2

Under strictly anaerobic conditions (methanogenic and sulfate-reducing conditions), homoacetogens, methanogens and sulfate reducers are potential H_2 scavengers. Consequently, any strategic delivery of H_2 should aim to favor dechlorination, while mitigating detrimental side effects of high electron donor surpluses, such as accumulation of volatile fatty acids (VFAs) or excess methane production (Aulenta et al., 2007). In the search of a balanced strategy for H_2 delivery, the type of the donor and the quantity added have been studied extensively and revealed key aspects of microbial competition for H_2.

As mentioned in Section 2.3, the addition of electron donor sources that produce H_2 at low levels (such as propionate or butyrate) can be selected to preferably channel H_2 to dechlorination and avoid competing metabolisms. Low H_2 levels are desirable for two reasons. First, reported H_2 thresholds for dechlorinators (0.1-24 nM Luijten et al., 2004) are lower than the corresponding thresholds for two of the three potential H_2 scavengers, namely acetogens (336-3640 nM, Löffler et al., 1999) and H_2-utilizing methanogens (5-100 nM, Löffler et al., 1999); H_2 thresholds for dechlorinators are comparable with thresholds reported for sulfate reduction (1-10 nM, Luijten et al., 2004). Second, dechlorinators have a competitive advantage over their competitors at low H_2 concentrations (i.e. below 50 nM), because they have a higher affinity for H_2, with reported half velocity coefficients ranging from 7 to 100 nM (Ballapragada et al., 1997; Smatlak et al., 1996;

Cupples et al., 2004), whereas half-velocity coefficients for methanogens range from 500-22,000 nM (Clapp et al., 2004) and for sulfate reducers from 57.9-4200 nM (Malaguerra et al, 2011; Stams et al., 2005). This competitive advantage could be diminished at greater H_2 levels, since dechlorinators are considered slow growers, especially when growing on cDCE and VC, while several methanogens and sulfate reducers can be relatively fast-growing species.

2.4.2 Competition for acetate

Following the addition of fermentable substrates another field for competition arises within the mixed culture, i.e. competition for acetate. Acetate is a common methanogenic substrate and it can also serve as a direct electron donor for sulfate reduction.

As already mentioned, only two genera are known to use acetate for methanogenesis, *Methanosaeta* and *Methanosarcina*. *Methanosaeta* is a slow-growing acetate utilizer (typical maximum specific growth rates for *Methanosaeta* are around 0.2 $days^{-1}$; De Vrieze et al., 2012), which can be efficient at low concentrations by consuming acetate at concentrations as low as 5 - 20 μM (Liu and Whitman, 2008). *Methanosarcina* is relatively fast growing (typical maximum specific growth rates for *Methanosarcina* around are 0.6 $days^{-1}$; De Vrieze et al., 2012) and dominant at greater concentrations, as it requires a minimum concentration of about 1000 nM (Liu and Whitman, 2008). In cultures with low acetate concentrations, as pristine subsurface environments are, only members of the genus *Methanosaeta* are expected to thrive. Yet, following biostimulation both species can find adequate acetate concentrations to support their growth.

Acetate in the presence of sulfate can be readily used by sulfate-reducers. Typically, acetate-utilizing sulfate reducers outcompete acetate-utilizing methanogens (Oude Elferink et al., 1994). But, as Muyzer and Stams (2008) point, competition for acetate is not as certain as it is for H_2. As the affinity of sulfate reducers for acetate is still ambiguous with few reported values (Stams et al., 2005), the outcome of competition cannot be clearly foreseen based solely on the reported maximum specific growth rates of sulfate reducers. Typically, sulfate reducers are slightly more rapidly growing compared to the members of the genus *Methanosaeta* (Stams et al., 2005), but the differences are not striking. As reported by Omil et al. (1998), it can take years for sulfate reducers to outcompete *Methanosaeta* species. Hence, in contaminated subsurface environments, they may be present simultaneously.

The outcome of this competition is meaningful for dechlorinators only if acetate can be oxidized towards H_2 production. Indeed, acetate oxidation can be energetically favorable at natural mesophilic habitats, if H_2 concentrations are maintained below 0.05 μM (Zinder, 1994); evidence of efficient acetate oxidation in natural habitats has been provided by Nüsslein et al. (2001) under low temperatures (15° C). In the presence of efficient H_2-scavenging species (such as dechlorinators, H_2-utilizing sulfate reducers or H_2-utilizing methanogens), acetate oxidation becomes energetically favorable and several syntrophic bacteria can grow on acetate producing H_2 (Hattori, 2008). Such low H_2 levels can be established when low H_2-ceiling donors, such as butyrate, are applied (Aulenta et al., 2008; Mao et al., 2015). Competition for acetate between acetate-utilizing sulfate reducers, acetate-utilizing methanogens and acetate-oxidizing syntrophs cannot be a priori predicted, as kinetic studies for acetate-oxidizing bacteria performed under low temperatures (below 35° C) and under low VFA concentrations are missing. For example, Qu et al. (2009) studied acetate oxidation kinetically, but under elevated temperatures (35° C and 55° C)

and high VFA concentrations in an anaerobic reactor; such conditions are very different to what acetate oxidizers would face in chloroethene-contaminated subsurface settings. The fact that acetate-oxidizing bacteria support their growth on a very limited amount of energy deriving from acetate oxidation implies that they should be considered slow growers (Hattori, 2008). Yet, their affinity to acetate is unknown.

2.4.3 Competition for fermentable organic substrates

In the presence of sulfate, sulfate reducers may compete with fermenting syntrophs for the available fermentable substrates. The outcome of this competition is important because sulfate reduction deprives reducing power from the dechlorinating species. In general, sulfate reducers grow faster than syntrophic butyrate oxidizers and, thus, they are expected to out-compete them (Muyzer and Stams, 2008). But, in the presence of sulfate-limiting conditions this competition is hard to predict. As indicated in laboratory studies where butyrate degradation is coupled with sulfate reduction, there can be no clear distinction between butyrate-dependent sulfate reduction and the syntrophic relationship between syntrophic acetogens and H_2-utilizing sulfate reducers (Stams et al. 2005). Hence, the experimental evidence regarding this competition are scarce.

2.5 Inhibition of dechlorinating activity by toxic compounds

2.5.1 Chlorinated compounds

Chlorinated compounds can be toxic to many populations thriving in the ecosystems of dechlorinating communities. Even the growth of dechlorinators can be inhibited at high concentrations of several chlorinated compounds. For example, Grostern and Edwards (2006) demonstrated that *Dehalococcoides mccartyi* dechlorinators were inhibited by 1,1,1-trichloroethane or chloroform, while Maymó-Gattell (2001) reported toxic effects of chloroform on cDCE and VC removal from *Dehalococcoides mccartyi* strain 195. Regarding partial dechlorinators, Futagami et al. (2006) reported chloroform and carbon tetrachloride inhibition on PCE dechlorination by *Desulfitobacterium hafniense* strain Y51. Interestingly, chloroethenes can be toxic to chloroethene-degrading species. This type of inhibition, namely self-inhibition, becomes relevant at molar concentrations higher than 1000 μM (Haest et al., 2010) and will be discussed in Section 3.2.

Methanogens have been shown to be inhibited by chlorinated compounds including chloroethenes. In few studies, chlorinated ethenes had inhibitory effects on methane formation at high concentrations resulting from the presence of NAPL PCE, i.e. molar concentrations greater than 900 μM (e.g. Yang and McCarty, 2000; Men et al., 2013).

2.5.2 Non-chlorinated compounds

Among the non-chlorinated compounds that have adverse effect on the detoxification of chloroethenes, sulfide is the most relevant compound under strictly anaerobic conditions. Sulfide is the daughter-product of sulfate, which is commonly reported as a co-contaminant of chloroethenes, with sulfate concentrations varying from 410 μM (39 mg/l) to 49,844 μM (4788 mg/l) (Pantazidou et al., 2012). Even if a mechanistic understanding of the toxic effects of sulfide on dechlorinators is absent, sulfide has been shown to inhibit enzymes involved in dechlorination at concentrations ranging from 2000 μM (68 mg/l) according to Sung (2005) to 5000 μM (170 mg/l) according to Mao et al. (2017). Yet, as Berggren et al. (2013) report, it remains questionable, if every *Dehaclococcoides mccartyi* strain is affected with the same way from the presence of sulfides.

2.6 Closing remarks

It is useful for what will follow to summarize and highlight herein the most salient findings with which this thesis converses.

Dechlorinators are members of complex ecosystems involving interspecies transfer of reducing power and multiple levels of competition, which are triggered following the supply of electron donor sources.

Dechlorination under methanogenic conditions has been systematically investigated, but still no firm conclusion can be drawn regarding the type and quantity of H_2 precursors that preferably enhance dechlorination. Low H_2 concentrations have been shown to provide a competitive advantage to dechlorinators over methanogens (Fennell et al., 1997; Yang and McCarty, 1998), but dechlorination has also been extensive under elevated H_2 concentrations both in the laboratory (Heimann et al., 2005; Aulenta et al., 2005) and in the field (Macbeth et al., 2004). The incomplete understanding concerning methane formation in conjunction with dechlorination results, at least partially, from the limited field and laboratory reports that shed light onto the make-up of methanogenic populations in dechlorinating communities (e.g. Macbeth et al., 2004; Duhamel and Edwards, 2006; Richardson et al., 2002; Rowe et al., 2008).

Dechlorination in the presence of sulfate has been studied less extensively. Contradictory findings in the literature range from positive or no effects on dechlorination (Harkness et al., 2012; Aulenta et al., 2007) to partial or complete inhibition (e.g. El Mamouni et al., 2002; Hoelen and Reinhard, 2004; Mao et al., 2017). Possible reasons for the adverse effect on dechlorination (when observed) are H_2 competition and sulfide toxicity (Hoelen and Reinhard, 2004; Berggren et al., 2013; Mao et al., 2017). Conclusions on the competitive fitness of sulfate reducers in dechlorinating communities are typically based on the performance characteristics of sulfate reducers in non-dechlorinating environments, which are substantially different from the typical conditions prevailing in chloroethene-contaminated subsurface environments. In addition, the effects of sulfide on dechlorinators have not been systematically evaluated to date.

The relevance of acetate as an electron donor source for dechlorination is also questionable. In the few studies considering acetate as an electron donor source, acetate has been shown either to support complete detoxification of chloroethenes (e.g. He et al., 2002; Harkness et al., 2012) or to result in accumulation of cDCE and VC (e.g. Aulenta et al., 2002; Lee et al., 2007). Competition for acetate has never been assessed in dechlorinating communities and, therefore, the outcome of the competition established between acetate-scavenging species can only be inferred by the competitive fitness they demonstrate in non-dechlorinating anaerobic reactors.

Chapter 3: Review on kinetic models simulating anaerobic reductive dechlorination in chloroethene-degrading consortia

3.1 Introduction

The value of modeling dechlorination kinetics has been recognized even from the early years of the investigation of dechlorination in the laboratory. Hence, over the last 20 years, numerical models of varying complexity have been developed to simulate the consumption of chlorinated ethenes in laboratory cultures and field sites. In the present chapter, an overview of the existing models is provided with emphasis being given in (a) the processes embodied within them (Section 3.2), (b) their mathematical formulation (Section 3.3) and (c) the methods implemented for parameter estimation (Section 3.4).

3.2 Conceptual development of kinetic models in the literature

Dechlorination models in the literature can be distinguished based on their conceptual designs in two groups: (a) models that account only for the activity of dechlorinators (Table 3.1), and (b) models that account for the activity of all the members of the mixed community (Table 3.2).

A significant share of modeling works that simulates solely dechlorination kinetics has been driven by the need to corroborate experimental efforts studying substrate inhibition. Experiments to quantify the magnitude and the mechanism of substrate inhibition are difficult to control and models are a useful tool for the study of inhibition (Wei et al., 2015).

The term "substrate inhibition" in the literature refers to any decrease in dechlorination rates resulting from the high concentrations of a substance. Two different concepts of substrate inhibition have been described regarding chloroethenes, competitive inhibition and self-inhibition.

Competitive inhibition refers to the preferential degradation of a specific chloroethene, when different chloroethenes are simultaneously available. Conceptually, competitive inhibition assumes that a common enzyme is responsible for multiple dechlorination steps and that chloroethenes compete for the active site of this enzyme. Competitive inhibition processes vary significantly in the literature, as different compounds have been shown to inhibit the activity of different dechlorination steps. Thus, some models account for the competitive inhibition of all chlorinated ethenes at each dechlorination step (e.g. Cupples et al., 2004a), while others consider that only higher chlorinated ethenes inhibit the degradation of less chlorinated ethenes (e.g. Yu and Semprini, 2004).

Self-inhibition (also referred to as Haldane inhibition) describes the stall of a dechlorination step resulting from the high concentrations of the chloroethene consumed. For example, high TCE concentrations can be inhibitory for the microorganisms mediating TCE dechlorination. Such inhibitory mechanisms are highly relevant when chloroethenes exceed molar concentrations of 1000 μM (Haest et al., 2010) and in the presence of a non-aqueous phase liquids (TCE solubility corresponds to molar concentrations of 8400 μM or 1100 mg/l).

The most sophisticated models (i.e. models included in Table 3.2) typically describe, aside from dechlorination, fermentation pathways of different electron donors (with or without thermodynamic limitations) and methanogenesis (e.g. Fennell and Gossett, 1998; Christ and Abriola, 2007). Only the modeling approaches of Kouznetsova et al. (2010) and Malaguerra et al. (2011) consider alternate electron accepting processes, such as sulfate and iron reduction. Nevertheless, all models developed to date consider one level of competition for reducing equivalents, i.e. competition for H_2.

Overall, there is a tendency in models to grow in complexity and capture the key biogeochemical mechanisms occurring in subsurface environments contaminated with chloroethenes. Kouznetsova et al. (2010) and Malaguerra et al. (2011) considered soil-water geochemistry, which is relevant in field settings. Yet, the use of more complex models for field applications is still limited. In the few efforts performed to simulate field applications, relatively simple models have been used (e.g. Clement et al., 2000; Viotti et al., 2014). Elaborate kinetic models create highly expensive optimization problems that are limited by computing capabilities (Manoli et al., 2012) and by the availability of field-measured data (Clement et al., 2000; Manoli et al., 2012).

Table 3.1. Overview of the existing models simulating dechlorination kinetics.

Reference	Dechlorination kinetics			Decay	NAPL dissolution	Transport	Data
	e^- donor limitation	Dechlorinating species	Substrate inhibition*				
Tandoi et al., 1994	-	PCE-to-ETH	-	-	-	-	Batch
Haston and McCarty, 1999	-	PCE-to-ETH	-	-	-	-	Batch
Carr et al., 2000	-	-	-	-	√	-	Batch
Clement et al., 2000	-	-	-	-	-	√	Field
Chu et al., 2003	√	PCE-to-cDCE	-	√	√	√	-
Cupples et al., 2004a	-	TCE-to-ETH	C	√	-	-	Batch
Cupples et al., 2004b	-	TCE-to-ETH	C	√	-	-	Batch
Yu and Semprini, 2004	-	PCE-to-ETH	C, S	√	-	-	Batch
Amos et al., 2007	√	PCE-to-cDCE	C, S	√	√	-	Batch
Friis et al., 2007	-	TCE-to-ETH	C	√	-	-	Batch
Schäffer et al., 2009	-	TCE-to-ETH	C	-	-	-	Batch
Haest et al., 2010	-	TCE-to-cDCE and TCE-to-ETH	C, S	√	-	-	Batch
Sabalowsky and Semprini, 2010	-	TCE-to-ETH	C, S	√	-	-	Batch
Huang and Becker, 2011	-	TCE-to-cDCE and TCE-to-ETH	S	√	-	-	Batch

C: Competitive inhibition, S: Self-inhibition, NAPL: non-aqueous phase liquid

Table 3.2. Overview of the existing models simulating dechlorination in conjunction with fermentation and alternate terminal electron-accepting processes (TEAPS).

Reference	H_2 production		Chloroethene inhibition	TEAPs	NAPL dissolution	Geochemistry	Transport	Data
	H_2 source	Limitations						
Bagley, 1998	Ethanol, H_2	Thermodynamic	-	M	-	-	-	-
Fennell and Gossett, 1998	H_2, Butyrate, ethanol, lactate, propionate, biomass	Thermodynamic	-	M	-	-	-	Batch
Clapp et al., 2004	H_2	-	C	M	-	-	√	-
Lee et al., 2004	Glucose, biomass	Thermodynamic	C	M	-	-	-	Batch
Christ and Abriola, 2007	H_2, Pentanol	-	C	M	√	-	√	-
Kouznetsova et al., 2010	Linoleic acid, acetate	Thermodynamic	C, S	SR	√	Mineral dissolution and precipitation, pH	-	-
Malaguerra et al., 2011	Lactate	Fermenting biomass	C	IR, SR, M	-	Mineral dissolution and precipitation	-	Batch
Manoli et al., 2012	Linoleic acid	-	C	IR, SR, M	-	-	√	Batch, Field
Chen et al., 2013	Lactate	-	C	-	√	-	√	Column
Heavner et al., 2013	Butyrate, biomass	Thermodynamic	C	M	-	-	-	Batch
Viotti et al., 2014	Lactate	Thermodynamic	-	-		-	√	Field

NAPL: non-aqueous phase liquid, C: Competitive inhibition, S: Self-inhibition, M: methane formation, SR: Sulfate reduction, IR: Iron reduction

3.3 Mathematical formulation of biochemical processes included in kinetic models

3.3.1 Reductive dechlorination

Reductive dechlorination of chloroethenes is typically modeled with dual Monod-type kinetic equations in the literature, in order to account for the limitation of both the electron donor (H_2) and the electron acceptor (chloroethenes). Thus, chloroethene degradation kinetics are modeled, as follows:

$$r_i = \frac{\mu_{\max}}{Y} \frac{S_i}{K_{S,i} + S_i} \frac{S_H - S_{\min,H}}{K_{S,H} + S_H - S_{\min,H}} X \quad (3.1)$$

where μ_{max} ($days^{-1}$) is the maximum specific growth rate of dechlorinators, Y (mg VSS or cells/μmol Cl^-) is the yield coefficient of microorganism, S_i (μM) is the concentration of chloroethene i, $K_{S,i}$ (μM) is the half-velocity coefficient for chloroethene i, S_H is the concentration of H_2 (μM), $S_{min,H}$ (μM) is an H_2 threshold for chloroethene consumption, $K_{S,H}$ (μM) is the half-velocity coefficient for H_2, and X (mg VSS or cells/l) is the concentration of active biomass.

Thresholds for H_2 consumption are marginal concentrations of H_2, below which dechlorination is infeasible. As Löffler et al. (1999) postulate, substrate thresholds are influenced (at least partially) by the thermodynamics of the electron-accepting process. The inclusion of a H_2 threshold, however, becomes a source of oscillatory behaviors and mathematical instabilities, when H_2 approaches its threshold (Ribes et al., 2004). Yet, this issue has never been addressed in models simulating dechlorination kinetics.

In models neglecting electron donor limitations (i.e. the majority of models in Table 3.1 that assume non-limiting H_2 conditions), Eq. (3.1) is simplified to the following expression (a single-substrate Monod equation):

$$r_i = \frac{\mu_{\max}}{Y} \frac{S_i}{K_{S,i} + S_i} X \quad (3.2)$$

As discussed in the previous section, the clear majority of dechlorination kinetic models employ competitive or self-inhibition mechanisms for some or all of the dechlorination steps. The general form for a competitive inhibition model is:

$$r_i = \frac{\mu_{\max}}{Y} \frac{S_i}{K_{S,i}\left(1 + \sum \frac{S_i}{K_{INH,i}}\right) + S_i} X \quad (3.3)$$

where K_{INH} (μM) is an inhibition coefficient. The values used for inhibition coefficient in the literature differ between studies. Inhibition coefficients fall within the range between of 2 to 75 μM (Lai and Becker, 2013). Values greater than 75 μM indicate poor inhibitory effects on dechlorination and, conversely, values below 10 μM indicate strong inhibitory effects. Typically, inhibition coefficients are estimated by batch tests performed with mixed dechlorinating cultures and not by enzyme kinetic assays. Thus, the fundamental underlying mechanisms are still poorly

understood and values should be perceived only as a relative measure of the significance of inhibition.

Alternative modeling approaches have been proposed to describe self-inhibition of dechlorination imposed by high concentrations of chloroethenes on dechlorinating bacteria. The most common approach is based on Haldane inhibition (Sabalowsky and Semprini, 2010; Yu and Semprini, 2004) and is formulated as follows:

$$r_i = \frac{\mu_{\max}}{Y} \frac{S_i}{K_{S,i} + S_i\left(1 + \frac{S_i}{K_{H,i}}\right)} X \tag{3.4}$$

where $K_{H,i}$ (μM) is the Haldane inhibition coefficient. In order to account for a more abrupt decline in the dechlorinating activity above a ceiling concentration for chloroethenes, Amos et al. (2007) introduced the following formulation:

$$r_i = \begin{cases} \frac{\mu_{\max}}{Y} \frac{S_i}{K_{S,i} + S_i}\left(1 - \frac{S_i}{S_{\max,i}}\right) \mathrm{X} & \text{if } S_i \le S_{\max,i} \\ 0 & \text{if } S_i > S_{\max,i} \end{cases} \tag{3.5}$$

where $S_{max,i}$ (μM)is a ceiling concentration for dechlorination. Haest et al. (2010) demonstrated that self-inhibition of TCE can be reproduced with a log-logistic dose–response term described as follows:

$$r_i = \frac{\mu_{\max}}{Y} \frac{S_i}{K_{S,i} + S_i\left(1 + \exp\left[s_i\left(\frac{S_i}{EC_{50,i}}\right)\right]\right)} X \tag{3.6}$$

where s_i is the slope of the dose-response curve and $EC_{50,i}$ (μM) is the concentration at which maximum specific growth rate is reduced by 50%. Finally, Sabalowsky and Semprini (2010) proposed the use of an increased decay rate calculated as follows:

$$b_i = b\left(1 + \frac{S_i}{K_{SINH,i}}\right) X \tag{3.7}$$

where $K_{SINH,i}$ (μM) is the self-inhibition coefficient.

The range of published kinetic and inhibition parameters used to describe these phenomena varies over four orders of magnitude (see Table 7.5 in Chapter 7 for a detailed presentation of literature-reported values on dechlorination kinetics). The correlated nature of parameters employed in Monod-type models (Liu and Zachara, 2001), the various mathematical formulations employed to model inhibition, the different conditions prevailing among the reported experimental works and the differences in the make-up of the dechlorinating consortia resulted in a lack of consistency in the estimated kinetic parameters. Inconsistent parameter values complicate parameter estimation efforts, as the modeler does not have a workable parameter range to deal with. Parameter values function more as measure of relative potency without necessarily reflecting the actual underlying mechanisms.

3.3.2 Fermentation processes

Fermentation of electron donor sources is modeled with single-substrate Monod-type kinetic equations similar to Eq. (3.2), in which Si is the concentration of the electron donor source. Thermodynamic limitations on fermentation have been considered in many studies, either directly by calculating the free Gibbs energy of the fermentation reaction (e.g. Fennell and Gossett, 1998; Lee et al., 2004; Heavner et al., 2013) or indirectly by using simple inhibition factors for the end-products of fermentation (Bagley, 1998; Kouznetsova et al., 2010; Manoli et al., 2012). Including thermodynamic limitations safeguards against reproducing unrealistically high H_2, i.e. concentrations above 2000 nM.

Fermentation models calculating the free Gibbs energy of the reaction are based upon the model proposed by Fennell and Gossett (1998), who employed an inhibition term for fermentation reactions calculated as follows:

$$I_{INH} = 1 - \exp\left(\frac{\Delta G_r - \Delta G_c}{RT}\right) \tag{3.8}$$

where ΔG_c (kJ/mol) is a marginally negative free Gibbs energy that fermenters require to grow, R is the gas constant, T is the absolute temperature, and ΔG_r (kJ/mol) is the free Gibbs energy available from fermentation calculated as follows:

$$\Delta G_r = \Delta G^o + RT\,ln\left(\frac{S_{products}}{S_{reactants}}\right) \tag{3.9}$$

in which ΔG_o (kJ/mol) is the free Gibbs energy at 25° C (i.e. the amount of energy available from the fermentation reaction). The inhibition term, I_{INH}, functions as a measure of the distance of the reaction from thermodynamic equilibrium; it expresses the thermodynamic driving force of the reaction. If the concentration of the fermentable substrate is high relative to the concentrations of the products, i.e. H_2 and acetate, the driving force is significant and the reaction proceeds uninhibited, while Eq. (3.8) approaches one. When H_2 and acetate accumulate, I_{INH} is calculated close to zero and fermentation ceases; the available energy from fermentation cannot support the growth of the fermenters. Equation (3.8) can, however, take negative values, when ΔG_r becomes lower than ΔG_c. This would be suitable for reversible reactions, but is problematic for fermentation kinetics and, especially, in parameter estimation efforts (see also Section 4.4). In addition, reports on the thermodynamic limitation of fermentation reactions (e.g. Jin, 2007) indicate that fermentation can occur even when Eq. (3.8) predicts that the thermodynamic driving force is zero. Thus, even if Eq. (3.8) is a theoretically sound formulation for the description of thermodynamic limitations on fermentation, fermentation enzymes appear not to be stringently related to thermodynamics.

In simpler models, fermentation kinetics are limited by H_2 concentrations only. For example, Kouznetsova et al. (2010) proposed an exponential inhibition term:

$$I_H = e^{(-S_H/S_{INH,H})} \tag{3.10}$$

in which $S_{INH,H}$ (μM) is an inhibitory H_2 concentration for fermentation. This equation functions as a ceiling for H_2 concentrations, above which the fermentation process is infeasible. With an

appropriate selection of $S_{INH,H}$, Eq. (3.10) can reproduce the levels of H_2 typically anticipated in dechlorinating consortia, i.e. H_2 concentrations in the range of 2 – 2000 nM H_2.

An alternative approach for limiting fermentation was proposed by Malaguerra et al. (2011). Thermodynamic limitations were not included, but growth of fermentative biomass was limited by a maximum acceptable biomass concentration. This restriction in the biomass growth of fermenters resulted in a modeled H_2 concentration in the range of a few nM, which was consistent with the observed values.

When complex organic substrates (such as linoleic acid) are used as H_2 precursors, direct fermentation of the substrate to acetate and H_2 is usually considered (e.g., Christ and Abriola, 2007; Kouznetsova et al., 2010; Manoli et al., 2012). The intermediate production of short-chain fatty acids during fermentation is modeled in a few studies (Bagley, 1998; Fennell and Gossett, 1998; Lee et al., 2004; Malaguerra et al., 2011).

3.3.3 Alternative terminal electron accepting processes

Competing electron accepting processes (e.g. methanogenesis, but also sulfate and iron reduction) are modeled using Monod-type kinetics.

Methanogenesis from H_2 is formulated with single-substrate Monod equations, employing an H_2 threshold:

$$r_M = \frac{\mu_{\max}}{Y} X \frac{S_H - S_{\min,H}}{K_{S,\mathrm{H}} + S_H - S_{\min,H}} \tag{3.11}$$

Values reported for maximum specific growth rates (μ_{max}) of H_2-utilizing methanogens in dechlorinating communities are inconsistent, varying within one order of magnitude. In some models H_2-utilizing methanogens are considered slow growers (e.g. μ_{max} = 0.13 days^{-1}, Malaguerra et al., 2011), while other models consider H_2-utilizing methanogens as fast growers (e.g. μ_{max} = 2.1 days^{-1}, Lee et al., 2004), which could easily outcompete dechlorinators in the presence of sufficient H_2.

Acetate-dependent methanogenesis is modeled by a single-substrate Monod-type equation of the form:

$$r_M = \frac{\mu_{\max}}{Y} X \frac{S_A}{K_{\mathrm{S,A-AM}} + S_A} \tag{3.12}$$

in which S_A (μM) is the concentration of acetate. Substrate thresholds are not employed in this case, even if acetate threshold values have been reported for acetate-utilizing methanogens (e.g. Yetten et al., 1990).

Other terminal electron-accepting processes, such as sulfate and iron reduction, are simulated with dual-substrate Monod equations, similar to those used for dechlorination; alternate electron acceptors substitute chloroethenes in Eq (3.1). For example, H_2-dependent sulfate reduction rates are described as follows:

$$r_S = \frac{\mu_{\max}}{Y} X \frac{S_S}{K_{S,S} + S_S} \frac{S_H - S_{\min,H}}{K_{S,H} + S_H - S_{\min,H}} \tag{3.13}$$

Again, H_2 threshold concentrations control the terminal electron-accepting processes (e.g. Kouznetsova et al., 2010).

3.3.4 Microbial growth and decay

Regardless of the microbial population, growth rates are uniformly regarded as a function of substrate degradation rates (dS/dt) and endogenous decay. Endogenous decay is typically simulated with first-order kinetic equations and, thus, the change of biomass is calculated as follows:

$$\frac{dX}{dt} = Y\frac{dS}{dt} - bX \tag{3.14}$$

where b (days^{-1}) is the first-order decay coefficient. Reported decay coefficients vary slightly in the literature and, for the populations considered in the context of the thesis, decay coefficients fall in the range of 0.01 days^{-1} to 0.09 days^{-1} (see also Chapters 7 and 10).

3.3.5 Endogenous decay contribution

Endogenous cell decay can be a source of electron equivalents (e.g. Yang and McCarty, 2000; Heavner et al., 2013) and, therefore, it is considered in some studies. Specifically, Fennell and Gossett (1998) considered that endogenous decay of microbial populations contributed to the pool of butyrate, while Lee et al. (2004) assumed that 30% of the electron equivalents associated with biomass were converted directly to H_2. Finally, Heavner et al. (2013) adopted the approach proposed by Fennell and Gossett (1998).

3.4 Parameter estimation in kinetic models simulating dechlorination

Parameter estimation methods in kinetic modeling of dechlorination is rarely addressed in the literature. In this section, all the different methods employed for parameter estimation are presented. Prior to the discussion on parameter estimation, the type of empirical observations available is discussed.

3.4.1 Data types

Kinetic models describing dechlorination are typically fitted to chemical observations comprising chloroethenes and occasionally H_2 (when H_2 limitation is considered, e.g. Cupples et al., 2004a). More complex kinetic models are also fitted to chemical data that comprise, aside from chloroethenes, concentrations of (a) electron donor sources and their fermentation daughter products, (b) methane (when produced, e.g. Lee et al., 2004) and (c) competing electron acceptors, such as iron and sulfate (Malaguerra et al., 2011). H_2 concentrations are not always available in batch studies (e.g. Lee et al., 2004) and model output cannot be compared with observed values.

Microbial data are often unavailable in laboratory data sets. Typically, an aggregate initial biomass concentration is available. A few recent studies include experiments where concentrations of *Dehalococcoides mccartyi* cells are observed over time (Haest et al., 2010; Schäfer et al., 2009; Chen et al., 2013).

Pilot or full scale efforts of engineered reductive dechlorination have been published (e.g. Major et al., 2002; Hood et al., 2008). Yet, observations comprise mostly chloroethene concentrations, while geochemical and microbial data are sparse.

3.4.2 Parameter estimation methods

The clear majority of parameter estimation methods falls in the category of least squares analysis (e.g. Schäfer et al., 2009). Rarely, manual fitting of the model output to observations has been performed via trial-and-error approaches (Yu and Semprini, 2004). Two of the most recent modeling studies, employed global optimization techniques for the estimation of kinetic parameters, (a) Malaguerra et al. (2011) and Haest et al. (2010). In the work of Haest et al. (2010), a genetically adaptive multi-objective method was implemented, while in the work of Malaguerra et al. (2011) a combination of a trial-and-error approach with a Shuffled Complex Evolution Metropolis algorithm was used. As Malaguerra et al. (2011) report, an extensive search for parameters over the whole model space was not feasible due to the computational burden. Yet, none of the modeling works has addressed the issue of non-uniqueness of solutions, which was addressed in the review paper of Chambon et al. (2013), who claimed that more than one parameter ensembles can possibly describe adequately experimental observations.

3.5 Closing remarks

In every modeling effort reported to date, only competition for H_2 is considered. Even if many models simulate the fate of H_2 precursors (e.g. lactate, butyrate or acetate), none of them has taken into account that they can serve as substrates for processes that are not producing H_2 and, thus, affect dechlorination extent indirectly. This is the first work that considers such possibility.

The issues addressed by the modeling approaches in the literature can be roughly divided in two groups. The first group comprises models that examine how efficiently can empirical observations be predicted (e.g. Fennell and Gossett, 1998; Clapp et al, 2004; Christ and Abriola, 2007; Manoli et al., 2012; Heavner et al., 2013). This type of model application is useful to supplement experimental efforts and is guided by the need to employ models in a predictive fashion. From these models, the work of Fennell and Gossett (1998) was the first to consider the complex interspecies transfers of reducing power in dechlorinating communities. Model application corroborated their previous experimental findings (Fennell et al., 1997) according to which efficient stimulation of dechlorinators is performed with low surpluses of low H_2-ceiling donors. Yet, their work focused solely on a specific dechlorinating community which was tested under a variety of electron donor sources; a more thorough examination on the function of non-dechlorinators was lacking. Following this work, discussion on the interplay of dechlorinators and non-dechlorinators was overlooked.

The second group of models contains efforts that were accompanied by sensitivity analyses (e.g. Kouznetsova et al., 2010; Malaguerra et al., 2011; Chen et al. 2013), indicating which parameters of the problem need more experimental observations and how models can be simplified. Kouznetsova et al. (2010) indicated that a more accurate estimation of cDCE- and VC-related parameters is needed for the efficient simulation of the dechlorination under sulfate-reducing conditions, while Malaguerra et al. (2011) postulated that sulfate concentrations and the kinetics of lactate fermentation were the most influential aspects of dechlorination performed under iron- and sulfate-reducing conditions.

The modeling approach of Lee et al. (2004) does not fall in either of the two groups. Lee et al. (2004) were the only to employ their calibrated model in designed "what-if" scenarios providing insight in parameters of the problem that cannot be easily observed on an experimental basis.

Simulations performed by Lee et al. (2004) indicated that the initial relative abundance of dechlorinators and H_2-utilizing methanogens affected the degree of dechlorination and confirmed that biomass decay can pose a sizeable source of reducing power. Finally, Lee et al. (2004) highlighted that the phased injection of electron donor sources can affect the latter stages of PCE dechlorination. Lee et al. (2004) were the first to examine systematically the quantitative characteristics of the make-up of dechlorinating cultures, but did not examine different functional characteristics. Yet, based on the type of the inquiry implemented, the current thesis is closer to the rationale employed by Lee et al. (2004).

PART 2. PARAMETER ESTIMATION - METHODOLOGICAL ISSUES

Chapter 4: Model set-up

4.1 Introduction

Fundamentally, the modeler should incorporate all the salient information available from the laboratory in the model structure and the model parameters, so that the model output conforms to reality. Hence, the conceptual design of the model was guided by the long-term monitoring of two *Dehalococcoides mccartyi*-dominated mixed cultures developed and maintained as described in Panagiotakis (2010) and Antoniou (2017). A chloroethene-degrading, methane-producing culture, denoted as culture NTUA-M, and a sulfate-reducing, methane-producing, chloroethene-degrading source culture, denoted as culture NTUA-S. All major symbiotic and antagonistic relationships that may have been established within the two cultures are considered in the conceptual design of the model. Therefore, before introducing the processes observed in the culture (Section 4.3) and the mathematical formulation of the model (Section 4.4), the performance and maintenance characteristics of the two source cultures are discussed (Section 4.2).

4.2 Experimental information

The two source cultures were developed, in replicates of two, by the combination of two dechlorinating cultures and one sulfate-reducing culture (Fig. 4.1, Panagiotakis et al., 2014), which were initially developed using as inoculum anaerobic sludge from a wastewater treatment plant receiving significant contribution of industrial discharges (Panagiotakis et al., 2014). As indicated by Figure 4.1, culture NTUA-M exhibited two distinctive phases with respect to dechlorination performance. Therefore, they will be referred to as if they are two different cultures, i.e. cultures NTUA-M1 and NTUA-M2. Possible explanations for the shift in their performance will be further discussed in Chapter 8.

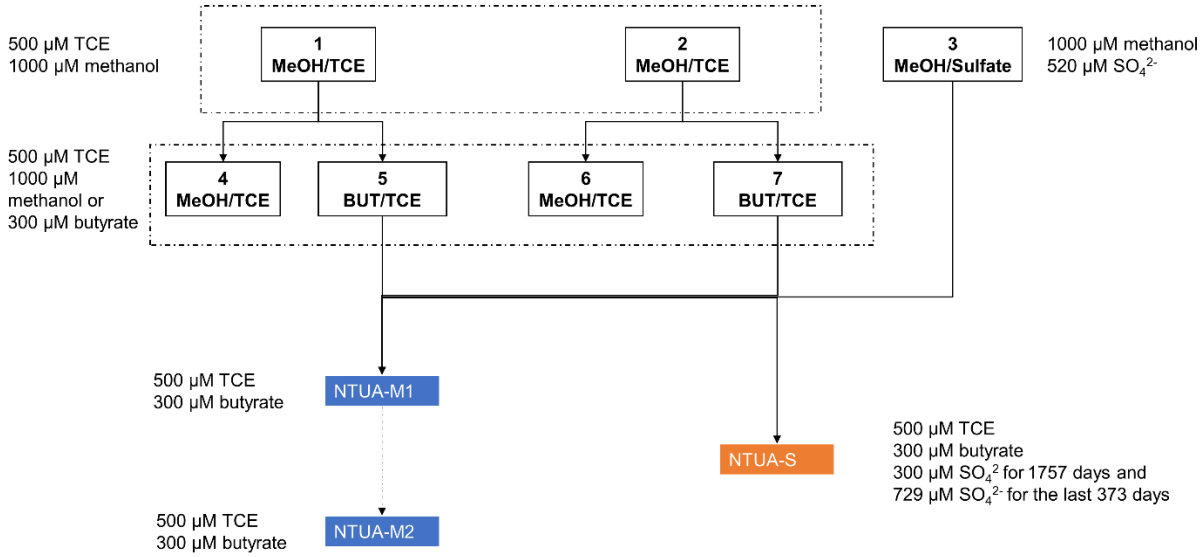

Fig. 4.1. Relationship between the cultures under consideration (NTUA-M1, NTUA-M2 and NTUA-S) and their ancestral cultures. TCE= trichloroethene, MeOH=methanol, BUT=butyrate.

4.2.1 Long-term monitoring of the methane-producing, chloroethene-degrading cultures NTUA-M1 and NTUA-M2

Source cultures NTUA-M1 and NTUA-M2 were maintained under limiting electron donor conditions in order to mimic the conditions typically encountered in the field. Particularly, they were maintained on a 7-day feeding cycle that included the addition of 500 μM (66.7 mg/l) trichloroethene (TCE) and 300 μM (27.5 mg/l) butyrate, which served as a low H_2-ceiling electron donor source. At the end of each feeding cycle, part of the culture was replaced by fresh medium to achieve a solid retention time of 48 days. With respect to their maintenance characteristics, these cultures differed only in the addition of yeast extract, which was routinely added in the case of NTUA-M1 at a concentration of 4.5 mg/l. Yeast extract is a nutritional supplement, which also serves as a source of slowly fermented volatile fatty acids (mainly butyrate and to a lesser degree acetate and propionate; Fennell and Gossett, 1998). However, the quantity of yeast extract added in culture NTUA-M1 is low; according to Yang and McCarty (1998), it yields an equivalent of 780 μe⁻eq/l, which corresponds to approximately a 10% increase of reducing power, if it is consumed within the 7-day feeding cycles. Hence, the addition of yeast extract changes mildly the electron equivalent surplus of culture NTUA-M1.

The two cultures operated at steady-state performance regarding dechlorination and butyrate consumption. On a weekly basis cultures NTUA-M1 and NTUA-M2 dechlorinated on average 64% and 71% of the overall available chloroethenes, respectively (Fig. 4.2a). Consequently, vinyl chloride (VC) was the main daughter product of TCE dechlorination followed by ethene (ETH). Since ETH is produced, both cultures should be classified as *Dehalococcoides mccartyi*-enriched cultures. Finally, the supplied butyrate was steadily consumed on each feeding cycle, indicating the existence of a robust butyrate-degrading community.

With respect to methane formation, the two cultures failed to reach a steady state (Fig. 4.2b). In both cultures, methane formation exhibited a sequence of two separate phases: a phase of reduced methane formation and a phase of elevated methane formation. These phases were accompanied by inversely fluctuating acetate concentrations (data not shown), i.e. elevated methanogenesis coincided with low acetate concentrations and vice versa. This correlation indicates that methanogenesis in both cultures is mainly of acetoclastic nature. The verity of this hypothesis will be checked in Chapters 7 and 8.

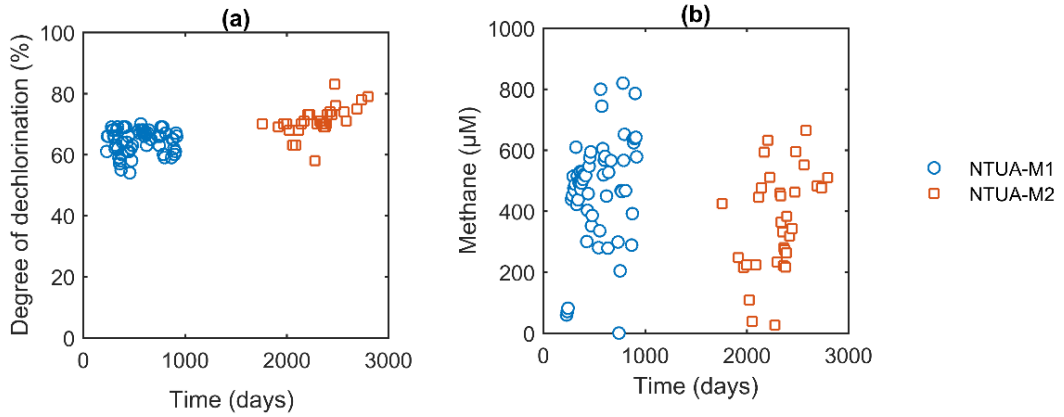

Fig. 4.2. Long-term performance, in terms of (a) the degree of dechlorination and (b) methane formation in cultures NTUA-M1 and NTUA-M2. The gap between the data points indicate a period without monitoring data.

A fluorescence in situ hybridization (FISH) analysis was performed during the operation of culture NTUA-M1 providing insight into the main microbial groups thriving within the culture (Panagiotakis et al., 2014). Specifically, the FISH analysis demonstrated that (a) *Dehalococcoides mccartyi* spp. was the predominant species (49% of the total bacteria), (b) two hydrogenotrophic dechlorinators were present (besides *Dehalococcoides mccartyi* spp., the partial dechlorinator *Sulfurospirillum* spp. was detected and comprised 8% of the total bacteria), and (c) methanogenic archaea were only a small proportion of the culture (around 10% of the total cell numbers). The FISH analysis underscored the relevance of dechlorinators and methanogens, but it could not (a) enumerate them rigorously and (b) provide definite answers as to which and how many other microbial groups should be considered. Even if this molecular analysis does not necessarily illustrate the exact composition of culture NTUA-M2, given the increase in dechlorinating performance (Fig. 4.2a), culture NTUA-M2 is certainly dominated by *Dehalococcoides mccartyi*.

The end-products of the 7-day feeding cycles indicated that the major processes occurring within the mixed culture are: dechlorination, butyrate oxidation and methanogenesis. What is more, dechlorination daughter products at the end of each feeding cycle indicated that syntrophic acetate oxidation should also be considered, since as already mentioned, ETH was observed at the end of each 7-day feeding cycle. Yet, based on the butyrate quantity added, direct H_2 formation (600 μM H_2 can be readily formed from 300 μM of butyrate) would justify cDCE and VC as the main daughter products of TCE dechlorination. Hence, it is reasonable to deduce that an H_2 source additional to butyrate sustained dechlorination, that is acetate. This is true for both NTUA-M1 and NTUA-M2, so the additional source cannot be solely the yeast extract. Decaying biomass does not provide the missing electron equivalents either, as it functions as a slowly-producing source of butyrate and, thus, it does not pose a readily available source of H_2 for dechlorinators or methanogens within the 7-day feeding cycles of the cultures.

4.2.2 Long-term monitoring of the sulfate-reducing, methane-producing, chloroethene-degrading source culture NTUA-S

Source culture NTUA-S was also maintained under limiting electron donor conditions. The culture was routinely fed with 500 μM TCE, 300 μM butyrate and (a) 300 μM (or 28 mg/l) sulfate for the first 1757 days and (b) 729 μM (or 70 mg/l) sulfate for the following 373 days. As in cultures NTUA-M1 and NTUA-M2, a solid retention time of 48 days was maintained. In this work, only the second period of the lifetime of culture NTUA-S will be examined, when 729 μM sulfate were added, since dechlorinators, despite the increase in sulfate supply, were more robust and achieved routinely a higher degree of dechlorination: 67% of chloroethenes was removed instead of the relatively low 58% in the first phase of the culture.

Culture NTUA-S demonstrated a robust dechlorinating, sulfate-reducing, butyrate-oxidizing performance and limited methane production. Dechlorinators removed completely TCE and cis-dichloroethene (cDCE) on a weekly basis, producing mainly VC and small quantities of ETH. The steady dechlorinating performance of the culture and the observed ethene production at the end of each feeding cycle indicate that culture NTUA-S is enriched with a *Dehalococcoides mccartyi* population. Additionally, culture NTUA-S reduced on average 470 μM of the available sulfate on a weekly basis. The 300 μM of butyrate were completely removed pointing out the existence of a butyrate-degrading population. Finally, methane formation is limited consuming around 1% of the supplied reducing equivalents.

A FISH analysis was performed during the first phase of the maintenance of culture NTUA-S, when the culture was maintained with lower sulfate concentration, unveiling the main microbial groups thriving within the culture (Panagiotakis et al., 2014). The FISH analysis demonstrated that *Dehalococcoides mccartyi* spp. was the predominant species and the only obligately H_2-consuming dechlorinator. Approximately 65% of the total bacteria are members of *Dehalococcoides mccartyi*. They were followed by the class of *Deltaproteobacteria* (40% of the total bacteria), which contains the clear majority of sulfate-reducing bacteria, butyrate-oxidizing syntrophs and a small number of partial dechlorinators (the acetate-utilizing *Desulfuromonas chloroethenica* and *Desulfuromonas michiganensis* and the H_2- or acetate-utilizing *Geobacter lovleyi*). Finally, the archaeal population was below detection limits supporting the findings of limited methane formation. Even if it the molecular analysis is not representative of the second period of the culture (the period which interests us mostly), provided that dechlorination was more extensive during this phase of the culture, we can reasonably deduce that *Dehalococcoides mccartyi* are still a substantial part of the culture.

The major processes occurring within the sulfate-reducing, methane-producing culture NTUA-S were signified by the weekly end-products of the feeding cycles. Obviously, dechlorination, butyrate oxidation, sulfate reduction and to a lesser degree methane formation were processes observed in the culture. The observed acetate consumption of approximately 511 μM out of the produced 600 μM acetate on a weekly basis, combined with the minimal methanogenic activity, indicate that acetate-dependent sulfate reduction and/or syntrophic acetate oxidation should be considered. Acetate oxidation is also supported by the daughter products of TCE dechlorination. At the end of each 7-day feeding cycle, low ETH production was observed. Yet, based on the butyrate quantity added, direct H_2 formation (600 μM H_2 can be readily formed from 300 μM of butyrate) doesn't justify ETH production unless acetate is oxidized and contributes to the H_2 pool. Hence, we can reasonably deduce that an H_2 source, additional to butyrate, sustained dechlorination, i.e. acetate. Finally, butyrate-dependent sulfate reduction cannot be excluded, but it cannot pose an important sulfate reducing pathway either; the amount of sulfate consumed each week (i.e. 470 μM sulfate) cannot be attributed solely to butyrate-utilizing sulfate reducers, as in that case they would have consumed 940 μM of butyrate, i.e. 3.1-fold more butyrate than supplied.

4.3 Conceptual development of the model

The model aims to describe dechlorination in complex microbial communities, which involve syntrophic and competitive interactions among dechlorinators, fermenters, methanogens and sulfate reducers. Therefore, a comprehensive kinetic model was designed to study dechlorination in conjunction with methane formation, sulfate reduction and the microbially mediated fermentation of butyrate and acetate, which serve as low H_2-ceiling electron donor sources. More specifically, apart from dechlorination, the model takes into account (a) the syntrophic oxidation of butyrate and acetate, (b) H_2- and acetate-dependent methanogenesis, and (c) H_2-, acetate- and butyrate-dependent sulfate reduction. In addition, composite organic substrates, comprising decaying biomass and yeast extract, were considered to contribute into the electron donor pool, as slowly-producing butyrate sources.

The processes occurring concurrently with the anaerobic degradation of chloroethenes in this modeling approach are schematically presented in Fig. 4.3, while Table 4.1 presents the associated reactions. According to the conceptual model, a syntrophic butyrate-oxidizing population

competes with butyrate-utilizing sulfate reducers for the available butyrate. The butyrate-oxidizing syntrophs produce H_2 and acetate, while butyrate-utilizing sulfate reducers produce sulfide and acetate. Acetate can be (a) converted to methane by acetate-utilizing methanogens, (b) sustain sulfate reduction by acetate-utilizing sulfate reducers or (c) be consumed by acetate-oxidizing bacteria to produce H_2. Subsequently H_2 is used by (a) TCE-to-ETH dechlorinators, (b) TCE-to-cDCE dechlorinators, (c) H_2-utilizing methanogens or (d) H_2-utilizing sulfate reducers. Finally, decaying cells and yeast extract (if supplied) contribute to the electron donor pool, as they are considered to yield slowly butyrate. Yeast extract has presumably the chemical composition of biomass ($C_5H_7O_2N$; Aulenta et al., 2005) and is provided in the beginning of each test. According to simulations performed herein (Chapter 8), the supplied 4.5 mg/l of yeast extract are depleted within two weeks offering 36 μM butyrate. Biomass on the other hand is relevant only in long-term simulations (exceeding 15 days). In simulations performed under low butyrate additions (i.e. 300 μM butyrate – see also Chapter 7), decaying biomass contributed nearly 2-fold greater quantities of electron equivalents relative to the addition of 4.5 mg/l of yeast extract.

Three levels of competition are considered, i.e. competition for H_2, acetate and butyrate. Competition for H_2 is critical, affecting directly the outcome of dechlorination. Any addition of electron donor sources can stimulate, besides the two H_2-utilizing dechlorinators considered, methanogens and sulfate reducers. Addition of butyrate in dechlorinating communities has resulted in H_2 concentrations varying from 0.05 μM (Fennell and Gossett, 1998) to 1.2 μM (Mao et al., 2015) and, therefore, all H_2-consuming processes are thermodynamically feasible (Löffler et al., 1999). As discussed in Chapter 2, following the supply of a fermentable substrate, competition for acetate can be established among methanogens, sulfate reducers and acetate-oxidizing syntrophs, if H_2 concentrations are maintained below 0.4 μM. The outcome of the competition among the three acetate-scavenging species has not been investigated thoroughly in the literature and, thus, it cannot be a priori predicted based on the informed judgment of the modeler. The same applies for the competition for butyrate. Even fewer studies have examined how butyrate oxidizers and butyrate-utilizing syntrophs compete for the available butyrate (Stams et al, 2005). Even if syntrophs are considered typically slow growers, in the presence of sulfate-limiting conditions they may outcompete sulfate reducers and produce H_2 (Muyzer and Stams, 2008).

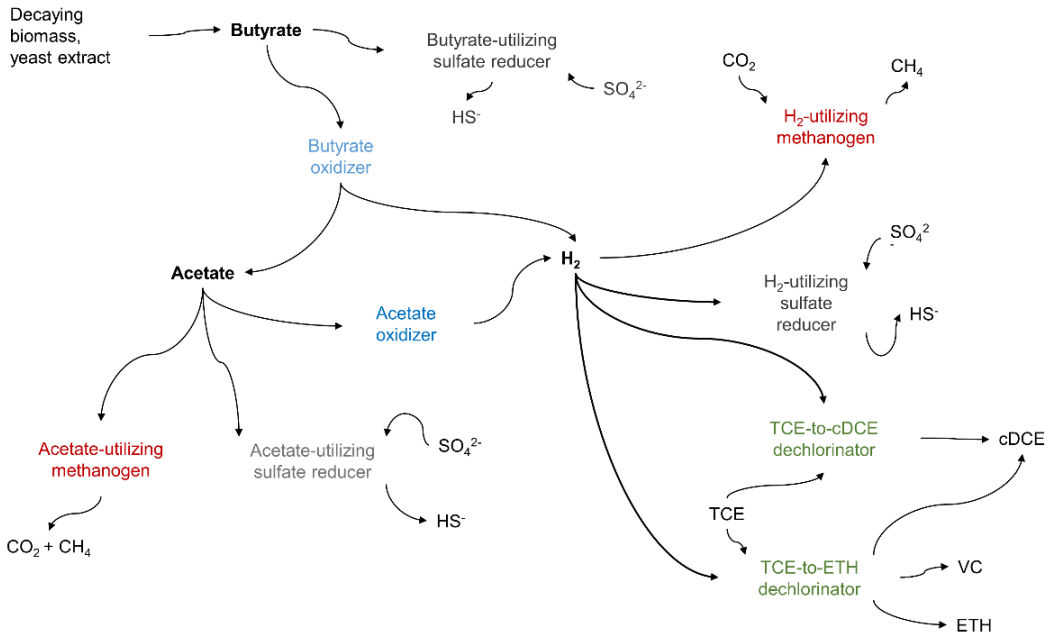

Fig. 4.3. Microbial processes considered in the model.

Table 4.1. Biological processes included in the conceptual model and the corresponding chemical reactions.

Process	Reaction
H_2 production	
Butyrate oxidation	$CH_3CH_2CH_2COO^- + 2H_2O \rightarrow 2CH_3COO^- + 2H_2 + H^+$
Acetate oxidation	$CH_3COO^- + 4H_2O \rightarrow 4H_2 + 2HCO_3^- + H^+$
Dechlorination	
TCE consumption	$C_2HCl_3 + H_2 \rightarrow C_2H_2Cl_2 + Cl^-$
DCE consumption	$C_2H_2Cl_2 + H_2 \rightarrow C_2H_3Cl + Cl^-$
VC consumption	$C_2H_3Cl + H_2 \rightarrow C_2H_4 + Cl^-$
Methane production	
H_2-dependent methanogenesis	$4H_2 + CO_2 \rightarrow 4CH_4 + 2H_2O$
Acetate-dependent methanogenesis	$CH_3COO^- + H_2O \rightarrow CH_4 + HCO_3^-$
Sulfate reduction	
H_2-dependent sulfate reduction	$4H_2 + SO_4^{2-} + H^+ \rightarrow HS^- + 4H_2O$
Acetate-dependent sulfate reduction	$CH_3COO^- + SO_4^{2-} \rightarrow 2HCO_3^- + HS^-$
Butyrate-dependent sulfate reduction	$CH_3CH_2CH_2COO^- + 0.5SO_4^{2-} \rightarrow 2CH_3COO^- + 0.5HS^- + 0.5H^+$

4.4 Mathematical formulation of the model

The kinetic equations describing the rate of each process described in Section 4.2 are presented in the following sections. In the mathematical formulation of the model, the concentration of biological components will be denoted as X_j, in which the indices j change for the nine microbial groups of interest as follows: j is D1 for TCE-to-ETH dechlorinators, D2 for TCE-to-cDCE dechlorinators, HM for H_2-utilizing methanogens, AM for acetate-utilizing methanogens, HSR for H_2-utilizing sulfate reducers, ASR for acetate-utilizing sulfate reducers, BSR for butyrate-utilizing sulfate reducers, BO for butyrate oxidizers and AO for acetate oxidizers. Dead biomass and yeast extract are maintained in the system as composite organic materials and their concentration will be denoted as X_{CM}. The concentration of chemical components will be denoted as S_i, in which the indices i change in order to designate the various chemical components of the model: i is TCE, cDCE, VC, ETH for the respective chloroethenes, M for methane, S for sulfate, H for H_2, B for butyrate, A for acetate and HS for hydrogen sulfide.

4.4.1 Biochemical reaction rates

4.4.1.1 Reductive dechlorination processes

Chloroethene consumption rates, r_{i-j}, are described by dual substrate Monod kinetic equations:

$$r_{i-j} = -\frac{\mu_{\max,i-j}}{Y_j} X_j \frac{S_i}{K_{S,i-j} + S_i} \frac{S_H - S_{\min,H-j} f_{d,j}}{K_{S,H-j} + S_H - S_{\min,H-j} f_{d,j}} F_{d,j} \quad (4.1)$$

where $\mu_{max,i-j}$ is the maximum specific growth rate of dechlorinator j on substrate i (days^{-1}), X_j is the biomass concentration of microorganism j (mg VSS/l), Y_j is the yield coefficient of microorganism j (mg VSS/μmol Cl^-), S_i is the concentration of substrate i (μM), $K_{S,i-j}$ is the half-velocity coefficient for chloroethene i of microorganism j (μM), S_H is the concentration of H_2 (μM), $K_{S,H-j}$ is the half-velocity coefficient for H_2 of microorganism j (μM), and $S_{min,H-j}$ is the threshold for H_2 use for dechlorinators (μM). Two sigmoid functions, $f_{d,j}$ and $F_{d,j}$, were used in order to avoid possible instabilities and oscillatory behavior when H_2 concentrations approach the H_2 threshold values (Ribes et al., 2004). These sigmoid functions are defined as follows:

$$f_{d,j} = \frac{1}{1 + \exp\left(\frac{100}{S_{\min,H-j}}\left(S_{\min,H-j} - S_H\right)\right)} \quad (4.2)$$

$$F_{d,j} = \frac{1}{1 + \exp\left(\frac{100}{S_{\min,H-j}}\left(1.1S_{\min,H-j} - S_H\right)\right)} \quad (4.3)$$

In Eq. (4.1) to (4.3) i = TCE or cDCE and j = D_1 for TCE-to-ETH dechlorinators or D_2 for TCE-to-cDCE dechlorinators. Concerning VC consumption, possible competitive inhibition of VC by cDCE was considered and, consequently, Eq. (4.1) was replaced by the following (Cupples et al., 2004a):

$$r_{VC-D1} = -\frac{\mu_{\max,VC-D1}}{Y_{D1}} X_{D1} \frac{S_{VC}}{K_{S,VC-D1}\left(1+\frac{S_{cDCE}}{K_{INH,cDCE}}\right)+S_{VC}} \frac{S_H - S_{\min,H-D1} f_{d,D1}}{K_{S,H-D1} + S_H - S_{\min,H-D1} f_{d,D1}} F_{d,D1} \quad (4.4)$$

where $K_{INH,cDCE}$ is an inhibition coefficient (μM). In Eq. (4.1) and (4.4), $\mu_{max,i-j}$ are considered both microorganism- and substrate-related parameters; they differ for each dechlorinator and each chloroethene. In many modeling applications (e.g. Lee et al., 2004, Clapp et al., 2004) and in order to simplify model structure, $\mu_{max,i-j}$ are considered only microorganism-related and, thus, independent from the chloroethene consumed. For the sake of simplicity, for cultures NTUA-M1 and NTUA-M2 (Chapters 5 to 9), this approach will be followed.

4.4.1.2 Alternative terminal electron-accepting processes - Methanogenesis

Methanogenesis is modeled using Monod-type kinetic equations, which incorporated substrate thresholds for H_2 or acetate use by the corresponding methanogens. Specifically, the rate of H_2 consumption from H_2-utilizing methanogens, r_{H-HM}, was calculated as follows:

$$r_{H-HM} = -\frac{\mu_{\max,HM}}{Y_{HM}} X_{HM} \frac{S_H - S_{\min,H-HM} f_{HM}}{K_{S,H-HM} + S_H - S_{\min,H-HM} f_{HM}} F_{HM} \quad (4.5)$$

where $\mu_{max,HM}$ is the maximum specific growth rate of H_2-utilizing methanogens ($days^{-1}$), Y_{HM} is the yield coefficient of H_2-utilizing methanogens (mg VSS/μmol H_2), X_{HM} is the biomass concentration of H_2-utilizing methanogens (mg VSS/l), $K_{S,H-HM}$ is the half-velocity coefficient for H_2 of H_2-utilizing methanogens (μM), and $S_{min,H-HM}$ is the threshold for H_2 use (μM). The sigmoid functions, f_{HM} and F_{HM}, which were defined by Eq. (4.2) and (4.3), were adjusted to account for the appropriate H_2 threshold ($S_{min,H-HM}$ instead of $S_{min,H-j}$).

Acetate consumption rate from acetate-utilizing methanogens, r_{A-AM}, is modeled by the following equation:

$$r_{A-AM} = -\frac{\mu_{\max,AM}}{Y_{AM}} X_{AM} \frac{S_A - S_{\min,A-AM} f_{AM}}{K_{S,A-AM} + S_A - S_{\min,A-AM} f_{AM}} F_{AM} \quad (4.6)$$

where $\mu_{max,AM}$ is the maximum specific growth rate of acetate-utilizing methanogens ($days^{-1}$), Y_{AM} is the yield coefficient of acetate-utilizing methanogens (mg VSS/μmol acetate), X_{AM} is the biomass concentration of acetate-utilizing methanogens (mg VSS/l), S_A is the concentration of acetate (μM), $K_{S,A-AM}$ is the half-velocity coefficient for acetate of acetate-utilizing methanogens (μM), and $S_{min,A-AM}$ is the threshold for acetate use (μM). Again, f_{AM} and F_{AM} are the two sigmoid functions defined by Eq. (4.2) and (4.3), and they were properly adjusted to account for the appropriate substrate (S_A and $S_{min,A-AM}$ instead of S_H and $S_{min,H-j}$, respectively).

4.4.1.3 Alternative terminal electron acceptor processes - Sulfate reduction

Sulfate reduction is modeled using dual substrate Monod kinetic equations. Specifically, the rate of H_2 consumption from H_2-utilizing sulfate reducers, r_{H-HS}, was calculated as follows:

$$r_{H-HSR} = -\frac{\mu_{\max,HSR}}{Y_{HSR}} X_{HSR} \frac{S_S}{K_{S,S-HSR} + S_S} \frac{S_H - S_{\min,H-HSR} f_{HSR}}{K_{S,H-HSR} + S_H - S_{\min,H-HSR} f_{HSR}} F_{HSR} \quad (4.7)$$

where $\mu_{max,HSR}$ is the maximum specific growth rate of H_2-utilizing sulfate reducers (days^{-1}), Y_{HSR} is the yield coefficient of H_2-utilizing sulfate reducers (mg VSS/μmol H_2), X_{HSR} is the biomass concentration of H_2-utilizing sulfate reducers (mg VSS/l), $K_{S,H\text{-}HSR}$ is the half-velocity coefficient for sulfate of H_2-utilizing sulfate reducers (μM), $K_{S,H\text{-}HSR}$ is the half-velocity coefficient for H_2 of H_2-utilizing sulfate reducers (μM), and $S_{min,H\text{-}HSR}$ is the threshold for H_2 use (μM). The sigmoid functions, f_{HSR} and F_{HSR}, which were defined by Eq. (4.2) and (4.3), were adjusted to account for the appropriate H_2 threshold ($S_{min,H\text{-}HSR}$ instead of $S_{min,H\text{-}j}$).

Acetate consumption rate from acetate-utilizing sulfate reducers, $r_{A\text{-}AS}$, is modeled by the following equation:

$$r_{A-ASR} = -\frac{\mu_{\max,ASR}}{Y_{ASR}} X_{ASR} \frac{S_S}{K_{S,S-ASR} + S_S} \frac{S_A - S_{\min,A-ASR} f_{ASR}}{K_{S,A-ASR} + S_A - S_{\min,A-ASR} f_{ASR}} F_{ASR} \quad (4.8)$$

where $\mu_{max,ASR}$ is the maximum specific growth rate of acetate-utilizing sulfate reducers (days^{-1}), Y_{ASR} is the yield coefficient of acetate-utilizing sulfate reducers (mg VSS/μmol acetate), X_{ASR} is the biomass concentration of acetate-utilizing sulfate reducers (mg VSS/l), $K_{S,S\text{-}ASR}$ is the half-velocity coefficient for sulfate of acetate-utilizing sulfate reducers (μM), and $K_{S,A\text{-}ASR}$ is the half-velocity coefficient for acetate of acetate-utilizing sulfate reducers (μM). The sigmoid functions, f_{ASR} and F_{ASR}, which were defined by Eq. (4.2) and (4.3), were adjusted to account for the appropriate acetate threshold ($S_{min,A\text{-}ASR}$ instead of $S_{min,H\text{-}j}$).

Butyrate consumption rate from butyrate-utilizing sulfate reducers, $r_{B\text{-}BS}$, is modeled by the following equation:

$$r_{B-BSR} = -\frac{\mu_{\max,BSR}}{Y_{BSR}} X_{BSR} \frac{S_S}{K_{S,S-BSR} + S_S} \frac{S_B}{K_{S,B-BSR} + S_B} \quad (4.9)$$

where $\mu_{max,BSR}$ is the maximum specific growth rate of butyrate-utilizing sulfate reducers (days^{-1}), Y_{BSR} is the yield coefficient of butyrate-utilizing sulfate reducers (mg VSS/μmol butyrate), X_{BS} is the biomass concentration of butyrate-utilizing sulfate reducers (mg VSS/l), $K_{S,S\text{-}BSR}$ is the half-velocity coefficient for sulfate of butyrate-utilizing sulfate reducers (μM), and $K_{S,B\text{-}BSR}$ is the half-velocity coefficient for butyrate of butyrate-utilizing sulfate reducers (μM).

4.4.1.4 Fermentation processes – butyrate oxidation

The rate of butyrate oxidation, $r_{B\text{-}BO}$, was described as follows:

$$r_{B-BO} = -\frac{\mu_{\max,BO}}{Y_{BO}} X_{BO} \frac{S_B}{K_{S,B-BO} + S_B} I_{H-BO} \quad (4.10)$$

where $\mu_{max,BO}$ is the maximum specific growth rate of butyrate oxidizers (days^{-1}), Y_{BO} is the yield coefficient of butyrate oxidizers (mg VSS/μmol butyrate), X_{BO} is the biomass concentration of butyrate oxidizers (mg VSS/l), S_B is butyrate concentration (μM), $K_{S,B\text{-}BO}$ is the half-velocity coefficient for butyrate (μM). $I_{H\text{-}BO}$ is an inhibition factor defined as follows:

$$I_{H-BO} = e^{(-S_H/S_{INH,H-BO})} \quad (4.11)$$

in which $S_{INH,H\text{-}BO}$ is an inhibitory H_2 concentration for butyrate oxidation (μM). As mentioned, Eq. (4.11) is an inhibition factor proposed by Kouznetsova et al. (2010) and describes the distance

of butyrate oxidation from thermodynamic equilibrium. More elaborate functions have been proposed in the literature to describe the distance of butyrate oxidation from thermodynamic equilibrium (e.g. Fennell and Gossett, 1998; Jin, 2007). When tested in parameter estimation efforts, when conditions near or beyond thermodynamic equilibrium were reached, the proposed more elaborate functions calculated a negative inhibition factor – this would be acceptable only if the reaction was reversible. To avoid such problems, the simplifying Eq. (4.11) was chosen. For the sake of completeness, in Appendix A the simplified factors employed herein are compared to the previously mentioned elaborate thermodynamic models.

4.4.1.5 Fermentation processes – acetate oxidation

The rate of acetate oxidation, $r_{A\text{-}AO}$, is modeled by the following kinetic equation:

$$r_{A-AO} = -\frac{\mu_{\max,AO}}{Y_{AO}} X_{AO} \frac{S_A}{K_{S,A-AO} + S_A} I_{H-AO} \tag{4.12}$$

where $\mu_{max,AO}$ is the maximum specific growth rate of acetate oxidizers (days^{-1}), Y_{AO} is the yield coefficient of acetate oxidizers (mg VSS/μmol acetate), X_{AO} is the biomass concentration of acetate oxidizers (mg VSS/l), $K_{S,A\text{-}AO}$ (μM) is the half-velocity coefficient for acetate of acetate oxidizers (μM), and $I_{H\text{-}AO}$ is an inhibition factor defined as follows:

$$I_{H-AO} = e^{(-s_H / s_{INH,H-AO})} \tag{4.13}$$

in which $S_{INH,H\text{-}AO}$ is an inhibitory H_2 concentration for acetate oxidation (μM). Again, this exponential inhibition factor is used to simulate thermodynamic limitations imposed by H_2 concentrations to acetate oxidation.

4.4.1.6 Microbial growth

Microbial growth and decay for each microorganism is described in the model as follows:

$$\frac{dX_j}{dt} = \sum_i \left(-Y_j r_{i-j}\right) - b_j X_j \tag{4.14}$$

where b_j is the first-order decay coefficient of microorganism j (days^{-1}).

4.4.1.7 Endogenous decay and yeast extract contribution

The contribution of complex organic materials to the electron equivalent pool is a complex process containing both abiotic and biotic steps. As depicted in Fig. 4.4a, complex material (comprising decaying biomass and yeast extract herein) first disintegrates to carbohydrates, proteins, lipids and inert material (particulate and soluble). Then, carbohydrates, proteins and lipids are hydrolyzed to monosaccharides, aminoacids and long-chain fatty acids. Subsequently, hydrolysis products are biotically converted into short-chain fatty acids (i.e. acidogenesis of propionate, butyrate and valerate), acetate and H_2 (i.e. acetogenesis).

In the present modeling approach, these processes were substituted by a simpler process during which the complex particulate materials ultimately yield butyrate (Fennel and Gossett, 1998) (Fig. 4.4b). Particularly, dead biomass and yeast extract are converted abiotically into butyrate, which can be subsequently transformed biotically into acetate and H_2 (process performed by butyrate oxidizers, BO). As mentioned in Section 4.3, yeast extract was assumed to have the chemical

composition of biomass ($C_5H_7O_2N$; Aulenta et al., 2005) and, therefore, it contributed to the butyrate pool in the same manner as biomass did.

Similar simplifying approaches have used H_2 as the daughter product of biomass (Lee et al., 2004). However, the biotic steps of biomass disintegration (e.g. acidogenesis from long-chain fatty acids) are subject to thermodynamic limitations and considering H_2 as their daughter product would neglect these limitations.

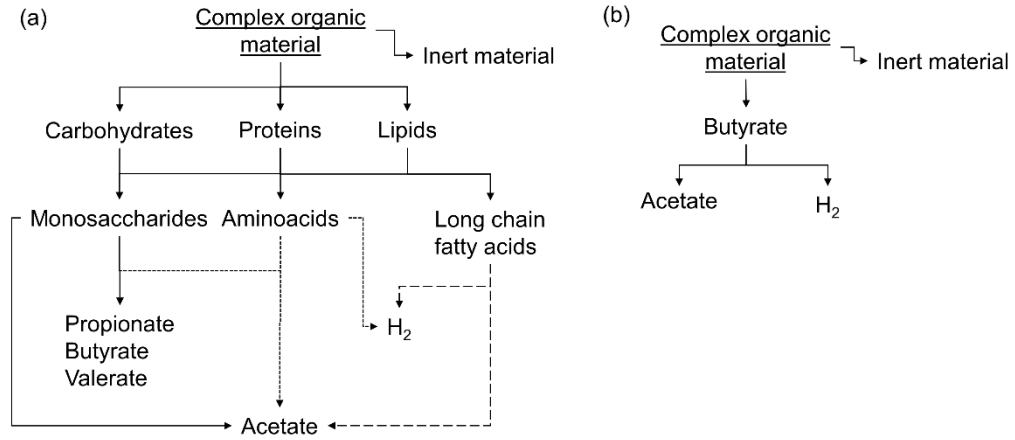

Fig. 4.4. (a) Conversion processes of dead biomass typically considered in anaerobic digestion models and (b) conversion processes of dead biomass used in the present modeling approach.

The rate of butyrate production from biomass decay, r_{CM}, was described by the following equation:

$$r_{B-CM} = F_s K_{ED} X_{CM} \tag{4.15}$$

where F_S is a stoichiometric coefficient for converting mg VSS (i.e. the units of decaying biomass) to μmol butyrate (μmol butyrate/mg VSS), K_{ED} is a first-order coefficient ($days^{-1}$) and X_{CM} is the concentration of decaying biomass (mg VSS/l). The coefficient F_S was set equal to 8.0 (i.e. 8.0 μmol butyrate produced from 1 mg of VSS) assuming (a) 90% of the decaying biomass is biodegradable, (b) 1 g of VSS equals 1.42 g COD, (c) 1 g of butyrate corresponds to 1.82 g of COD, and (d) 1 mole of butyrate weighs 87.11 g.

4.4.2 Model overview

The model contains 56 kinetic parameters and 20 dynamic state variables (i.e. chemical and microbial concentrations). Thus, model solution requires solving the following system of 20 ordinary equations:

$$\frac{dS_B}{dt} = +r_{B-BO} + r_{B-BS} + r_{B-CM} \tag{4.16a}$$

$$\frac{dS_A}{dt} = -2r_{B-BO} - 2r_{B-BS} + r_{A-AO} + r_{A-AM} + r_{A-ASR} \tag{4.16b}$$

$$\frac{dS_H}{dt} = -2r_{B-BO} - 4r_{A-AO} + r_{TCE-D1} + r_{TCE-D2} + r_{cDCE-D1} + r_{VC-D1} + r_{H-HM} + r_{H-HSR} \tag{4.16c}$$

$$\frac{dS_{TCE}}{dt} = r_{TCE-D1} + r_{TCE-D2} \tag{4.16d}$$

$$\frac{dS_{cDCE}}{dt} = -r_{TCE-D1} - r_{TCE-D2} + r_{cDCE-D1} \tag{4.16e}$$

$$\frac{dS_{VC}}{dt} = r_{cDCE-D1} - r_{VC-D1} \quad (4.16f)$$

$$\frac{dS_{ETH}}{dt} = r_{VC-D1} \quad (4.16g)$$

$$\frac{dS_{M}}{dt} = -r_{A-AM} - \frac{1}{4} r_{H-HM} \quad (4.16h)$$

$$\frac{dS_{S}}{dt} = \frac{1}{4} r_{H-HSR} + r_{A-ASR} + \frac{1}{2} r_{B-BSR} \quad (4.16i)$$

$$\frac{dS_{HS}}{dt} = -\frac{1}{4} r_{H-HSR} - r_{A-ASR} - \frac{1}{2} r_{B-BSR} \quad (4.16j)$$

$$\frac{dX_{BO}}{dt} = -r_{B-BO} Y_{BO} - b_{BO} X_{BO} \quad (4.16k)$$

$$\frac{dX_{AO}}{dt} = -r_{A-AO} Y_{AO} - b_{AO} X_{AO} \quad (4.16l)$$

$$\frac{dX_{D1}}{dt} = (-r_{TCE-D1} - r_{cDCE-D1} - r_{VC-D1}) Y_{D1} - b_{D1} X_{D1} \quad (4.16m)$$

$$\frac{dX_{D2}}{dt} = -r_{TCE-D2} Y_{D2} - b_{D2} X_{D2} \quad (4.16n)$$

$$\frac{dX_{HM}}{dt} = -r_{H-HM} Y_{HM} - b_{HM} X_{HM} \quad (4.16o)$$

$$\frac{dX_{AM}}{dt} = -r_{M-AM} Y_{AM} - b_{AM} X_{AM} \quad (4.16p)$$

$$\frac{dX_{HSR}}{dt} = -r_{H-HSR} Y_{HSR} - b_{HSR} X_{HSR} \quad (4.16q)$$

$$\frac{dX_{ASR}}{dt} = -r_{A-ASR} Y_{ASR} - b_{HSR} X_{ASR} \quad (4.16r)$$

$$\frac{dX_{BSR}}{dt} = -r_{B-BSR} Y_{BSR} - b_{BSR} X_{BSR} \quad (4.16s)$$

$$\frac{dX_{CM}}{dt} = \sum b_j X_j - r_{B-CM} \quad (4.16t)$$

In order to provide an overview of the model, a matrix model presentation is provided in Tables 4.2 and 4.3. In Tables 4.2 and 4.3, when moving across the matrix lines, the biochemical processes change (they are given in the left-hand column of the matrix), while when moving horizontally and across the matrix columns, the biochemical components of the model change. In the right-hand column, the process rates are presented, while each cell of the matrix contains rate coefficients, which describe the influence of that row's process on each component. The overall reaction rate for each component is the sum of products of reaction rate coefficients and process rates. For example, according to Table 4.2, cDCE reaction rate is the following:

$$\frac{dS_{cDCE}}{dt} = -r_{TCE-D1} - r_{TCE-D2} + r_{cDCE} \quad (4.17)$$

Similarly, the overall reaction rate of X_{D1} according to Table 4.3 is calculated as follows:

$$\frac{dX_{D1}}{dt} = -Y_{D1} r_{TCE-D1} - Y_{D1} r_{cDCE-D1} - Y_{D1} r_{VC-D1} - b_{D1} X_{D1} \quad (4.18)$$

Table 4.2. Rate coefficients for the chemical components of the model.

Component S_i →	B	H	A	TCE	cDCE	VC	ETH	M	S	HS	Rate
Process ↓	S_B	S_H	S_A	S_{TCE}	S_{cDCE}	S_{VC}	S_{ETH}	S_M	S_S	S_{HS}	
TCE dechlorination		+1		+1	-1						$r_{TCE\text{-}D1}$
		+1		+1	-1						$r_{TCE\text{-}D2}$
cDCE dechlorination		+1			+1	-1					$r_{cDCE\text{-}D1}$
VC dechlorination		+1				+1	-1				$r_{VC\text{-}D1}$
H_2-dependent methanogenesis		+1						-0.25			$r_{H\text{-}HM}$
Acetotrophic methanogenesis			+1					-1			$r_{A\text{-}AM}$
Butyrate oxidation	+1	-2	-2								$r_{B\text{-}BO}$
Acetate oxidation		-4	+1								$r_{A\text{-}AO}$
H_2-dependent sulfate reduction		+1							+0.25	-0.25	$r_{H\text{-}HSR}$
Acetate-dependent sulfate reduction			+1						+1	-1	$r_{A\text{-}ASR}$
Butyrate-dependent sulfate reduction	+1		-2						+0.5	-0.5	$r_{B\text{-}BSR}$
Biomass disintegration	-1										$r_{B\text{-}CM}$
Decay of TCE-to-ETH dechlorinators											$b_{D1}X_{D1}$
Decay of TCE-to-cDCE dechlorinators											$b_{D2}X_{D2}$
Decay of H_2-utilizing methanogens											$b_{HM}X_{HM}$
Decay of acetate-utilizing methanogens											$b_{AM}X_{AM}$
Decay of butyrate oxidizers											$b_{BO}X_{BO}$
Decay of acetate oxidizers											$b_{AO}X_{AO}$
Decay of H_2-utilizing sulfate reducers											$b_{HSR}X_{HSR}$
Decay of acetate-utilizing sulfate reducers											$b_{ASR}X_{ASR}$
Decay of butyrate-utilizing sulfate reducers											$b_{BSR}X_{BSR}$
Units →	μM butyrate	μM H_2	μM acetate	μM TCE	μM cDCE	μM VC	μM ETH	μM methane	μM SO^{2-}_4	μM HS^-	

Table 4.3. Rate coefficients for the microbial components of the model.

Component X_J→	D1	D2	HM	AM	BO	AO	HSR	ASR	BSR	CM	Rate
Process ↓	X_{D1}	X_{D2}	X_{HM}	X_{AM}	X_{BO}	X_{AO}	X_{HSR}	X_{ASR}	X_{BSR}	X_{CM}	
TCE dechlorination	$-Y_{D1}$										$r_{TCE\text{-}D1}$
		$-Y_{D2}$									$r_{TCE\text{-}D2}$
cDCE dechlorination	$-Y_{D1}$										$r_{cDCE\text{-}D1}$
VC dechlorination	$-Y_{D1}$										$r_{VC\text{-}D1}$
H_2-dependent methanogenesis			$-Y_{HM}$								$r_{H\text{-}HM}$
Acetotrophic methanogenesis				$-Y_{AM}$							$r_{A\text{-}AM}$
Butyrate oxidation					$-Y_{BO}$						$r_{B\text{-}BO}$
Acetate oxidation						$-Y_{AO}$					$r_{A\text{-}AO}$
H_2-dependent sulfate reduction							$-Y_{HSR}$				$r_{H\text{-}HSR}$
Acetate-dependent sulfate reduction								$-Y_{ASR}$			$r_{A\text{-}ASR}$
Butyrate-dependent sulfate reduction									$-Y_{BSR}$		$r_{B\text{-}BSR}$
Biomass disintegration										$-1/F_S$	$r_{B\text{-}CM}$
Decay of TCE-to-ETH dechlorinators	-1									+1	$b_{D1}X_{D1}$
Decay of TCE-to-cDCE dechlorinators		-1								+1	$b_{D2}X_{D2}$
Decay of H_2-utilizing methanogens			-1							+1	$b_{HM}X_{HM}$
Decay of acetate-utilizing methanogens				-1						+1	$b_{AM}X_{AM}$
Decay of butyrate oxidizers					-1					+1	$b_{BO}X_{BO}$
Decay of acetate oxidizers						-1				+1	$b_{AO}X_{AO}$
Decay of H_2-utilizing sulfate reducers							-1			+1	$b_{HSR}X_{HSR}$
Decay of acetate-utilizing sulfate reducers								-1		+1	$b_{ASR}X_{ASR}$
Decay of butyrate-utilizing sulfate reducers									-1	+1	$b_{BSR}X_{BSR}$
Units →	mg VSS/l	mg VSS/l	mg VSS/l	mg VSS/l	mg VSS/l	mg VSS/l	mg VSS/l	mg VSS/l	mg VSS/l	mg VSS/l	

Chapter 5: Developing a multistart optimization strategy for parameter estimation

5.1 Introduction

Parameter estimation in kinetic models (also referred to as the inverse problem) is a process aiming to develop data-driven models of biological systems that resonate with reality. In the present chapter, problems that typically plague parameter estimation efforts in kinetic models are addressed (Section 5.2). Then, a heuristic multistart-based strategy is designed in order to circumvent these pitfalls (Section 5.3). Finally, this heuristic strategy is tested with three different models (Section 5.4): a simplified version of the model developed in Chapter 4 and two literature-reported models.

5.2 Definition of the parameter estimation problem in kinetic models

As we saw in Chapter 4, deterministic kinetic models constitute a nonlinear system of differential equations of the form:

$$\frac{dS(t,p)}{dt} = f\left(t, S(t,p), X(t,p), p\right) \tag{5.1a}$$

$$\frac{dX(t,p)}{dt} = g\left(t, S(t,p), X(t,p), p\right) \tag{5.1b}$$

$$S(t_0,p) = S_0(p) \tag{5.1c}$$

$$X(t_0,p) = X_0(p) \tag{5.1d}$$

$$s\left(t, S(t,p), X(t,p), p\right) \tag{5.1e}$$

$$x\left(t, S(t,p), X(t,p), p\right) \tag{5.1f}$$

in which t is the time ranging from t_0 (time of the first observation) to t_f (time of the last observation), $\boldsymbol{p}$ is the m-dimensional vector of the unknown parameters, $\boldsymbol{S}$ is the n-dimensional vector of the chemical concentrations, $\boldsymbol{X}$ is the r-dimensional vector of biomass concentrations, and $\boldsymbol{f}$ and $\boldsymbol{g}$ are the vector functions describing biochemical reaction rates. If some of the components of the initial vectors $\boldsymbol{S_0}$ (n-dimensional) and $\boldsymbol{X_0}$ (r-dimensional) are not measured, they are considered as unknown parameters, and hence they are treated as components of the parameter vector $\boldsymbol{p}$. Finally, $\boldsymbol{s}$ is the vector of observed chemical concentrations and $\boldsymbol{x}$ is the vector of observed microbial concentrations.

The objective of parameter estimation is to minimize the discrepancy between model output (described by vectors $\boldsymbol{S}$, $\boldsymbol{X}$) and experimental observations (contained in vectors $\boldsymbol{s}$, $\boldsymbol{x}$). In principle, the unknown parameter vector $\boldsymbol{p}$ is estimated by minimizing a function (an objective function), J, which is a quantitative measure of the aforementioned discrepancy. Hence, the parameter estimate $\boldsymbol{p^*}$ is calculated as follows:

$$\boldsymbol{p^* = \arg\min J(p)} \tag{5.2}$$

Solving Eq. (5.2) can be performed manually by a trial-and-error approach or automatically with the use of a search algorithm (an optimization algorithm). In both cases, an initial parameter vector $\boldsymbol{p'}$ is assumed prior to the search for a smaller $J(\boldsymbol{p})$.

In Monod-type kinetic models the problem of parameter estimation is frequently ill-posed. Multiple and ambiguous mathematical solutions (i.e. vectors $\boldsymbol{p^*}$) can be estimated, reproducing equally well the vectors $\boldsymbol{s}$ and $\boldsymbol{x}$ of the experimental observations [practically equal $J(\boldsymbol{p})$ values]. Non-uniqueness of the solutions derives from the linear correlation of the model parameters (Liu and Zachara, 2001), parameter insensitivity (Malaguerra et al., 2011) or the limited availability of the information content that could constrain the model behavior (e.g. microbial concentrations are seldom available, as discussed in Chapter 3). Ultimately, one of those equivalent, good-fit parameter sets has a marginally lower objective function value and is considered the global optimum solution of the parameter estimation problem.

Non-uniqueness of the problem has two implications. First, different behavior models may be harbored in the family of equivalent good-fit solutions, especially when models with multiple functionality are considered (Beven, 2006). For example, a model with multiple functionality is the fully kinetic model discussed in Chapter 4. In the present model, methane can be produced by two pathways, whereas sulfate may be reduced by three different sulfate-reducers. Hence, the same output may be produced by different mechanisms. Consequently, non-uniqueness gives little confidence on the global optimum solution. Second, the existence of multiple solutions does not guarantee that all of them reproduce the experimental observations with acceptable accuracy. Finding a parameter set that produces an acceptable fit to the data requires providing the optimization algorithm with a good starting point. Providing a proper starting point necessitates prior knowledge of the system under consideration, which is rarely available. In addition, a poor fit of the model to the experimental observations may falsely lead to the conclusion that the conceptual model is erroneous, when poor fit may be attributed to the failure of the optimization algorithm.

Multistart global optimization algorithms (will be simply referred to as multistart algorithms from this point onwards) have two advantages when applied for parameter estimation. First, they are conceptually simple methods that allow the modeler to circumvent the difficulty of providing a single starting point (Mugunthan et al., 2005), as local searches are performed from randomly generated starting points of the parameter space. Second, the multistart approaches provide the opportunity to detect solutions of the problem that are equivalent to the best-fit solution. Thus, the modeler can map and examine distinctive parameter sets, which may represent different behavior models. Estimating a single solution (even if it is indeed the global optimum solution) may conceal differences in processes that are insignificant during the identification phase of the model, but may become important during the prediction phase, when different initial conditions are considered. Even if multistart strategies are considered inefficient for large parameter vectors (Moles et al., 2003; Gabor and Banga, 2015), they were implemented in this work for their ability to detect functionally distinctive approximations of mixed dechlorinating consortia.

5.3 Formulation of the multistart algorithm for parameter estimation

A prerequisite for any parameter estimation problem is to solve quickly and robustly the forward problem. In models describing dechlorination kinetics, the forward problem requires a robust time integrator in order to avoid numerical instability issues that may occur. As Fennell and Gossett (1998) and Lee et al. (2004) report, simulating H_2 concentrations is a source of instabilities due to the rapid changes in H_2 production and consumption. Thus, small time-steps are required. In this work, a MATLAB® initial value problem solver was utilized, *ode15s* function, the time steps of which were adjusted to yield a relative tolerance smaller than 10^{-6} (the m-file containing the MATLAB® code for solving the forward problem is available in Appendix B).

The multistart algorithm is typically performed in three steps (Fig 5.1). First, a feasible starting point (a vector $\boldsymbol{p}'$) is generated. Second, a local search method is implemented searching for a solution that minimizes the objective function, *J*. Third, a stopping criterion is checked, and if it is not met, the algorithm returns to the first step and generates another vector $\boldsymbol{p}'$. For the set-up of the multistart algorithm, we should: (a) select an appropriate objective function, (b) define the feasible area of the parameter space, (c) specify a way to generate feasible starting points, (d) choose a local search method, and (e) impose a stopping criterion to prevent the algorithm reiterating perpetually. These decisions are discussed in the following sections.

Procedure Multistart
While *stopping criterion not satisfied* **do**
Generate a parameter set, *p',* from the feasible area of the parameter space
Calculate the objective function, *J(p')*, and apply a local search method to improve the solution *J(p')*
Store the solution *J(p*)* obtained from the local search routine
End

Fig. 5.1. The algorithmic procedure of the multistart optimization algorithm.

5.3.1 Choice of an objective function

The most prevalent objective function is the sum of weighted squares of errors, *J(p)* (μM^2), and is calculated as follows (Ashyraliyev et al., 2008):

$$J(t,p)=\sum_{0}^{t_f} W\left(v_{test}(t)-v_{model}(t,p)\right)^2 \tag{5.3}$$

where $\boldsymbol{p}$ is the parameter vector (containing the kinetic parameters of the model and the unknown chemical and microbial initial concentrations), $\boldsymbol{v_{test}}$ is the vector of observed data (described by vectors $\boldsymbol{s}$ and $\boldsymbol{x}$), $\boldsymbol{v_{model}}$ is the vector of model outputs (containing vectors $\boldsymbol{S}$ and $\boldsymbol{X}$), and $\boldsymbol{W}$ is a *N*x*N* weighting matrix assuming that *N* measurements are available. Objective functions using the squares of errors are preferred over alternative objective functions (e.g. the mean absolute error of the model), because squared errors create smooth objective functions, a feature required for several optimization algorithms (Bennett et al., 2013).

Objective functions for kinetic models describing dechlorination are also based on functions employing the squares of errors. Apart from the sum of weighted squares of errors (used by Manoli et al., 2012), the root mean of squared errors has been used (e.g. Schneidewind et al., 2014 or Haest et al., 2010), or a simple sum of squared errors (e.g. Cupples et al., 2004 or Heavner et al., 2013). The only exception is the work of Amos et al. (2007), where the Nash-Sutcliffe index was

calculated, since it was considered preferable to weighted functions in cases where components with different magnitudes are considered.

The role of weighting matrixes in objective functions varies. In many applications, the weighting matrix is set equal to the inverse of the covariance matrix of the experimental measurements, i.e. $W_{ii} = 1/\sigma^2_{ii}$. Hence, the weighting matrix favors observations that are relatively more reliable. Often, the weighting matrix functions as a normalization matrix safeguarding against biases towards large concentration measurements. The diagonal elements of such weighting matrixes are calculated as follows (Englezos and Kalogerakis, 2000):

$$W_{ii} = \frac{1}{\left(\frac{1}{N}\sum_{i=1}^{N} v_{test}(i)\right)^2} \tag{5.4}$$

In the present thesis, the weighting matrix described by Eq. (5.4) was adopted in order to deal with possible differences in the observed values between chloroethenes, methane, sulfate and volatile fatty acids and because the covariance matrix of the measurements was not always accessible, due to lack of repeated measurements.

5.3.2 Generation of starting points

When the number of parameters grows, it seems a pointless effort to randomly create a set of starting points that covers sufficiently an unlimited parameter space. In order to simplify the optimization problem and reduce the computational burden, constraining the parameter space and, thereafter, creating a feasible area is inevitable.

There are two ways to constrain the parameter space, (a) to fix a parameter to a certain value (a fixed parameter) or (b) to confine a parameter within specific bounds (an adjustable parameter). The first way typically refers to measurable parameters. In kinetic modeling, readily measurable parameters comprise part of the initial conditions (chemical or, less often, microbial initial concentrations). With respect to kinetic parameters, growth yields, decay coefficients or substrate thresholds are typically considered fixed. Typically, they are experimentally determined and, hence, considered more reliable. On the contrary, maximum specific growth rates, half-velocity coefficients and inhibition coefficients are inversely estimated and, thus, their values are not trustworthy, because of the limited transferability of Monod kinetic parameters between diverse experimental conditions (Chambon et al., 2013). Consequently, they are usually considered adjustable and are treated as part of the parameter vector $\boldsymbol{p}$ of the optimization problem.

A feasible parameter vector $\boldsymbol{p}'$ can be generated randomly or systematically. The first approach depends solely on the probability distribution of each parameter, it is simple to implement, but provides limited control on the level of diversification of the initial starting points. Hence, many starting points may coexist in regions of the parameter space from which the local search algorithm ultimately leads to the same local optimum solution (regions of attraction). The second approach is based on controlled randomization, including heuristic local searches to improve the starting points (Marti et al., 2013). This approach is more complicated to implement, but it helps the algorithm to become more efficient. An uncontrolled random restart approach was implemented in the multistart algorithm for the generation of starting points, as we opted for simplicity. Since

no prior knowledge is available regarding the probability distribution of each parameter, we assumed that each parameter is uniformly distributed between its boundaries.

Regarding the random number generator, two options are available: (a) a pseudo-random number generator and (b) a quasi-random number generator. The main difference of these two options is that in the case of quasi-random sequences each successive number is set as far away as possible from the existing numbers in the set, avoiding clustering and achieving uniformity (Kucherenko and Sytsko, 2005). Two built-in functions of MATLAB® were tested in a simple two-dimensional problem in order to investigate the relevance of the random number generators in the construction of starting parameter sets. A quasi-random Sobol sequence was created by the *sobolset* function of MATLAB®, which was tested against a pseudo-random sequence created by the *rand* function of MATLAB®. For both cases, 1000 points were created with variables being uniformly distributed between 0 and 1. When all random points are considered, the pseudo-random numbers are unevenly distributed, as there are areas more densely populated than others (compare Fig. 5.2a versus Fig. 5.2b). Yet, one could argue that this is only an issue of efficiency; many areas of the available space have been revisited many times (the dense black areas of Fig. 5.2b), but all the available space has been covered. The relevance of random sampling technique is more pronounced, when only the first 100 points of each sequence are considered. The pseudo-random sequence left many areas of the available space unvisited (Fig. 5.2c compared to the pseudo-random Fig. 5.2d); in this case, the sampling technique is not sufficient. For high dimensional problems, the lack of uniformity would lead to inadequate local searches, when only a small number of starting points is drawn from the feasible area of the parameter space. Therefore, the *sobolset* built-in function of MATLAB® was implemented for the construction of sets of quasi-random starting points.

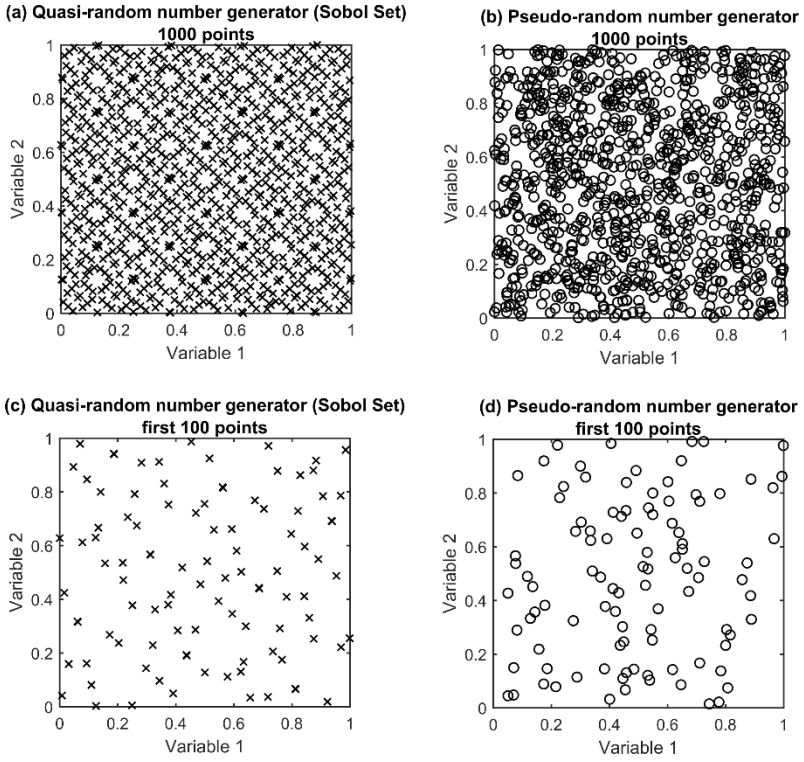

Fig. 5.2. Comparison of a quasi-random number sequence (a Sobol sequence created by the *sobolset* function of Matlab®) and a pseudo-random number sequence (created by the *rand* function of Matlab®) for a two-dimensional problem for 1000 points (a, b) and 100 points (c, d).

5.3.3 Choice of a local search routine

Local search methods can be classified in two broad classes: gradient-based methods, which make use of the first- and second-order derivatives of the objective function, and gradient-free methods, which rely solely on objective function evaluations, and, thus, they do not require the differentiability of the objective function. In general, gradient-based methods converge faster to local optimum solutions (Lewis et al., 2000), but in complex models analytical derivatives are not available and their numerical approximation is computationally expensive. When many costly function evaluations are needed per iteration, gradient-free methods should be considered as a reasonable alternative. The modeler should investigate a trade-off between the convergence rate and the time required at each step of the local search. In the case of multistart algorithms this trade-off becomes important considering the large number of required local searches. Therefore, two local search routines were tested, a derivative-based algorithm and a derivative-free algorithm.

A sequential quadratic programming (SQP) algorithm was used as a derivative-based algorithm for the solution of the parameter estimation problem. The SQP method is considered as a generalization of Newton's method for constrained optimization, since it calculates steps by minimizing quadratic subproblems. SQP is one of the most effective methods for nonlinear constrained optimization problems, since it is robust when dealing with (a) active constraints as large as the number of variables (b) significant nonlinearities, and (c) badly scaled problems, i.e. problems in which parameters differ by orders of magnitude (Nocedal and Wright, 2006). SQP algorithms have already been used for parameter estimation in anaerobic digestion models (e.g. Sales-Cruz and Gani, 2004; Aceves-Lara et al., 2005), which are models structurally similar to those dealing with dechlorination kinetics in mixed cultures. In these cases, SQP algorithms provided better and faster estimates compared to classical local search algorithms, such as the Levenberg-Marquardt algorithm. The SQP algorithm was implemented in a line-search strategy using the *fmincon* function in Matlab® (the m-file containing the MATLAB® code of the SQP-based algorithm is available in Appendix B).

Several classes of derivative-free methods exist, such as pattern-search methods, simplex methods and methods with adaptive sets of search directions (Lewis et al., 2000). We implemented the simple and intuitive method of generalized pattern search (GPS) through the *patternsearch* built-in function of Matlab® (the m-file containing the MATLAB® code of the GPS-based algorithm is available in Appendix B). The GPS method evaluates J at a mesh of candidate points, which form a stencil around the current iterate. If a point has a lower function value, it is considered as the new iterate, the center of the stencil is shifted to this new point and the size of the stencil is altered.

It is beyond the scope of this work to search thoroughly the performance characteristics of each algorithm or to provide an in-depth overview of all the possible local search algorithms that could have been implemented. The aim of this chapter is to find which of the two local optimization routines (i.e. the SQP method and the GPS method) gives the opportunity to study more complex systems (and, thus, more computationally demanding) efficiently and reliably. Therefore, both local search routines will be compared in the application of a multistart strategy for parameter estimation in models studying dechlorination kinetics.

5.3.4 Selection of a stopping criterion

In multistart algorithms when the number of local minima to be discovered is unknown in advance, a stopping criterion must be applied to prevent the algorithm from generating starting points and searching for solutions endlessly. The efficiency of the stopping criterion is critical for the overall efficiency of the algorithm (Marti et al., 2013). An intuitive and simple stopping criterion would be the maximum allowable number of starting points; the multistart algorithm will be put to an end when its local searches reach that ceiling. However, more sophisticated probabilistic stopping criteria have been proposed in the literature (e.g. Ribeiro et al., 2011).

In this work a Bayesian stopping criterion is applied and, if not met, the multistart algorithm will stop when 1000 local searches are performed. The imposed Bayesian stopping criterion terminates the algorithm when all the local optimum solutions of the problem have been discovered. As proposed by Boender and Rinooy-Kan (1987), the Bayesian estimate of local optimum solutions for a problem, $\hat{o}$, is calculated as follows:

$$\hat{o} = \frac{o(l-1)}{l-o-2} \tag{5.5}$$

where o is the number of discovered optimum solutions and l is the number of performed local searches. Hence, the Bayesian stopping criterion is formulated as follows:

$$\frac{o(l-1)}{l-o-2} \leq o \tag{5.6}$$

The proposed Bayesian stopping criterion, however, may necessitate many local searches to be triggered, especially if the objective function is rugged and many local minimum solutions exist. In order to prevent from such computationally intensive efforts, a supplementary stopping criterion was imposed based on the maximum number of local searches performed: the multistart algorithm will stop if 1000 starting points are examined.

Since the same local minimum can be found from more than one starting points (i.e. starting points belonging in the same region of attraction), it is important to define when two local optimum solutions should be considered distinctive. In this multistart strategy, two local optima, $\boldsymbol{p_k^*}$ and $\boldsymbol{p_m^*}$, were considered distinctive when their relative Euclidean distance (Eq. 5.7a) or the relative difference in the objective function value (Eq. 5.7b) were greater than 10%, i.e.:

$$\frac{\left|p_k^* - p_m^*\right|}{\left|p_k^*\right|} \geq 10\% \tag{5.7a}$$

$$\frac{\left|J\left(p_k^*\right) - J\left(p_m^*\right)\right|}{\left|J\left(p_k^*\right)\right|} \geq 10\% \tag{5.7b}$$

Therefore, after each local search that produced a local solution, the matrix that contained all the discovered local solutions was sorted by the objective value from the lowest to the highest and then those matrix lines (i.e. vectors $\boldsymbol{p_k^*}$) that do not satisfy both (5.7a) and (5.7b) were removed from the solution matrix. Then, the algorithm proceeded to the next local search.

When all the existing local solutions of the problem are not discovered (i.e. when the ceiling of 1000 local searches has been reached), a different quantitative measure was used to examine how

exhaustive the search for a global solution was. Boender and Rinooy-Kan (1987) propose to quantify the total relative volume of the observed regions of attraction, R_V, which is calculated as follows:

$$R_V = \frac{(l-o-1)(l+o)}{l(l-1)} \tag{5.8}$$

Ideally, R_V is 100% when l is significantly greater than o and all the regions of attraction of the problem have been searched. In the present multistart algorithm this measure was not used as a stopping criterion, nevertheless, it was calculated as an indication of how extensive the generation of starting points was.

5.4 Application of the multistart strategy for dechlorination kinetics

The aim of the application of the multistart strategy is two-fold. First, it aims to test the two main features of the multistart strategy: (a) the local search routine and (b) the stopping criterion. The performance of each local search routine will dictate its selection, which will not be reviewed in the following chapters, where the multistart strategy will be implemented for parameter estimation in more complex models. Second, the application of the multistart strategy aims to investigate how detecting distinctive local solutions of the problem can enhance understanding on the underlying mechanisms of dechlorination.

For the first aim, two MATLAB-based multistart algorithms were designed. Their pseudocode is given in Fig.5.3 (as already mentioned their m-files are available in Appendix B). The only difference of these approaches lies in the local search routine employed: an SQP method (derivative-based routine) and a GPS method (derivative-free routine) were used. The remaining features of the algorithm are the same: a Sobol set of quasi-random points is generated from the feasible area of the parameter space and the same stopping criterion is applied. These multistart algorithms will be implemented for the estimation of the kinetic parameters of a model describing dechlorination in culture NTUA-M2.

Procedure Multistart
Provide boundaries for the parameter vector $\boldsymbol{p}$, i.e. $\boldsymbol{p}^{lb}<\boldsymbol{p}<\boldsymbol{p}^{ub}$
Construct a quasi-random Sobol set of 1000 starting points $\boldsymbol{p}_l$
Set $o=0$;
for l=1…1000
    Calculate the objective function, $J(p_l)$ and apply a local search routine to improve the solution $J(p_l^*)$
    if $\boldsymbol{p}_l^*$ is a distinctive local optimum solution
        Store the local optimum solution $\boldsymbol{p}_l^*$, $J(p_l^*)$ obtained from the local search routine
        $o=o+1$;
    else $o=o$;
    end
    if $o(l-1)/(l-o-2)-0.5 = o$
        break for loop
    end
end
Return the solution with the lowest objective function value

Fig. 5.3. The pseudocode describing the algorithmic procedure of the multistart algorithm implemented in MATLAB®.

5.4.1 Dechlorinating culture NTUA-M2

For the application of the multistart optimization strategy in culture NTUA-M2, a simpler version of the full model described in Chapter 4 was used. The parameter estimation problem was solved twice, one time for the SQP-based approach and one time for the GPS-based approach. Then, the two applications of the multistart strategy were compared based on (a) the fit of the respective global optimum solutions and (b) the computation time required to reach a global optimum solution (parameter estimation problems were solved in a quad-core Intel i7-4790® processor). Since the sum of weighted squared errors is not expressed in units readily comparable to the units of experimental measurements, the mean absolute simulation error will be used to express the quality of fit in a readily interpretable way. The mean absolute simulation error, E_i, will be evaluated for each chloroethene separately according to the following equation:

$$E_i = \frac{1}{N}\sum\left|V_{test,i} - V_{model,i}\right| \tag{5.9}$$

in which i = TCE, cDCE, VC and ETH for chloroethene and ethene concentrations. Then, simulation errors are readily comparable with the mean absolute experimental errors, $\hat{E}_i$, which can be estimated by Eq. (5.9), if we substitute V_{test} and V_{model} values with the values of the measurements of each duplicate batch reactor.

5.4.1.1 Model development

Conceptually the model describes chloroethene consumption along with the growth of two dechlorinating species, a TCE-to-cDCE dechlorinator and a TCE-to-ETH dechlorinator. The model ignores any interactions occurring between the dechlorinating community and non-dechlorinators that are present in the mixed culture, provided that the supplied electron donor is provided in excess and that chloroethenes are the sole limiting factor for the growth of dechlorinators (the verity of these assumptions will be further assessed in Chapter 7). Thus, chloroethene consumption rates, r_{i-j}, were modeled with single substrate Monod kinetic equations:

$$r_{i-j} = -\frac{\mu_{\max,j}}{Y_j} X_j \frac{S_i}{K_{S,i-j} + S_i} \tag{5.10}$$

where $\mu_{max,j}$ is the maximum specific growth rate of microorganism j (days^{-1}), X_j is the biomass concentration of microorganism j (mg VSS/l), Y_j is the yield coefficient of microorganism j (mg VSS/μmol Cl$^-$), S_i is the concentration of chloroethene i (μM), and $K_{S,i-j}$ is the half-velocity coefficient for chloroethene i of microorganism j (μM). In Eq. (5.10), i = TCE or cDCE and j = D1 for TCE-to-ETH dechlorinators or D2 for TCE-to-cDCE dechlorinators. For the sake of simplicity, maximum specific growth rates in this application were considered microorganism-related and, thus, independent of the consumed chloroethene.

Concerning VC consumption, potential competitive inhibition of VC by cDCE was considered and, consequently, r_{VC-D1}, is estimated as follows:

$$r_{VC-D1} = -\frac{\mu_{\max,D1}}{Y_{D1}} X_{D1} \frac{S_{VC}}{K_{S,VC-D1}\left(1 + \frac{S_{cDCE}}{K_{INH,cDCE}}\right) + S_{VC}} \tag{5.11}$$

where $K_{INH,cDCE}$ is an inhibition coefficient (μM). Finally, microbial growth supported by chloroethene consumption is simulated as follows:

$$\frac{dX_j}{dt} = \sum_i (-Y_j \cdot r_i) - \left(b_j \cdot X_j\right) \quad (5.12)$$

where b_j is the decay coefficient (days^{-1}).

5.4.1.2 Experimental information

Two sources of experimental information are available: (a) the long-term performance data of the source culture and (b) a six-day long batch test performed with material from culture NTUA-M2 (Antoniou, 2017). This batch test was selected for two reasons. First, it is an H_2-fed batch test, which minimizes the dependence of dechlorinators to butyrate oxidizers. Second, considering the amount of methane produced at the end of the dechlorination (560 μM), almost 60% of the reducing equivalents remained unused (accumulated in the form of acetate and butyrate), indicating that dechlorination proceeded without significant electron donor limitation.

Experimental observations of the source culture were used to specify the steady-state biomass concentrations for the two dechlorinating species. Steady-state biomass concentrations can be calculated using the steady-state end-products of dechlorination on a weekly basis according to the following equation:

$$X_{j,SS} = \frac{\theta_c}{f} \frac{Y_j dS_{i-j}}{1 + b_j \theta_c} \quad (5.13)$$

where $X_{j,SS}$ is the steady-state biomass concentration of microorganism j (mg VSS/l), θ_c is the solid retention time (48 days), f is the duration of the feeding cycles of the culture (7 days), and dS_{i-j} is the quantity of substrate i consumed by dechlorinator j during each feeding cycle (μM).

The source culture reached a steady state with respect to dechlorination, producing mainly VC and to a lesser extent ETH at the end of the weekly feeding cycles (see also Chapter 4.1.1 for a more detailed discussion on the source culture maintenance and monitoring). As two dechlorinating species grow on TCE within culture NTUA-M2 (a *Dehalococcoides mccartyi* dechlorinator and a *Sulfurospirillum* partial dechlorinator), an assumption was made for the calculation of dS_{TCE-j}. It was assumed that 80% of the supplied TCE was consumed by TCE-to-cDCE dechlorinators (dS_{TCE-D2}=400 μM TCE). Hence, for TCE-to-ETH dechlorinators, dS_{i-D1} is the sum of chloroethenes consumed on a weekly basis and, thus, comprises the remaining 20% of TCE, and all of cDCE and VC [$\Sigma(dS_{i-D1})$=1050 μM Cl^-]. This assumption is consistent with the findings of Duhamel and Edwards (2007) and Lai and Becker (2013), who reported that partial dechlorinators are efficient TCE scavengers. Duhamel and Edwards (2007) estimated that partial dechlorinators (the acetotrophic *Geobacter*) consumed 80% of TCE in their mixed dechlorinating community, whereas Lai and Becker (2013) reported that *Dehalobacter restrictus* (hydrogenotrophic partial dechlorinators) outperformed *Dehalococcoides mccartyi 195* (TCE-to-ETH dechlorinators) in the competition for TCE.

Chloroethene concentrations of a batch test performed (in duplicates) were used as input for the parameter estimation process. The duplicate batch reactors were fed with 3000 μM H_2 and 300 μM butyrate as electron donor sources and 596 μM TCE as electron acceptor. The resulting electron donor surplus equals 3.4, assuming that 1 mol H_2 yields 2 e^-eq, 1 mol butyrate yields 20 e^-eq and 1 mol TCE requires 6 e^-eq for its complete dechlorination. What is more, significant

quantities of acetate were measured initially (900 μM acetate or 7200 μe⁻eq/l), providing an extra electron donor source and a carbon source.

5.4.1.3 The feasible area of the solutions of the problem

The first step of the multistart strategy is to define the parameter vector and its boundaries. Four kinetic parameters were treated as fixed in the problem, the growth yields and decay coefficients (Y_j and b_j, two parameters per dechlorinating group). Growth yields and decay coefficients are typically determined experimentally and, hence, they are considered more reliable. What is more, fixing their values gives the opportunity to specify and fix the steady-state biomass concentrations and, hence, the respective initial biomass concentrations of the two dechlorinators using Eq. (5.13) (Table 5.1). As shown in Table 5.2, growth yields and decay coefficients vary within a relatively narrow range of values reported in the literature. Their values were selected so that biomass concentrations are consistent with the results of the FISH analysis performed for culture NTUA-M1 (Panagiotakis et al., 2014) and steady-state biomass concentrations would not exceed the measured biomass concentration of the source culture (23.3 mg VSS/l). The initial biomass concentration of TCE-to-ETH dechlorinators was estimated equal to 10.21 mg VSS/l (44% of the overall steady-state biomass). Considering that one *Dehalococcoides mccartyi* cell corresponds to 1.6×10^{-14} g of VSS (Cupples et al., 2003), this concentration is equal to 1.6×10^{10} cells/l, a value within the range of concentrations reported for *Dehalococcoides mccartyi*-enriched cultures.

Additionally, chloroethene initial concentrations were also treated as fixed parameters, since they were measured at the beginning of the batch test. The remaining kinetic parameters (7 parameters), comprising maximum specific growth rates ($\mu_{max,j}$), half-velocity coefficients ($K_{S,i-1}$) and the competitive inhibition coefficient of cDCE ($K_{INH,cDCE}$), constitute the adjustable parameter vector $\boldsymbol{p}$. These parameters were constrained by the wide range of literature reported values presented in Table 5.2.

Table 5.1. Initial chemical and biomass concentrations for the batch test performed with source culture NTUA-M2.

Component	Symbol	Value [units]
TCE	$S_{TCE}(t=0)$	596 μM
TCE-to-ETH dechlorinators	$X_{D1}(t=0)$	10.21 mg VSS/l
TCE-to-cDCE dechlorinators	$X_{D2}(t=0)$	3.89 mg VSS/l

Table 5.2. Fixed and adjustable kinetic parameters implemented in the multistart strategy for the two dechlorinating species present in dechlorinating culture NTUA-M2.

Substrate	Parameter (units)	Type	Range of values	Feasible Area/Value	Reference
TCE, cDCE, VC	Maximum specific growth rate, $\mu_{max,j}$ (days^{-1})	Adjustable	0.01-4.30 [1]	0.01-4.30	(a)-(b)
TCE, cDCE, VC	Half-velocity coefficient, $K_{S,i-j}$ (μM)	Adjustable	0.05-602.00 [2]	0.05-602.00	(c)-(a)
VC	Inhibition coefficient, $K_{INH,cDCE}$ (μM)	Adjustable	0.05-602.00 [3]	0.05-602.00	-
TCE, cDCE, VC	Growth yield, Y_{D1} x10^{-3} (mg VSS/μmol)	Fixed	0.07-9.60	4.96	(d)-(e)
TCE	Growth yield, Y_{D2} x10^{-3} (mg VSS/μmol)	Fixed	2.80	2.80	(f)
-	Decay coefficient, b_j (days^{-1})	Fixed	0.024-0.090	0.024	(g)-(h)

[1]: Reported values of μ_{max} for TCE range from 0.33 days^{-1} (Cupples et al., 2004b) to 4.30 days^{-1} (Christ and Abriola, 2007), for cDCE from 0.04 days^{-1} (Yu and Semprini, 2004) to 0.46 days^{-1} (Cupples et al., 2004b), and for VC from 0.01 days^{-1} (Yu and Semprini, 2004) to 0.49 days^{-1} (Cupples et al., 2004b). In this approach μ_{max} is a microorganism-related parameter and, hence, the three subranges were merged into the one presented herein.

[2]: Reported values of $K_{S,i-j}$ for TCE range from 0.05 μM (Lee et al., 2004) to 12.40 μM (Cupples et al., 2004a), for cDCE from 0.54 μM (Fennell and Gossett, 1998) to 99.70 μM (Haest et al., 2010), and for VC from 2.60 μM (Haston and McCarty, 1999) to 602.00 μM (Yu and Semprini, 2004). The three subranges were merged into the one presented herein.

[3]: In the literature inhibition coefficients are typically set equal to the half-velocity coefficient for the respective chloroethene, i.e. $K_{INH,cDCE} = K_{S,cDCE-j}$. Consequently, the range of values for the inhibition coefficient was set equal to the range of values for the half-velocity coefficients.

[4]: Yield coefficients are demonstrated in mg VSS/μmol assuming that one *Dehalococcoides mccartyi* cell corresponds to 1.6 x 10^{-14} g of VSS (Cupples et al., 2003) and that 1 mg VSS corresponds to 0.5 mg protein. (a) Yu and Semprini (2004), (b) Christ and Abriola (2007), (c) Lee et al. (2004), (d) Schaffer et al. (2009), (e) Maymo-Gatell et al. (1997), (f) Scholz-Muramatsu et al. (1995), (g) Fennell and Gossett (1998), (h) Cupples et al. (2003)

5.4.1.4 The solutions of the parameter estimation problem

The multistart procedure described in Fig.5.3 yielded one global optimum solution for each multistart application. Both solutions simulated successfully all dechlorination steps (Fig. 5.4), if we compare model errors and experimental errors obtained by the duplicate batch tests. Particularly, the mean absolute simulation errors were: E_{TCE} was 9 μM, E_{cDCE} was 12 μM, E_{VC} was equal to 20 μM and E_{ETH} was equal to 17 μM. Based on the available duplicate measurements, the mean absolute errors of the measured concentrations were equal to $\hat{E}_{TCE}$=4 μM, $\hat{E}_{cDCE}$=6 μM, $\hat{E}_{VC}$=19 μM and $\hat{E}_{ETH}$=17 μM.

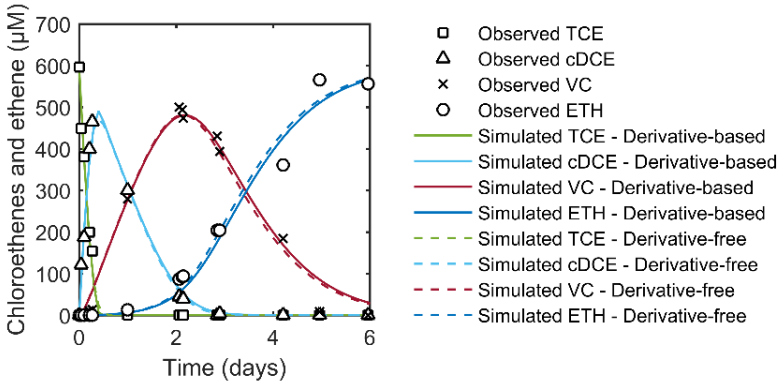

Fig. 5.4. Observed and simulated sequential dechlorination of TCE in dechlorinating culture NTUA-M2. Simulations correspond to the global optimum solutions obtained from the SQP-based multistart strategy (solid lines) and the GPS-based multistart strategy (dashed lines).

Parameter values estimated for both global optimum solutions were similar (Table 5.3). The only discrepancy lies in the half-velocity coefficients for TCE of TCE-to-ETH dechlorinators ($K_{S,TCE-D1}$). However, these differences are trivial from a functional point of view for this experimental conditions. In the global optimum solution deriving from the SQP-based approach partial dechlorinators consumed approximately 70% of the supplied TCE, whereas in the solution deriving from the GPS-based algorithm partial dechlorinators consumed 84% of TCE. Both solutions were close to what it was assumed to be the outcome of competition for TCE in the source culture. The behavior of the model was insensitive to changes in $K_{S,TCE-D1}$ values.

Table 5.3. Estimated kinetic parameters of dechlorinating culture NTUA-M2 estimated by the SQP-based multistart strategy and the GPS-based multistart strategy.

	TCE-to-cDCE dechlorinator		**TCE-to-ETH dechlorinator**				
	$\mu_{max,D2}$ ($days^{-1}$)	$K_{S,TCE-D2}$ (μM)	$\mu_{max,D1}$ ($days^{-1}$)	$K_{S,TCE-D1}$ (μM)	$K_{S,cDCE-D1}$ (μM)	$K_{S,VC-D1}$ (μM)	$K_{INH,cDCE}$ (μM)
SQP-based	2.71	602.00	0.18	0.07	153.32	474.32	20.89
GPS-based	2.73	561.00	0.18	54.95	131.92	454.78	22.36

The behavior of the two best-fit solutions diverged, when a numerical test with low TCE was performed. In this numerical test, a concentration of 50 μM TCE was initially supplied in the culture. At such low TCE concentrations, growth rates of dechlorinators are significantly lower than their maximum values (i.e. μ_{max} values), as they are severely limited by the availability of TCE. Thus, half-velocity coefficients become more relevant and TCE-to-ETH dechlorinators more efficient competitors than TCE-to-cDCE dechlorinators. Therefore, during the first day of the test, the simulated patterns of TCE consumption are dictated by the kinetic abilities of TCE-to-ETH dechlorinators (Fig. 5.5.a). In the SQP-based solution, TCE is sharply consumed within 2.4 hours, due to the low half-velocity coefficient for TCE ($K_{S,TCE-D1}$=0.07 μM). In the GPS-based solution, TCE is consumed in 10 hours, as TCE-to-ETH dechlorinators had a relatively lower affinity for TCE ($K_{S,TCE-D1}$=54.95 μM). Following the depletion of TCE, both solutions converged to the same simulated VC and ETH concentrations (Fig. 5.5b). This shift in the competition for TCE did not alter the consumption patterns of cDCE and VC, which were dictated by the

respective high half-velocity coefficients. Hence, despite the difference occurring under low TCE concentrations, we are confident that the overall behavior of the two best-fit solutions is similar in a large span of TCE concentrations. The bottleneck of dechlorination in this dechlorinating culture (i.e. cDCE and VC consumption) is described with similar accuracy.

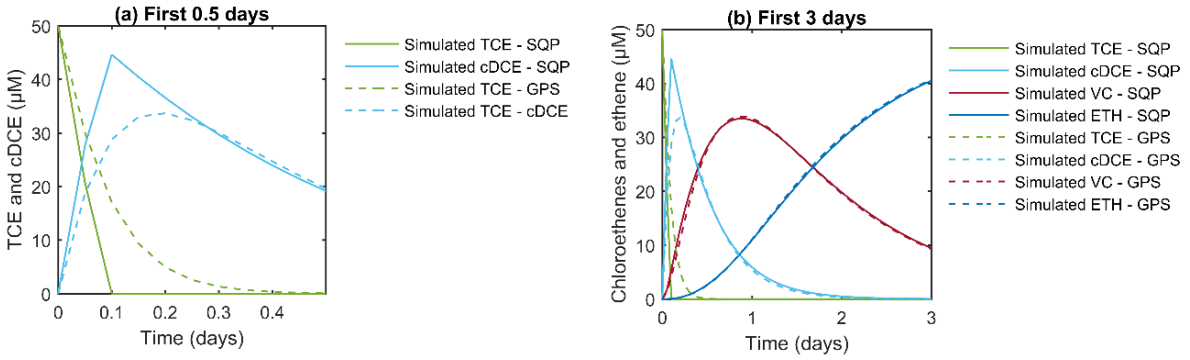

Fig. 5.5. Simulated sequential dechlorination of 50 μM TCE in dechlorinating culture NTUA-M2. Simulations correspond to the best-fit solutions obtained from the SQP-based multistart strategy (solid lines) and the GPS-based multistart strategy (dashed lines).

The SQP-based algorithm was superior in terms of efficiency. In this case, the generation of starting points stopped when the multistart strategy reached the maximum allowable number of starting points. From these 1000 starting points, the SQP-based approach estimated 487 distinctive local optimum solutions of the problem and required 45 minutes of computation time. According to Eq. (5.5), 952 local solutions exist in the problem. Conversely, in order to estimate 952 distinctive solutions an enormous amount of starting points is needed (several millions of starting points); this indicates that the Bayesian stopping criterion is useful in problems with few solutions. The relative volume of the observed regions of attraction was 76%, indicating that a significant portion of the existing regions of attraction has been searched. On the other hand, the GPS-based approach required 10 times greater computation time to perform 1000 local searches and estimate 472 local optimum solutions. The difference in the required computational time is mainly attributed to the low convergence rate of the GPS-based algorithm. The GPS-based algorithm necessitated an average of 200 iterations to converge to a local solution, whereas the SQP-based approach would typically converge within 10 iterations.

The best-fit solutions were in fact only marginally better than the remaining members of the family of good-fit local solutions. It is reasonable to claim that if the starting point of the best-fit solution had not been selected from the feasible parameter space, the best-fit solution would have been another member of the family of good-fit solutions. Hence, it is necessary to investigate how different these equivalently good fit solutions behave under different initial conditions.

All the local optimum solutions discovered from both multistart approaches were investigated thoroughly. Approximately 25% and 45% of the estimated local optimum solutions provided an acceptable fit to the data (green-shaded parts of the subplots in Fig. 5.6a and 5.6b) in the SQP-based and the GPS-based multistart algorithms, respectively. In these good-fit solutions, E_{TCE} was equal to 9 μM, E_{cDCE} ranged from 9 μM to 13 μM, E_{VC} ranged from 19 μM to 22 μM and E_{ETH} ranged from 14 to 18 μM. Parameter variability was significant mainly for half-velocity coefficients for TCE and cDCE (e.g. $K_{S,cDCE\text{-}D1}$ ranged from 73 μM to 270 μM) and to a lesser degree for

maximum specific growth rates (e.g. $\mu_{max,D1}$ ranged from 0.15 days^{-1} to 0.25 days^{-1}), half-velocity coefficients for VC ($K_{S,VC\text{-}D1}$ ranged from 356 μM to 580 μM) and inhibition coefficients ($K_{INH,cDCE}$ ranged from 17 μM to 27 μM). The functional characteristics of the solutions were, however, the same: (a) TCE-to-cDCE dechlorinators were fast-growers ($\mu_{max,D2}$ values were at least equal to 1.93 days^{-1}) and consumed most of the supplied TCE (from 68% to 88% of initial TCE), (b) TCE-to-ETH dechlorinators were slow growers ($\mu_{max,D2}$ values were at most equal to 0.25 days^{-1}) and grew mostly on the expense of cDCE and VC and (c) cDCE inhibited VC consumption, as indicated by the relatively low inhibition coefficients.

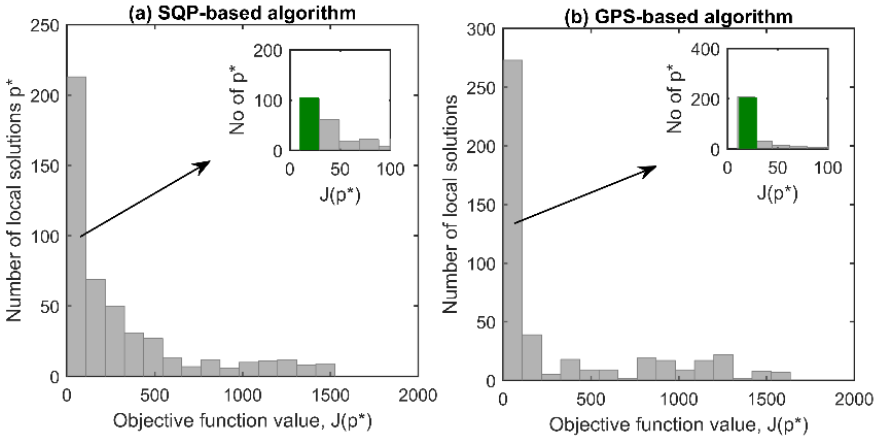

Fig. 5.6. Distribution of the objective function values of the 1000 local solutions obtained from (a) the SQP-based algorithm and (b) the GPS-based algorithm. Green-shaded local solutions in each subplot are those that produce a good fit to the experimental observations.

The family of good-fit solutions was tested under varying TCE and biomass concentrations, in order to investigate whether parameter variability results in a proportionately variable behavior, when the initial conditions deviate from those considered in the parameter estimation phase. We used only the good-fit solutions of the SQP-based algorithm, since parameter variability in the solutions of the GPS-based algorithm were practically the same as in the solutions of the SQP-based algorithm. Apart from the test used for parameter estimation (Fig. 5.7b), three numerical tests were performed: (a) a test with 50 μM TCE (Fig. 5.7a), (b) a test with 1800 μM TCE (Fig. 5.7c), and (c) a test with 1800 μM TCE and a dechlorinating community with biomass concentration four times sparser than the dechlorinating community used for parameter estimation (Fig. 5.7d); such differences in biomass concentrations could be encountered in contaminated subsurfaces given the observed spatial variability of dechlorinators (Dowideit et al., 2010). Numerical tests (b) and (c) are performed under the assumption that TCE is not inhibitory for dechlorinators at such concentrations.

The progress of dechlorination over time in these tests was assessed in an aggregate manner with the degree of dechlorination, *DoD*, which is calculated from the concentrations of chloroethenes and ETH as follows (Manoli et al., 2012):

$$DoD = \frac{S_{cDCE} + 2S_{VC} + 3S_{ETH}}{3\left(S_{TCE} + S_{cDCE} + S_{VC} + S_{ETH}\right)} \tag{5.14}$$

Parameter variability in the family of good-fit solutions resulted in relatively low variability in the model output at the lower TCE concentrations (Fig. 5.7a and 5.7b). At such low TCE concentrations, the consumption rates of chloroethenes were dictated by the specific affinity for each chloroethene, i.e. the ratio μ_{max}/K_S. In the good-fit solutions, the specific affinity for each chloroethene is not significantly different among the family of good-fit solutions, as μ_{max} values were correlated with K_S values; increased μ_{max} were coupled with increased K_S.

When tested under high TCE supply (Fig. 5.7c and 5.7d), good-fit solutions demonstrated moderate variability in the simulated degrees of dechlorination. At elevated chloroethene concentrations, μ_{max} values are dictating the simulated dechlorination rates and their variability contributed to the overall variability of the modeled degrees of dechlorination. In addition, when fewer dechlorinators were present in the culture and high chloroethene quantities were available (Fig. 5.7d), μ_{max} values became even more relevant in the simulated dechlorination rates and, thus, variability in the degree of dechlorination became larger. Considering the above, all the good-fit solutions can be trusted in a specific span of TCE concentrations (from low TCE to moderate TCE concentrations), but if the model is intended to be used in a predictive mode under elevated TCE concentrations or sparser biomass concentrations they are not equally adequate. At this case, extra empirical observations of the culture are needed to confirm which solution (contained within the light green areas of Fig. 5.7c and 5.7d) can capture the behavior of the culture.

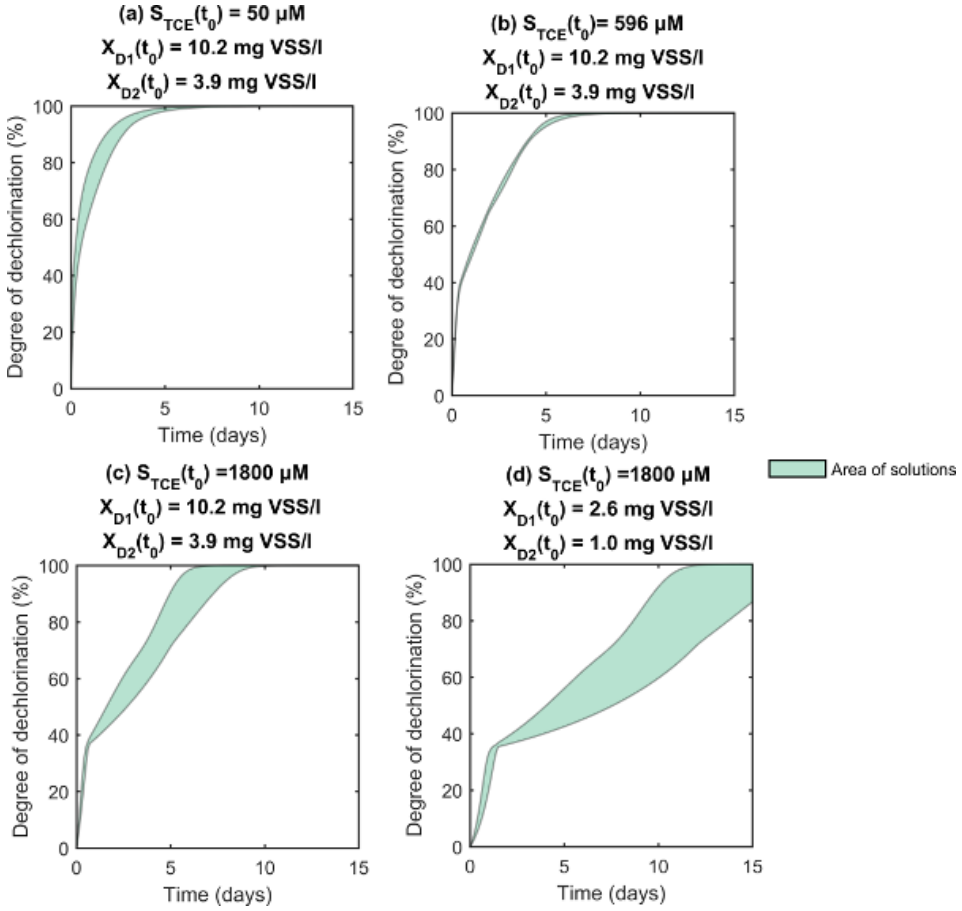

Fig. 5.7. Simulated degrees of dechlorination in dechlorinating culture NTUA-M2 of: (a) 50 μM TCE, (b) 596 μM TCE, (c) 1800 μM TCE and (d) 1800 μM with a four times less dense biomass concentration. Simulations correspond to the best-fit solutions obtained from the SQP-based multistart only.

The remaining local optimum solutions were trapped in regions of the parameter space that could not reproduce sufficiently the experimental observations. Hence, a choice of an improper starting point is probable. Parameters varied significantly in the family of poor-fit solutions. Distinctive behavior models were harbored in these solutions. For example, there were local solutions in which TCE-to-cDCE dechlorinators were outcompeted by TCE-to-ETH dechlorinators, consuming significantly less than 50% of the supplied TCE. In addition, there were local solutions in which competitive inhibition between cDCE and VC was insignificant ($K_{INH,cDCE}$ greater than 500 μM). Hence, the investigation of poor-fit solutions provided evidence that the behavior described by the best-fit solutions is probably an adequate approximation of the true behavior of the dechlorinating community.

5.5 Gaining confidence in the multistart strategy using models reported in the literature

In order to build trust in the application of the multistart strategy, the performance of both multistart algorithms (the SQP- and the GPS-based algorithm) was tested with Monod-type kinetic models reported in the literature. Two models were selected describing dechlorination at different TCE concentration levels. The first model was developed by Schäfer et al. (2009) and it was calibrated with data from batch tests performed with the commercial dechlorinating culture SDC-9 (Shaw Environmental, Inc., Lawrenceville, NJ). The levels of TCE in this culture remained relatively low (lower than 150 μM or 19.7 mg/l). The second model was developed by Yu and Semprini (2004) and tested against observations from batch tests performed with a culture enriched with material from Point Mugu Naval Weapon Facility, California (dechlorinating culture PM). In this case, a possible self-inhibition of chloroethenes was examined, as TCE concentrations were half of its solubility (initial TCE concentrations were equal to 3875 μM or 509 mg/l).

5.5.1 Dechlorinating culture SDC-9

5.5.1.1 Model development

The models developed by Schäfer et al. (2009) and herein are conceptually similar. The stepwise dechlorination of TCE, along with the growth of dechlorinators, is modeled using Monod-type kinetics. Competitive inhibition is included in the model, as the more chlorinated cDCE inhibits VC consumption. The only difference lies in the concept of biomass decay, since Schäfer et al. (2009) considered decay negligible in culture SDC-9 for the reported time period.

With respect to the mathematical formulation, the model proposed by Schäfer et al. (2009) is different to model developed herein in two ways. First, a single aggregate dechlorinating population is considered in their model (*j*=D1), performing each step of dechlorination. Second, μ_{max} values are substrate-specific parameters and, hence, they differ among the various chloroethenes. As a result, Eq.(5.10) should be calculated as follows:

$$r_{i-D1} = -\frac{\mu_{\max,i-D1}}{Y_{D1}} X_{D1} \frac{S_i}{K_{S,i-D1} + S_i} \tag{5.15}$$

in which $\mu_{max,i\text{-}D1}$ is the maximum specific growth rate of microorganism D1 for chloroethene *i* (*i*= TCE or cDCE). Likewise, Eq. (5.11) is now written as:

$$r_{VC-D1} = -\frac{\mu_{\max,VC-D1}}{Y_{D1}} X_{D1} \frac{S_{VC}}{K_{S,VC-D1}\left(1+\frac{S_{cDCE}}{K_{INH,cDCE}}\right)+S_{VC}} \quad (5.16)$$

5.5.1.2 Experimental information

Schäfer et al. (2009) performed five batch tests supplying SDC-9 culture with different chloroethene mixtures (four of them are shown in Fig 5.8). Particularly, the five batch tests were performed with: (a) only cDCE (80 μM), (b) VC (140 μM) and cDCE (80 μM), (c) only TCE (80 μM), (d) a mixture of TCE (4 μM), cDCE (6 μM) and VC (10 μM), and (e) only VC (data not available in the original paper). Lactate was used as an electron donor source and it was supplied in excess (lactate concentrations are not mentioned in Schäfer et al., 2009). Finally, for validation purposes, a duplicate batch experiment was performed with 60 μM TCE (Fig. 5.9), with one reactor used for measuring chloroethene concentrations and the other reactor for observing the growth of dechlorinators. The initial conditions of the batch tests performed with dechlorinating culture SDC-9 are given in Table 5.4.

Table 5.4. Initial chemical and biomass concentrations for the five batch tests performed by Schäfer et al. (2009) with dechlorinating culture SDC-9.

	Component			
	$S_{TCE}(t=0)$ [μM]	$S_{cDCE}(t=0)$ [μM]	$S_{VC}(t=0)$ [μM]	$X_{D1}(t=0)$ [cells/l]
cDCE-only	-	80	-	2.8×10^{10}
cDCE-VC mixture	-	140	80	2.8×10^{10}
TCE-only (a)	80	-	-	2.8×10^{10}
TCE-cDCE-VC mixture	4	6	10	3.3×10^{9}
TCE-only (b)	60	-	-	9.5×10^{7}

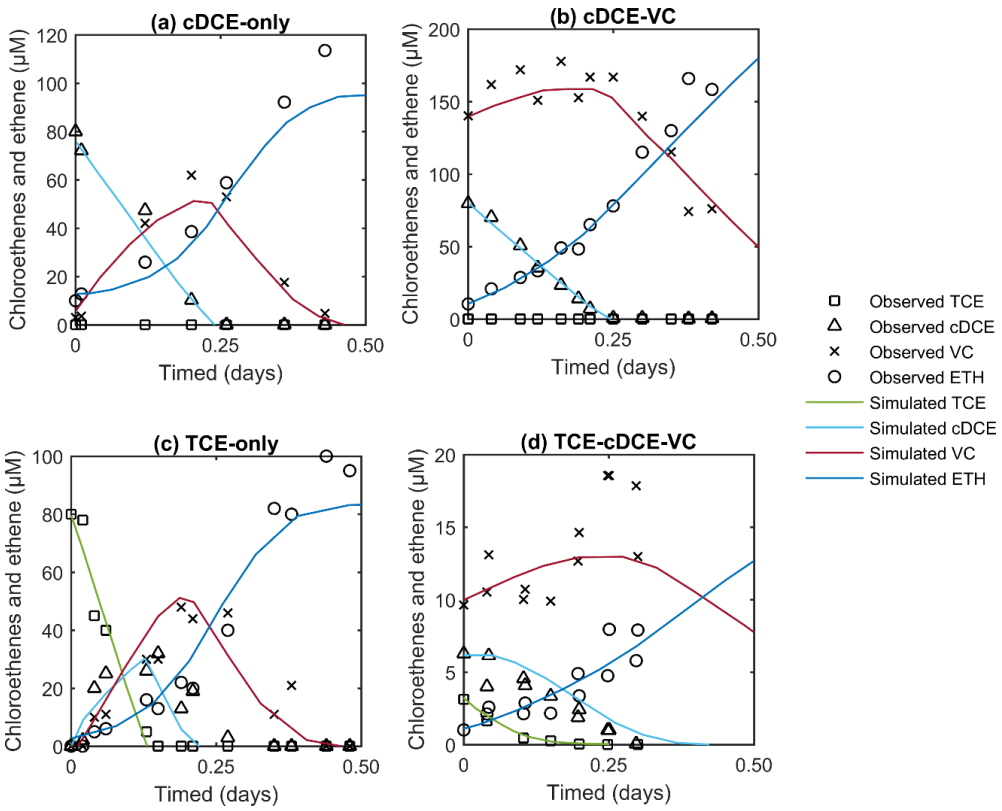

Fig. 5.8. Observed and simulated chloroethene degradation of (a) cDCE, (b) a mixture of cDCE and VC, (c) TCE, and (d) a mixture of TCE, cDCE and VC in dechlorinating culture SDC-9. Simulated concentrations correspond to the parameter set obtained from the sequential parameter estimation approach employed by Schäfer et al. (2009).

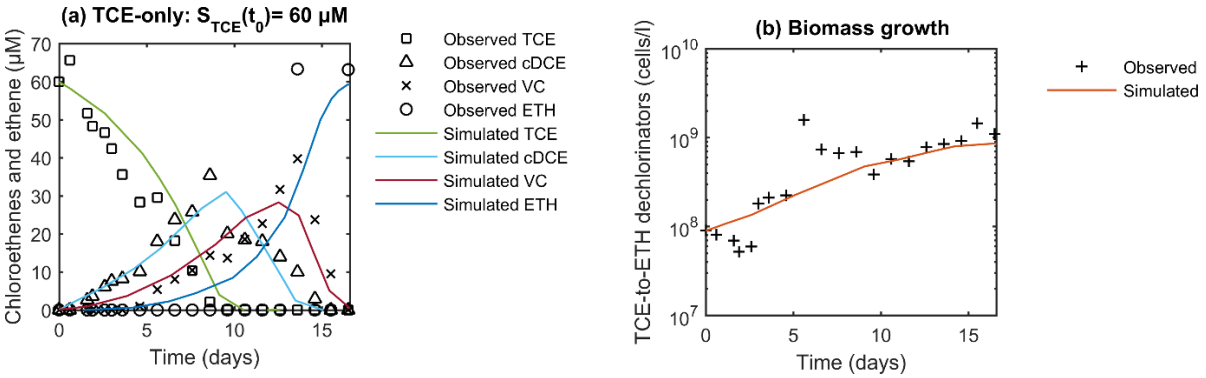

Fig. 5.9. Observed and simulated (a) sequential dechlorination of TCE and (b) growth of dechlorinators in dechlorinating culture SDC-9. Simulated concentrations correspond to the parameter set obtained from the sequential parameter estimation approach employed by Schäfer et al. (2009).

5.5.1.3 Sequential parameter estimation for culture SDC-9 by Schäfer et al. (2009)

Seven kinetic parameters were considered adjustable (the same number of parameters as in culture NTUA-M2) by Schäfer et al. (2009): $\mu_{max,i\text{-}D1}$ (3 parameters) $K_{S,i\text{-}D1}$ (3 kinetic parameters) and $K_{INH,cDCE}$ (1 parameter). The growth yield for dechlorinators was fixed (Y_{D1}= 4.4x10^6 cells/μmol Cl$^-$), since it was experimentally determined. Chloroethene and biomass concentrations were also measured initially for each batch test and, hence, they were considered fixed.

The parameter estimation technique employed by Schäfer et al. (2009) was based on the Microsoft Excel Solver® function and a nonlinear least-squares analysis, previously described by Cupples et al. (2004). The parameter estimation problem was solved five times (one time per batch test), so that only two parameters were simultaneously estimated. From the TCE-only experiment $\mu_{max,TCE-D1}$ and $K_{S,TCE-D1}$ were estimated, from the VC-only batch test $\mu_{max,VC-D1}$ and $K_{S,VC-D1}$ were estimated and, finally, from the cDCE-only experiment $\mu_{max,Cdce-D1}$ and $K_{S,VC-D1}$ were estimated. Competitive inhibition coefficient for cDCE was determined from the cDCE-VC batch experiment, while the TCE-cDCE-VC test was used to investigate for a possible cDCE inhibition by TCE (none was observed).

The parameter set obtained by the sequential parameter estimation process of Schäfer et al. (2009) described accurately the experimental observations (Fig. 5.8 and Fig. 5.9). Parameter estimates (Table 5.5) were on the same order of magnitude with previously reported values for different dechlorinating cultures, even if the optimization algorithm employed by Schäfer et al. (2009) let the adjustable parameters unconstrained in the parameter space. When compared to the kinetic parameters estimated for culture NTUA-M2, the most striking feature is the high affinity of TCE-to-ETH dechlorinators for VC demonstrated for culture SDC-9. The *Dehalococcoides mccartyi* strains present in culture SDC-9 will probably remove VC at higher rates compared to culture NTUA-M2.

Table 5.5. Estimated kinetic parameters of dechlorinating culture SDC-9 estimated by the sequential parameter estimation approach of Schäfer et al. (2009).

	Kinetic parameter		
	$\mu_{max,i-D1}$ ($days^{-1}$)	$K_{S,i-D1}$ (μM)	$K_{INH,i-D1}$ (μM)
TCE	0.14	3.20	-
cDCE	0.06	2.00	-
VC	0.15	14.00	5.20

5.5.1.4 Multistart parameter estimation strategy for culture SDC-9

The multistart strategy implemented for culture NTUA-M2 was also applied herein. Hence, all the unknown parameters were collectively fitted to the chemical concentrations of a single batch test performed with TCE. The batch test performed for validation purposes (Fig. 5.6) was preferred to the batch tests depicted in Fig. 5.5c or 5.5d, as it exhibited a better total chloroethene molar balance (the sum of chloroethenes was close to the initially supplied chloroethenes). Only chloroethene concentrations were considered from the available data. The available biomass concentrations were ignored, in order to solve a parameter estimation problem with input similar to what is considered as typical for dechlorination modeling; temporal microbial data are seldom accessible. Nonetheless, biomass concentration data from the batch test, as well as the batch tests performed with different initial chloroethene mixtures, were used for the cross-confirmation of the parameter sets considered as the global minimum solutions.

The vector of unknown parameters, $\boldsymbol{p}$, comprises seven kinetic parameters, $\mu_{max,i-D1}$ (3 parameters), $K_{S,i-D1}$ (3 parameters) and $K_{INH,cDCE}$ (1 parameter). The adjustable parameters were bounded by the range of values presented in Table 5.6. Note that Tables 5.2 and 5.6 are different, as in Table 5.6 the feasible areas of the parameter space for maximum specific growth rates and half-velocity coefficients are distinctive for each chloroethene, as Schäfer et al. (2009) postulated that both

parameters are chloroethene-specific. Finally, we fixed all the measured parameters of the problem. Growth yield for dechlorinators, initial chloroethene concentrations and initial biomass concentrations were fixed to their experimentally measured values.

Table 5.6. Fixed and adjustable kinetic parameters implemented in the multistart strategy for the aggregate dechlorinating community in culture SDC-9.

Substrate	Parameter (units)	Type	Range of values	Feasible Area/Value	Reference
TCE	Maximum specific growth rate, $\mu_{max,i\text{-}D1}$ (days^{-1})	Adjustable	0.33-4.30	0.33-4.30	(a)-(b)
cDCE	Maximum specific growth rate, $\mu_{max,i\text{-}D1}$ (days^{-1})	Adjustable	0.04-0.46	0.04-0.46	(c)-(a)
VC	Maximum specific growth rate, $\mu_{max,i\text{-}D1}$ (days^{-1})	Adjustable	0.01-0.49	0.01-0.49	(c)-(a)
TCE	Half-velocity coefficient, $K_{S,i\text{-}D1}$ (μM)	Adjustable	0.05-12.40	0.05-12.40	(d)-(e)
cDCE	Half-velocity coefficient, $K_{S,i\text{-}D1}$ (μM)	Adjustable	0.04-99.70	0.04-99.70	(f)-(g)
VC	Half-velocity coefficient, $K_{S,i\text{-}D1}$ (μM)	Adjustable	2.60-602.00	2.60-602.00	(h)-(c)
VC	Inhibition coefficient, $K_{INH,cDCE}$ (μM)	Adjustable	0.04-99.70 [1]	0.04-99.70	(f)-(g)
TCE, cDCE, VC	Growth yield, Y_{D1}x10^7 (cells/μmol)	Fixed	0.44-60.00 [2]	0.44	(h)-(i)

[1]: In the literature inhibition coefficients are typically set equal to the half-velocity coefficient for the respective chloroethene, i.e. $K_{INH,cDCE} = K_{S,cDCE\text{-}f}$. Consequently, the range of values for the inhibition coefficient was set equal to the range of values for the half-velocity coefficients.
[2]: Yield coefficients are reported in cells/μmol assuming that one *Dehalococcoides mccartyi* cell corresponds to 1.6 x 10^{-14} g of VSS (Cupples et al., 2003) and that 1 mg VSS corresponds to 0.5 mg protein.
(a) Cupples et al. (2004b), (b) Christ and Abriola (2007), (c) Yu and Semprini (2004), (d) Lee et al. (2004), (e) Cupples et al. (2004a), (f) Fennell and Gossett (1998), (g) Haest et al. (2010), (h) Schäfer et al. (2009), (i) Maymó-Gatell et al. (1997)

Both global optimum solutions described chloroethene concentrations with accuracy similar to the one achieved by Schäfer et al. (2009) (compare Fig. 5.10 to Fig. 5.9). Mean absolute simulation errors were approximately equal to 4.0 μM for TCE, 2.4 μM for cDCE, 2.9 μM for VC and 10.0 μM for ETH. Note that the lower simulation errors compared to the errors in NTUA-M2 should be attributed to the lower chloroethene concentrations of the batch test performed with culture SDC-9. Biomass concentrations were also reproduced adequately (Fig. 5.10b). Both simulations predicted that dechlorinators would be almost an order of magnitude denser at the end of the batch test.

Kinetic parameters obtained from the best-fit solutions agreed to those estimated by Schäfer et al. (2009), apart from the half-velocity coefficient for TCE and the VC-related parameters (Table 5.7). The four-fold greater half-velocity coefficients for TCE in our solutions resulted in slightly lower TCE consumption rates, which were closer to the actual consumption rate of TCE. With regard to VC-related parameters, we estimated lower $\mu_{max,VC\text{-}D1}$ values, which were accompanied by lower $K_{S,VC\text{-}D1}$ values. Yet, the consumption rates of VC were unaffected, as the impact of the lower growth rates was offset by the higher affinity for VC consumption. This interchange of maximum specific growth rates and half-velocity coefficients indicates the parameter correlation issue, which

has been reported in the literature as a significant reason for the lack of unique and reliable parameter sets in Monod-type kinetic models (Liu and Zachara, 2001).

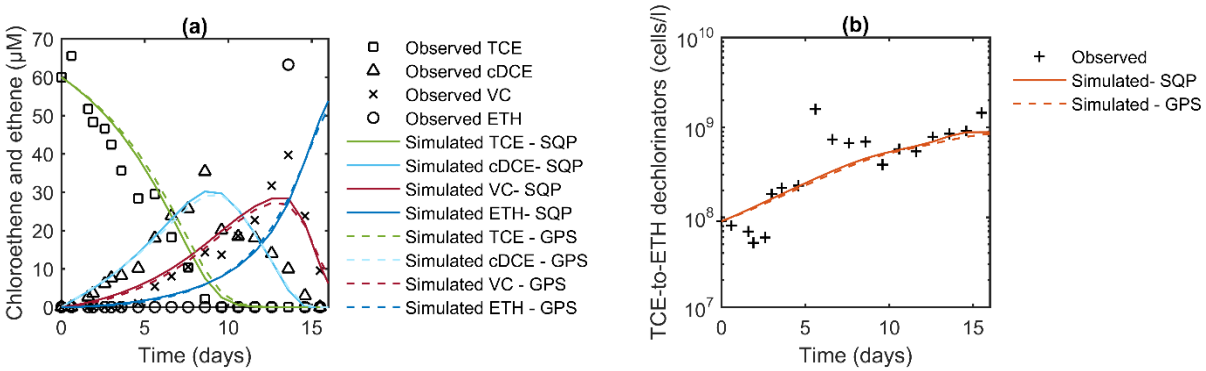

Fig. 5.10. Observed and simulated (a) sequential dechlorination of TCE and (b) growth of dechlorinators in dechlorinating culture SDC-9. Simulations were performed with parameter sets obtained from the best-fit solutions obtained by the SQP-based multistart strategy (solid lines) and the GPS-based multistart strategy (dashed lines).

Table 5.7. Estimated kinetic parameters of dechlorinating culture SDC-9 estimated by the SQP-based and the GPS-based multistart algorithms.

	TCE		**cDCE**		**VC**		
	$\mu_{max,i\text{-}D1}$ (days^{-1})	$K_{S,i\text{-}D1}$ (μM)	$\mu_{max,i\text{-}D1}$ (days^{-1})	$K_{S,i\text{-}D1}$ (μM)	$\mu_{max,i\text{-}D1}$ (days^{-1})	$K_{S,i\text{-}D1}$ (μM)	$K_{INH,i\text{-}D1}$ (μM)
SQP-based multistart	0.17	12.40	0.05	0.70	0.08	2.60	1.50
GPS-based multistart	0.17	12.40	0.06	2.50	0.08	6.30	4.56
Schäfer et al. (2009)	0.14	3.20	0.06	2.00	0.15	14.00	5.20

In terms of efficiency, the SQP-based approach was found superior again. Both multistart algorithms ran for 1000 starting points due to the large number of existing local minima. The SQP-based algorithm estimated 184 local solutions and required 46 minutes of computation time, while the GPS-based algorithm estimated 125 local solutions in almost 10 hours. Nevertheless, in both cases the estimated total relative volume of the observed regions of attraction was greater than 97%, indicating that practically all regions of attraction had been investigated. The large difference in the required computation time is attributed again to the low convergence rates exhibited by the GPS-based algorithm, which required at least 200 iterations per local search to reach a local solution.

In both multistart applications, we were close to finding all the existing local solutions. For example, based on Eq. (5.5) and the results of the SQP-based algorithm, the Bayesian estimate of the total number of local solutions of the problem is equal to 226. Therefore, we re-implemented the SQP-based multistart algorithm, without using a maximum allowable number of local searches. This time the algorithm was terminated only when all local solutions were discovered. As a result, the algorithm required nearly a day of computer time, generated 27,251 starting points and discovered 192 distinctive local solutions. The global solution (i.e. the "true" global solution) was

slightly different than the best-fit solution derived from the 1000 starting points (Table 5.8); the TCE-related parameters were close to the parameters reported by Schäfer et al. (2009). In terms of simulation errors, the differences were trivial. Hence, the extra computational time required for estimating a true global solution was not accompanied by a proportionately improved fit to the data.

Table 5.8. Estimated kinetic parameters of dechlorinating culture SDC-9 estimated by the SQP-based multistart algorithm for 1000 starting points ("best-fit" solution) and 27,251 starting points ("true" global solution).

	TCE		cDCE		VC		
	$\mu_{max,i\text{-}D1}$ ($days^{-1}$)	$K_{S,i\text{-}D1}$ (μM)	$\mu_{max,i\text{-}D1}$ ($days^{-1}$)	$K_{S,i\text{-}D1}$ (μM)	$\mu_{max,i\text{-}D1}$ ($days^{-1}$)	$K_{S,i\text{-}D1}$ (μM)	$K_{INH,i\text{-}D1}$ (μM)
"Best-fit" solution	0.17	12.40	0.05	0.70	0.08	2.60	1.50
"True" global solution	0.14	2.66	0.05	0.60	0.07	2.60	1.88

The two best-fit solutions were tested against the four batch tests performed with culture SDC-9 under varying initial chloroethene and biomass concentrations. The two solutions reproduced the four batch tests with adequate accuracy, as shown in Fig. 5.11. The relative performance of the two multistart-based solutions was still indistinguishable. Compared to the fit achieved by the approach of Schäfer et al. (2009) (compare Fig. 5.8 to Fig.5.11), our parameter sets produced equivalent results, as well. Parameter variability in multistart-derived solutions was not accompanied by variability in the model responses, even when tested under different initial conditions. Hence, both solutions are functionally similar approximations of the true behavior of dechlorinating culture SDC-9.

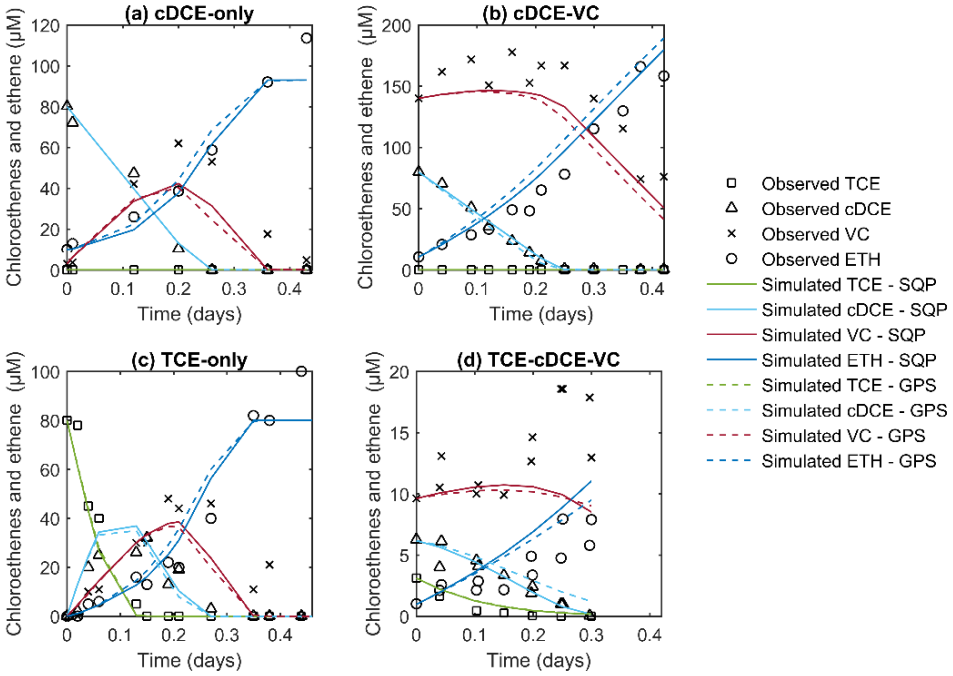

Fig. 5.11. Observed and simulated chloroethene degradation of (a) cDCE, (b) a mixture of cDCE and VC, (c) TCE, and (d) a mixture of TCE, cDCE and VC in dechlorinating culture SDC-9. Simulations were performed with parameter sets obtained from the best-fit solutions obtained by the SQP-based multistart strategy (solid lines) and the GPS-based multistart strategy (dashed lines).

As in culture NTUA-M2, all the local solutions of the problem were investigated thoroughly. From the 184 and 125 local solutions, approximately half of them demonstrated mean absolute simulation errors like those of the best-fit solutions: E_{TCE} ranged from 3.0 μM to 5.7 μM, E_{cDCE} ranged from 2.0 μM to 2.8 μM, E_{VC} ranged from 2.7 μM to 4.0 μM and E_{ETH} ranged from 8.5 to 10.0 μM. In these solutions, differences occurred due to the correlation of VC-related parameters. In the 184 solutions from the SQP-based algorithm, $\mu_{max,VC\text{-}D1}$ values varied between 0.07 days^{-1} and 0.46 days^{-1} and were inversely correlated with $K_{S,VC\text{-}D1}$ values, which in turn varied between 2.6 μM and 127 μM.

The significant variability of VC-related parameters in the family of good-fit solutions was coupled with different model responses only when elevated chloroethene concentrations were present in the culture (Fig. 5.8b and 5.12b). For the test with high chloroethene concentrations the corresponding consumption rates were controlled by the maximum specific growth rates. Thus, the discrepancies in $\mu_{max,VC\text{-}D1}$ values was the reason for the differentiated behavior of the good-fit solutions. In fact, only three solutions reproduced the experimental data sufficiently apart from the best-fit solutions. Finally, under low chloroethene concentrations, when the specific affinity for VC is critical, all solutions were again more or less equivalent (Fig. 5.12a, 5.12c and 5.12d).

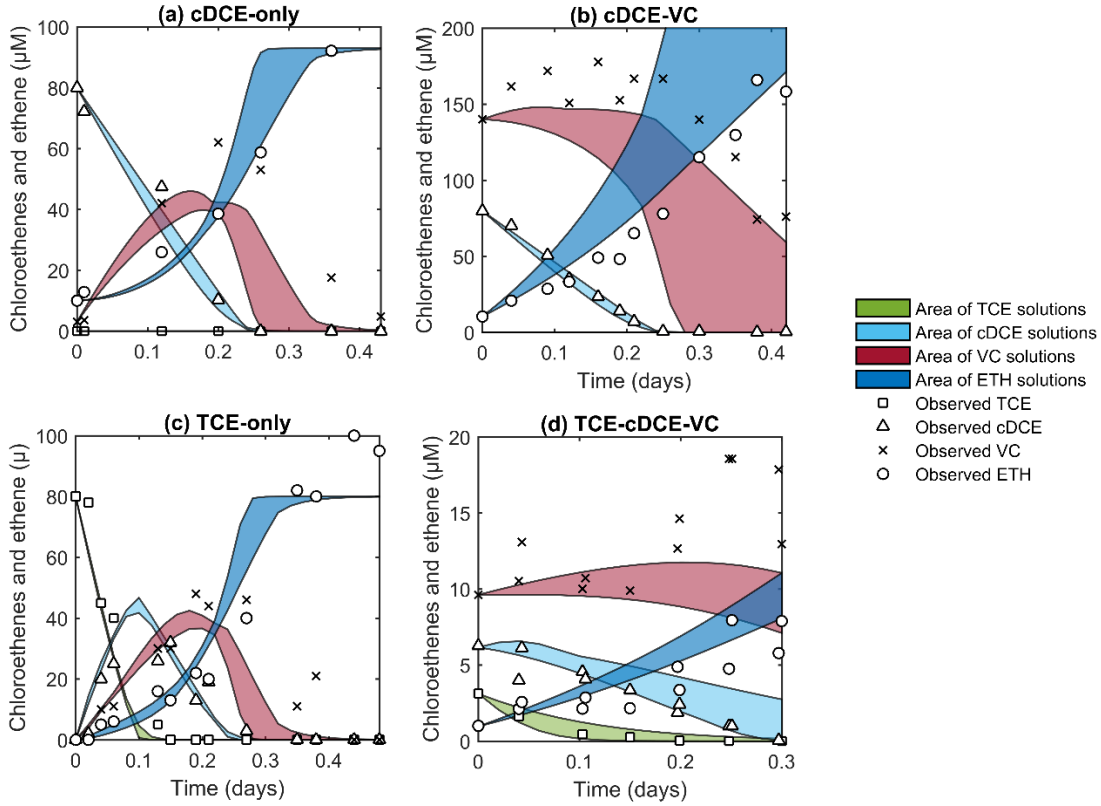

Fig. 5.12. Observed and simulated chloroethene degradation of (a) cDCE, (b) a mixture of cDCE and VC, (c) TCE, and (d) a mixture of TCE, cDCE and VC in dechlorinating culture SDC-9. Simulations were performed with parameter sets obtained from the good-fit solutions obtained by the SQP-based multistart strategy. Data points from Schäfer et al. (2009).

5.5.2 Dechlorinating culture PM

5.5.2.1 Model development

Conceptually, the model developed by Yu and Semprini (2004) describes PCE and TCE dechlorination, employing competitive inhibition and Haldane inhibition kinetics. Haldane inhibition kinetics were used to describe the self-inhibition of TCE, cDCE or VC dechlorination caused by their own high concentrations. In their modeling approach, Yu and Semprini (2004) considered a single aggregate dechlorinating population, growing from each step of the sequential dechlorination of PCE or TCE, apart from VC; they assumed that culture PM consumed VC commetabolically. The existence of a dechlorinating population was backed by molecular analysis, which indicated that culture PM was enriched with *Dehalococcoides mccartyi* bacteria (a later work on PM culture indicated that at least three strains were present, belonging to the Pinellas and the Cornell group of strains; Berggren et al., 2013).

The mathematical formulation of the model proposed by Yu and Semprini (2004) is like the formulation employed by Schäfer et al. (2009), with the addition of Haldane inhibition coefficients. The only discrepancy is found in the competitive inhibition coefficients ($K_{INH,i}$), which were set equal to the half-velocity coefficients of the more chlorinated compounds ($K_{S,(i-1)}$) in the model of Yu and Semprini (2004). This assumption reduced the number of parameters of the problem and was supported by previous work on culture PM performed by Yu (2003). Thus, chloroethene consumption rates were estimated as follows:

$$r_{PCE-D1} = -\frac{\mu_{\max,PCE-D1}}{Y_{D1}} X_{D1} \frac{S_{PCE}}{K_{S,PCE-D1} + S_{PCE}} \tag{5.17}$$

$$r_{i-D1} = -\frac{\mu_{\max,i-D1}}{Y_{D1}} X_j \frac{S_i}{K_{S,i-D1}\left(1+\frac{S_{(i-1)}}{K_{S,(i-1)-D1}}\right) + S_i\left(1+\frac{S_i}{K_{H,i}}\right)} \tag{5.18}$$

where $K_{H,i}$ is the Haldane inhibition coefficient (μM) and i =TCE, cDCE or VC. When $K_{H,i}$ is significantly greater than S_i, then Eq. (5.17) is practically a competitive inhibition model similar to the two previously described models. Finally, biomass growth was modeled by the following equation:

$$\frac{dX_{D1}}{dt} = \sum_i (-Y_{D1} \cdot r_{i-D1}) - \left(b_{D1} \cdot X_{D1}\right) \tag{5.19}$$

in which i = PCE, TCE or CDCE, as Yu and Semprini (2004) assumed that culture PM consumed VC commetabolically.

5.5.2.2 Experimental information

Four batch tests were performed with dechlorinating culture PM (Table 5.9 and Fig. 5.13): (a) three batch tests were performed using PCE with concentrations ranging from 92 μM (or 15 mg/l) to 1128 μM (or 187 mg/l), which is higher than PCE solubility limit at 25° C(900 μM or 150 mg/l), and (b) one batch test where TCE was supplied with a concentration equal to 3875 μM (or 509 mg/l), which is almost half of TCE solubility in water at 25° C (Fig. 5.13d). In the batch test where PCE concentration exceeded its solubility limit, simulations were performed using the total mass added to yield a computed aqueous concentration of 1128 μM. H_2 and 1-butanol were used as

electron donors and were supplied in excess (concentrations were not mentioned in the Yu and Semprini, 2004). The initial measured cell concentration of the culture on a protein basis was 35 mg protein/l and it was used as the initial biomass concentration of the dechlorinators (X_{D1}=35 mg protein/l, which is a value corresponding to high-density dechlorinating cultures).

Table 5.9. Initial chemical and biomass concentrations for the four batch tests performed with dechlorinating culture PM.

	Component		
	$S_{PCE}(t=0)$ [µM]	$S_{TCE}(t=0)$ [µM]	$X_{D1}(t=0)$ [mg protein/l]
PCE – low	92	-	25
PCE – medium	282	-	34
PCE – high	1128 [1]	-	34
TCE – high	-	3875	35

[1]: Simulations were performed using the total mass added to yield a computed aqueous concentration of 1128 µM.

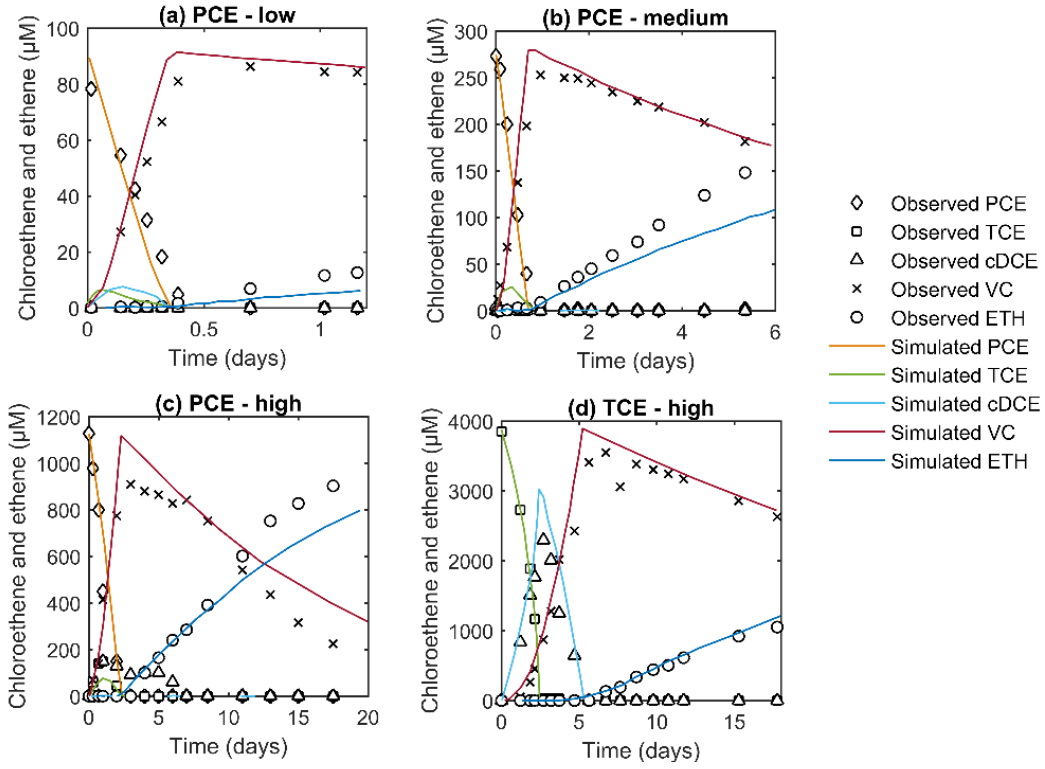

Fig. 5.13. Observed and simulated sequential dechlorination of PCE (a to c) and TCE (d) in dechlorinating culture PM. Simulations were performed with the parameter set obtained from the parameter estimation approach of Yu and Semprini (2004).

5.5.2.3 Trial-and-error parameter estimation by Yu and Semprini (2004)

Yu and Semprini (2004) estimated the parameters of the kinetic model through a trial-and-error analysis comparing the model output with the experimental observations obtained from batch tests performed with culture PM. The values of $\mu_{max,i-j}$, $K_{S,i-j}$ and $K_{H,i}$ were estimated from this heuristic curve-fitting approach. The growth yield and the decay coefficient were fixed to literature reported values: Y_{D1} = 0.006 mg protein/l and b_{D1} = 0.024 days^{-1}.

Results reported by Yu and Semprini (2004) indicate that the Haldane inhibition model and the estimated parameters described sufficiently chloroethene consumption at high concentrations (Fig. 5.13). TCE was self-inhibited by its high concentrations, as indicated by the low $K_{H,TCE}$ values (Table 5.10). The consumption of cDCE and VC was dictated solely by the kinetic properties of dechlorinators; according to the model results, self-inhibition could be neglected, as $K_{H,cDCE}$ and $K_{H,VC}$ were two-fold greater than the respective maximum chloroethene concentrations. Finally, VC-related parameters were extremely unfavorable for dechlorinators in culture PM. Dechlorinators could grow slowly and demonstrated with a low affinity for VC. The VC-related parameters were in the range of values reported for *Dehalococcoides mccartyi* strain 195 (Fennell and Gossett, 1998), which grows commetabolically on VC. Compared to the VC-related parameters estimated for culture NTUA-M2, even if the half-velocity coefficients are comparable, the maximum specific growth rate of dechlorinators is 18 times higher compared to the maximum specific growth rate of culture PM. Hence, this difference implies that VC dechlorination in culture NTUA-M2 is commetabolic.

Table 5.10. Estimated kinetic parameters for dechlorinating culture PM estimated by the heuristic parameter estimation approach of Yu and Semprini (2004).

	Parameter		
	$\mu_{max,i\text{-}D1}$ **(days^{-1})**	$K_{S,i\text{-}D1}$ **(μM)**	$K_{H,i}$ **(μM)**
PCE	0.08	3.86	-
TCE	0.74	2.76	900
cDCE	0.13	1.90	6000
VC	0.01	602.00	7000

5.5.2.4 Multistart parameter estimation strategy for culture PM

Similar to the previous multistart applications, all unknown parameters were collectively fitted to the observations from the batch test performed with TCE (Fig. 5.13d). The PCE-fed batch reactors were used for cross-confirmation purposes only.

The set of unknown parameters comprised $\mu_{max,i\text{-}D1}$, $K_{S,i\text{-}D1}$ and $K_{H,i\text{-}D1}$ (nine parameters, two more than the problems of culture NTUA-M2 and SDC-9). The adjustable parameters were bounded by the range of reported values presented in Table 5.6. In the absence of literature reported values, bounding $K_{H,i\text{-}D1}$ was not feasible and reasonable assumptions were made. Thus, $K_{H,i\text{-}D1}$ ranged from 500 μM to 10,000 μM. Only two kinetic parameters were considered fixed. The growth yield and the decay coefficient were fixed to the values used by Yu and Semprini (2004), i.e. Y_{D1} = 0.006 mg protein/l and b_{D1} = 0.024 days^{-1}. Finally, the initial biomass concentration for the aggregate dechlorinating community was equal to X_{D1}=35 mg protein/l.

The best-fit solutions of both multistart applications reproduced the observations of the batch test adequately (Fig. 5.14). Their mean absolute simulation errors were similar and equal to 14 μM for TCE, 40 μM for cDCE, 290 μM for VC and 18 μM for ETH. Simulation errors for VC are almost an order of magnitude greater than the respective errors for culture NTUA-M2 and SDC-9. This is a result of the large VC concentrations encountered in this batch test (almost an order of magnitude greater than the VC concentrations in NTUA-M2 and SDC-9 as well).

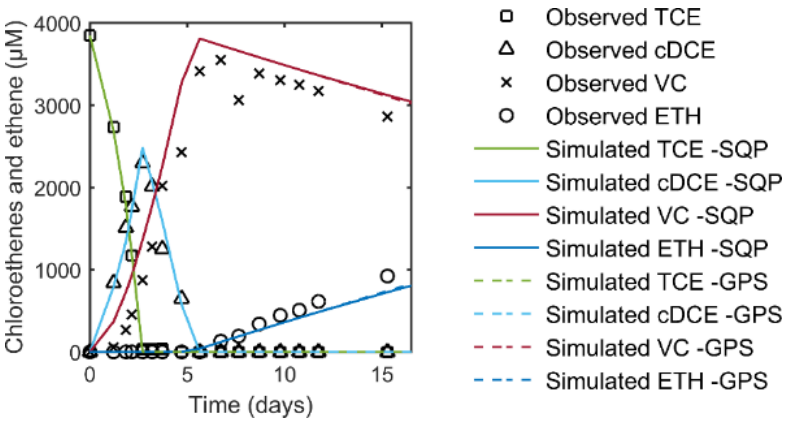

Fig. 5.14. Observed and simulated sequential dechlorination of TCE in culture PM. Simulations were performed with parameter sets obtained from the best-fit solutions obtained by the SQP-based multistart strategy (solid lines) and the GPS-based multistart strategy (dashed lines).

In terms of efficiency, the multistart approach employing the SQP search routine was again preferable in this problem as well. It ran for 1000 starting points, estimated 289 distinctive local solutions and required 2.6 hours of computation time. On the other hand, the GPS-based algorithm estimated 320 local solutions after 1000 local searches, which required 27 hours of computation time. The GPS-based approach demonstrated significantly lower convergence rates, as an average of 700 iterations per local search were needed for the estimation of a local solution. Even if both multistart approaches failed to locate all the local minima of the problem, the estimated total relative volume of the observed regions of attraction were greater than 90%. Thus, significant parts of the regions of attractions were investigated.

The multistart-obtained parameter sets are different to the parameters reported by Yu and Semprini (2004), except from the cDCE-related parameters (Table 5.11). With respect to TCE consumption, both solutions provided parameters distinctive to those specified by Yu and Semprini (2004). Particularly, in both best-fit solutions, low consumption rates of TCE were a result of low $\mu_{max,TCE\text{-}D1}$ values and high $K_{S,TCE\text{-}D1}$ values (i.e. low affinity for TCE). Haldane inhibition coefficients were two times greater than the coefficient specified by Yu and Semprini (2004), indicating a weaker self-inhibition of TCE. The multistart-obtained self-inhibition coefficients are closer to the findings of Yang and McCarty (2000), who reported that TCE was degraded to concentrations up to 2260 μM without apparent self-inhibition. With respect to VC-related parameters, in the results obtained by the GPS-based multistart approach, incomplete dechlorination of VC was attributed to the impact of self-inhibition, as indicated by the low $K_{I\text{-}VC}$ values. Models with diverse functionalities were obtained by the multistart strategy. Thus, conclusions on the underlying mechanisms drawn exclusively on parameter estimates may be erroneous, unless they are cross-confirmed by supplementary experimental observations.

Table 5.11. Estimated kinetic parameters for dechlorinating culture PM estimated by the SQP-based and the GPS-based multistart algorithms.

	TCE			cDCE			VC		
	$\mu_{max,i\text{-}D1}$ (days^{-1})	$K_{S,i\text{-}D1}$ (μM)	$K_{H,i\text{-}D1}$ (μM)	$\mu_{max,i\text{-}D1}$ (days^{-1})	$K_{S,i\text{-}D1}$ (μM)	$K_{H,i\text{-}D1}$ (μM)	$\mu_{max,i\text{-}D1}$ (days^{-1})	$K_{S,i\text{-}D1}$ (μM)	$K_{H,i\text{-}D1}$ (μM)
SQP-based multistart	0.40	11.69	1929	0.10	1.28	8961	0.01	602	8532
GPS-based multistart	0.42	8.57	1789	0.10	0.98	8995	0.03	465	1124
Yu and Semprini (2004)	0.74	2.76	900	0.13	1.90	6000	0.01	602	7000

For the sake of completeness, the PCE-fed batch tests were simulated using the PCE-related parameters estimated by Yu and Semprini (2004) (see Table 5.10). As indicated by Fig. 5.15, both best-fit solutions reproduced all the batch tests sufficiently and in a comparable accuracy to the parameter set of Yu and Semprini (2004). The relative performance of the two best-fit solutions changed at the two batch tests with elevated PCE concentrations. Yet, simulation errors were still comparable and, thus, it was still hard to discriminate among the two multistart-provided solutions and the solution given by Yu and Semprini (2004).

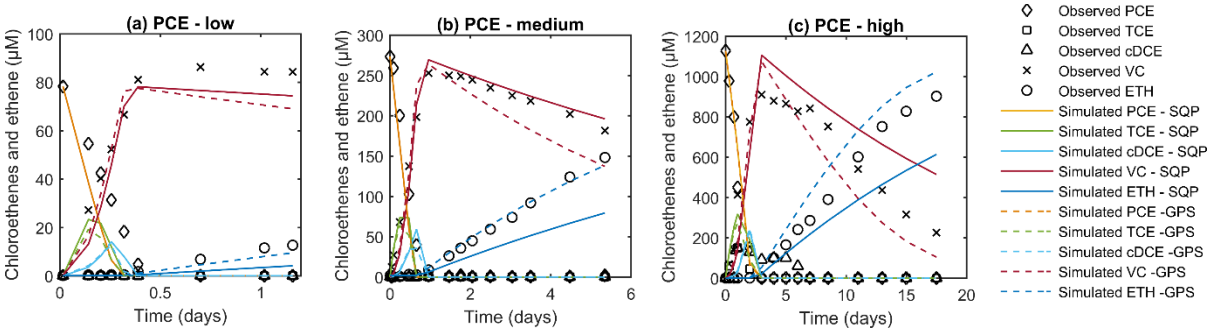

Fig. 5.15. Observed and simulated sequential dechlorination of PCE in culture PM. Simulations were performed with parameter sets obtained from the best-fit solutions obtained by the SQP-based multistart strategy (solid lines) and the GPS-based multistart strategy (dashed lines).

It was possible to discriminate among the solutions, when a numerical test with low TCE initial concentration was used ($S_{TCE}(t_0)$ =300 μM). At such low chloroethene concentrations, Haldane inhibition is irrelevant and, hence, differences in the remaining kinetic properties of dechlorinators can be highlighted. Indeed, the GPS solution was significantly different than the solution of Yu and Semprini (2004) and the solution of the SQP-based multistart approach: due to its greater μ_{max} value for VC, the GPS-based solution predicted a faster VC removal compared to the solution of Yu and Semprini (Fig. 5.16). On the other hand, the SQP-based solution had a similar output to the one predicted by Yu and Semprini (2004). All solutions were completely equivalent during the first two steps of dechlorination, i.e. TCE and cDCE consumption. Therefore, differences in TCE-related parameters cannot be distinguished under these initial conditions.

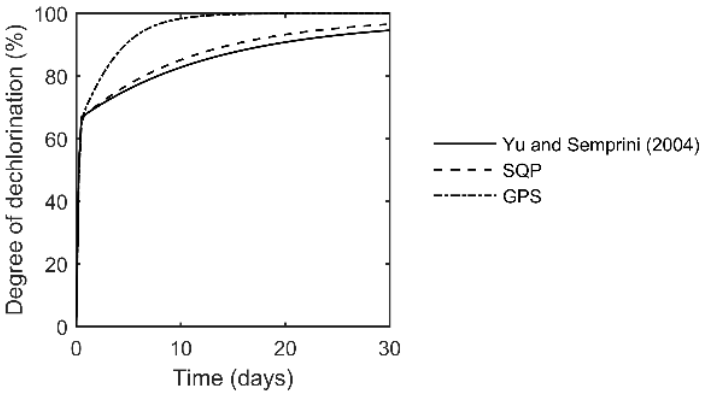

Fig. 5.16. Simulated degrees of dechlorination in dechlorinating culture PM fed with 300 μM TCE. Simulations correspond to the best-fit solutions of the two multistart algorithms and the solution of Yu and Semprini (2004).

Trusting that the solution of Yu and Semprini (2004) is a good approximation of the true behavior of culture PM, a search within the good-fit solutions of the GPS-based algorithm was performed in order search for solutions with behavior similar to the one of Yu and Semprini (2004). Almost 30% of the local optimum solutions demonstrated mean absolute simulation errors comparable to those of the best-fit solution. For the good-fit solutions, E_{TCE} ranged from 18 μM to 22 μM, E_{cDCE} ranged from 40 μM to 70 μM, E_{VC} ranged from 290 μM to 330 μM and E_{ETH} ranged from 12 to 20 μM. In these solutions, $K_{H\text{-}VC}$ values varied from 500 μM, indicating severe self-inhibition of VC should be considered to 9000 μM, indicating that self-inhibition could have been neglected. In these solutions, the impact of self-inhibition was compensated by combinations of the maximum specific growth rates and half-velocity coefficients. The good-fit solutions were also tested in a numerical experiment performed with a moderate initial TCE concentration, $S_{TCE}(t_0)$ = 300 μM. In the family of good-fit solutions of the GPS-based algorithm (Fig. 5. 17b), there were solutions that were closer to the solution of Yu and Semprini (2004). Conversely, in the SQP-based solutions, there were many parameter sets that deviated from the best-fit solution when tested with low TCE concentrations (Fig. 5. 17a).

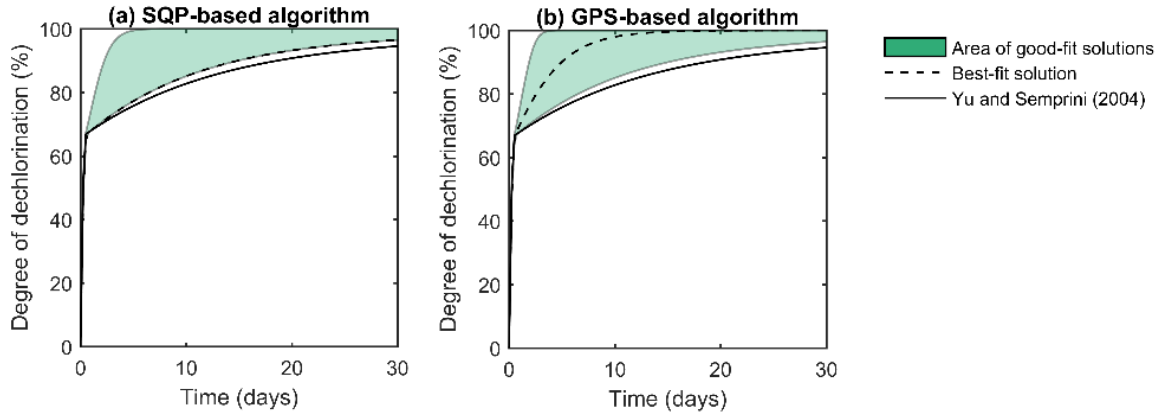

Fig. 5.17. Simulated degrees of dechlorination in dechlorinating culture PM fed with 300 μM TCE. Simulations correspond to the solution of Yu and Semprini (2004) and the good-fit solutions of (a) the SQP-based multistart algorithm and (b) the GPS-based multistart algorithm.

5.6 Concluding remarks

In this chapter a multistart optimization strategy was designed for the estimation of parameters employed in Monod-type kinetic models describing dechlorination. The multistart optimization strategy was tested on three kinetic models considering dechlorination and the growth of dechlorinators, with distinctive mathematical formulations under varying TCE concentrations: (a) a simple version of the model developed in Chapter 4, (b) the competitive inhibition model of Schäfer et al. (2009), and (c) the competitive and self-inhibition model developed by Yu and Semprini (2004). Two local search routines were examined, a derivative-based routine (an SQP method) and a derivative-free routine (a GPS method).

The application of the multistart strategy identified adequate models of dechlorinating cultures NTUA-M2, SDC-9 and PM, without being trapped in areas of the parameter space that contained erroneous local solutions.

Based on the application of the multistart approach in the three kinetic models, the SQP derivative-based routine was found superior in terms of efficiency compared to the GPS derivative-free routine. Nonetheless, both local search routines were equally reliable and produced solutions with good quality of fit.

The use of the proposed Bayesian stopping criterion was ineffectual and the multistart algorithm was terminated when the maximum allowable number of iterations was reached (i.e. 1000 starting points). Due to parameter correlation, the objective function is significantly rugged having, thus, many local solutions. The computational effort to find the true global minimum is rather heavy and not accompanied by a clearly better fit of the model output to the experimental observations. Considering the above, in the more complicated models of the following chapters, the SQP-based multistart algorithm will be employed for a workable maximum number of local searches.

Investigating large areas of the parameter space provided confidence that the conceptualization embodied in the best-fit solution of the multistart strategy is not flawed. For culture NTUA-M2, the common functional characteristics of the good-fit solutions provided evidence that TCE-to-cDCE dechlorinators consume most of the supplied TCE and that cDCE has inhibitory effect on VC removal. For culture PM, the good-fit solutions question the finding of Yu and Semprini (2004) who concluded on the toxic effect of high TCE concentrations based on their parameter estimates.

The application of the multistart strategy delineated a frame into which to work with complex models. It demonstrated that many diverse-yet-equivalent local solutions can be specified from collective parameter estimation efforts. These solutions should be tested under diverse observations in order to discriminate among them and detect those that have a good probability of being acceptable approximations of the true behavior of a culture. In both literature-reported models, such acceptable approximations were harbored in the families of these equivalently good-fit solutions without being necessarily the best-fit solutions. In the absence of observations with discriminating power (e.g. culture NTUA-M2 or PM), the survey of good-fit solutions illustrates the limits of trust for the estimated parameter ensembles and guides the selection of initial conditions with high discriminating power.

Chapter 6: Choosing among candidate conceptual models for the make-up of the dechlorinating community

6.1 Introduction

Kinetic models are growing in complexity and even more often they are employed to corroborate the study of inhibitory impacts induced by chloroethenes to dechlorinators (e.g. Yu and Semprini, 2004) or the competition for chloroethenes among dechlorinators and the respective population dynamics (e.g. Becker, 2006; Lai and Becker, 2013). As models grow in complexity, the need for more knowledge on the underlying inhibitory or competitive mechanisms inevitably becomes more profound. Even if this need has already been addressed (Chambon et al., 2013), such microbial mechanisms are difficult to analyze experimentally, because batch tests performed to assess the magnitude of inhibition and the dynamics of dechlorinating populations are difficult to control. It is hard to deconvolute experimentally the inhibitory mechanisms and populations dynamics, as concentration of chloroethenes are constantly changing during the stepwise dechlorination reactions, while dechlorinators cannot be easily maintained in pure cultures (Adrian and Löffler, 2016). Thus, complex models are frequently overfitted to information-poor data sets, i.e. data sets deriving from batch tests with mixed microbial communities, in which the functional structure of the dechlorinating community is largely unknown (e.g. NTUA-M2, Antoniou, 2017; PM culture, Yu and Semprini, 2004; SDC-9 culture, Schäffer et al. 2009). Overfitted models describe experimental observations sufficiently, yet, their predictive value is low. Thus, when the models are to be extended to field scale, kinetic parameters should be treated as place to begin, rather than as an unquestionable proof for the relevance of a microbial mechanism. Then, the design of parsimonious models becomes an option, as model reduction may result in more trustworthy parameters and reliable predictions.

Culture NTUA-M2 is a typical case of dechlorinating cultures accompanied by information-poor data. Despite being monitored for years and analyzed at a molecular level, it is unclear which and how many different chloroethene-respiring microorganisms perform each step of the sequential dechlorination of TCE. Dechlorinating bacteria have a rather pronounced strain and enzyme specialization and, as Duhamel and Edwards (2006) report, inferring the functional redundancy based on phylogenetic abundance needs caution. Thus, even the concept of two dechlorinating populations thriving in the culture may approximate crudely the real structure of dechlorinators.

In the set-up of the model (Chapter 4), we incorporated the information provided by the FISH analysis performed (Panagiotakis et al., 2014). Two hydrogenotrophic dechlorinators were included in the model, a TCE-to-cDCE dechlorinator (as *Sulfurospirillum* which were equal to 8% of the overall cell count) and a TCE-to-ETH dechlorinator (as *Dehalococcoides mccartyi,* which comprised 49% of the overall cell count). As discussed in Chapter 5, using data from a batch study performed with excessive H_2 and butyrate supply, a simple Monod-type kinetic model was calibrated and the kinetic parameters of the two dechlorinators were estimated (Chapter 5). The model described adequately chloroethene consumption rates. Simulation results indicated that

TCE-to-cDCE dechlorinators consumed most of the supplied TCE (almost 70% of TCE) and that cDCE inhibited VC consumption (a low inhibition coefficient was calculated).

The model used in Chapter 5 may have been overfitted, as seven parameters were adjustable and estimated by a single batch test. Thus, the estimated parameters may be unreliable. Therefore, two candidate conceptual models for dechlorination with decreasing complexity were designed, in order to mitigate the impact of overparameterization. Then, apart from the quality of fit, we employed a Monte Carlo scheme and assessed parameter and prediction reliability deriving from experimental noise in the models. In the search for a balance between model performance and prediction reliability in chloroethene biodegradation models, we used a measure of applied interest and investigated whether model reduction would entail performance reduction.

6.2 Candidate models of the make-up of the dechlorinating community

Three candidate conceptual models were considered for the description of the dechlorinating community. The first model (referred to as the reference model) is the two-dechlorinator model described in Chapter 5. In addition, two alternative models of decreasing complexity were considered. Both models are knowingly less accurate approximations of culture NTUA-M2.

The first simplified modeling approach (referred to as model variation 1) also employs two dechlorinating species, a TCE-to-cDCE dechlorinator growing exclusively on TCE and a cDCE-to-ETH dechlorinator growing on cDCE and ETH. Hence, we ignore any competition among the dechlorinators for TCE, assuming that partial dechlorinators consume all the supplied TCE. What is more, inhibition induced by the presence of more chlorinated ethenes to their less chlorinated daughter compounds is ignored. Any possible stall on VC consumption will be described by a change in the half-velocity coefficient of VC. Considering the above-mentioned assumptions, chloroethene consumption rates are calculated as follows:

$$r_{i-j} = -\frac{\mu_{\max,j}}{Y_j} X_j \frac{S_i}{K_{S,i-j} + S_i} \tag{6.1}$$

in which (a) when i = TCE, then j = D2 (TCE-to-cDCE dechlorinators) and (b) when i= cDCE or VC, then j = D1 (cDCE-to-ETH dechlorinators).

The second simplified modeling approach (referred to as model variation 2) considers a single aggregate dechlorinating population and neglects any inhibitory mechanisms. Chloroethene consumption rates are described by the following equation:

$$r_{i-j} = -\frac{\mu_{\max,j}}{Y_j} X_j \frac{S_i}{K_{S,i-j} + S_i} \tag{6.2}$$

in which i = TCE, cDCE or VC and j = D1 (TCE-to-ETH dechlorinators).

6.3 Application of the multistart strategy for parameter estimation

In this section, we will concentrate on the application of the multistart strategy for the parameter estimation of the two simpler models, as parameter estimation of the reference model has been discussed in Chapter 5. Both models were fitted to the data obtained from the batch experiment described in Chapter 5. Chemical initial concentrations (chloroethene concentrations), growth yields and decay coefficients were considered as fixed parameters. Initial biomass concentrations

for each model were calculated as described in Section 5.4 and are presented in Table 6.1. Only maximum specific growth rates ($\mu_{max,j}$) and half-velocity coefficients ($K_{S,i-j}$) were considered adjustable and they were constrained by the range of literature reported values. For model variation 1 five kinetic parameters have to be estimated, while for model variation 2 only four parameters are adjustable.

Table 6.1. Model input and estimated initial biomass concentrations for the two simpler models.

	Model variation 1		**Model variation 2**
	cDCE-to-ETH dechlorinator	TCE-to-ETH dechlorinator	TCE-to-cDCE dechlorinator
Yield, Y_j (mg VSS/μmol Cl$^-$)	2.80 x 10^{-3}	4.96 x 10^{-3}	4.96 x 10^{-3}
Decay coefficient, b_j (d^{-1})	0.024	0.024	0.024
Initial biomass, X_j (mg VSS/l)	8.4	4.8	17.1

The first variation of the model resulted in calculated curves that fitted the observed concentration values with fair accuracy (Fig. 6.1b), resulting in mean absolute errors equal to 10 μM for TCE, 19 μM for cDCE, 52 μM for VC and 37 μM for ETH. Compared to the reference model (compare Fig. 6.1a to Fig. 6.1b), this simplification reproduced the data less accurately and failed to predict VC degradation. The multistart strategy needed only 300 starting points to return a global optimum solution and, thus, consumed a lower computation time.

The one-dechlorinator model failed to provide an adequate fit to the chloroethene observations, with mean absolute errors equal to 86 μM for TCE, 89 μM for cDCE, 77 μM for VC and 53 μM for ETH. Yet, it described ethene production satisfactorily (Fig. 6.1c). The local search routine was performed for only 110 starting points and required approximately 5 minutes of computer time. This is a 7-fold decrease of computational burden compared to the reference model.

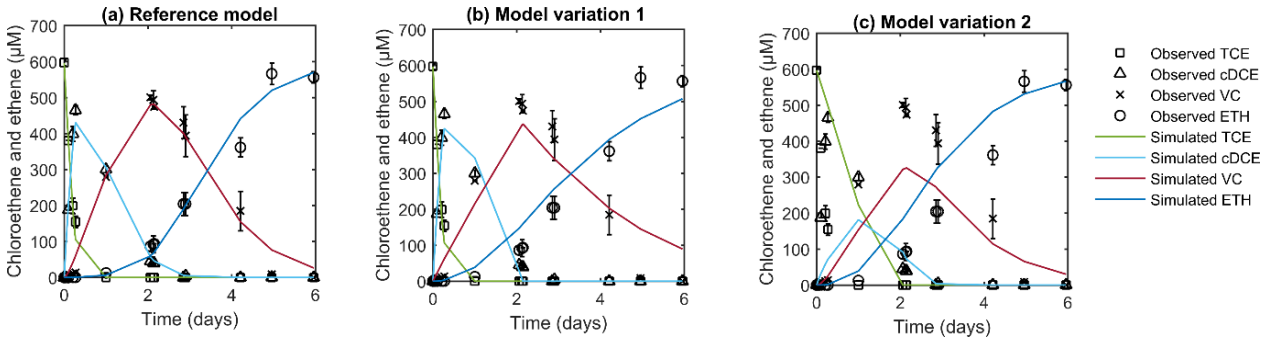

Fig. 6.1. Observed and simulated sequential dechlorination of TCE in dechlorinating culture NTUA-M2. Simulations were performed with the best-fit solutions of (a) the reference model, (b) model variation 1, (c) model variation 2.

6.4 Assessment of parameter and prediction reliability

The effect of experimental noise on the reliability of estimated parameters was assessed by a Monte Carlo scheme proposed by Nickerel et al. (2009): in the data set used for parameter estimation, a normally distributed error was injected and the multistart parameter estimation approach was performed using the noisy data set. As information on the standard deviation of each measurement is known, noisy data sets were created by introducing a normally distributed relative standard deviation (RSD) equal to the RSD of each measurement (3% for TCE, 4% for cDCE, 13% for

VC and 12% for ETH). Nickerel et al. (2009) used 500 synthetic, noisy data sets for the estimation of parameter reliability, but in our approach, a workable number of 200 synthetic data sets was constructed. The magnitude of the parameter ensembles may be not significant (200 parameters), but it can give a crude estimate of the practical reliability of each parameter. Based on the 200 global optimum solutions for each model, the RSD of each parameter was calculated as a measure of parameter reliability. Finally, it should be noted that for reproducibility purposes, the initial starting points used for parameter estimation were also used for each multistart application in the synthetic noisy data sets.

An overall opposite trend of model complexity and parameter reliability can be observed for most of the model parameters. As simpler models are employed (moving from the reference model towards model variation 2) tighter parameters are estimated, with the exception of the half-velocity coefficients for TCE and cDCE. For the reference model, half-velocity coefficients and the inhibition coefficient of cDCE were significantly affected by the experimental noise as indicated by the RSD values in Table 6.2. Only maximum specific growth rates were estimated with relative confidence. TCE consumption was overfitted in this modeling approach, as four kinetic parameters (two for each dechlorinating species) were fitted to the TCE concentrations of the first day of the experiment. In addition, the poor reliability of the inhibition coefficient underscores the possibility that cDCE inhibition may not be necessary to describe the observed VC consumption rates. Ignoring competitive inhibition and the competition for TCE (model variation 1), improved the reliability of the parameters, except for the half-velocity coefficient for cDCE. Finally, the one-dechlorinator model (model variation 2) has more certain parameter estimates, apart from the half-velocity coefficient for TCE. Thus, from the current data set, tight parameters cannot be calculated even for the most parsimonious model.

Table 6.2. The relative standard deviation (%) for each parameter assessed from randomly generated noisy data sets.

		Reference model	Model variation 1	Model variation 2
TCE-to-cDCE dechlorinator	$\mu_{max,D2}$ (days^{-1})	26.0	2.3	-
	$K_{S,TCE-D2}$ (μM)	151.4	14.8	-
TCE-to-ETH dechlorinator	$\mu_{max,D1}$ (days^{-1})	14.0	9.3	3.4
	$K_{S,TCE-D1}$ (μM)	17.6	-	64.0
	$K_{S,cDCE-D1}$ (μM)	75.8	232.7	20.8
	$K_{S,VC-D1}$ (μM)	28.8	3.9	0.0
	$K_{INH,cDCE-D1}$ (μM)	57.5	-	-

As Gutenkunst et al. (2007) mention, loose parameters may produce tight predictions. Unreliable parameters may not affect significantly the predictive abilities of the model. Therefore, we have to quantify the reliability of each prediction and not use parameter reliability as a performance criterion. To this end, we specified a quantitative measure that would assist us compare the predictive abilities of the alternate conceptual models. The time to achieve complete dechlorination (i.e. the time required for VC to reach concentrations less than 0.03 μM or 2 μg/l, which is the maximum contaminant level for drinking water) was used. Then, based on the 200 values of each parameter, their empirical probability distributions were calculated (using the fitdist function of MATLAB®). Then, a sample of 1000 random parameter ensembles was created for each model, consistent with the respective empirical probability distributions. Finally, the four numerical tests

performed in Chapter 5 (Table 6.3) were repeated for 1000 times using the randomly created parameters and calculated prediction uncertainty for the estimated time of complete chloroethene detoxification. As only one numerical test coincides with an actual batch experiment (Test 1 in Table 6.3), for the three remaining numerical tests we will be discussing only the relative performance of the three alternate models.

Table 6.3. Initial chemical and biomass concentrations for the four numerical tests performed with the three dechlorination models of culture NTUA-M2.

	Component						
	$S_{TCE}(t=0)$ [μM]	$X_{D1}(t=0)$ [mg VSS/l]			$X_{D2}(t=0)$ [mg VSS/l]		
		Reference	Variation 1	Variation 2	Reference	Variation 1	Variation 2
Test 1	596	10.2	8.4	17.1	3.9	4.8	-
Test 2	50	10.2	8.4	17.1	3.9	4.8	-
Test 3	1800	10.2	8.4	17.1	3.9	4.8	-
Test 4	1800	2.6	2.1	4.3	1.0	1.2	-

The reference model provided a relatively accurate prediction of chloroethene detoxification time (Fig. 6.2a); the mean predicted chloroethene elimination time was 7.1 days, whereas the observed chloroethene elimination time was 6 days. The prediction was unreliable though, as the 90% confidence intervals varied significantly from 4.1 to 12.1 days. Model variation 1 missed to predict chloroethene elimination accurately. The mean predicted time was 10.5 days, a 1.7-fold greater value than the observed. It provided, however, a very tight prediction. On the other hand, model variation 2 also provided a tight estimation of the chloroethene elimination time, which was only slightly inaccurate (mean calculated time was 8.1 days, whereas observed time was 6 days). Overall, even if not every step of dechlorination is simulated accurately with model variation 2, it predicted that the dechlorinating culture would pass the bottleneck of VC consumption at a time comparable to the observed. Hence, a slightly inaccurate prediction with greater confidence and lower computational burden derived from the simple kinetic model employing an aggregate dechlorinating population.

For the remaining three numerical tests, predictions for chloroethene elimination times from model variation 2 were close to the predictions calculated from the reference model (Fig. 6.2b to 6.2d). If we assume that the reference model approximates accurately chloroethene elimination under the conditions prevailing in the three numerical tests, then model variation 2 is again more accurate compared to model variation 1 and slightly less precise (i.e. wider confidence intervals). Nonetheless, when higher TCE values were introduced the differences in prediction accuracy were diminished among the three models. Given the availability of chloroethenes, chloroethene removal is more sensitive to maximum specific growth rates, which were close for all conceptual models. Considering the above, again model simplification was not accompanied by performance reduction.

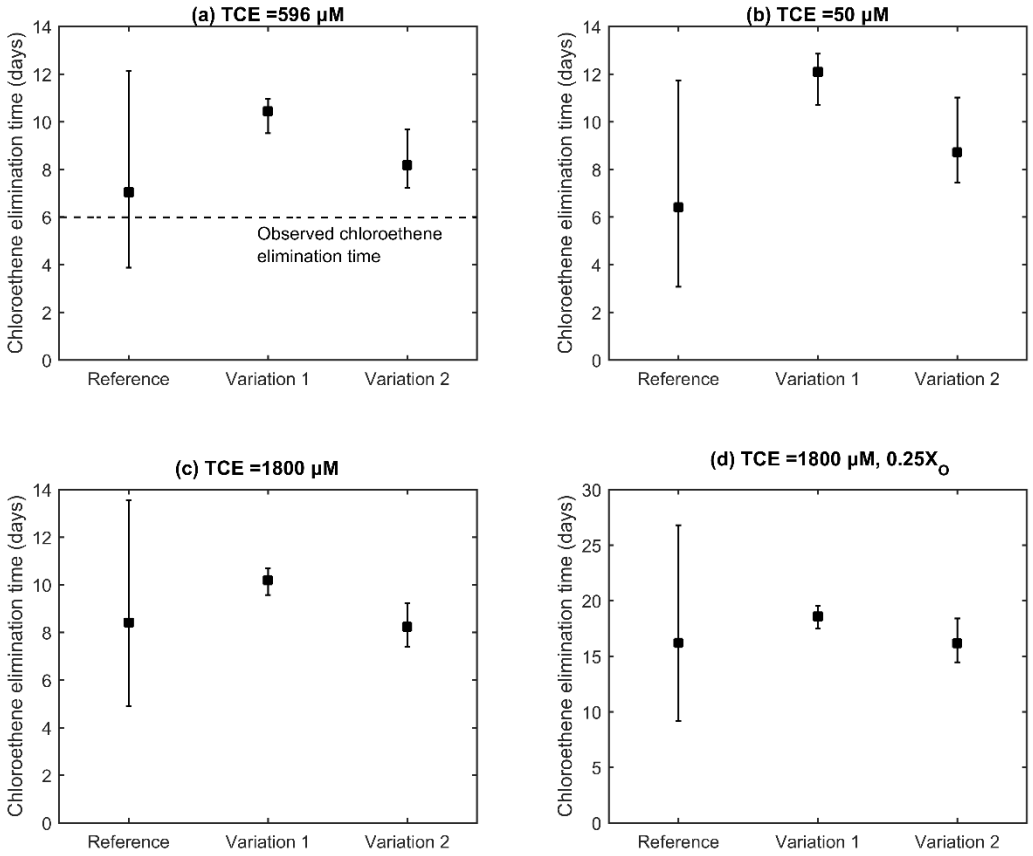

Fig. 6.2. Predicted and observed chloroethene elimination times for the four numerical experiments performed with dechlorinating culture NTUA-M2 and the three alternate models of the dechlorinating consortium. The error bars correspond to the 90% confidence intervals of each prediction.

For every model considered herein parameter uncertainty was not directly proportional to prediction uncertainty. For example, in the reference model the RSD of the prediction of chloroethene elimination time in Test 1 was approximately equal to 20%, which is lower than most of the calculated RSD for the model parameters. Model behavior depended mainly on specific parameter combinations. For example, model variation 1 was insensitive to the poorly identified half-velocity coefficient for cDCE. Thus, even if these parameters could be precisely measured, the predictive ability of the model wouldn't be significantly enhanced.

6.5 Concluding remarks

From the preceding findings, it was shown that when the model is intended for predictive purposes that do not require drastic extrapolation outside the conditions used for parameter estimation, the modeler is advised to examine more simplifying approaches, even if it they are knowingly less accurate approximations of reality. To answer questions of applied interest, the computational burden resulting from more complex models may not be accompanied by proportionally significant improvements in their predictive abilities. The computational burden may seem workable when single batch tests are modeled, but it would be heavier when the model is extended for field applications and transport is also considered. What is more, it can be argued that it may be unnecessary to insist on the measurement of kinetic parameters, as not all of them enhance model predictivity; the difficulty of deconvoluting inhibitory or competitive microbial mechanisms

in mixed cultures may be greater than the profit of knowing the exact value of the respective kinetic parameters.

The findings of this chapter are based on the comparison of three models of one dechlorinating culture, while model evaluation was based on a specific question of applied interest. Thus, these findings should not be regarded as if they are applicable for every kinetic model of dechlorination. Nonetheless, the preceding analysis puts forth two concepts that should be considered in kinetic modeling of dechlorination: (a) model reduction and (b) the necessity of direct parameter measurements.

PART 3. A MODELING APPROACH FOR THE STUDY OF THE FUNCTIONAL STRUCTURE OF MIXED CHLOROETHENE-DEGRADING COMMUNITIES

Chapter 7: Elucidating the composition of non-dechlorinators in a methane-producing, chloroethene-degrading mixed culture

7.1 Introduction

In mixed methane-producing, chloroethene-degrading cultures, dechlorinators may thrive alongside with distinctive methanogenic species and syntrophic bacteria that mediate the use of H_2. In such cultures, the primary (and obvious) concern is how to strategically supply the H_2 sources and channel H_2 to dechlorinators. Hence, we focus on the competition for H_2 between dechlorinators and methanogens. This perception implies that methane formation in dechlorinating consortia is primarily hydrogenotrophic. This could be a valid assumption in a significant share of microbial communities reported in the literature (e.g. KB-1: Duhamel and Edwards, 2006; ANAS: Richardson et al., 2002; VS enrichment culture: Yang and McCarty, 1998), in which molecular analyses support the existence of H_2-utilizing methanogens. Yet, methane formation in chloroethene-degrading cultures is not solely H_2-dependent. Acetate-dependent methanogenesis has been reported as the main methanogenic pathway in mixed chloroethene-degrading communities (DonnaII dechlorinating culture: Rowe et al., 2008), while acetate-utilizing methanogens have been reported as the major methanogenic population in dechlorinating communities developed under laboratory conditions (Dennis et al., 2003) and established in the field (Macbeth et al., 2004). Therefore, if methane is produced concurrently with dechlorination, acetate-utilizing methanogens should not be neglected. Concurrently, another field of competition arises within the mixed culture, i.e. competition for acetate. This level of competition is frequently overlooked. Yet, if low H_2-ceiling electron donor sources are used and acetoclastic activity is evident, acetate can be oxidized towards H_2 production. Considering all the above, describing the dynamics of H_2 production and consumption is performed in a context of uncertainty.

The goal of the present chapter is to investigate the composition and the functional role of the non-dechlorinating community present in the mixed dechlorinating culture NTUA-M2. As described in Chapter 4, culture NTUA-M2 demonstrated a robust dechlorinating performance accompanied by an unsteady methanogenic activity. Methane variations coincided with acetate fluctuations, indicating a correlation between methane formation and acetate consumption and, hence, providing evidence that the main methanogenic pathway in this culture may be acetate-dependent. However, the same outcome may have been produced by an alternative pathway, i.e. the syntrophic association of acetate oxidizers and H_2-utilizing methanogens. With the application of our model, we will seek for evidence that corroborate the hypothesis that methane formation is of acetoclastic nature and shed light in the make-up of the non-dechlorinating community.

To this end, a cross-confirmation strategy was implemented, in which different-yet-equivalent approximations of the non-dechlorinating community were tested under varying initial conditions. First, the multistart strategy was applied using a six-month long batch test conducted under limiting electron donor conditions with material from source culture NTUA-M2. Then, taking advantage of the non-uniqueness of the solutions, plausible mixed cultures were specified with differences in

the functional structure and the relative abundance of non-dechlorinators; all these cultures provided a good fit to the data of the batch test. Finally, two batch experiments with different electron donors in elevated surplus quantities were simulated, in order to find which realization of the source culture gives the most probable explanation of the make-up of non-dechlorinators.

7.2 Experimental information

7.2.1 Long-term monitoring of dechlorinating culture NTUA-M2

Long-term observations of the source culture offered two types of evidence. First, they offered a quantitative description of the most relevant parts of the catabolic food web established in the culture. Based on the electron balance of the source culture, we found in Section 4.1 that syntrophic acetate oxidation is an integral part of the food webs of culture NTUA-M2, along with dechlorination, butyrate oxidation and methanogenesis. Second, long-term monitoring of the source culture gave the opportunity to estimate steady-state biomass concentrations for the various microbial groups, provided that a steady-state performance has been established for the respective microbial activity.

Culture NTUA-M2 reached a steady state only with respect to dechlorination and butyrate oxidation. Regarding methane and acetate, the culture reached a pseudo-state phase, which was interrupted by periods of suppressed methane formation and inversely elevated acetate concentrations (inhibited steady state). Thus, steady-state biomass concentrations can be estimated for the two dechlorinating species and butyrate oxidizers, but not for methanogens or acetate oxidizers.

For dechlorinators, steady-state (SS) biomass concentrations were calculated in Chapter 5, according to the following equation:

$$X_{j,\mathrm{SS}} = \frac{\theta_c}{f}\frac{Y_j dS_{i-j}}{1+b_j\theta_c} \tag{7.1}$$

where $X_{j,SS}$ is the steady-state biomass concentration of microorganism j (mg VSS/l), θ_c is the solid retention time (48 days), f is the duration of the feeding cycles of the culture (7 days), and dS_{i-j} is the quantity of substrate i consumed by microorganism j during each feeding cycle (μM). In Chapter 5, we selected Y_j and b_j from the literature, assumed a reasonable dS_{i-j} value for each dechlorinating group (Table 7.1) and estimated the respective biomass concentrations. The assumptions on dS_{i-j} for dechlorinators were backed by the simulations with culture NTUA-M2 in Chapter 5. Regarding butyrate oxidizers, the same approach was followed; we selected Y_{BO} and b_{BO} from the literature and calculated $X_{BO,SS}$ according to Eq. (7.1); $dS_{B\text{-}BO}$ in Eq. (7.1) is the quantity of butyrate supplied on a weekly basis, i.e. 300 μM butyrate (Table 7.1).

Table 7.1. Steady-state substrate consumption for dechlorinators and butyrate oxidizers in culture NTUA-M2.

Microorganism	Substrate consumed on a weekly basis, dS_{i-j} (μM)
TCE-to-ETH dechlorinators – D1 [1]	647.9
TCE-to-cDCE dechlorinators – D2 [1]*	437.6
Butyrate oxidizers – BO	300.0

* It is assumed that 20% of the supplied TCE (a mean concentration of 547 μM was supplied on a weekly basis) is consumed by partial dechlorinators. This assumption is supported by the results of the kinetic model estimated in Chapter 5. [1]: dS_{i-j} is expressed in μM of H_2

Since methanogens never reached a steady state, a similar estimation of their biomass concentrations cannot be performed. The same problem applies for acetate-oxidizing bacteria, as the quantity of acetate consumed by them on a weekly basis cannot be estimated with certainty. Therefore, initial biomass concentrations of methanogens and acetate oxidizers for the batch test were treated as adjustable parameters. Nevertheless, upper and lower boundaries of these biomass concentrations could be calculated by Eq. (7.1) by estimating the respective maximum and minimum $dS_{i\text{-}j}$ values (Table 7.2). The lowest possible boundary for each methanogenic biomass concentration is zero (assuming that the corresponding $dS_{i\text{-}j}$ is zero). On the other hand, the upper boundary was calculated assuming that, during the pseudo-steady state of elevated methanogenesis, methane production was completely attributable either to H_2-utilizing methanogens or to acetate-utilizing methanogens. For the acetate oxidizers (AO), the minimum and maximum $dS_{A\text{-}AO}$ values were calculated from the mass balance for acetate (A): maximum $dS_{A\text{-}AO}$ was calculated assuming that methanogenesis was entirely hydrogenotrophic (i.e. all acetate yielding from butyrate oxidation is consumed by acetate oxidizers), whilst minimum $dS_{A\text{-}AO}$ was calculated when the culture demonstrated increased methanogenic activity and methanogenesis was presumed entirely acetotrophic.

Table 7.2. Minimum and maximum substrate consumption for H_2-utilizing methanogens, acetate-utilizing methanogens and acetate oxidizers in culture NTUA-M2.

Microorganism	Substrate consumed on a weekly basis, $dS_{i\text{-}j}$ (μM)	
	Min	Max
H_2-utilizing methanogens – HM [1]	0.00	1898.80
Acetate-utilizing methanogens – AM [2]	0.00	474.70
Acetate oxidizers – AO [2]	155.10	600.00

[1]: $dS_{i\text{-}j}$ is expressed in μM of H_2
[2]: $dS_{i\text{-}j}$ is expressed in μM of acetate

7.2.2 Batch tests performed with culture NTUA-M2

A total of three batch experiments were available for dechlorinating culture NTUA-M2 (Panagiotakis et al., 2015; Antoniou, 2017). The experiments were performed with varying initial electron donor types and quantities (Table 7.3). We divided these experiments in two groups. The first group was used for the collective fitting of unknown parameters and the identification of candidate approximations of the non-dechlorinating community. The second group was used to cross-validate the identified candidate approximations of the culture.

Experimental observations of a batch test performed under a low electron donor surplus (LEDS-B) was used as input for the solution of the parameter estimation problem. The experiment lasted 184 days and samples were taken periodically for the analysis of chloroethenes, ethene, methane and VFAs. Initially 567 μM TCE and 300 μM butyrate were added. At the beginning of the experiment, acetate was measured equal to 270 μM. The resulting electron donor surplus was equal to 2.4 assuming that 1 mol TCE requires 6 μe^- eq for its removal, 1 mol butyrate yields 20 μe^- eq and 1 mol acetate produces 8 μe^- eq. This experiment was used for parameter estimation due to its low electron donor surplus; the limited availability for H_2 makes feasible to study competition for H_2 and estimate the affinity for H_2 of H_2-scavenging species (dechlorinators and H_2-utilizing methanogens). It should be noted, that this experiment was performed when the source culture

had revived from an inhibited steady-state phase and, thus, it is close to the typical methanogenic performance of culture.

Two experiments were used for cross-checking purposes, a butyrate-fed experiment with a relatively high electron donor surplus (HEDS-B2), and a H_2-fed (MEDS-H2) experiment performed with a moderate electron donor surplus. The H_2-fed experiment is the experiment used for the parameter estimation problem of the simple model in Chapter 5, and it was performed when the culture was at inhibited steady state, i.e. experiencing acetate accumulation and low methanogenic activity. On the contrary, the butyrate-fed experiment (HEDS-B2) was performed, when methanogenesis was not suppressed, like the experiment used for parameter estimation (MEDS-B2).

Table 7.3. Initial donor and TCE concentrations and electron donor surplus for the batch experiments used for parameter estimation (experiment LEDS-B2) and model cross-examination (experiments HEDS-B2, MEDS-H2).

Batch test	Butyrate (μM)	Acetate (μM)	H_2 (μM)	TCE (μM)	Electron donor surplus[1]	Duration (days)
LEDS-B2	300	270	-	567	2.4	184.0
HEDS- B2	2230	258	-	601	12.9	9.2
MEDS-H2	300	900	3000	597	5.4	6.0

[1]: Electron donor surplus is calculated assuming that 1 mol butyrate yields 20 e^- eq.

7.3 Model development

Fig. 7.1 demonstrates the processes occurring concurrently with the anaerobic degradation of chloroethenes in our modeling approach for culture NTUA-M2. Table 7.4 presents the associated reactions. According to our conceptual design, a butyrate-oxidizing community consumes the supplied butyrate and produces H_2 and acetate. H_2 is subsequently used by (a) TCE-to-ETH dechlorinators, (b) TCE-to-cDCE dechlorinators, and (c) H_2-utilizing methanogens. Acetate is either converted to methane by acetate-utilizing methanogens or it is consumed by acetate-oxidizing bacteria for the production of H_2. Finally, decaying cells contribute to the electron donor pool, as they are considered to yield butyrate. The non-linear system of differential equations that constitutes the model and the mathematical formulation of the reaction rates have been presented in Chapter 4.

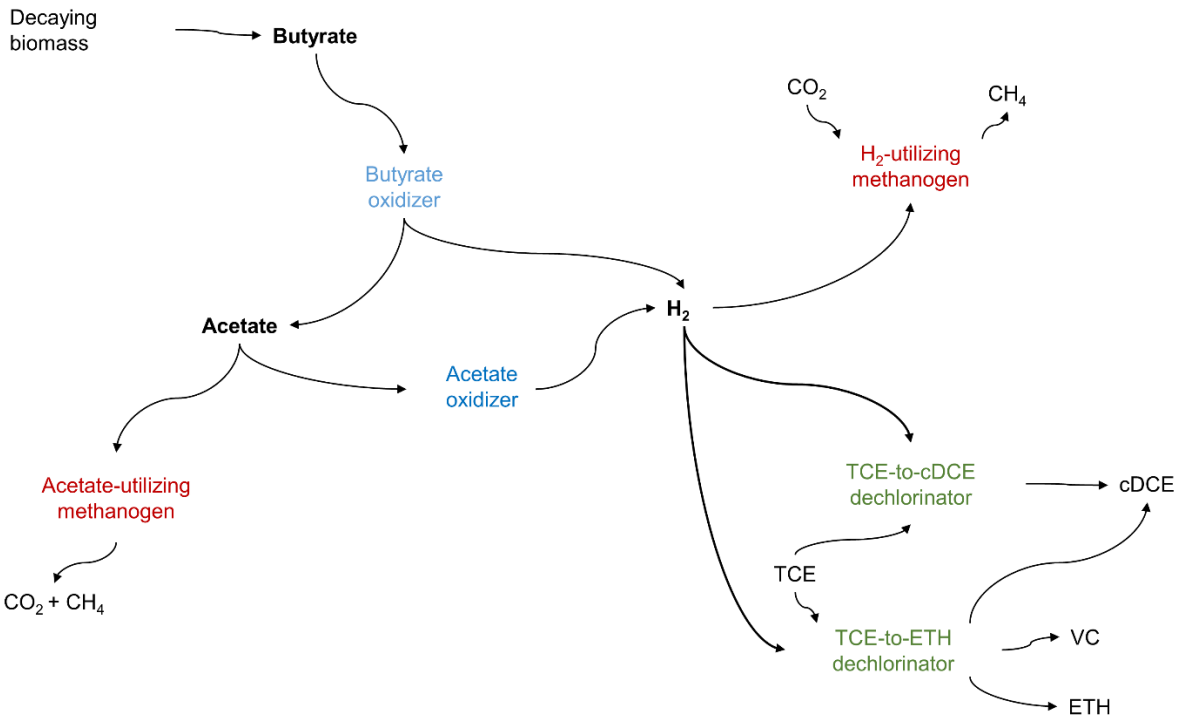

Fig. 7.1. Microbial processes considered in the model.

Table 7.4. Biological processes included in the conceptual model and the corresponding chemical reactions (subset of processes included in Table 4.1).

Process	Reaction
H_2 production	
Butyrate oxidation	$CH_3CH_2CH_2COO^- + 2H_2O \rightarrow 2CH_3COO^- + 2H_2 + H^+$
Acetate oxidation	$CH_3COO^- + 4H_2O \rightarrow 4H_2 + 2HCO_3^- + H^+$
Dechlorination	
TCE consumption	$C_2HCl_3 + H_2 \rightarrow C_2H_2Cl_2 + Cl^-$
DCE consumption	$C_2H_2Cl_2 + H_2 \rightarrow C_2H_3Cl + Cl^-$
VC consumption	$C_2H_3Cl + H_2 \rightarrow C_2H_4 + Cl^-$
Methane production	
H_2-dependent methanogenesis	$4H_2 + CO_2 \rightarrow 4CH_4 + 2H_2O$
Acetate-dependent methanogenesis	$CH_3COO^- + H_2O \rightarrow CH_4 + HCO_3^-$

7.4 Application of the multistart optimization strategy

The aim of parameter estimation is two-fold. Parameter estimation aims to specify the kinetic properties and the unknown initial biomass concentrations of microbial groups, which (a) reproduce sufficiently the observed data and (b) constitute different microbial communities with respect to the non-dechlorinating bacteria (i.e. H_2-utilizing methanogens, acetate-utilizing methanogens and acetate oxidizers). Therefore, the goal of parameter estimation is to identify solutions with (a) common biomass concentrations and kinetic parameters for dechlorinators and

butyrate oxidizers (i.e. the fixed part of the culture), (b) diverse biomass concentrations for the non-dechlorinating species, and (c) diverse kinetic properties for the non-dechlorinating species.

A heuristic approach was designed in which the multistart optimization algorithm was used in three phases. Each phase coincided with the three previously described goals. After the first phase, the kinetic parameters of dechlorinators and butyrate oxidizers, which were the fixed part of the candidate cultures, were specified. Following the second phase, three cultures with distinctive biomass distributions with respect to non-dechlorinators were identified. Finally, after the third phase cultures containing diverse functional characteristics were estimated. Schematically this ad-hoc approach is given in Fig. 7.2. Every modeling decision taken en route to the estimation of all the model parameters will be discussed thoroughly in the following sections.

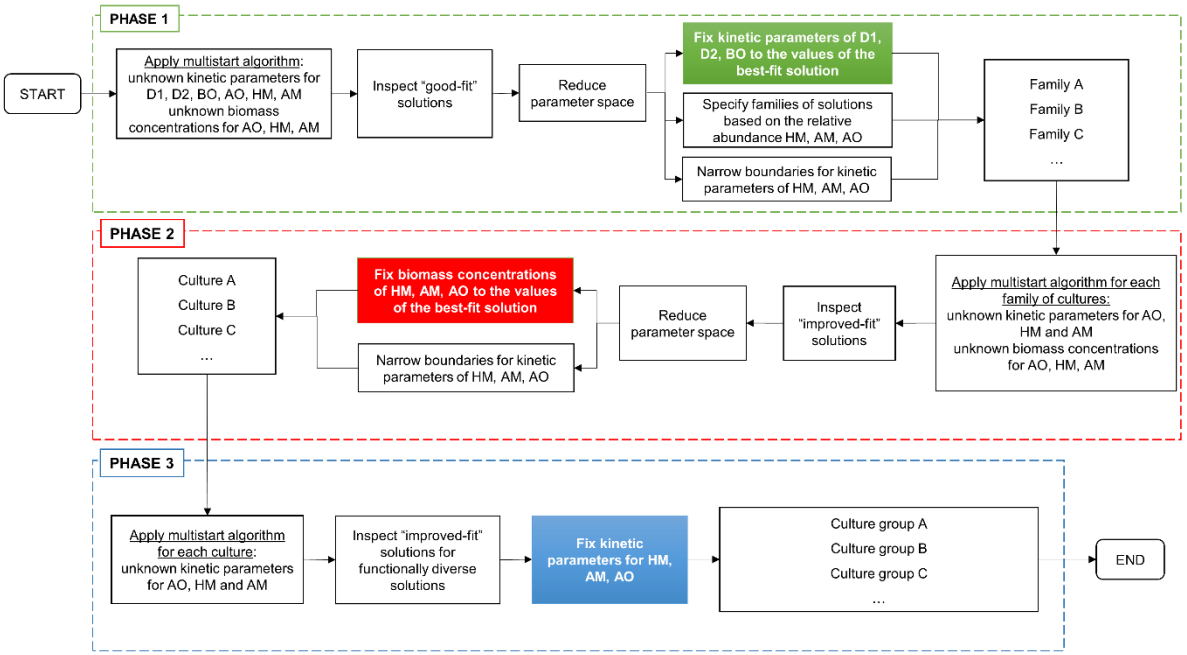

Fig. 7.2. Schematic representation of the ad hoc parameter estimation approach and the modeling decisions taken to detect the candidate approximations of culture NTUA-M2.

The specifics of the multistart algorithm have been decided and discussed in Chapter 5. Thus, during each phase of the parameter estimation problem, a sequence of 1000 quasi-random starting points from the feasible area of the parameter space was created and local searches with the SQP routine were performed. Following the execution of 1000 local searches, the Bayesian estimate of total local solutions was calculated, giving an inkling of how exhaustively the multistart algorithm had searched the parameter space.

The model was fitted to experimental observations comprising chloroethenes (TCE, cDCE, VC), ETH, methane, and volatile fatty acids (VFAs), i.e. butyrate and acetate. The output of each local search solution is expressed in units not readily comparable to the units of experimental measurements (the objective function, $J(p)$, returns results in squared concentrations). Therefore, for every local solution and for convenience purposes, the quality of fit was assessed with the mean absolute error calculated for chloroethenes, ethene, methane and VFAs (it was calculated as described in Section 5.4). Finally, the progress of dechlorination over time in these tests will be demonstrated with an aggregate measure, i.e. the degree of dechlorination (*DoD*). The degree of

dechlorination, *DoD*, was calculated from the concentrations of chloroethenes and ETH as follows (Manoli et al., 2012):

$$DoD = \frac{S_{cDCE} + 2S_{VC} + 3S_{ETH}}{3\left(S_{TCE} + S_{cDCE} + S_{VC} + S_{ETH}\right)} \quad (7.2)$$

Comparisons between observed and simulated observations of chloroethenes for each simulated batch test are available in Appendix A.

Preparing the multistart algorithm

The problem is certainly ill-posed, as its complexity relative to the quantity of available experimental information does not allow for rigorous estimation of all the components of the model. A total of 39 parameters are needed, i.e. 36 kinetic parameters, three initial biomass concentrations (for the two methanogens and acetate oxidizers). In order to simplify the problem and reduce the computational burden of our staged optimization strategy, 18 of the 36 of the kinetic parameters were fixed to specific values.

First, the 12 growth yields and decay coefficients were fixed (two parameters per microbial group), because (a) this decision allowed to specify steady-state biomass concentrations from Eq. (7.1) and (b) these parameters vary within a relatively narrow range of values reported in the literature, as shown in Tables 7.5, 7.6 and 7.7. What is more, we fixed the thresholds for acetate ($S_{min,A\text{-}AO}$) and H_2 utilization ($S_{min,H\text{-}D1}$, $S_{min,H\text{-}D2}$ and $S_{min,H\text{-}HM}$), as they also demonstrated a relatively narrow range of values in the literature (Tables 7.5 and 7.6). Finally, we calculated and fixed H_2 inhibition factors ($S_{INH,H\text{-}BO}$ and $S_{INH,H\text{-}AO}$). H_2 inhibition factor for butyrate oxidation was set equal to 0.25 and it was estimated from the results of a syntrophic TCE-degrading coculture of *Dehalococcoides mccartyi* and butyrate oxidizers reported by Mao et al. (2015); in their work, butyrate oxidation was thermodynamically infeasible at an H_2 concentration of 1.2 μM. H_2 inhibition factor for acetate oxidizers was set equal to 0.08 μM. The inhibitory H_2 concertation $S_{INH,H\text{-}AO}$ was estimated from the standard Gibbs energy 25° C under conditions typically encountered in the source culture (calculations were performed for pH 6.8, 750 μM acetate and 357 μM bicarbonate). According to the calculations, acetate oxidation is no longer thermodynamically feasible for H_2 concentrations exceeding 0.4 μM.

The remaining kinetic parameters (18 parameters), comprising maximum specific growth rates ($\mu_{max,j}$), half-velocity coefficients ($K_{S,i\text{-}j}$) and the first-order coefficient for endogenous decay contribution (K_{ED}), were considered adjustable. These parameters were constrained by the wide range of literature reported values presented in Tables 7.5, 7.6 and 7.7; note that in Table 7.5 due to the presence of two dechlorinators the number of adjustable parameters is nine (two μ_{max} values, two K_S values for TCE, two K_S values for H_2, one K_S value for cDCE, VC and one $K_{INH,cDCE}$ value).

Table 7.5. Fixed and adjustable kinetic parameters implemented for the two dechlorinators for the first phase of the parameter estimation strategy.

Substrate	Parameter (units)	Type	Range of values	Feasible Area/Value	Reference
TCE-to-ETH dechlorinators (*j*=D1) and TCE-to-cDCE dechlorinators (*j*=D2)					
TCE, cDCE, VC	Maximum specific growth rate, $\mu_{max,j}$ ($days^{-1}$)	Adjustable	0.01-4.30 [1]	0.01-4.30	(a)-(b)
TCE, cDCE, VC	Half-velocity coefficient, $K_{S,i\text{-}j}$ (μM)	Adjustable	0.05-602.00 [2]	0.05-602.00	(c)-(a)
VC	Inhibition coefficient, $K_{INH,cDCE}$ (μM)	Adjustable	0.05-602.00 [3]	0.05-602.00	-
H_2	Half-velocity coefficient, $K_{S,H\text{-}j}$ (μM)	Adjustable	0.007-0.100	0.007-0.100	(d)-(e)
H_2	H_2 threshold, $S_{min,H\text{-}j}$ (μM)	Fixed	0.001-0.024	0.002	(f)
TCE, cDCE, VC	Growth yield, Y_{D1} x10^{-3} (mg VSS/μmol)	Fixed	0.18-9.60 [4]	4.96	(g)-(h)
TCE	Growth yield, Y_{D2} x10^{-3} (mg VSS/μmol)	Fixed	2.80 [5]	2.80	(i)
-	Decay coefficient, b_j ($days^{-1}$)	Fixed	0.024-0.090	0.024	(j)-(k)

[1]: Reported values of μ_{max} for TCE range from 0.33 d^{-1} (Cupples et al., 2004b) to 4.30 d^{-1} (Christ and Abriola, 2007), for cDCE from 0.04 d^{-1} (Yu and Semprini, 2004) to 0.46 d^{-1} (Cupples et al., 2004b), and for VC from 0.01 d^{-1} (Yu and Semprini, 2004) to 0.49 d^{-1} (Cupples et al., 2004b). In our approach μ_{max} is a microorganism-related parameter and, hence, we merged the three subranges into the one presented herein.

[2]: Reported values of $K_{S,i\text{-}j}$ for TCE range from 0.05 μM (Lee et al., 2004) to 12.40 μM (Cupples et al., 2004a), for cDCE from 0.54 μM (Fennell and Gossett, 1998) to 99.70 μM (Haest et al., 2010), and for VC from 2.60 μM (Haston and McCarty, 1999) to 602.00 μM (Yu and Semprini, 2004). We merged the three subranges into the one presented herein.

[3]: In the literature inhibition coefficients are typically set equal to the half-velocity coefficient for the respective chloroethene, i.e. $K_{INH,cDCE} = K_{S,cDCE\text{-}j}$. Consequently, the range of values for the inhibition coefficient was set equal to the range of values for the half-velocity coefficients.

[4]: Yield coefficients are reported in mg VSS/μmol assuming that one *Dehalococcoides mccartyi* cell corresponds to 1.6 x 10^{-14} g of VSS (Cupples et al., 2003).

[5]: Only yields for *Sulfurospirillum* partial dechlorinators were considered.

(a) Yu and Semprini (2004), (b) Christ and Abriola (2007), (c) Lee et al. (2004), (d) Cupples et al. (2004b), (e) Smatlak et al. (1996), (f) Luijten et al. (2004), (g) Holmes et al. (2006), (h) Maymó-Gatell et al. (1997), (i) Scholz-Muramatsu et al. (1995), (j) Fennell and Gossett (1998), (k) Cupples et al. (2003)

Table 7.6. Fixed and adjustable kinetic parameters implemented for methanogens for the first phase of the parameter estimation strategy.

Substrate	Parameter (units)	Type	Range of values	Feasible Area/Value	Reference
		H_2-utilizing methanogens			
H_2	Maximum specific growth rate, $\mu_{max,HM}$ (days^{-1})	Adjustable	0.02-1.98 [1]	0.02-1.98	(a), (b)
H_2	Half-velocity coefficient, $K_{S\text{-}H,HM}$ (μM)	Adjustable	0.50-18.40 [1]	0.50-18.40	(a), (b)
H_2	Growth yield, Y_{HM} x10^{-3} (mg VSS/μmol)	Fixed	0.30-2.20	0.78	(a), (b)
-	Decay coefficient, b_{HM} (days^{-1})	Fixed	0.011-0.080 [1]	0.024	(a), (c)
H_2	Substrate threshold, $S_{H,min\text{-}HM}$ (μM)	Fixed	0.005-0.950	0.011	(d)
		Acetate-utilizing methanogens			
Acetate	Maximum specific growth rate, $\mu_{max,AM}$ (days^{-1})	Adjustable	0.04-0.38 [1]	0.04-0.38	(a), (b)
Acetate	Half-velocity coefficient, $K_{S,A\text{-}AM}$ (μM)	Adjustable	370-2031 [1]	370-2031	(a), (b)
Acetate	Growth yield, Y_{AM} x10^{-3} (mg VSS/μmol)	Fixed	1.10-1.40	1.40	(a), (b)
-	Decay coefficient, b_{AM} (days^{-1})	Fixed	0.007-0.029 [1]	0.024	(a), (c)
Acetate	Substrate threshold, $S_{A,min\text{-}AM}$ (μM)	Fixed	7-69 [2]	15	(e)

[1]: Parameter values were corrected from a temperature T to a temperature of 25°C according to the equations (Rittmann and McCarty, 2001): $\mu_{max,j}^{25} = \mu_{max,j}^{T} e^{0.06(25-T)}$, $K_{S,i-j}^{25} = K_{S,i-j}^{T} e^{-0.077(25-T)}$, $b_j^{25} = b_j^T e^{0.14(25-T)}$.

[2]: Reported values for *Methanosaeta* spp. are considered, since *Methanosarcina* spp. are expected to be dominant at acetate concentrations greater than 1000 μM (Liu and Whitman, 2008).

(a) Pavlostathis and Giraldo-Gomez (1991), (b) Oude Elferink et al. (1994), (c) Clapp et al. (2004), (d) Löffler et al. (1999), (e) Aulenta et al. (2006)

Table 7.7. Fixed and adjustable kinetic parameters for butyrate and acetate oxidizers for the first phase of the parameter estimation strategy.

Substrate	Parameter (units)	Type	Range of values	Feasible Area/Value	Reference
		Butyrate oxidizers			
Butyrate	Maximum specific growth rate, $\mu_{max,BO}$ (days^{-1})	Adjustable	0.21-0.60 [1]	0.21-0.60	(a)
Butyrate	Half-velocity coefficient, $K_{S,B}$ (μM)	Adjustable	160-3676 [1]	160-3676	(a), (b)
Butyrate	Growth yield, Y_{BO} x10^{-3} (mg VSS/μmol)	Fixed	1.50-4.90	3.10	(c)
H_2	H_2 inhibition coefficient, $S_{H,INH-BO}$ (μM)	Fixed	-	0.25	-
-	Decay coefficient, b_{BO} (days^{-1})	Fixed	0.020-0.054 [1]	0.024	(a)
-	First-order coefficient for endogenous decay contribution, K_{ED} (days^{-1})	Adjustable	-	0.001-0.010	-
		Acetate oxidizers			
Acetate	Maximum specific growth rate, $\mu_{max,AO}$ (days^{-1})	Adjustable	0.07-0.26 [2]	0.07-0.26	(d)
Acetate	Half-velocity coefficient, $K_{S,A-AO}$ (μM)	Adjustable	-	500-2500 [3]	-
Acetate	Growth yield, Y_{AO} x10^{-3} (mg VSS/μmol)	Fixed	-	0.70 [4]	-
H_2	H_2 inhibition coefficient, $S_{H,INH-AO}$ (μM)	Fixed	-	0.08	-
-	Decay coefficient, b_{AO} (days^{-1})	Fixed	-	0.024	-

[1]: Parameter values were corrected to a temperature of 25°C assuming that an increase of 10°C doubles maximum specific growth rates and decay coefficients, while it reduces half-velocity coefficients by half.
[2]: The values were calculated by the reported doubling times and were corrected to a temperature of 25°C assuming that an increase of 10°C doubles maximum specific growth rates.
[3]: Qu et al. (2009) reported a $K_{S,A-AO}$ value of 339 μM estimated under thermophilic conditions (55°C).
[4]: Yield for acetate oxidizers has been thermodynamically predicted according to Duhamel and Edwards (2007) assuming S_H = 50 nM and S_A = 750 μM.
(a) Pavlostathis and Giraldo-Gomez (1991), (b) Oude Elferink et al. (1994), (c) Kleerebezem and Stams (2000), (d) Hattori (2008)

Bounding parameters was infeasible for two out of the 18 adjustable kinetic parameters. Reasonable assumptions were made regarding their lower and upper limits. Following the literature review, the first-order coefficient for endogenous decay contribution (K_{ED}) remained unbounded, as the mathematical formulation employed for biomass disintegration has not been previously utilized in kinetic models. In this case, the boundary values were assumed based on the disintegration and hydrolytic rate coefficients reported by Batstone et al. (2002). In addition, half-velocity coefficients for acetate oxidizers ($K_{S,A-AO}$) have not been reported in the literature, with the exception of Qu et al. (2009), who estimated a $K_{S,A-AO}$ of 339 μM for thermophilic conditions (55° C) in a anaerobic reactor with high VFA concentrations. The lack of reported values reflects the absence of kinetic studies considering acetate oxidation specifically under low organic loads and temperatures, i.e. conditions normally anticipated at contaminated sites. Despite being isolated mainly in thermophilic conditions (Hattori, 2008), acetate oxidizers have been efficient acetate

scavengers in natural habitats at temperatures as low as 15° C (Nüsslein et al., 2001). Hence, boundaries for $K_{S,A\text{-}AO}$ were assumed to be comparable to those of acetate-utilizing methanogens (compare $K_{S,Aj}$ values in Tables 7.6 and 7.7) and specifically to the members of the genus *Methanosaeta*, as members of the genus *Methanosarcina* are expected to thrive with greater acetate concentrations than those observed in the source culture (Liu and Whitman, 2008).

Chemical initial concentrations were measured at the beginning of the batch test and, hence, were treated as fixed parameters. Regarding biomass concentrations, only the initial biomass concentrations of dechlorinators and butyrate oxidizers were calculated from Eq. (7.1) and, hence, were treated as fixed parameters (Table 7.8). On the contrary, initial biomass concentrations of H_2-utilizing methanogens, acetate-utilizing methanogens and acetate oxidizers were treated as constrained adjustable parameters. Their constraints were calculated from Eq. (7.1) and the end-products of the culture during the achieved pseudo-steady states. Finally, in order to safeguard against unrealistically high overall biomass concentrations, solutions producing an overall biomass concentration greater than the 90% of the measured steady-state biomass concentration of the source culture (i.e. 20.9 mg VSS/l) were ruled out. Hence, every culture may contain populations, other than the six major groups considered herein, equal to at least 10% of the overall biomass concentration (i.e. 2.3 mg VSS/l). This part of the biomass mostly consists from primary fermenters that mediate the conversion of decaying cells to short-chain fatty acids, and inert cells.

Table 7.8. Initial biomass concentrations for the six microbial groups considered.

Component	Symbol	Value (mg VSS/l)	Type
TCE-to-ETH dechlorinators	$X_{D1,o}$	10.21	Fixed
TCE-to-cDCE dechlorinators	$X_{D2,o}$	3.89	Fixed
H_2-utilizing methanogens	$X_{HM,o}$	0.00-4.59	Adjustable
Acetate-utilizing methanogens	$X_{AM,o}$	0.00-2.11	Adjustable
Butyrate oxidizers	$X_{BO,o}$	2.95	Fixed
Acetate oxidizers	$X_{AO,o}$	0.26-1.34	Adjustable

Phase 1: The fixed part of the candidate approximations of culture NTUA-M2

In the first phase of parameter estimation we fixed the kinetic parameters of dechlorinators (D1 and D2) and butyrate oxidizers (BO), i.e. the bacteria that constitute the fixed part of the mixed community. In addition, we segregated the parameter space into three pieces based on the relative abundance of non-dechlorinators; each segment of the parameter space now represents a family of cultures. Before discussing every modeling decision made and each result obtained, phase 1 is schematically presented in Fig. 7.3.

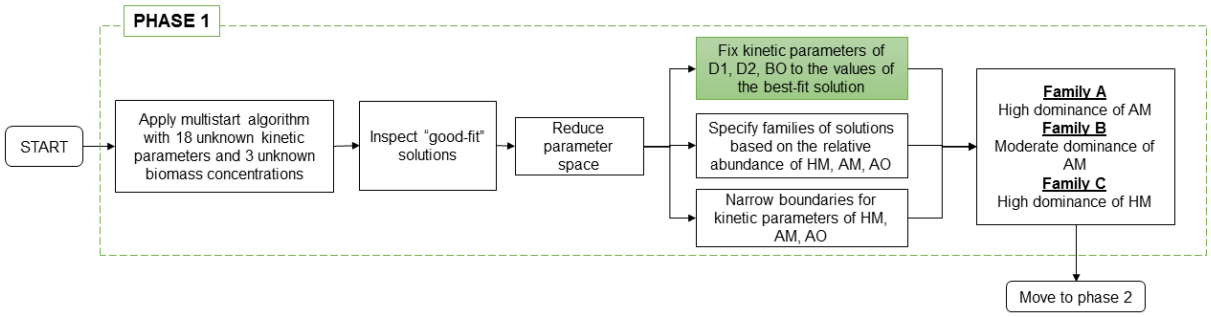

Fig. 7.3. Modeling decisions and results of the first phase of the parameter estimation strategy.

During the first phase of our heuristic parameter estimation approach, 1000 local searches were performed, with 21 adjustable parameters (i.e. 18 kinetic parameters and three initial biomass concentrations). Based on the 930 local minima discovered from the 1000 iterations, 12,903 local minima are estimated to exist in the problem. In addition, the total relative volume of the observed regions of attraction is equal to 13%, indicating that there is a rather significant part of the regions of attraction that has not been investigated. Yet, based on the distribution of the values of the objective functions of each local solution (Fig. 7.4), it is reasonable to deduce that there is a small possibility to discover better local solutions from new starting points. Hence, emphasis was given on the 52 local searches (approximately the top 5% of local solutions), that produced a fair fit to the data according to the achieved mean absolute simulation errors. The best-fit solution and the family of good-fit solutions are compared to experimental observations in Fig. 7.5 (parameter values estimated for the best-fit solution are provided in Appendix A). Simulation errors for dechlorination were less than 30 μM, less than 41 μM for VFAs, but were in the range of 220 μM to 260 μM for methane formation.

The 52 good-fit local solutions described dechlorination and VFA consumption with fair accuracy (Fig. 7.5a, 7.5c and 7.5d). Yet, they failed to reproduce the final levels of methane production (Fig. 7.5b). The good-fit solutions reproduced poorly methane formation, because in the batch experiment the end-products accounted for 47% more electron equivalents than those offered. The batch test appears to be deficient from day 7 in an electron equivalent basis, indicating that a significantly better fit cannot be achieved for this data set; the model by defaults produces balanced electron equivalent production and consumption and, therefore, it can simulate adequately either dechlorination or methane formation. The remaining 95% of the local searches was trapped in regions of the parameter space with local optimum solutions that couldn't reproduce sufficiently the experimental observations (see Appendix A for an example of poor-fit solutions).

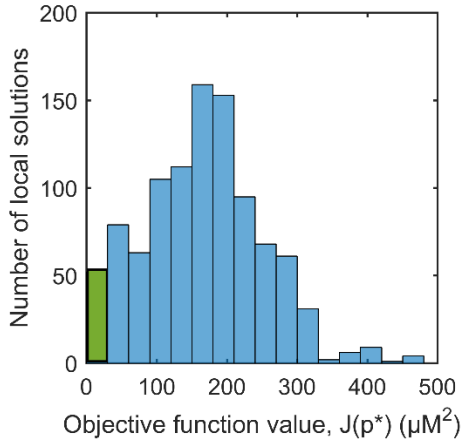

Fig. 7.4. Distribution of the objective function values of the 930 local solutions obtained from the first phase of the parameter estimation strategy. The green-shaded bar is the family of good-fit solutions.

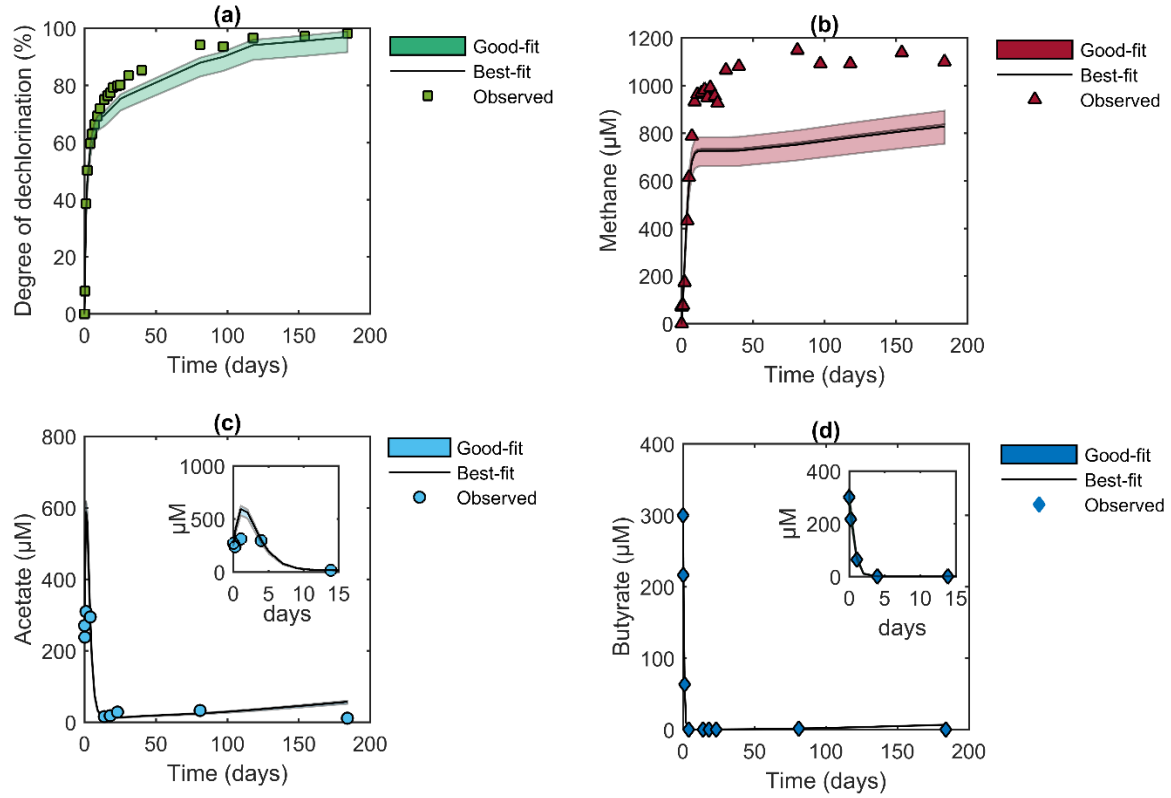

Fig. 7.5. Comparison between the best-fit solution obtained from the first phase of the parameter estimation strategy and the observed values from the batch test for (a) the degree of dechlorination, (b) methane formation, (c) acetate concentrations and (d) butyrate concentrations.

On the basis of the parameter values of these 52 local solutions, insignificant reduction of the parameter space was achieved concerning the kinetic parameters (compare Table 7.9 with Tables 7.6 and 7.7), with the exception of the kinetic parameters of butyrate oxidizers (i.e. $\mu_{max,BO}$, $K_{S,B\text{-}BO}$), the first-order coefficient for the contribution of endogenous decay, K_{ED}, and to some lesser extent the kinetic parameters of dechlorinators (i.e. $\mu_{max,D1}$, $K_{S,TCE\text{-}D1}$, $K_{S,cDCE\text{-}D1}$, $K_{S,VC\text{-}D1}$, K_{INH}, $K_{S,H\text{-}D1}$ for TCE-to-ETH dechlorinators and $\mu_{max,D2}$, $K_{S,TCE\text{-}D2}$, $K_{S,H\text{-}D2}$ for TCE-to-cDCE dechlorinators). The

kinetic parameters related to butyrate-oxidizers and dechlorinators (the latter were in good agreement with those determined for the same culture in Chapter 5) were set equal to the parameters of the best-fit solution and treated as fixed onwards (Table 7.10). This decision is in accordance with our initial aim of producing alternate cultures with the same dechlorinators and butyrate oxidizers.

Table 7.9. Range of values for the family of good-fit solutions of the first phase of the parameter estimation strategy for methanogens and acetate oxidizers.

Substrate	Parameter (units)	Range of values
	H_2-utilizing methanogens	
H_2	Maximum specific growth rate, $\mu_{max,HM}$ ($days^{-1}$)	0.05-1.98
H_2	Half-velocity coefficient, $K_{S\text{-}H,HM}$ (μM)	0.50-5.50
Acetate-utilizing methanogens		
Acetate	Maximum specific growth rate, $\mu_{max,AM}$ ($days^{-1}$)	0.06-0.38
Acetate	Half-velocity coefficient, $K_{S,A\text{-}AM}$ (μM)	500-1920
	Acetate oxidizers	
Acetate	Maximum specific growth rate, $\mu_{max,AO}$ ($days^{-1}$)	0.07-0.26
Acetate	Half-velocity coefficient, $K_{S,A\text{-}AO}$ (μM)	500-1650

Table 7.10. Fixed kinetic parameters for dechlorinators and butyrate oxidizers deriving from the best-fit solution of the first phase of the parameter estimation strategy.

Substrate	Parameter (units)	Symbol	Value
	TCE-to-ETH dechlorinators		
TCE, DCE, VC	Maximum specific growth rate ($days^{-1}$)	$\mu_{max,D1}$	0.19
TCE	Half-velocity coefficient (μM)	$K_{S,TCE\text{-}D1}$	58.10
DCE	Half-velocity coefficient (μM)	$K_{S,cDCE\text{-}D1}$	148.66
VC	Half-velocity coefficient (μM)	$K_{S,VC\text{-}D1}$	466.87
VC	Inhibition coefficient (μM)	$K_{INH,cDCE}$	20.00
H_2	Half-velocity coefficient (μM)	$K_{S,H\text{-}D1}$	0.079
	TCE-to-cDCE dechlorinators		
TCE	Maximum specific growth rate ($days^{-1}$)	$\mu_{max,\ D2}$	2.85
TCE	Half-velocity coefficient (μM)	$K_{S,TCE\text{-}D2}$	602.00
H_2	Half-velocity coefficient (μM)	$K_{S,H\text{-}D2}$	0.051
	Butyrate oxidizers		
Butyrate	Maximum specific growth rate ($days^{-1}$)	$\mu_{max,BO}$	0.52
Butyrate	Half-velocity coefficient (μM)	$K_{S,B\text{-}BO}$	213.00
Butyrate	1st-order coefficient for endogenous decay ($days^{-1}$)	K_{ED}	0.004

Concerning the unknown initial biomass concentrations, a negative correlation between the concentrations of H_2-utilizing methanogens and acetate-utilizing methanogens was detected (Fig. 7.6). In order to capture this correlation four values of the concentrations of acetate-utilizing methanogens were selected and delimited three subranges, creating, thus, three families of cultures, one with high dominance of acetate-utilizing methanogens (family A), one with moderate dominance of acetate-utilizing methanogens (family B) and one with dominance of H_2-utilizing methanogens (family C). In these three families of cultures, acetate oxidizers were uniformly distributed within a narrowed range of values, i.e. X_{AO} ranged between 0.50 mg VSS/l and 0.80 mg VSS/l (Table 7.11). Creating these three families of cultures gives us the opportunity to

perform a targeted search for solutions with (a) diverse non-dechlorinating communities and (b) an improved fit of the model output to the observations.

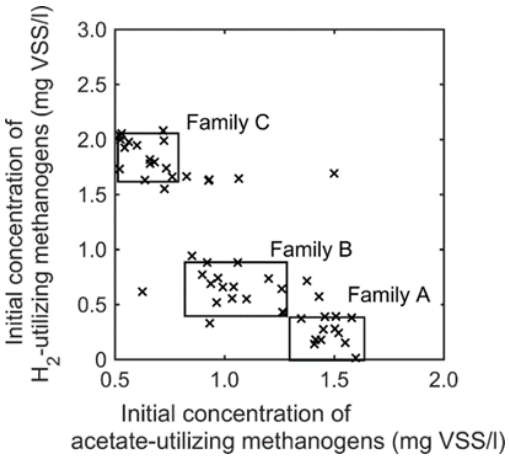

Fig. 7.6. Initial biomass concentrations of methanogens for the 52 good-fit solutions, illustrating the three families of cultures used during the second phase of the parameter estimation strategy.

Table 7.11. Fixed and adjustable initial biomass concentrations following the first phase of the optimization strategy.

Microorganism	Symbol	Type	Range of values (mg VSS/l)			Value (mg VSS/l)
			Family A	Family B	Family C	
TCE-to-ETH dechlorinators	$X_{D1,o}$	Fixed	-	-	-	10.21
TCE-to-cDCE dechlorinators	$X_{D2,o}$	Fixed	-	-	-	3.89
H_2-utilizing methanogens	$X_{HM,o}$	Adjustable	0.01-0.40	0.40-0.80	1.60-2.10	-
Acetate-utilizing methanogens	$X_{AM,o}$	Adjustable	1.20-1.60	0.70-1.20	0.50-0.70	-
Butyrate oxidizers	$X_{BO,o}$	Fixed	-	-	-	2.95
Acetate oxidizers	$X_{AO,o}$	Adjustable		0.50-0.80		-

Phase 2: The relative abundance of the candidate approximations of culture NTUA-M2

In the second phase of parameter estimation, we performed a targeted search for local optimum solutions within the three families of cultures. Ultimately, we specified three cultures with distinctive biomass distributions and improved fit to the observed data. An overview of phase 2 is provided in Fig. 7.7.

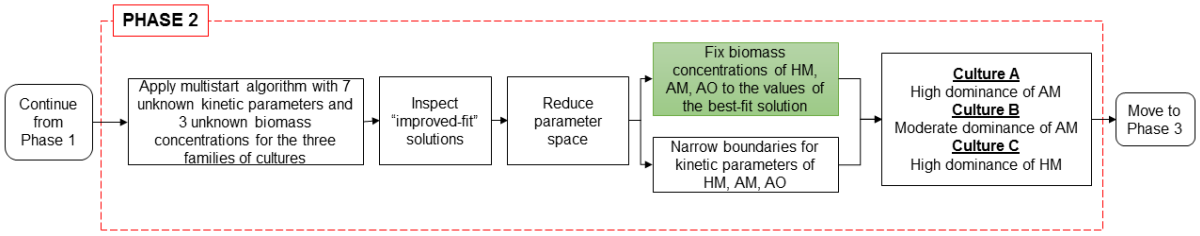

Fig. 7.7. Modeling decisions and results of the second phase of the parameter estimation strategy.

During the second phase of our strategy, we performed 1000 iterations with 41 fixed, 10 adjustable parameters for each one of the three families of cultures. The feasible area of the parameter space is defined by the range of values of the good-fit solutions of the previous phase (Table 7.9 and 7.11). Out of the 1000 local searches performed 910, 918 and 915 local optima were estimated for families A, B and C, respectively. The best-fit points for each family of cultures were slightly improved with respect to the achieved mean absolute simulation errors. More specifically, for the best-fit solution of the three families, E_c was 24 μM, while E_m was 227 μM, 224 μM and 211 μM for families A, B and C, respectively.

For families A, B and C the sets of improved-fit points included 162, 120 and 156 local optima, respectively. Insignificant reduction of the parameter space was observed (compare Table 7.12 with Table 7.9). In order to further decrease the size of the problem, the values for the initial concentrations of acetate-oxidizing bacteria, acetate-utilizing methanogens and H_2-utilizing methanogens from the respective best-fit solutions were treated as fixed onwards. Hence, the initial biomass distributions for each family of cultures were determined from this stage of the optimization strategy (Table 7.13).

Table 7.12. Range of values for the family of good-fit solutions of the second phase of the parameter estimation strategy for methanogens and acetate oxidizers.

Substrate	Parameter (units)	Range of values
H_2-utilizing methanogens		
H_2	Maximum specific growth rate, $\mu_{max,HM}$ ($days^{-1}$)	0.08-1.98
H_2	Half-velocity coefficient, $K_{S\text{-}H,HM}$ (μM)	0.50-3.13
Acetate-utilizing methanogens		
Acetate	Maximum specific growth rate, $\mu_{max,AM}$ ($days^{-1}$)	0.11-0.31
Acetate	Half-velocity coefficient, $K_{S,A\text{-}AM}$ (μM)	500-1890
Acetate oxidizers		
Acetate	Maximum specific growth rate, $\mu_{max,AO}$ ($days^{-1}$)	0.09-0.26
Acetate	Half-velocity coefficient, $K_{S,A\text{-}AO}$ (μM)	500-1650

Table 7.13. Initial biomass concentrations of the best-fit solutions of the three families of cultures considered during the second phase of the parameter estimation strategy.

Microorganism	Symbol (mg VSS/l)	Value Family A	Family B	Family C
TCE-to-ETH dechlorinators	$X_{D1,o}$	10.21	10.21	10.21
TCE-to-cDCE dechlorinators	$X_{D2,o}$	3.89	3.89	3.89
H_2-utilizing methanogens	$X_{HM,o}$	0.03	0.52	2.09
Acetate-utilizing methanogens	$X_{AM,o}$	1.59	1.34	0.64
Butyrate oxidizers	$X_{BO,o}$	2.95	2.95	2.95
Acetate oxidizers	$X_{AO,o}$	0.51	0.57	0.76
Overall biomass concentration		19.18	19.48	20.54

As already mentioned, each culture contains an unaccounted part corresponding to microorganisms besides the six major groups considered herein (mostly primary fermenters and inert cells). This part of the culture was at least equal to 10% of the overall biomass concentration. Families A, B and C were not estimated to have precisely the same percentage of unaccounted biomass and, therefore, the overall biomass concentration of the six populations considered also differs (from 19.2 to 20.5 mg VSS/l according to Table 7.13). Nevertheless, these differences are trivial.

Phase 3: Functionally diverse candidate approximations of culture NTUA-M2

In the last phase of parameter estimation, we searched for functionally diverse consortia with fixed initial biomass concentrations by adjusting only the kinetic parameters of methanogens and acetate oxidizers. Finally, we specified four candidate approximations of culture NTUA-M2 with different relative abundances and functionally diverse non-dechlorinators. Phase 3 is schematically presented in Fig. 7.8.

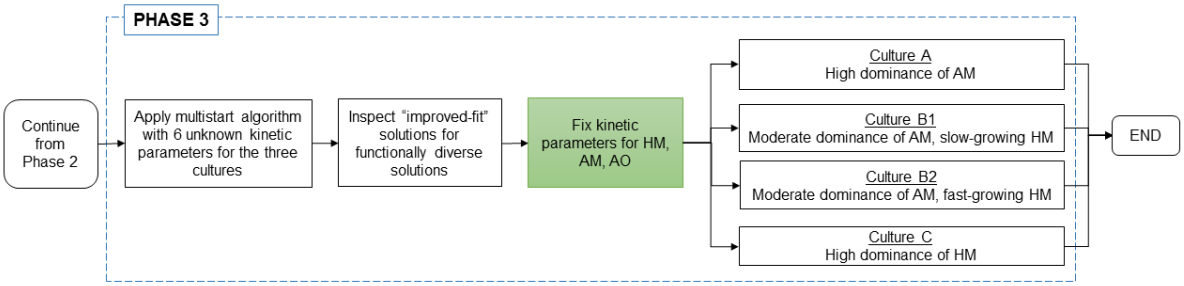

Fig. 7.8. Modeling decisions and results of the third phase of the parameter estimation strategy.

After the third phase, the remaining 6 adjustable parameters (i.e. the kinetic parameters of methanogen, $\mu_{max,HM}$, $K_{S,H\text{-}HM}$, $\mu_{max,AM}$, and $K_{S,A\text{-}AM}$, and acetate oxidizers, $\mu_{max,AO}$, $K_{S,A\text{-}AO}$) for each one of the three families of cultures were estimated. As in the previous phase of the optimization strategy, the majority of local searches converged to a local optimum solution; for families A, B and C, 295, 283 and 285 local optima were estimated, respectively. Again, during this phase, only local optima with simulation errors smaller than those in the best-fit solution of the previous phase will be considered. For families A, B and C the sets of these optimum points included 15, 18 and 12 solutions, respectively. The best-fit points for each family of cultures were slightly improved with respect to the achieved E_a. More specifically, E_c was 21 μM, 20 μM and 20 μM for the best-fit solution of families A, B and C, respectively. In addition, E_m was 222 μM, 222 μM and 208 μM

for families A, B and C, respectively. Hence, any further search of local optima with the specific relative abundances would be inefficient; the reduction of simulation errors is disproportionate to the computation effort required.

In the three sets of good-fit points created, parameter variability was significant. However, functional variability of the solutions of families A and C declined; the relative contribution of the two methanogenic pathways and the efficiency of acetate-oxidizing bacteria was more or less the same within the local solutions. At this point, the parameters of the best-fit solution were selected and, thus, one representative of each one of the two families of cultures was fully described. In contrast, functional variability remained in family B; many functionally diverse solutions could reproduce the experimental observations adequately. In order to capture this variability, two solutions were selected and defined two cultures, B_1 and B_2, which differed mainly in the maximum specific growth rates of H_2-utilizing methanogens and kinetic properties of acetate oxidizers (Tables 7.14 and 7.15).

Table 7.14. Kinetic parameters of the two methanogens for the four candidate approximations.

Substrate	Parameter (units)	Symbol	Value			
			Culture A	Culture B_1	Culture B_2	Culture C
H_2-utilizing methanogens						
H_2	Maximum specific growth rate (days^{-1})	$\mu_{max,HM}$	1.93	0.14	1.24	1.96
H_2	Half-velocity coefficient (μM)	$K_{S,H\text{-}HM}$	0.50	0.51	0.79	0.83
H_2	H_2 threshold (μM)	$S_{min,H\text{-}HM}$	0.011			
H_2	Growth yield x10^{-3} (mg VSS/μmol)	Y_{HM}	0.76			
-	Decay coefficient (days^{-1})	b_{HM}	0.024			
Acetate-utilizing methanogens						
Acetate	Maximum specific growth rate (days^{-1})	$\mu_{max,AM}$	0.29	0.28	0.34	0.20
Acetate	Half-velocity coefficient (μM)	$K_{S,A\text{-}AM}$	811	680	740	553
Acetate	Acetate threshold (μM)	$S_{min,A\text{-}AM}$	15			
Acetate	Growth yield x10^{-3} (mg VSS/μmol)	Y_{AM}	1.40			
-	Decay coefficient (days^{-1})	b_{AM}	0.024			

Table 7.15. Kinetic parameters of acetate oxidizers for the four candidate approximations.

Substrate	Parameter (units)	Symbol	Value			
			Culture A	Culture B_1	Culture B_2	Culture C
Acetate oxidizers						
Acetate	Maximum specific growth rate ($days^{-1}$)	$\mu_{max,AO}$	0.21	0.17	0.26	0.26
Acetate	Half-velocity coefficient (μM)	$K_{S,A-AO}$	1286	1304	839	519
Acetate	H_2 inhibition factor (μM)	$S_{H,INH-AO}$	0.08			
Acetate	Growth yield $x10^{-3}$ (mg VSS/μmol)	Y_{AO}	0.70			
-	Decay coefficient ($days^{-1}$)	b_{AO}	0.024			

7.5 The four alternate approximations of culture NTUA-M2

The kinetic parameters of the six microbial groups of each culture have been presented in Tables 7.10, 7.14 and 7.15. The initial compositions of the four alternate cultures are depicted in Fig. 7.9. In this section, only the salient features of the cultures will be discussed.

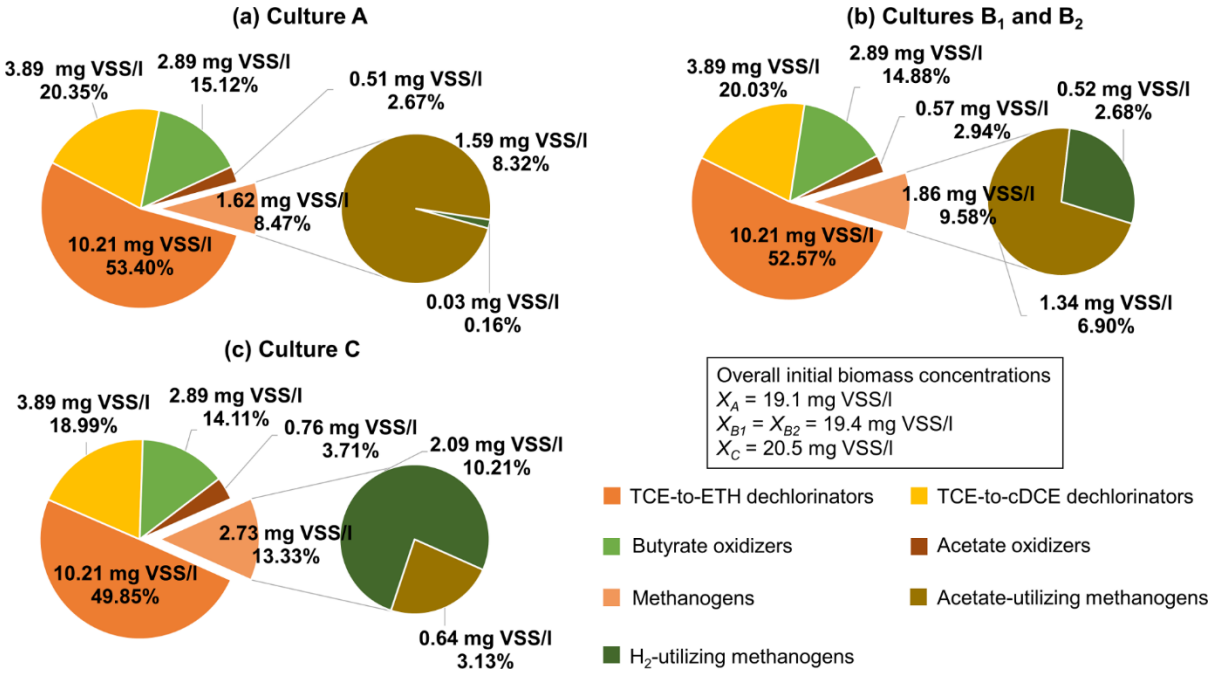

Fig. 7.9. Initial biomass distributions deriving from the optimization strategy followed for the four plausible approximations of culture NTUA-M2.

Dechlorinators and butyrate oxidizers in the four cultures are identical, both in quantitative (i.e. initial biomass concentrations) and in qualitative terms (i.e. the metabolic capabilities of the respective microbial groups). The slow-growing TCE-to-ETH dechlorinators ($\mu_{max,D1}$=0.19 $days^{-1}$), followed by the fast-growing TCE-to-cDCE dechlorinators ($\mu_{max,D2}$=2.85 $days^{-1}$) and the butyrate oxidizers, are the dominant microbial groups comprising at least 83% of the biomass concentration of the six microbial groups considered in each culture (as depicted in Fig. 7.9 the four cultures do

not have the same overall initial concentration of biomass, so naturally the initial relative abundances may differ among the cultures).

The main differences of the cultures derive from the initial relative abundance of the two methanogens, the maximum specific growth rates of H_2-utilizing methanogens and the efficiency of the two acetate-scavenging species. Culture A is characterized by the high dominance of acetate-utilizing methanogens and the presence of few, fast-growing H_2-utilizing methanogens ($\mu_{max,HM}$=1.94 days^{-1}). What is more, acetate-utilizing methanogens are more competitive than acetate oxidizers, considering that they were calculated with a higher specific affinity for acetate (greater $\mu_{max,j}/K_{S,A-j}$ ratio). In cultures B_1 and B_2, acetate-utilizing methanogens are moderately dominant. In culture B_1, H_2-utilizing methanogens are estimated to be slow growers ($\mu_{max,HM}$=0.14 days^{-1}), while in culture B_2 they are estimated as fast growers ($\mu_{max,HM}$=1.24 days^{-1}). In both cultures, acetate-utilizing methanogens are more competitive than acetate oxidizers with respect to acetate consumption. Culture C is a considerably different culture, as the fast-growing H_2-utilizing methanogens ($\mu_{max,HM}$=1.96 days^{-1}) are the dominant methanogenic population and acetate oxidizers are estimated with a greater specific affinity for acetate than acetate-utilizing methanogens.

The behavior of the four cultures in the batch test with low electron donor surplus is practically indistinguishable when dechlorination, methane and VFA concentrations are examined. Simulation fit in terms of the *DoD* is comparable for the four cultures (simulation error, E_c, was 21 μM, 24 μM, 20 μM and 20 μM for cultures A, B_1, B_2 and C, respectively); simulated chloroethene and ETH concentrations are compared to their corresponding observed concentrations in Appendix A. All cultures reproduced dechlorination sufficiently, predicting that *DoD* would ultimately plateau at 98% (Fig.7.10a); Concerning methanogenesis the four cultures are also equivalent (Fig.7.10b); the cultures reproduced poorly methane formation (E_m was 222 μM, 220 μM, 220 μM and 208 μM for cultures A, B_1, B_2 and C, respectively), because, as already discussed, in the batch experiment the end products accounted for 47% more electron equivalents than those offered. Based on simulation results, only 25% of these extra consumed electron equivalents may be attributable to biomass decay, which became a significant electron donor source for all cultures following day 14. Finally, with regard to VFA concentrations, all candidate cultures predicted the complete VFA consumption by day 14 and the slow VFA production from the decaying biomass (Fig. 7.9c and 7.9d).

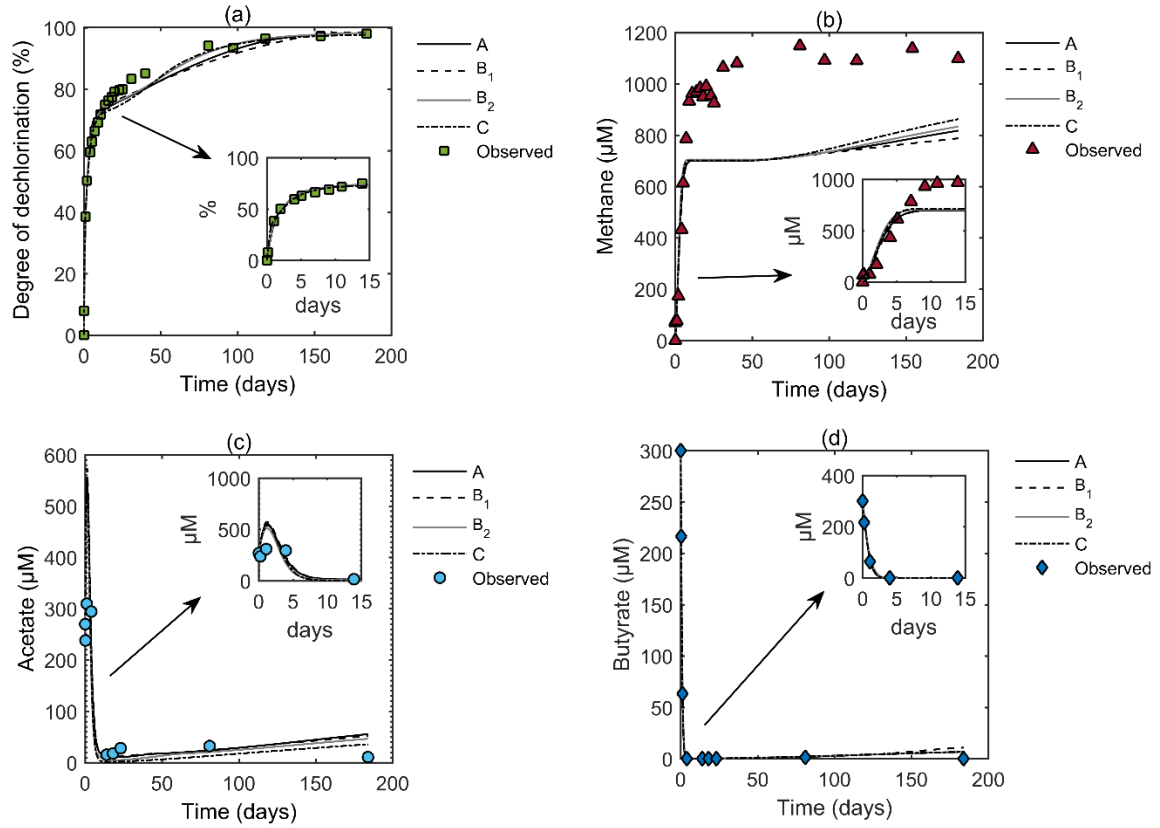

Fig. 7.10. Comparison between the four equivalent solutions of the inverse problem and the observed values from the batch test for (a) the degree of dechlorination, (b) methane formation, (c) acetate concentrations and (d) butyrate concentrations.

Differences among the four alternate cultures are highlighted when the detailed behavior of each culture is investigated for the first 14 days, as demonstrated in Fig. 7.11. Cultures A and B_1 demonstrated nearly identical behavior, considering that (a) the relative contribution of the two methanogenic pathways (Fig. 7.11a) and (b) the efficiency of acetate oxidation (Fig. 7.11c) were equivalent in the two cultures. However, the same end-point was reached by two different trajectories; the very few fast-growing H_2-utilizing methanogens of culture A produced the same quantity of methane as the slow-growing H_2-utilizing methanogens in culture B_1. Cultures B_1 and B_2 have the same relative abundance of methanogens, but in culture B_2 the fast-growing H_2-utilizing methanogens produced more methane (15% of the overall methane production was hydrogenotrophic). Culture C behaved differently: fast-growing H_2-utilizing methanogens outcompeted dechlorinators (Fig. 7.11b) and produced 65% of the total methane. Nevertheless, dechlorinators produced the same *DoD* as in cultures A, B_1 and B_2, as a greater H_2 quantity was available to them. Due to the poor competitive fitness of acetate-utilizing methanogens in culture C, acetate oxidation became an important acetoclastic metabolism and more H_2 was eventually produced from butyrate (Fig. 7.11c).

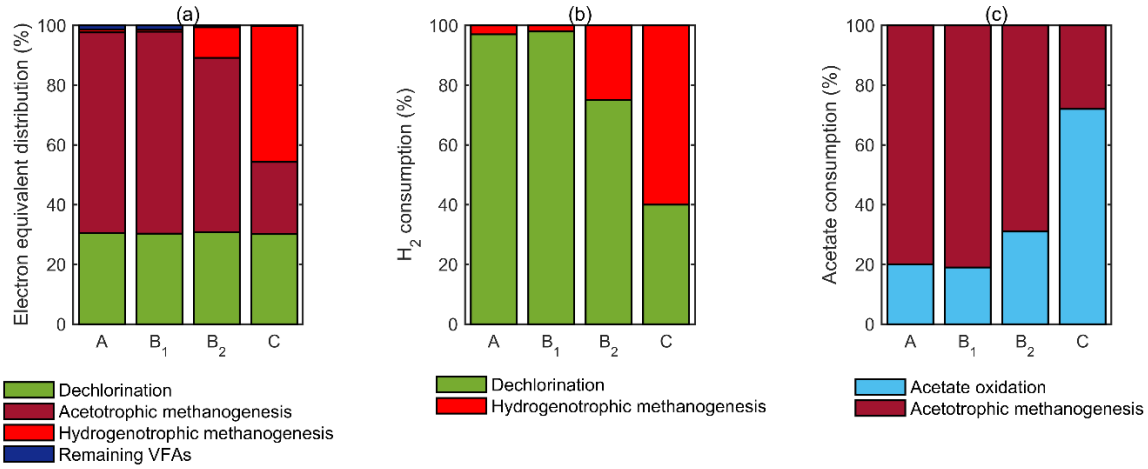

Fig. 7.11. Distribution of (a) electron equivalents, (b) consumed H_2 by dechlorinators and H_2-utilizing methanogens, and (c) consumed acetate by acetate oxidizers and acetate-utilizing methanogens at 14 days for an initial supply of 300 μM butyrate to cultures A, B_1, B_2 and C. The total available H_2 for cultures A, B_1, B_2 and C was 1131 μM, 1104 μM, 1425 μM and 2520 μM, respectively.

In terms of the quality of fit, the stepwise approach implemented herein did not produce remarkably better results from best-fit solution obtained from its first step (observe the mild improvement of the four solutions in Fig. 7.10 relative to the best-fit solution in Fig. 7.5). Yet, as indicated from the simple models tested in Chapter 5, there is no guarantee that the best-fit solution of the problem during phase 1 is a good approximation of the actual culture. Therefore, this stepwise approach provides confidence that the most probable behavior models that approximate culture NTUA-M2 under a low butyrate supply were identified. The cross-confirmation technique presented in the following section will demonstrate if any of the four candidate approximations of culture NTUA-M2 is acceptable.

7.6 Cross-confirmation of the alternate approximations of culture NTUA-M2

The four candidate approximations of culture NTUA-M2 described equivalently the batch test under the low electron donor surplus. In order to discriminate among them, we simulated two experiments performed at different instances of the life of the culture, with different electron donors and different surplus quantities (experiments HEDS-B2, MEDS-H2).

The initial biomass concentration of non-dechlorinators may differ from experiment to experiment, since methanogenic activity fluctuated significantly over time in the source culture. As discussed in Section 7.2, the culture exhibited periods of suppressed methane formation. During these periods, mean methane formation was 40% lower than the typically observed methane. Therefore, for each candidate approximation of culture NTUA-M2, forward simulations were performed 10,000 times under random initial biomass concentrations, in order to consider the variations of methanogenesis exhibited during the maintenance of the culture. Initial biomass concentrations of methanogens and acetate-oxidizers were assumed to be uniformly distributed around their estimated values. Minimum and maximum biomass concentrations for each microbial group was set equal to -40% and +40% of the estimated biomass concentrations from experiment LEDS-B2. On the other hand, dechlorinators and butyrate oxidizers were considered constant, based on the robustness of dechlorination and butyrate oxidation in the long-term performance of culture NTUA-M2.

7.6.1 Non-limiting electron donor conditions: butyrate-fed experiment

Every candidate culture that included fast-growing H_2-utilizing methanogens (i.e. cultures A, B_2 and C) failed to approximate the behavior of culture NTUA-M2 under elevated butyrate supply. They failed to represent methane formation and VFA consumption patterns sufficiently (Fig. 7.12b to 7.12d, Fig. 7.13b to 7.13d and Fig. 7.14b to 7.14d). In these simulations, significant amounts of methane were produced: e.g. minimum simulated methane production reached 5000 μM for cultures A and C, which is nearly four times greater than the observed concentration of 1400 μM. Moreover, butyrate was completely oxidized, as the fast-growing H_2-utilizing methanogens increased H_2 consumption rates, maintained H_2 levels low (around 0.15 μM) and, thus, made butyrate oxidation thermodynamically feasible. Therefore, simulated acetate concentrations reached a peak by day 6 (when all butyrate was removed) that was at least two-fold greater than the observed acetate concentrations. In addition, dechlorinators exploited this extra available H_2 from butyrate and approached *DoD* values close to 100%.

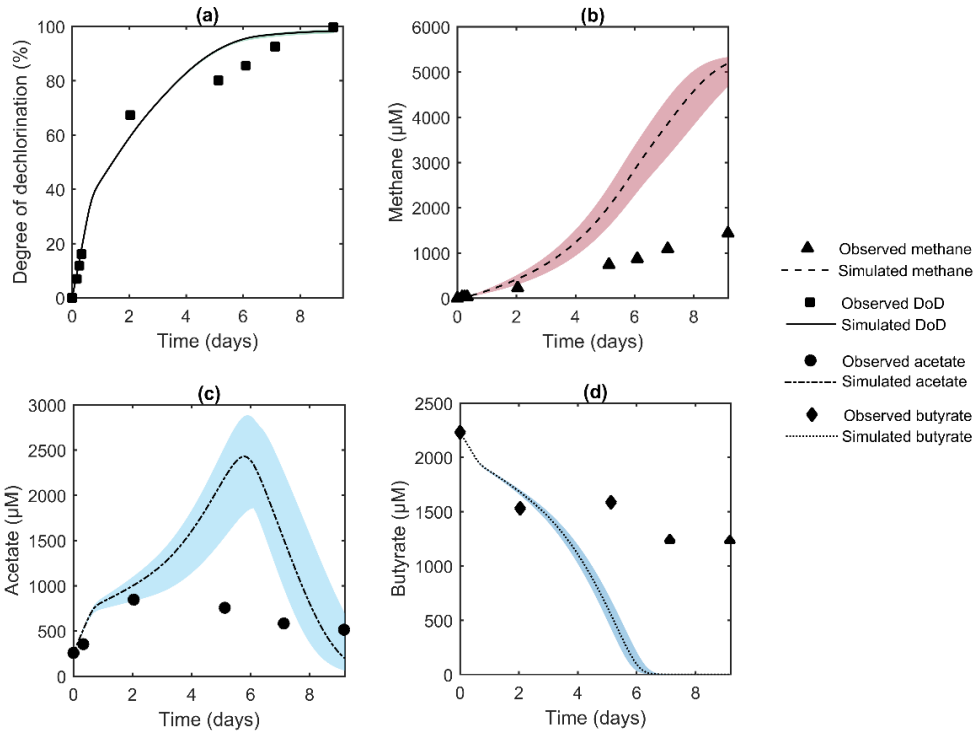

Fig. 7.12. Observed and simulated (a) degree of dechlorination, (b) methane concentration, (c) acetate concentration, and (d) butyrate concentration for batch test HEDS-B2 and candidate culture A. The results of 10,000 simulations performed under random initial conditions are included within the color-shaded areas of each graph.

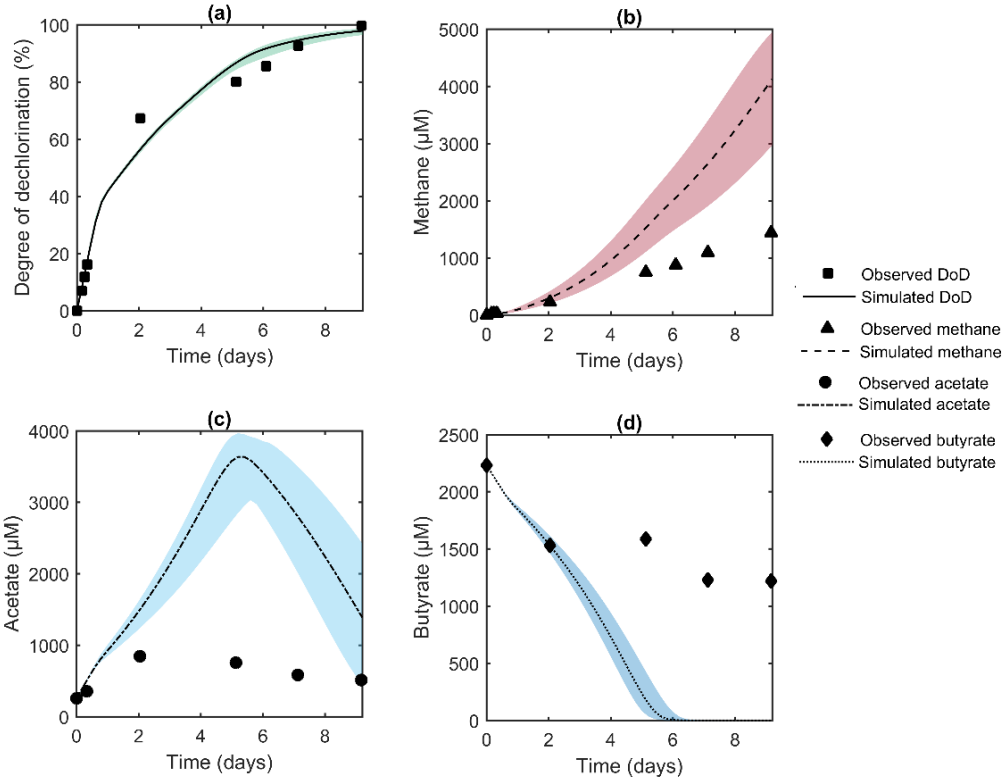

Fig. 7.13. Observed and simulated (a) degree of dechlorination, (b) methane concentration, (c) acetate concentration, and (d) butyrate concentration for batch test HEDS-B2 and candidate culture B_2. The results of 10,000 simulations performed under random initial conditions are included within the color-shaded areas of each graph.

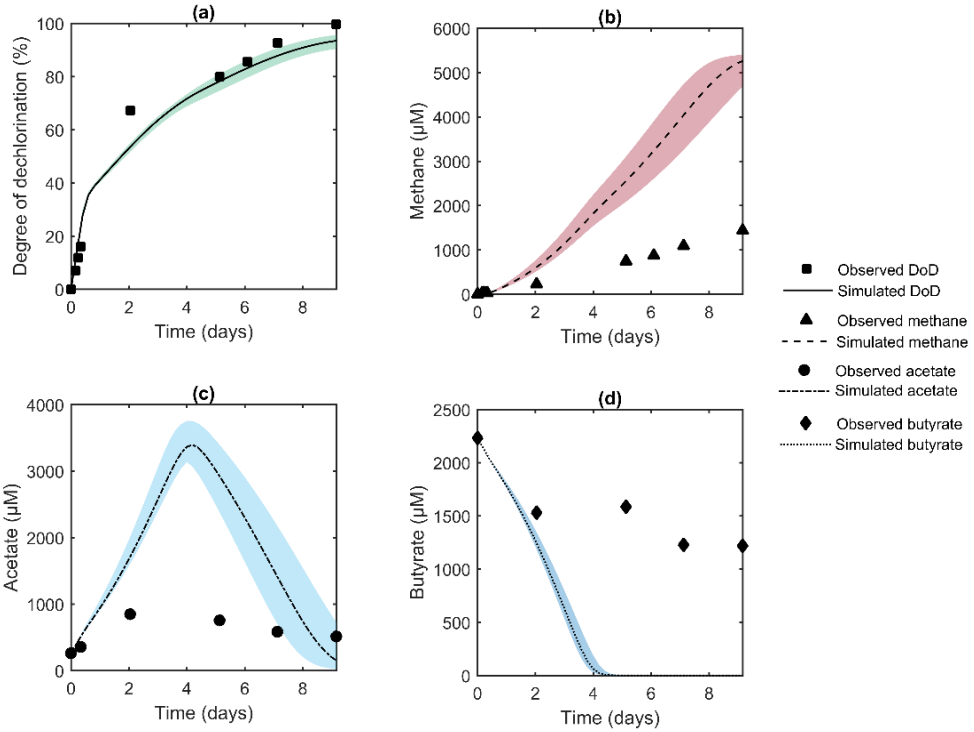

Fig. 7.14. Observed and simulated (a) degree of dechlorination, (b) methane concentration, (c) acetate concentration, and (d) butyrate concentration for batch test HEDS-B2 and candidate culture C. The results of 10,000 simulations performed under random initial conditions are included within the color-shaded areas of each graph.

Simulations performed with culture B_1, which contained few, slow-growing H_2-utilizing methanogens, yielded results closer to the experimental observations (Fig. 7.15). This approximation of culture NTUA-M2 predicted the completion of dechlorination by day 9 (Fig. 7.15a), the accumulation of butyrate (Fig. 7.15d), while it described adequately the smooth increase of acetate during the first two days and its relatively low consumption rate thereafter (Fig. 7.15c). Culture B_1 predicted the lowest methane formation among the candidate cultures. Yet, the mean simulated methane concentration at the end of the simulation was 1.7-fold greater than the observed concentration. This discrepancy, however, could be attributed again to the poor electron equivalent balance of the batch experiment, in which the offered electron equivalents at the beginning of the experiment were 1.7-fold more than the sum of consumed and unused electron equivalents at the end of the experiment.

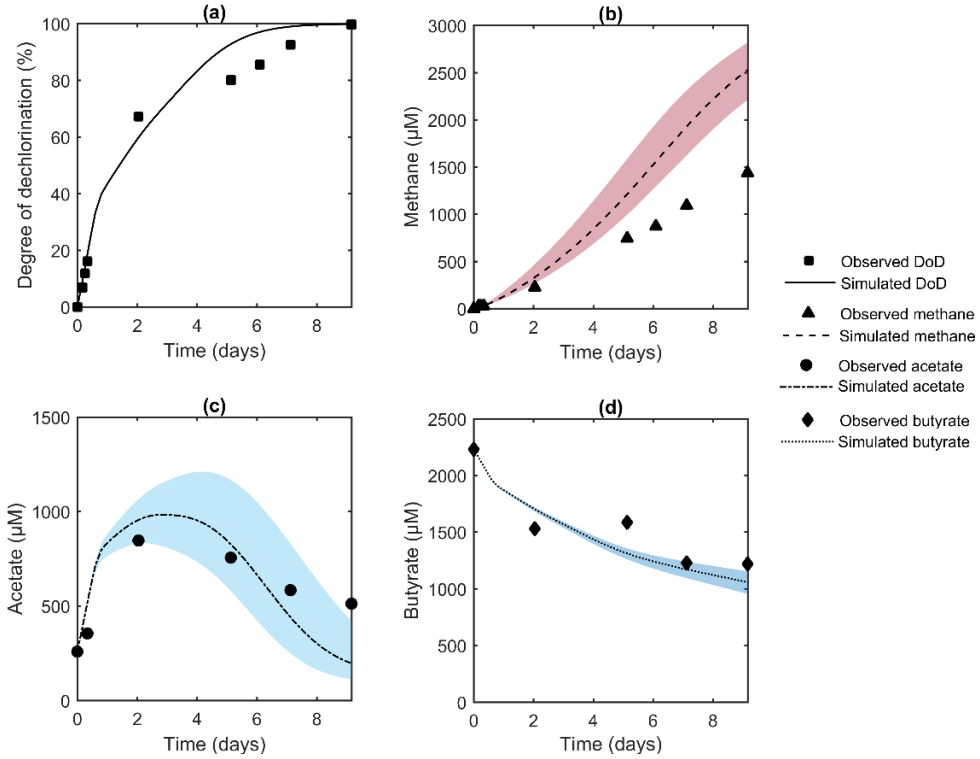

Fig. 7.15. Observed and simulated (a) degree of dechlorination, (b) methane concentration, (c) acetate concentration, and (d) butyrate concentration for batch test HEDS-B2 and candidate culture B_1. The results of 10,000 simulations performed under random initial conditions are included within the color-shaded areas of each graph.

7.6.2 Non-limiting electron donor conditions: H_2-fed experiment

Cultures A, B_2 and C, that include fast-growing H_2-utilizing methanogens, failed to reproduce the observed behavior of the culture under a direct H_2 supply. Simulations performed with cultures A, B_2 and C failed to predict the complete chloroethene removal by day 6 (Fig. 7.16a to Fig. 7.18a). In addition, they failed to represent methane formation and VFA consumption patterns. Simulated methane concentrations were at least 2.5 times greater than the observed concentration of 500 μM (Fig. 7.16b, 7.17b and Fig. 7.18b), because H_2-utilizing methanogens became important H_2-scavengers regardless of their initial relative abundance. Moreover, butyrate was completely consumed in cultures A, B_2 and C (Fig. 7.16d, 7.17d and Fig. 7.18d), since fast-growing H_2-utilizing methanogens poised H_2 levels lower than the H_2-ceiling of butyrate oxidation.

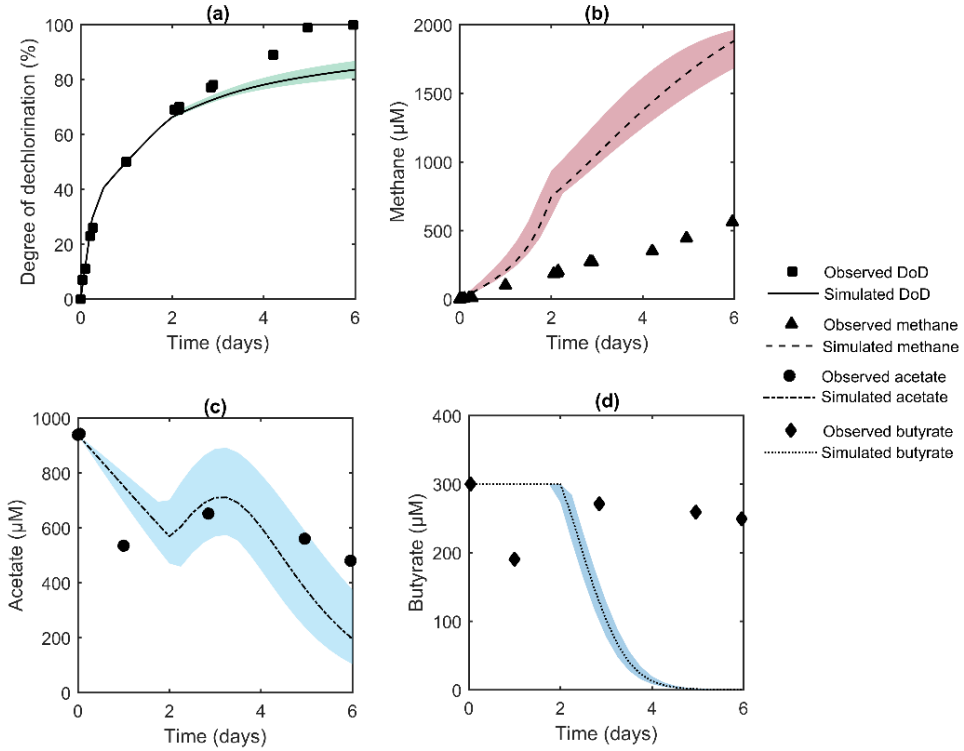

Fig. 7.16. Observed and simulated (a) degree of dechlorination, (b) methane concentration, (c) acetate concentration, and (d) butyrate concentration for batch test MEDS-H2 and candidate culture A. The results of 10,000 simulations under random initial conditions are included within the color-shaded areas of each graph.

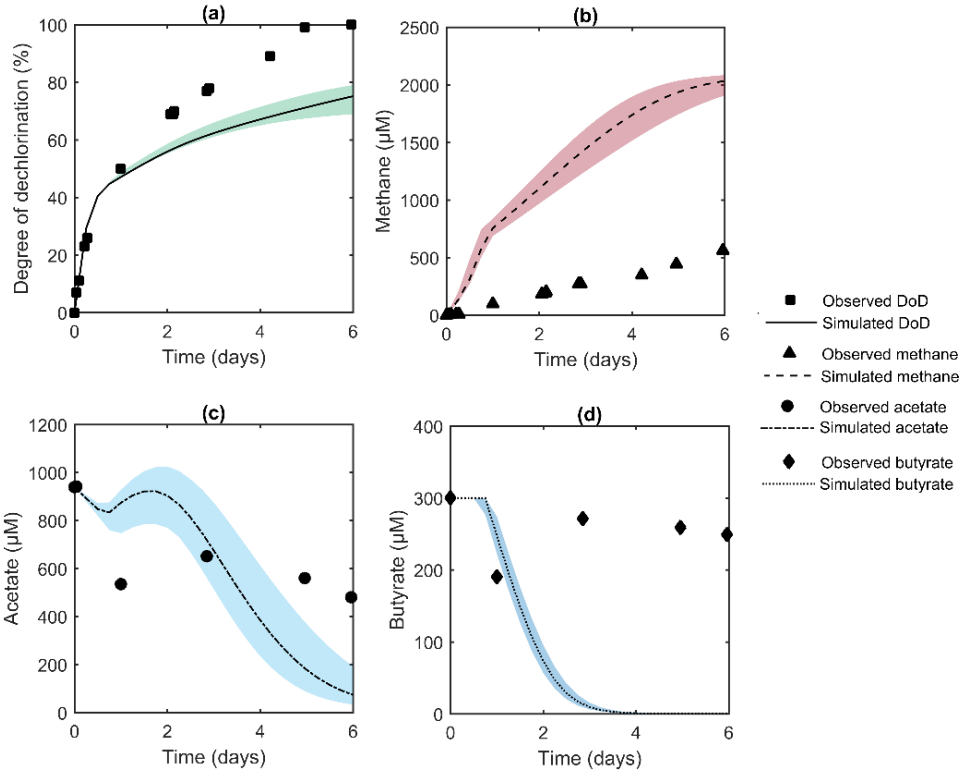

Fig. 7.17. Observed and simulated (a) degree of dechlorination, (b) methane concentration, (c) acetate concentration, and (d) butyrate concentration for batch test MEDS-H2 and candidate culture B_2. The results of 10,000 simulations performed under random initial conditions are included within the color-shaded areas of each graph.

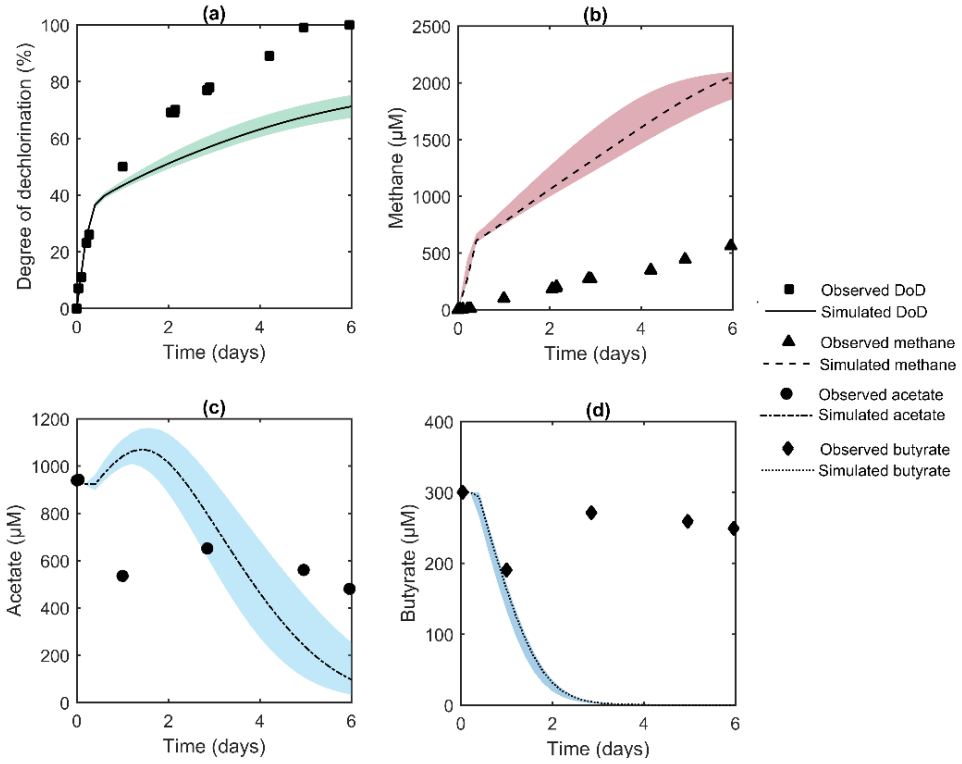

Fig. 7.18. Observed and simulated (a) degree of dechlorination, (b) methane concentration, (c) acetate concentration, and (d) butyrate concentration for batch test MEDS-H2 and candidate culture C. The results of 10,000 simulations performed under random initial conditions are included within the color-shaded areas of each graph.

Culture B_1, which contained slow-growing H_2-utilizing methanogens, described the behavior of the culture sufficiently (Fig. 7.19). Simulations with culture B_1 predicted the fast and complete removal of TCE (Fig. 7.19a) and the thermodynamic inhibition of butyrate consumption (Fig. 7.19d); dechlorinators failed to poise H_2 at low levels. Culture B_1 predicted the lowest methane formation among the candidate cultures, but still overpredicted methanogenic activity (Fig. 7.19b) and underpredicted acetate concentrations (Fig. 7.19c).

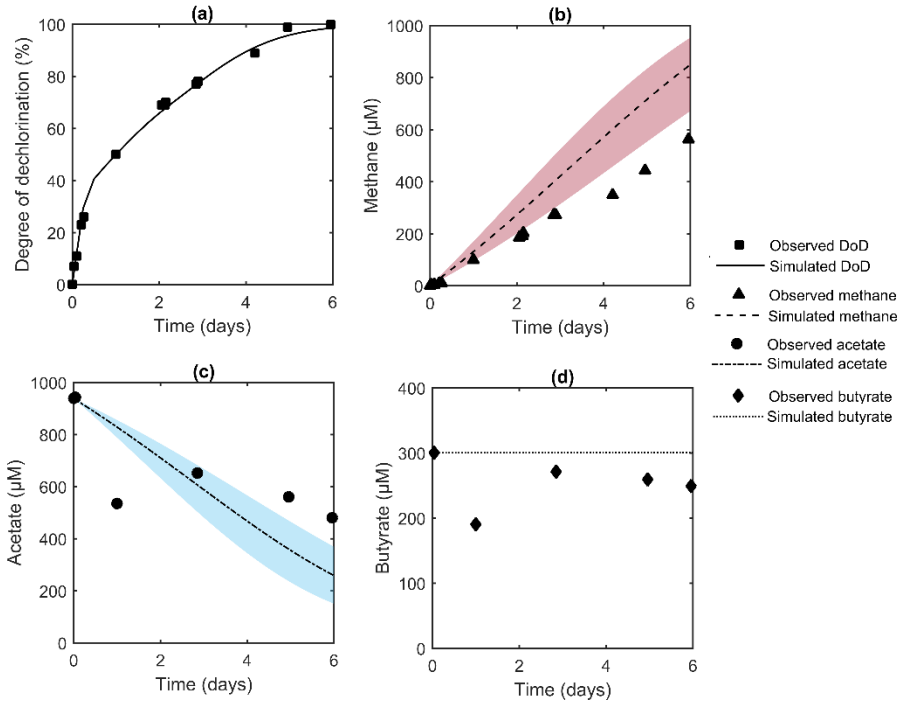

Fig. 7.19. Observed and simulated (a) degree of dechlorination, (b) methane concentration, (c) acetate concentration, and (d) butyrate concentration for batch test MEDS-H2 and candidate culture B_1. The results of 10,000 simulations performed under random initial conditions are included within the color-shaded areas of each graph.

The discrepancy between simulated and observed methanogenesis may be attributed to the fact that experiment MEDS-H2 was performed when the culture was under the inhibited state for methanogenesis. Hence, along with biomass concentrations, kinetic properties of methanogens may differ during this phase of the culture. A 20% lower maximum specific growth rate of acetate-utilizing methanogens simulated better both methane formation and the low acetate consumption rates (Fig. 7.20). In order to assess whether the other candidate solutions could have behaved adequately with a different μ_{max} value, experiment MEDS-H2 was re-simulated for culture A, which was the most promising approximation of the remaining three. A 20% lower μ_{max} for both methanogenic species was considered. Results are not significantly different despite the lower μ_{max} for methanogens (compare Fig. 7.16 to 7.21). Dechlorinators were more efficient due to the diminished competitive fitness of H_2-utilizing methanogens, but still failed to completely remove the existing chloroethenes. H_2-utilizing methanogens were still competent H_2 scavengers and, therefore, deprived from dechlorinators the requisite H_2. Methane was produced at lower concentrations, but it remained three-fold greater from the observed values at the end of the test. Finally, butyrate became thermodynamically favorable by day 3 (whereas previously its consumption initiated by day 2), as it took almost three days for H_2-utilizing methanogens to grow and keep H_2 low enough for butyrate-oxidizing syntrophs to thrive.

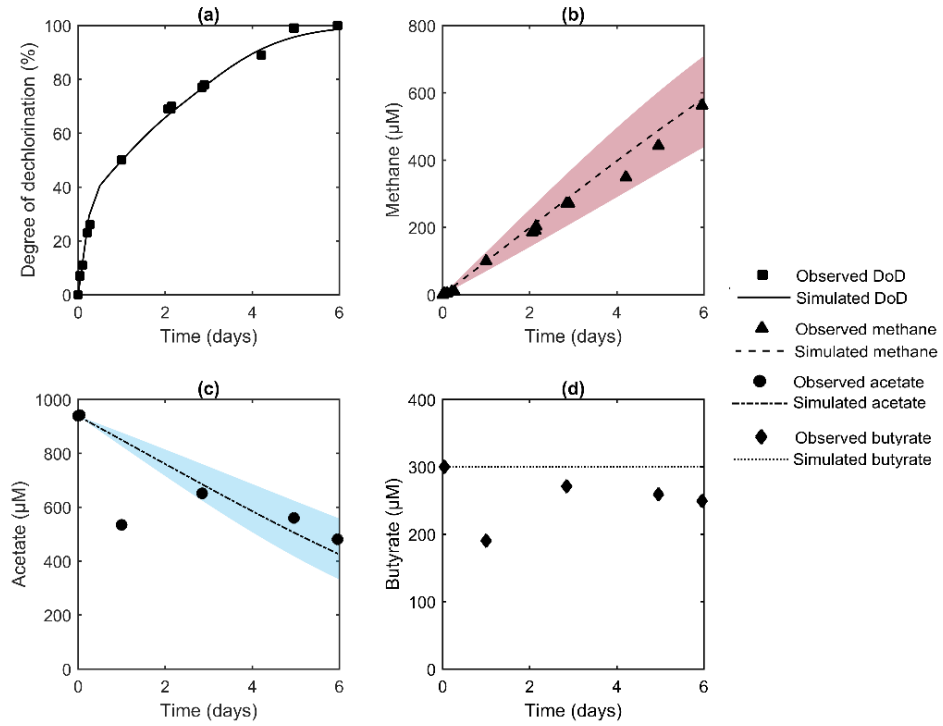

Fig. 7.20. Observed and simulated (a) degree of dechlorination, (b) methane concentration, (c) acetate concentration, and (d) butyrate concentration for batch test MEDS-H2 and candidate culture B_1. The results of 10,000 simulations performed under random initial conditions are included within the color-shaded areas of each graph. Simulations were performed with a 20% lower μ_{max} value for methanogens.

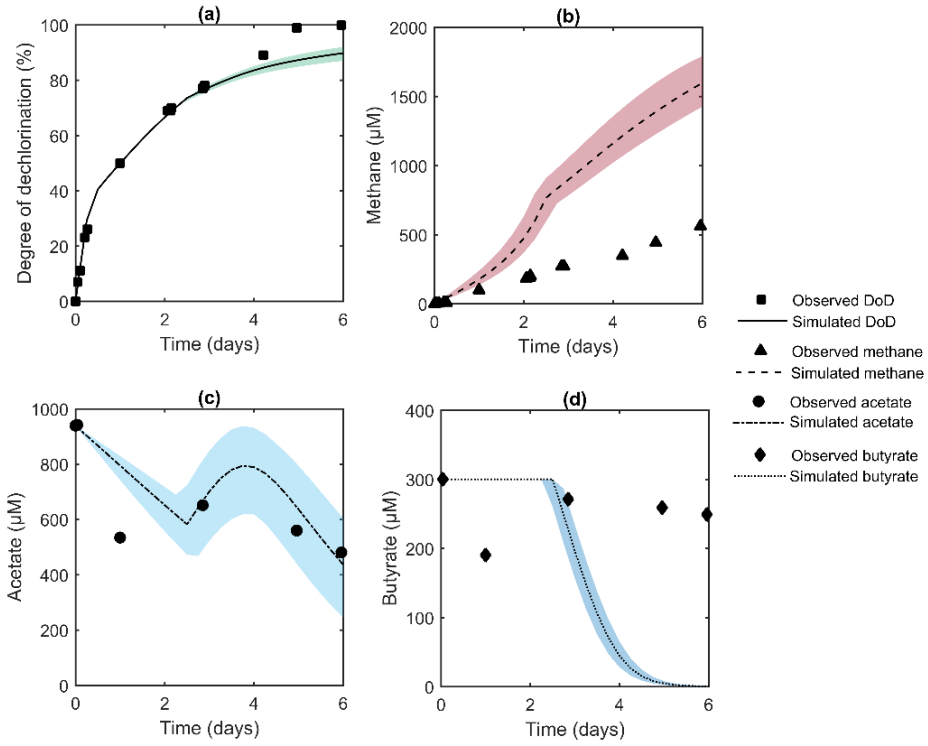

Fig. 7.21. Observed and simulated (a) degree of dechlorination, (b) methane concentration, (c) acetate concentration, and (d) butyrate concentration for batch test MEDS-H2 and candidate culture A. The results of 10,000 simulations performed under random initial conditions are included within the color-shaded areas of each graph. Simulations were performed with a 20% lower μ_{max} value for methanogens.

7.7 Concluding remarks

The model developed herein simulated the behavior of the culture with satisfactory accuracy, despite the simplifying approaches employed for the thermodynamic limitations on VFA oxidation and the contribution of decaying biomass. The successful simulation of the experimental observations collected under different electron donor supply scenarios and distinctive phases of the culture provides confidence that the model described by the formulation and the parameters of culture B_1 can capture the complex dynamics of reducing power in culture NTUA-M2.

Through a stepwise application of the multistart algorithm, small and distinct neighborhoods of the model space were investigated thoroughly in search of behavior models that could be plausible approximations of the functional composition of culture NTUA-M2. This heuristic approach provided confidence that significant processes that underlie experimental observations were not omitted and, ultimately, offered a solution that approximates the behavior of culture NTUA-M2.

Results from the preceding cross-confirmation analysis indicate that in culture NTUA-M2 methanogenesis is almost exclusively acetate-dependent even following the direct supply of H_2 or the addition of high electron donor surpluses. The presence of H_2-utilizing methanogens cannot be excluded, but if they are extant, they are a minority population of the consortium and they should be considered slow-growing.

Simulations underscored the relevance of acetate-oxidizing syntrophs in the distribution of reducing power. Their presence offered evidence that, apart from the competition for H_2, competition for acetate should not be overlooked, especially under limiting electron donor conditions.

This modeling effort is one of the few (especially compared with the significant number of robust dechlorinating consortia) that examines the dechlorinating community collectively and the first that inspects the functional characteristics of non-dechlorinators. Even if the relevance of the latter has been recognized in the literature, only recently have experimental efforts focused on their phylogenetic determination. Yet, inferring the metabolic activities of microbial populations based on phylogenetic analyses can lead to erroneous conclusions regarding the functional structure of non-dechlorinators. The impact of such errors on the extent and efficiency of dechlorination will be examined in Chapter 9, with the help of the four candidate approximations identified herein.

Chapter 8: Examining microbial community shifts in mixed chloroethene-degrading cultures maintained under steady growth conditions

8.1 Introduction

As demonstrated in Chapter 7, mixed dechlorinating consortia constitute complex food webs containing, apart from dechlorinators, methanogens (H_2- and acetate-utilizing species), acetate- and H_2-producing syntrophs. These food webs involve interspecies exchange of reducing power, expressed as transfers of H_2 and acetate among the members of the consortium. Any disturbance in the population of any of the members of the consortium would expectedly impact the entire community. A possible accumulation of substances or a change in the efficiency of a process reflects the impact of such disturbances.

A change in the efficiency of dechlorination has been observed between the two generations of culture NTUA-M, i.e. culture NTUA-M1 and culture NTUA-M2 (see Fig. 4.1 and 4.2). Particularly, an increase in the efficiency of dechlorinators can be observed in culture NTUA-M2 (Antoniou, 2017) when compared to culture NTUA-M1 (Panagiotakis, 2010), both under limiting and under non-limiting electron donor conditions. Given the complexity of culture NTUA-M2, a definite answer for this change cannot be given. Is this change the result of a disturbance in the composition of non-dechlorinators or is it the outcome of the evolution of the dechlorinators? To answer this question, a modeling approach was implemented in search of supporting evidence. Specifically, the model (including the formulation and the kinetic parameters of culture B_1) that described the food web established in culture NTUA-M2 was used as a starting point for the investigation of culture NTUA-M1. Then, using three batch tests performed with the culture NTUA-M1 and the model in inverse mode, we searched for changes in the μ_{max} values and the initial biomass concentrations for each microbial group considered. Specific patterns in the estimated kinetic properties and the relative abundances support that a combined change in the functional characteristics of dechlorinators and H_2-utilizing methanogens could explain the increased performance of dechlorination in culture NTUA-M2.

8.2 Performance differences between culture NTUA-M1 and culture NTUA-M2

The differences in the long-term performance of the two dechlorinating consortia are not striking. First, a systematically increased dechlorinating performance in culture NTUA-M2 is observed. The mean *DoD* for NTUA-M1 is 64%, while the mean *DoD* for NTUA-M2 is 71%. In terms of reducing power this difference is equivalent to 105 μM H_2, which in turn would necessitate the fermentation of 52.5 μM butyrate to acetate and H_2, i.e. almost 18% of the initially supplied quantity. Hence, it should be considered a moderate improvement in the dechlorinating performance of the culture. Regarding methane formation, both cultures had a similarly unstable activity during their maintenance, which coincided with the inversely fluctuating acetate concentrations, that we discussed in Chapter 4. In both cultures, methanogens are systematically unstable (see Fig. 4.2b). Yet, as Fernandes et al. (1999) report, consistency in the behavior of a

methanogenic consortium does not imply an equally stable community composition, as will be explained in Section 8.4.

Apart from the long-term monitoring results, three butyrate-fed batch experiments are available for culture NTUA-M1 (Table 8.1). These tests were performed at different instances of the life of culture NTUA-M1 and under varying electron donor surpluses: (a) test LEDS-B1 (Panagiotakis et al., 2014) was under a low surplus, (b) test MEDS-B1 (Panagiotakis et al., 2015) was performed under a moderate surplus, and (c) HEDS-B1 (Panagiotakis et al., 2015) was performed under a high surplus. As the batch tests were not performed simultaneously, changes in the initial relative abundance of the microbial groups should be anticipated.

In the first two experiments, dechlorinators failed to consume the chloroethenes after 14 days; they achieved a similar *DoD* approximately equal to 70% (Table 8.1), with VC as the main daughter product of dechlorination, followed by ETH. Methane formation in the moderate surplus experiment was 1.8-fold higher than the low surplus experiment, revealing that the extra butyrate provided stimulated mainly methanogens. In the third experiment, dechlorinators removed TCE and its daughter products completely after almost 50 days of operation. But, due to the excessive supply of butyrate, dechlorination was accompanied by excessive methane formation (6000 μM methane).

The high surplus experiment reveals the most notable difference of the two cultures. As described in Chapter 7, when supplied with 2230 μM butyrate (HEDS-B2 test), culture NTUA-M2 dechlorinated completely the provided TCE within nine days, nearly five times faster relative to NTUA-M1. What is more, in NTUA-M2 butyrate accumulated in large quantities and acetate was only moderately increased. On the contrary, in NTUA-M1, butyrate was oxidized completely in almost 10 days and significant amounts of acetate were produced. Methane levels were comparable during the first nine days of each test. But, following day 9, culture NTUA-M1 took advantage of the overabundance of acetate and produced a four-fold higher methane concentration compared to NTUA-M2. This difference in methane production provided the incentive to investigate possible differences in community structure.

Table 8.1. Initial donor and TCE concentrations and electron donor surplus for the numerical batch experiments.

Batch test	Butyrate (μM)	Acetate (μM)	TCE (μM)	Electron donor surplus[1]	Duration (days)	Terminal *DoD* (%)
LEDS-B1	302	142	505	2.4	14	69
MEDS- B1	750	185	495	5.5	14	71
HEDS- B1	3313	317	468	24.5	48	100

[1]: Electron donor surplus is calculated assuming that 1 mol butyrate yields 20 e^- eq. The addition of yeast extract is considered in the model as a source of butyrate, but is not accounted for in the electron donor surplus.

8.3 A modeling approach to investigate community shifts

We aim to search for possible functional differences between cultures NTUA-M1 and NTUA-M2 that would support a probable explanation for the increase in the efficiency of dechlorination in culture NTUA-M2. If such differences exist, they should be reflected in changes in the kinetic properties and the relative abundance of each microbial group thriving in the culture. Therefore, we will use the model developed in Chapter 7 in an inverse mode for each of the batch tests

performed with culture NTUA-M1 in the search for patterns in the kinetic properties and the biomass concentrations of the groups constituting the food web of the two cultures.

Based on an H_2 balance of the culture NTUA-M1, it is evident that syntrophic acetate oxidation is an integral part of the food web established in culture NTUA-M1, along with dechlorination, butyrate oxidation and methanogenesis. The routinely achieved DoD cannot be sustained by the H2 quantities supplied solely by butyrate oxidation. Hence, apart from dechlorination, butyrate oxidation and methanogenesis, acetate oxidation is an integral part of the model. The conceptual model and the mathematical formulation designed in Chapter 4 and applied in Chapter 7 for culture NTUA-M2 are also applicable for culture NTUA-M1. In this application, however, the addition of yeast extract (4.5 mg/l) is also accounted for. Yeast extract is modeled as an input of composite organic material at the beginning of the test, assuming it has the typical chemical composition of biomass ($C_5H_7O_2N$). Thereafter, it contributes to the butyrate pool functioning as an extra source of butyrate. Based on simulation results, the contribution 4.5 mg/l of yeast extract yielded 36 μM butyrate, which was a relatively small contribution compared to that of decaying cells in experiments that lasted more than 14 days.

8.3.1 Preparing the multistart algorithm

The multistart algorithm developed in Chapter 5 and implemented in Chapter 7 will be used in this chapter as well. Hence, at each problem of parameter estimation, we will create a sequence of quasi-random starting points from the feasible area of the parameter space and we will perform local searches with the SQP routine. The hybrid stopping criterion will be checked after each local solution.

Maximum specific growth rates ($\mu_{max,j}$) and initial biomass concentrations of dechlorinators, methanogens and acetate oxidizers will be treated as adjustable parameters in the parameter estimation problems. A similar approach has been previously used by Berggren et al. (2013) and confirmed the microbial shifts occurring in dechlorinating culture PM, after its long-term exposure in sulfides. In that case, changes in the microbial composition were reflected in changes of μ_{max} values and initial biomass concentrations. A limitation of this approach is that changes in the half-velocity coefficients (K_S) resulting from community shifts will not be detected. But, given the correlated nature of μ_{max} and K_S, a change in K_S will be reflected, up to a point, in a change of μ_{max}. Apart from K_S values, the kinetic properties of butyrate oxidizers will be fixed to the values estimated for culture NTUA-M2 in Chapter 7 (Table 8.2). Butyrate oxidizers had a stable performance in both generations of the culture and, hence, insignificant changes are anticipated in butyrate oxidation rates. Only their biomass concentration was considered increased in culture NTUA-M1 taking into account that the added yeast extract constitutes an extra source of butyrate. According to simulations, nearly half of the 4.5 mg/l of yeast extract routinely added is consumed within the weekly feeding cycles offering 18 μM butyrate. Therefore, the initial concentration of butyrate oxidizers in culture NTUA-M1 is equal to 3.2 mg VSS/l, whereas in culture NTUA-M2 was 2.95 mg VSS/l. This value will be treated as fixed in the multistart application.

Table 8.2. Fixed parameters used in the kinetic model for culture NTUA-M1.

Substrate	Microorganism	Symbol	Value
Half-velocity coefficient [μM]			
TCE	TCE-to-ETH dechlorinator	$K_{S,TCE\text{-}D1}$	58.10
TCE	TCE-to-cDCE dechlorinator	$K_{S,TCE\text{-}D2}$	602.00
cDCE	TCE-to-ETH dechlorinator	$K_{S,cDCE\text{-}D1}$	148.66
VC	TCE-to-ETH dechlorinator	$K_{S,VC\text{-}D1}$	466.87
H_2	TCE-to-ETH dechlorinator	$K_{S,H\text{-}D1}$	0.079
H_2	TCE-to-cDCE dechlorinator	$K_{S,H\text{-}D2}$	0.055
H_2	H_2-utilizing methanogen	$K_{S,H\text{-}HM}$	0.51
Acetate	Acetate-utilizing methanogen	$K_{S,A\text{-}AM}$	680
Butyrate	Butyrate oxidizer	$K_{S,B\text{-}BO}$	213.00
Acetate	Acetate oxidizer	$K_{S,A\text{-}AO}$	1304
Growth yield x10^{-3} [mg VSS/μmol]			
TCE, cDCE, VC	TCE-to-ETH dechlorinator	Y_{D1}	4.96
TCE	TCE-to-cDCE dechlorinator	Y_{D2}	2.80
H_2	H_2-utilizing methanogen	Y_{HM}	0.76
Acetate	Acetate-utilizing methanogen	Y_{AM}	1.40
Butyrate	Butyrate oxidizer	Y_{BO}	3.10
Acetate	Acetate oxidizer	Y_{AO}	0.70
Decay coefficient and contribution [$days^{-1}$]			
-	TCE-to-ETH dechlorinator	b_{D1}	0.024
-	TCE-to-cDCE dechlorinator	b_{D2}	0.024
-	H_2-utilizing methanogen	b_{HM}	0.024
-	Acetate-utilizing methanogen	b_{AM}	0.024
-	Butyrate oxidizer	b_{BO}	0.024
-	Acetate oxidizer	b_{AO}	0.024
	-	K_{ED}	0.004
Substrate threshold [μM]			
H_2	TCE-to-ETH or TCE-to-cDCE dechlorinator	$S_{H,min\text{-}D1}$ or $S_{H,min\text{-}D2}$	0.002
H_2	H_2-utilizing methanogen	$S_{H,min\text{-}HM}$	0.011
Acetate	Acetate-utilizing methanogen	$S_{A,min\text{-}AM}$	15.00
Inhibition coefficients [μM]			
cDCE	TCE-to-ETH dechlorinator	$K_{INH,cDCE}$	20.00
H_2	Butyrate oxidizer	$S_{H,INH\text{-}BO}$	0.25
H_2	Acetate oxidizer	$S_{H,INH\text{-}AO}$	0.08
Initial biomass concentration [mg VSS/l]			
Butyrate	Butyrate oxidizer [1]	X_{BO}	3.20

[1]: The initial biomass concentration of butyrate oxidizers has been calculated from Eq. (8.1) assuming that the overall butyrate supply is equal to 318 μM, assuming that half of the routinely added 4.5 mg/l of yeast extract offered extra 18 μM butyrate within the weekly feeding-cycles of the culture.

For the initial biomass concentrations, upper and lower boundaries were calculated by the steady-state biomass concentration of each microbial group, assuming the respective maximum and minimum mass of substrates consumed during each feeding cycle (Table 8.3):

$$X_{j,\mathrm{SS}} = \frac{\theta_c}{f} \frac{Y_j dS_{i-j}}{1 + b_j \theta_c} \tag{8.1}$$

where $X_{j,SS}$ is the steady-state biomass concentration of microorganism j (mg VSS/l), θ_c is the solid retention time (48 days), f is the duration of the feeding cycles of the culture (7 days), and dS_{i-j} is the molar mass of substrate i consumed by microorganism j during each feeding cycle (μM).

For partial dechlorinators, the lowest possible boundary is zero, under the assumption that they are not active in culture NTUA-M1. This assumption provides the upper boundary for TCE-to-ETH dechlorinators, as they would consume every available chloroethene on a weekly basis. Conversely, the upper boundary for partial dechlorinators is calculated if we assume that they consume all the available TCE on a weekly basis. For TCE-to-ETH dechlorinators, this assumption provides the lowest boundary, as they should grow solely on cDCE and VC.

The lowest possible boundary for each methanogenic biomass concentration is zero. On the other hand, the upper boundary was calculated assuming that, the mean methane production in culture NTUA-M1 was completely attributable either to H_2-utilizing methanogens or to acetate-utilizing methanogens. For the acetate oxidizers, the minimum and maximum dS values are calculated from the mass balance for acetate: maximum dS was calculated assuming that methanogenesis was entirely hydrogenotrophic (i.e. all acetate yielding from butyrate oxidation is consumed by acetate oxidizers), whilst minimum dS was calculated when methanogenesis was presumed entirely acetotrophic. Finally, we excluded from our local searches those combinations of initial biomass concentrations that added an overall biomass concentration greater than the average concentration of culture NTUA-M1 (26-27 mg VSS/l).

Table 8.3. Minimum and maximum substrate consumption for dechlorinators, H_2-utilizing methanogens, acetate-utilizing methanogens and acetate oxidizers in culture NTUA-M1.

Microorganism	Substrate consumed on a weekly basis, dS_{i-j} (μM)	
	Min	Max
TCE-to-ETH dechlorinator[1]	455.00	957.5
TCE-to-cDCE dechlorinator[1]	0.00	503.00
H_2-utilizing methanogens[1]	0.00	1898.80
Acetate-utilizing methanogens[2]	0.00	474.70
Acetate oxidizers[2]	227.50	688.00

[1]: dS_{i-j} is expressed in μM of H_2

[2]: dS_{i-j} is expressed in μM of acetate

The boundaries used for μ_{max} values are those dictated by the values reported in the literature. Thus, they coincide with the boundaries used in Chapter 7 for the parameter estimation problem of culture NTUA-M2 (Table 8.4).

Table 8.4. Adjustable parameters of the kinetic model for culture NTUA-M1.

Substrate	Microorganism	Symbol	Range	Constraints	Reference
Maximum specific growth rate (days^{-1})					
TCE	TCE-to-ETH or TCE-to-cDCE dechlorinator	$\mu_{max,D1}$ or $\mu_{max,D2}$	0.33-4.30		(a), (b)
cDCE	TCE-to-ETH dechlorinator	$\mu_{max,\ D1}$	0.04-0.46	0.01-4.30	(c), (a)
VC	TCE-to-ETH dechlorinator	$\mu_{max,\ D1}$	0.01-0.49		(c), (a)
H_2	H_2-utilizing methanogen	$\mu_{max,HM}$	0.02-1.98 [1]	0.02-1.98	(d), (e)
Acetate	Acetate-utilizing methanogen	$\mu_{max,AM}$	0.04-0.38 [1]	0.04-0.38	(d), (e)
Butyrate	Butyrate oxidizer	$\mu_{max,BO}$	0.21-0.52 [2]	0.21-0.52	(d)
Acetate	Acetate oxidizer	$\mu_{max,AO}$	0.04-0.26 [3]	0.04-0.26	(f)
Initial biomass concentration (mg VSS/l)					
-	TCE-to-ETH dechlorinator	X_{D1}	7.20-15.10	7.20-15.10	Eq. (8.1)
-	TCE-to-cDCE dechlorinator	X_{D2}	0.0-4.50	0.0-4.50	Eq. (8.1)
-	H_2-utilizing methanogen	X_{HM}	0.0-4.50	0.0-4.50	Eq. (8.1)
-	Acetate-utilizing methanogen	X_{AM}	0.0-2.10	0.0-2.10	Eq. (8.1)
-	Acetate oxidizer	X_{AO}	0.25-1.53	0.25-1.53	Eq. (8.1)

[1]: Parameter values were corrected from a temperature T to a temperature of 25°C according to the equations (Rittmann and McCarty, 2001): $\mu_{max,j}^{25} = \mu_{max,j}^{T} e^{0.06(25-T)}$, $K_S^{25} = K_S^T e^{-0.077(25-T)}$, $b_j^{25} = b_j^T e^{0.14(25-T)}$

[2]: Parameter values were corrected to a temperature of 25°C assuming that an increase of 10°C doubles maximum specific growth rates and decay coefficients, while it reduces half-velocity coefficients by half.

[3]: The values were calculated by the reported doubling times and were corrected to a temperature of 25°C assuming that an increase of 10°C doubles maximum specific growth rates.

(a) Cupples et al. (2004a), (b) Christ and Abriola (2007), (c) Yu and Semprini (2004), (d) Pavlostathis and Giraldo-Gomez (1991), (e) Oude Elferink et al., (1994), (f) Hattori (2008)

8.3.2 Application of the multistart strategy for culture NTUA-M1

Despite the constrained nature of the problem, many local solutions were found for each batch test: 840 local solutions for LEDS-B1, 921 local solutions for MEDS-B1 and 939 local solutions for HEDS-B1. Yet, less than 1% of the local solutions provided an adequate-fit to each set of observations. These small families of good-fit solutions had similar performance characteristics and, therefore, only the best-fit solutions will be examined for each test. Similar to Chapter 7 and for convenience purposes, the stepwise removal of TCE will be presented in an aggregate manner using the degree of dechlorination (*DoD*) which is calculated as described in Chapter 7 and Eq. (7.2). Simulated curves for each chloroethene are available in Appendix A.

The best-fit solutions reproduced the observed data sets sufficiently (Fig. 8.3 to Fig. 8.5). For the low-donor test LEDS-B1, the model simulated accurately dechlorination in conjunction with methane formation (Fig. 8.3a and Fig. 8.3b), with mean absolute errors for chloroethenes equal to

22 μM and for methane equal to 17 μM. The best-fit solution reproduced the pattern of acetate consumption and production, but overpredicted slightly the peak of acetate concentrations at day 2, possibly due to the poor electron equivalent balance of the test during the first three days. For the same reason, it predicted constantly greater acetate values for the moderate-donor test MEDS-B1 (Fig. 8.4bc). Yet, dechlorination and methane formation were simulated adequately (Fig. 8.4a and 8.4b); mean absolute errors were 21 μM for chloroethenes and 87 μM for methane. Finally, the best-fit solution reproduced with fair accuracy all the observed quantities for the high-donor HEDS-B1, apart from the terminal methane levels. Methane formation plateaued at a concentration almost 30% higher than the concentration observed in the batch test. This discrepancy, could be attributed (at least partially) to the poor electron equivalent balance of the batch experiment. The offered electron equivalents at the beginning were 36% more than those consumed or accumulated at the end. Overall, based on the simulations, we are confident that the conceptual model still captures the most important metabolic processes in culture NTUA-M1 and, that changes in μ_{max} values and the relative abundances of the microbial groups of the consortium can capture the differences observed in dechlorination efficiency.

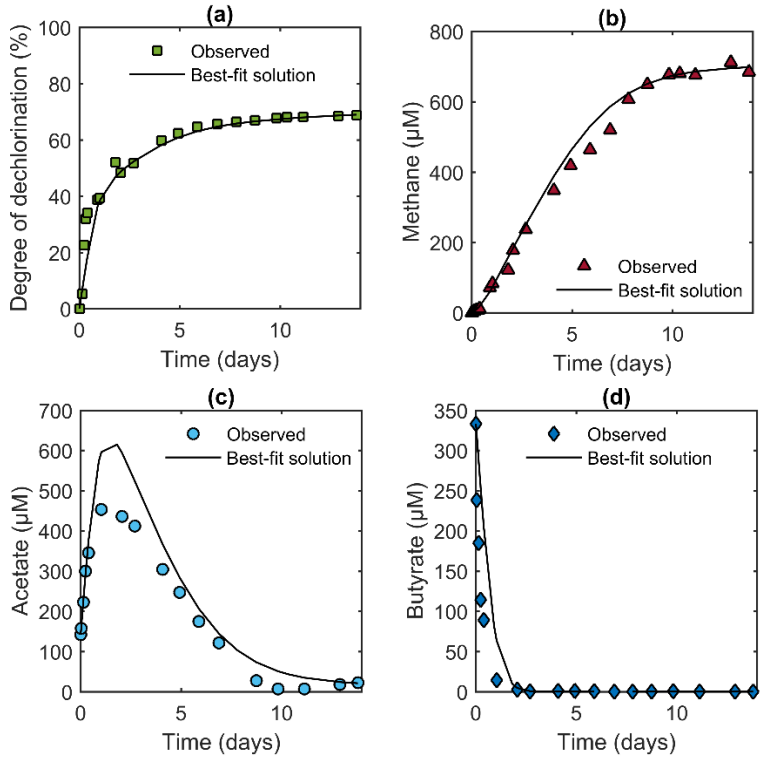

Fig. 8.1. Observed and simulated (a) degree of dechlorination, (b) methane concentration, (c) acetate concentration, and (d) butyrate concentration for batch test LEDS-B1 and culture NTUA-M1.

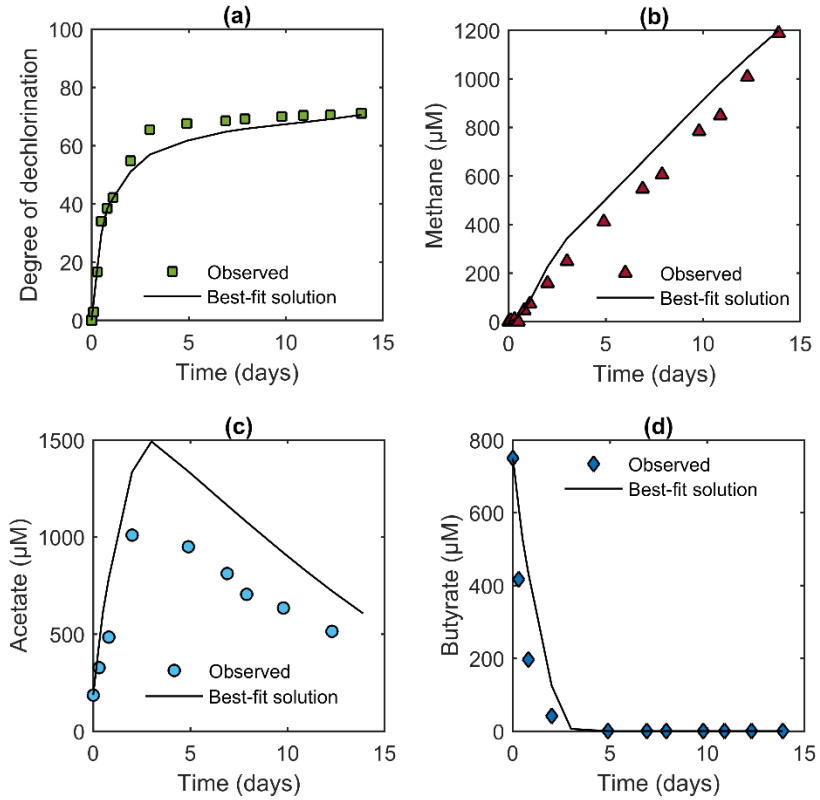

Fig. 8.2. Observed and simulated (a) degree of dechlorination, (b) methane concentration, (c) acetate concentration, and (d) butyrate concentration for batch test MEDS-B1 and culture NTUA-M1.

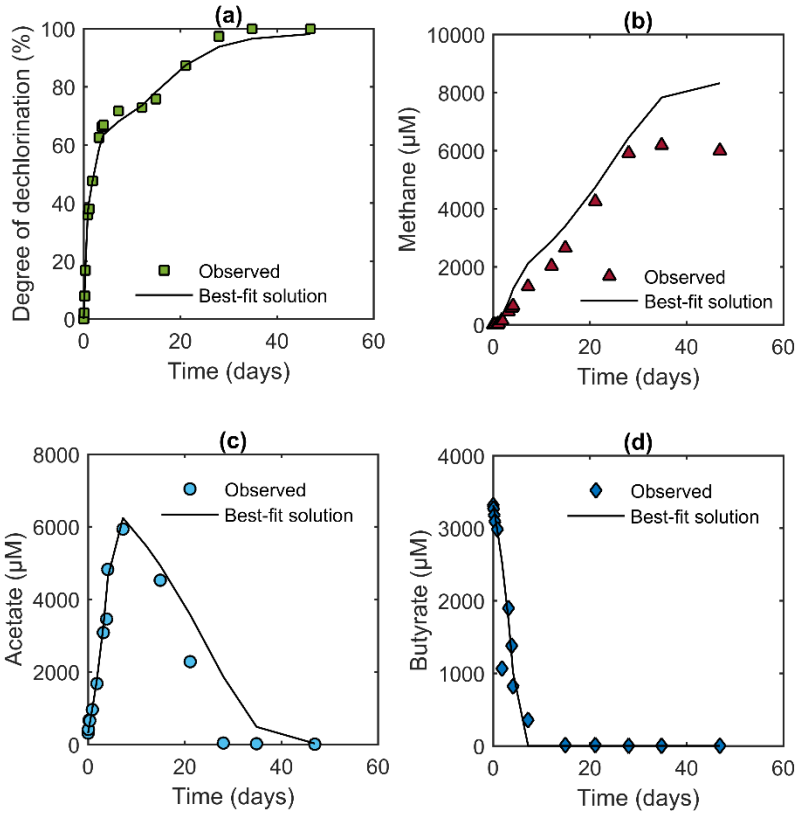

Fig. 8.3. Observed and simulated (a) degree of dechlorination, (b) methane concentration, (c) acetate concentration, and (d) butyrate concentration for batch test HEDS-B1 and culture NTUA-M1.

8.3.3 Gaining insight in the functional differences between NTUA-M1 and NTUA-M2

In this section, we are searching for patterns in the kinetic properties and the biomass concentrations of the populations constituting the food web of the two cultures, NTUA-M1 and NTUA-M2. To this end, the group of green bars (NTUA-M1) will be compared to the red bars (NTUA-M2) in Fig. 8.4.

The most noticeable difference between the two generations of dechlorinating culture NTUA-M1 is reflected in the μ_{max} (Fig. 8.4a) values and relative abundance of H_2-utilizing methanogens (Fig. 8.4b). The lowest $\mu_{max,HM}$ estimated for NTUA-M1 is seven-fold greater than the corresponding value for culture NTUA-M2. In culture NTUA-M1 a dense and faster-growing population of H_2-utilizing methanogens can explain the behavior of the culture under every butyrate supply scenario, i.e. from the low-surplus test LEDS-B1 to the high-surplus test HEDS-B1. Especially in the high-surplus test, this difference underscores that two nearly identical cultures can behave differently following biostimulation, if the make-up of non-dechlorinators is neglected.

A milder difference derives also from the metabolic properties of partial dechlorinators (Fig. 8.4a, D2 bars). In culture NTUA-M1, partial dechlorinators are consistently more competent TCE scavengers (nearly 1.5-fold greater $\mu_{max,D2}$ values, as shown in Fig. 8.4a). Concurrently, TCE-to-ETH dechlorinators demonstrate systematically lower initial concentrations (approximately 20% lower initial biomass concentrations – Fig. 8.4b, D1 bars). Based on these findings, it is reasonable to deduce that in culture NTUA-M1, partial dechlorinators outcompeted TCE-to-ETH dechlorinators, which in turn would grow almost exclusively on cDCE and VC. As they consume a lower quantity of chloroethenes in a weekly basis relative to NTUA-M2 culture (in that case TCE-to ETH dechlorinators consumed almost 20% of the available TCE), steady-state biomass concentrations of TCE-to-ETH dechlorinators should be lower, as indicated by our results (Fig. 8.4b, D1 bars).

Small differences are found in the μ_{max} values and the relative abundance of acetate-scavenging species. Acetate-oxidizing syntrophs (AO) are relatively stable in both cultures. They were a minor and slow-growing population. The behavior of acetate-utilizing methanogens (AM) in the two cultures is also stable, apart from the HEDS-B1 test, in which acetate-utilizing methanogens were a minority population with a low μ_{max}. This inconsistency follows the overall unsteady behavior of the culture regarding methane formation and acetate concentrations. Indeed, HEDS-B1 test was performed in a phase of culture NTUA-M1, when methanogenesis was significantly lower than its mean performance and, thus, the active methanogens could have been fewer and less competent.

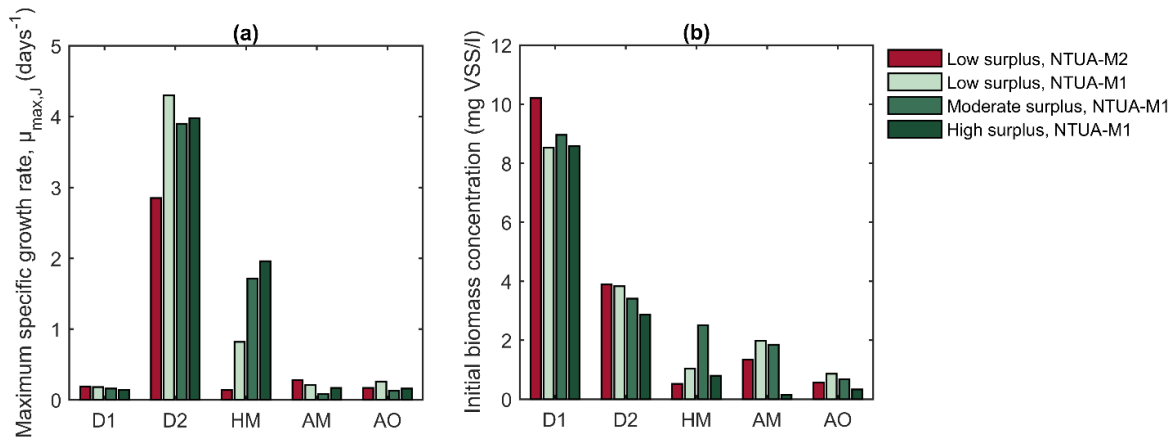

Fig. 8.4. (a) Maximum specific growth rates and (b) initial biomass concentrations for cultures NTUA-M2 and NTUA-M1 under varying electron donor surpluses. D1=TCE-to-ETH dechlorinators, D2=TCE-to-cDCE dechlorinators, HM=H_2-utilizing methanogens, AM=acetate-utilizing methanogens, AO=acetate oxidizers.

Further insight in the functional differences of the two cultures is gained, when observing their behavior under a low electron donor surplus, which resembles the maintenance conditions of the cultures. The differences are mild. In terms of the electron equivalent distribution, both cultures gave a similar outcome (Fig. 8.7a). Acetoclastic methanogenesis was the most efficient metabolism followed by dechlorination. In culture NTUA-M1, acetate-oxidizers were slightly more efficient acetate scavengers compared to culture NTUA-M2 and consumed 19% of the available acetate (in culture NTUA-M1 the respective percentage was 16%). This little, extra available H_2 did not make a change for dechlorinators, as they had to outperform a more efficient H_2-utilizing methanogenic population. The relatively fast-growing H_2-utilizing methanogens ($\mu_{max,HM}$=0.82 days^{-1}) were a considerable part of the culture (5% of the overall biomass concentration of NTUA-M1) and consumed 11% of the available H_2. This consumption contributed only 5% to the overall methane formation, but was adequate to explain the decline in the efficiency of dechlorination. Acetate-utilizing methanogens were still the dominant methanogenic species, as in culture NTUA-M2.

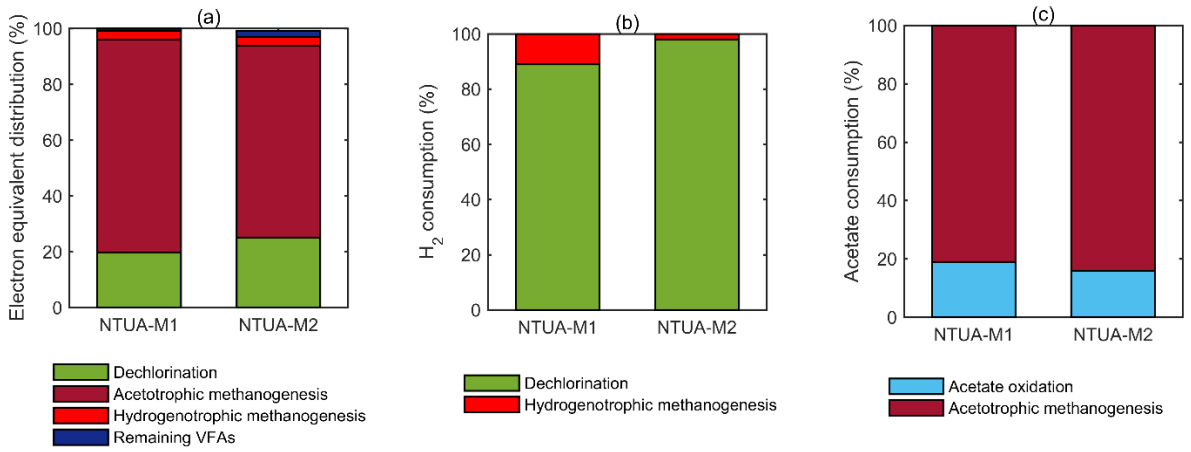

Fig. 8.5. Distribution of (a) electron equivalents, (b) consumed H_2 by dechlorinators and H_2-utilizing methanogens, and (c) consumed acetate by acetate oxidizers and acetate-utilizing methanogens in cultures NTUA-M1 and NTUA-M2 after 14 days for batch tests with low electron donor surpluses.

Simulated results of the LEDS-B1 test in culture NTUA-M1 support the finding of a diverse TCE consumption pattern relative to culture NTUA-M2. In culture NTUA-M1, TCE-to-cDCE dechlorinators (D2) consumed all the available TCE, as a result of their high $\mu_{max,D2}$ value. Hence, TCE-to-ETH dechlorinators (D1) starved during the first day of experiment. Consequently, the active dechlorinating biomass consuming cDCE and VC in NTUA-M1 was sparser than in NTUA-M2 and, thus, it dechlorinated at a slower pace, without being functionally different ($\mu_{max,D1}$ values are practically equal in both cultures). It seems that gradually, the competitive fitness of TCE-to-cDCE dechlorinators deteriorated, TCE-to-ETH dechlorinators grew and filled their role in TCE consumption, leading the overall dechlorinating community to function more effectively. Unfortunately, the reason for this changeover cannot be indicated by our modeling approach.

The existence of fast-growing H_2-utilizing methanogens (HM) also explains the behavior of culture NTUA-M1 under the high electron donor surplus, which constitutes the most profound difference of the two cultures. H_2-utilizing methanogens consumed 92% of the available H_2 rapidly and maintained H_2 concentrations in the range of 0.1 μM for the first week of the experiment (Fig. 8.8c). During this period, butyrate oxidation was thermodynamically feasible and, thus, butyrate was completely removed within the first week of the experiment. Following the first week, the prevailing H_2 concentrations were even lower, in the range of 0.02-0.03 μM, allowing acetate to function as a source of H_2. Acetate oxidizers then consumed 32% of the available acetate, but, due to their poor kinetic properties, they were still outcompeted by acetate-utilizing methanogens. H_2 never went higher than 30 μM and dechlorinating species exploited these conditions. They grew faster from day 7 to day 48 and eventually dechlorinated cDCE and VC. During this period H_2-dependent methanogenesis became slower and acetate-dependent methanogenesis become the main methanogenic pathway, as the initially few acetate-utilizing methanogens grew in numbers.

Under a comparably high electron donor surplus (i.e. 2230 μM butyrate, HEDS-B2), culture NTUA-M2 behaved differently. The slow-growing H_2-utilizing methanogens did not pose a significant threat to dechlorinators. The latter were also denser compared to NTUA-M1 and on that account dechlorinated TCE rapidly within nine days. The fast dechlorination combined with the slow pace of H_2-dependent methanogenesis poised H_2 concentrations at 0.9 μM, inhibited butyrate oxidation and, consequently, left much of the supplied butyrate unused. This seemingly mild difference in the properties of H_2-utilizing methanogens invoked two remarkably different behavior following biostimulation with the same electron donor quantity and type.

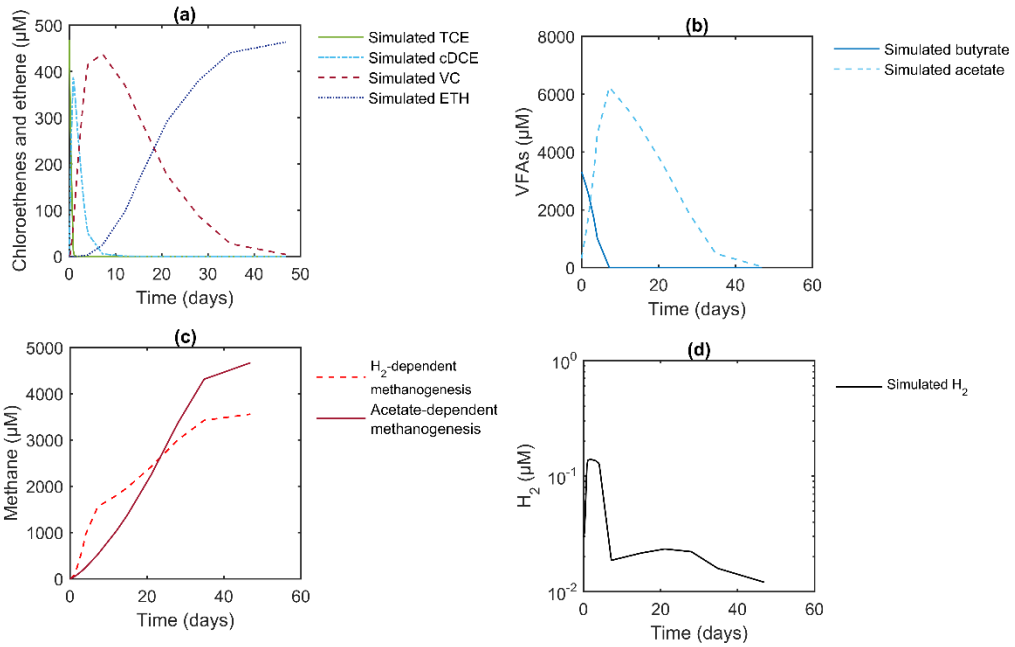

Fig. 8.6. (a) Sequential dechlorination of TCE, (b) VFA concentrations, (c) H_2- and acetate-dependent methanogenesis, and (d) H_2 concentration versus time for culture NTUA-M1 and the HEDS-B1 batch test.

8.4 Concluding remarks

This chapter helped to appreciate a probable cause of the different behavior exhibited by dechlorinating cultures in the literature fed with the similar electron donor types and surpluses. The model was used in an inverse mode and found evidence that outline a probable explanation of the performance differences observed between the two generations of culture NTUA-M in terms of dechlorination efficiency under low electron donor surpluses and, mostly, under elevated surpluses. Based on model results, the differences could be attributed mainly to shifts in the functional properties of H_2-utilizing methanogens and to some extent to a shift in the dechlorinating populations that consume TCE.

Regarding non-dechlorinators, this work suggests that in the first generation of the culture the presence of fast-growing H_2-utilizing methanogens is probable. Under low electron donor surpluses, fast-growing H_2-utilizing methanogens may not be competent H_2 scavengers and, thus, the overall behavior of the cultures will not be dramatically different. But, under excessive butyrate supply the presence of fast-growing H_2-utilizing methanogens is detrimental and the differences, that were previously concealed, became dramatic.

Changes in the functional characteristics of methanogenic consortia are not rare, neither easily detectable. Fernandez et al. (1999) reported a drastic shift in a methanogenic consortium, with a H_2- and formate-utilizing methanogen being replaced by a methylotrophic methanogen in an ecosystem with steady methanogenic performance. With respect to dechlorinating consortia, Hug et al. (2012) showed that in three of the most prominent dechlorinating cultures (KB-1, DonnaII and ANAS) the identities of non-dechlorinators also varied significantly, filling, however, the same niche within each consortium. Each metabolic pathway in these cultures (e.g. VFA fermentation or methane formation) was functionally redundant, with key processes encoded by multiple taxonomic groups. Thus, an extremely diverse and dynamic community could co-exist with

dechlorinators. This community could be rearranged in several different ways and still demonstrate a seemingly stable behavior, but only under specific conditions. However, under extrapolating conditions these differences may become important. The implications of these changes will be re-visited in the following chapter.

According to the simulations, it is probable that the outcome of the competition for TCE has changed over time. In culture NTUA-M1, partial dechlorinators were almost exclusively responsible for TCE consumption. With time, competition for TCE changed, with TCE-to-ETH dechlorinators consuming around 30% of TCE in culture NTUA-M2 and, thus, growing in numbers. Such a change in a mixed dechlorinating consortium should be anticipated. For example, Duhamel and Edwards (2007) reported that the make-up of the dechlorinating community in KB1 subcultures evolved differently and varied significantly even within subcultures maintained with the same substrate. This variability implies that if one dechlorinating species is somehow inhibited, another may grow opportunistically and fill its role to keep dechlorination functioning. In our case, this change was in favor of TCE-to-ETH dechlorinators who improved the overall performance of the culture. Considering the above, the competition for TCE and the dynamics of TCE-consuming dechlorinators should not be neglected, as it could affect the populations performing the latter and, usually, most critical steps of dechlorination.

Chapter 9: Investigating how non-dechlorinators impact dechlorination efficiency in *Dehalococcoides mccartyi*-dominated, methane-producing, chloroethene-degrading cultures

9.1 Introduction

The relevance of non-dechlorinators has been addressed in the literature, with many reports trying to profile phylogenetically and metagenomically various dechlorinating consortia (e.g. for KB-1 subcultures from Duhamel and Edwards, 2006; for KB-1, ANAS and DonnaII consortia from Hug et al., 2012). Yet, the detailed molecular characterization of dechlorinating consortia fueled discussions mainly on reactions mediated by non-dechlorinators that do not affect directly the dynamics of reducing equivalents, such as the provision of cofactors to dechlorinators (e.g. corrinoids). The competitive fitness of non-dechlorinators is rarely addressed.

In Chapters 7 and 8 the make-up of cultures NTUA-M1 and NTUA-M2 put forth a discussion regarding dechlorination performance and the functional structure of non-dechlorinators. Therefore, in this chapter the developed kinetic model will be applied in order to elucidate how the composition and the metabolic properties of non-dechlorinators affect the dynamics of reducing power and, thus, dechlorination. The methodology implemented in Chapter 7 identified four different candidate approximations of the behavior of dechlorinating culture NTUA-M2, one of which was found the most probable of being a good realization of the true behavior of the culture. In addition, the four candidate approximations offer the opportunity to investigate how non-dechlorinators influence dechlorination under varying scenarios of electron donor supply. Therefore, these candidate approximations of culture NTUA-M2 will be treated in this chapter as four different cultures and they will be used in numerical experiments performed with different electron donor surpluses and types. Some of these numerical experiments coincide with the real batch tests performed with the culture and, hence, we will gain insight into the reasons for the distinctive behavior of these four alternate cultures. These numerical experiments provide a chance to question the consensus regarding observations from dechlorination in enrichment cultures and *in situ* with different electron donor types and surpluses.

9.2 Alternate methane-producing, dechlorinating consortia

The four cultures, A, B_1, B_2 and C, differ regarding the relative abundance and the kinetic properties of methanogens (H_2- and acetate-utilizing methanogens) and acetate oxidizers (see also Fig. 7.8). This part of the community will be referred to as the non-dechlorinating part of the cultures and adds up to 20% of the overall biomass concentration. The remaining 80% is dominated by TCE-to-ETH dechlorinators, TCE-to-cDCE dechlorinators and butyrate oxidizers. A detailed discussion on the characteristics of the four cultures was given in Chapter 7. In this section, their main differences will be briefly revisited.

In culture A, the non-dechlorinating fraction is dominated by acetate-utilizing methanogens (75% of non-dechlorinators), followed by the acetate-oxidizing syntrophs (24% of non-dechlorinators). Only few, fast-growing H_2-utilizing methanogens are present ($\mu_{max,HM}$=1.94 $days^{-1}$). In this culture, acetate-utilizing methanogens are more competent acetate-scavengers than acetate oxidizers, consuming, thus, most of the available acetate.

In cultures B_1 and B_2, acetate-utilizing methanogens are moderately dominant (55% of non-dechlorinators); acetate oxidizers are 24% of the non-dechlorinating community, while H_2-utilizing methanogens are the remaining 21%. In both cultures, acetate-utilizing methanogens outperform acetate oxidizers with respect to acetate consumption. The difference of cultures B_1 and B_2 is the competitive fitness of H_2-utilizing methanogens. In culture B_1 they are slow growers ($\mu_{max,HM}$=0.14 $days^{-1}$), while in culture B_2 they are fast growers ($\mu_{max,HM}$=1.24 $days^{-1}$).

Culture C is a considerably different culture. The fast-growing H_2-utilizing methanogens ($\mu_{max,HM}$=1.96 $days^{-1}$) are the dominant methanogenic population (60% of non-dechlorinators). Acetate oxidizers are the denser acetate-scavenging group (22% of non-dechlorinators), while they are estimated with a greater maximum specific growth rate than acetate-utilizing methanogens.

9.3 Behavior of the alternate methane-producing, dechlorinating consortia under varying strategies for the supply of H_2

The behavior of the four alternate cultures will be tested under different donor delivery strategies employing different electron donor types and quantities (Table 9.1); some of these strategies coincide with the actual tests performed with culture NTUA-M2. First, the behavior of these cultures will be examined under increasing electron donor surpluses, i.e. under (a) a low electron donor surplus of 300 μM butyrate (an electron donor surplus equal to 2.4; LEDS-B2), (b) a moderate electron donor surplus resulting from the addition of 750 μM butyrate (i.e. an electron donor surplus equal to 5.0; MEDS-B2), and (c) a high electron donor surplus resulting from the addition of 2230 μM butyrate (an electron donor surplus equal to 12.9; HEDS-B2). Second, the behavior of the four cultures will be examined when the electron donor source (i.e. butyrate) is supplied periodically in small doses (MEDS-BD2), aiming to produce a smoother H_2 flux towards the H_2-scavenging species that could potentially favor dechlorinators. Third, we will examine a scenario of direct H_2 supply, simulating the test used in Chapter 7 for discrimination purposes (batch test MEDS-H2). Finally, the possibility of acetate supporting dechlorinating activity when supplied as the sole electron donor source will be examined. Two tests with different acetate quantities will be performed: a moderate acetate supply (electron donor surplus equivalent to MEDS-B2; MEDS-A2), and a high acetate supply (electron donor surplus equivalent to HEDS-B2; HEDS-A2). All numerical tests lasted 184 days, in order to examine whether biomass decay could eventually promote complete chloroethene detoxification.

Table 9.1. Initial concentrations of electron donor and TCE and electron donor surplus for the numerical batch experiments performed with cultures A, B_1, B_2 and C.

Batch test	Butyrate(μM)	Acetate (μM)	H_2 (μM)	TCE (μM)	Electron donor surplus[1]
Butyrate-fed tests					
LEDS-B2 [2]	300	270	-	567	2.4
MEDS-B2	750	270	-	567	5.0
MEDS-BD2	150 (x5)	270	-	567	5.0
HEDS-B2 [2]	2230	258	-	601	12.9
H_2-fed test					
MEDS-H2 [2]	300.0	900.0	3000.0	597	5.4
Acetate-fed tests					
MEDS-A2	-	2126	-	567	5.0
HEDS-A2	-	5486	-	567	12.9

[1]: Electron donor surplus is calculated assuming that 1 mol of butyrate yields 20 e^- equivalents.

[2]: Actual batch test performed with dechlorinating culture NTUA-M2

9.3.1 Butyrate supply

9.3.1.1 Instantaneous addition of butyrate at the beginning of the experiment

LEDS-B2

As expected, since all four cultures correspond to good-fit solutions for this electron donor surplus, the performance of dechlorination is practically indistinguishable (Fig. 9.1a). They achieved a moderate *DoD* (76%, which means that VC was the main daughter product) in 14 days, with dechlorinators consuming almost 30% of the available electron equivalents. Dechlorination is the most efficient hydrogenotrophic metabolism in all cultures, with the exception of culture C (Fig. 9.2b; note that Fig. 9.2 is Fig. 7.10 repeated herein for the convenience of the reader).

Most of the electron equivalents were channeled to methane formation (Fig. 9.2a). Yet, the relative distribution of equivalents towards the two methanogenic pathways differentiates the four cultures. In culture A, the H_2-utilizing methanogens, despite their remarkably low initial concentration, consumed around 1% of the total electron equivalents and produce almost 1.5% of the observed methane. For culture B_1, the efficiency of the H_2-utilizing methanogens is the same, despite constituting the 2.68% of the overall biomass. In this case, they also contributed slightly to methane production (1% of the overall methane concentration) and acetoclastic methanogenesis was the main methanogenic pathway. In culture B_2, H_2-utilizing methanogens were fast-growing and, thus, they produced around 15% of methane. Acetoclastic methanogenesis was the most efficient metabolic pathway of the mixed culture, consuming around 55% of the available electron equivalents. Finally, in culture C the H_2-utilizing methanogens took advantage of their kinetic properties and their denser population and became the most efficient methanogenic species; 65% of methane production was H_2-dependent.

Another functional difference of the four cultures derives from the competition for acetate (Fig. 9.2c). In cultures A and B_1, the acetate oxidizing species are consuming around 20% of the available acetate, as they are fewer than acetate-utilizing methanogens and with a lower specific affinity for acetate (i.e. they exhibited lower μ_{max}/K_s ratio than acetate-utilizing methanogens). Consequently, the initial supply of 300 μM butyrate provided only 2160 μe^-eq in terms of H_2 (the e^- eq conversion

factor was 7.2). For culture B_2, the acetate oxidizing culture was more efficient (it demonstrated an increased specific affinity) and consumed around 32% (an e^-eq conversion factor of 8.8 was calculated). Finally, for culture C, acetate oxidation was the main acetoclastic pathway, as acetate oxidizers were denser than the acetate-utilizing methanogens and had a higher specific affinity for acetate. Hence, more than 4608 μe^-eq in terms of H_2 were provided from butyrate to the hydrogenotrophic species, resulting in an e^- eq conversion factor of 15.36. Therefore, despite the elevated competition for H_2, dechlorination in culture C demonstrated the same extent as in the other communities; dechlorination was sustained due to the electron equivalents deriving from acetate oxidation.

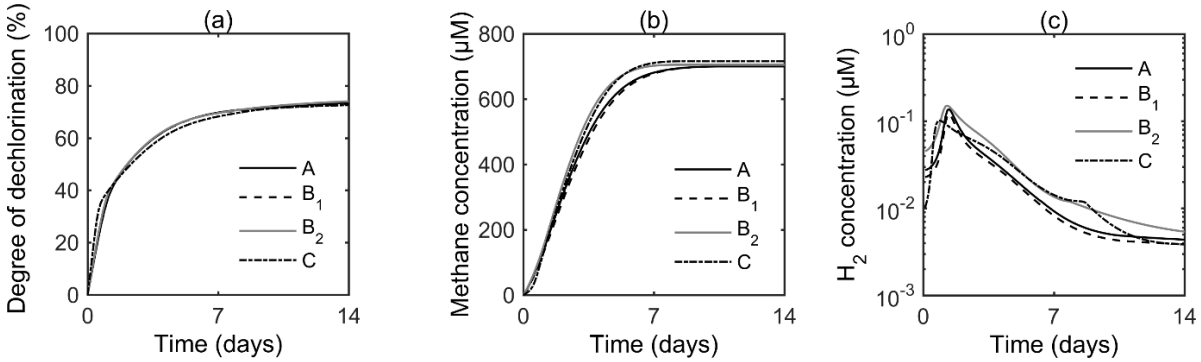

Fig. 9.1. (a) Degree of dechlorination, (b) methane production, and (c) H_2 concentration versus time for an initial supply of 300 μM butyrate (LEDS-B2 test) to cultures A, B_1, B_2 and C.

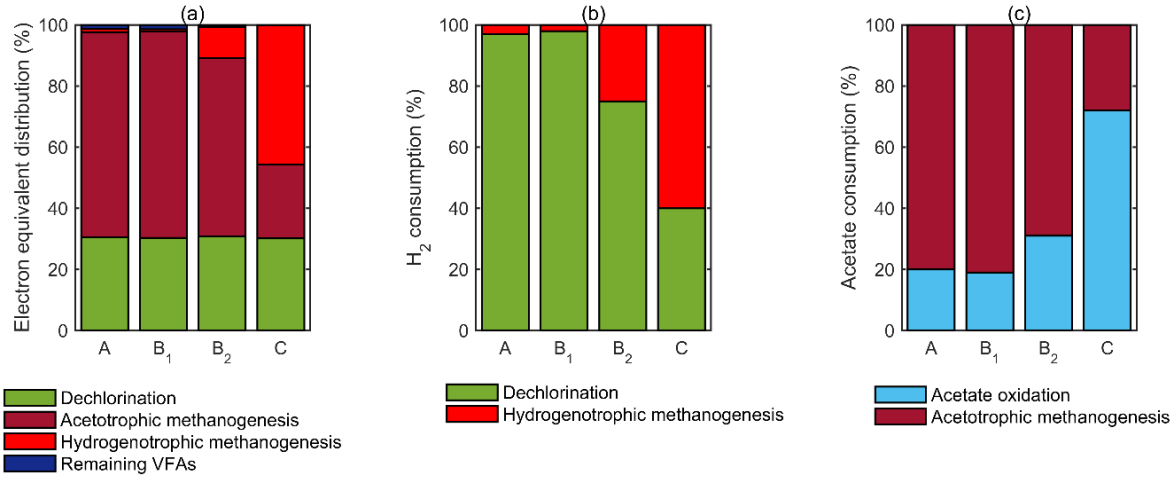

Fig. 9.2. Distribution of (a) electron equivalents, (b) consumed H_2 by dechlorinators and H_2-utilizing methanogens, and (c) consumed acetate by acetate oxidizers and acetate-utilizing methanogens after 14 days for an initial supply of 300 μM butyrate (LEDS-B2 test) to cultures A, B_1, B_2 and C. The total available H_2 for cultures A, B_1, B_2 and C was 1291 μM, 1271 μM, 1677 μM and 3103 μM, respectively.

MEDS-B2

The performance of the four cultures was distinctive during this numerical experiment. Culture B_1 was the only to achieve dechlorination within 14 days. Despite the elevated H_2 concentrations, the slow-growing H_2-utilizing methanogens in culture B_1 did not deprive the requisite electron equivalents for dechlorination. This was not the case for the other cultures, since the fast-growing H_2-utilizing methanogens consumed the major fraction of the extra supplied H_2. Eventually, apart from culture B_1, only culture A dechlorinated around day 84, taking advantage of the contribution of decaying biomass (results regarding the 184-day long simulations are presented in Appendix A). In cultures B_2 and C the simulated degree of dechlorination plateaued at 99.8% and 99.5%, respectively.

Following the addition of 750 μM butyrate (electron donor surplus is equal to 5.0), dechlorination rates were increased (Fig. 9.3a). However, electron equivalent distribution was less favorable for dechlorination in comparison with the supply of 300 μM butyrate; overall methane production was 2.2-fold greater, as a result of an increase in both hydrogenotrophic and acetoclastic methanogenesis. H_2-utilizing methanogens took advantage of the elevated H_2 concentrations and became more efficient H_2-scavengers (Fig. 9.4b), while acetate-utilizing methanogens consumed a greater share of acetate (Fig. 9.4c), as acetate-oxidizers were thermodynamically limited by the elevated H_2 concentrations (contrast Fig. 9.3c to Fig. 9.1c). Thus, the estimated e^- eq conversion factors for butyrate were: 5.8 for community A, 5.0 for community B_1, 7.4 for community B_2. Again, acetate was an important H_2 source in community C (the e^- eq conversion factor for butyrate was 14.4) and sustained dechlorination after day 3, when butyrate was depleted.

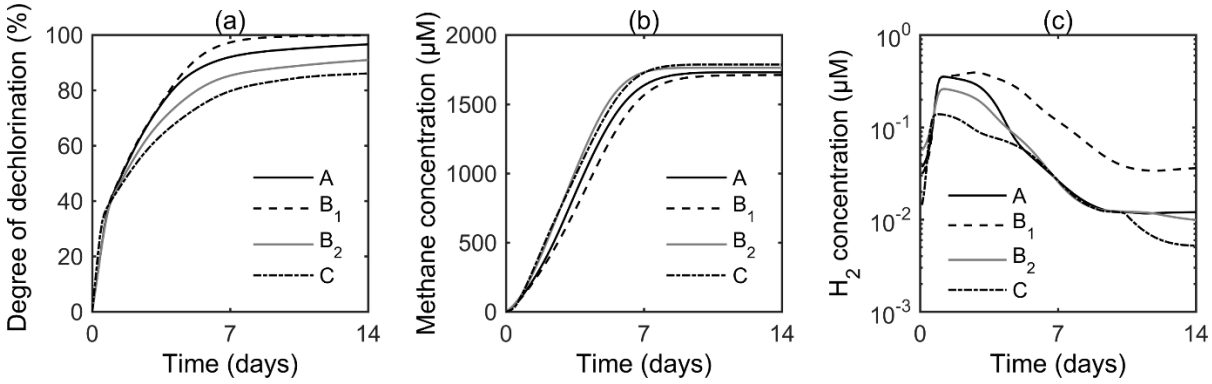

Fig. 9.3. (a) Degree of dechlorination, (b) methane production, and (c) H_2 concentration versus time for an initial supply of 750 μM butyrate (MEDS-B2 test) to cultures A, B_1, B_2 and C.

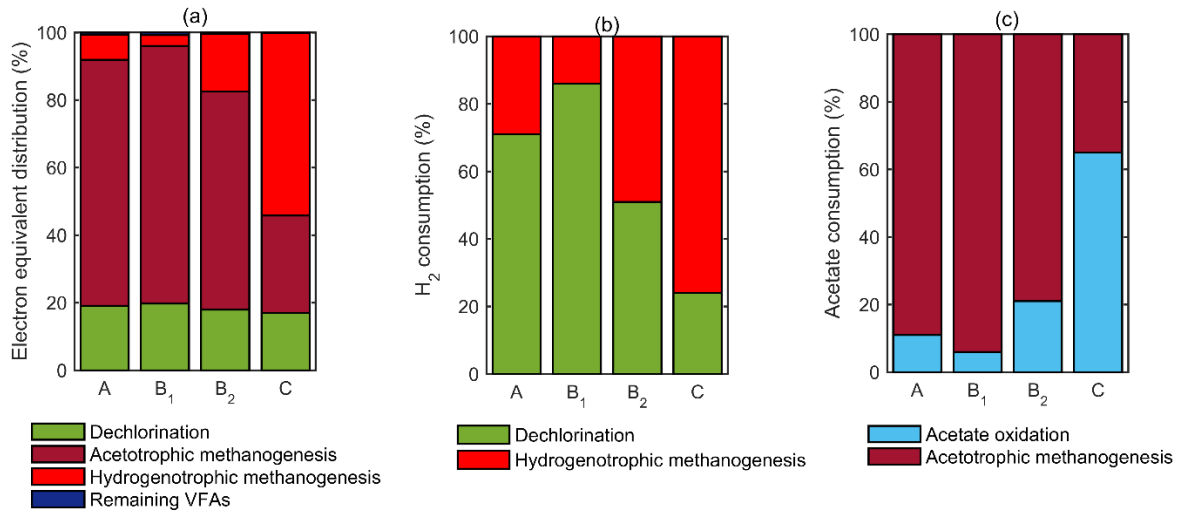

Fig. 9.4. Distribution of (a) electron equivalents, (b) consumed H_2 by dechlorinators and H_2-utilizing methanogens, and (c) consumed acetate by acetate oxidizers and acetate-utilizing methanogens after 14 days for an initial supply of 750 μM butyrate (MEDS-B2 test) to cultures A, B_1, B_2 and C. The total available H_2 for cultures A, B_1, B_2 and C was 2275 μM, 1970 μM, 3012 μM and 6116 μM, respectively.

HEDS-B2

After the initial supply of 2230 μM butyrate (electron donor surplus equal to 12.9), the performance of culture B_1 was distinctly better, because, despite the donor abundance, clearly less methane was produced (Fig. 9.5b), while butyrate accumulated due to thermodynamic inhibition of its oxidation (Fig. 9.6a). At the same time, acetate oxidation is almost completely inhibited, because of the H_2 abundance (Fig. 9.6c). For all the cultures, dechlorination was faster and approached completion, but in terms of efficiency, dechlorination deteriorated. Cultures A and B_2 detoxified TCE completely after 56 and 150 days, respectively. Degrees of dechlorination as high as 99.9% were achieved in culture C due to biomass disintegration, which however, resulted in VC concentrations which were orders of magnitude greater than the maximum contaminant levels for VC (i.e. 0.032 μM).

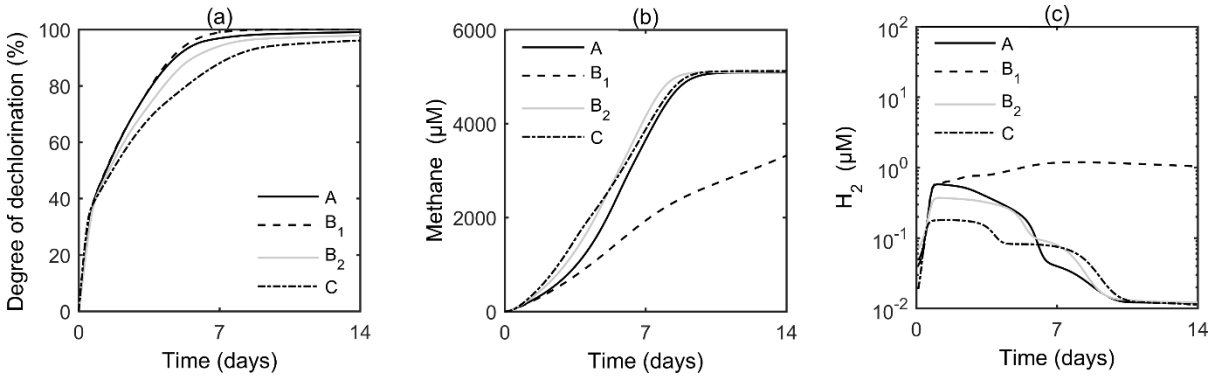

Fig. 9.5. (a) Degree of dechlorination, (b) methane production, and (c) H_2 concentration versus time for an initial supply of 2230 μM butyrate (HEDS-B2 test) to cultures A, B_1, B_2 and C.

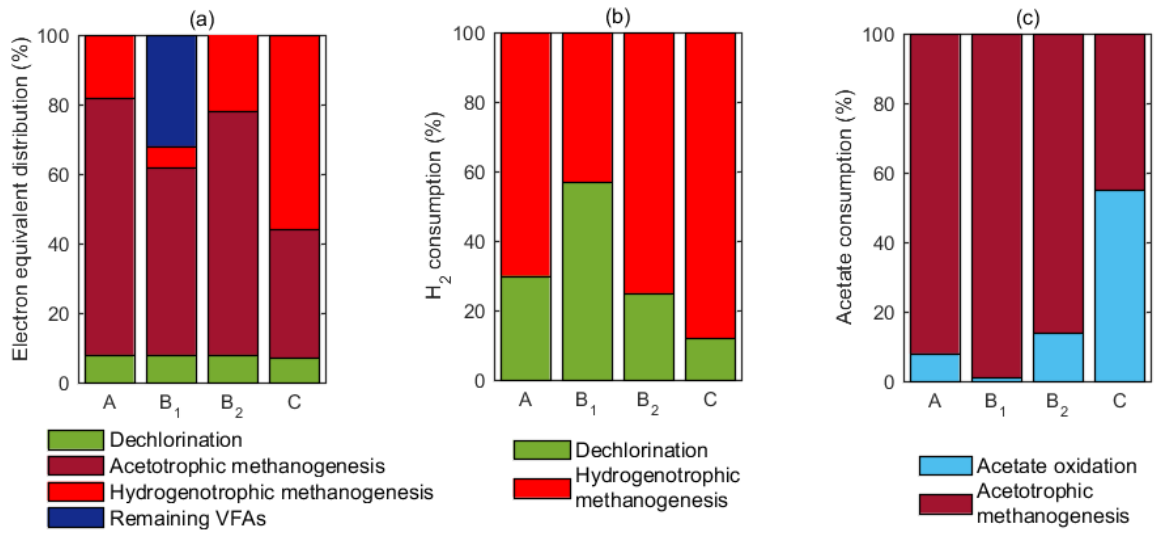

Fig. 9.6. Distribution of (a) electron equivalents, (b) consumed H_2 by dechlorinators and H_2-utilizing methanogens, and (c) consumed acetate by acetate oxidizers and acetate-utilizing methanogens after 14 days for an initial supply of 2230 μM butyrate (HEDS-B2 test) to cultures A, B_1, B_2 and C. The total available H_2 for cultures A, B_1, B_2 and C was 5947 μM, 3102 μM, 7015 μM and 14,672 μM, respectively.

According to the simulations, the high electron donor supply induced a drastic shift in the relative abundance of the cultures favoring methanogens (Fig. 9.7). After 14 days, in cultures A, B_1 and B_2 methanogens were significantly increased accounting for almost 25% of the overall biomass. In culture C, the shift was more pronounced. The concentration of H_2-utilizing methanogens was comparable to the concentration of dechlorinators comprising 80% of the overall biomass concentration (Fig. 9.7c). Hence, the quantitative advantage of dechlorinators was diminished due to the elevated butyrate supply. This is why culture C did not achieve complete dechlorination even with a slow-releasing electron donor source, such as the decaying biomass.

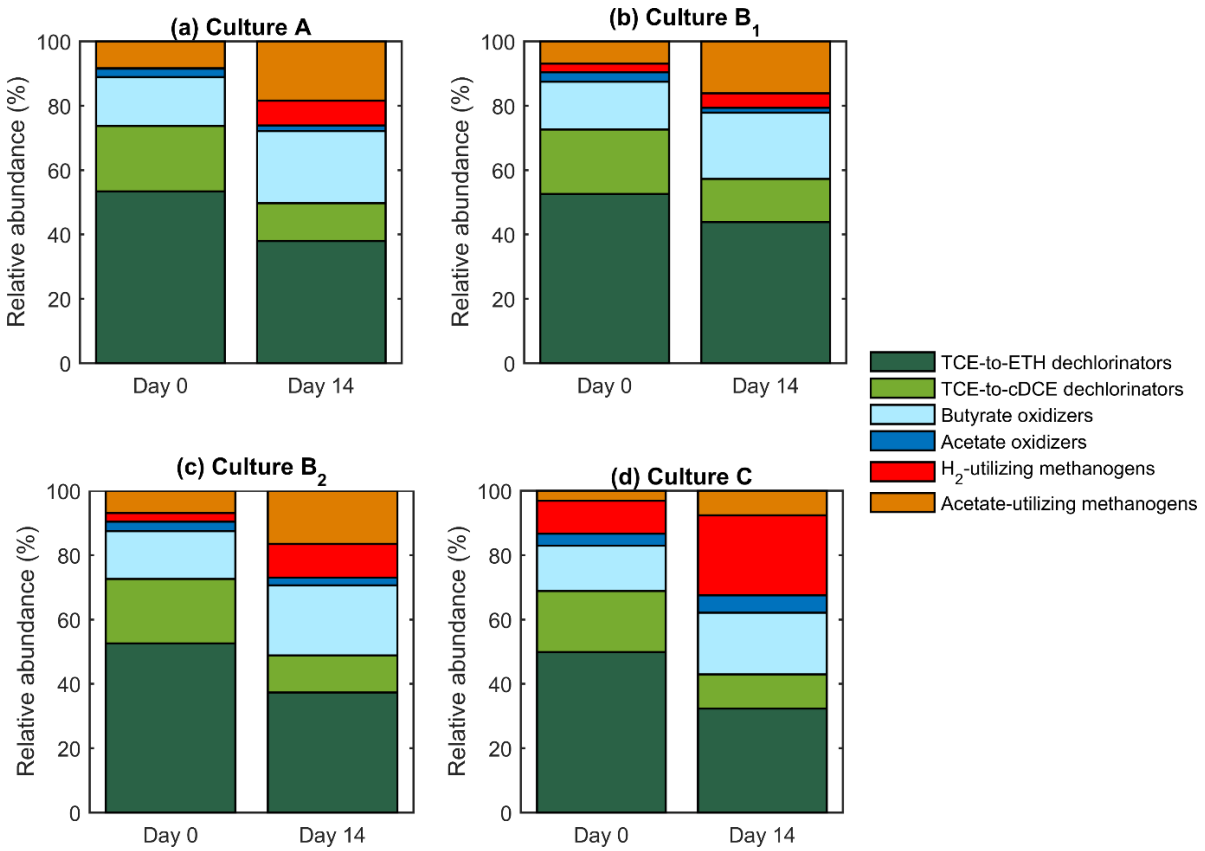

Fig. 9.7. Simulated biomass distributions at the beginning and after 14 days for cultures A, B_1, B_2 and C following the supply of 2230 µM butyrate (HEDS-B2 test).

9.3.1.2 Incremental addition of butyrate

MEDS-BD2

A different feeding pattern was explored, namely a periodic butyrate injection with five doses of 150 µM butyrate at a 2-day interval (overall butyrate supply equals 750 µM). This scenario follows the rationale behind the utilization of slow-release anaerobic substrates, such as TBOS (Yang and McCarty, 2000), which yield fermentable electron donor sources continuously and, hence, favor dechlorinators through the fixation of H_2 at low levels.

The change in the feeding pattern of butyrate enhanced dechlorination slightly and only when dechlorinators had to compete with a sizeable community of fast-growing H_2-utilizing methanogens, i.e. cultures B_2 and C (Fig. 9.8c and 9.8d). Simulated H_2 concentrations reveal that the incremental injection of butyrate moderated peak H_2 concentrations occurring during the first three days of the test performed with an instantaneous initial addition of butyrate. H_2 concentrations were evenly distributed during the first 8 days of the test (Fig. 9.10). Thus, H_2-utilizing methanogens grew with lower rates and H_2 availability was a less limiting factor for dechlorination at the later and slower stages of the reaction (cDCE and VC consumption). These findings are in accordance with the model results of Lee et al. (2004), who also reported that the incremental supply of electron donor resulted in an improved sequential dechlorination of the two final stages of dechlorination, i.e. cDCE and VC consumption.

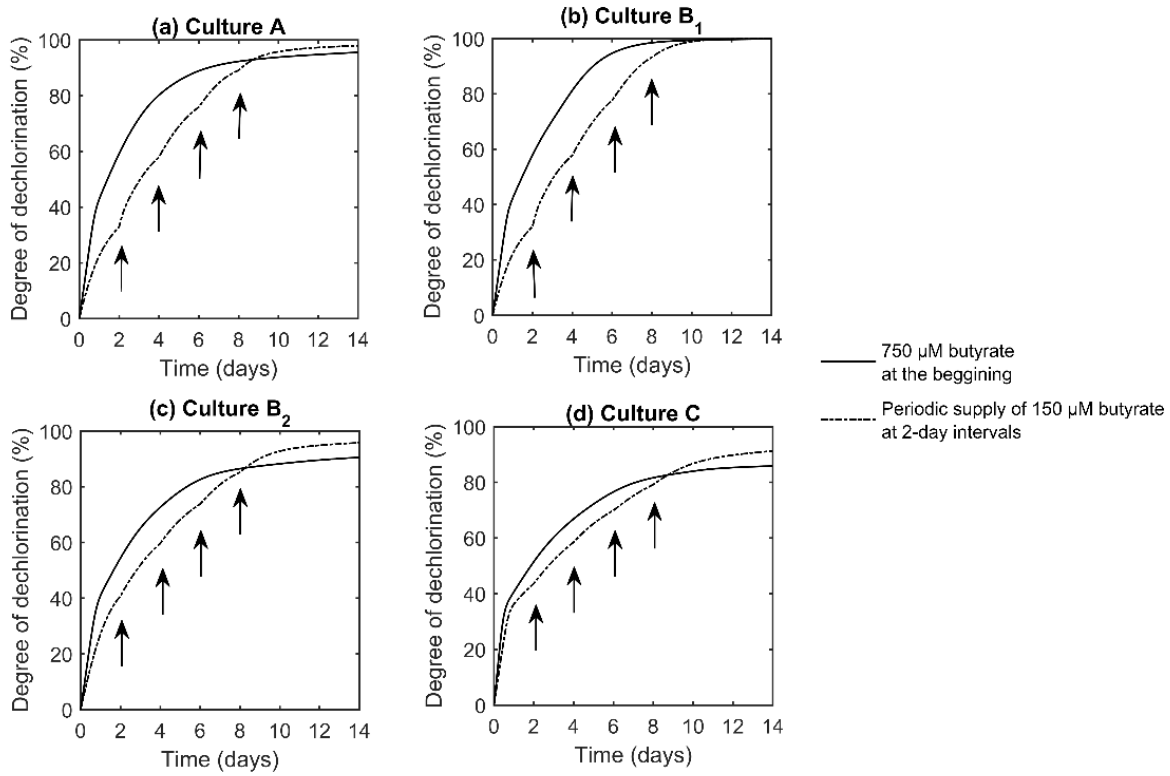

Fig. 9.8. Comparison of simulated degrees of dechlorination between the periodic addition of butyrate (five doses of butyrate were supplied from day 0 to day 8 in a 2-day interval, adding a total butyrate supply of 750 μM) and a single addition of 750 μM butyrate in the beginning for cultures A, B_1 and B_2 and C.

For cultures A and B_1, the profit of this alternative feeding pattern was trivial (Fig. 9.8a and 9.8b). The change in the prevailing H_2 profiles did not affect dechlorination, as dechlorinators in these cultures and under these surpluses were already more competent H_2 scavengers than methanogens; dechlorinator growth was limited more by chloroethene availability and to a lesser degree by H_2 availability. As a result, the outcome was more or less the same. Culture A dechlorinated TCE around day 80 and culture B_1 in 14 days. These findings support the experimental observations of Panagiotakis et al. (2015), who also found that for a similar injection pattern the improvement of TCE performance was minor in culture NTUA-M1.

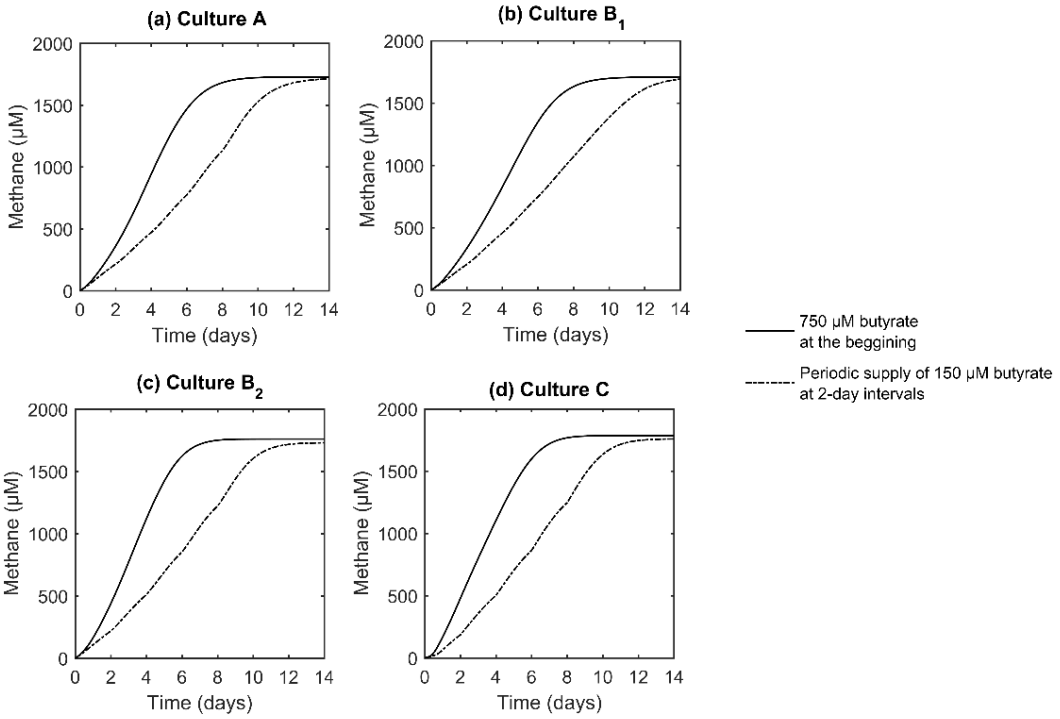

Fig. 9.9. Comparison of simulated methane formation between the periodic addition of butyrate (MEDS-BD2: five doses of butyrate were supplied from day 0 to day 8 in a 2-day interval, adding a total butyrate supply of 750 μM) and a single addition of 750 μM butyrate in the beginning for cultures A, B_1 and B_2 and C.

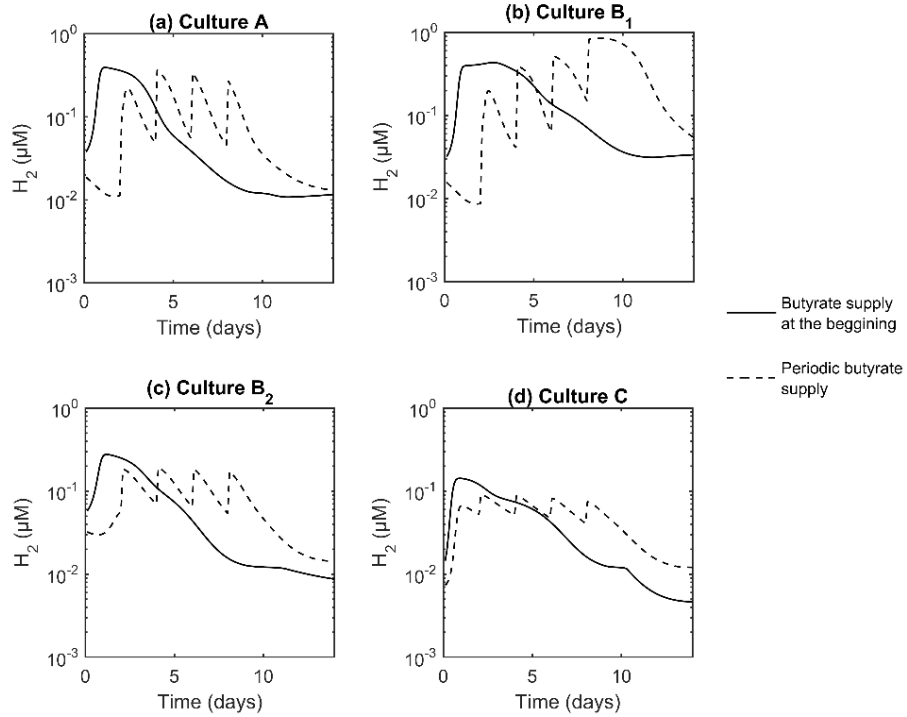

Fig. 9.10. Comparison of simulated H_2 concentrations between the periodic addition of butyrate (MEDS-BD2: five doses of butyrate were supplied from day 0 to day 8 in a 2-day interval, adding a total butyrate supply of 750 μM) and a single addition of 750 μM butyrate in the beginning for cultures A, B_1 and B_2 and C.

9.3.2 H_2 supply

MEDS-H2

When H_2 was supplied directly as an electron donor, the relative performance of the four cultures remained unchanged, as culture B_1 performed better followed by cultures A, B_2 and C. However, the absolute difference in the performance of the four cultures increased (Fig. 9.11a). Despite the elevated competition for H_2, dechlorinators in culture B_1 were efficient and outcompeted the slow-growing H_2-utilizing methanogens (Fig. 9.12b). This indicates that a non-fermentable donor would be preferable for stimulating dechlorinators in culture B_1. When fast-growing H_2-utilizing methanogens were present (cultures A, B_2 and C), direct addition of H_2 was detrimental for the extent of dechlorination, regardless of their initial relative abundance. This behavior is in accordance with the experimental findings that claim that direct H_2 supply promotes methanogenesis (Ballapragada et al., 1997; Ma et al., 2003; Aulenta et al., 2005). Dechlorination in these cultures was sustained by butyrate and acetate oxidation, which were thermodynamically favorable after the first two days of the simulations (H_2 concentrations were constantly below 0.10 μM – see Fig. 9.11c) and contributed to the pool of electron equivalents.

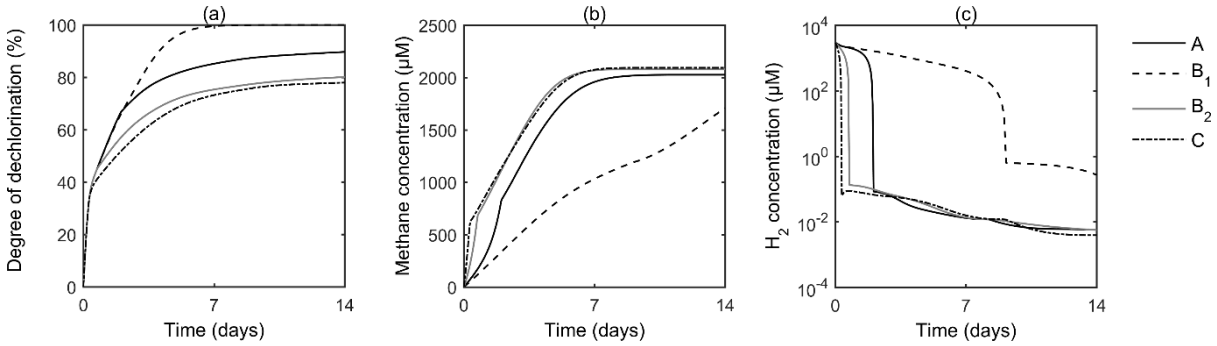

Fig. 9.11. (a) Degree of dechlorination, (b) methane production, (c) H_2 concentration versus time for an initial supply of 3000 μM of H_2 (MEDS-H2) to the cultures A, B_1, B_2 and C.

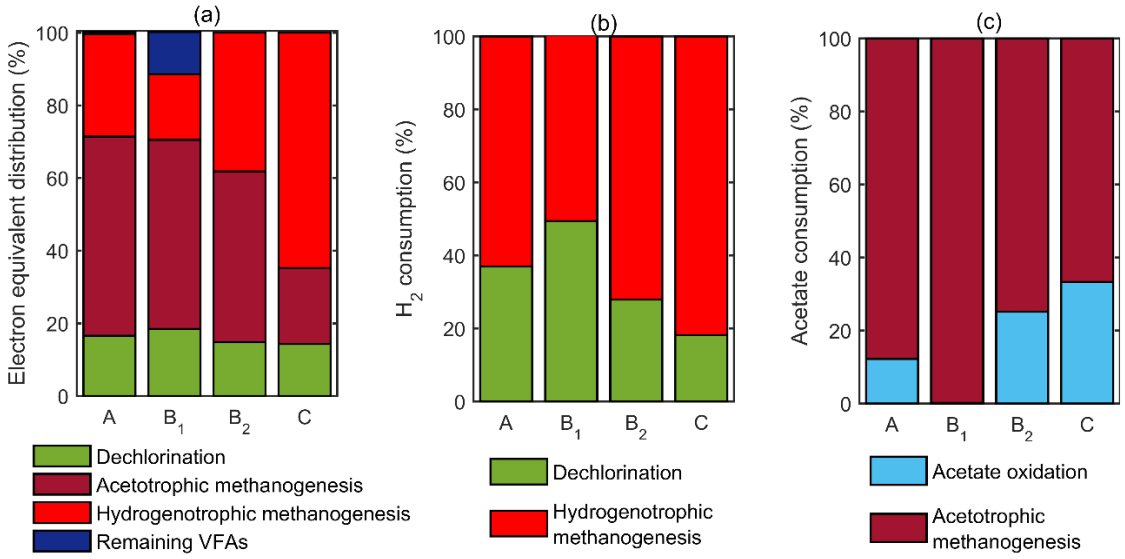

Fig. 9.12. Distribution of (a) electron equivalents, (b) consumed H_2 by dechlorinators and H_2-utilizing methanogens, and (c) consumed acetate by acetate oxidizers and acetate-utilizing methanogens after 14 days for an initial supply of 3000 μM H_2 (MEDS-H2) to cultures A, B_1, B_2 and C. The total available H_2 for cultures A, B_1, B_2 and C was 4369 μM, 3560 μM, 5166 μM and 7728 μM, respectively.

After the first 14 days, dechlorination was mainly sustained by the contribution of decaying biomass; endogenous decay contributed almost 24% of the total electron equivalents consumed by the four cultures. Yet, dechlorination never reached completion for cultures A, B_2 and C, as the achieved degrees of dechlorination were equal to 95%, 94% and 94% respectively (lower values than those achieved for 300 μM butyrate – see also a comparison of the terminal *DoD* in Appendix A).

9.3.3 Acetate supply

MEDS-A2

The extent of dechlorination in the four cultures converged to the same levels after the supply of 2126 μM (Fig. 9.13a), which resulted in an electron surplus equal to 5.0 (equivalent to the addition of 750 μM butyrate). The four cultures achieved a moderate *DoD* (82%, which means that dechlorination stalled at VC consumption) in 14 days, which was also lower than the achieved *DoD* following the supply of 750 μM butyrate (contrast Fig. 9.3a to Fig. 9.13a). The deterioration of performance compared to butyrate supply was more evident in cultures A, B_1 and B_2. In these cultures, due to the low H_2 quantities that resulted from acetate oxidation, dechlorinators failed to remove VC, even if they outperformed H_2-utilizing methanogens clearly (Fig. 9.14b). The total available H_2 for cultures A, B_1, B_2 and C was 1505 μM, 1513 μM, 2211 μM and 3027 μM, respectively. It was the competition for acetate that dictated the final degree of dechlorination by day 14. Ultimately, none of the cultures removed the existing chloroethenes completely within the 184 days of the simulation and *DoD* plateaued at values ranging from 99.2 % (culture C) to 99.8 % (culture B_1); the decline of butyrate oxidizers led to a very low production rate of electron equivalents from the decaying biomass and, thus, dechlorination was incomplete.

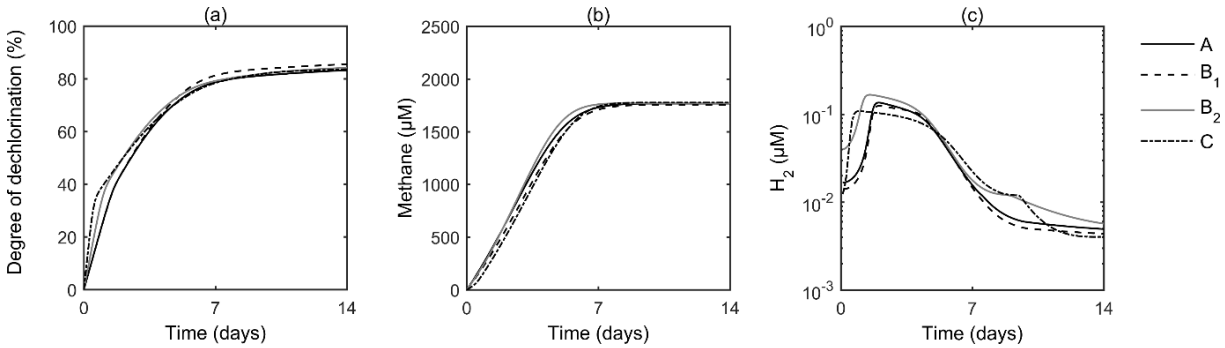

Fig. 9.13. (a) Degree of dechlorination, (b) methane production, (c) H_2 concentration versus time for an initial supply of 2126 μM acetate (MEDS-A2) to the cultures A, B_1, B_2 and C.

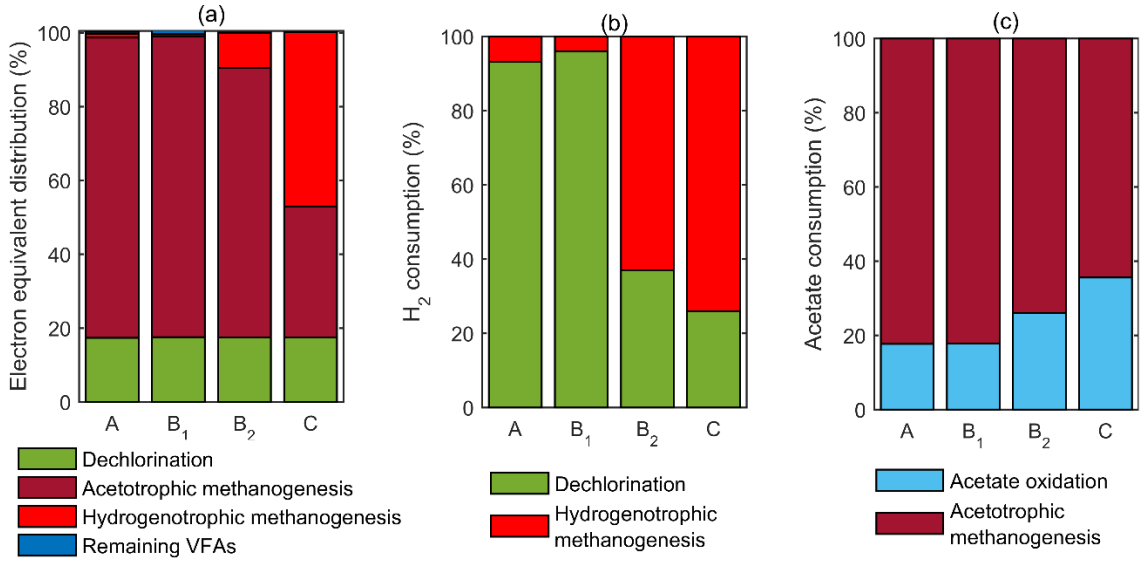

Fig. 9.14. Distribution of (a) electron equivalents, (b) consumed H_2 by dechlorinators and H_2-utilizing methanogens, and (c) consumed acetate by acetate oxidizers and acetate-utilizing methanogens after 14 days for an initial supply of 2126 μM acetate (MEDS-A2) to cultures A, B_1, B_2 and C. The total available H_2 for cultures A, B_1, B_2 and C was 1520 μM, 1515 μM, 1270 μM and 5502 μM, respectively.

HEDS-A2

When a high acetate initial supply was tested (5486 μM acetate, which resulted in an electron donor surplus of 12.9), dechlorination approached completion (Fig. 9.15a) in all cultures during the first 14 days. Culture B_1 was marginally better. In terms of efficiency, dechlorination got worse in every culture compared to the more moderate acetate supply (Fig. 9.16a); most of the reducing power was channeled to methanogenesis (Fig. 9.15b). In this case, culture B_1 detoxified TCE completely by day 29, as the little extra H_2 needed, was provided by the decaying biomass. For cultures A, B_2 and C, 42 days, 74 days and 87 days were needed for complete TCE removal, respectively.

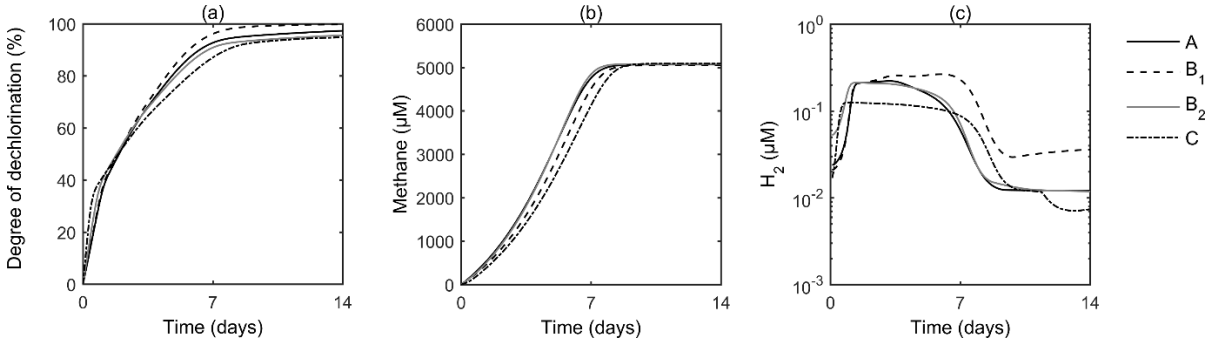

Fig. 9.15. (a) Degree of dechlorination, (b) methane production, (c) H_2 concentration versus time for an initial supply of 5750 μM acetate (HEDS-A2) to cultures A, B_1, B_2 and C.

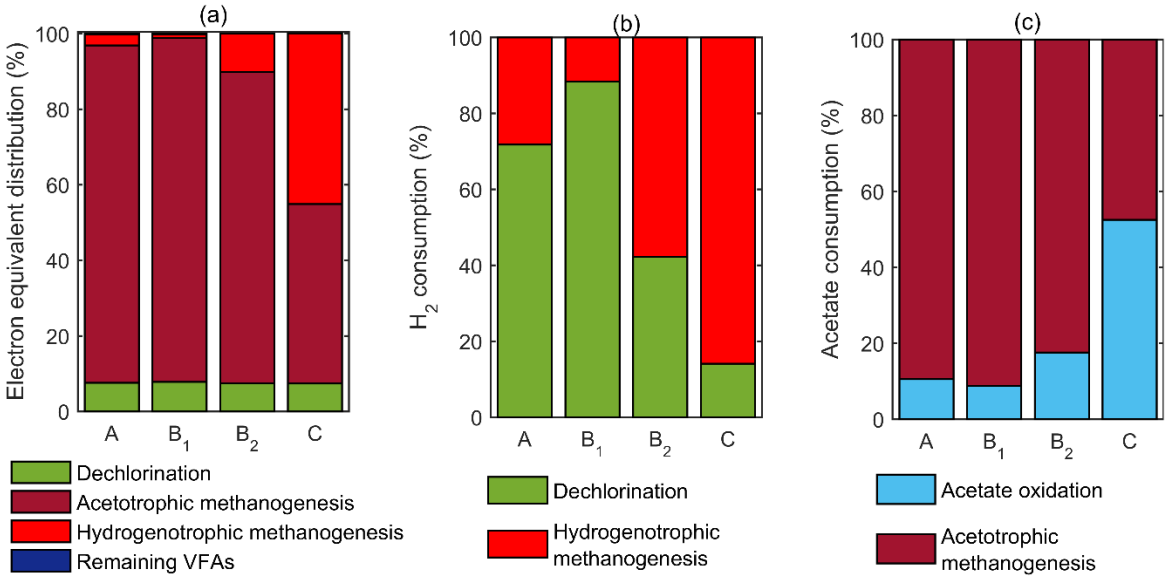

Fig. 9.16. Distribution of (a) electron equivalents, (b) consumed H_2 by dechlorinators and H_2-utilizing methanogens, and (c) consumed acetate by acetate oxidizers and acetate-utilizing methanogens after 14 days for an initial supply of 5750 μM acetate (HEDS-A2) to cultures A, B_1, B_2 and C. The total available H_2 for cultures A, B_1, B_2 and C was 2330 μM, 1937 μM, 3921 μM and 11,663 μM, respectively.

Considering the above, acetate was an equivalent electron donor source to butyrate only in culture C. Due to the high competitive fitness of acetate-oxidizing syntrophs in this culture, acetate produced only slightly fewer reducing equivalents compared to butyrate. In the remaining three cultures, acetate was not equivalent to butyrate. Despite the lower H_2 concentrations established, dechlorination was not as extensive as in the butyrate-fed tests, as acetate-utilizing methanogens consumed most of the available acetate and, thus, the available H_2 was insufficient.

9.4 Concluding remarks

The numerical simulations performed with four alternative cultures resulting from the heuristic approach of Chapter 7 demonstrated that mild changes in the composition and the metabolic abilities of non-dechlorinators in a *Dehalococcoides mccartyi*-dominated culture would ultimately require different strategies for the preferential stimulation of dechlorinators.

In cultures where acetate-dependent methane formation is dominant, direct addition of H_2 (or perhaps a high H_2-ceiling donor) would be the optimal strategy for stimulating the performance of the slow-growing dechlorinators. The presence H_2-utilizing methanogens is not necessarily problematic, as they could be slow growers, as for example specific strains of *Methanobacterium spp.* are (Jain et al., 1987), and, therefore, do not compete efficiently within a *Dehalococcoides mccartyi*-dominated culture following biostimulation.

When fast-growing H_2-utilizing methanogens were present within the mixed culture, complete dechlorination was feasible only if methanogens were severely outnumbered by the dechlorinating community. If this was not the case, adding excessive levels of a slowly fermentable substrate in order to overcome the competition for H_2 had a negative impact to the efficiency of dechlorination, since the resulting H_2 concentrations became high enough to diminish the competitive advantage of dechlorinators over H_2-utilizing methanogens. In such cases, the incremental supply of electron donor sources was found promising. Hence, a more complex

organic substrate (which would slowly yield butyrate or another fermentable electron donor source) would be more appropriate for the preferential stimulation of dechlorinators.

Competition for acetate was assessed systematically and it was found relevant in cultures with efficient H_2-utilizing species and low electron donor surpluses. Particularly, when acetate oxidizers were coupled with a robust, fast-growing community of H_2-utilizing methanogens, H_2 concentrations were maintained constantly low enough allowing acetate to function as an H_2 source almost equivalent to butyrate. Thereby, any loss of reducing power towards methane formation can be partially compensated for dechlorinators. The need for constantly low H_2 concentrations explains why acetate oxidizing syntrophs are usually sustaining dechlorination in the field (He et al., 2002 or Harkness et al., 2012) and scarcely in the laboratory, where excessive surpluses are supplied and possibly inhibit their function.

This chapter highlighted that in order to fully describe the fate of electron donors in mixed dechlorinating consortia, it is important (a) to specify the methanogenic pathways and the functional roles of the associated methanogenic species and (b) to illuminate possible symbiotic interactions established between acetate oxidizers and H_2-scavenging populations. The type of inquiry presented in this chapter holds the promise to offer a framework through which to interpret the varied research results reported in the literature, by thinking of groups of cultures and their collective activities, characterized not exclusively by the activity of dechlorinators, but also by the type of methanogens and the competitive fitness of syntrophs mediating H_2 supply.

Chapter 10: Gaining insight into functional structure of a methane-producing, sulfate-reducing, chloroethene-degrading culture

10.1 Introduction

Dechlorination in conjunction with sulfate reduction has been studied less extensively compared to dechlorination under methanogenic conditions. The available studies considering competition between dechlorination and sulfate reduction in the field or in the laboratory have not established a firm consensus on how the presence of sulfate affects dechlorination rate and extent. Considering that only few reports describe no or positive impact of sulfate on dechlorination (e.g. Aulenta et al., 2007 or Harkness et al., 2012), the majority of laboratory works shows that: (a) complete chloroethene removal can be achieved slowly in the presence of sulfate (e.g. Aulenta et al., 2008 or Heimann et al., 2005), (b) sulfate must be depleted before the initiation of the two terminal steps of dechlorination (e.g. Azizian et al., 2008 or Malaguerra et al., 2011), or (c) dechlorination cannot be complete in the presence of sulfate (El Mamouni et al., 2002). Nonetheless, the common ground of the reported laboratory and field studies is that sulfate has an adverse effect on the dechlorination rates of the later stages of dechlorination, i.e. cDCE and VC degradation (Pantazidou et al., 2012). Nevertheless, the underlying mechanisms that can explain the stall of cDCE and VC removal under sulfate-reducing conditions are still unclear.

From a modeling perspective, competition between dechlorination and sulfate reduction has been even less studied. Only two modeling efforts have been made to date, i.e. the works of Malaguerra et al. (2011) and Kouznetsova et al. (2010). In both modeling studies, the competition for H_2 between sulfate reducers and dechlorinators was the major concern. Consequently, the only possible explanation for any stall in dechlorination was the direct competition for H_2. But, sulfate reducers can reduce sulfate via alternative metabolic pathways, using a large variety of electron donors, from H_2 to volatile fatty acids (such as butyrate, propionate or acetate). Thus, the presence of sulfate and the metabolic versatility of sulfate reducers add complexity to the food webs established in the dechlorinating consortia, with many metabolic pathways explaining a possible inefficiency of dechlorinators. The relevance of the alternative sulfate-reducing pathways in dechlorinating consortia remains also unknown.

This chapter will attempt to shed light onto the functional structure of the methane-producing, sulfate-reducing, chloroethene-degrading culture NTUA-S. Thereby, it aims to investigate which sulfate-reducing pathways may have been established in the culture allowing dechlorinators to remove TCE and cDCE similarly with culture NTUA-M2, but slowing down the consumption of VC, even at ample electron donor conditions.

As discussed in Chapter 4, culture NTUA-S was developed using as inoculum the same dechlorinating and sulfate-reducing cultures as NTUA-M2 and it has been maintained with comparably limiting electron donor conditions. Thus, they can be regarded as closely related consortia. The culture established a robust ethene-producing community, achieving a weekly, long-

term degree of dechlorination close to the one observed for NTUA-M2. However, it failed to dechlorinate rapidly even at excessive butyrate supplies. In order to consider more than one sulfate-reducing pathways that could explain this delay in dechlorination, two models regarding the make-up of the sulfate-reducing community were designated: (a) in the first scenario, a consortium of H_2- and acetate-utilizing sulfate reducers was assumed to be present, and (b) in the second scenario, a dominant acetate-utilizing population of sulfate reducers was supplemented with a population of butyrate-utilizing sulfate reducers.

The selection of two separate models describing culture NTUA-S should be regarded as a variation of the stepwise application of the multistart-based strategy employed in Chapter 7. Herein, as the conceptual design of the model is even more complex, instead of identifying distinctive models through the stepwise application of the multistart algorithm, models were pre-selected based on the performance characteristics of the culture (see also the discussion in Section 10.3). Practically, the first step of the stepwise implementation of the multistart algorithm followed in Chapter 7 was omitted. Then, the two models were fitted with the multistart-based algorithm simultaneously to observations collected from two batch tests, one performed for 149 days with a low electron donor surplus (300 μM butyrate), and another performed for 83 days with a high electron surplus (2200 μM butyrate).

10.2 Experimental information

10.2.1 Long-term monitoring of culture NTUA-S

The long-term performance data of the culture elucidate the relevance of the microbial groups present and the corresponding processes constituting the catabolic food web of culture NTUA-S. The steady dechlorinating performance of the culture and the observed ethene production at the end of each feeding cycle indicate that the culture is enriched with a *Dehalococcoides mccartyi*-like population. Additionally, the observed acetoclastic activity (approximately 511 μM acetate are consumed on a weekly basis) combined with the minimal methanogenic activity indicate that acetate-dependent sulfate reduction and syntrophic acetate oxidation should be considered. What is more, butyrate-dependent sulfate reduction cannot be the major sulfate reducing pathway; the amount of sulfate consumed each week (i.e. 470 μM sulfate) cannot be attributed solely on butyrate-utilizing sulfate reducers, as in that case they would have consumed 940 μM of butyrate, i.e. 3.1-fold more butyrate than the supplied. Finally, methane formation is limited consuming around 1% of the supplied reducing equivalents and, therefore, methanogens are a minority population of the culture.

10.2.2 Batch tests performed with culture NTUA-S

Two batch tests are available with culture NTUA-S (Table 10.1), one test performed under a low electron donor surplus (LEDS-BS; 300 μM butyrate) and one test under a high electron donor surplus (HEDS-BS; 2200 butyrate). The LEDS-BS test lasted 149 days at which time dechlorination and sulfate reduction being both incomplete; dechlorination reached and plateaued at a degree of dechlorination (*DoD*) equal to 80.5% and sulfate plateaued following the removal of 84% of sulfate. Methane formation was negligible. On the other hand, in the HEDS-BS, which lasted 83 days, sulfate was completely consumed and dechlorination halted at a *DoD* equal to 99%. Interestingly, methane formation was significant, but it commenced following a 45-day lag-phase.

Both tests were performed after a year from the increase of sulfate concentrations in the parent culture from 300 μM to 729 μM, having reached a steady-state regarding all major functions. Both tests were performed on the same day and, hence, the model can be simultaneously fitted to the observations of both tests. There is no need to perform the cross-confirmation technique followed in Chapter 7, as the source material in the batch tests should be qualitatively and quantitatively the same.

Table 10.1. Initial concentrations of electron donor sources (butyrate and acetate), TCE and sulfate for the batch experiments used for parameter estimation (experiment LEDS-BS, HEDS-BS).

Batch test	Butyrate (μM)	Acetate (μM)	TCE (μM)	Sulfate (μM)	Electron donor surplus[1]	Duration (days)	Final *DoD* (%)
LEDS-BS	300	40	533	729	2	149	80.5
HEDS-BS	2000	40	516	729	13	83	99.0

[1]: Electron donor surplus is calculated assuming that 1 mol butyrate yields 20 e^- eq.

10.3 Model development

The kinetic model developed in Chapter 4 is a comprehensive modeling approach containing all the possible interactions occurring in the food web established in the methane-producing, sulfate-reducing, chloroethene-degrading culture NTUA-S (the associated reactions are presented in Table 10.2, same as in Table 4.1). The model considers: (a) chloroethene consumption by two dechlorinating species (one species can grow on every chloroethene ranging from trichloroethene to vinyl chloride, while the other grows exclusively on trichloroethene), (b) sulfate reduction by hydrogen-, acetate- and butyrate-utilizing sulfate reducers, (c) methane production by hydrogen- and acetate-utilizing methanogens, (d) hydrogen and acetate production by butyrate-oxidizing bacteria, (e) hydrogen production by acetate-oxidizing bacteria, (f) thermodynamic limitations of butyrate and acetate oxidization reactions, and (g) endogenous decay contribution to the electron donor pool. Based on the parameter estimation efforts of the previous chapters with simpler models, considering all the above-mentioned microbial mechanisms would create an extremely overparameterized problem and a costly parameter estimation problem. Thus, a series of decisions were taken, aiming to simplify the model and allow it to corroborate specific hypotheses regarding the composition of the sulfate-reducing community. As already mentioned, these decisions led to the development of two separate conceptual designs, which differed only in the pathways accounted for sulfate reduction. These designs are discussed in the following sections.

Table 10.2. Biological processes included in the conceptual model and the corresponding chemical reactions.

Process	Reaction
	H_2 production
Butyrate oxidation	$CH_3CH_2CH_2COO^- + 2H_2O \rightarrow 2CH_3COO^- + 2H_2 + H^+$
Acetate oxidation	$CH_3COO^- + 4H_2O \rightarrow 4H_2 + 2HCO_3^- + H^+$
	Dechlorination
TCE consumption	$C_2HCl_3 + H_2 \rightarrow C_2H_2Cl_2 + Cl^-$
DCE consumption	$C_2H_2Cl_2 + H_2 \rightarrow C_2H_3Cl + Cl^-$
VC consumption	$C_2H_3Cl + H_2 \rightarrow C_2H_4 + Cl^-$
	Methane production
H_2-dependent methanogenesis	$4H_2 + CO_2 \rightarrow 4CH_4 + 2H_2O$
Acetate-dependent methanogenesis	$CH_3COO^- + H_2O \rightarrow CH_4 + HCO_3^-$
	Sulfate reduction
H_2-dependent sulfate reduction	$4H_2 + SO_4^{2-} + H^+ \rightarrow HS^- + 4H_2O$
Acetate-dependent sulfate reduction	$CH_3COO^- + SO_4^{2-} \rightarrow 2HCO_3^- + HS^-$
Butyrate-dependent sulfate reduction	$CH_3CH_2CH_2COO^- + 0.5SO_4^{2-} \rightarrow 2CH_3COO^- + 0.5HS^- + 0.5H^+$

10.3.1 Conceptual design

Two separate conceptual models were developed regarding the composition of sulfate reducers. In both models, only two sulfate-reducers are assumed to be present, reasoning that the supplied sulfate concentration cannot sustain three sulfate-reducing populations. In both conceptual models, acetate-utilizing sulfate reducers are thriving. Considering (a) the acetoclastic activity in the culture (a mean value of 511 μM acetate are consumed weekly), (b) the negligible methane formation (only 7 μM methane are observed), and (c) the low probability of acetate-oxidizing syntrophs being the most efficient acetate scavengers (this was also the case in the common-ancestry cultures NTUA-M1 and NTUA-M2), acetate-dependent sulfate reduction should be considered as a relevant sulfate reducing pathway in the culture. For the first conceptual model (namely variation 1, Fig. 10.1), H_2-utilizing sulfate reducers are also considered in the sulfate-reducing community. The outcome of the competition for sulfate among sulfate reducers is generally unknown (Muyzer and Stams, 2008), but given the dominance of H_2-utilizing *Dehalococcoides mccartyi* dechlorinators, we can reasonably deduce that H_2-utilizing sulfate reducers are not the dominant sulfate-reducing population. In the second conceptual model (namely variation 2, Fig. 10.2), acetate-utilizing sulfate reducers were supplemented by butyrate-degrading sulfate reducers. Any possible delay in dechlorination rates should be attributed to the loss of electron equivalents from the competition of butyrate-oxidizing syntrophs with butyrate-utilizing

sulfate reducers. If butyrate is channeled to sulfate reduction rather than H_2 production, dechlorinators would ultimately have lower H_2 quantities available.

In both variations, the methanogenic activity was considered acetate-dependent. This is a reasonable assumption considering that in the common-ancestry cultures of NTUA-S (i.e. NTUA-M1 and NTUA-M2) methanogenic activity was primarily acetate-dependent. Moreover, in variation 1, H_2-utilizing sulfate reducers would easily outcompete H_2-utilizing methanogens (Stams et al., 2005). Especially under the substrate-limiting conditions prevailing in the culture, it would be improbable for H_2-utilizing methanogens to survive.

With respect to dechlorination, only one dechlorinating population was considered gaining energy from every step of dechlorination. Apart from convenient, this decision is also in accordance with the molecular analysis performed in culture NTUA-S, when maintained with 300 μM sulfate. Then, it was indicated the *Dehalococcoides mccartyi* bacteria were dominant. The existence of partial dechlorinators (H_2- or acetate-utilizing) cannot be excluded. There are three dechlorinating species belonging in the class of *Deltaproteobacteria,* which were a significant part of the culture according to the molecular analysis. Yet, the dominance of *Dehalococcoides mccartyi* indicates that even if partial dechlorinators existed, they would consume only a small fraction of TCE; conversely, if TCE-to-ETH dechlorinators consumed mainly cDCE during each weekly feeding cycle, they would not be dominant. Therefore, we opted for simplicity in our model and considered only a *Dehalococcoides mccartyi* aggregate population present.

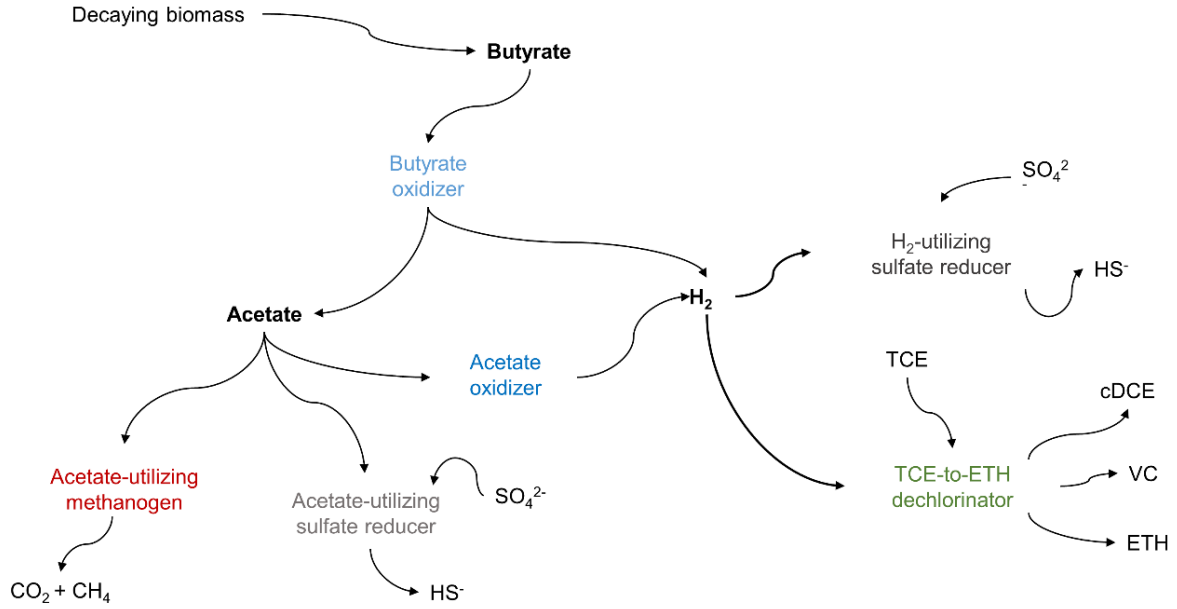

Fig. 10.1. Microbial processes considered in the first conceptual model of culture NTUA-S (variation 1).

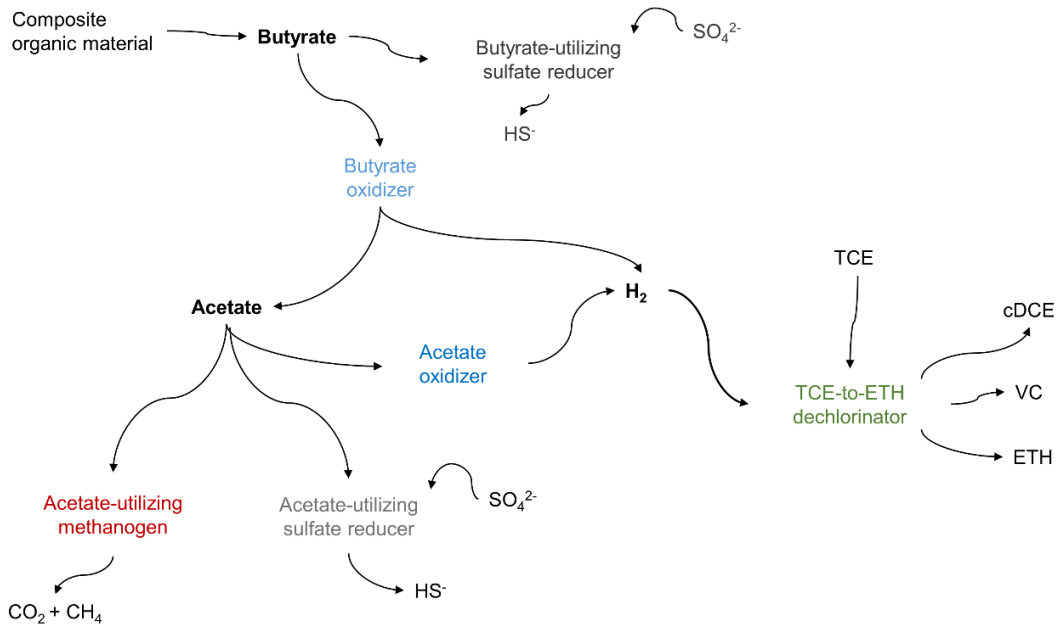

Fig. 10.2. Microbial processes considered in the second conceptual model of culture NTUA-S (variation 2).

10.3.2 Mathematical formulation

Both models are mathematically formulated on the basis of the system of differential equations and the reaction rates described in Chapter 4. Nevertheless, the rate of acetate-dependent methanogenesis is modified herein. During the high-surplus HEDS-BS test, a low rate of methane formation was observed that coincided with acetate accumulation after sulfate was depleted. Then, methane formation was coupled with acetate consumption. This lag in the formation of methane is an indication of either (a) inhibition of methanogens due to the presence of elevated VFA concentrations, or (b) inhibition due to sulfide toxicity. The first option is not rare in methanogenic reactors, in which VFA accumulation typically inhibits the members of *Methanosaeta* (Demirel, 2008), which are expected to thrive in reactors with acetate concentrations as low as those observed in our culture. Even a small pH shock (transient changes in the range of 0.5-1.0 pH units) induced by VFA overloading may affect the growth rate of *Methanosaeta* (De Vrieze et al., 2012). But, since these systems are presumably buffered and demonstrate relatively steady pH values, the most probable inhibitory mechanism is the presence of sulfide. In order to capture this lag phase in methane formation due to sulfide presence, we utilized an inhibition correction factor, $I_{HS\text{-}AM}$, that would decrease the maximum specific growth rates of methanogens in the presence of high sulfide concentrations:

$$I_{HS-AM} = \frac{1}{1+\frac{S_{HS}}{S_{INH,HS-AM}}} \tag{10.1}$$

where $S_{INH,HS\text{-}AM}$ is the inhibition factor of acetate-utilizing methanogens (μM) and S_{HS} is the concentration of sulfide (μM). Acetate consumption rates from acetate-utilizing methanogens now read as follows:

$$r_{A-AM} = -\frac{\mu_{\max,AM}}{Y_{AM}} X_{AM} \frac{S_A - S_{\min,A-AM} f_{AM}}{K_{S,A-AM} + S_A - S_{\min,A-AM} f_{AM}} F_{AM} I_{HS-AM} \tag{10.2}$$

10.4 Application of the multistart strategy for culture NTUA-S

The multistart algorithm that has been developed in Chapter 5 and employed in Chapters 7 and 8 (for methanogenic cultures NTUA-M1 and NTUA-M2) was utilized herein. Specifically, for each conceptual model, a sequence of 1000 quasi-random starting points was generated from the feasible area of the parameter space and local searches with the SQP local search routine were performed. The models were fitted to experimental observations from two batch tests comprising chloroethenes (TCE, cDCE, VC), ETH, sulfate, methane, and VFAs, i.e. butyrate and acetate. Following the application of the multistart algorithm, the quality of fit for each local solution was assessed with the mean absolute errors for chloroethenes and ethene only (calculated as in Section 5.4). Thus, only solutions capturing the removal of chloroethenes comprised the family of good-fit solutions. Given the relatively few available observations of sulfate, methane and VFAs, the fit to these observations was assessed based on visual proximity of model output and observed values. If any solution failed to approximate these observations, it was subsequently ruled out of the family of good-fit solutions. Similar to Chapters 7 and 8 and for the sake of convenience, the stepwise dechlorination of TCE will be presented in an aggregate fashion with the degree of dechlorination, *DoD*, calculated as described in section 7.4 by Eq. (7.2).

Preparing the multistart algorithm

Given the complexity of the catabolic food webs described in both model variations, it is hard to estimate rigorously all the components of each model: 41 kinetic parameters should be estimated for variation 1 and 40 kinetic parameters for variation 2. Therefore, 19 kinetic parameters were treated as fixed for variation 1 and 18 kinetic parameters for variation 2. Similar to the previous modeling efforts and in order to simplify the parameter estimation problem, growth yields, decay coefficients and substrate thresholds were fixed to specific values. These parameters vary within a relatively narrow range of values reported in the literature, as shown in Tables 10.3, 10.4, 10.5 and 10.6. Additionally, fixing growth yields and decay coefficients allows for the estimation of steady-state biomass concentrations or at least their respective lower and upper boundaries (if they are treated as adjustable). Growth yields and decay coefficients were selected from the range of reported values, in order to reproduce the main features of the performed molecular analysis (see also Section 4.2): moderate dominance of dechlorinators, which was accompanied by a dense community of sulfate-reducers and butyrate oxidizers. Finally, H_2 inhibition factors ($S_{INH,H\text{-}BO}$ and $S_{INH,H\text{-}AO}$) for syntrophic reactions were fixed to the values used for the model describing dechlorination under methanogenic conditions and the first-order coefficient for endogenous decay contribution to the value estimated for cultures NTUA-M1 and NTUA-M2.

The remaining kinetic parameters (22 parameters for both variations), comprising maximum specific growth rates ($\mu_{max,j}$), half-velocity coefficients ($K_{S,i\text{-}j}$) were considered adjustable. These parameters were constrained by the wide range of literature reported values presented in Tables 10.3, 10.4, 10.5 and 10.6. Nevertheless, boundaries for the sulfide inhibition coefficient for methanogens ($S_{INH,HS\text{-}AM}$) differed from the corresponding literature-reported values. Values of $S_{INH,HS\text{-}AM}$ vary from 1500 to 8500 μM according to Oude Elferink et al. (1994), but methane formation in culture NTUA-S appeared to be inhibited at lower sulfide concentrations. Therefore, $S_{INH,HS\text{-}AM}$ was constrained between 500 to 1500 μM of sulfides.

Bounding parameters was infeasible for two kinetic parameters and the corresponding boundaries were based on assumptions. As discussed in Chapter 7, the literature review did not yield boundaries for the half-velocity coefficients for acetate oxidizers ($K_{S,A\text{-}AO}$) remained unbounded. In this parameter estimation problem, we will be using the boundaries assumed in Chapter 7. Additionally, we could not locate boundaries for the half-velocity coefficient for butyrate of butyrate-utilizing sulfate reducers; only one value has been reported in two modeling efforts performed by Kalyuzhnyi et al. (1998) and Fedorovich et al (2003). Hence, we utilized the wide range of $K_{S,B\text{-}j}$ values employed for the syntrophic butyrate-oxidizing community in Chapter 7.

Table 10.3. Fixed and adjustable kinetic parameters of dechlorinators implemented in the parameter estimation problem.

Substrate	Parameter (units)	Type	Range of values	Feasible Area/Value	Reference
TCE	Maximum specific growth rate, $\mu_{max,D1}$ (days^{-1})	Adjustable	0.33-4.30	0.33-4.30	(a), (b)
cDCE	Maximum specific growth rate, $\mu_{max,\,D1}$ (days^{-1})	Adjustable	0.04-0.46	0.04-0.46	(c)-(a)
VC	Maximum specific growth rate, $\mu_{max,\,D1}$ (days^{-1})	Adjustable	0.01-0.49	0.01-0.49	(c)-(a)
TCE	Half-velocity coefficient, $K_{S,i\text{-}D1}$ (µM)	Adjustable	0.05-12.40	0.05-12.40	(d) –(e)
cDCE	Half-velocity coefficient, $K_{S,i\text{-}D1}$ (µM)	Adjustable	0.54-99.70	0.54-99.70	(f)-(g)
VC	Half-velocity coefficient, $K_{S,i\text{-}D1}$ (µM)	Adjustable	2.60-602.00	2.60-602.00	(h) –(c)
VC	Inhibition coefficient, $K_{INH,cDCE}$ (µM)	Adjustable	0.05-602.00	0.05-602.00	-
H_2	Half-velocity coefficient, $K_{S,H\text{-}D1}$ (µM)	Adjustable	0.007-0.100	0.007-0.100	(a)-(i)
H_2	H_2 threshold, $S_{min,H\text{-}D1}$ (µM)	Fixed	0.001-0.024	0.002	(j)
TCE, cDCE, VC	Growth yield, Y_{D1} x10^{-3} (mg VSS/µmol)	Fixed	0.18-9.60 [1]	2.40	(k)-(l)
-	Decay coefficient, b_{D1} (days^{-1})	Fixed	0.024-0.090	0.024	(f)-(m)

[1]: Yield coefficients are reported in mg VSS/µmol assuming that one *Dehalococcoides mccartyi* cell corresponds to 1.6 x 10^{-14} g of VSS (Cupples et al., 2003).

(a) Cupples et al. (2004b), (b) Christ and Abriola (2007), (c) Yu and Semprini (2004), (d) Lee et al. (2004), (e) Cupples et al. (2004a), (f) Fennell and Gossett (1998), (g) Haest et al. (2010), (h) Haston and McCarty (1999), (i) Smatlak et al. (1996), (j) Luijten et al. (2004), (k) Holmes et al. (2006), (l) Maymó-Gatell et al. (1997), (m) Cupples et al. (2003)

Table 10.4. Fixed and adjustable kinetic parameters of methanogens implemented in the parameter estimation problem.

Substrate	Parameter (units)	Type	Range of values	Feasible Area/Value	Reference
Acetate	Maximum specific growth rate, $\mu_{max,AM}$ (days^{-1})	Adjustable	0.04-0.38 [1]	0.04-0.38	(a), (b)
Acetate	Half-velocity coefficient, $K_{S,A-AM}$ (μM)	Adjustable	370-2031 [1]	370-2031	(a), (b)
Butyrate, acetate	VFA inhibition coefficient, $S_{INH,VFA-AM}$ (μM)	Adjustable	-	2500-5000	-
Acetate	Growth yield, Y_{AM} x10^{-3} (mg VSS/μmol)	Fixed	1.10-1.40	1.40	(a), (b)
-	Decay coefficient, b_{AM} (days^{-1})	Fixed	0.007-0.029 [1]	0.024	(a), (c)
Acetate	Substrate threshold, $S_{A,min-AM}$ (μM)	Fixed	7-69 [2]	15	(e)
Sulfide	Sulfide inhibition coefficient, $S_{INH,HS-AM}$ (μM)	Adjustable	1500-8500	500-1500	(b)

[1]: Parameter values were corrected from a temperature T to a temperature of 25°C according to the equations (Rittmann and McCarty, 2001): $\mu_{\max,j}^{25} = \mu_{\max,j}^{T} e^{0.06(25-T)}$, $K_{S,i-j}^{25} = K_{S,i-j}^{T} e^{-0.077(25-T)}$, $b_j^{25} = b_j^{T} e^{0.14(25-T)}$

[2]: Reported values for *Methanosaeta* spp. are considered, since *Methanosarcina* spp. are expected to be dominant at acetate concentrations greater than 1000 μM (Liu and Whitman, 2008).

(a) Pavlostathis and Giraldo-Gomez (1991), (b) Oude Elferink et al. (1994), (c) Clapp et al. (2004), (d) Löffler et al. (1999), (e) Aulenta et al. (2006)

Table 10.5. Fixed and adjustable kinetic parameters of butyrate and acetate oxidizers implemented in the parameter estimation problem.

Substrate	Parameter (units)	Type	Range of values	Feasible Area/Value	Reference
		Butyrate oxidizers			
Butyrate	Maximum specific growth rate, $\mu_{max,BO}$ (days^{-1})	Adjustable	0.21-0.60 [1]	0.21-0.60	(a)
Butyrate	Half-velocity coefficient, $K_{S,B\text{-}BO}$ (μM)	Adjustable	160-3676 [1]	160-3676	(a), (b)
Butyrate	Growth yield, Y_{BO} x10^{-3} (mg VSS/μmol)	Fixed	1.50-4.90	3.10	(c)
H_2	H_2 inhibition coefficient, $S_{H,INH\text{-}BO}$ (μM)	Fixed	-	0.25	-
-	Decay coefficient, b_{BO} (days^{-1})	Fixed	0.020-0.054 [1]	0.024	(a)
-	First-order coefficient for endogenous decay contribution, K_{ED} (days^{-1})	Fixed	-	0.004	-
		Acetate oxidizers			
Acetate	Maximum specific growth rate, $\mu_{max,AO}$ (d^{-1})	Adjustable	0.07-0.26 [2]	0.07-0.26	(d)
Acetate	Half-velocity coefficient, $K_{S,A\text{-}AO}$ (μM)	Adjustable	-	500-2500 [3]	-
Acetate	Growth yield, Y_{AO} x10^{-3} (mg VSS/μmol)	Fixed	-	0.70 [4]	-
H_2	H_2 inhibition coefficient, $S_{H,INH\text{-}AO}$ (μM)	Fixed	-	0.08	-
-	Decay coefficient, b_{AO} (days^{-1})	Fixed	-	0.024	-

[1]: Parameter values were corrected to a temperature of 25°C assuming that an increase of 10°C doubles maximum specific growth rates and decay coefficients, while it reduces half-velocity coefficients by half.

[2]: The values were calculated by the reported doubling times and were corrected to a temperature of 25°C assuming that an increase of 10°C doubles maximum specific growth rates.

[3]: Qu et al. (2009) reported a $K_{S,A\text{-}AO}$ value of 339 μM estimated under thermophilic conditions (55°C)

[4]: Yield for acetate oxidizers has been thermodynamically predicted according to Duhamel and Edwards (2007) assuming S_H = 50 nM and S_A = 750 μM.

(a) Pavlostathis and Giraldo-Gomez (1991), (b) Oude Elferink et al. (1994), (c) Kleerebezem and Stams (2000), (d) Hattori (2008)

Table 10.6. Fixed and adjustable kinetic parameters of sulfate-reducing bacteria implemented in the parameter estimation problem.

Substrate	Parameter (units)	Type	Range of values	Feasible Area/Value	Reference
	H_2-utilizing sulfate reducers				
H_2, sulfate	Maximum specific growth rate, $\mu_{max,HSR}$ (days^{-1})	Adjustable	0.23-5.50	0.23-5.50	(a)
H_2	Half-velocity coefficient, $K_{S,H\text{-}HSR}$ (μM)	Adjustable	0.05-2.6	0.05-2.6	(b)-(a)
Sulfate	Half-velocity coefficient, $K_{S,S\text{-}HSR}$ (μM)	Adjustable	5-200	5-200	(c)-(d)
H_2	Substrate threshold, $S_{H,min\text{-}HSR}$ (μM)	Fixed	1-10	2	(e)
H_2	Growth yield, Y_{HSR} x10^{-3} (mg VSS/μmol)	Fixed	0.6-2.6	1.60	(b)
-	Decay coefficient, b_{HSR} (days^{-1})	Fixed	0.01-0.06	0.05	(d)-(f)
	Acetate-utilizing sulfate reducers				
Acetate, sulfate	Maximum specific growth rate, $\mu_{max,ASR}$ (days^{-1})	Adjustable	0.14-1.39	0.14-1.39	(a)
Acetate	Half-velocity coefficient, $K_{S,A\text{-}ASR}$ (μM)	Adjustable	70-600	70-600	(a)
Sulfate	Half-velocity coefficient, $K_{S,S\text{-}ASR}$ (μM)	Adjustable	5-200	5-200	(c)-(d)
Acetate	Substrate threshold, $S_{A,min\text{-}ASR}$ (μM)	Fixed	-	15	(a)
Acetate	Growth yield, Y_{ASR} x10^{-3} (mg VSS/μmol)	Fixed	4.30-5.60	4.30	(a)
-	Decay coefficient, b_{ASR} (days^{-1})	Fixed	0.01-0.04	0.03	(d)-(f)
	Butyrate-utilizing sulfate reducers				
Butyrate, sulfate	Maximum specific growth rate, $\mu_{max,BSR}$ (days^{-1})	Adjustable	0.17-1.58	0.17-1.58	(a)-(g)
Butyrate	Half-velocity coefficient, $K_{S,B\text{-}BSR}$ (μM)	Adjustable	631	160-3676	(c)-(e)
Sulfate	Half-velocity coefficient, $K_{S,S\text{-}BSR}$ (μM)	Adjustable	5-200	5-200	(c)-(d)
Butyrate	Growth yield, Y_{BSR} x10^{-3} (mg VSS/μmol)	Fixed	4.75	4.75	(d)-(f)
-	Decay coefficient, b_{BSR} (days^{-1})	Fixed	0.01-0.04	0.03	(d)-(f)

(a) Stams et al. (2005), (b) Malaguerra et al. (2011), (c) Ingvorsen and Jørgensen (1984), (d) Fedorovich et al. (2003), (e) Luijten et al. (2004), (f) Kalyuzhnyi et al. (1998), (g) Oude Elferink et al. (1994)

Chemical initial concentrations were fixed at their measured values at the beginning of each batch test. Concerning initial biomass concentrations, based on the steady-state performance of the source culture, biomass concentrations were estimated and fixed for (a) dechlorinators and acetate-utilizing methanogens in both variations, and (b) butyrate-oxidizing bacteria for variation 1. These values were calculated from the following equation:

$$X_{j,SS} = \frac{\theta_c}{f} \frac{Y_j dS_{i-j}}{1 + b_j \theta_c} \quad (10.3)$$

where $X_{j,SS}$ is the steady-state biomass concentration of microorganism j (mg VSS/l), θ_c is the solid retention time (48 days), f is the duration of the feeding cycles of the culture (7 days), and dS_{i-j} is the quantity of substrate i consumed by microorganism j during each feeding cycle (μM).

The remaining initial biomass concentrations (i.e. concentrations of sulfate reducers and acetate oxidizers) were treated as constrained adjustable parameters. Their constraints were calculated from Eq. (10.3) and the end-products of the culture during the achieved steady state of the culture by assuming the respective maximum and minimum dS_{i-j} values (Tables 10.7 and 10.8).

For model variation 1, the lower boundary for H_2-utilizing sulfate reducers is zero, assuming that they are absent. The upper boundary corresponds to 50% of the observed sulfate reduction. These assumptions entail that acetate-utilizing sulfate reducers are responsible for at least 50% of the weekly sulfate reduction. This is consistent with the significant acetoclastic activity observed within the culture, which cannot be attributed solely to the slow-growing acetate-oxidizing syntrophs (as supported by the findings regarding acetate oxidizers in the common-ancestry cultures NTUA-M1 and NTUA-M2).

For model variation 2, the lowest possible boundary for butyrate-utilizing sulfate reducers is zero (i.e. they are not active in the culture) and the upper boundary corresponds to 100% of the available butyrate or equivalently to 32% of the observed sulfate-reducing activity. This means that acetate-utilizing sulfate reducers in model variation 2 consume at least 68% of the consumed sulfate on a weekly basis.

For both variations, the minimum and maximum dS_{A-AO} values for acetate oxidizers were calculated from the mass balance for acetate on a weekly basis, i.e. the 600 μM of produced acetate from butyrate oxidation minus the acetate consumed for sulfate reduction. As shown in Table 10.7, at least 20% (120 μM) of acetate should be consumed by acetate oxidizers on an average basis.

Table 10.7. Fixed and adjustable initial biomass concentrations for the microbial groups considered in variation 1.

Component	Type	Substrate consumed on a weekly basis, $dS_{i\text{-}j}$ (μM)	Growth yield, Y_j x10^{-3} (mg VSS/μmol*)	Decay coefficient, b_j (days^{-1})	Range of values/Value (mg VSS/l)
TCE-to-ETH dechlorinators	Fixed	1051	2.35	0.024	7.85
Butyrate oxidizers	Fixed	300	3.10	0.024	2.96
Acetate oxidizers	Adjustable	120-358	0.70	0.024	0.27-0.80
Acetate-utilizing methanogens	Fixed	7	1.40	0.024	0.03
H_2-utilizing sulfate reducers	Adjustable	0-235	1.70	0.050	0.00-3.22
Acetate-utilizing sulfate reducers	Adjustable	235-470	4.30	0.030	2.83-5.67

*: μmol H_2 for dechlorinators and H_2-utilizing sulfate reducers, μmol butyrate for butyrate oxidizers and butyrate-utilizing sulfate reducers, and μmol acetate for acetate-utilizing methanogens, acetate-utilizing sulfate reducers and acetate oxidizers.

Table 10.8. Fixed and adjustable initial biomass concentrations for the microbial groups considered in variation 2.

Component	Type	Substrate consumed on a weekly basis, $dS_{i\text{-}j}$ (μM)	Growth yield, Y_j x10^{-3} (mg VSS/μmol)	Decay coefficient, b_j (days^{-1})	Range of values/Value (mg VSS/l)
TCE-to-ETH dechlorinators	Fixed	1051	2.35	0.024	7.85
Butyrate oxidizers	Adjustable	0-300	3.10	0.024	0.00-2.96
Acetate oxidizers	Adjustable	123-198	0.70	0.024	0.27-0.66
Acetate-utilizing methanogens	Fixed	7	1.40	0.024	0.03
Butyrate-utilizing sulfate reducers	Adjustable	0-75	4.75	0.030	0.00-4.00
Acetate-utilizing sulfate reducers	Adjustable	395-470	4.30	0.030	3.86-5.67

10.5 The two alternate approximations of culture NTUA-S

10.5.1 Acetate- and H_2-dependent sulfate reduction

The simultaneous fitting of the model to observations from two batch tests constrained the behavior of the model and gave a small family of 43 local solutions. Only five of them could be grouped in a family of good-fit solutions, which contained those local solutions that achieved mean absolute errors for dechlorination lower than 30 μM for each test. This is a reasonable error given that (a) parameter estimation efforts for cultures NTUA-M1 and NTUA-M2 resulted in similar errors, and (b) total chloroethene molar balance (i.e. the deviation of the sum of chloroethenes at

each measurement from the initial TCE concentration) varied from 2 μM to 38 μM. These good-fit solutions were not substantially different in terms of their behavior: they had almost identical kinetic properties for dechlorinators and similar functional features for the sulfate-reducing community. Hence, only the relative abundance and the kinetic properties of the microbial groups considered in the best-fit solution will be discussed herein.

Acetate-utilizing sulfate reducers were estimated as a substantial part of the culture and as the denser sulfate-reducing population ($X_{ASR,0}$=5.0 mg VSS/l, Fig. 10.3). H_2-utilizing sulfate reducers constitute only 8% of the biomass of culture NTUA-S ($X_{HSR,0}$=1.5 mg VSS/l, Fig. 10.3), as their growth was limited by the availability of both their substrates, i.e. H_2 and sulfate. Finally, 3% of the culture ($X_{AO,0}$=0.60 mg VSS/l) belonged to acetate-oxidizing syntrophs. Acetate oxidizers were limited by the presence of the acetate-utilizing sulfate reducers, which outcompeted them.

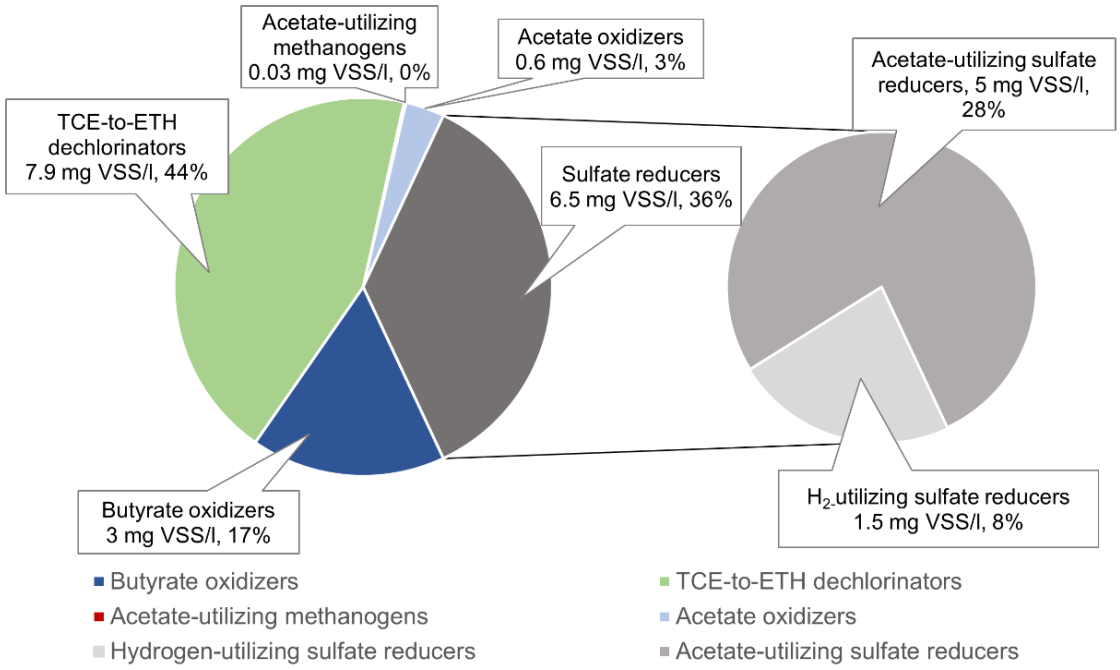

Fig. 10.3. Initial biomass distributions resulting from the optimization strategy for variation 1.

Dechlorinators were competent TCE, cDCE and H_2 scavengers, as indicated by the low half-velocity coefficients for the corresponding substrates ($K_{S,TCE\text{-}D1}$, $K_{S,cDCE\text{-}D1}$ and $K_{S,H\text{-}D1}$ in Table 10.9). The high affinity to these substrates probably explains why the long-term performance of NTUA-S is similar to the performance of culture NTUA-M2; on a weekly basis dechlorinators in both cultures consumed TCE and cDCE. Regarding VC, dechlorinators were calculated with poor kinetic properties; they could grow with a low $\mu_{max,VC\text{-}D1}$ (0.01 $days^{-1}$, which coincides with the lower boundary of $\mu_{max,VC\text{-}D1}$ values), they had a low affinity for VC ($K_{S,VC\text{-}D1}$=507.4 μM, which is close to the upper boundary of 602 μM), while VC consumption was strongly inhibited by cDCE ($K_{INH,Cdce}$ =2.0 μM, a value suggesting that VC consumption will commence, when all cDCE is removed).

The kinetic properties estimated for the dechlorinating species in culture NTUA-S revealed a significant difference compared to the dechlorinating consortia in cultures NTUA-M1 or NTUA-M2. In these cultures, dechlorinators grew with a 18-fold greater $\mu_{max,VC\text{-}D1}$, had a slightly greater affinity for VC and a 10-fold lower inhibition coefficient of cDCE. The VC-related parameters

estimated for the dechlorinating population thriving within culture NTUA-S are close to the reported values for culture PM (which was examined in Chapter 5) or culture Donna II (Fennel and Gossett, 1998), which were enriched *Dehalococooides mccartyi 195* (Cornell group of *Dehalococcoides mccartyi* strains*),* a *Dehalococcoides mccartyi* strain growing commetabolically on VC. Given that cultures NTUA-M2 and NTUA-S originated from the same material, we can surmise that the long-term exposure to sulfides played a role as to which chloroethene-respiring microorganisms would eventually thrive in each culture. This effect of sulfides in the make-up of the dechlorinating community has been reported by Berggren et al. (2013), who postulated that the presence of sulfide probably induced a shift from the dominance of Pinellas group of *Dehalococcoides mccartyi* strains to the dominance of *Dehalococcoides mccartyi 195* strain, which removes VC commetabolically and, thus, slower than any other *Dehalococcoides mccartyi* strain isolated.

Table 10.9. Kinetic parameters for dechlorinators resulting from the best-fit solution of the parameter estimation strategy employed for variation 1.

Substrate	Parameter	Symbol (units)	Value
TCE	Maximum specific growth rate	$\mu_{max,TCE\text{-}D1}$ ($days^{-1}$)	1.07
DCE	Maximum specific growth rate	$\mu_{max,cDCE\text{-}D1}$ ($days^{-1}$)	0.08
VC	Maximum specific growth rate	$\mu_{max,VC\text{-}D1}$ ($days^{-1}$)	0.01
TCE	Half-velocity coefficient	$K_{S,TCE\text{-}D1}$ (μM)	3.9
DCE	Half-velocity coefficient	$K_{S,cDCE\text{-}D1}$ (μM)	65.1
VC	Half-velocity coefficient	$K_{S,VC\text{-}D1}$ (μM)	507.4
VC	Inhibition coefficient	$K_{INH,cDCE}$ (μM)	2.0
H_2	Half-velocity coefficient	$K_{S,H\text{-}D1}$ (μM)	0.007

Acetate-utilizing sulfate reducers were the dominant sulfate-reducing population. They could grow rapidly on the available acetate, as they had to outcompete only the inefficient acetate-oxidizing syntrophs (as indicated by their low specific affinity for acetate, $\mu_{max,j}/K_{s,Aj}$ ratio, see Tables 10.10 and 10.11). On the other hand, H_2-utilizing sulfate reducers had to surpass the obstacle of a dense dechlorinating population, that exhibited a higher affinity for H_2 ($K_{S,S\text{-}D1}$ is 54-fold lower than $K_{S,H\text{-}HSR}$). Thus, despite being a fast-growing and good sulfate scavengers (with $\mu_{max,HSR}$ = 4.5 $days^{-1}$ and $K_{S,S\text{-}HSR}$ being lower than $K_{S,S\text{-}ASR}$, Table 10.10), H_2-utilizing sulfate reducers were limited mainly by the availability of H_2.

Table 10.10. Kinetic parameters for sulfate reducers deriving from the best-fit solution of the parameter estimation strategy employed for variation 1.

Substrate	Parameter	Symbol (units)	Value
H_2-utilizing sulfate reducers			
H_2, sulfate	Maximum specific growth rate	$\mu_{max,HSR}$ ($days^{-1}$)	4.5
H_2	Half-velocity coefficient	$K_{S,H\text{-}HSR}$ (μM)	1.2
Sulfate	Half-velocity coefficient	$K_{S,S\text{-}HSR}$ (μM)	37
Acetate-utilizing sulfate reducers			
Acetate, sulfate	Maximum specific growth rate	$\mu_{max,ASR}$ ($days^{-1}$)	0.48
Acetate	Half-velocity coefficient	$K_{S,A\text{-}ASR}$ (μM)	163
Sulfate	Half-velocity coefficient	$K_{S,S\text{-}ASR}$ (μM)	83

Butyrate-oxidizing syntrophs were a substantial part of the culture (Fig. 10.3) given the absence of competition for butyrate. Acetate-oxidizing syntrophs were a relatively small part of the culture, due to their low poor competitive fitness for acetate. Yet, they make their living from the available acetate, since (a) the existence of two H_2-scavenging groups maintains H_2 concentrations significantly below inhibiting levels (H_2 concentrations higher than 0.4 μM are inhibiting), and (b) acetate-dependent methanogenesis is negligible (one competitor less). Likely, acetate-dependent methanogenesis is negligible as a result of the combined effect of competition for acetate and the poor kinetic properties of methanogens (low $\mu_{max,AM}$, especially compared to the methanogens of NTUA-M2 culture). The poor kinetic characteristics of methanogens result perhaps by their long-term exposure to sulfides, which are a knowingly inhibiting substance for acetate-utilizing methanogens of the genus *Methanosaeta* (Demirel, 2008).

Table 10.11. Kinetic parameters for butyrate oxidizers and acetate oxidizers resulting from the best-fit solution of the parameter estimation strategy for variation 1.

Substrate	Parameter	Symbol (units)	Value
Butyrate oxidizers			
Butyrate	Maximum specific growth rate	$\mu_{max,BO}$ ($days^{-1}$)	0.60
Butyrate	Half-velocity coefficient	$K_{S,B\text{-}BO}$ (μM)	485
Acetate oxidizers			
Acetate	Maximum specific growth rate	$\mu_{max,AO}$ ($days^{-1}$)	0.26
Acetate	Half-velocity coefficient	$K_{S,A\text{-}AO}$ (μM)	1094

Table 10.12. Kinetic parameters for acetate-utilizing methanogens resulting from the best-fit solution of the parameter estimation strategy for variation 1.

Substrate	Parameter	Symbol (units)	Value
Acetate-utilizing methanogens			
Acetate	Maximum specific growth rate	$\mu_{max,AM}$ ($days^{-1}$)	0.20
Acetate	Half-velocity coefficient	$K_{S,A\text{-}AM}$ (μM)	936
Sulfide	Sulfide inhibition coefficient	$S_{INH,HS\text{-}AM}$ (μM)	830

The best-fit solution for model variation 1 reproduced all the important features of the behavior of culture NTUA-S under low butyrate supply (Fig. 10.4). The mean absolute error for dechlorination was 26 μM. The model described adequately the rapid depletion of TCE and cDCE within the first five days, while it simulated sufficiently the stall of VC consumption that followed

from day 5 to day 150 (Fig. 10.4a). Additionally, the simulated results reproduced the pattern of sulfate reduction: a quick initial decline of sulfate followed by a long period of slow sulfate reduction, which ultimately resulted in the accumulation of sulfate (Fig. 10.4b). Model variation 1 was also fitted fairly to the limited VFA observations (Fig. 10.4c), while it predicted the minimal methane formation (data not shown, as methane was below 5 μM).

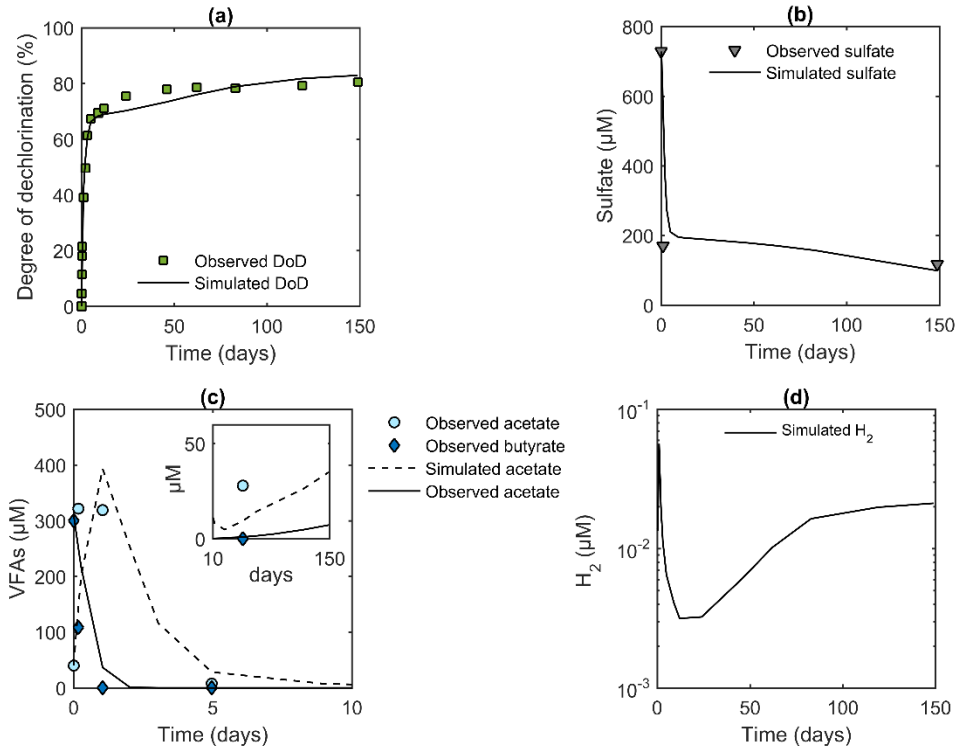

Fig. 10.4. Observed and simulated (a) degree of dechlorination, (b) sulfate concentration, (c) VFA concentrations, and (d) H_2 concentration for batch test LEDS-BS and variation 1. Methane concentrations are negligible (below 5 μM) and, hence, not shown.

The culture was mostly active during the first five days, when dechlorinators consumed all the available TCE and cDCE, and sulfate-reducers consumed 73% of the overall consumed sulfate. During this period, dechlorinators took advantage of their competitive fitness at the low prevailing H_2 concentrations (below 0.08 μM – Fig. 10.4d) and consumed 78% of the available H_2 and 35% of the overall reducing equivalents (Fig 10.5a and 10.5b). Despite their high $\mu_{max,HSR}$ values, H_2-utilizing sulfate reducers were outcompeted by dechlorinators, due to (a) their low affinity for H_2 compared to dechlorinators (3 orders of magnitude greater $K_{S,H\text{-}J}$ value), and (b) the competition for sulfate (they are responsible for 12% of the reduced sulfate by day five – Fig. 10.5d). Acetate-utilizing sulfate reducers were, consequently, the most efficient metabolism and the most capable sulfate-scavengers. Nevertheless, the competition for sulfate delayed the growth of acetate-utilizing sulfate reducers and gave room for acetate-oxidizing syntrophs to thrive; they consumed 27% of the available acetate (Fig. 10.5c) providing extra H_2 to dechlorinators and H_2-utilizing sulfate reducers; 717 μM H_2 were produced from acetate oxidation, which is 1.2-fold more H_2 compared to butyrate oxidation. Thus, acetate oxidizers, despite being a minority population, contributed significantly to the extent of dechlorination.

Following the first five days, dechlorination and sulfate reduction occurred with the reducing power of decaying biomass. Approximately 20% of the final reducing equivalents came from biomass disintegration. Yet, these electron equivalents did not enhance dechlorination significantly, at least not at the extent that they enhanced dechlorination in culture NTUA-M2. Dechlorinator growth was limited by their poor kinetic properties regarding VC and, thus, despite the kinetic advantage that they had over H_2-utilizing sulfate reducers at the low H_2 concentrations that prevailed (biomass functioned as a slow-releasing H_2 source maintaining H_2 concentrations around 0.02 μM), they did not consume much of the available H_2. During this period, sulfate reduction was almost entirely H_2-dependent given the competitive advantage of H_2-utilizing sulfate reducers over acetate-utilizing reducers at sulfate-limiting conditions. This shift in the sulfate-reducing pathway deprived the requisite reducing power from dechlorinators.

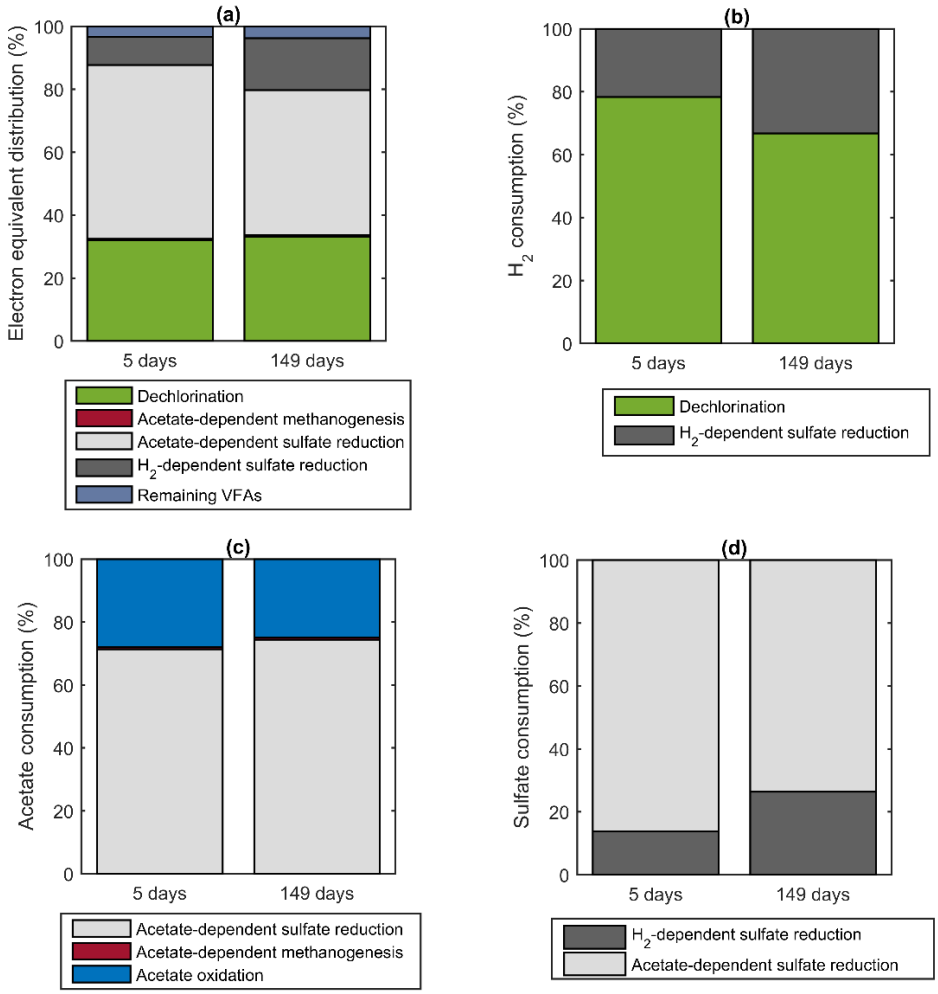

Fig. 10.5. Distribution of (a) electron equivalents, (b) consumed H_2 by dechlorinators and H_2-utilizing sulfate reducers, (c) consumed acetate by acetate-utilizing sulfate reducers, acetate-utilizing methanogens and acetate oxidizers, (d) reduced sulfate by acetate-utilizing sulfate reducers and H_2-utilizing sulfate reducers after five days and at the end of batch test LEDS-BS for variation 1.

The best-fit solution of the problem failed to reproduce the collective behavior of culture NTUA-S under high sulfate concentrations. There are discrepancies between the model output and (a) the observed VFA concentrations (Fig. 10.6c) and (b) the final levels of methane formation (Fig. 10.6d); the lag-phase of methane formation was reproduced. According to our simulations,

butyrate plateaued at 1000 μM following its initial rapid decline. Butyrate fermentation was thermodynamically inhibited, because of the high H_2 concentrations that prevailed following sulfate depletion (around 1.2 μM, data available in Appendix A). Being limited by VC availability, dechlorinators grew slowly and, thus, consumed the available H_2 in a low pace. Consequently, H_2 never dropped at levels that could make butyrate oxidation feasible. Because of butyrate accumulation, acetate never reached the levels observed in the laboratory and, hence, the final simulated concentration of methane deviated from the observed.

The model predicted that dechlorinators would consume nearly all the available chloroethenes by day 83 (Fig. 10.6a) and captured the rapid removal of sulfate (Fig. 10.6b). The mean absolute error for dechlorination was 28 μM. Simulated *DoD* deviated mildly from the observed *DoD* following cDCE removal and until day 60. The observed VC consumption rate was lower. But, as VC-related parameters were estimated very close to the respective lower boundaries, a slower VC consumption rate cannot be reproduced by our model. Nonetheless, we consider this deviation of the model from the observations as not critical, because regardless of the mechanism that caused it, it was no longer applicable following day 60. For the last 23 days of the experiment, VC consumption rate was higher and resulted in an observed *DoD* equal to 99%.

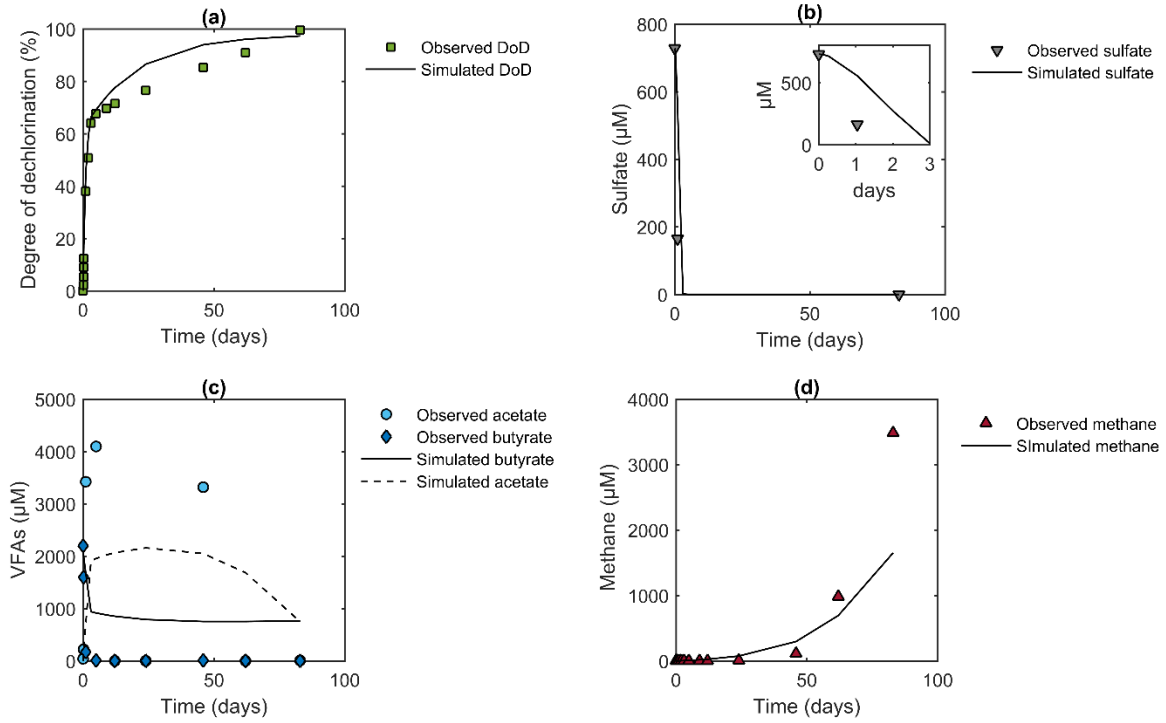

Fig. 10.6. Observed and simulated (a) degree of dechlorination, (b) sulfate concentration, (c) VFA concentrations, and (d) methane concentration for batch test HEDS-BS and variation 1.

Due to the increased quantity of butyrate as an electron donor source, the fast-growing H_2-utilizing sulfate reducers became more competent sulfate scavengers consuming 40% of the available sulfate (Fig. 10.7d). They also outcompeted dechlorinators consuming 57% of H_2 produced through butyrate and acetate oxidation (Fig. 10.7d). Their enhanced performance, however, was inadequate to cause the complete oxidation of butyrate. The presence of fast-growing H_2-utilizing sulfate reducers failed to constitute butyrate oxidation thermodynamically feasible, as nearly half of the initially supplied butyrate functioned as an H_2 source. Thinking in terms of electron balances,

only if sulfate reduction depended entirely on H_2 it would have caused the complete removal of butyrate: 730 µM sulfate require 2920 µM H_2 and 515 µM TCE require 1545 µM H_2. These quantities of H_2 add up to the quantities of butyrate that are readily available from the oxidation of 2230 µM butyrate. Thus, the make-up of the sulfate-reducing community that was estimated by the parameter estimation process appears to be inadequate to predict the true behavior of the culture under elevated butyrate supply.

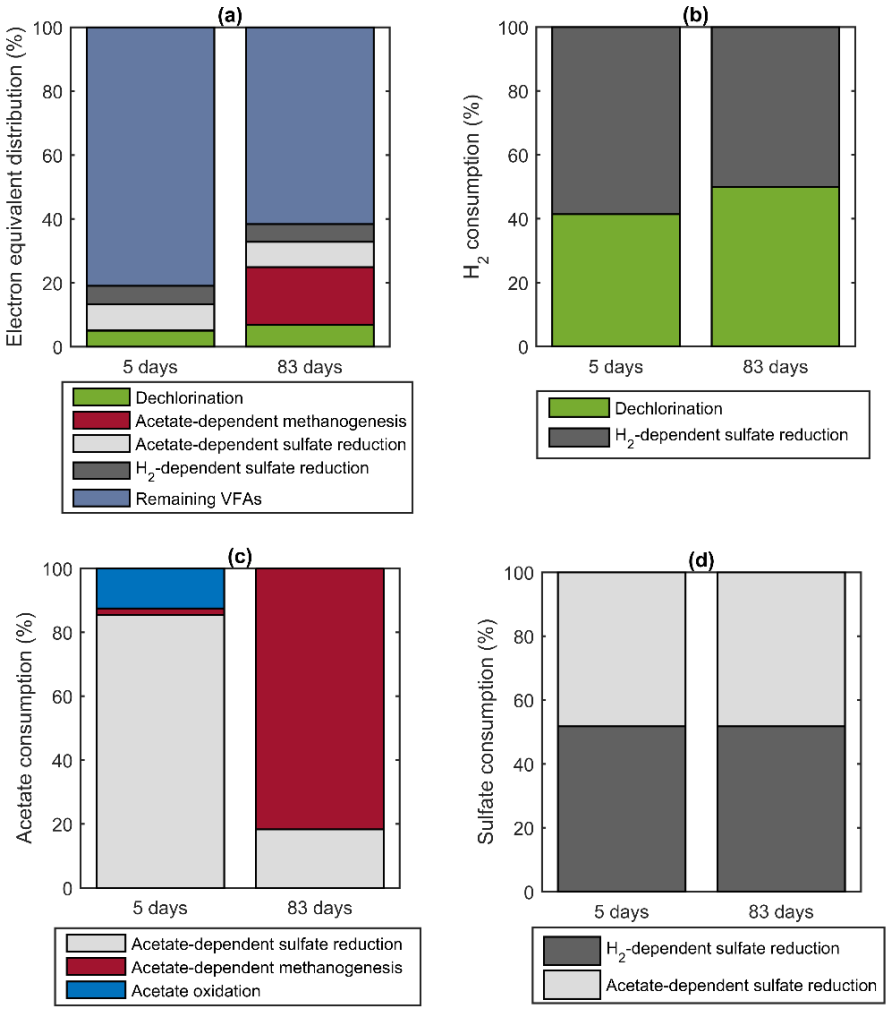

Fig. 10.7. Distribution of (a) electron equivalents, (b) consumed H_2 by dechlorinators and H_2-utilizing sulfate reducers, (c) consumed acetate by acetate-utilizing sulfate reducers, acetate-utilizing methanogens and acetate oxidizers, (d) reduced sulfate by acetate-utilizing sulfate reducers and H_2-utilizing sulfate reducers after five days and at the end of batch test HEDS-BS for variation 1.

In an attempt to improve the fit for the high-donor test HEDS-BS, variation 1 was modified, assuming that H_2-utilizing sulfate reducers did not have to compete for sulfate; they were the only sulfate-reducing population with an initial biomass concentration equal to the sum of both sulfate-reducing species, i.e. $X_{HSR,0}$ = 6.5 mg VSS/l. This shift implies that in the presence of significant butyrate quantities acting as an H_2 source, acetate-utilizing sulfate reducers preferably chose to use the resulting H_2 as an electron donor rather than acetate. Is this shift in the function of sulfate reducers probable? Theoretically, it is probable. According to Madigan et al. (2014), the majority of sulfate reducers that are capable of utilizing acetate can also utilize H_2 as an electron donor (e.g. *Desulfosarcina*, *Desulfonema*, *Desulfococcus*, *Desulfobacterium*, *Desulfotomaculum* and some members of

Desulfovibrio). The conditions under which this shift should be anticipated are, however, unclear. Perhaps it is thermodynamics that can induce such a shift, as H_2-dependent sulfate reduction is typically yielding more energy than acetate-dependent sulfate reduction to sulfate-reducing bacteria (151.9 kJ per mol sulfate of reduced instead of 47.7 kJ per mol of sulfate reduced).

In the absence of acetate-utilizing sulfate reducers, model output was closer to the observed behavior of culture NTUA-S, but it was still inaccurate regarding butyrate depletion (Fig. 10.8c). Butyrate was not entirely removed under these conditions, as well. All the available sulfate was consumed by H_2-utilizing sulfate reducers, which grew faster and consumed 73% of the produced H_2 (Fig. 10.9b). Exactly due to their performance, they established a mutually beneficial syntrophic relationship with butyrate oxidizers, which consumed 78% of the available butyrate within the first five days. Therefore, even if dechlorinators had to compete with a stronger and more competent H_2-utilizing population, they also had more H_2 readily available during the first five days. But, butyrate oxidizers were not the only population that benefited from the H_2-scavenging species. Acetate oxidizers consumed 174 μM acetate (96% of the observed acetoclastic activity, Fig. 10.9c) producing nearly 25% of the total H_2 quantity. Therefore, 2200 μM butyrate were not completely used again; they are not needed as a H_2 source, as acetate-oxidizing syntrophs stepped in and gave the requisite H_2.

After the first five days, dechlorinators consumed the available VC under non-limiting H_2 concentrations, as H_2 plateaued at 1.2 μM (results available in Appendix A). Hence, the low dechlorination rates should be attributed to the poor growth characteristics of dechlorinators on VC. Finally, acetate-utilizing methanogens exploited the high quantities of available acetate and the absence of competition, and grew slowly, overcoming the inhibitory effects of the produced sulfides (Fig. 10.8d).

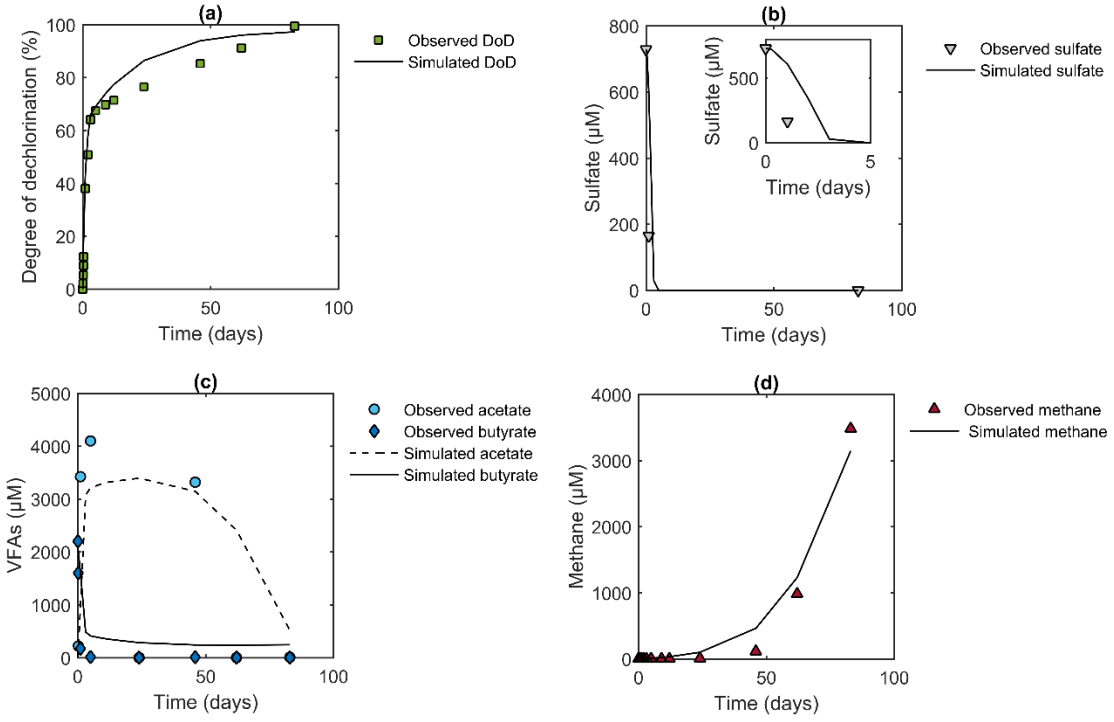

Fig. 10.8. Observed and simulated (a) degree of dechlorination, (b) sulfate concentration, (c) VFA concentrations, and (d) methane concentration for batch test HEDS-BS and variation 1 assuming that all sulfate reducers utilize H_2 as an electron donor.

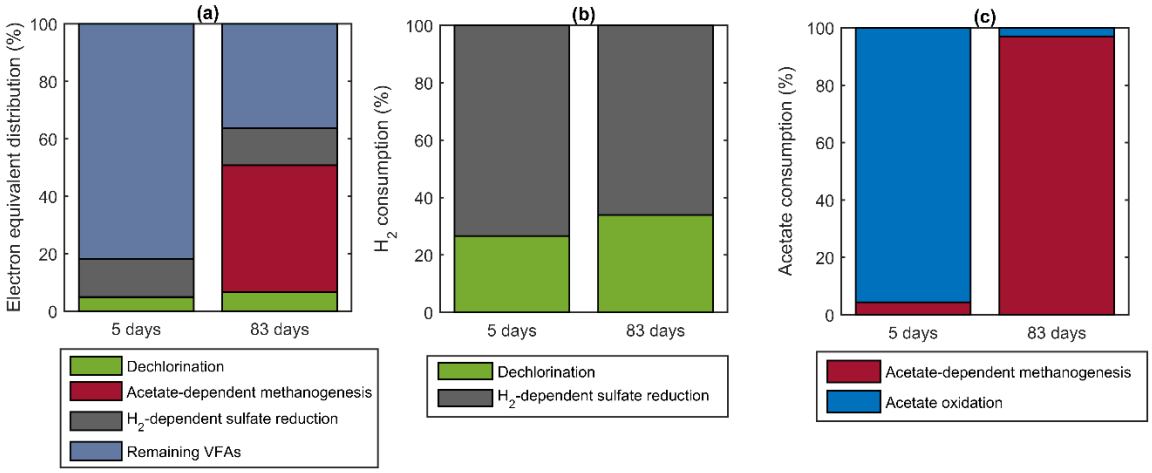

Fig. 10.9. Distribution of (a) electron equivalents, (b) consumed H_2 by dechlorinators and H_2-utilizing sulfate reducers, (c) consumed acetate by acetate-utilizing sulfate reducers, acetate-utilizing methanogens and acetate oxidizers after five days and at the end of batch test HEDS-BS for variation 1 assuming that all sulfate reducers utilize H_2 as an electron donor.

10.5.2 Acetate- and butyrate-dependent sulfate reduction

Like variation 1, fitting the model to observations from two batch tests constrained its behavior and few distinctive local solutions were estimated, with parameter estimates being close to the imposed boundaries (especially kinetic parameters for dechlorinators and the syntrophic H_2-producing species). The multistart algorithm ran for 1000 starting points and located 89 distinctive local solutions. Yet, only nine of the local solutions are considered adequate, achieving mean absolute errors for dechlorination lower than 30 μM in each experiment. These solutions were functionally similar (i.e. the outcome of the competitions for butyrate and sulfate) and had nearly identical relative abundances for the microbial species considered. Thus, we will be commenting on the performance and the characteristics of the best-fit solution.

In terms of the initial relative abundance of the microbial groups, the main difference between variation 1 and variation 2 is the make-up of the sulfate-reducing community (compare Fig. 10.3 to Fig. 10.10). Practically, H_2-utilizing sulfate reducers were replaced by butyrate-utilizing sulfate reducers. Butyrate-utilizing sulfate reducers were the minority sulfate-reducing population ($X_{BSR,0}$=2.9 mg VSS/l, which is 42% of sulfate reducers), but their function within culture NTUA-S deprived butyrate from butyrate-oxidizing syntrophs, who were fewer than in variation 1 (2.4 mg VSS/l instead of 3.0 mg VSS/l).

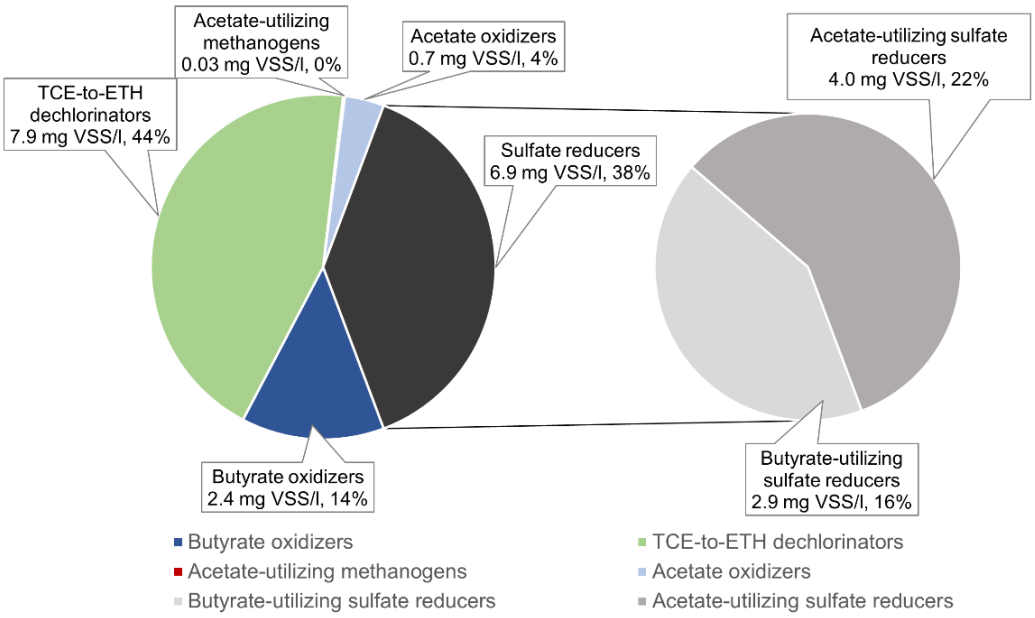

Fig. 10.10. Initial biomass distributions resulting from the optimization strategy for variation 2.

Dechlorinators in variation 2 have similar functional characteristics to those calculated for variation 1 (Table 10.13). Again, dechlorinators were competent TCE, cDCE and H_2 scavengers (low $K_{s,i\text{-}D1}$ values estimated for each substrate), but they could grow poorly on VC with a low calculated $\mu_{max,VC\text{-}D1}$ and a high $K_{S,VC\text{-}D1}$. This finding provides confidence that behavior approximates the actual functional features of dechlorinators in culture NTUA-S. The main discrepancy between the dechlorinating species in variation 2 and variation 1 is the maximum specific growth rate for TCE. In variation 2, dechlorinators had to be even more fast-growing to maintain H_2 concentrations below inhibitory levels for syntrophic butyrate and acetate oxidations. In the absence of H_2-utilizing sulfate reducers, dechlorinators are the only species capable of maintaining H_2 low. Nevertheless, the kinetic properties estimated for dechlorinating species in culture NTUA-S highlight the differences compared to the dechlorinating consortium in cultures NTUA-M1 or NTUA-M2, in which dechlorinators could grow rapidly during VC consumption ($\mu_{max,VC\text{-}D1}$ for NTUA-M1 and NTUA-M2 was 18-fold greater).

Table 10.13. Kinetic parameters for dechlorinators resulting from the best-fit solution of the parameter estimation strategy for model variation 2.

Substrate	Parameter (units)	Symbol	Value
TCE	Maximum specific growth rate	$\mu_{max,TCE\text{-}D1}$ ($days^{-1}$)	4.30
DCE	Maximum specific growth rate	$\mu_{max,cDCE\text{-}D1}$ ($days^{-1}$)	0.18
VC	Maximum specific growth rate	$\mu_{max,VC\text{-}D1}$ ($days^{-1}$)	0.01
TCE	Half-velocity coefficient	$K_{S,TCE\text{-}D1}$ (μM)	3.4
DCE	Half-velocity coefficient	$K_{S,cDCE\text{-}D1}$ (μM)	55.6
VC	Half-velocity coefficient	$K_{S,VC\text{-}D1}$ (μM)	568.0
VC	Inhibition coefficient	$K_{INH,cDCE}$ (μM)	4.7
H_2	Half-velocity coefficient	$K_{S,H\text{-}D1}$ (μM)	0.025

Acetate-utilizing sulfate reducers had comparable affinity for sulfate to butyrate-utilizing sulfate reducers (compare $K_{S,S\text{-}ASR}$ to $K_{S,S\text{-}BSR}$ values, Table 10.14). But, they outcompeted butyrate-utilizing sulfate reducers, as the latter had to compete for butyrate with an efficient syntrophic butyrate-

oxidizing community. Butyrate-oxidizing syntrophs were significant in numbers and demonstrated a comparable specific affinity for butyrate with sulfate-reducers (compare $\mu_{max,BO}/K_{S,B\text{-}BO}$ to $\mu_{max,BSR}/K_{S,B\text{-}BSR}$ ratios based on Tables 10.14 and 10.15). On the other hand, acetate-utilizing sulfate reducers had to overcome a minor obstacle, i.e. the competition with acetate-oxidizing syntrophs. Acetate-oxidizing syntrophs were a relatively small part of the culture, since they had a low specific affinity for acetate (as in variation 1). Nonetheless, they were extant within the culture, since (a) dechlorinators poised H_2 concentrations way below inhibiting levels, and (b) acetate-dependent methanogenesis was practically negligible. Methanogenesis was not a competitive acetate-utilizing metabolism, due to the remarkably low affinity of methanogens for acetate (Table 10.16). As discussed for variation 1, limited methane formation may be the outcome of the long-term exposure of methanogens to sulfides.

Table 10.14. Kinetic parameters for sulfate reducers deriving from the best-fit solution of the parameter estimation strategy employed for variation 2.

Substrate	Parameter	Symbol (units)	Value
Butyrate-utilizing sulfate reducers			
Butyrate, sulfate	Maximum specific growth rate	$\mu_{max,BSR}$ ($days^{-1}$)	1.58
Butyrate	Half-velocity coefficient	$K_{S,B\text{-}BSR}$ (μM)	296
Sulfate	Half-velocity coefficient	$K_{S,S\text{-}BSR}$ (μM)	75
Acetate-utilizing sulfate reducers			
Acetate, sulfate	Maximum specific growth rate	$\mu_{max,ASR}$ ($days^{-1}$)	0.35
Acetate	Half-velocity coefficient	$K_{S,A\text{-}ASR}$ (μM)	127
Sulfate	Half-velocity coefficient	$K_{S,S\text{-}ASR}$ (μM)	96

Table 10.15. Kinetic parameters for butyrate oxidizers and acetate oxidizers resulting from the best-fit solution of the parameter estimation strategy for variation 2.

Substrate	Parameter	Symbol (units)	Value
Butyrate oxidizers			
Butyrate	Maximum specific growth rate	$\mu_{max,BO}$ ($days^{-1}$)	0.60
Butyrate	Half-velocity coefficient	$K_{S,B\text{-}BO}$ (μM)	160
Acetate oxidizers			
Acetate	Maximum specific growth rate	$\mu_{max,AO}$ ($days^{-1}$)	0.26
Acetate	Half-velocity coefficient	$K_{S,A\text{-}AO}$ (μM)	854

Table 10.16. Kinetic parameters for acetate-utilizing methanogens resulting from the best-fit solution of the parameter estimation strategy for variation 2.

Substrate	Parameter	Symbol (units)	Value
Acetate-utilizing methanogens			
Acetate	Maximum specific growth rate	$\mu_{max,AM}$ ($days^{-1}$)	0.25
Acetate	Half-velocity coefficient	$K_{S,A\text{-}AM}$ (μM)	1928
Sulfide	Sulfide inhibition coefficient	$S_{INH,HS\text{-}AM}$ (μM)	845

Variation 2 simulated with fair accuracy the salient characteristics of the behavior of culture NTUA-S under low butyrate supply (Fig. 10.11). This modeling approach described adequately the fast consumption of TCE and cDCE within the first five days. It simulated sufficiently the

hindrance of VC consumption that was observed from day 5 to day 150 (Fig. 10.11a). Apart from dechlorination, simulated results reproduced (a) the pattern of sulfate reduction, i.e. the initial rapid removal of sulfate that was succeeded by a long period of a practically negligible sulfate reduction rate (Fig. 10.11b), (b) VFA concentrations (Fig. 10.11c), and (c) the negligible methane formation (methane concentrations were below 5 μM).

During the first five days, dechlorinators consumed all the available TCE and cDCE, and sulfate-reducers consumed 73% of the overall consumed sulfate. During this period, dechlorinators, in the absence of competing H_2-scavengers, consumed all the available H_2, that resulted mainly from butyrate oxidation and to a lesser degree from acetate oxidation. Despite the absence of competing H_2-scavengers, dechlorinators did not drive dechlorination to a higher degree, as a smaller quantity of butyrate served as an H_2 source directly; nearly 70% of butyrate was channeled to sulfate reduction (Fig. 10.12b). Fortunately for dechlorinators, the fast-growing butyrate-utilizing sulfate reducers were slowed down, apart from their lower affinity for butyrate, from the limited availability of sulfate; the consumed only 20% of sulfate. Thus, acetate-utilizing sulfate reducers were the most efficient metabolism during these first five days, consuming 65% of the available acetate (Fig. 10.12c) and 80% of the available sulfate (Fig. 10.12d). This high efficiency of acetate-utilizing sulfate reducers gave limited space for acetate-oxidizing syntrophs to thrive; they consumed 35% of the available acetate, which, however, compensated for the loss of H_2 that resulted from butyrate being channeled to sulfate reduction. Again, the activity of acetate oxidizers was critical for the extent of dechlorinators.

Following the first five days, dechlorination and sulfate reduction proceeded with the reducing power resulting from decaying biomass. Yet, these electron equivalents were not adequate to drive dechlorination towards completion. Likely, two factors contributed to dechlorination stall. First, part of the available butyrate and acetate that resulted from biomass disintegration was consumed by butyrate- and acetate-utilizing sulfate-reducers, respectively. Thus, the H_2-producing syntrophs failed to provide the requisite H_2 to dechlorinators. The second factor is the poor kinetic properties of dechlorinators on VC. As H_2 concentrations are increasing from day 25 to day 149, we can deduce that H_2 production is higher than H_2 consumption. Hence, dechlorinators would not have consumed VC significantly faster, even in the absence of sulfate reduction.

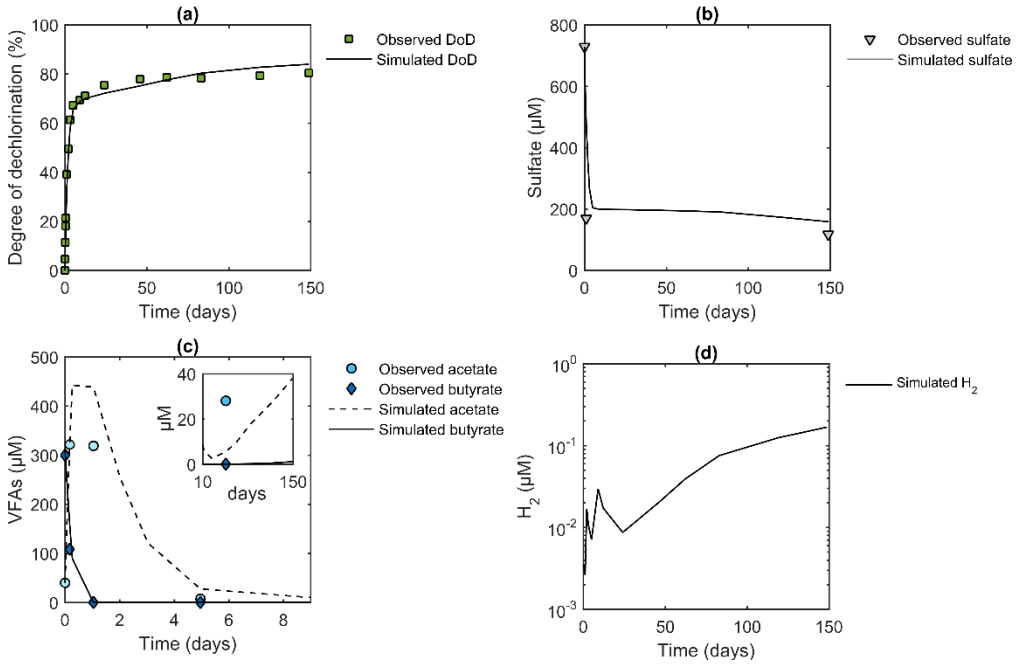

Fig. 10.11. Observed and simulated (a) degree of dechlorination, (b) sulfate concentration, (c) VFA concentrations, and (d) H_2 concentration for batch test LEDS-BS and variation 2. Methane concentrations are negligible (below 5 µM) and, hence, not shown.

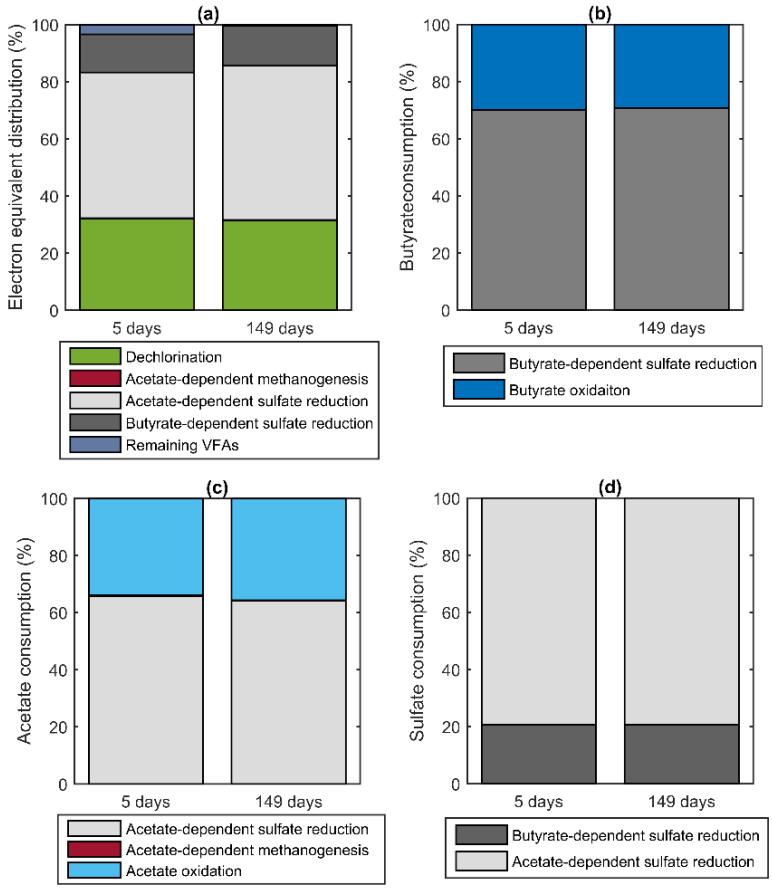

Fig. 10.12. Distribution of (a) electron equivalents, (b) consumed butyrate by butyrate oxidizers and butyrate-utilizing sulfate reducers, (c) consumed acetate by acetate-utilizing sulfate reducers, acetate-utilizing methanogens and acetate oxidizers, (d) reduced sulfate by acetate-utilizing and butyrate-utilizing sulfate reducers after five days and at the end of batch test LEDS-BS for variation 2.

Similar to variation 1, variation 2 failed to reproduce the collective behavior of culture NTUA-S under ample electron donor conditions. Although it correctly predicted that dechlorinators would slowly consume nearly all the available chloroethenes within 83 days (Fig. 10.13a) and it captured the fast reduction of sulfate (Fig. 10.13b), it failed to simulate butyrate depletion. Butyrate consumption stopped following its initial rapid decline because (a) butyrate-oxidizing syntrophs were thermodynamically inhibited from the high H_2 concentrations that prevailed (around 1.2 μM – results are available in Appendix A), and (b) butyrate-utilizing SRBs were inhibited by the absence of sulfate. Following sulfate removal, dechlorinators grew slowly on VC and, thus, consumed the available H_2 without any competition. Because of butyrate accumulation, acetate plateaued at lower concentrations than those observed in the laboratory and, hence, acetate-dependent methanogenesis was less extensive (Fig. 10.13d).

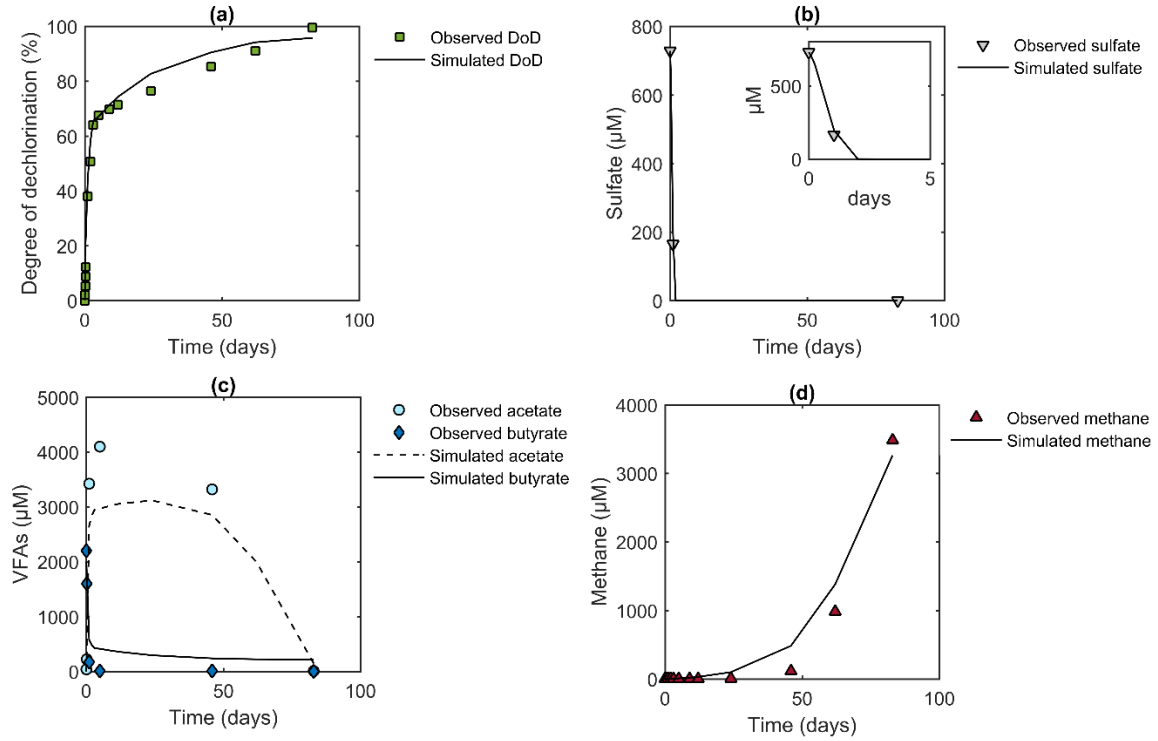

Fig. 10.13. Observed and simulated (a) degree of dechlorination, (b) sulfate concentration, (c) VFA concentrations, and (d) methane concentration for batch test HEDS-BS and variation 2.

Given the availability of butyrate as a readily available electron donor for sulfate-reduction, the fast-growing butyrate-utilizing sulfate reducers became the most competent sulfate scavengers of the culture consuming almost 65% of the available sulfate, i.e. 473 μM (Fig. 10.14d). This amount of sulfate requires 946 μM butyrate. Combined with the syntrophic butyrate oxidation, which is thermodynamically feasible during the first five days of the batch test, butyrate-scavengers removed most of the initially available butyrate. But, some of the initially supplied butyrate remained unused. Considering the stoichiometry of butyrate-dependent sulfate reduction (1 mol of butyrate reduces 0.5 mol of sulfate, Table 10.1), it is reasonable to deduce that butyrate could have been completely consumed only in the absence of acetate-dependent sulfate reduction. In such case, 730 μM sulfate would consume 1460 μM butyrate and 515 μM TCE would require 1545 μM H_2 or equivalently 772.5 μM butyrate. This assumption implies that in the presence of significant butyrate quantities, acetate-utilizing sulfate reducers would preferably use butyrate

directly as an electron donor, rather than grow on the acetate deriving from syntrophic butyrate oxidation. Again, this versatile behavior of sulfate reducers is probable for sulfate reducers belonging to the genus *Desulfosarcina*, *Desulfonema*, *Desulfococcus*, or *Desulfobacterium*, and *Desulfotomaculum* (Madigan et al., 2014; Rabus et al., 2013).

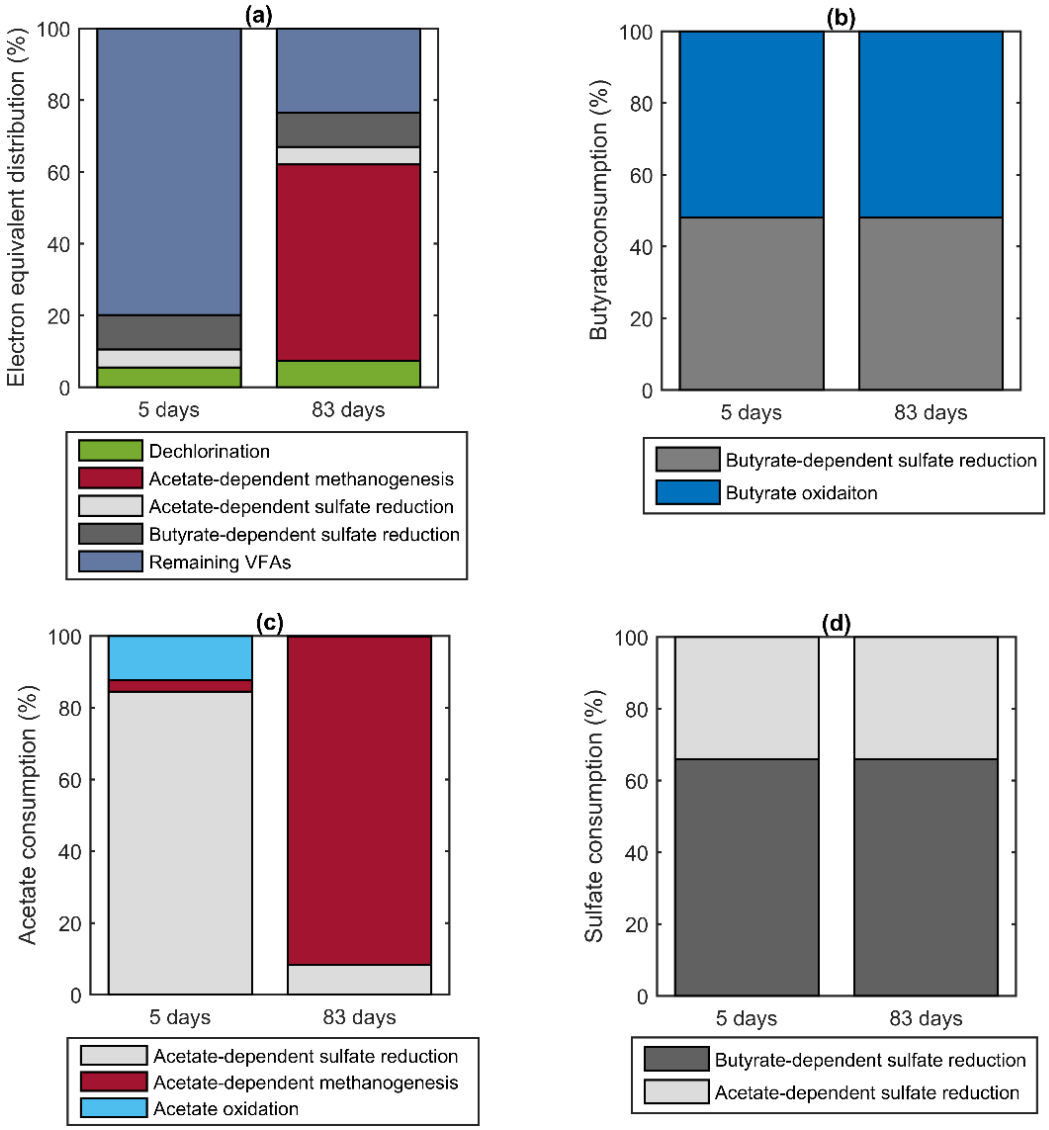

Fig. 10.14. Distribution of (a) electron equivalents, (b) consumed H_2 by dechlorinators and H_2-utilizing sulfate reducers, (c) consumed acetate by acetate-utilizing sulfate reducers, acetate-utilizing methanogens and acetate oxidizers and (d) reduced sulfate by acetate-utilizing and butyrate-utilizing sulfate reducers after five days and at the end of batch test HEDS-BS for variation 2.

Again, in the search of a better fit to the observations from the high-surplus test HEDS-BS, it was re-simulated assuming that butyrate-utilizing sulfate reducers were the only sulfate-reducing population with an initial biomass concentration equal to the sum of both sulfate-reducing species, i.e. $X_{BSR,0}$ = 6.9 mg VSS/l.

In the absence of acetate-utilizing sulfate reducers, model variation 2 simulated the observed behavior of culture NTUA-S adequately (Fig. 10.15). Sulfate-reducers consumed rapidly 95% of the available butyrate and 100% of sulfate within the first three days (Fig. 10.15c and 10.15b, respectively). Then, the remaining butyrate was slowly oxidized, as dechlorinators failed to poise

H_2 at low levels and, thus, to establish a favorable environment for butyrate-oxidizing syntrophs. These H_2 levels also cancelled the activity of acetate oxidizers. Even if they appear to be efficient in the first four days of the experiment (Fig. 10.16c), they consumed only 50 µM of acetate. Acetoclastic activity was almost completely inhibited at the beginning of the batch test. Acetate consumption commenced practically after day 25, when acetate-utilizing methanogens started to grow in numbers taking advantage of the available acetate, the absence of sulfate reduction and the thermodynamic limitations for acetate oxidation. Acetate became an important methanogenic substrate and, thus, eventually significant methane quantities were produced.

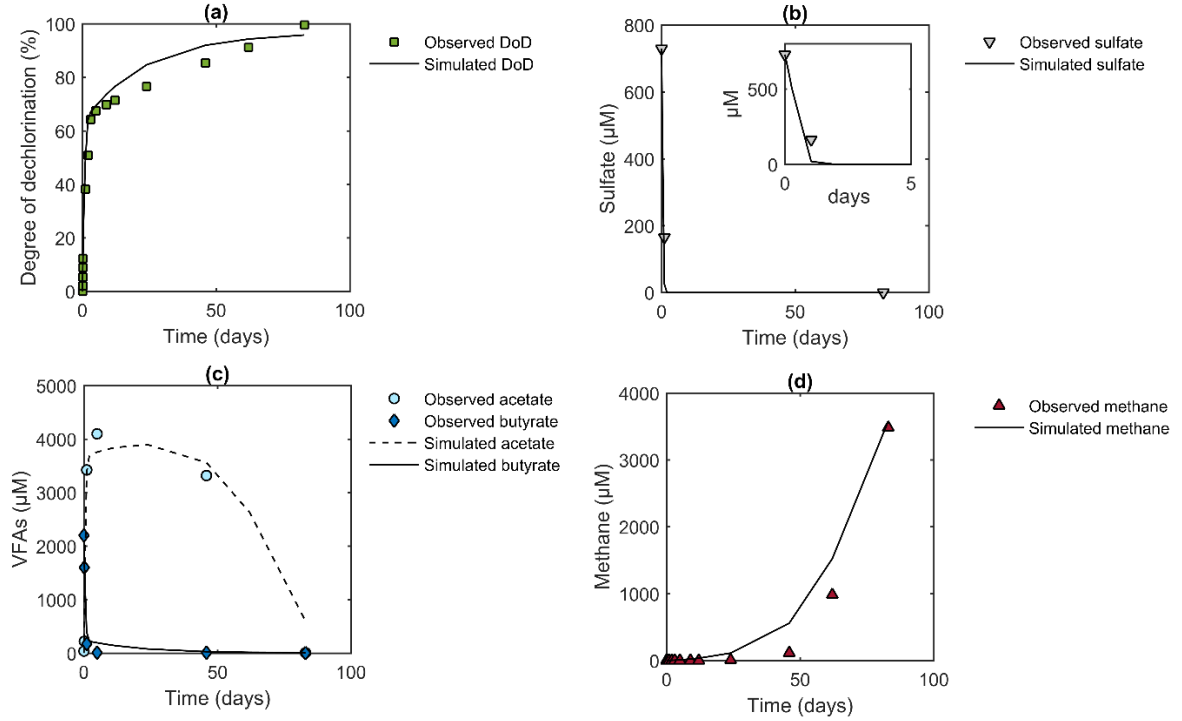

Fig. 10.15. Observed and simulated (a) degree of dechlorination, (b) sulfate concentration, (c) VFA concentrations, and (d) methane concentration for batch test HEDS-BS and variation 2 assuming that all sulfate reducers utilize butyrate as an electron donor.

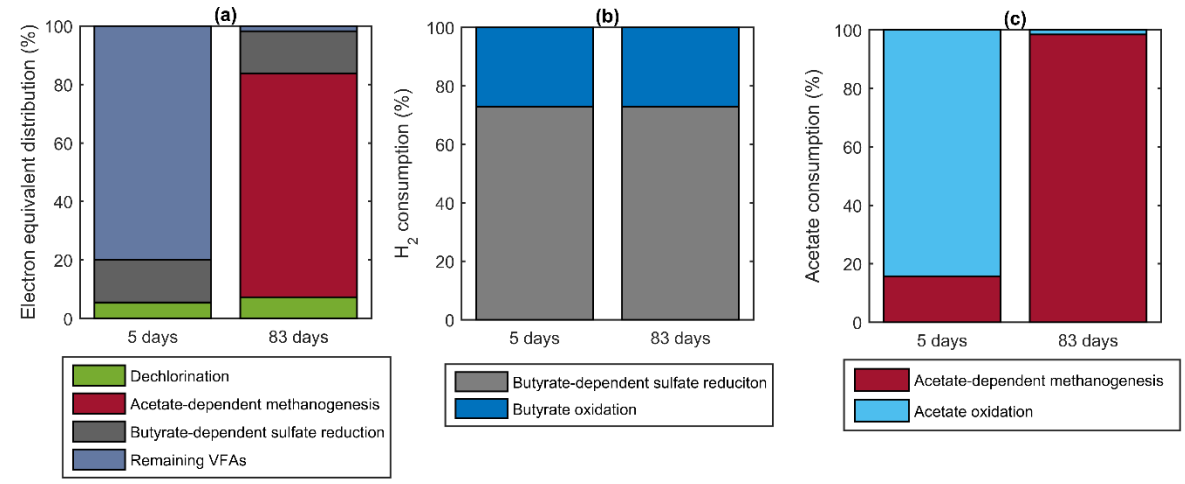

Fig. 10.16. Distribution of (a) electron equivalents, (b) consumed butyrate by butyrate oxidizers and butyrate-utilizing sulfate reducers, (c) consumed acetate by acetate-utilizing sulfate reducers, acetate-utilizing methanogens and acetate oxidizers after five days and at the end of batch test HEDS-BS for variation 2 assuming that all sulfate reducers utilize butyrate as an electron donor.

10.6 Concluding remarks

Two candidate approximations of culture NTUA-S were examined herein. Both could explain adequately the performance of culture NTUA-S under limiting electron donor conditions. In the light of the existing experimental observations, it is hard to deduce which of them is more likely to be true. As the profiles of H_2 concentrations were different in the two variations of NTUA-S (compare Fig. 10.4d with Fig. 10.11d), it seems that H_2 measurements could be useful to discriminate among the two candidate approximations of culture NTUA-S. Nevertheless, following an ample butyrate supply, the presence of butyrate-utilizing sulfate reducers is needed to capture the behavior of culture NTUA-S. Thereby, the approximation that contained a sulfate reducing community containing acetate- and butyrate-utilizing sulfate reducers is the most probable approximation of culture NTUA-S between the two examined herein.

The present modeling effort is the first to account for and indicate the relevance of acetate- and butyrate-dependent sulfate reduction in sulfate-reducing, chloroethene-degrading consortia. Even if H_2-utilizing sulfate reducers should be an obvious concern in sulfate-reducing, chloroethene-degrading communities, acetate- and butyrate-utilizing sulfate reducers can be also active and, thus, dictate the distribution of reducing power and affect dechlorination.

The metabolic versatility of sulfate reducers was accentuated by this modeling approach. A shift from acetate- towards butyrate-dependent sulfate reduction was needed to explain the behavior of the culture. This finding underscores that when VFAs are utilized as H_2 precursors for dechlorination, direct consumption of VFAs as electron donors for sulfate reduction can jeopardize biostimulation efforts. This pronounced metabolic flexibility of sulfate reducers adds complexity in the modeling efforts for sulfate reduction increasing the feasible descriptions of reality. This might seem an undermining for the development of models, but, on the other hand, it adds a possible explanation for the conflicting findings in the literature, while it guides the need for further examination of the functional structure of sulfate reducers in dechlorinating consortia.

The kinetic analysis performed for culture NTUA-S revealed that the presence of sulfate has affected the make-up of the dechlorinating community. In culture NTUA-S, dechlorinators were estimated with (a) increased affinity for H_2, and (b) decreased kinetic properties for VC consumption relative to the dechlorinators of the common-ancestry cultures NTUA-M1 and NTUA-M2. The increased affinity for H_2 explains why dechlorination of TCE and cDCE proceeded fast, regardless of the presence of sulfate, that acted as a competing electron accepting. On the other hand, the poor kinetic properties regarding VC consumption, explain the low VC consumption rates, even at an excessive electron donor surplus. It is likely that long-term exposure to sulfides has caused this difference between the dechlorinators prevailing in culture NTUA-S and the dechlorinators prevailing cultures NTUA-M1 and NTUA-M2. A similar finding has already been reported by Berggren et al. (2013), who postulated that when sulfate was introduced in a dechlorinating culture, a shift to the qualitative characteristics of the dechlorinating community occurred from a more efficient VC-degrader to a slower, commetabolic VC-degrader. The relevance of these changes in the dechlorinating population will be further assessed in Chapter 11.

Finally, the findings of this chapter exhibited the role of acetate-oxidizing syntrophs, especially at low electron donor surpluses. As in cultures NTUA-M1 and NTUA-M2, this typically neglected H_2-producing pathway was relevant under limiting electron donor conditions, i.e. conditions

usually encountered in contaminated subsurface environments. Acetate is seemingly an important source of H_2 and aside from the relative abundance of acetate-oxidizing syntrophs, their metabolic properties can be an important factor affecting dechlorination. The impact of the competitive fitness of acetate oxidizers on dechlorination in sulfate-reducing, chloroethene-degrading consortia will be examined in Chapter 11.

Chapter 11: Questioning the factors that impact reductive dechlorination in a methane-producing, sulfate-reducing, chloroethene-degrading culture

11.1 Introduction

Chapter 10 was an attempt to elucidate the functional composition of culture NTUA-S by investigating (a) the roles of dechlorinators and H_2-producing syntrophic populations and (b) the make-up of sulfate reducers. Model results indicated that, relative to the methanogenic, chloroethene-degrading cultures NTUA-M1 and NTUA-M2, culture NTUA-S has undergone (a) a decline in the kinetic properties of VC consumption, (b) an increase in the affinity of dechlorinators for H_2, that gave them the opportunity to thrive in a more competitive environment, and (c) an improvement in the ability of acetate oxidizers to grow on acetate and produce H_2, compensating, thus, for any loss of reducing equivalents towards the competing sulfate-reducing process. It is probable that the presence of sulfide led specific strains of dechlorinators to thrive within the culture and result in such different dechlorinating groups compared to cultures NTUA-M1 and NTUA-M2.

In the present Chapter, the alternate approximations of culture NTUA-S will be used in forward simulations to execute specific what-if scenarios that can highlight the relevance of such changes. This Chapter performs a targeted sensitivity analysis in search of microbial shifts that were influential in the outcome of dechlorination. To this end, this Chapter cancels the shift observed within culture NTUA-S and evaluates the outcome of dechlorination if (a) efficient VC-degraders were present, (b) dechlorinators had a lower affinity for H_2, and (c) acetate-oxidizing syntrophs were less efficient. Finally, a series of numerical experiments is performed examining how would the alternate approximations of culture NTUA-S behave under increased sulfate concentrations, which has been indicated by Malaguerra et al. (2011) as an important factor regarding the extent and the rate of dechlorination.

11.2 Alternate sulfate-reducing, dechlorinating consortia and electron donor supply scenarios

We will be working on the two batch tests performed with culture NTUA-S (Table 11.1), i.e. test LEDS-BS (limiting electron donor supply) and test HEDS-BS (non-limiting electron donor supply). The first test mimics the conditions typically encountered under the natural attenuation of chloroethenes in contaminated environments, as dechlorination and sulfate reduction were sustained for nearly 140 days with the reducing power resulting from biomass disintegration. The second test resembles the conditions anticipated following the stimulation of a dechlorinating consortium, i.e. a high initial butyrate injection that to aims rapidly deplete sulfate and, therefore, minimize competition between dechlorinators and sulfate reducers.

Table 11.1. Initial donor, TCE and sulfate concentrations for the batch performed with culture NTUA-S (experiment LEDS-BS, HEDS-BS).

Batch test	Butyrate (μM)	Acetate (μM)	TCE (μM)	Sulfate (μM)	Electron donor surplus[1]	Duration (days)
LEDS-BS	300	40.0	533	728	2.0	149
HEDS-BS	2200	40.0	516	728	14.3	83

[1]: Electron donor surplus is calculated assuming that 1 mol butyrate yields 20 e^- eq.

The two experiments will be re-simulated using the four approximations of culture NTUA-S that were tested against the true behavior of the culture in Chapter 10 (two per batch test). The relative abundances of the four alternate dechlorinating consortia are given in Figure 11.1. The major difference between these dechlorinating communities is the make-up of the sulfate-reducing consortium, which comprises nearly 40% of the overall biomass concentration. The H_2-utilizing sulfate reducers present in variations 1a and 1b are substituted by a population of butyrate-utilizing sulfate reducers in variations 2a and 2b, respectively. In all the variations considered, dechlorinators are dominant, H_2-producing syntrophs (i.e. butyrate oxidizers and acetate oxidizers) are present and comprise almost 20% of the culture, while acetate-utilizing methanogens are a minority population (less than 1% of the overall biomass). Even if approximation 1b ended up reproducing inadequately the behavior of culture NTUA-S under non-limiting electron donor conditions, it is interesting to examine it, as it is an exemplar case of how sulfate-reducing, chloroethene-degrading consortia are considered in the literature (e.g. Kouznetsova et al., 2010): a dense H_2-utilizing population of sulfate reducers competing with a comparably dense population of dechlorinators.

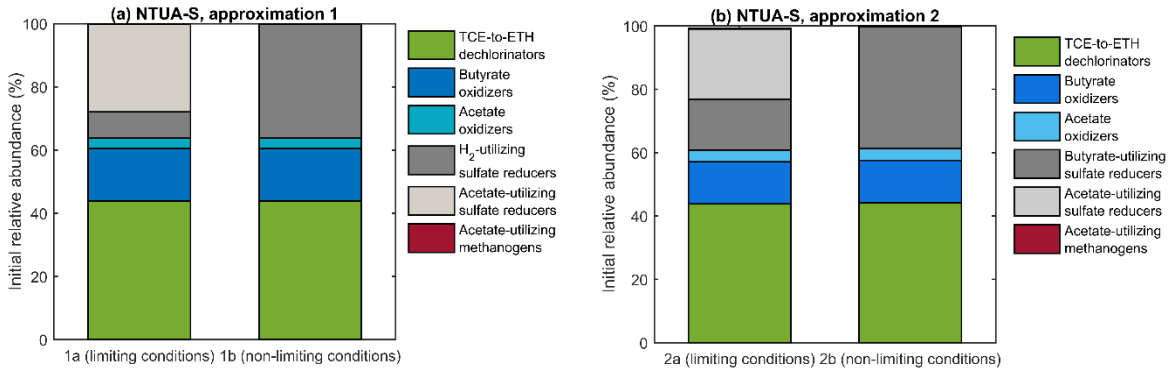

Fig. 11.1. Initial biomass distributions resulting for approximation 1 (overall biomass concentration equal to 18.0 mg VSS/l) and approximation 2 (overall biomass concentration equal to 17.8 mg VSS/l) of culture NTUA-S.

The kinetic properties of the microbial groups considered in each consortium are presented in Tables 11.2 to 11.5. Dechlorinators are characterized by their high specific affinity for TCE and cDCE, their high affinity for H_2 consumption and their poor kinetic properties regarding VC consumption. With respect to sulfate-reducers, they were all calculated as relatively fast-growing with a high affinity for sulfate. Regarding the H_2-producing microbial groups of the culture, both butyrate- and acetate-oxidizing syntrophs were calculated with the maximum allowable μ_{max} values, indicating that they are efficient H_2 producers given that they are not inhibited thermodynamically or by microbial competition. Finally, acetate-utilizing methanogens are characterized by their low

affinity for acetate and the significant inhibition by sulfides. As indicated by the low inhibition coefficient ($S_{INH,HS\text{-}AM}$=830-845 μM sulfide), sulfide concentrations in the range of 470 μM (typically the concentrations prevailing within culture NTUA-S) can cause a decrease of 64% to the μ_{max} of methanogens.

Table 11.2. Kinetic parameters for dechlorinators in the four alternate approximations of culture NTUA-S.

Substrate	Parameter	Symbol (units)	Value	
			Approximation 1 (a and b)	**Approximation 2 (a and b)**
TCE	Maximum specific growth rate	$\mu_{max,TCE\text{-}D1}$ ($days^{-1}$)	1.07	4.30
DCE	Maximum specific growth rate	$\mu_{max,cDCE\text{-}D1}$ ($days^{-1}$)	0.08	0.18
VC	Maximum specific growth rate	$\mu_{max,VC\text{-}D1}$ ($days^{-1}$)	0.01	0.01
TCE	Half-velocity coefficient	$K_{S,TCE\text{-}D1}$ (μM)	3.9	3.4
DCE	Half-velocity coefficient	$K_{S,cDCE\text{-}D1}$ (μM)	65.1	55.6
VC	Half-velocity coefficient	$K_{S,VC\text{-}D1}$ (μM)	507.4	568.0
VC	Inhibition coefficient	$K_{INH,cDCE}$ (μM)	2.0	4.7
H_2	Half-velocity coefficient	$K_{S,H\text{-}D1}$ (μM)	0.007	0.025
TCE, cDCE, VC	Growth yield	Y_{D1} x10^{-3} (mg VSS/μmol)	2.40	
-	Decay coefficient	b_{D1} ($days^{-1}$)	0.024	

Table 11.3. Kinetic parameters for sulfate reducers in the four alternate approximations of culture NTUA-S.

Substrate	Parameter	Symbol (units)	Value	
			Approximation 1 (a and b)	**Approximation 2 (a and b)**
Acetate-utilizing sulfate reducers				
Acetate, sulfate	Maximum specific growth rate	$\mu_{max,ASR}$ (days^{-1})	0.48	0.35
Acetate	Half-velocity coefficient	$K_{S,A\text{-}ASR}$ (μM)	163	127
Sulfate	Half-velocity coefficient	$K_{S,S\text{-}ASR}$ (μM)	83	96
Acetate	Growth yield	Y_{ASR} x10^{-3} (mg VSS/μmol)	4.30	
-	Decay coefficient	b_{ASR} (days^{-1})	0.03	
H_2-utilizing sulfate reducers				
H_2, sulfate	Maximum specific growth rate	$\mu_{max,HSR}$ (days^{-1})	4.5	-
H_2	Half-velocity coefficient	$K_{S,H\text{-}HSR}$ (μM)	1.2	-
Sulfate	Half-velocity coefficient	$K_{S,S\text{-}HSR}$ (μM)	37	-
H_2	Growth yield	Y_{HSR} x10^{-3} (mg VSS/μmol)	1.60	
-	Decay coefficient	b_{HSR} (days^{-1})	0.05	
Butyrate-utilizing sulfate reducers				
Butyrate, sulfate	Maximum specific growth rate	$\mu_{max,BSR}$ (days^{-1})	-	1.58
Butyrate	Half-velocity coefficient	$K_{S,B\text{-}BSR}$ (μM)	-	254
Sulfate	Half-velocity coefficient	$K_{S,S\text{-}BSR}$ (μM)	-	177
Butyrate	Growth yield	Y_{BSR} x10^{-3} (mg VSS/μmol)	4.75	
-	Decay coefficient	b_{BSR} (days^{-1})	0.03	

Table 11.4. Kinetic parameters for butyrate oxidizers and acetate oxidizers in the four alternate approximations of culture NTUA-S.

Substrate	Parameter	Symbol (units)	Value	
			Approximation 1 (a and b)	Approximation 2 (a and b)
Butyrate oxidizers				
Butyrate	Maximum specific growth rate	$\mu_{max,BO}$ (days^{-1})	0.60	0.60
Butyrate	Half-velocity coefficient	$K_{S,B\text{-}BO}$ (μM)	485	160
Butyrate	Growth yield	Y_{BO} x10^{-3} (mg VSS/μmol)	3.10	
-	Decay coefficient	b_{BO} (days^{-1})	0.024	
Acetate oxidizers				
Acetate	Maximum specific growth rate	$\mu_{max,AO}$ (days^{-1})	0.26	0.26
Acetate	Half-velocity coefficient	$K_{S,A\text{-}AO}$ (μM)	1094	854
Acetate	Growth yield	Y_{AO} x10^{-3} (mg VSS/μmol)	0.70	
-	Decay coefficient	b_{AO} (days^{-1})	0.024	

Table 11.5. Kinetic parameters for acetate-utilizing methanogens in the four alternate approximations of culture NTUA-S.

Substrate	Parameter	Symbol (units)	Value	
			Approximation 1 (a and b)	Approximation 2 (a and b)
Acetate-utilizing methanogens				
Acetate	Maximum specific growth rate	$\mu_{max,AM}$ (days^{-1})	0.20	0.25
Acetate	Half-velocity coefficient	$K_{S,A\text{-}AM}$ (μM)	936	1928
Sulfide	Sulfide inhibition coefficient	$S_{INH,HS\text{-}AM}$ (μM)	830	845
Acetate	Growth yield	Y_{AM} x10^{-3} (mg VSS/μmol)	1.40	
-	Decay coefficient	b_{AM} (days^{-1})	0.024	

11.3 The impact of VC-related parameters on dechlorination

Findings in Chapter 10 provided evidence that the extent of dechlorination was affected mainly by how effectively dechlorinators could grow on VC. In this section, the two experiments of culture NTUA-S will be re-simulated hypothesizing that dechlorinators grow on VC with the same properties as the dechlorinators thriving in culture NTUA-M2 (Table 11.6). The most salient change in the VC-related properties is the 18-fold increase in maximum specific growth rates. There is also a two-fold greater growth yield, a slightly higher affinity for VC, whereas cDCE is less inhibitory on VC consumption. Yet, these changes are less extensive compared to the change in maximum specific growth rates.

Table 11.6. Kinetic parameters of VC consumption for dechlorinators in the four approximations of culture NTUA-S (substituting parameters presented in Table 11.2).

Substrate	Parameter	Symbol (units)	Previous values (Table 11.2 values)				Current values (NTUA-M2 values)			
			1a	1b	2a	2b	1a	1b	2a	2b
VC	Maximum specific growth rate	$\mu_{max,VC\text{-}D1}$ (days^{-1})	0.01		0.01		0.18			
VC	Half-velocity coefficient	$K_{S,VC\text{-}D1}$ (μM)	507.4		568.0		466.87			
VC	Inhibition coefficient	$K_{INH,cDCE}$ (μM)	2.0		4.7		20.00			
VC	Growth yield	Y_{D1} x10^{-3} (mg VSS/μM)	2.40				4.96			

Under electron donor limiting conditions, the change in VC-related parameters influenced substantially the extent of dechlorination (Fig. 11.2a and 11.3a). In variation 1a, TCE was completely detoxified by day 120, as dechlorinators grew faster and consumed at a faster pace the available H_2 resulting from biomass disintegration. They outcompeted the H_2-utilizing sulfate reducers, who started to remove sulfate, following VC detoxification. In variation 2a, dechlorinators did not achieve the complete removal of chloroethenes, but reached a degree of dechlorination equal to 97% by day 149. In this culture, dechlorinators did not have to outcompete any H2-scavenging population, but they assisted acetate-oxidizing syntrophs to grow uninhibited by maintaining low H2 concentrations. Hence, acetate oxidizers were even more efficient acetate scavengers and competed efficiently with acetate-utilizing sulfate reducers.

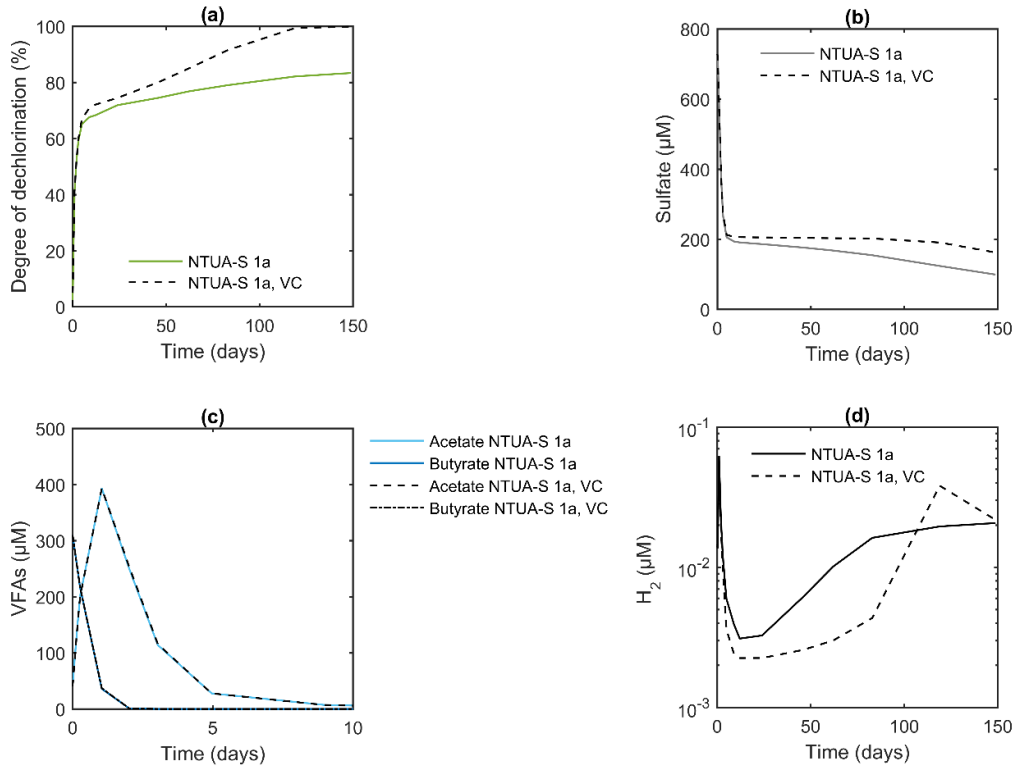

Fig. 11.2. Simulated (a) degree of dechlorination, (b) sulfate concentration, (c) VFA concentrations, and (d) H_2 concentration for batch test LEDS-BS and approximation 1a. The dashed lines correspond to simulations performed with the VC-related parameters estimated for TCE-to-ETH dechlorinators in culture NTUA-M2.

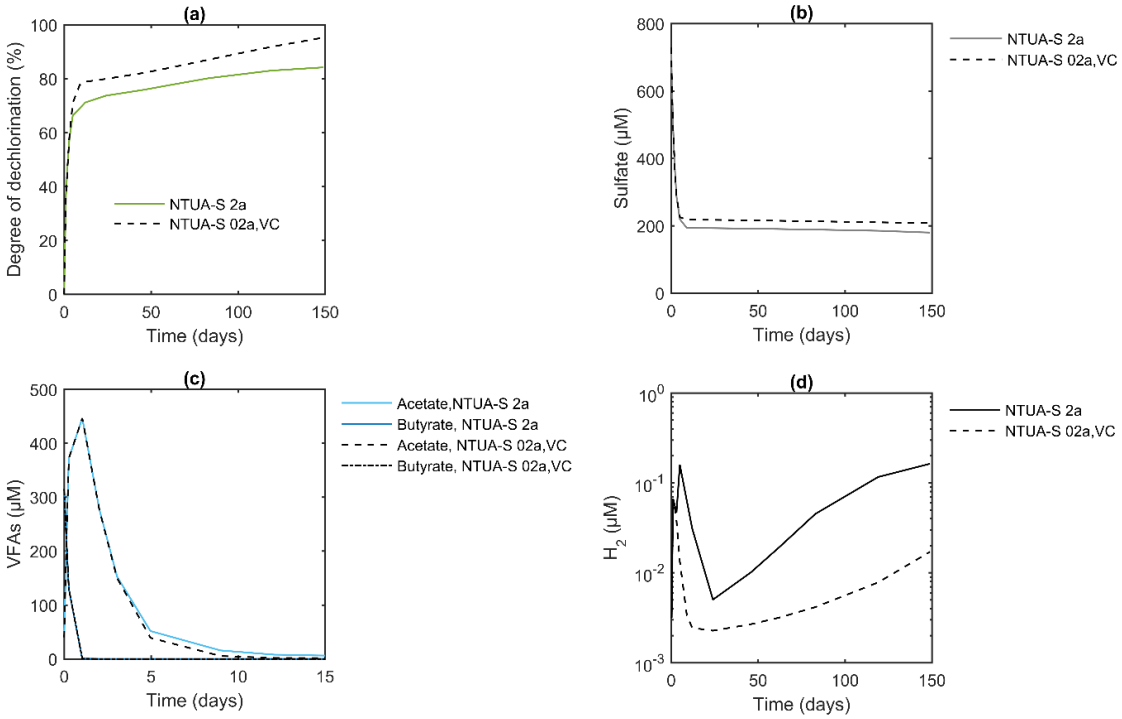

Fig. 11.3. Simulated (a) degree of dechlorination, (b) sulfate concentration, (c) VFA concentrations, and (d) H_2 concentration for batch test LEDS-BS and approximation 2a. The dashed lines correspond to simulations performed with the VC-related parameters estimated for TCE-to-ETH dechlorinators in culture NTUA-M2.

When tested under non-limiting electron donor conditions, the effect of VC-related parameters on dechlorination extent was significant (Fig. 11.4a and 11.5a). Regardless of the make-up of the sulfate-reducing community, dechlorinators removed all the available chloroethenes within 10 days. The timespan required for complete detoxification of TCE is comparable with the observed chloroethene elimination times in culture NTUA-M2 under non-limiting electron donor conditions. Hence, these simulations provide evidence that corroborate the hypothesis claiming that the observed VC-stall in culture NTUA-S results from the drastic differences exhibited in the kinetic properties of dechlorinators rather than competition for reducing power.

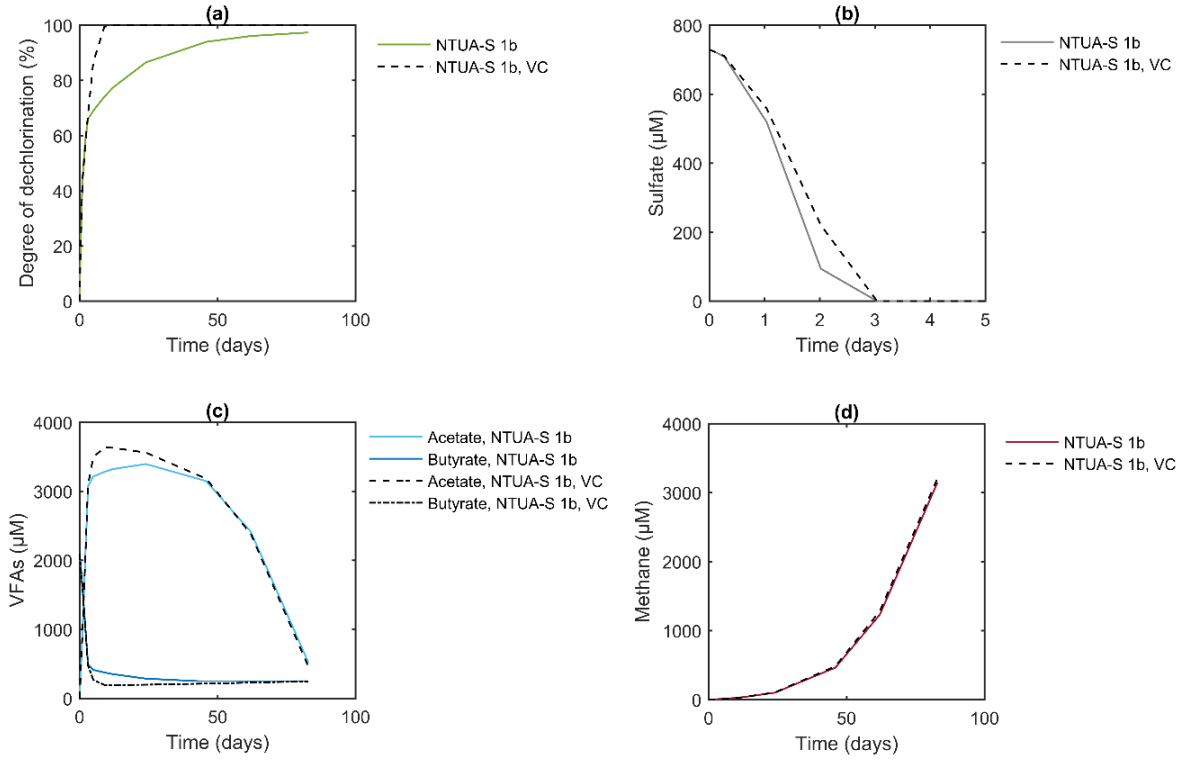

Fig. 11.4. Simulated (a) degree of dechlorination, (b) sulfate concentration, (c) VFA concentrations, and (d) H_2 concentration for batch test HEDS-BS and approximation 1b. The dashed lines correspond to simulations performed with the VC-related estimated for TCE-to-ETH dechlorinators in culture NTUA-M2.

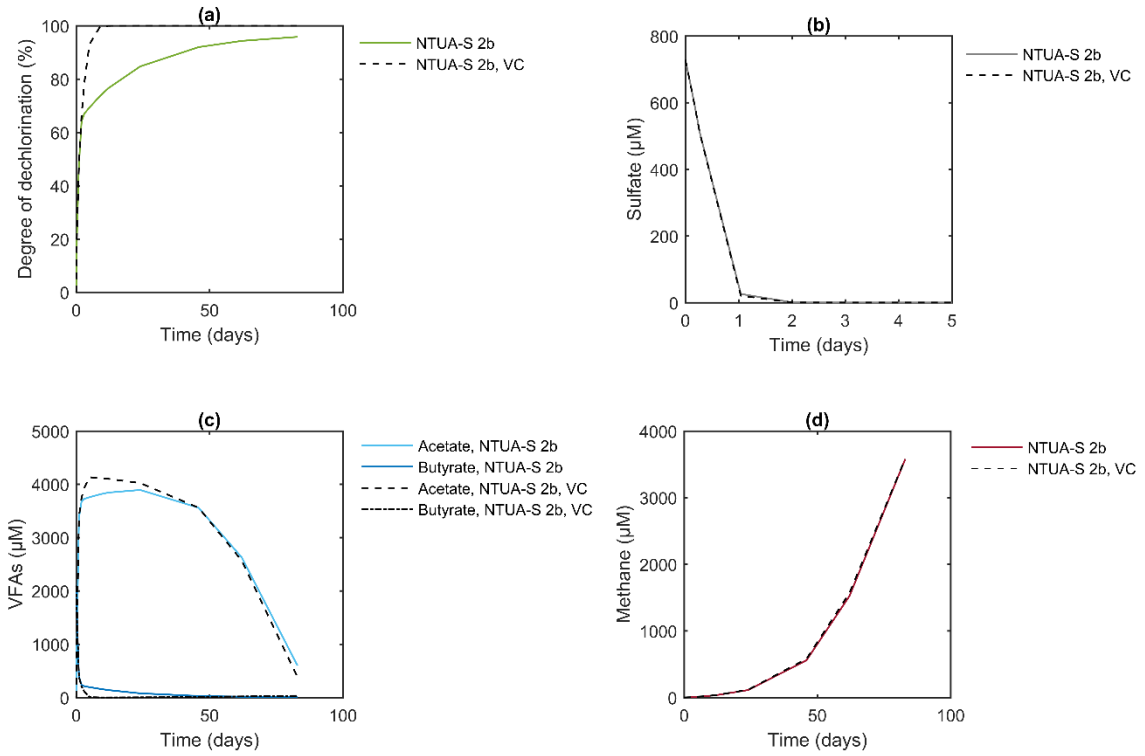

Fig. 11.5. Simulated (a) degree of dechlorination, (b) sulfate concentration, (c) VFA concentrations, and (d) H_2 concentration for batch test HEDS-BS and approximation 2b. The dashed lines correspond to simulations performed with VC-related parameters estimated for TCE-to-ETH dechlorinators in culture NTUA-M2.

11.4 The impact of the affinity for H_2 of dechlorinators on dechlorination

Consumption rates of TCE and cDCE in culture NTUA-S were comparable with consumption rates observed in culture NTUA-M2. This is why, during their long-term monitoring, the observed dechlorination daughter-products on a weekly basis were only slightly different. In Chapter 10 the ability of dechlorinators to remove TCE and cDCE rapidly was attributed to their high affinity for H_2, probably reflecting the prevalence of different dechlorinating strains between cultures NTUA-S and NTUA-M2.

In this section, the higher affinity for H_2 will be offset and simulations will assess how different would the outcome of dechlorination be, if dechlorinators demonstrated affinity for H_2 like the one estimated for culture NTUA-M2. Hence, the two tests with the four alternate approximations of culture NTUA-S will be re-performed, using the $K_{S,H\text{-}D1}$ value estimated for dechlorinators in culture NTUA-M2 (0.079 μM – see Table 11.7), which is a 11-fold increase for approximation 1 and a 3-fold increase for approximation 2.

Table 11.7. Kinetic parameters of VC consumption for dechlorinators in the four approximations of culture NTUA-S.

Substrate	Parameter	Symbol (units)	Previous values (Table 11.2 values)				Current values (NTUA-M2 values)			
			1a	1b	2a	2b	1a	1b	2a	2b
H_2	Half-velocity coefficient	$K_{S,H\text{-}D1}$ (μM)	0.007		0.025		0.079			

Under limiting electron donor conditions, the decreased affinity for H_2 affected significantly approximation 1a (Fig. 11.6a). In this case, dechlorinators were outcompeted by H_2-utilizing sulfate reducers from the early stages of dechlorination. As a result, cDCE was never completely removed, even after 149 days. H_2 was mainly channeled to sulfate reduction, which was nearly complete by day 149. On the other hand, the shift in the affinity for H_2, influenced to a smaller degree the consumption of VC for approximation 2a (Fig. 11.7a). In the absence of competing H_2-scavengers, the relevance of the affinity for H_2 became less important. In this approximation, the lower $K_{S,H\text{-}D1}$ values allowed H_2 concentrations to become higher and, thus, the thermodynamic driving force for butyrate and acetate oxidation to become weaker.

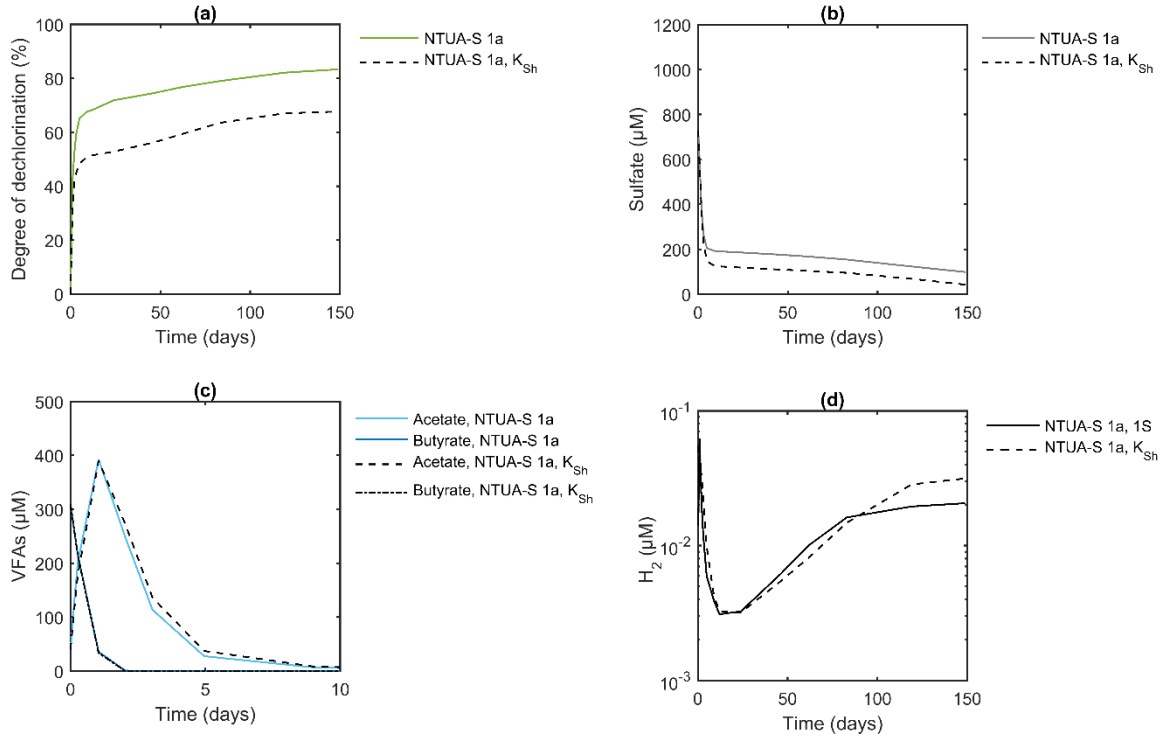

Fig. 11.6. Simulated (a) degree of dechlorination, (b) sulfate concentration, (c) VFA concentrations, and (d) H_2 concentration for batch test LEDS-BS and approximation 1a. The dashed lines correspond to simulations performed with the $K_{S,H\text{-}D1}$ values estimated for TCE-to-ETH dechlorinators in culture NTUA-M2.

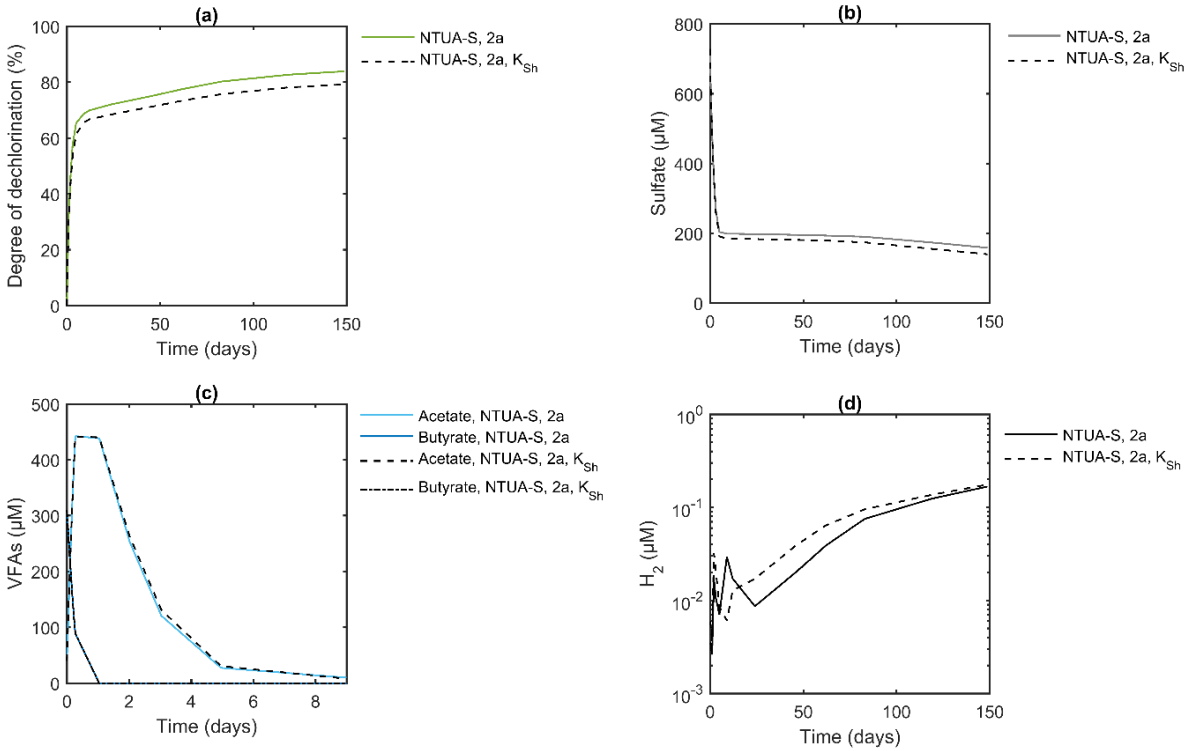

Fig. 11.7. Simulated (a) degree of dechlorination, (b) sulfate concentration, (c) VFA concentrations, and (d) H_2 concentration for batch test LEDS-BS and approximation 2a. The dashed lines correspond to simulations performed with the $K_{S,H\text{-}D1}$ values estimated for TCE-to-ETH dechlorinators in culture NTUA-M2.

Following a high initial butyrate supply, the influence of the affinity of dechlorinators for H_2 in dechlorination extent and rates was minor (Fig. 11.8a and 11.9a). Eventually, chloroethenes were almost completely removed within 89 days, regardless of $K_{S,H\text{-}D1}$ values. Given the high surplus of H_2 sources available and the quick depletion of sulfate (Fig. 11.8b and 11.9b), dechlorination of VC proceeded without any competing electron-accepting process for both approximations. Hence, under a typical bio-stimulation effort in a sulfate-reducing, chloroethene-degrading community, the affinity of dechlorinators becomes H_2 becomes insignificant, as chloroethenes were the limiting factor for VC removal.

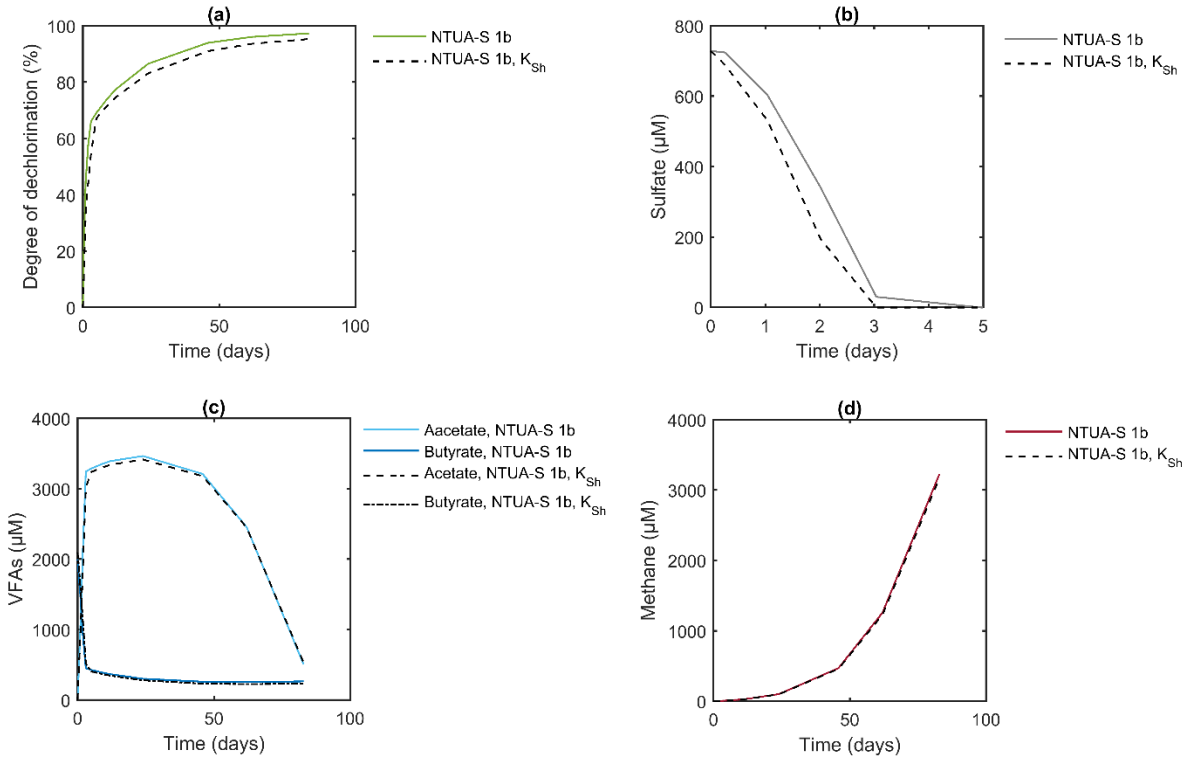

Fig. 11.8. Simulated (a) degree of dechlorination, (b) sulfate concentration, (c) VFA concentrations, and (d) H_2 concentration for batch test HEDS-BS and approximation 1b. The dashed lines correspond to simulations performed with the $K_{S,H\text{-}D1}$ values estimated for TCE-to-ETH dechlorinators in culture NTUA-M2.

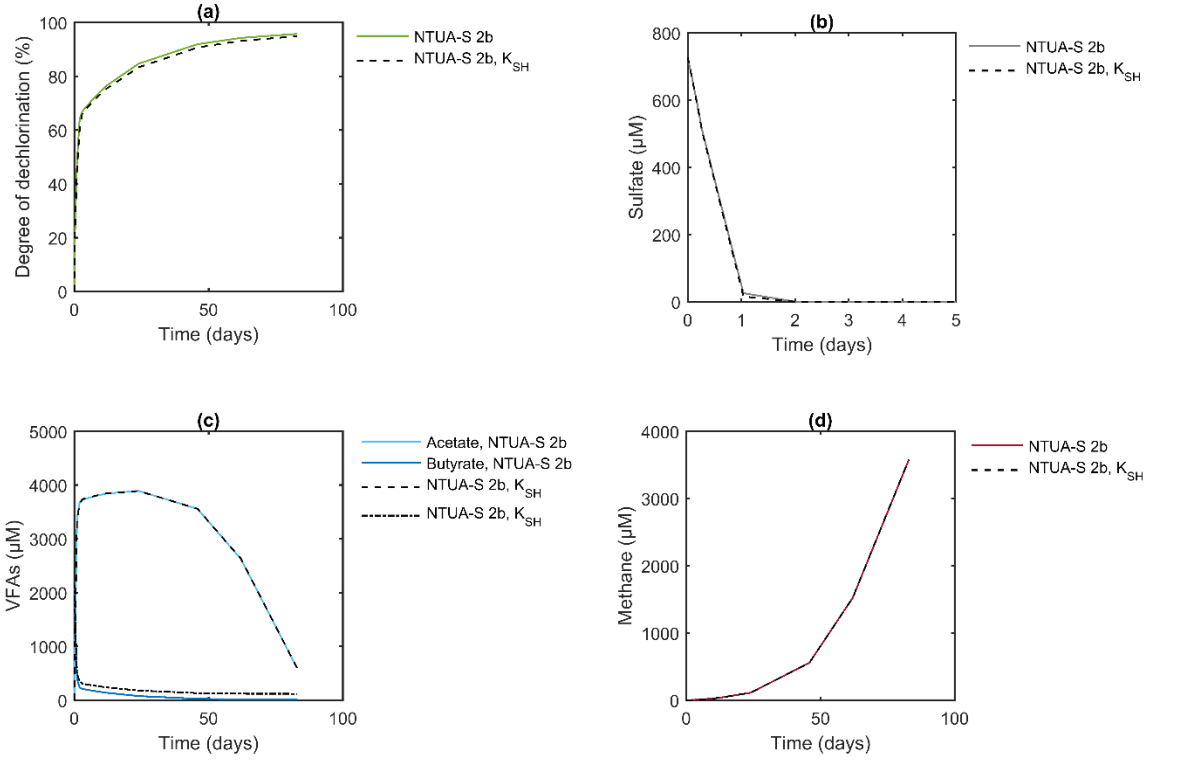

Fig. 11.9. Simulated (a) degree of dechlorination, (b) sulfate concentration, (c) VFA concentrations, and (d) H_2 concentration for batch test HEDS-BS and approximation 2b. The dashed lines correspond to simulations performed with $K_{S,H\text{-}D1}$ values parameters estimated for TCE-to-ETH dechlorinators in culture NTUA-M2.

11.5 The impact of the performance of acetate-oxidizing syntrophs on dechlorination

In many instances of the previous analyses, the relevance of acetate-oxidizing syntrophs in the extent and the rate of dechlorination was highlighted. Particularly, regardless of the variation of culture NTUA-S, the presence of acetate-oxidizing syntrophs was needed to explain the collective behavior of the culture. Therefore, in this section, we will review how the four alternate approximations of culture NTUA-S would have behaved, if acetate oxidizers were less efficient acetate scavengers. The two batch tests with the four alternate approximations of culture NTUA-S will be re-simulated, assuming that acetate oxidizers grow with a lower maximum specific growth rate and demonstrate a lower affinity for acetate. Specifically, acetate oxidizers will have the kinetic properties estimated in culture NTUA-M2 (see Table 11.8), i.e. $\mu_{max,AO}$ =0.17 days^{-1} (instead of 0.26 days^{-1} in NTUA-S approximations) and $K_{S,A\text{-}AO}$ = 1304 μM (instead of 1094 μM and 854 μM for NTUA-S variation 1 and 2, respectively).

Under limiting butyrate supply, the impact of acetate oxidation was significant, especially for variation 2a (Fig. 11.10 and 11.11a). In variation 1a, acetate oxidizers with their modified kinetic properties, consumed 2.5% of the overall available acetate, instead of 24% that they had consumed with their previous properties. This loss of acetate resulted in a diminished production of H_2 and, therefore, dechlorination was not extensive. Nonetheless, this loss of H_2, that resulted from the change in the consumption pattern of acetate, was compensated to a small degree by the fact that sulfate reduction became almost entirely acetate-dependent. Hence, dechlorinators had to outcompete a less efficient H_2-utilizing sulfate-reducing population. Thus, dechlorinators consumed a smaller quantity of H_2, but more efficiently. In variation 2a, the change of the kinetic properties of acetate oxidizers had a consequential impact on dechlorination. The significant loss of acetate was not compensated by any other rearrangement of reducing equivalents within the culture. Limited acetate oxidation was coupled with a severe loss of reducing power and dechlorinators failed to completely remove cDCE.

Table 11.8. Kinetic parameters of VC consumption for dechlorinators in the four approximations of culture NTUA-S.

Substrate	Parameter	Symbol (units)	Previous values (Table 11.4)				Current values (NTUA-M2)			
			1a	1b	2a	2b	1a	1b	2a	2b
Acetate	Maximum specific growth rate	$\mu_{max,AO}$ (days^{-1})	0.26		0.26		0.17		0.17	
Acetate	Half-velocity coefficient	$K_{S,A\text{-}AO}$ (μM)	1094		854		1304		1304	

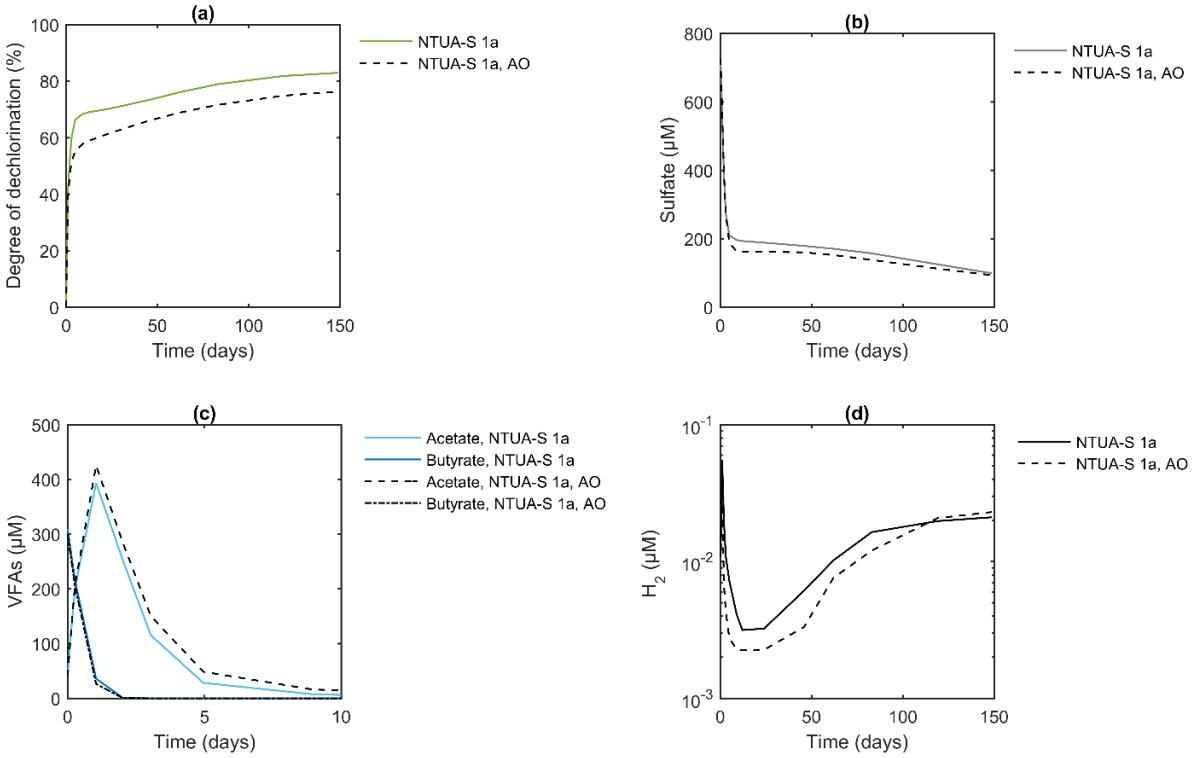

Fig. 11.10. Simulated (a) degree of dechlorination, (b) sulfate concentration, (c) VFA concentrations, and (d) H_2 concentration for batch test LEDS-BS and approximation 1a. The dashed lines correspond to simulations performed with the acetate-oxidizing syntrophs estimated for culture NTUA-M2.

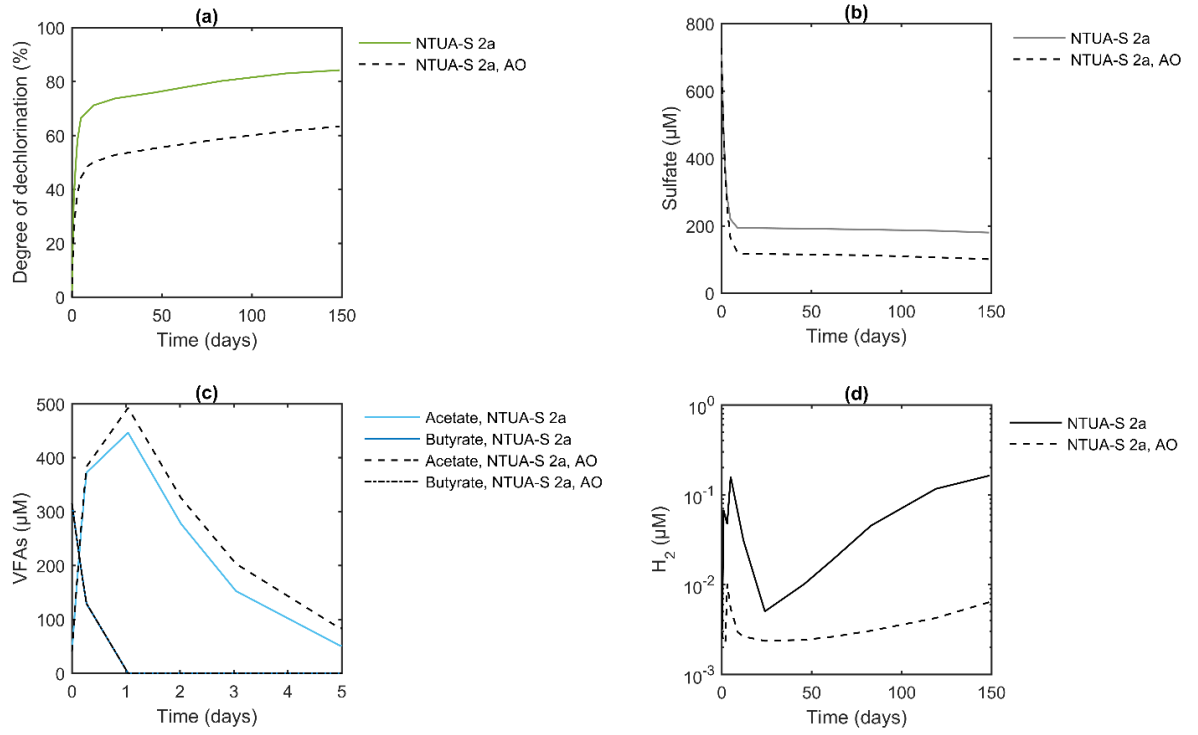

Fig. 11.11. Simulated (a) degree of dechlorination, (b) sulfate concentration, (c) VFA concentrations, and (d) H_2 concentration for batch test LEDS-BS and variation 2a. The dashed lines correspond to simulations performed with the acetate-oxidizing syntrophs estimated for culture NTUA-M2.

In the simulations performed with excessive butyrate supply, the change in acetate oxidation did not change the outcome of dechlorination (Fig. 11.12a and 11.13a). In both variations, butyrate was the main H_2-producing substrate and acetate functioned mainly as a methanogenic substrate. As in the methanogenic culture NTUA-M2, it is evident that when excessive electron donor is supplied, acetate oxidation is irrelevant. Therefore, acetate oxidation should be anticipated mainly in conditions when H_2 is the limiting factor.

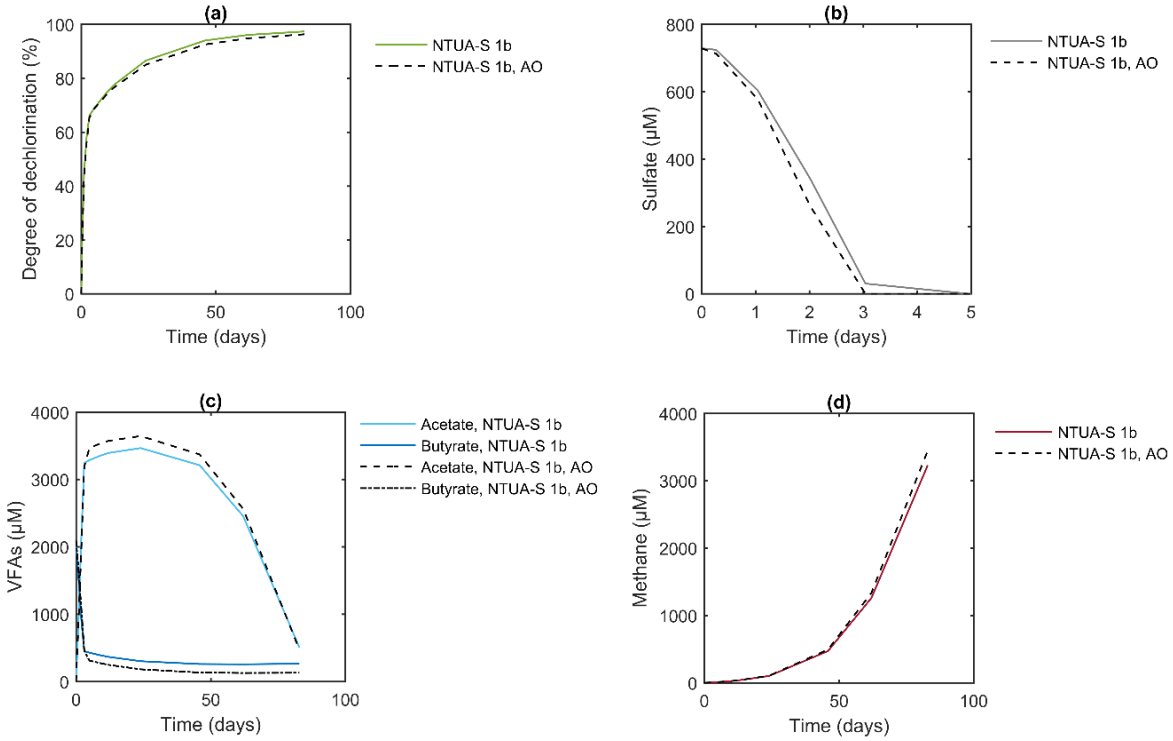

Fig. 11.12. Simulated (a) degree of dechlorination, (b) sulfate concentration, (c) VFA concentrations, and (d) H_2 concentration for batch test HEDS-BS and approximation 1b. The dashed lines correspond to simulations performed with the acetate-oxidizing syntrophs estimated for culture NTUA-M2.

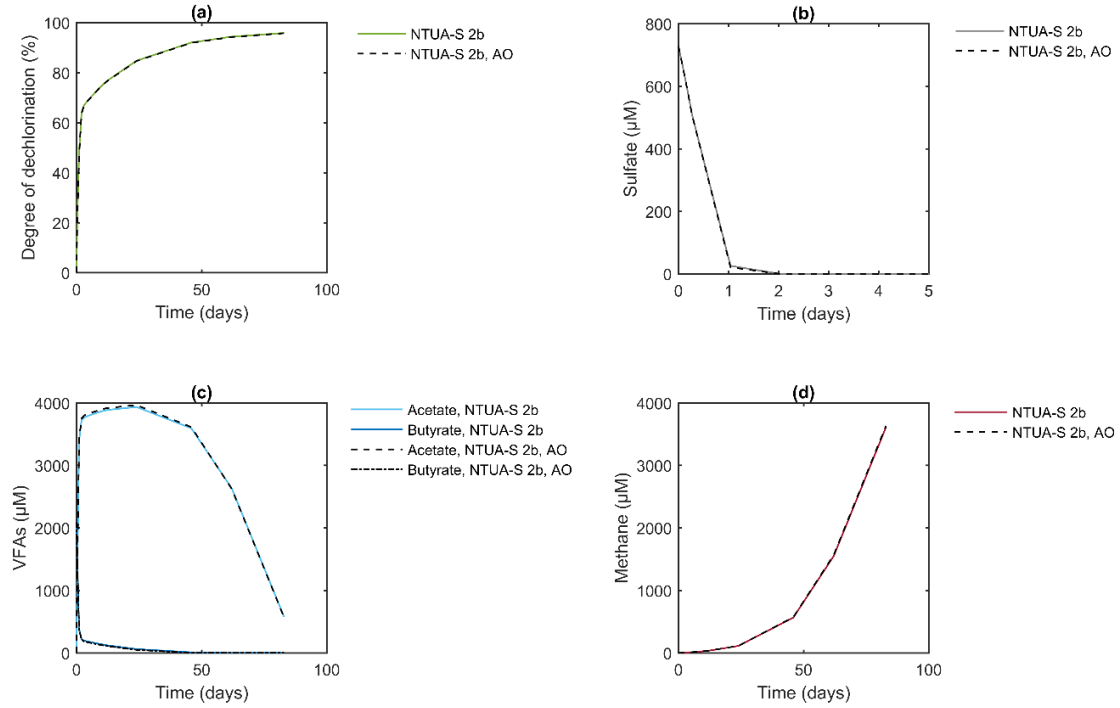

Fig. 11.13. Simulated (a) degree of dechlorination, (b) sulfate concentration, (c) VFA concentrations, and (d) H_2 concentration for batch test HEDS-BS and approximation 2b. The dashed lines correspond to simulations performed with the acetate-oxidizing syntrophs estimated for culture NTUA-M2.

11.6 The impact of sulfate concentration on dechlorination

In this series of numerical experiments, the impact of initial sulfate concentrations on the extent of dechlorination will be assessed. To this end, the two batch tests performed with culture NTUA-S will be re-simulated using higher initial sulfate concentrations. For the low-surplus LEDS-BS and variations 1a and 2a, a 50% higher sulfate concentration ($S_{S,0}$ =1092 μM) was introduced, creating, thus, a higher demand for reducing power; the complete reduction of sulfate and TCE would necessitate almost 600 μM butyrate, instead of the 300 μM offered. For high-donor HEDS-BS and variations 1b and 2b, a 6.9-fold greater initial sulfate concentration was added ($S_{S,0}$ =5000 μM), reaching the limits of the available reducing power resulting from 2200 μM butyrate; the complete reduction of 5000 μM sulfate and 515 μM TCE require 43,090 μe^- eq., i.e. 2155 μM butyrate.

Under electron donor limiting conditions, the effect of sulfate concentration was practically negligible to the extent of dechlorination (Fig. 11.14a and 11.15a). The increase in sulfate concentrations favored slightly the sulfate-reducing communities. In both variations, sulfate reducers following the supply of 1092 μM reduced only 5-6% more sulfate compared to the supply with 728 μM sulfate. They were not limited by sulfate availability, but by the availability of the electron donor (H_2, acetate or butyrate). Under these starvation conditions (H_2 concentrations following day 5 were in the range of 3 to 30 nM), dechlorinators, due to their high affinity for H_2, were limited largely from their poor kinetic properties on VC.

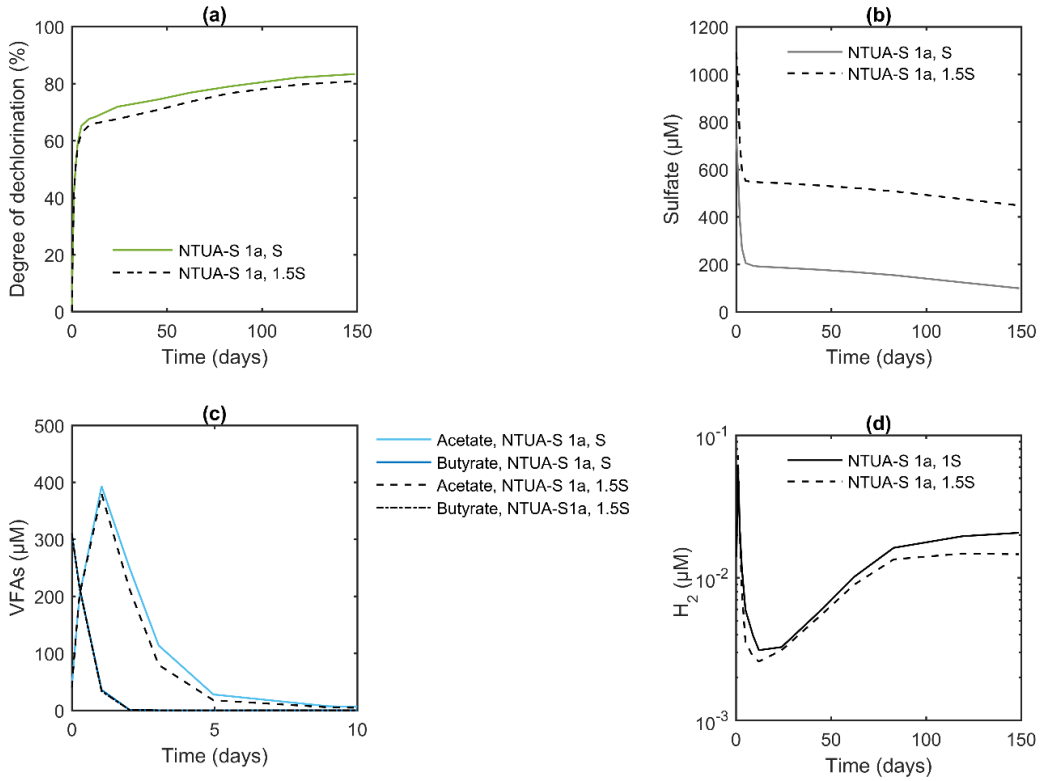

Fig. 11.14. Simulated (a) degree of dechlorination, (b) sulfate concentration, (c) VFA concentrations, and (d) H_2 concentration for batch test LEDS-BS and approximation 1a for an initial sulfate concentration of 728 μM (S) and 1092 μM (1.5S).

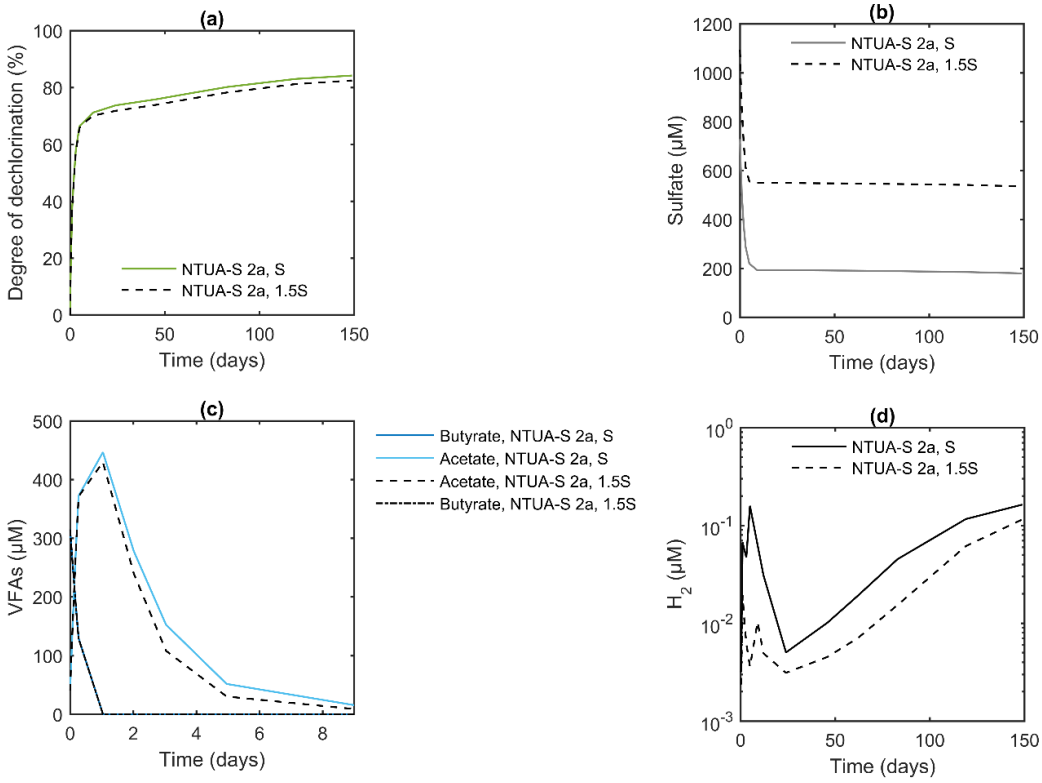

Fig. 11.15. Simulated (a) degree of dechlorination, (b) sulfate concentration, (c) VFA concentrations, and (d) H_2 concentration for batch test LEDS-BS and approximation 2a for an initial sulfate concentration of 728 μM (S) and 1092 μM (1.5S).

Under ample electron donor conditions, the effect of sulfate concentration to the extent of dechlorination in approximation 1b was again trivial (Fig. 11.16a). The significant sulfate and butyrate concentrations allowed sulfate reducers (only H_2-utilizing sulfate reducers are available) to grow rapidly and deplete sulfate within 25 days. The performance of the fast-growing H_2-utilizing sulfate reducers, poised H_2 concentrations low (below 300 nM). Therefore, butyrate and acetate oxidation remained far from their thermodynamic equilibria during the first 25 days and, hence, all the reducing power of butyrate was available to dechlorinators, apart from sulfate reducers. As acetate functioned as a secondary source of H_2, dechlorinators were unaffected by the loss of electrons to sulfate reduction. Acetate oxidation was feasible for one more reason. The excessive sulfides produced inhibited methane formation completely. Hence, in the absence of competing acetate scavengers, acetate oxidizes produced the requisite H_2 for dechlorination. Following day 25, H_2 concentrations were poised at 400 nM, causing acetate to accumulate. Thus, at these H_2 concentrations, dechlorinators are not limited by the availability for H_2, but by their growth rate and the low affinity for VC.

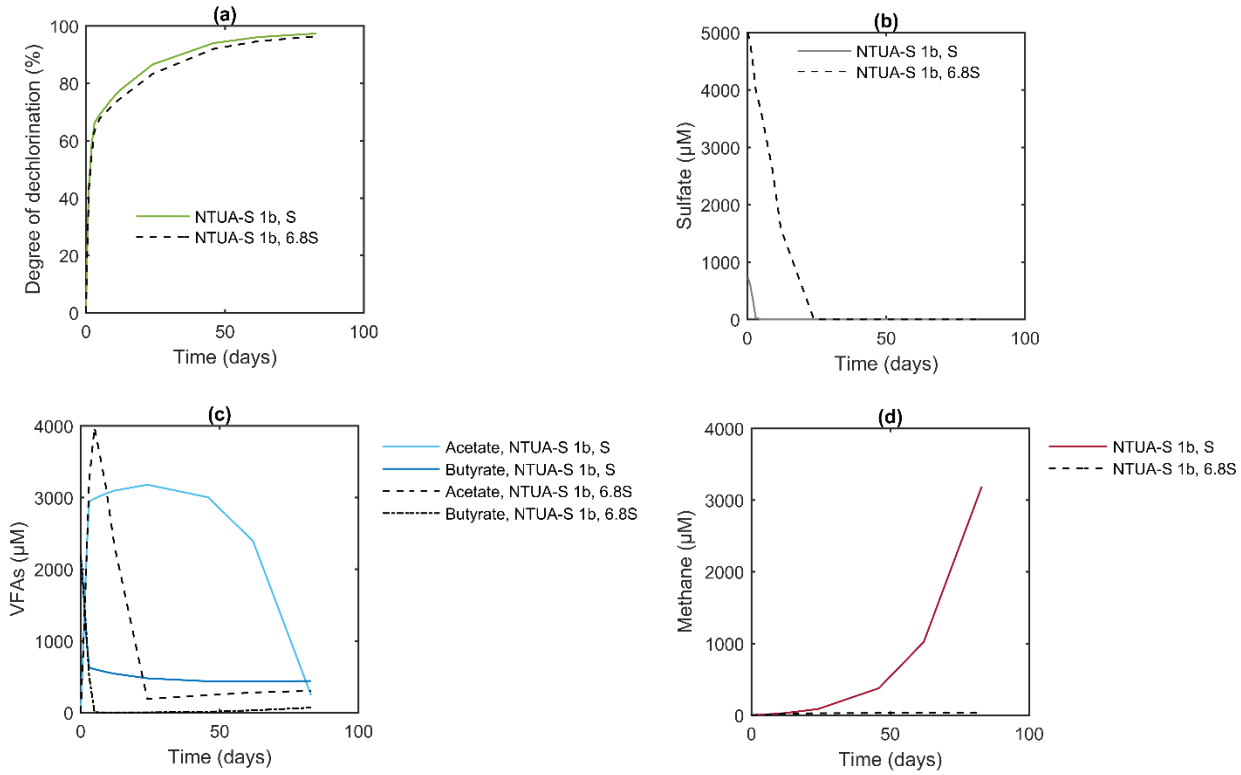

Fig. 11.16. Simulated (a) degree of dechlorination, (b) sulfate concentration, (c) VFA concentrations, and (d) H_2 concentration for batch test HEDS-BS and approximation 1b for an initial sulfate concentration of 728 μM (S) and 5000 μM (6.8S).

In approximation 2a and under non-limiting electron donor conditions, the effect of sulfate concentration to the extent of dechlorination was imperceptible (Fig. 11.17a). The butyrate-utilizing sulfate reducers (they are the only sulfate reducers extant in this variation) consumed 90% of the available butyrate and reduced 1000 μM sulfate. The remaining butyrate was oxidized at the first 5 days, when dechlorinators managed to maintain H_2 concentrations at the range of 200-300 nM. Following these first days, acetate oxidizers were the only H_2-producing population. The H_2 high concentrations that prevailed within the culture was in the range of 400 nM and

thermodynamically inhibited acetate oxidizers. But, their thermodynamic disadvantage was partially compensated by the presence of sulfides, which inhibited their competitors, i.e. acetate-utilizing methanogens. Once again, it was not H_2 limitation that stalled VC consumption.

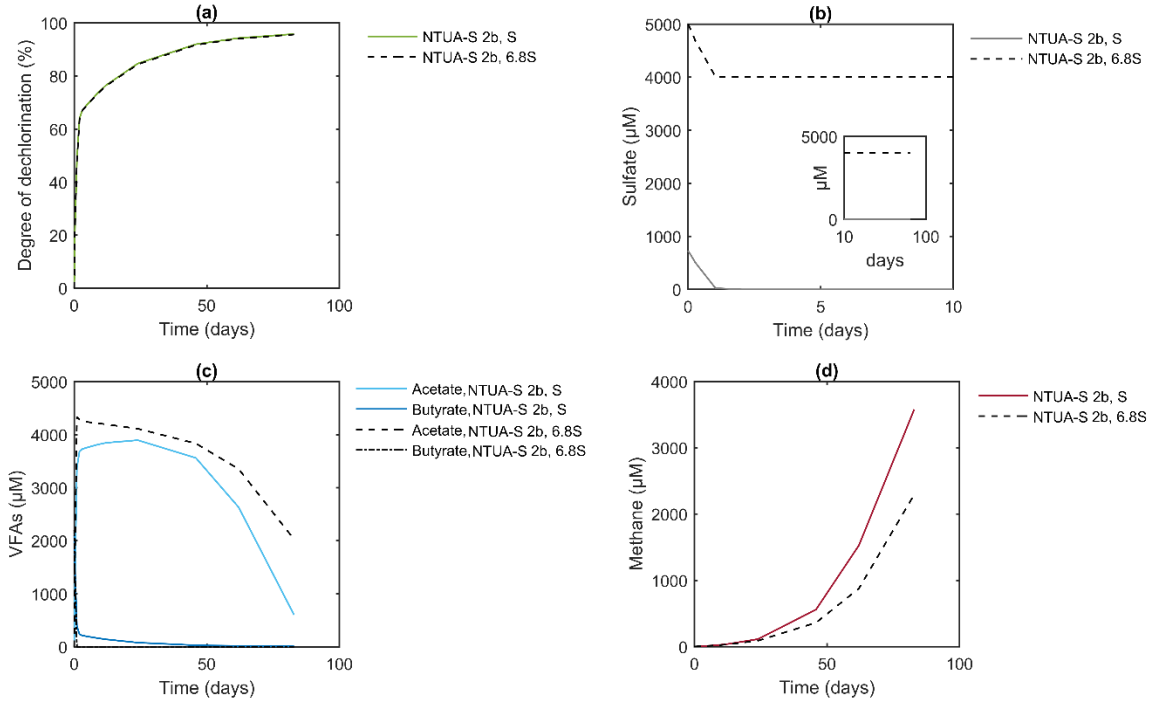

Fig. 11.17. Simulated (a) degree of dechlorination, (b) sulfate concentration, (c) VFA concentrations, and (d) H_2 concentration for batch test HEDS-BS and approximation 2b for an initial sulfate concentration of 728 μM (S) and 5000 μM (6.8S).

Even if the mechanism of inhibition of dechlorinators in sulfate-reducing conditions is unclear, for the high sulfate concentrations tested in the last two simulations, it is highly probable that the produced sulfides may have affected dechlorinators, apart from methanogens. As Mao et al. (2017) reported, for *Dehalococcoides mccartyi* strain 195 the cell yield Y_{D1} decreased by 65% when sulfides reached a concentration of 5000 μM. Therefore, we re-simulated the last two tests, considering that sulfides may further repress the activity of dechlorinators. To this end, we introduced a non-competitive inhibition term, similar to the one used for acetate-utilizing methanogens:

$$I_{HS-D1} = \frac{1}{1+\frac{S_{HS}}{S_{INH,HS-D1}}} \tag{11.1}$$

in which S_{HS} is the concentration of sulfides (μM) and $S_{INH,HS-D1}$ is the sulfide inhibition factor for dechlorinators. In our simulations, $S_{INH,HS-D1}$ =9000 μM, so that when sulfides reach 5000 μM, the inhibition term would be equal to 0.65, as indicated by the work of Mao et al. (2017).

Sulfide inhibition was noticeable only for the case of H_2-dependent sulfate reduction (Fig. 11.18a). In that case, excessive sulfide concentrations reduced the extent of dechlorination by 7% (compare the two cases with 5000 μM initial sulfate concentrations). When butyrate-dependent sulfate reduction is considered (Fig. 11.18b), the impact of sulfide was trivial. The incomplete reduction of sulfate produced sulfides at non-inhibitory levels. Hence, the pathway of sulfate reduction is relevant, as it dictates the levels of the ultimately produced sulfides.

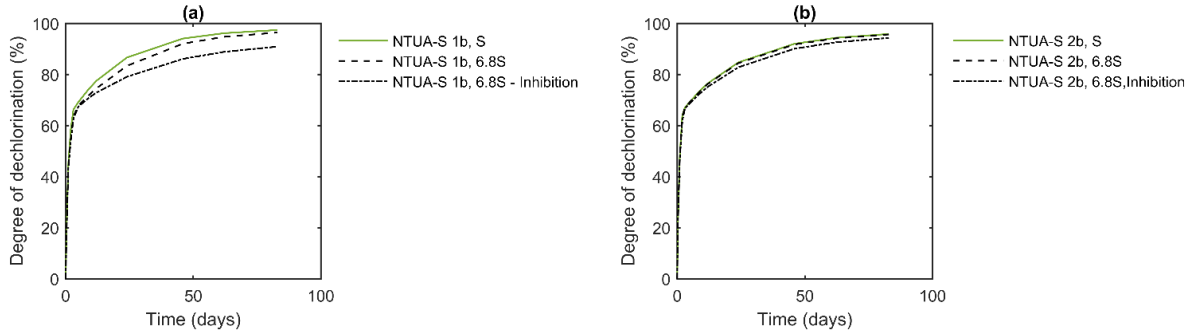

Fig. 11.18. Simulated degree of dechlorination for batch test HEDS-BS performed with a 6.8-fold higher sulfate concentration for (a) approximation 1b and (b) approximation 2b, with or without considering sulfide inhibition for dechlorinators.

Considering the above, initial sulfate concentrations were not critical in culture NTUA-S for the outcome of dechlorination, unless excess sulfide (>5000μM) is produced. This finding contradicts the sensitivity analysis performed by Malaguerra et al. (2011), who postulated that initial sulfate concentrations are the most prominent parameter of such systems. Regardless of the make-up of the sulfate-reducing community or the initial dosage of butyrate, eventually dechlorination stalled due to the poor performance characteristics of dechlorinators.

11.7 Concluding remarks

Dechlorination extent and rate in culture NTUA-S were dictated by VC-related parameters regardless of the electron donor supply or the composition of sulfate reducers. This finding supplements the work of Kouznetsova et al. (2010) who also highlighted the relevance of VC-related parameters, based solely on simulation findings. Considering that the long-term exposure of dechlorinators to sulfides (even at low concentrations) had seemingly favored specific dechlorinating strains that grow slowly on VC, more inhibition studies are required to shed light onto which *Dehalococcoides mccartyi* strains are more tolerant to the present of sulfides.

The affinity of dechlorinators for H_2 is relevant only when dechlorination proceeds under limiting electron donor conditions. Under such conditions, dechlorinators that have high affinity for H_2 (such as *Dehalococcoides mccartyi* strains belonging to the Victoria subgroup of strains) can (a) compete effectively with the relatively the fast-growing H_2-utilizing sulfate reducers, if the latter are present, and (b) maintain H_2 concentrations at levels below the thermodynamic equilibrium for butyrate and acetate oxidation and, thus, exploit most of the available reducing power. Yet, following biostimulation, the affinity for H_2 becomes irrelevant.

Simulations performed with high butyrate supply justify the typical field approaches, which involve excessive supply of electron donor sources in order to deplete sulfate swiftly and allow dechlorinators to grow without competition afterwards. Model simulations performed herein indicated that in such cases it is important (a) to elucidate the main pathway of sulfate reduction, and (b) to examine any possible repression of the dechlorinating performance due to excessive sulfide production. If sulfide inhibition is probable, then the presence of sulfate reducers that degrade organic compounds (such as butyrate) incompletely to acetate is preferable, as lower sulfide concentrations will be produced.

Like in the methanogenic, chloroethene-degrading consortia NTUA-M1 and NTUA-M2, simulations highlighted that competition for acetate should not be neglected under limiting electron donor conditions. In order to capture the collective behavior of cultures, it is important to illuminate any possible synergies established between acetate oxidizers and H_2-scavenging populations and shed light onto the pathway that sulfate is reduced, as acetate-dependent sulfate reduction can deprive significant quantities of acetate from syntrophic populations.

The what-if scenarios executed with culture NTUA-S demonstrated that chloroethene-degrading cultures that undergo natural dechlorination under sulfate-reducing conditions are complex ecosystems, in which synergies among microbial groups do not allow for their simplification without omitting important microbial processes. Yet, following biostimulation, the outcome of dechlorination is mainly affected by the kinetic properties of dechlorinators, indicating that even simple models can approximate dechlorination adequately.

Chapter 12: Contribution and recommendations

This final chapter presents the main findings of the thesis. They are accompanied by examples from and references to previous Chapters, but, by design, they do not follow strictly the structure of the thesis. Finally, specific aspects of the problem that require further study are recommended, as underscored by the modeling approach employed.

12.1 Main findings

The main findings are presented in two sections. The first section describes the main findings deriving from the methodological issues addressed during parameter estimation efforts. The second section discusses the findings related to understanding dechlorination in mixed cultures.

12.1.1 Methodological issues on parameter estimation

Parameter estimation was performed with a heuristic approach that entailed a series of decisions aiming to reduce the dimensions of the parameter space and identify models of the mixed dechlorinating consortia that can be trusted. The main findings from these decisions are discussed herein.

The judicious constraint of model parameters reduced the complexity of the parameter estimation problem. Following an exhaustive literature review on the kinetic parameters of the problem, parameters typically measured in the laboratory (i.e. growth yields, decay coefficients, substrate thresholds) were fixed to specific values. On the other hand, parameters typically resulting from curve-fitting processes were found to vary significantly in the literature and, hence, were considered less reliable. Therefore, they were treated as constrained adjustable parameters.

Parameter estimation avoided entrapment in regions of erroneous solutions with the application of a multistart parameter estimation strategy. This is the first effort employing a multistart strategy for the estimation of kinetic parameters in Monod-type models simulating dechlorination in mixed microbial communities. The multistart strategy was repeatedly tested with models of varying complexity and data sets obtained from distinctive cultures. Multistart application not only found acceptable models of the examined cultures, but highlighted that even in simple kinetic models (specifically, in Chapter 5 and culture PM), multiple behavior models can explain experimental observations, questioning the confidence in the estimated solutions.

The application of the multistart strategy facilitated the identification of distinct-yet-equivalent models for the behavior of a culture. Through a stepwise application of the multistart algorithm (Chapter 7), smaller neighborhoods of the model space were investigated thoroughly in search of different behavior models that offer plausible approximations of the composition and metabolic behavior of the mixed culture. This heuristic approach provided confidence that significant processes that underlie experimental observations were not omitted and provided candidate solutions that were subsequently tested in a cross-confirmation mode against experimental data other than those used for calibration.

A trustworthy model of the methane-producing, dechlorinating culture was identified with a cross-confirmation technique developed in Chapter 7. The identified plausible models of the culture

were used in a forward fashion under random initial conditions to simulate the performance of the culture under (a) different electron donor amendment scenarios and (b) diverse phases of the culture. Models that failed to pass the cross-confirmation test were rejected.

Confidence in the models describing the sulfate-reducing, methane-producing, dechlorinating culture was built by simultaneously fitting them to observations obtained under diverse electron donor supply scenarios. Experimental observations corresponded to the same steady state of the culture and allowed for the simultaneous curve-fitting process employed. Ultimately, this approach constrained the output of each behavior model tested providing trustworthy solutions. Due to the large computational effort of this approach, the cross-confirmation approach followed in Chapter 7 was found superior in terms of efficiency.

The indisputable problem of non-uniqueness of solutions was used as an opportunity in this thesis. It posed an opportunity to explore the levels of complexity entailed in dechlorinating consortia and, thereby, to enhance process understanding, thus offering plausible explanations for confusing field and laboratory evidence.

12.1.2 Dechlorination understanding

Methane-producing, chloroethene-degrading cultures

By focusing on the non-dechlorinating part of the cultures, this work revealed that moderate variations in the composition and the metabolic properties of non-dechlorinating species can induce sizeable differences in the behavior of dechlorinators following biostimulation. Therefore, efficient enhanced dechlorination requires not only analysis for the abundance of key microorganisms in mixed cultures, but also elucidation of their metabolic properties. The findings of this work underscore the necessity to consider the collective activities of mixed cultures, rather than focusing solely on the activity of dechlorinators. Re-examining empirical observations from this viewpoint offers plausible explanations for behaviors that appeared as conflicting, when attempting to explain them on the basis of the characteristics of dechlorinators.

The type of inquiry followed for methane-producing, chloroethene-degrading cultures frames the consensus of stimulating dechlorinators at low H_2 concentrations to cultures where efficient H_2-utilizing methanogens are present. In cultures where acetate-dependent methane formation is dominant, higher H_2 fluxes would be the optimal strategy for accelerating chloroethene removal.

This is the first modeling attempt that considers the competition for acetate in a dechlorinating consortium and assesses the relevance of acetate as an H_2 source. Under limiting electron donor conditions, i.e. conditions anticipated in pristine environments undergoing natural dechlorination, acetate-oxidizing syntrophs were shown to be competent acetate scavengers and mediated the use of H_2 for dechlorinators, thus mitigating the negative impact of H_2-scavenging competitors. Therefore, models intended to describe adequately natural dechlorination should consider competition for acetate.

Model application corroborated experimental findings postulating that mixed dechlorinating communities accommodate multiple populations being able to perform the same functions within the community. Thus, robustness in the performance of dechlorination may conceal functional differences in the underlying populations of dechlorinators (especially those mediating the first steps of dechlorination), which when tested under distinctive conditions may respond differently

than expected. The same applies for methanogens. Dynamic populations of methanogens can develop along with dechlorinators constituting a seemingly stable methanogenic consortium. But, what appears as a stable methanogenic community may harbor populations with distinctive functional properties, the relevance of which was highlighted in this thesis.

Sulfate-reducing, methane-producing, chloroethene-degrading cultures

This work is the first to indicate the relevance of sulfate-reducing pathways using electron donors besides H_2 in mixed dechlorinating communities. The relevance of this finding is two-fold. First, it underscores the need to examine competition for H_2 precursors and not exclusively direct competition for H_2. None of the existing modeling efforts considers such fields of microbial competition. Second, sulfate-reducing pathways dictate the levels of produced sulfides, that can inhibit microbial activity; sulfate reduction that uses complex organic substrates as electron donors results in lower sulfide levels and, thus, lesser inhibitory environments for dechlorinators.

Model simulations confirmed the metabolic flexibility of sulfate reducers that has been observed in non-dechlorinating cultures. Under limiting electron donor conditions acetate-dependent sulfate reduction was dominant, while under non-limiting conditions butyrate-dependent sulfate reduction was the only active sulfate-reducing pathway. Hence, models describing sulfate reduction in problems of natural attenuation of chloroethenes may be conceptually inadequate to simulate problems of enhanced dechlorination.

Model results strengthened the trust in electron donor supply strategies followed when dechlorination occurs under sulfate-reducing conditions. The addition of excessive supply of electron donor sources is preferable in order to exploit the relatively fast-growing sulfate reducers, remove sulfate swiftly and allow dechlorinators to perform the later and typically slower dechlorination steps without competition. Simplified models describing solely dechlorination kinetics can become reasonable approximations of the behavior of the culture, as dechlorination performance is dictated by the physiological properties of dechlorinators.

Model results indicate that sulfides do not inhibit *Dehalococcoides mccartyi* strains in a consistent manner. Preferential inhibition of sulfides to specific *Dehalococcoides mccartyi* strains is, however, consistent with the conflicting reports regarding the impact of sulfate reduction on dechlorination. According to model simulations, the long-term exposure to sulfides lead to the prevalence of *Dehalococcoides mccartyi* strains with kinetic properties similar to *Dehalococcoides mccartyi* strain 195, which removes VC in slow rates. The prevalence of *Dehalococcoides mccartyi* strains that grow slowly on VC is a probable explanation of the observed VC stall in the field, where dechlorinators have been exposed for a sizeable amount of time to sulfides.

The complexity of food webs established in dechlorinating communities may seemingly be a hindrance for kinetic modeling efforts. This work, however, supports the usefulness of kinetic modeling, which is three-fold: (a) to integrate complex simultaneous phenomena into a common framework, (b) to question hypotheses and existing biases, and (c) either strengthen what has been established through empirical observations or reveal significant questions to be considered.

12.2 Recommendation for future research

This work provided valuable insight into the relevance of non-dechlorinators under methanogenic conditions and described a specific need. It is relevant to systematically investigate the specific activities of methanogens and H_2-producing syntrophs in enrichment cultures and field settings and search for trends between the distribution of reducing power, the relative abundance of mixed cultures and dechlorinating performance. Currently, such investigations revealed patterns regarding biochemical interactions (e.g. the provision of corrinoids) besides the distribution of reducing power, which is typically overlooked. The findings of the thesis, point out that classical phylogenetic analyses are inadequate to reveal the functional structure of methanogens. Yet, the increasing accuracy of metagenomic sequencing methods can shed light on the ecology of mixed chloroethene-degrading communities.

Regarding the relevance of sulfate in mixed dechlorinating consortia, the need to move down to the enzyme level of dechlorination has been revealed. A more mechanistic understanding of inhibition induced by sulfides is needed.

From a modeling perspective, priority for improved modeling results is the shift towards biomarker-based models that can accurately capture population-specific activities. Models must move from aggregate measures of dechlorinating activity (expressed in mg VSS or cell counts) to gene copies that actually capture population-specific activities.

References

Abrahamsson, K., Ekdahl, A., Collen, J., & Pedersen, M. (1995). Marine algae-a source of trichloroethylene and perchloroethylene. *Limnology and Oceanography*, *40*(7), 1321-1326.

Aceves-Lara, C. A., Aguilar-Garnica, E., Alcaraz-Gonzalez, V., Gonzalez-Reynoso, O., Steyer, J. P., Dominguez-Beltran, J. L., & Gonzalez-Alvarez, V. (2005). Kinetic parameters estimation in an anaerobic digestion process using successive quadratic programming. *Water Science and Technology*, *52*(1-2), 419-426.

Adrian, L., & Löffler, F. E. (2016). *Organohalide Respiring Bacteria*. Springer, Berlin.

Amos, B. K., Christ, J. A., Abriola, L. M., Pennell, K. D., & Löffler, F. E. (2007). Experimental evaluation and mathematical modeling of microbially enhanced tetrachloroethene (PCE) dissolution. *Environmental science & technology*, *41*(3), 963-970.

Antoniou, K., (2017, unpublished manuscript). Investigation of the applicability of in situ biological remediation of soil and groundwater contaminated with chlorinated hydrocarbons. PhD thesis, National Technical University of Athens (in Greek).

Ashyraliyev, M., Fomekong-Nanfack, Y., Kaandorp, J. A., & Blom, J. G. (2009). Systems biology: parameter estimation for biochemical models. *Febs Journal, 276*(4), 886-902.

Aulenta, F., Majone, M., Verbo, P., & Tandoi, V. (2002). Complete dechlorination of tetrachloroethene to ethene in presence of methanogenesis and acetogenesis by an anaerobic sediment microcosm. *Biodegradation*, 13(6), 411-424.

Aulenta, F., Gossett, J. M., Papini, M. P., Rossetti, S., & Majone, M. (2005). Comparative study of methanol, butyrate, and hydrogen as electron donors for long-term dechlorination of tetrachloroethene in mixed anerobic cultures. *Biotechnology and bioengineering*, *91*(6), 743-753.

Aulenta, F., Majone, M., & Tandoi, V. (2006). Enhanced anaerobic bioremediation of chlorinated solvents: environmental factors influencing microbial activity and their relevance under field conditions. *Journal of Chemical Technology and Biotechnology*, *81*(9), 1463-1474.

Aulenta, F., Catervi, A., Majone, M., Panero, S., Reale, P., & Rossetti, S. (2007). Electron transfer from a solid-state electrode assisted by methyl viologen sustains efficient microbial reductive dechlorination of TCE. *Environmental science & technology*, *41*(7), 2554-2559.

Azizian, M. F., Behrens, S., Sabalowsky, A., Dolan, M. E., Spormann, A. M., & Semprini, L. (2008). Continuous-flow column study of reductive dehalogenation of PCE upon bioaugmentation with the Evanite enrichment culture. *Journal of contaminant hydrology*, *100*(1), 11-21.

Azizian, M. F., Marshall, I. P., Behrens, S., Spormann, A. M., & Semprini, L. (2010). Comparison of lactate, formate, and propionate as hydrogen donors for the reductive dehalogenation of trichloroethene in a continuous-flow column. *Journal of contaminant hydrology*, *113*(1), 77-92.

Bagley, D. M. (1998). Systematic approach for modeling tetrachloroethene biodegradation. *Journal of environmental engineering*, *124*(11), 1076-1086.

Ballapragada, B. S., Stensel, H. D., Puhakka, J. A., & Ferguson, J. F. (1997). Effect of hydrogen on reductive dechlorination of chlorinated ethenes. *Environmental science & technology*, *31*(6), 1728-1734.

Batstone, D. J., Keller, J., Angelidaki, I., Kalyuzhnyi, S. V., Pavlostathis, S. G., Rozzi, A., ... & Vavilin, V. A. (2002). The IWA anaerobic digestion model no 1 (ADM1). *Water Science and Technology*, *45*(10), 65-73.

Becker, J. G. (2006). A modeling study and implications of competition between Dehalococcoides ethenogenes and other tetrachloroethene-respiring bacteria. *Environmental science & technology*, *40*(14), 4473-4480.

Bennett, N. D., Croke, B. F., Guariso, G., Guillaume, J. H., Hamilton, S. H., Jakeman, A. J., ... & Pierce, S. A. (2013). Characterising performance of environmental models. *Environmental Modelling & Software*, *40*, 1-20.

Berggren, D. R., Marshall, I. P., Azizian, M. F., Spormann, A. M., & Semprini, L. (2013). Effects of sulfate reduction on the bacterial community and kinetic parameters of a dechlorinating culture under chemostat growth conditions. *Environmental science & technology*, *47*(4), 1879-1886.

Beven, K. (2006). A manifesto for the equifinality thesis. *Journal of hydrology*, *320*(1), 18-36.

Boender, C.G.E., & Rinooy-Kan, A. (1987). Bayesian stopping rules for multistart global optimization methods. *Mathematical Programming*, *37*(1), pp.59-80.

Bradley, P. M. (2003). History and ecology of chloroethene biodegradation: a review. *Bioremediation Journal*, *7*(2), 81-109.

Brisson, V. L., West, K. A., Lee, P. K., Tringe, S. G., Brodie, E. L., & Alvarez-Cohen, L. (2012). Metagenomic analysis of a stable trichloroethene-degrading microbial community. *The ISME journal*, *6*(9), 1702-1714.

Caccavo, F., Lonergan, D. J., Lovley, D. R., Davis, M., Stolz, J. F., & McInerney, M. J. (1994). Geobacter sulfurreducens sp. nov., a hydrogen-and acetate-oxidizing dissimilatory metal-reducing microorganism. *Applied and environmental microbiology*, *60*(10), 3752-3759.

Carr, C. S., Garg, S., & Hughes, J. B. (2000). Effect of dechlorinating bacteria on the longevity and composition of PCE-containing nonaqueous phase liquids under equilibrium dissolution conditions. *Environmental Science & Technology*, *34*(6), 1088-1094.

Chambon, J. C., Bjerg, P. L., Scheutz, C., Bælum, J., Jakobsen, R., & Binning, P. J. (2013). Review of reactive kinetic models describing reductive dechlorination of chlorinated ethenes in soil and groundwater. *Biotechnology and bioengineering*, *110*(1), 1-23.

Chen, M., Abriola, L. M., Amos, B. K., Suchomel, E. J., Pennell, K. D., Löffler, F. E., & Christ, J. A. (2013). Microbially enhanced dissolution and reductive dechlorination of PCE by a mixed culture: model validation and sensitivity analysis. *Journal of contaminant hydrology*, *151*, 117-130.

Christ, J.A., & Abriola, L.M. (2007). Modeling metabolic reductive dechlorination in dense non-aqueous phase liquid source-zones. *Advances in Water Resources*, *30*(6), pp.1547-1561.

Chu, M., Kitanidis, P. K., & McCarty, P. L. (2003). Effects of biomass accumulation on microbially enhanced dissolution of a PCE pool: a numerical simulation. *Journal of Contaminant Hydrology*, *65*(1), 79-100.

Clapp, L. W., Semmens, M. J., Novak, P. J., & Hozalski, R. M. (2004). Model for in situ perchloroethene dechlorination via membrane-delivered hydrogen. *Journal of environmental engineering*, *130*(11), 1367-1381.

Clement, T. P., Johnson, C. D., Sun, Y., Klecka, G. M., & Bartlett, C. (2000). Natural attenuation of chlorinated ethene compounds: model development and field-scale application at the Dover site. *Journal of Contaminant Hydrology*, *42*(2), 113-140.

Cord-Ruwisch, R., Lovley, D. R., & Schink, B. (1998). Growth of *Geobacter sulfurreducens* with acetate in syntrophic cooperation with hydrogen-oxidizing anaerobic partners. *Applied and environmental microbiology*, *64*(6), 2232-2236.

Cupples, A. M., Spormann, A. M., & McCarty, P. L. (2003). Growth of a Dehalococcoides-like microorganism on vinyl chloride and cis-dichloroethene as electron acceptors as determined by competitive PCR. *Applied and environmental microbiology*, *69*(2), 953-959.

Cupples, A. M., Spormann, A. M., & McCarty, P. L. (2004). Vinyl chloride and cis-dichloroethene dechlorination kinetics and microorganism growth under substrate limiting conditions. *Environmental science & technology*, *38*(4), 1102-1107.

Cupples, A. M., Spormann, A. M., & McCarty, P. L. (2004). Comparative evaluation of chloroethene dechlorination to ethene by Dehalococcoides-like microorganisms. *Environmental science & technology*, *38*(18), 4768-4774.

De Vrieze, J., Hennebel, T., Boon, N., & Verstraete, W. (2012). Methanosarcina: the rediscovered methanogen for heavy duty biomethanation. *Bioresource technology*, *112*, 1-9.

Demirel, B., & Scherer, P. (2008). The roles of acetotrophic and hydrogenotrophic methanogens during anaerobic conversion of biomass to methane: a review. *Reviews in Environmental Science and Bio/Technology*, *7*(2), 173-190.

Dennis, P. C., Sleep, B. E., Fulthorpe, R. R., & Liss, S. N. (2003). Phylogenetic analysis of bacterial populations in an anaerobic microbial consortium capable of degrading saturation concentrations of tetrachloroethylene. *Canadian journal of microbiology*, *49*(1), 15-27.

Dowideit, K., Scholz-Muramatsu, H., Miethling-Graff, R., Vigelahn, L., Freygang, M., Dohrmann, A. B., & Tebbe, C. C. (2010). Spatial heterogeneity of dechlorinating bacteria and limiting factors for in situ trichloroethene dechlorination revealed by analyses of sediment cores from a polluted field site. *FEMS microbiology ecology*, *71*(3), 444-459.

Drake, H. L., Küsel, K., & Matthies, C. (2006). Acetogenic prokaryotes. In *The prokaryotes* (pp. 354-420). Springer New York.

Duhamel, M., & Edwards, E. A. (2006). Microbial composition of chlorinated ethene-degrading cultures dominated by *Dehalococcoides*. *FEMS Microbiology Ecology*, *58*(3), 538-549.

Duhamel, M., & Edwards, E. A. (2007). Growth and yields of dechlorinators, acetogens, and methanogens during reductive dechlorination of chlorinated ethenes and dihaloelimination of 1, 2-dichloroethane. *Environmental science & technology*, *41*(7), 2303-2310.

El Mamouni, R., Jacquet, R., Gerin, P., & Agathos, S. N. (2002). Influence of electron donors and acceptors on the bioremediation of soil contaminated with trichloroethene and nickel: laboratory- and pilot-scale study. *Water science and technology*, *45*(10), 49-54.

Englezos, P., & Kalogerakis, N. (2000). *Applied parameter estimation for chemical engineers*. CRC Press.

Fedorovich, V., Lens, P., & Kalyuzhnyi, S. (2003). Extension of Enaerobic Digestion Model No. 1 with processes of sulfate reduction. *Applied biochemistry and biotechnology*, *109*(1), 33-45.

Fennell, D. E., Gossett, J. M., & Zinder, S. H. (1997). Comparison of butyric acid, ethanol, lactic acid, and propionic acid as hydrogen donors for the reductive dechlorination of tetrachloroethene. *Environmental Science & Technology*, *31*(3), 918-926.

Fennell, D. E., & Gossett, J. M. (1998). Modeling the production of and competition for hydrogen in a dechlorinating culture. *Environmental Science & Technology*, *32*(16), 2450-2460.

Fernández, A., Huang, S., Seston, S., Xing, J., Hickey, R., Criddle, C., & Tiedje, J. (1999). How stable is stable? Function versus community composition. *Applied and environmental microbiology*, *65*(8), 3697-3704.

Friis, A. K., Heimann, A. C., Jakobsen, R., Albrechtsen, H. J., Cox, E., & Bjerg, P. L. (2007). Temperature dependence of anaerobic TCE-dechlorination in a highly enriched Dehalococcoides-containing culture. *Water research*, *41*(2), 355-364.

Futagami, T., & Furakawa, K. (2016). The Genus *Deslulfitobacterium*. In *Organohalide Respiring Bacteria*. Springer, Berlin.

Futagami, T., Yamaguchi, T., Nakayama, S. I., Goto, M., & Furukawa, K. (2006). Effects of chloromethanes on growth of and deletion of the pce gene cluster in dehalorespiring Desulfitobacterium hafniense strain Y51. *Applied and environmental microbiology*, *72*(9), 5998-6003.

Gábor, A., & Banga, J. R. (2015). Robust and efficient parameter estimation in dynamic models of biological systems. *BMC systems biology*, *9*(1), 74.

Goris, T., & Diekert, G. (2016). The Genus *Sulfurospirillum*. In *Organohalide Respiring Bacteria*. Springer, Berlin.

Grostern, A., & Edwards, E. A. (2006). A 1, 1, 1-trichloroethane-degrading anaerobic mixed microbial culture enhances biotransformation of mixtures of chlorinated ethenes and ethanes. *Applied and environmental microbiology*, *72*(12), 7849-7856.

Gutenkunst, R. N., Waterfall, J. J., Casey, F. P., Brown, K. S., Myers, C. R., & Sethna, J. P. (2007). Universally sloppy parameter sensitivities in systems biology models. *PLoS Comput Biol*, *3*(10), e189.

Haest, P. J., Springael, D., & Smolders, E. (2010). Modelling reactive CAH transport using batch experiment degradation kinetics. *Water research*, *44*(9), 2981-2989.

Harkness, M., Fisher, A., Lee, M. D., Mack, E. E., Payne, J. A., Dworatzek, S., ... & Possolo, A. (2012). Use of statistical tools to evaluate the reductive dechlorination of high levels of TCE in microcosm studies. *Journal of contaminant hydrology*, *131*(1), 100-118.

Haston, Z. C., & McCarty, P. L. (1999). Chlorinated ethene half-velocity coefficients (Ks) for reductive dehalogenation. *Environmental Science & Technology*, *33*(2), 223-226.

Hattori, S. (2008). Syntrophic acetate-oxidizing microbes in methanogenic environments. *Microbes and Environments*, *23*(2), 118-127.

He, J., Sung, Y., Dollhopf, M. E., Fathepure, B. Z., Tiedje, J. M., & Löffler, F. E. (2002). Acetate versus hydrogen as direct electron donors to stimulate the microbial reductive dechlorination process at chloroethene-contaminated sites. *Environmental Science & Technology*, *36*(18), 3945-3952.

Heavner, G. L., Rowe, A. R., Mansfeldt, C. B., Pan, J. K., Gossett, J. M., & Richardson, R. E. (2013). Molecular biomarker-based biokinetic modeling of a PCE-dechlorinating and methanogenic mixed culture. *Environmental science & technology*, *47*(8), 3724-3733.

Heimann, A. C., Friis, A. K., & Jakobsen, R. (2005). Effects of sulfate on anaerobic chloroethene degradation by an enriched culture under transient and steady-state hydrogen supply. *Water research*, *39*(15), 3579-3586.

Heimann, A. C., Batstone, D. J., & Jakobsen, R. (2006). Methanosarcina spp. drive vinyl chloride dechlorination via interspecies hydrogen transfer. *Applied and environmental microbiology*, *72*(4), 2942-2949.

Heimann, A. C., Friis, A. K., Scheutz, C., & Jakobsen, R. (2007). Dynamics of reductive TCE dechlorination in two distinct H2 supply scenarios and at various temperatures. *Biodegradation*, *18*(2), 167-179.

Hendrickson, E. R., Payne, J. A., Young, R. M., Starr, M. G., Perry, M. P., Fahnestock, S., ... & Ebersole, R. C. (2002). Molecular analysis of Dehalococcoides 16S ribosomal DNA from chloroethene-contaminated sites throughout North America and Europe. *Applied and Environmental Microbiology*, *68*(2), 485-495.

Hoelen, T. P., & Reinhard, M. (2004). Complete biological dehalogenation of chlorinated ethylenes in sulfate containing groundwater. *Biodegradation*, *15*(6), 395-403.

Holmes, V. F., He, J., Lee, P. K., & Alvarez-Cohen, L. (2006). Discrimination of multiple Dehalococcoides strains in a trichloroethene enrichment by quantification of their reductive dehalogenase genes. *Applied and Environmental Microbiology*, *72*(9), 5877-5883.

Hood, E. D., Major, D. W., Quinn, J. W., Yoon, W. S., Gavaskar, A., & Edwards, E. A. (2008). Demonstration of enhanced bioremediation in a TCE source area at Launch Complex 34, Cape Canaveral Air Force Station. *Groundwater Monitoring & Remediation*, *28*(2), 98-107.

Huang, D., & Becker, J. G. (2009). Determination of intrinsic Monod kinetic parameters for two heterotrophic tetrachloroethene (PCE)-respiring strains and insight into their application. *Biotechnology and bioengineering*, *104*(2), 301-311.

Huang, D., & Becker, J. G. (2010). Dehalorespiration model that incorporates the self-inhibition and biomass inactivation effects of high tetrachloroethene concentrations. *Environmental science & technology*, *45*(3), 1093-1099.

Hug, L. A., Beiko, R. G., Rowe, A. R., Richardson, R. E., & Edwards, E. A. (2012). Comparative metagenomics of three Dehalococcoides-containing enrichment cultures: the role of the non-dechlorinating community. *BMC genomics*, *13*(1), 327.

Ingvorsen, K., & Jørgensen, B. B. (1984). Kinetics of sulfate uptake by freshwater and marine species ofDesulfovibrio. *Archives of Microbiology*, *139*(1), 61-66.

Jain, M. K., Thompson, T. E., De Macario, E. C., & Zeikus, J. G. (1987). Speciation of Methanobacterium strain Ivanov as Methanobacterium ivanovii, sp. nov. *Systematic and applied microbiology*, *9*(1-2), 77-82.

Jin, Q. (2007). Control of hydrogen partial pressures on the rates of syntrophic microbial metabolisms: a kinetic model for butyrate fermentation. *Geobiology*, *5*(1), 35-48.

Kalyuzhnyi, S., Fedorovich, V., Lens, P., Pol, L. H., & Lettinga, G. (1998). Mathematical modelling as a tool to study population dynamics between sulfate reducing and methanogenic bacteria. *Biodegradation*, *9*(3-4), 187-199.

Kleerebezem, R., & Stams, A. J. (2000). Kinetics of syntrophic cultures: a theoretical treatise on butyrate fermentation. *Biotechnology and bioengineering*, *67*(5), 529-543.

Kouznetsova, I., Mao, X., Robinson, C., Barry, D. A., Gerhard, J. I., & McCarty, P. L. (2010). Biological reduction of chlorinated solvents: Batch-scale geochemical modeling. *Advances in Water Resources*, *33*(9), 969-986.

Kucherenko, S., & Sytsko, Y. (2005). Application of deterministic low-discrepancy sequences in global optimization. *Computational Optimization and Applications*, *30*(3), 297-318.

Lai, Y., & Becker, J. G. (2013). Compounded effects of chlorinated ethene inhibition on ecological interactions and population abundance in a Dehalococcoides-Dehalobacter coculture. *Environmental science & technology*, *47*(3), 1518-1525.

Lee, I. S., Bae, J. H., Yang, Y., & McCarty, P. L. (2004). Simulated and experimental evaluation of factors affecting the rate and extent of reductive dehalogenation of chloroethenes with glucose. *Journal of Contaminant Hydrology*, *74*(1), 313-331.

Lee, I. S., Bae, J. H., & McCarty, P. L. (2007). Comparison between acetate and hydrogen as electron donors and implications for the reductive dehalogenation of PCE and TCE. *Journal of contaminant hydrology*, *94*(1), 76-85.

Lewis, R. M., Torczon, V., & Trosset, M. W. (2000). Direct search methods: then and now. *Journal of computational and Applied Mathematics*, *124*(1), 191-207.

Liu, Y., & Whitman, W. B. (2008). Metabolic, phylogenetic, and ecological diversity of the methanogenic archaea. *Annals of the New York Academy of Sciences*, *1125*(1), 171-189.

Liu, C., & Zachara, J. M. (2001). Uncertainties of Monod kinetic parameters nonlinearly estimated from batch experiments. *Environmental science & technology*, *35*(1), 133-141.

Löffler, F. E., Tiedje, J. M., & Sanford, R. A. (1999). Fraction of electrons consumed in electron acceptor reduction and hydrogen thresholds as indicators of halorespiratory physiology. *Applied and Environmental Microbiology*, *65*(9), 4049-4056.

Löffler, F.E., Ritalahti, K.M., & Zinder S.H. (2013). *Dehalococcoides* and reductive dechlorination of chlorinated solvents. In *Bioaugmentation for groundwater remediation*. Springer Science & Business Media.

Luijten, M. L., Roelofsen, W., Langenhoff, A. A., Schraa, G., & Stams, A. J. (2004). Hydrogen threshold concentrations in pure cultures of halorespiring bacteria and at a site polluted with chlorinated ethenes. *Environmental microbiology*, *6*(6), 646-650.

Ma, X., Novak, P. J., Clapp, L. W., Semmens, M. J., & Hozalski, R. M. (2003). Evaluation of polyethylene hollow-fiber membranes for hydrogen delivery to support reductive dechlorination in a soil column. *Water research*, *37*(12), 2905-2918.

Ma, X., Novak, P. J., Semmens, M. J., Clapp, L. W., & Hozalski, R. M. (2006). Comparison of pulsed and continuous addition of H 2 gas via membranes for stimulating PCE biodegradation in soil columns. *Water research*, *40*(6), 1155-1166.

Ma, X., Novak, P. J., Ferguson, J., Sadowsky, M., LaPara, T. M., Semmens, M. J., & Hozalski, R. M. (2007). The impact of H2 addition on dechlorinating microbial communities. *Bioremediation journal*, *11*(2), 45-55.

Macbeth, T. W., Cummings, D. E., Spring, S., Petzke, L. M., & Sorenson, K. S. (2004). Molecular characterization of a dechlorinating community resulting from in situ biostimulation in a trichloroethene-contaminated deep, fractured basalt aquifer and comparison to a derivative laboratory culture. *Applied and Environmental Microbiology*, *70*(12), 7329-7341.

Madigan, M. T., Martinko, J. M., & Parker, J. (2003). Microbial growth. *Brock biology of microorganisms*, 137-166.

Maillard, J., & Holliger, C (2016). The Genus *Dehalobacter*. In *Organohalide Respiring Bacteria*. Springer, Berlin.

Major, D. W., McMaster, M. L., Cox, E. E., Edwards, E. A., Dworatzek, S. M., Hendrickson, E. R., ... & Buonamici, L. W. (2002). Field demonstration of successful bioaugmentation to achieve dechlorination of tetrachloroethene to ethene. *Environmental Science & Technology*, *36*(23), 5106-5116.

Malaguerra, F., Chambon, J. C., Bjerg, P. L., Scheutz, C., & Binning, P. J. (2011). Development and sensitivity analysis of a fully kinetic model of sequential reductive dechlorination in groundwater. *Environmental science & technology*, *45*(19), 8395-8402.

Manoli, G., Chambon, J. C., Bjerg, P. L., Scheutz, C., Binning, P. J., & Broholm, M. M. (2012). A remediation performance model for enhanced metabolic reductive dechlorination of chloroethenes in fractured clay till. *Journal of contaminant hydrology*, *131*(1), 64-78.

Mao, X., Stenuit, B., Polasko, A., & Alvarez-Cohen, L. (2015). Efficient metabolic exchange and electron transfer within a syntrophic trichloroethene-degrading coculture of Dehalococcoides mccartyi 195 and Syntrophomonas wolfei. *Applied and environmental microbiology*, *81*(6).

Mao, X., Polasko, A., & Alvarez-Cohen, L. (2017). The Effects of sulfate reduction on TCE dechlorination by Dehalococcoides-containing microbial communities. *Applied and Environmental Microbiology*, AEM-03384.

Martí, R., Resende, M. G., & Ribeiro, C. C. (2013). Multi-start methods for combinatorial optimization. *European Journal of Operational Research*, *226*(1), 1-8.

Maymó -Gatell, X., Chien, Y. T., Gossett, J. M., & Zinder, S. H. (1997). Isolation of a bacterium that reductively dechlorinates tetrachloroethene to ethene. *Science*, *276*(5318), 1568-1571.

Maymó-Gatell, X., Nijenhuis, I., & Zinder, S. H. (2001). Reductive dechlorination of cis-1, 2-dichloroethene and vinyl chloride by "Dehalococcoides ethenogenes". *Environmental science & technology*, *35*(3), 516-521.

Men, Y., Lee, P. K., Harding, K. C., & Alvarez-Cohen, L. (2013). Characterization of four TCE-dechlorinating microbial enrichments grown with different cobalamin stress and methanogenic conditions. *Applied microbiology and biotechnology*, *97*(14), 6439-6450.

Moles, C. G., Mendes, P., & Banga, J. R. (2003). Parameter estimation in biochemical pathways: a comparison of global optimization methods. *Genome research*, *13*(11), 2467-2474.

Mugunthan, P., Shoemaker, C. A., & Regis, R. G. (2005). Comparison of function approximation, heuristic, and derivative-based methods for automatic calibration of computationally expensive groundwater bioremediation models. *Water resources research*, *41*(11).

Muyzer, G., & Stams, A. J. (2008). The ecology and biotechnology of sulphate-reducing bacteria. *Nature Reviews Microbiology*, *6*(6), 441-454.

Nikerel, I. E., van Winden, W. A., Verheijen, P. J., & Heijnen, J. J. (2009). Model reduction and a priori kinetic parameter identifiability analysis using metabolome time series for metabolic reaction networks with linlog kinetics. *Metabolic engineering*, *11*(1), 20-30.

Nocedal, J., & Wright, S. J. (2006). Numerical optimization: Springer Science & Business Media.

Nüsslein, B., Chin, K. J., Eckert, W., & Conrad, R. (2001). Evidence for anaerobic syntrophic acetate oxidation during methane production in the profundal sediment of subtropical Lake Kinneret (Israel). *Environmental microbiology*, *3*(7), 460-470.

Omil, F., Lens, P., Visser, A., Hulshoff Pol, L. W., & Lettinga, G. (1998). Long-term competition between sulfate reducing and methanogenic bacteria in UASB reactors treating volatile fatty acids. *Biotechnology and Bioengineering*, *57*(6), 676-685.

Oude Elferink, S.J.W.H., Visser, A., Pol, L.W.H. & Stams, A.J. (1994). Sulfate reduction in methanogenic bioreactors. *FEMS Microbiology Reviews*, *15*(2-3), pp.119-136.

Panagiotakis, I. (2010). The effect of electron donor and sulfate on in situ bioremediation of chloroethene-contaminated aquifers. PhD thesis, National Technical University of Athens (in Greek).

Panagiotakis, I., Mamais, D., Pantazidou, M., Rossetti, S., Aulenta, F., & Tandoi, V. (2014). Predominance of Dehalococcoides in the presence of different sulfate concentrations. *Water, Air, & Soil Pollution*, *225*(1), 1785.

Panagiotakis, I., Antoniou, K., Mamais, D., & Pantazidou, M. (2015). Effects of Different Electron Donor Feeding Patterns on TCE Reductive Dechlorination Performance. *Bulletin of environmental contamination and toxicology*, *94*(3), 289-294.

Pantazidou, M., Panagiotakis, I., Mamais, D., & Zikidi, V. (2012). Chloroethene biotransformation in the presence of different sulfate concentrations. *Groundwater Monitoring & Remediation*, *32*(1), 106-119.

Pavlostathis, S.G., & Giraldo-Gomez, E. (1991). Kinetics of anaerobic treatment: a critical review. *Critical Reviews in Environmental Science and Technology*, *21*(5-6), pp.411-490.

Qu, X., Vavilin, V.A., Mazéas, L., Lemunier, M., Duquennoi, C., He, P.J. & Bouchez, T. (2009). Anaerobic biodegradation of cellulosic material: batch experiments and modelling based on isotopic data and focusing on aceticlastic and non-aceticlastic methanogenesis. *Waste Management*, *29*(6), pp.1828-1837.

Rabus, R., Hansen, T. A., & Widdel, F. (2013). Dissimilatory sulfate-and sulfur-reducing prokaryotes. In *The prokaryotes* (pp. 309-404). Springer Berlin Heidelberg.

Ribeiro, C. C., Rosseti, I., & Souza, R. C. (2011, January). Effective probabilistic stopping rules for randomized metaheuristics: GRASP implementations. In *International Conference on Learning and Intelligent Optimization* (pp. 146-160). Springer Berlin Heidelberg.

Ribes, J., Keesman, K., & Spanjers, H. (2004). Modelling anaerobic biomass growth kinetics with a substrate threshold concentration. *Water research*, *38*(20), 4502-4510.

Richardson, R. E., Bhupathiraju, V. K., Song, D. L., Goulet, T. A., & Alvarez-Cohen, L. (2002). Phylogenetic characterization of microbial communities that reductively dechlorinate TCE based upon a combination of molecular techniques. *Environmental Science & Technology*, *36*(12), 2652-2662.

Richardson, R. (2016). Organohalide-respiring bacteria as members of microbial communities: Catabolic food webs and biochemical interactions. In *Organohalide Respiring Bacteria*. Springer, Berlin.

Rittmann, B.E., & McCarty, P.L. (2001). Environmental Biotechnology: Principles and Applications. McGraw-Hill Book Co., New York.

Rowe, A. R., Lazar, B. J., Morris, R. M., & Richardson, R. E. (2008). Characterization of the community structure of a dechlorinating mixed culture and comparisons of gene expression in

planktonic and biofloc-associated "*Dehalococcoides*" and *Methanospirillum* species. *Applied and environmental microbiology*, *74*(21), 6709-6719.

Sabalowsky, A. R., & Semprini, L. (2010). Trichloroethene and cis-1, 2-dichloroethene concentration-dependent toxicity model simulates anaerobic dechlorination at high concentrations: I. batch-fed reactors. *Biotechnology and bioengineering*, *107*(3), 529-539.

Sales-Cruz, M., & Gani, R. (2004). Aspects of modelling and model identification for bioprocesses through a computer-aided modelling system. *Computer Aided Chemical Engineering*, *18*, 1123-1128.

Sanford, R.A., Chowdhary, J. & Löffler, F.E. (2016). The organohalide-respiring *Deltaproteobacteria*. In *Organohalide Respiring Bacteria*. Springer, Berlin.

Schäfer, C. E., Condee, C. W., Vainberg, S., & Steffan, R. J. (2009). Bioaugmentation for chlorinated ethenes using Dehalococcoides sp.: Comparison between batch and column experiments. *Chemosphere*, *75*(2), 141-148.

Schneidewind, U., Haest, P. J., Atashgahi, S., Maphosa, F., Hamonts, K., Maesen, M., ... & Dejonghe, W. (2014). Kinetics of dechlorination by Dehalococcoides mccartyi using different carbon sources. *Journal of contaminant hydrology*, *157*, 25-36.

Scholz-Muramatsu, H., Neumann, A., Meßmer, M., Moore, E. & Diekert, G. (1995). Isolation and characterization of Dehalospirillum multivorans gen. nov., sp. nov., a tetrachloroethene-utilizing, strictly anaerobic bacterium. *Archives of Microbiology*, *163*(1), pp.48-56.

Smatlak, C.R., Gossett, J.M. & Zinder, S.H. (1996). Comparative kinetics of hydrogen utilization for reductive dechlorination of tetrachloroethene and methanogenesis in an anaerobic enrichment culture. *Environmental Science and Technology*, *30*(9), pp.2850-2858.

Stams, A. J. M., Plugge, C. M., De Bok, F. A. M., Van Houten, B. H. G. W., Lens, P., Dijkman, H., & Weijma, J. (2005). Metabolic interactions in methanogenic and sulfate-reducing bioreactors. *Water Science and Technology*, *52*(1-2), 13-20.

Stroo, H. F., Leeson, A., & Ward, C. H. (Eds.). (2013). *Bioaugmentation for groundwater remediation*. Springer Science & Business Media.

Tandol, V., DiStefano, T. D., Bowser, P. A., Gossett, J. M., & Zinder, S. H. (1994). Reductive dehalogenation of chlorinated ethenes and halogenated ethanes by a high-rate anaerobic enrichment culture. *Environmental Science & Technology*, *28*(5), 973-979.

Taş, N., Eekert, V., Miriam, H. A., De Vos, W. M., & Smidt, H. (2010). The little bacteria that can–diversity, genomics and ecophysiology of 'Dehalococcoides' spp. in contaminated environments. *Microbial biotechnology*, *3*(4), 389-402.

Viotti, P., Di Palma, P. R., Aulenta, F., Luciano, A., Mancini, G., & Papini, M. P. (2014). Use of a reactive transport model to describe reductive dechlorination (RD) as a remediation design tool:

application at a CAH-contaminated site. *Environmental Science and Pollution Research*, *21*(2), 1514-1527.

Wei, N., & Finneran, K. T. (2011). Influence of ferric iron on complete dechlorination of trichloroethylene (TCE) to ethene: Fe (III) reduction does not always inhibit complete dechlorination. *Environmental science & technology*, *45*(17), 7422-7430.

Wei, N., Oh, E. J., Million, G., Cate, J. H., & Jin, Y. S. (2015). Simultaneous utilization of cellobiose, xylose, and acetic acid from lignocellulosic biomass for biofuel production by an engineered yeast platform. *ACS synthetic biology*, *4*(6), 707-713.

Weissflog, L., Lange, C. A., Pfennigsdorff, A., Kotte, K., Elansky, N., Lisitzyna, L., ... & Krueger, G. (2005). Sediments of salt lakes as a new source of volatile highly chlorinated C1/C2 hydrocarbons. *Geophysical research letters*, *32*(1).

Yang, Y., & McCarty, P. L. (1998). Competition for hydrogen within a chlorinated solvent dehalogenating anaerobic mixed culture. *Environmental Science & Technology*, *32*(22), 3591-3597.

Jetten, M. S., Stams, A. J., & Zehnder, A. J. (1990). Acetate threshold values and acetate activating enzymes in methanogenic bacteria. *FEMS Microbiology Ecology*, *6*(4), 339-344.

Yu, S. (2003). Kinetics and modeling investigations of the anaerobic reductive dechlorination of chlorinated ethylenes using single and binary mixed cultures and silicon-based organic compounds as slowrelease substrates. Ph.D. thesis, Oregon State University, Corvallis.

Yu, S., & Semprini, L. (2004). Kinetics and modeling of reductive dechlorination at high PCE and TCE concentrations. *Biotechnology and Bioengineering*, 88(4), pp.451-464.

Zinder, S.H. (1994). Syntrophic acetate oxidation and "reversible acetogenesis". In *Acetogenesis* (pp. 386-415). Springer US.

Ziv-El, M., Delgado, A. G., Yao, Y., Kang, D. W., Nelson, K. G., Halden, R. U., & Krajmalnik-Brown, R. (2011). Development and characterization of DehaloR^ 2, a novel anaerobic microbial consortium performing rapid dechlorination of TCE to ethene. *Applied microbiology and biotechnology*, *92*(5), 1063-1071.

Appendix A

Appendix A provides supplementary material for Chapters 4, 7, 8, 9 and 10.

A1. Supplementary material for Chapter 4

Product inhibition for butyrate and acetate oxidation

A simple exponential term was used in order to simulate possible inhibition of syntrophic metabolisms by H_2, as proposed by Kouznetsova et al. (2010):

$$I_{H-j} = e^{\left(-S_H / S_{INH,H-j}\right)} \quad \text{(A1.1)}$$

where $S_{INH,H-J}$ is an inhibitory H_2 concentration for the syntrophic microorganism j (μM). Regarding butyrate oxidizers (j=BO) this H_2 concentration was calculated based on the results of a syntrophic TCE-degrading coculture of *Dehalococcoides mccartyi* and butyrate oxidizers reported by Mao et al. (2015). With respect to acetate oxidizers (j=AO), the inhibitory H_2 concertation $S_{INH,H-AO}$ was estimated from the standard Gibbs energy 25° C under conditions typically encountered in the source culture (calculations were performed for pH 6.8, 750 μM acetate and 357 μM bicarbonate).

Alternatively, more complex functions have been proposed in the literature describing the thermodynamic limitations imposed to syntrophic reactions. For butyrate oxidation, Jin (2007) proposed the following equation:

$$I_{H-BO} = 1 - P_H^{0.5} S_A \left(\frac{S_{H^+}}{S_B}\right)^{0.5} \exp\left(\frac{\Delta G^o - 17.8 \pm 2.9}{2RT}\right) \quad \text{(A1.2)}$$

where P_H is the partial pressure of H_2 (atm), ΔG_o is the standard Gibbs free energy change at 25° C (89.89 kJ/mol butyrate), R is the gas constant, and T is the absolute temperature. Likewise, Fennell and Gossett (1998) proposed a modeling approach, which for acetate oxidation is formulated as follows:

$$I_{H-AO} = 1 - \exp\left(\frac{\Delta G_r - \Delta G_c}{RT}\right) \quad \text{(A1.3)}$$

where ΔG_c is a marginally negative free energy that acetate oxidizers must have available to grow (in the absence of reported values, we hypothesized that ΔG_c =-10 kJ/mol) and ΔG_r is the free energy available from acetate oxidation calculated as follows:

$$\Delta G_r = \Delta G^o + RT \ln\left(\frac{P_H^4 S_{H^+} S_{HCO_3^-}^2}{S_A}\right) \quad \text{(A1.4)}$$

in which ΔG_o is set 140 kJ/mol acetate.

The exponential inhibition factor (Eq. A1.1) and the proposed approaches of Jin (2007) and Fennell and Gossett (1998) were tested during the solution of the inverse problem. The exponential inhibition factor was more suitable for the solution of the inverse problem, because the more complex functions for butyrate and acetate oxidation (Eq. A1.2 to A1.3) evoked stability issues in several local searches during the optimization.

For confirmation purposes, we compared our simplifying approach with the aforementioned sophisticated functions for conditions near thermodynamic equilibrium; the supply of 1500 μM

butyrate to culture B_1 (see also Chapter 7 for the make-up of culture B_1) was tested resulting in maximum simulated H_2 concentrations in the range of 1 μM. Simulated VFA concentrations were comparable between the different modeling approaches (Fig. A1.1).

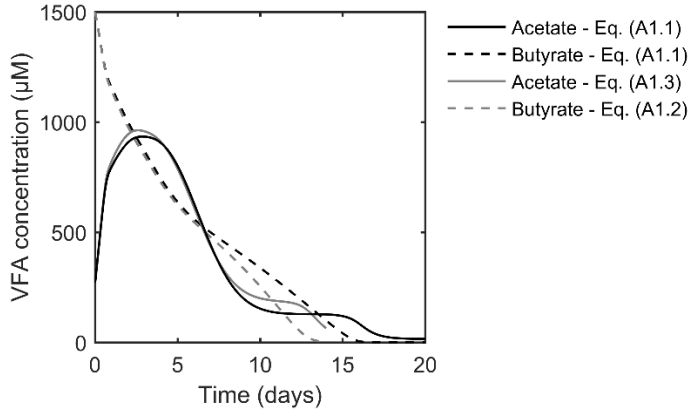

Fig. A1.1. Acetate and butyrate concentrations calculated with either the exponential inhibition function (Eq. A1.1) or the modeling approaches proposed by Fennell and Gossett (1998) and Jin (2007) (Eq. A1.2 and A1.3 for acetate and butyrate oxidation, respectively).

A2. Supplementary material for Chapter 7

Table A2.1. Kinetic parameters of the best-fit solution obtained from the first phase of the parameter estimation strategy for dechlorinators, butyrate oxidizers, methanogens and acetate oxidizers.

Substrate	Parameter (units)	Symbol	Value
TCE-to-ETH dechlorinators			
TCE, DCE, VC	Maximum specific growth rate ($days^{-1}$)	$\mu_{max,D1}$	0.19
TCE	Half-velocity coefficient (μM)	$K_{S,TCE\text{-}D1}$	58.10
DCE	Half-velocity coefficient (μM)	$K_{S,cDCE\text{-}D1}$	148.66
VC	Half-velocity coefficient (μM)	$K_{S,VC\text{-}D1}$	466.87
VC	Inhibition coefficient (μM)	$K_{INH,cDCE}$	20.00
H_2	Half-velocity coefficient (μM)	$K_{S,H\text{-}D1}$	0.079
TCE-to-cDCE dechlorinators			
TCE	Maximum specific growth rate ($days^{-1}$)	$\mu_{max,\ D2}$	2.85
TCE	Half-velocity coefficient (μM)	$K_{S,TCE\text{-}D2}$	602.00
H_2	Half-velocity coefficient (μM)	$K_{S,H\text{-}D2}$	0.051
Butyrate oxidizers			
Butyrate	Maximum specific growth rate ($days^{-1}$)	$\mu_{max,BO}$	0.52
Butyrate	Half-velocity coefficient (μM)	$K_{S,B\text{-}BO}$	213.00
Butyrate	1st-order coefficient for endogenous decay ($days^{-1}$)	K_{ED}	0.004
H_2-utilizing methanogens			
H_2	Maximum specific growth rate($days^{-1}$)	$\mu_{max,HM}$	1.96
H_2	Half-velocity coefficient (μM)	$K_{S\text{-}H,HM}$	0.76
Acetate-utilizing methanogens			
Acetate	Maximum specific growth rate ($days^{-1}$)	$\mu_{max,AM}$	0.38
Acetate	Half-velocity coefficient (μM)	$K_{S,A\text{-}AM}$	962
Acetate oxidizers			
Acetate	Maximum specific growth rate ($days^{-1}$)	$\mu_{max,AO}$	0.18
Acetate	Half-velocity coefficient (μM)	$K_{S,A\text{-}AO}$	1120

Table A2.2. Initial biomass concentrations of the best-fit solution of the first phase of the parameter estimation strategy.

Microorganism	Symbol	Value (mg VSS/l)
TCE-to-ETH dechlorinators	$X_{D1,o}$	10.2
TCE-to-cDCE dechlorinators	$X_{D2,o}$	3.9
H_2-utilizing methanogens	$X_{HM,o}$	0.05
Acetate-utilizing methanogens	$X_{AM,o}$	1.4
Butyrate oxidizers	$X_{BO,o}$	3.0
Acetate oxidizers	$X_{AO,o}$	0.4
Overall biomass concentration		19.0

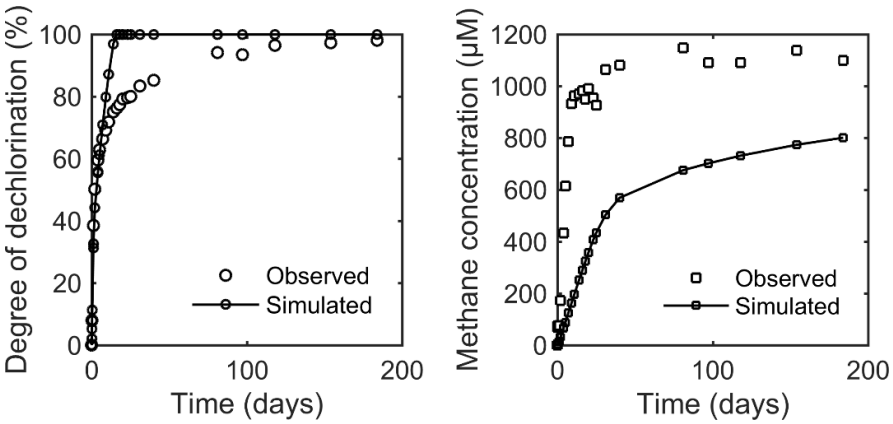

Fig. A2.1. An example of a local optimum solution that resulted in a poor fit of the model output to (a) the observed degree of dechlorination (E_c = 90 μM) and (b) methane production (E_m = 439 μM).

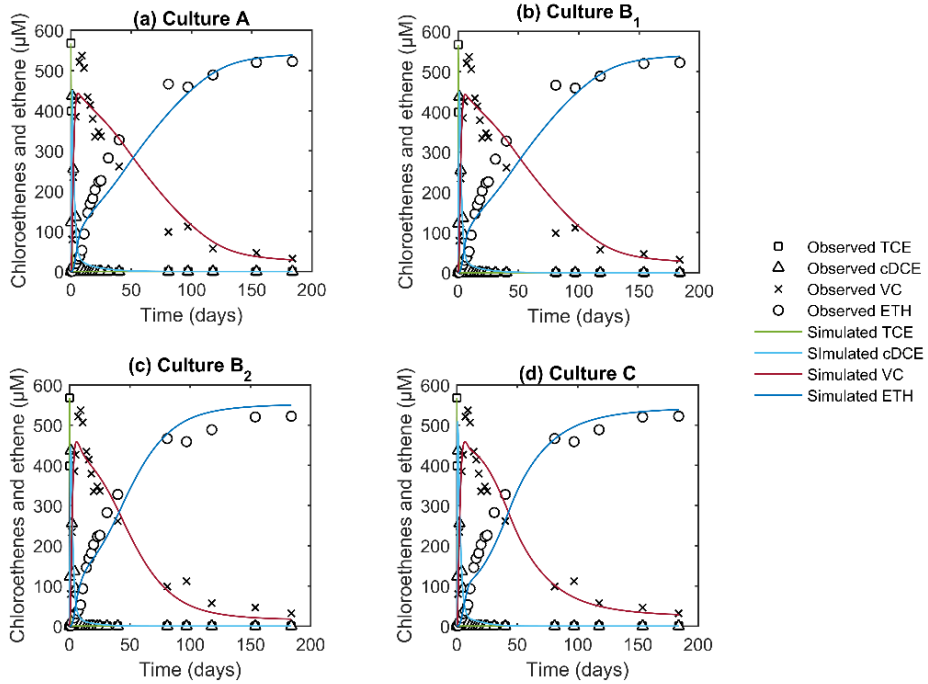

Fig. A2.3. Comparison between the four equivalent solutions of the inverse problem and the observed values from the batch test for chlorinated ethenes and ethene.

A3. Supplementary material for Chapter 8

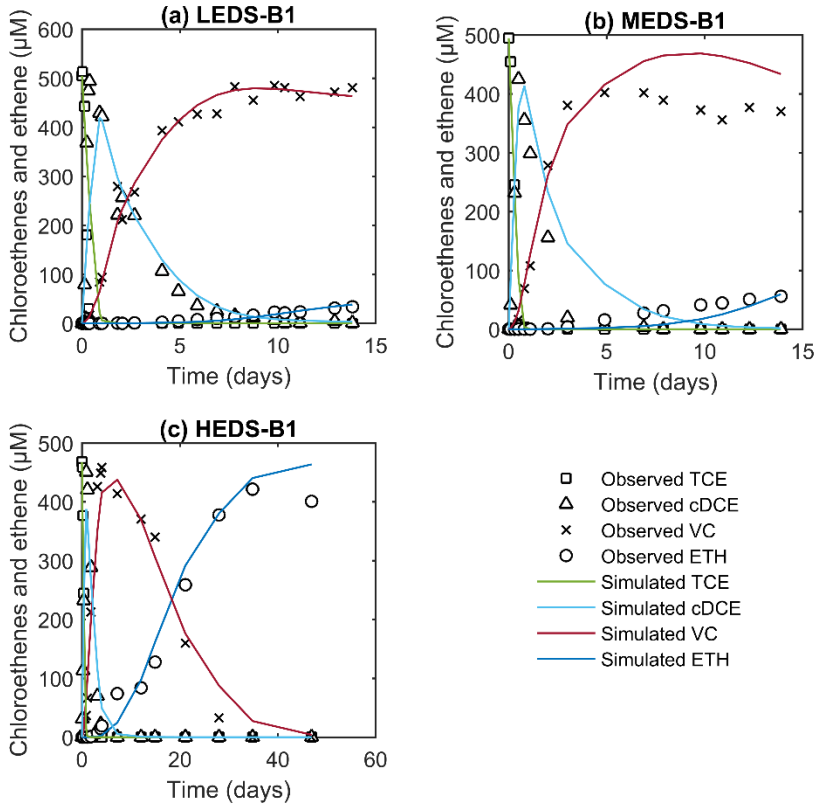

Fig. A3.1. Comparison between the best-fit solutions of the inverse problem and the observed values for chlorinated ethenes and ethene and the batch tests (a) LEDS-B1, (b) MEDS-B1 and (c) HEDS-B1 performed with culture NTUA-M1.

A4. Supplementary material for Chapter 9

Table A4.1. Degrees of dechlorination achieved at day 14 and day 184 for cultures A, B_1, B_2 and C for the numerical tests performed with butyrate, H_2 or acetate as electron donor sources.

Test	Degree of dechlorination, *DoD* (%)							
	Culture A		Culture B_1		Culture B_2		Culture C	
	Day 14	Day 184	Day 14	Day 184	Day 14	Day 184	Day 14	Day 184
LEDS-B2	73.5	98.3	73.0	98.2	74.0	98.2	72.8	97.8
MEDS-B2	95.5	100.0	100.0	100.0	89.7	99.8	85.6	99.5
MEDS-BD2	97.2	100.0	100.0	100.0	95.1	99.8	90.1	99.5
HEDS-B2	99.3	100.0	100.0	100.0	99.1	100.0	97.6	99.9
MEDS-H2	88.0	95	100.0	100.0	80.1	94	78.5	94
MEDS-A2	82.1	99.7	83.4	99.8	82.0	99.3	82.0	99.2
HEDS-A2	97.3	100.0	99.8	100.0	97.0	100.0	96.9	100.0

A5. Supplementary material for Chapter 10

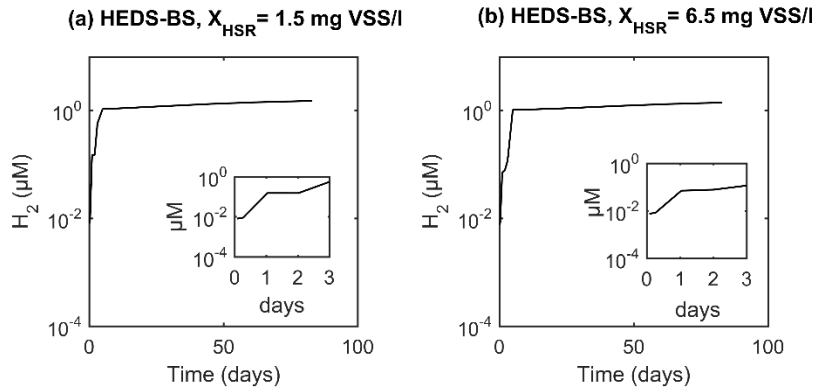

Fig. A5.1. Concentrations of H_2 versus time for the HEDS-BS test performed with different initial concentrations for H_2-utilizing sulfate reducers: (a) X_{HSR}=1.5 mg VSS/l and (b) X_{HSR}=6.5 mg VSS/l.

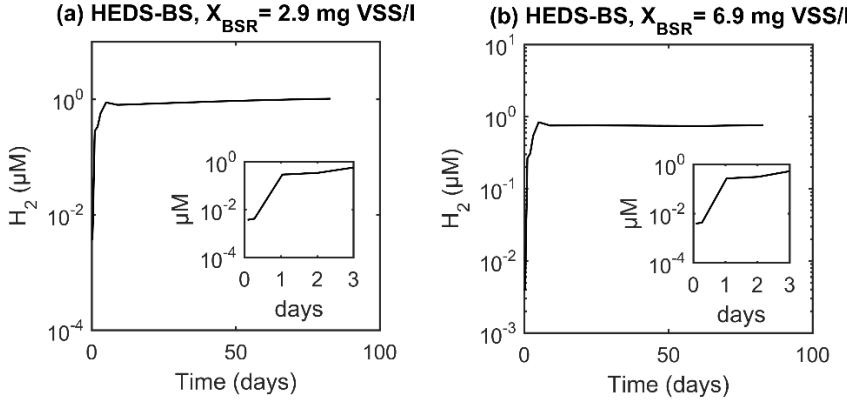

Fig. A5.2. Concentrations of H_2 versus time for the HEDS-BS test performed with different initial concentrations for butyrate-utilizing sulfate reducers: (a) X_{BSR}=2.9 mg VSS/l and (b) X_{BSR}=6.9 mg VSS/l.

Appendix B

Appendix B provides the m-files developed in MATLAB® for the solution of the forward and the inverse problems of the thesis employing the developed kinetic model. The m-files require the Optimization Toolbox ™ and the Global Optimization Toolbox ™ of MATLAB® for their execution.

B1. A simple model for dechlorination kinetics in culture NTUA-M2 – Chapter 5

This section provides the requisite m-files for the estimation of parameters in the simple model developed in Chapter 5 using (a) an SQP-based multistart algorithm (*InvDecSQP*.m), and (b) a GPS-based multistart algorithm (*InvDecGPS*.m). The forward problem can be solved using the *ode15s* function with *SysDef*.m as an input argument.

B1.1 The SQP-based multistart approach

B1.1.1 InvDecSQP.m

Load the input data of the problem: Chloroethene and initial biomass concentrations

```
global x
tic % start the timer
% TCE, DCE, VC, ETH are the input chloroethene concentrations.
% Xd1 and Xd2 are the initial biomass concentrations of TCE-to-ETH and
% TCE-to-cDCE dechlorinators, respectively. T is the time vector.
% Use a proper filename as input for the importdata function.
TCE = importdata('filename'); DCE = importdata('filename');
VC = importdata('filename'); ETH = importdata('filename');
Xd1 = importdata('filename'); Xd2 = importdata('filename');
T = importdata('filename');
```

Define the feasible area of the parameter space

```
% MaxStPts is the maximum number of starting points for the multistart algorithm
% ub and lb are the upper and lowere boundaries creating the feasible
% area of the parameter space
MaxStPts = 1000;
ub = [4.30, ... mmax,D1 k1
4.30,... mmax, D2 k2
602,... Ks,TCE-D1 k3
602, ... Ks,TCE-D2 k4
602,... Ks,cDCE-D1 k5
602, ... Ks,VC-D1 k6
602];% KINH,cDCE/VC k7
lb = [0.01, ... mmax,D1 k1
0.01,... mmax, D2 k2
0.05,... Ks,TCE-D1 k3
0.05, ... Ks,TCE-D2 k4
0.05,... Ks,cDCE-D1 k5
0.05,... Ks,VC-D1 k6
0.05]; % KINH,cDCE/VC k7
```

Initialize vectors of the local solutions of the problem

```
K=zeros(MaxStPts,length(ub)); % parameter vector
F=zeros(MaxStPts,1); % objective function value
```

Create the Sobol set of starting points

```
K0=zeros(MaxStPts,length(ub)); % Vector of starting points for the multistart
algorithm
SbSet=sobolset(length(ub));
spts = net(SbSet,MaxStPts);
for i=1:MaxStPts
for j=1:length(ub)
K0(i,j) = lb(j)+spts(i,j).*(ub(j)-lb(j));
end
end
```

Set-up the optimization problem

```
tol = 0.10; % tolerance for the solution matrix
MaxIterLS = length(ub)*100;  % number of maximum iterations per local search, 100 per
each parameter
MaxFevals = MaxIterLS*20; % number of maximum function evaluations per local search
opt2=optimset
('Display','iter','MaxFunEvals',MaxFevals,'maxiter',MaxIterLS,'TolFun',1e-3,'TolX',1e-
3,'TolCon',1e-6,'FinDiffType','central','Algorithm','sqp'); % choose SQP algorithm
specifics
```

Solve the optimization problem using *fmincon*

```
for i =1:MaxStPts
k0 = K0(i,:);
problem=createOptimProblem('fmincon','objective',@(k)
ObjF(k,iv,TCE,DCE,VC,ETH,Xd1,Xd2,T),'lb', lb,'ub', ub, 'x0', k0,'options', opt2);
[k,fval,exitflag,output] = fmincon(problem);
K(i,:)=k;
F(i,1)=fval;
Solutions = [F,K];
Solutions = uniquetol(Solutions,tol,'ByRows',true); % Find unique solutions of the
inverse problem
Solutions = sortrows(Solutions,1); %
 if (i-size(Solutions,1)-2)>0
     if ((size(Solutions,1)*(i-1))/(i-size(Solutions,1)-2))<=size(Solutions,1) % Check
Bayesian stopping rule
         break
     end
 end
end
ElapsedTime = toc; % Evaluate the time consumed by the algorithm
```

B1.1.2 ObjF.m

The *fmincon* function calls the function *ObjF.m*, which calculates the objective function value, as follows:

```
function J = ObjF(k,iv,TCE,DCE,VC,ETH,Xd1,Xd2,T)
global x
```

Solve the forward problem

```
iv = [TCE(1);DCE(1);VC(1);ETH(1);Xd1(1);Xd2(1)]; % Initial values of the system of ODEs
opt1 = odeset('Abstol', 1e-8, 'Reltol', 1e-6);
[t,x] = ode15s(@(t,x)SysDef(t,x,k,iv,TCE,DCE,VC,ETH,Xd1,Xd2,T), T, iv, opt1);
```

Calculate the objective function value, *J*

```
J = 0;
N = length(T);
for i= 1:N;
        J = J+((TCE(i)-x(i,1))^2+(DCE(i)-x(i,2))^2+(VC(i)-x(i,3))^2 +(ETH(i)-
x(i,4))^2);
end
```

```
end
```

B1.1.3 SysDef.m

During the solution of the forward problem, function *ode15s* calls the function *SysDef*.m, which contains the system of ordinary differential equations of the model. The corresponding m-file is the following:

```
function dx = SysDef(t,x,k,iv,TCE,DCE,VC,ETH,Xd1,Xd2,T)
```

Chloroethene limitation & dce/vc inhibition for dechlorination

```
climtdin = zeros(4,1);
climtdin(1) = (x(1)/(k(3)+x(1))); % TCE: TCE-to-ETH dechlorinator
climtdin(2) = (x(1)/(k(4)+x(1))); % TCE: TCE-to-cDCE dechlorinator
climtdin(3) = (x(2)/(k(5)+x(2))); % cDCE: TCE-to-ETH dechlorinator
climtdin(4) = (x(3)/(k(6)*(1+(x(2)/k(7)))+x(3))); % VC: TCE-to-ETH dechlorinator
```

Growth and decay rates for dechlorinators

```
r = ones(4,1);
r(1) = k(1)*x(5); % growth of TCE-to-ETH dechlorinator
r(2) = k(2)*x(6); % growth of TCE-to-cDCE dechlorinator
r(3) = 0.024*x(5); % decay of TCE-to-ETH dechlorinator
r(4) = 0.024*x(6); % decay of TCE-to-cDCE dechlorinator
```

Define the system of ODEs that describes the rates of substrate consumption and biomass growth

```
dx=zeros(6,1);
dx(1) = (-r(1)*climtdin(1)/4.96e-3) - (r(2)*climtdin(2)/2.80e-3); %TCE
dx(2) = (r(1)*climtdin(1)/4.96e-3) + (r(2)*climtdin(2)/2.80e-3)...
    - (r(1)*climtdin(3)/4.96e-3); % cDCE
dx(3) = (r(1)*climtdin(3)/4.96e-3) - (r(1)*climtdin(4)/4.96e-3); % VC
dx(4) = r(1)*climtdin(4)/4.96e-3; % ETH
dx(5) = (r(1)*climtdin(1)) + (r(1)*climtdin(3)) + (r(1)*climtdin(4)) - r(3); %D1
dx(6) = r(2)*climtdin(2) - r(4); % D2
```

```
end
```

B1.2 The GPS-based multistart approach - InvDecGPS.m

For the GPS-based approach, the m-file containing the solution of the inverse problem is different, as it is based on a different local search method. On the contrary, the called functions *ObjF*.m and *SysDef*.m are the same as in the previous section and, therefore, they will not be presented herein.

Load the input data of the problem: Chloroethene and initial biomass concentrations

```
global x
tic % start the timer

% TCE, DCE, VC, ETH are the input chloroethene concentrations.
% Xd1 and Xd2 are the initial biomass concentrations of TCE-to-ETH and
% TCE-to-cDCE dechlorinators, respectively. T is the time vector.
% Use a proper filename as input for the importdata function.
TCE = importdata('filename');
DCE = importdata('filename');
VC = importdata('filename');
ETH = importdata('filename');
Xd1 = importdata('filename');
Xd2 = importdata('filename');
T = importdata('filename');
```

Define the feasible area of the parameter space

```
% _MaxStPts_ is the maximum number of starting points for the multistart algorithm
% _ub_ and _lb_ are the lower and upper boundaries creating the feasible
% area of the parameter space

MaxStPts = 1000;
ub = [4.30, ... mmax,D1 k1
4.30,... mmax, D2 k2
602,... Ks,TCE-D1 k3
602, ... Ks,TCE-D2 k4
602,... Ks,cDCE-D1 k5
602, ... Ks,VC-D1 k6
602];% KINH,cDCE/VC k7
lb = [0.01, ... mmax,D1 k1
0.01,... mmax, D2 k2
0.05,... Ks,TCE-D1 k3
0.05, ... Ks,TCE-D2 k4
0.05,... Ks,cDCE-D1 k5
0.05,... Ks,VC-D1 k6
0.05]; % KINH,cDCE/VC k7
```

Initialize vectors of the local solutions of the problem

```
K=zeros(MaxStPts,length(ub)); %parameter vector
F=zeros(MaxStPts,1); %objective function value
```

Create the Sobol set of starting points

```
K0=zeros(MaxStPts,length(ub)); %Vector of starting points for the multistart algorithm
SbSet=sobolset(length(ub));
spts = net(SbSet,MaxStPts);
for i=1:MaxStPts
for j=1:length(ub)
K0(i,j) = lb(j)+spts(i,j).*(ub(j)-lb(j));
end
end
```

Construct the optimization problem for the pattern search algorithm

```
% Use the psoptimset function to specify mesh parameters (initial mesh size, mesh
scaling etc.) and,
% stopping criteria and tolerances (TolFun,TolMesh)

tol = 0.10; % tolerance for the solution matrix
opt = psoptimset
('Display','iter','maxiter',length(ub)*100,'PlotFcns',{@psplotbestx,@psplotbestf},
'CompletePoll','on','PollingOrder','Random','InitialMeshSize',291,'TolFun',1e-3,
'TolMesh',0.01,'TolCon',1e-
4,'UseParallel','always','CompletePoll','on','Vectorized','off',
    'MeshContraction',0.25,'MeshExpansion',4,'ScaleMesh','on');
```

Solve the optimization problem using the *patternsearch* function

```
for i =1:MaxStPts
k0 = K0(i,:);
[k,fval,exitflag,output] = patternsearch(@(k)ObjF(k,iv,TCE,DCE,VC,ETH,Xd1,Xd2,T),...
    k0,[],[],[],[],lb,ub,[],opt);
if exitflag == 1
    K(i,:)=k;
    F(i,1)=fval;
    Solutions = [F,K];
    Solutions = uniquetol(Solutions,tol,'ByRows',true); % Find unique solutions of the
inverse problem
    Solutions = sortrows(Solutions,1); %
    if (i-size(Solutions,1)-2)>0
        if ((size(Solutions,1)*(i-1))/(i-size(Solutions,1)-2))<=size(Solutions,1) %
Check Bayesian stopping rule
            break
        end
    end
end
end
ElapsedTime = toc; % Evaluate the time consumed by the algorithm
```

B2. A fully kinetic model for cultures NTUA-M1 and NTUA-M2 – Chapters 7, 8 and 9

This section provides the requisite m-file for solving the inverse problem using an SQP-based multistart algorithm for cultures NTUA-M1 and NTUA-M2, *InvMth*.m. As the Bayesian stopping rule is not checked after each local search, the algorithm is based on the *multistart* built-in function of MATLAB®. Again, the forward problem can be solved using the *ode15s* function with *SysDef*.m as an input argument.

B2.1 InvMth.m

Load the input data of the problem

```
global x
rng('shuffle')
MaxStPts = input('Number of starting points:'); % Define the maximum number of starting
points = 1000
% Use a proper filename for the importdata function
TCE = importdata('filename'); DCE = importdata('filename');
VC = importdata('filename'); ETH = importdata('filename');
BUT = importdata('filename'); AC = importdata('filename');
MTH = importdata('filename'); H=0;
W = importdata('filename'); % Weighting factors for the objective function
Xbo = importdata('filename');
Xd1 = importdata('filename');
Xd2 = importdata('filename');
T = importdata('filename');
```

Set the feasible area of the parameter space

```
% The upper and lower boundaries for each parameter can be altered
% to define a different feasible area of the parameter space, if necessary.
ub=[0.52,... mmax,BO ,k1
    4.30,...mmax,D1 ,k2
    4.30,... mmax,D2 ,k3
    1.98,... mmax,HM ,k4
    0.38,... mmax,AM ,k5
    0.26,...mmax,AO ,k6
    3676, ... Ks,B-BO ,k7
    602.00, ...Ks,tce-D1 ,k8
    602.00, ...Ks,tce-D2 ,k9
    602.00, ... Ks,dce-D1 ,k10
    602.00, ... Ks,vc-D1 ,k11
    0.100, ... Ks,H-D1 ,k12
    0.100, ... Ks,H-D2 ,k13
    602.00,... Kinh,cDCE/VC ,k14
    18.40,... Ks,H-HM ,k15
    2031,... Ks,A-AM ,k16
    2500,... Ks,A-AO ,k17
    0.010,... KED ,k18
    1.31,... X,AO ,k19
    4.50,... X,HM ,k20
    2.10]; % X, AM ,k21
lb =[0.21,... mmax,BO,k1
    0.01,... mmax,D1,k2
    0.01,... mmax,D2,k3
    0.02,... mmax,HM,k4
    0.04,... mmax,AM,k5
    0.07,... mmax,AO,k6
    160, ...  Ks,B-BO, k7
    0.05, ... Ks,tce-D1,k8
    0.05, ... Ks,tce-D2,k9
    0.05, ... Ks,dce-D1,k10
    0.05, ... Ks,vc-D,k11
    0.007, ... Ks,h-D1,k12
    0.007, ... Ks,h-D2,k13
    0.05,... Kinh,cDCE/VC ,k14
    0.500,... Kshmeth,k15
    370,... Ksacm,k16
    500,... Ksach,k17
    0.001,... KED, k18
    0.25,... XAO, k19
    0.0,... XHM, k20
    0.0];% XAM, k21
```

Create the Sobol set of starting points

```
K0=zeros(MaxStPts,length(ub)); %Matrix of starting points for the multistart algorithm
SbSet=sobolset(length(ub));
spts = net(SbSet,MaxStPts);

for i=1:MaxStPts
for j=1:length(ub)
K0(i,j) = lb(j)+spts(i,j).*(ub(j)-lb(j));
end
end
```

Set the optimization problem using the built-in *MultiStart* function using *fmincon*

```
MaxIterLS = length(ub)*100;  % number of maximum iterations per local search, 100 per
each parameter
MaxFevals = MaxIterLS*20; % number of maximum function evaluations per local search
opt2 = optimset ('Display','iter','MaxFunEvals',MaxFevals,'maxiter',MaxIterLS,...
    'TolFun',1.0e-3,'TolX',1e-3,...
    'TolCon', 1e-5, 'FinDiffType', 'central', 'Algorithm', 'sqp',
'PlotFcns','optimplotfval');
problem = createOptimProblem ('fmincon', 'objective', @(k)ObjF(k, iv, BUT, AC, H, TCE,
DCE,...
    VC, ETH, MTH, T,W), 'lb', lb, 'ub', ub,'x0', k,'options', opt2);
ms = MultiStart('UseParallel', 'always', 'StartPointsToRun',...
    'bounds','TolFun',0.01,'TolX',0.01);
stpts = CustomStartPointSet(K0); % Use the Sobol set of starting points
```

Solve the optimization problem

```
[xmin, fminm, flagm, outputm, solutions] = run(ms,problem,stpts);
```

B2.2 *ObjF*.m

The *fmincon* function calls function *ObjF* which calculates the objective function value, as follows:

```
function J= ObjF(k, iv, BUT, AC, H, TCE, DCE, VC, ETH, MTH, T,W)
```

Solve the forward problem

```
global x
iv = [BUT(1), AC(1), H(1), TCE(1), DCE(1), VC(1), ETH(1), MTH(1),Xbo(1),...
    Xd1(1),Xd2(1),k(20),k(21),k(19),0];

opt1 = odeset('Abstol', 1e-8, 'Reltol', 1e-6);
[t,x] = ode15s(@(t,x) SysDef(t, x, k, iv, BUT, AC, H, TCE, DCE, VC, ETH, MTH, T,W), T,
iv, opt1);
```

Calculate the objective function value, *J*

```
J = 0;
N = length(T);
for i= 1:N
    J = J + (W(i,1)*((TCE(i)-x(i,4)))^2 + W(i,2)*((DCE(i)-x(i,5)))^2 + W(i,3)*((VC(i)-
x(i,6)))^2         +W(i,4)*((ETH(i)-x(i,7)))^2+W(i,5)*((MTH(i)-
x(i,8))^2)+W(i,7)*((BUT(i)-x(i,1)))^2 + W(i,6)*((AC(i)-x(i,2)))^2);
end
```

```
end
```

B2.3 *SysDef*.m

During the solution of the forward problem, function *ode15s* calls *SysDef* function which contains the system of ordinary differential equations that describe the problem. The corresponding m-file is the following:

```
function dx = SysDef(t, x, k, iv, BUT, AC, H, TCE, DCE, VC, ETH, MTH, T,W)
```

Hydrogen limitation for D1, D2 and HM

```
% Calculate hydrogen threshold functions according to Ribes et al. (2004)

fm = zeros(2,1); % methanogenesis
fm(1,1) = 1/(1+exp(100*(11e-3-x(3))/11e-3));
fm(2,1) = 1/(1+exp(100*((1.1*11e-3)-x(3))/11e-3));
ft = zeros(2,1); % TCE dechlorination
ft(1,1) = 1/(1+exp(100*(2e-3-x(3))/2e-3));
ft(2,1) = 1/(1+exp(100*((1.1*2e-3)-x(3))/2e-3));
fd = zeros(2,1); % DCE dechlorination
fd(1,1) = 1/(1+exp(100*(2e-3-x(3))/2e-3));
fd(2,1) = 1/(1+exp(100*((1.1*2e-3)-x(3))/2e-3));
fv = zeros(2,1); % VC dechlorination
fv(1,1) = 1/(1+exp(100*(2e-3-x(3))/2e-3));
fv(2,1) = 1/(1+exp(100*((1.1*2e-3)-x(3))/2e-3));

Hlim = zeros(5,1);
Hlim(1,1) = ((x(3)-11e-3*fm(1))*fm(2)/(k(15)+x(3)-11e-3*fm(1))); % methanogenesis
Hlim(2,1) = ((x(3)-2e-3*ft(1))*ft(2)/(k(12)+x(3)-2e-3*ft(1))); % TCE dechlorination
Hlim(3,1) = ((x(3)-2e-3*ft(1))*ft(2)/(k(13)+x(3)-2e-3*ft(1))); %TCE dechlorination
Hlim(4,1) = ((x(3)-2e-3*fd(1))*fd(2)/(k(12)+x(3)-2e-3*fd(1))); % DCE dechlorination
Hlim(5,1) = ((x(3)-2e-3*fv(1))*fv(2)/(k(12)+x(3)-2e-3*fv(1))); % VC dechlorination
```

Butyrate limitation for BO

```
bf = zeros(1,1);
bf(1,1) = x(1)/(k(7)+x(1));
% Inhibition by hydrogen
bi = zeros(1,1);
bi(1,1) = exp(-(x(3)/0.25));
```

Chloroethene limitation for D1 and D2 dechlorinators

```
dec = zeros(4,1);
dec(1) = (x(4)/(k(8)+x(4))); % TCE
dec(2) = (x(4)/(k(9)+x(4))); % TCE
dec(3) = (x(5)/(k(10)+x(5))); % cDCE
dec(4) = (x(6)/(k(11)*(1+(x(5)/k(14)))+x(6))); %VC
```

Acetate limitation for AM

```
% Calculate acetate threshold functions - Ribes et al. (2004)
am = zeros(2,1);
am(1,1) = 1/(1+exp(100*(15-x(2))/15));
am(2,1) = 1/(1+exp(100*((1.1*15)-x(2))/15));
acm = zeros(1,1);
acm(1,1) = ((x(2)-15*am(1))*am(2)/(k(16)+x(2)-15*am(1)));
```

Acetate limitation for AO

```
ach = zeros(1,1);
ach(1,1) = x(2)/(k(17)+x(2));
% Inhibition by hydrogen
ai = zeros(1,1);
ai(1,1) = exp(-(x(3)/0.08));
```

Growth and decay rates for microbial groups considered

```
r = ones(14,1);
r(1) = k(1)*x(9); % growth of BO
r(2) = k(2)*x(10);% growth of D1
r(3) = k(3)*x(11); % growth of D2
r(4) = k(4)*x(12); % growth of HM
r(5) = k(5)*x(13); % growth of AM
r(6) = k(6)*x(14); % growth of AO
r(7) = 0.024*x(9); % decay of BO
r(8) = 0.024*x(10);% decay of D1
r(9) = 0.024*x(11); %decay of D2
r(10) = 0.024*x(12); % decay of HM
r(11) = 0.024*x(13); % decay of AM
r(12) = 0.024*x(14); % decay of AO
r(13) = (0.024*x(9)+0.024*x(10)+0.024*x(11)+0.024*x(12)+0.024*x(13)+0.024*x(14)); %
Decay by-products
r(14) = k(18)*x(15); % Composite material consumption
```

Define the system of ODEs that describes the rates of substrate consumption and biomass growth

```
dx=zeros(15,1);
dx(1) = 8.0*r(14)-r(1)*bf(1,1)*bi(1,1)/3.10e-3; % Butyrate
dx(2) = 2*r(1)*bf(1,1)*bi(1,1)/3.10e-3-r(5)*acm(1,1)/1.40e-3-...
    r(6)*ach(1,1)*ai(1,1)/(0.70e-3); % Acetate
dx(3) = 2*r(1)*bf(1,1)*bi(1,1)/3.10e-3+4*r(6)*ach(1,1)*ai(1,1)/0.70e-3-...
    r(2)*dec(1)*Hlim(2,1)/4.96e-3 - r(3)*dec(2)*Hlim(3,1)/2.80e-3-...
    r(2)*dec(3)*Hlim(4,1)/4.96e-3-r(2)*dec(4)*Hlim(5,1)/4.96e-3-...
    r(4)*Hlim(1,1)/0.76e-3; % Hydrogen
dx(4) = -r(2)*dec(1)*Hlim(2,1)/4.96e-3 - r(3)*dec(2)*Hlim(3,1)/2.80e-3; % TCE
dx(5) = r(2)*dec(1)*Hlim(2,1)/4.96e-3 + r(3)*dec(2)*Hlim(3,1)/2.80e-3-...
    r(2)*dec(3)*Hlim(4,1)/4.96e-3;% cDCE
dx(6) =  r(2)*dec(3)*Hlim(4,1)/4.96e-3 - r(2)*dec(4)*Hlim(5,1)/4.96e-3; % VC
dx(7) =  r(2)*dec(4)*Hlim(5,1)/4.96e-3; % ETH
dx(8) = 0.25*r(4)*Hlim(1,1)/0.76e-3+r(5)*acm(1,1)/1.40e-3; % MTH
dx(9) = r(1)*bf(1,1)*bi(1,1) - r(7); % XBO
dx(10) = r(2)*dec(1)*Hlim(2,1)+r(2)*dec(3)*Hlim(4,1)+r(2)*dec(4)*Hlim(5,1)-r(8);% XD1
dx(11) = r(3)*dec(2)*Hlim(3,1)- r(9);% XD2
dx(12) = r(4)*Hlim(1,1)-r(10); % XHM
dx(13) = r(5)*acm(1,1)-r(11); % XAM
dx(14) = r(6)*ach(1,1)*ai(1,1)-r(12); % XAO
dx(15) = r(13)-r(14); % XCM
```

```
end
```

B3. A fully kinetic model for culture NTUA-S – Chapters 10 and 11

This section provides the m-file for solving the inverse problem using an SQP-based multistart algorithm for culture NTUA-S (*InvS*.m). Like the previous section, the algorithm is based on the *multistart* built-in function of MATLAB®. As the inverse problem in Chapter 10 requires input from two batch tests, there are two m-files describing the system of ordinary differential equations of the model, *SysDef1*.m and *SysDef2*.m.

B3.1 *InvS*.m

Load the input data of the problem

```
global x y
rng('shuffle')
MaxStPts = input('Number of starting points:'); % Maximum number of starting points
% Import input data collected from two batch tests
TCE1 = importdata('filename'); DCE1 = importdata('filename'); VC1 =
importdata('filename'); ETH1 = importdata('filename'); BUT1 = importdata('filename');
AC1 = importdata('filename'); MTH1 = importdata('filename'); SUL1 =
importdata('filename');W1 = importdata('filename');
TCE2 = importdata('filename'); DCE2 = importdata('filename'); VC2=
importdata('filename'); ETH2 = importdata('filename'); BUT2 =
importdata('filename');AC2 = importdata('filename');
MTH2 = importdata('filename'); SUL2 = importdata('filename');
W2 = importdata('filename'); Xbo = importdata('filename'); Xd1 =
importdata('filename'); Xd2 = importdata('filename');T1 = importdata('filename'); T2 =
importdata('filename');
```

Set the feasible area of the parameter space

```
ub =[0.60,... mmax,BO k1
    4.30, ... mmax,TCE-D1 k2
    0.46, ... mmax,DCE-D1 k3
    0.49, ... mmax,VC-D1 k4
    0.38, ... mmax,AM k5
    0.26,... mmax,AO k6
    5.50,... mmax,HSR k7
    1.39,... mmax,ASR k8
    1.58,... mmax,BSR k9
    3676,... Ks,B-BO, k10
    12.40, ... Ks,tce-D1 k11
    99.70,... Ks,dce-D1  k12
    602,... Ks,vc-D1 k13
    0.10,... Ks,H-D1 k14
    602,...  Kinh,cDCE/VC k15
    2031,... Ks,A-AM k16
    2500,... Ks,A-AO k17
    200, ... Ks,S-HSR k18
    200, ... Ks,S-ASR k19
    200, ... Ks,S-BSR k20
    2.6, ... Ks,H-HSR k21
    600, ... KS,A-ASR k22
    3676, ... KS,B-BSR k23
    0.004,... KED k24
    1500,... Kinh,Sulfide k25
    2.96,... XBO k26
    0.66,... XAO k27
    5.50,... XHSR k28
    5.67, ... XASR k29
    4.00]; %XBSR k30
lb=[0.21,... mmax,BO k1
    0.33, ... mmax,TCE-D1 k2
    0.04, ... mmax,DCE-D1 k3
    0.01, ... mmax,VC-D1 k4
    0.04, ... mmax,AM k5
    0.07, ... mmax,AO k6
    0.23, ... mmax,HSR k7
    0.14, ... mmax,ASR k8
    0.17, ... mmax,BSR k9
    160, ... Ks,B-BO, k10
    0.05, ... Ks,tce-D1 k11
    0.54, ... Ks,dce-D1  k12
    2.60, ... Ks,vc-D1 k13
    0.007, ... Ks,H-D1 k14
    0.05, ...  Kinh,cDCE/VC k15
    370, ... Ks,A-AM k16
    500, ... Ks,A-AO k17
    5, ... Ks,S-HSR k18
    5, ... Ks,S-ASR k19
    5, ... Ks,S-BSR k20
    0.05, ... Ks,H-HSR k21
    70, ... KS,A-ASR k22
    160, ... KS,B-BSR k23
    0.004,... KED k24
    500,... Kinh,S k25
    0.00,... XBO k26
```

```
    0.27,... XAO k27
    0.00,... XHSR k28
    2.83, ... XASR k29
    0.00]; %XBSR k30
```

Create the Sobol set of starting points

```
K0=zeros(MaxStPts,length(ub)); %Matrix of starting points for the multistart algorithm
SbSet=sobolset(length(ub));
spts = net(SbSet,MaxStPts);
for i=1:MaxStPts
for j=1:length(ub)
K0(i,j) = lb(j)+spts(i,j).*(ub(j)-lb(j));
end
end
```

Set the optimization problem using the built-in *MultiStart* function and *fmincon*

```
MaxIterLS = length(ub)*100; % number of maximum iterations per local search
MaxFevals = MaxIterLS*20; % number of maximum function evaluations per local search
opt2 = optimset ('Display','iter','MaxFunEvals',MaxFevals,'maxiter',MaxIterLS,...
    'TolFun',1e-3,'TolX',1e-3,...
    'TolCon', 1e-
5,'FinDiffType','central','Algorithm','sqp','PlotFcns','optimplotfval');
problem = createOptimProblem ('fmincon', 'objective',...
    @(k)ObjF(k,iv1,iv2,BUT1,AC1,H1,TCE1,DCE1,VC1,ETH1,MTH1,SUL1,W1,T1,...
    BUT2,AC2,H2,TCE2,DCE2,VC2,ETH2,MTH2,SUL2,W2,T2), ..'lb', lb, 'ub', ub,'x0',
k,'options', opt2);
ms =
MultiStart('UseParallel','always','StartPointsToRun','bounds','TolFun',0.10,'TolX',0.10
);
stpts = CustomStartPointSet(K0); % Use the Sobol set of starting points
```

Solve the optimization problem

```
[xmin, fminm, flagm, outputm, solutions] = run(ms,problem,stpts);
```

B3.2 *ObjF*.m

The *fmincon* function requires the m-file *ObjF*.m, which calculates the objective function value, as follows:

```
function J=
ObjF(k,iv1,iv2,BUT1,AC1,H1,TCE1,DCE1,VC1,ETH1,MTH1,SUL1,W1,T1,BUT2,AC2,H2,TCE2,DCE2,VC2,ETH2,
MTH2,SUL2,W2,T2)
```

Solve the forward problem for each batch test

```
global x y
iv = [BUT1(1),AC1(1),H1(1),TCE1(1),DCE1(1),VC1(1),ETH1(1),MTH1(1),...
    SUL1(1),0,k(26),7.85,0.031,k(27),k(28),k(29),k(30),0.00];
iv2 = [BUT2(1),AC2(1),H2(1),TCE2(1),DCE2(1),VC2(1),ETH2(1),MTH2(1),...
    SUL2(1),0,k(26),7.85,0.031,k(27),k(28),k(29),k(30),0.00];
opt1 = odeset('Abstol',1e-8, 'Reltol', 1e-6);
[t1,x] = ode15s(@(t1,x)SysDef1(t1,x,k,iv1,iv2,BUT1,AC1,H1,TCE1,DCE1,VC1,ETH1,...
    MTH1,SUL1,W1,T1,BUT2,AC2,H2,TCE2,DCE2,VC2,ETH2,MTH2,SUL2,W2,T2), T1, iv, opt1);
[t2,y] = ode15s(@(t2,y)SysDef2(t2,y,k,iv1,iv2,BUT1,AC1,H1,TCE1,DCE1,VC1,ETH1,...
    MTH1,SUL1,W1,T1,BUT2,AC2,H2,TCE2,DCE2,VC2,ETH2,MTH2,SUL2,W2,T2), T2, iv2, opt1);
```

Calculate the objective function value, J

```
J1 = 0;
N1 = length(T1);
for i= 1:N1
J1 = J1 + (W1(i,8)*((TCE1(i)-x(i,4)))^2 + W1(i,7)*((DCE1(i)-x(i,5)))^2 + ...
    W1(i,6)*((VC1(i)-x(i,6)))^2 + W1(i,5)*((ETH1(i)-x(i,7)))^2+W1(i,3)*((MTH1(i)-
x(i,8))^2)+ W1(i,2)*((BUT1(i)-x(i,1)))^2 + W1(i,1)*((AC1(i)-
x(i,2)))^2+W1(i,4)*((SUL1(i)-x(i,15)))^2);
end
J2 = 0;
N2 = length(T2);
for i= 1:N2
J2 = J2 + (W2(i,8)*((TCE2(i)-y(i,4)))^2 + W2(i,7)*((DCE2(i)-y(i,5)))^2 + ...
    W2(i,6)*((VC2(i)-y(i,6)))^2 + W2(i,5)*((ETH2(i)-y(i,7)))^2+W2(i,3)*((MTH2(i)-
y(i,8))^2)+W2(i,2)*((BUT2(i)-y(i,1)))^2 + W2(i,1)*((AC2(i)-
y(i,2)))^2+W2(i,4)*((SUL2(i)-y(i,15)))^2);
end
J = J1+J2;
```

```
end
```

B3.3 *SysDef1*.m and *SysDef2*.m

During the solution of the forward problem for each batch test, function *ode15s* calls *SysDef1*.m and *SysDef2*.m functions, which contain the system of ordinary differential equations that describe the problem.

```
function dx =
SysDef1(t1,x,k,iv1,iv2,BUT1,AC1,H1,TCE1,DCE1,VC1,ETH1,MTH1,SUL1,W1,T1,BUT2,AC2,H2,TCE2,DCE2,V
C2,ETH2,MTH2,SUL2,W2,T2)
```

Hydrogen limitation for D1, D2 and HSR

```
% Calculate hydrogen threshold functions according to Ribes et al. (2004)

ft = zeros(2,1); % TCE dechlorination
ft(1,1) = 1/(1+exp(100*((2e-3)-x(3))/(2e-3)));
ft(2,1) = 1/(1+exp(100*((1.1*(2e-3))-x(3))/(2e-3)));
fd = zeros(2,1); % DCE dechlorination
fd(1,1) = 1/(1+exp(100*((2e-3)-x(3))/(2e-3)));
fd(2,1) = 1/(1+exp(100*((1.1*(2e-3))-x(3))/(2e-3)));
fv = zeros(2,1); % VC dechlorination
fv(1,1) = 1/(1+exp(100*((2e-3)-x(3))/(2e-3)));
fv(2,1) = 1/(1+exp(100*((1.1*(2e-3))-x(3))/(2e-3)));
fs = zeros(2,1); %sulfate reduction
fs(1,1) = 1/(1+exp(100*((2e-3)-x(3))/(2e-3)));
fs(2,1) = 1/(1+exp(100*((1.1*(2e-3))-x(3))/(2e-3)));
Hlim = zeros(6,1);
Hlim(2,1) = ((x(3)-(2e-3)*ft(1))*ft(2)/(k(14)+x(3)-(2e-3)*ft(1))); % TCE
Hlim(4,1) = ((x(3)-(2e-3)*fd(1))*fd(2)/(k(14)+x(3)-(2e-3)*fd(1))); % DCE
Hlim(5,1) = ((x(3)-(2e-3)*fv(1))*fv(2)/(k(14)+x(3)-(2e-3)*fv(1))); % VC
Hlim(6,1) = ((x(3)-(2e-3)*fs(1))*fs(2)/(k(21)+x(3)-(2e-3)*fs(1))); % Sulfate reduction
```

Butyrate limitation for BO

```
bf = zeros(1,1);
bf(1,1) = x(1)/(k(10)+x(1));
% Inhibition by hydrogen
bi = zeros(1,1);
bi(1,1) = exp(-(x(3)/0.25));
```

Chloroethene limitation for D1 dechlorinators

```
dec = zeros(4,1);
dec(1) = (x(4)/(k(11)+x(4))); % tce
dec(3) = (x(5)/(k(12)+x(5))); %dce
dec(4) = (x(6)/((k(13))*(1+(x(5)/k(15)))+x(6))); %vc
```

Acetate limitation for AM

```
% Calculate acetate threshold functions according to Ribes et al. (2004)
at = zeros(2,1);
at(1,1) = 1/(1+exp(100*(15-x(2))/15));
at(2,1) = 1/(1+exp(100*((1.1*15)-x(2))/15));
acm = zeros(1,1);
acm(1,1) = ((x(2)-15*at(1))*at(2)/(k(16)+x(2)-15*at(1)));
```

Sulfide inhibition for acetoclastic methanogenesis

```
SulfideInh=zeros(1,1);
SulfideInh(1,1)=1/(1+((x(1)+x(2))/k(25)));
```

Acetate limitation for AO

```
ach = zeros(1,1);
ach(1,1) = x(2)/(k(17)+x(2));
% Inhibition by hydrogen
ai = zeros(1,1);
ai(1,1) = exp(-(x(3)/0.08));
```

Sulfate limitation for sulfate reducers

```
Sl = zeros(3,1);
Sl(1,1) = x(9)/((k(18))+x(9)); % HSR
Sl(2,1) = x(9)/((k(19))+x(9)); % ASR
Sl(3,1) = x(9)/((k(20))+x(9)); % BSR
```

Acetate limitation for ASR

```
Sac = ((x(2)-15*at(1))*at(2)/(k(22)+x(2)-15*at(1)));
```

Butyrate limitation for BSR

```
Sb = x(1)/(k(23)+x(1)); %
```

Growth and decay rates for microbial species

```
r = zeros(18,1);
r(1) = k(1)*x(11); %  Growth BO
r(2) = k(2)*x(12);%  Growth D1/TCE
r(3) = k(3)*x(12); % Growth D1/DCE
r(4) = k(4)*x(12); % Growth D1/VC
r(5) = k(5)*x(13); % Growth AM
r(6) = k(6)*x(14); % Growth AO
r(7) = k(7)*x(15); % Growth HSR
r(8) = k(8)*x(16); % Growth ASR
r(9) = k(9)*x(17); % Growth BSR
r(10) = 0.024*x(11); % decay BO
r(11) = 0.024*x(12);% decay D1
r(12) = 0.024*x(13); % decay AM
r(13) = 0.024*x(14); % decay AO
r(14) = 0.050*x(15); % decay HSR
r(15) = 0.030*x(16); % decay ASR
r(16) = 0.030*x(17); % decay BSR
r(17) = (r(10)+r(11)+r(12)+r(13)+r(14)+r(15)+r(16)); % decay by-products
r(18) = k(24)*x(18); % Composite material consumption
```

Define the system of ODEs that describes the rates of substrate consumption and biomass growth

```
dx=zeros(18,1);
dx(1) = 8.0*r(20)-r(1)*bf(1,1)*bi(1,1)/(3.10e-3)-r(9)*Sb(1,1)*Sl(3,1)/(4.30e-3); %
Butyrate
dx(2) = 2*r(1)*bf(1,1)*bi(1,1)/(3.10e-3)+2*r(9)*Sb(1,1)*Sl(3,1)/(4.30e-3)-...
    r(5)*acm(1,1)*SulfideInh(1)/(1.40e-3)-r(6)*ach(1,1)*ai(1,1)/(0.70e-3)-...
    r(8)*Sac*Sl(2,1)/(4.30e-3); % Acetate
dx(3) = 2*r(1)*bf(1,1)*bi(1,1)/(3.10e-3)+4*r(6)*ach(1,1)*ai(1,1)/(0.70e-3)-...
    r(2)*dec(1)*Hlim(2,1)/(2.35e-3)-r(3)*dec(3)*Hlim(4,1)/(2.35e-3)-...
    r(4)*dec(4)*Hlim(5,1)/(2.35e-3)-r(7)*Hlim(6,1)*Sl(1,1)/(1.70e-3); %Hydrogen
dx(4) = -r(2)*dec(1)*Hlim(2,1)/(2.35e-3); % TCE
dx(5) = r(2)*dec(1)*Hlim(2,1)/(2.35e-3)-r(3)*dec(3)*Hlim(4,1)/(2.35e-3); % DCE
dx(6) = r(3)*dec(3)*Hlim(4,1)/(2.35e-3)-r(4)*dec(4)*Hlim(5,1)/(2.35e-3);% VC
dx(7) = r(4)*dec(4)*Hlim(5,1)/(2.35e-3); % ETH
dx(8) = r(5)*acm(1,1)*SulfideInh(1)/(1.40e-3); %MTH
dx(9) = -r(8)*Sac*Sl(2,1)/(4.30e-3)-0.25*r(7)*Hlim(6,1)*Sl(1,1)/(1.70e-3)-...
    0.5*r(9)*Sb(1,1)*Sl(3,1)/(4.30e-3); % Sulfate
dx(10) = r(8)*Sac*Sl(2,1)/(4.30e-3)+0.25*r(7)*Hlim(6,1)*Sl(1,1)/(1.70e-3)+...
    0.5*r(9)*Sb(1,1)*Sl(3,1)/(4.30e-3); % Sulfide
dx(11) = r(1)*bf(1,1)*bi(1,1)-r(10); % BO
dx(12) = r(2)*dec(1)*Hlim(2,1)+r(2)*dec(3)*Hlim(4,1)+r(2)*dec(4)*Hlim(5,1)-r(11);%D1
dx(13) = r(5)*acm(1,1)*SulfideInh(1)-r(12); %AM
dx(14) = r(6)*ach(1,1)*ai(1,1)-r(13); % AO
dx(15) = r(7)*Hlim(6,1)*Sl(1,1)-r(14); % HSR
dx(16) = r(8)*Sac*Sl(2,1)-r(15); % ASR
dx(17) = r(9)*Sb(1,1)*Sl(3,1)-r(16); % BSR
dx(18) = r(17)-r(18); % Composite material
```

```
end
```

```
function dy =
SysDef2(t2,y,k,iv1,iv2,BUT1,AC1,H1,TCE1,DCE1,VC1,ETH1,MTH1,SUL1,W1,T1,BUT2,AC2,H2,TCE2,DCE2,V
C2,ETH2,MTH2,SUL2,W2,T2)
```

Hydrogen limitation for D1, D2 and HSR

```
% Calculate hydrogen threshold functions according to Ribes et al. (2004)
fty = zeros(2,1); % TCE dechlorination
fty(1,1) = 1/(1+exp(100*((2e-3)-y(3))/(2e-3)));
fty(2,1) = 1/(1+exp(100*((1.1*(2e-3))-y(3))/(2e-3)));
fdy = zeros(2,1); % DCE dechlorination
fdy(1,1) = 1/(1+exp(100*((2e-3)-y(3))/(2e-3)));
fdy(2,1) = 1/(1+exp(100*((1.1*(2e-3))-y(3))/(2e-3)));
fvy = zeros(2,1); % VC dechlorination
fvy(1,1) = 1/(1+exp(100*((2e-3)-y(3))/(2e-3)));
fvy(2,1) = 1/(1+exp(100*((1.1*(2e-3))-y(3))/(2e-3)));
fsy = zeros(2,1); % sulfate reduction
fsy(1,1) = 1/(1+exp(100*((2e-3)-y(3))/(2e-3)));
fsy(2,1) = 1/(1+exp(100*((1.1*(2e-3))-y(3))/(2e-3)));
Hlimy = zeros(6,1);
Hlimy(2,1) = ((y(3)-(2e-3)*fty(1))*fty(2)/(k(14)+y(3)-(2e-3)*fty(1))); % TCE
dechlorination
Hlimy(4,1) = ((y(3)-(2e-3)*fdy(1))*fdy(2)/(k(14)+y(3)-(2e-3)*fdy(1))); % DCE
dechlorination
Hlimy(5,1) = ((y(3)-(2e-3)*fvy(1))*fvy(2)/(k(14)+y(3)-(2e-3)*fvy(1))); % VC
dechlorination
Hlimy(6,1) = ((y(3)-(2e-3)*fsy(1))*fsy(2)/(k(21)+y(3)-(2e-3)*fsy(1))); % sulfate
reduction
```

Butyrate limitation for BO

```
bfy = zeros(1,1);
bfy(1,1) = y(1)/(k(10)+y(1));
% inhibition by hydrogen
biy = zeros(1,1);
biy(1,1) = exp(-(y(3)/0.25));
```

Chloroethene limitation for D1 dechlorinators

```
decy = zeros(4,1);
decy(1) = (y(4)/(k(11)+y(4))); % tce
decy(3) = (y(5)/(k(12)+y(5))); %dce
decy(4) = (y(6)/((k(13))*(1+(y(5)/k(15)))+y(6))); %vc
```

Acetate limitation for AM

```
% Calculate acetate threshold functions according to Ribes et al. (2004)
aty = zeros(2,1);
aty(1,1) = 1/(1+exp(100*(15-y(2))/15));
aty(2,1) = 1/(1+exp(100*((1.1*15)-y(2))/15));
acmy = zeros(1,1);
acmy(1,1) = ((y(2)-15*aty(1))*aty(2)/(k(16)+y(2)-15*aty(1)));
```

Sulfide inhibition for acetoclastic methanogenesis

```
SulfideInhy=zeros(1,1);
SulfideInhy(1,1)=1/(1+((y(1)+y(2))/k(25)));
```

Acetate limitation for AO

```
achy = zeros(1,1);
achy(1,1) = y(2)/(k(17)+y(2));
% inhibition by hydrogen
aiy = zeros(1,1);
aiy(1,1) = exp(-(y(3)/0.08));
```

Sulfate limitation for sulfate reducers

```
Sly = zeros(3,1);
Sly(1,1) = y(9)/((k(18))+y(9)); % HSR
Sly(2,1) = y(9)/((k(19))+y(9)); % ASR
Sly(3,1) = y(9)/((k(20))+y(9)); % BSR
```

Acetate limitation for ASR

```
Sacy = ((y(2)-15*aty(1))*aty(2)/(k(22)+y(2)-15*aty(1)));
```

Butyrate limitation for BSR

```
Sby = y(1)/(k(23)+y(1));
```

Growth and decay rates for the microbial population considered

```
ry = zeros(18,1);
ry(1) = k(1)*y(11); % growth BO
ry(2) = k(2)*y(12);% growth D1/TCE
ry(3) = k(3)*y(12); % growth D1/DCE
ry(4) = k(4)*y(12); % growth D1/VC
ry(5) = k(5)*y(13); % growth AM
ry(6) = k(6)*y(14); % growth AO
ry(7) = k(7)*y(15); % growth HSR
ry(8) = k(8)*y(16); % growth ASR
ry(9) = k(9)*y(17); % growth BSR
ry(10) = 0.024*y(11); % decay BO
ry(11) = 0.024*y(12);% decay D1
ry(12) = 0.024*y(13); % decay AM
ry(13) = 0.024*y(14); % decay AO
ry(14) = 0.050*y(15); % decay HSR
ry(15) = 0.030*y(16); % decay ASR
ry(16) = 0.030*y(17); % decay BSR
ry(17) = (ry(10)+ry(11)+ry(12)+ry(13)+ry(14)+ry(15)+ry(16)); % decay by-products
ry(18) = k(24)*y(18); % Composite material consumption
```

Define the system of ODEs that describes the rates of substrate consumption and biomass growth

```
dy=zeros(18,1);
dy(1) = 8.0*ry(20)-ry(1)*bfy(1,1)*biy(1,1)/(3.10e-3)-...
    ry(9)*Sby(1,1)*Sly(3,1)/(4.30e-3); %Butyrate
dy(2) = 2*ry(1)*bfy(1,1)*biy(1,1)/(3.10e-3)+2*ry(9)*Sby(1,1)*Sly(3,1)/(4.30e-3)-...
    ry(5)*acmy(1,1)*SulfideInhy(1)/(1.40e-3)-...
    ry(6)*achy(1,1)*aiy(1,1)/(0.70e-3)-ry(8)*Sacy*Sly(2,1)/(4.30e-3); %Acetate
dy(3) = 2*ry(1)*bfy(1,1)*biy(1,1)/(3.10e-3)+4*ry(6)*achy(1,1)*aiy(1,1)/(0.70e-3)-...
    ry(2)*decy(1)*Hlimy(2,1)/(2.35e-3)-ry(3)*decy(3)*Hlimy(4,1)/(2.35e-3)-...
    ry(4)*decy(4)*Hlimy(5,1)/(2.35e-3)-ry(7)*Hlimy(6,1)*Sly(1,1)/(1.70e-3); %Hydrogen
dy(4) = -ry(2)*decy(1)*Hlimy(2,1)/(2.35e-3); % TCE
dy(5) = ry(2)*decy(1)*Hlimy(2,1)/(2.35e-3)-ry(3)*decy(3)*Hlimy(4,1)/(2.35e-3);% DCE
dy(6) = ry(3)*decy(3)*Hlimy(4,1)/(2.35e-3)-ry(4)*decy(4)*Hlimy(5,1)/(2.35e-3);% VC
dy(7) = ry(4)*decy(4)*Hlimy(5,1)/(2.35e-3); % ETH
dy(8) = ry(5)*acmy(1,1)*SulfideInhy(1)/(1.40e-3); % MTH
dy(9) = -ry(8)*Sacy*Sly(2,1)/(4.30e-3)-0.25*ry(7)*Hlimy(6,1)*Sly(1,1)/(1.70e-3)-...
    0.5*ry(9)*Sby(1,1)*Sly(3,1)/(4.30e-3); % Sulfate
dy(10) = ry(8)*Sacy*Sly(2,1)/(4.30e-3)+0.25*ry(7)*Hlimy(6,1)*Sly(1,1)/(1.70e-3)+...
    0.5*ry(9)*Sby(1,1)*Sly(3,1)/(4.30e-3);% Sulfide
dy(11) = ry(1)*bfy(1,1)*biy(1,1)-ry(10); % BO
dy(12) = ry(2)*decy(1)*Hlimy(2,1)+ry(2)*decy(3)*Hlimy(4,1)+...
    ry(2)*decy(4)*Hlimy(5,1)-ry(11); % D1
dy(13) = ry(5)*acmy(1,1)*SulfideInhy(1)-ry(12); % AM
dy(14) = ry(6)*achy(1,1)*aiy(1,1)-ry(13); % AO
dy(15) = ry(7)*Hlimy(6,1)*Sly(1,1)-ry(14); % HSR
dy(16) = ry(8)*Sacy*Sly(2,1)-ry(15); % ASR
dy(17) = ry(9)*Sby(1,1)*Sly(3,1)-ry(16); % BSR
dy(18) = ry(17)-ry(18); % Composite material
```

```
end
```